frontiers | Research Topics

Personalized immunotherapy: Advancing processes to extend patient collectives

Edited by
Patrick Schmidt, Stefan B. Eichmüller, Yun-Fan Sun and Jonathan Scolnick

Published in
Frontiers in Immunology
Frontiers in Oncology

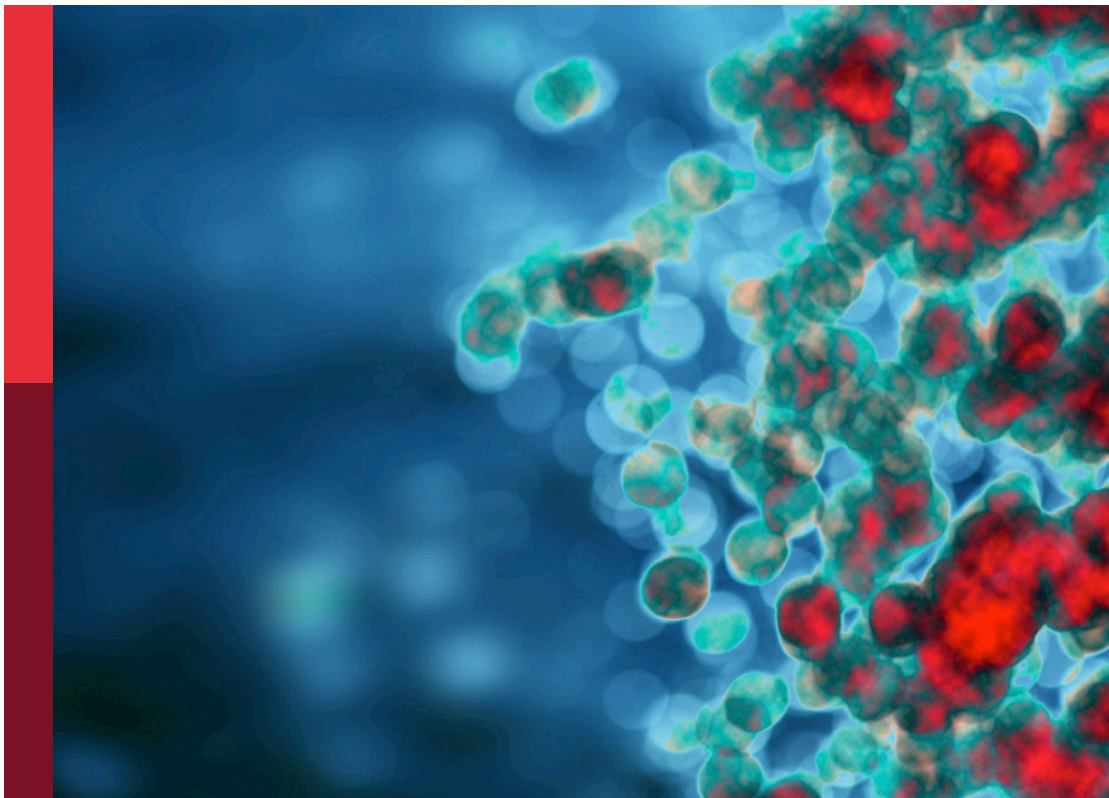

ISSN 1664-8714
ISBN 978-2-8325-4491-4
DOI 10.3389/978-2-8325-4491-4

About Frontiers

Frontiers is more than just an open access publisher of scholarly articles: it is a pioneering approach to the world of academia, radically improving the way scholarly research is managed. The grand vision of Frontiers is a world where all people have an equal opportunity to seek, share and generate knowledge. Frontiers provides immediate and permanent online open access to all its publications, but this alone is not enough to realize our grand goals.

Frontiers journal series

The Frontiers journal series is a multi-tier and interdisciplinary set of open-access, online journals, promising a paradigm shift from the current review, selection and dissemination processes in academic publishing. All Frontiers journals are driven by researchers for researchers; therefore, they constitute a service to the scholarly community. At the same time, the *Frontiers journal series* operates on a revolutionary invention, the tiered publishing system, initially addressing specific communities of scholars, and gradually climbing up to broader public understanding, thus serving the interests of the lay society, too.

Dedication to quality

Each Frontiers article is a landmark of the highest quality, thanks to genuinely collaborative interactions between authors and review editors, who include some of the world's best academicians. Research must be certified by peers before entering a stream of knowledge that may eventually reach the public - and shape society; therefore, Frontiers only applies the most rigorous and unbiased reviews. Frontiers revolutionizes research publishing by freely delivering the most outstanding research, evaluated with no bias from both the academic and social point of view. By applying the most advanced information technologies, Frontiers is catapulting scholarly publishing into a new generation.

What are Frontiers Research Topics?

Frontiers Research Topics are very popular trademarks of the *Frontiers journals series*: they are collections of at least ten articles, all centered on a particular subject. With their unique mix of varied contributions from Original Research to Review Articles, Frontiers Research Topics unify the most influential researchers, the latest key findings and historical advances in a hot research area.

Find out more on how to host your own Frontiers Research Topic or contribute to one as an author by contacting the Frontiers editorial office: frontiersin.org/about/contact

Personalized immunotherapy: Advancing processes to extend patient collectives

Topic editors

Patrick Schmidt — Department of Medical Oncology, National Center for Tumor Diseases (NCT), Germany

Stefan B. Eichmüller — German Cancer Research Center (DKFZ), Germany

Yun-Fan Sun — Fudan university, China

Jonathan Scolnick — Singleron biotechnologies, Singapore

Citation

Schmidt, P., Eichmüller, S. B., Sun, Y.-F., Scolnick, J., eds. (2024). *Personalized immunotherapy: Advancing processes to extend patient collectives*. Lausanne: Frontiers Media SA. doi: 10.3389/978-2-8325-4491-4

Table of contents

frontiers | Frontiers in Immunology

TYPE Review
PUBLISHED 09 February 2023
DOI 10.3389/fimmu.2023.1105420

OPEN ACCESS

EDITED BY
Patrick Schmidt,
National Center for Tumor Diseases (NCT), Germany

REVIEWED BY
Michael Volkmar,
German Cancer Research Center (DKFZ), Germany
Zeynep Kosaloglu Yalcin,
La Jolla Institute for Immunology (LJI), United States

*CORRESPONDENCE
Nupur Biswas
nupur@rhenix.org;
nupurbiswas@gmail.com

SPECIALTY SECTION
This article was submitted to Cancer Immunity and Immunotherapy, a section of the journal Frontiers in Immunology

RECEIVED 22 November 2022
ACCEPTED 30 January 2023
PUBLISHED 09 February 2023

CITATION
Biswas N, Chakrabarti S, Padul V, Jones LD and Ashili S (2023) Designing neoantigen cancer vaccines, trials, and outcomes. *Front. Immunol.* 14:1105420. doi: 10.3389/fimmu.2023.1105420

Designing neoantigen cancer vaccines, trials, and outcomes

Nupur Biswas[1]*, Shweta Chakrabarti[1], Vijay Padul[1], Lawrence D. Jones[2] and Shashaanka Ashili[2]

[1]Rhenix Lifesciences, Hyderabad, India, [2]CureScience, San Diego, CA, United States

Neoantigen vaccines are based on epitopes of antigenic parts of mutant proteins expressed in cancer cells. These highly immunogenic antigens may trigger the immune system to combat cancer cells. Improvements in sequencing technology and computational tools have resulted in several clinical trials of neoantigen vaccines on cancer patients. In this review, we have looked into the design of the vaccines which are undergoing several clinical trials. We have discussed the criteria, processes, and challenges associated with the design of neoantigens. We searched different databases to track the ongoing clinical trials and their reported outcomes. We observed, in several trials, the vaccines boost the immune system to combat the cancer cells while maintaining a reasonable margin of safety. Detection of neoantigens has led to the development of several databases. Adjuvants also play a catalytic role in improving the efficacy of the vaccine. Through this review, we can conclude that the efficacy of vaccines can make it a potential treatment across different types of cancers.

KEYWORDS

neoantigen vaccine, cancer immunotherapy, clinical trials, WES, NGS - next generation sequencing

1 Introduction

Cancer is an outcome of the abnormal proliferation of cells. The abnormal proliferation leads to the unrestricted growth of cells in the form of a tumor. If the abnormally proliferating cells invade surrounding normal tissue and/or spread all over the body, then it turns into cancer (1). Normal somatic cells turn into cancer cells due to genetic alterations. The divergent nature of genetic alterations, which mostly include mutations, has made cancer a complex disease. Several types of mutations are accumulated within the cells, starting from the embryonic state. But only a combination of mutations in multiple genes leads to cancer (2). Those mutations, translated to changes in the amino acid arrangement, create mutated proteins that are new to the body's adaptive immune system. The mutant peptides, usually ~ 8-25 mer long peptides around the mutated sites are considered as neoantigens. According to Xia et al. a neoantigen with validated immunogenicity is termed as neoepitope and a neoantigen with uncertain immunogenicity is termed as neopeptide (3).

Broadly there are two types of tumor antigens, Tumor Associated Antigens (TAA) and Tumor-Specific Antigens (TSA) (4). Neoantigens are a subclass of TSAs and differ from

TAAs. TAAs are not unique to tumor cells but neoantigens are. TAAs are derived from over-expressed proteins which may also be present in normal cells (5). Neoantigens are tumor-specific and expressed in tumor cells only. There were attempts at cancer vaccines targeting TAAs as well; however, the results were not so promising (6). Trials have also been conducted targeting differentiation antigens which appear at particular phases of cell differentiation but they can be expressed in both tumor and normal cells (7). Neoantigens arise from different types of mutations in DNA which include point mutations, insertions, deletions, gene fusions (8–10), and even frameshift mutations in genes that may or may not be oncogenes or tumor suppressor genes. As point mutations are more frequent, they are more often used as neoantigen candidates.

Neoepitopes are already present in the patient's body but only localized in the tumor cells. In neoantigen immunotherapy, synthetically made neopeptides are administered to the patients. The goal is to stimulate the immune system to recognize the neoantigens so that CD8+ and CD4+ T cells are activated to recognize and to destroy the cancer cells. However, the success of this process depends on several factors, the foremost among them being the successful loading and presentation of the neopeptides on human leukocyte antigens (HLA) proteins. Personalized neoantigen vaccines may train the immune system to identify and kill the neopeptide-presenting cancer cells. Apart from provoking immunogenicity, other advantages of the neoantigen vaccine are that it can be given to outpatients and side effects are not significant (11). Neoantigens are patient-specific, however, few of them may be shared among multiple patients (4). Mutations are not always random, driver mutations often appear in multiple patients. It opens up the possibility of shared neoepitopes for at least in the subgroup of patients sharing common mutations (12, 13).

In the last few years due to the cost-effectiveness of sequencing technologies, neoantigen vaccines have appeared as emergent immunotherapy. In this review, we are addressing the criteria, processes, and challenges associated with neoantigen vaccine design. We observed that several clinical trials are ongoing. A few research groups have also reported their trial results. Although the number of enrolled patients is less, several clinical trials are reporting encouraging results. Utilizing the national clinical trial website of NIH (https://clinicaltrials.gov/ct2/home), a search afforded 126 results using a combination of keywords 'cancer', 'neoantigen vaccine', and 'neoepitope', of which 39 trials were either active, terminated or completed (searched on December 20, 2022). Among them, we have discussed 26 trials in this review which involve the extraction of mutated peptides from sequence data, with the administration of them to the patients for evaluation. In order to determine the outcomes from these neoantigen vaccine therapy clinical trials, we completed a keywords search in PubMed using combinations of keywords 'neoantigen', 'neoepitope', 'cancer', 'vaccine', and 'clinical trials'. We identified 79 articles for article type 'clinical trial' to date (PubMed accessed on December 19, 2022). We included clinical trials where neoantigens were administered on human subjects only. Figure 1 shows our selection procedure for reviewing the outcomes. Based on these conditions, we summarized the ongoing clinical trials. Below we have discussed the reported outcomes in the neoantigen vaccine research.

2 Neoantigen design

The neoantigen design process starts with the identification of all types of somatic mutations from the whole genome or the exome sequencing of tumor samples. All mutations do not lead to effective neoantigens. For being identified as a neoepitope as well as a successful candidate for neoantigen vaccine therapy, the peptide must bind with the HLA molecules and the neoantigen-HLA complex must be able to stimulate neopeptide-specific T cells of the immune system (14). Hence, after the identification of various neopeptides, the potentially effective neopeptides are selected based on the predicted probability of neopeptide-HLA binding (15). These predictions are done using different algorithms which often use existing data of experimentally validated peptides which are available in the databases like Immune Epitope Database and Analysis Resource (IEDB) (16). Multiple combinations of algorithms are followed to identify the key parameters behind the neopeptide-HLA binding (17). Structural modeling considering spatial features has also been used to predict HLA binding energies as well as CD8+ T cell responses towards neoantigen (18, 19).

2.1 Criteria

As previously indicated, the primary requirement of designing a neoantigen is that the peptide must bind with the HLA molecules and the peptide-HLA complex must be able to stimulate T cells of the immune system (14). However, there are additional criteria that should be considered for effective design. These criteria include proper selection of target somatic mutations, the exclusivity of the

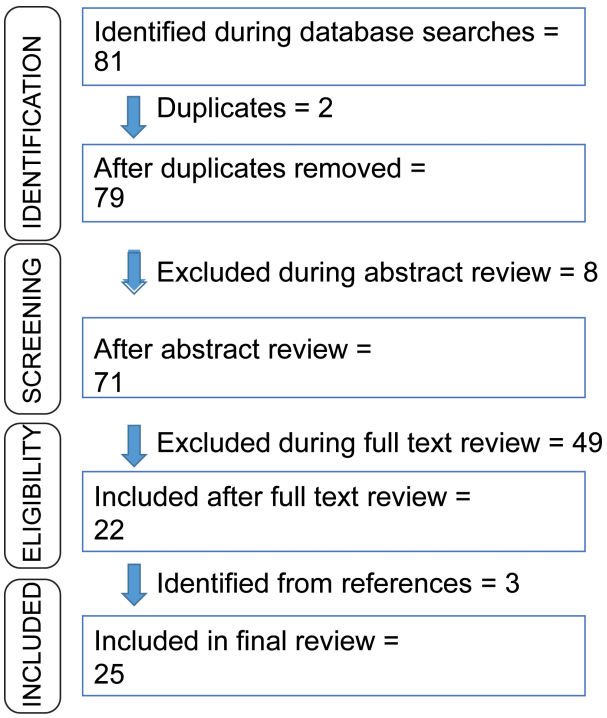

FIGURE 1
Flow chart describing the article selection process for this review.

peptide production in the cancer cells, abundant expression, processing by antigen presentation pathway, binding of the peptide fragment to host specific HLA proteins, and mutated allele frequency. All of these criteria are difficult to satisfy and a compromised or prioritized choice is made using immunoinformatics approaches (20). Researchers have developed multiple pipelines for the selection of neopeptides, such as pVACtools (21), Vaxrank (22), MuPeXI (23), TSNAD (24), and pTuneos (25). Each of these pipelines has its selection process and results in the lists of neopeptides. However, these lists very often differ from each other. In the following section, we will discuss the generalized approach required for vaccine design.

2.2 Processes

The personalized neopeptide vaccine design requires information on the mutations in proteins which are translated from the mutation sites of the DNA in cancer cells. This information is extracted by comparing the DNA sequences of normal and tumor cells. Either whole genome sequencing (WGS) or whole exome sequencing (WES) data of DNA of both tumor and normal cells is required. However, since of the entire genome, only exonic parts are only translated to peptides, WES is sufficient to detect somatic mutations. Moreover, compared to WGS, WES is more economical considering both clinical and computational costs. Additionally, the mutated proteins should be expressed in the tumor cells, to ensure that mRNA sequencing of tumor cell mRNAs is also performed.

Figure 2 shows the schematic of the bioinformatics process of vaccine design. The sequence reads, available in fastq file format, contain sequences and a quality score for each base representing the accuracy of the sequencer in identifying that base. The fastq files are pre-processed by trimming out low-quality bases and adapter sequences. Software like fastp (26), Trimmomatic (27), Cutadapt (28), and Prinseq (29) are used for trimming and FastQC (30) is very often used for quality checks. To identify tumor specific somatic nucleotide variants, both normal and tumor sequence reads are aligned or mapped to the reference human genome sequence assembly, available at NCBI and Ensembl (31) database. There are multiple aligner software available based on different algorithms. These algorithms include BWA, BWA-MEM (32), and Novoalign (33). The genome analysis tool kit (GATK) provides a bundle of software required for sequence analysis (34). Among different algorithms, BWA works for shorter sequences and BWA-MEM works for longer sequences. So for aligning WES, the BWA-MEM algorithm is preferred. mRNA sequence is also aligned in a similar fashion against the reference genome using specialized aligners. mRNAs are transcribed only from the exon parts of the genome by removing introns, but the reference genome contains both introns and exons. Hence, while aligning mRNA sequences, the splicing of exons should be taken care of. Among the mRNA sequence aligner software, STAR (35), GMAP (36), and Tophat2 (37) are splice-aware whereas Bowtie2 (38) is not splice-aware. For both WGS/WES and mRNA sequence alignment, the information is obtained in the form of a sequence alignment map (SAM) file or its binary counterpart BAM file. For mRNA sequences, expression count values of different mRNAs are extracted from the BAM file using software like HTSeq2 (39). For WES, the mapped sequences require post-processing, for

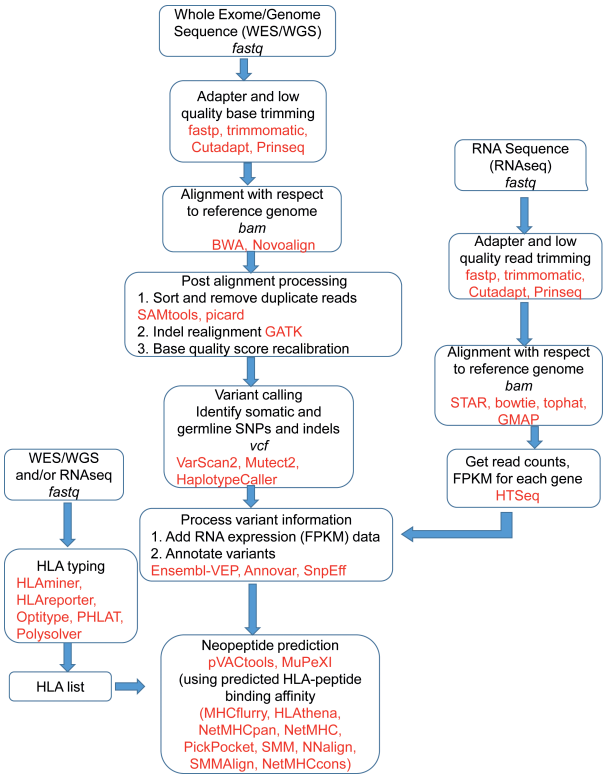

FIGURE 2
A schematic of the bioinformatics process of neoantigen vaccine design. Frequently used software and tools are in red. The file formats are in italics.

which software like GATK, Picard (40), SAMtools (41) are often used. This post-processing includes the removal of duplicate reads, which originate from the same fragment of the DNA. Indel realignment is also recommended by realigning reads near detected indels to remove alignment artifacts. After the removal of duplicate reads, the base quality score recalibration (BQSR) is performed using GATK. In the BQSR process, using machine learning algorithms, the systematic errors made by the sequencer while calling the bases are estimated and base quality scores are calibrated accordingly. These recalibrated BAM files are further used for identifying different genetic variants.

The variant calling software identifies single nucleotide polymorphisms (SNPs) and small insertions and deletions (indels). The software includes VarScan2 (42), Mutect2 (43), HaplotypeCaller (44) and each of them provides output in a variant call format (vcf). The vcf files contain nucleotide mutations and other information like chromosome position and quality scores associated with variant detection. Since neoantigens are based on somatic mutations, germline variants are often excluded. However, software like pVACtools considers germline variants and other somatic variants which are proximal to the 'somatic variant of interest' for which neoantigen is being predicted (45). To identify the germline variants, the BAM file from a normal DNA sample is used. Also, some known variants are removed to isolate tumor specific variants. The known variants can be obtained from resources like the GATK resource bundle in a user friendly format (46) and also from dbSNP (47).

The vcf files containing variant information are further annotated which effectively tags the variants with other necessary information

from different databases. This information includes gene information, transcript information, variant location, variant consequence (mutation type), and associated minor allele frequency (MAF), depending on the annotation and software used. The commonly used annotation software are Ensembl-VEP (48), ANNOVAR (49), SnpEff (50), and the databases are dbSNP (47), 1000 Genomes (51), etc. Since a vcf file may contain hundreds of mutations, the associated information is used for prioritizing the possible neopeptides.

These annotated vcf files are used for peptide prediction using software like pVACtools (21), MuPeXI (23). The prediction process is based on the binding with MHC molecules which is predicted by different software like MHCflurry (52), HLAthena (53), MixMHCpred (54), NetMHC (55), NetMHCpan (56), NetMHCcons (57), PickPocket (58), and SMM for MHC-I type whereas NetMHCIIPan (56), SMMAlign (59), and NNalign (60) are used for MHC-II molecules. Mei et al. observed that MixMHCpred 2.0.1, NetMHCpan 4.0, and NetMHCcons 1.1 perform well for predicting peptides binding to most of the HLA-I allomorphs (61). For a robust prediction of neopeptides, the list of relevant alleles, corresponding mRNA expression status of the mutated genes are required. The relevant alleles are predicted by HLA typing process which may be a clinical approach or analytical approach based on the WGS, WES or mRNA sequence data. The neopeptides, targeted for binding with MHC-I molecules are usually of 8-10 mer lengths whereas peptides targeted for binding with MHC-II molecules are usually longer, 13-25 mers (62). The neopeptide prediction software usually provides a large number of peptides that are further shortlisted based on the strength of peptide-MHC binding which is expressed in terms of IC50 values. IC50 < 50 nM is considered strong binding and IC50 >500 nM is considered non-binder (63). The mRNA expression strength and variant allele frequency are also considered for the final selection of peptides.

The peptides are further formulated following different strategies considering peptide solubility and stability. Oosting et al. developed a formulation that maintains stability for up to 32 weeks (64). The delivery strategy includes the use of mRNA vaccine (65), DNA vaccine (66), pulsed dendritic cells (67), and recombinant viruses (68). It also includes direct injection of unformulated vaccines (69). Different adjuvants like poly-ICLC, and helper peptides like tetanus are also used in the formulation. The administration process includes subcutaneous, intramuscular, and intravenous injections mostly in limbs.

2.3 Challenges

The neoantigen vaccine-based immunotherapy is a complex process involving several challenges (68). As the multistep design process involves the use of several computational tools, each of them containing an algorithm and each with advantages and disadvantages. This situation often results in wide variability in the output neopeptide sequences. For each analysis step, multiple software exists. The optimized combination of the software is required for building the pipeline for vaccine design. There is wide variability in identifying the mutations based on the WGS/WES data using different variant callers (70, 71). In case of high variance in mutations called by different variant callers, the consensus outputs can be considered as more reliable mutations (70–72). Similar high variability is observed in the process of HLA typing to identify MHC molecules from the sequence data (73, 74). Many HLA typing software exist, and they identify the HLA molecules in diverse ways using different computational and statistical approaches. The results of this software can be compared with the clinical HLA typing tests based on antigenic reactions, using the blood sample of patients. Here, the miscalled HLAs can be avoided for peptide binding. Also, for HLA class II typing, the number of HLA typing callers is less. The computational approach will identify a large number of neopeptides. Even, for a given mutation site, multiple peptides may be detected which may have varying lengths, and differ starting and ending positions of the sequence. Among them, the list of effective peptides need to be optimized based on criteria like HLA-peptide binding strength. Moreover, the neopeptide may not be effective if the corresponding HLA allele is deleted, not expressed, or epigenetically silenced as it reduces the possibility of its binding with the neoepitopes (75), so ideally these also should be verified.

There are also multiple biological implications. The binding is mediated between T cell exposed motifs (TCEM) of neopeptides with groove exposed motif HLA molecules. For better binding, and hence better T cell activation, Bremel et al. used peptides whose amino acids are altered maintaining TCEM core conservation (76). Tumors with a high mutational burden are more likely to have more number of neoantigenic peptides, which may lead to more neoepitope choices and better outcomes (77). The targeted somatic mutations should ideally be present in all cancer cells. These can be founder mutations that initiated cancer and thus possibly may be present in all lineage cells that form the bulk of cancer tissue. There may exist multiple subclonal mutations; consequently it may be better to target the dominant clone which may be present in the bulk of the cancer tissue. Selection of clonal and subclonal mutations can be achieved by establishing cancer cell content in the tissue used for sequencing and comparing mutant allele frequency with wild type/normal allele frequency. Also, the mutation may be heterozygous, present in one allele, the variant allele frequency should be preferably up to 50%, for the mutation to be considered for the vaccine target. In the case of homozygous mutation, the maximum allele frequency will approach 1.0. The designed peptide, synthesized *in vitro*, should be compatible with the physiological environment.

The neoepitopes can be formulated and administered in different vaccine formats (69), like mRNA vaccine (65), DNA vaccine (66), pulsed dendritic cells (67), and recombinant viruses (68). A proper choice is required. *In vitro* transcribed (IVT) mRNA vaccines have multiple advantages over other choices. As it does not integrate into the genome, the risk of insertional mutagenesis and infection is less (65). Apart from pulsed dendritic cells, B cells, macrophages, and splenocytes have also been tried which also act as adjuvants (78). Finally, the entire process should be cost-effective in terms of time, instrumental resources, and human resources.

3 Ongoing clinical trials

We noted that there are many clinical trials currently ongoing and can be accessed *via* the NIH ClinicalTrials website (https://www.clinicaltrials.gov/ct2/home). The trials which involve the

administration of vaccines on human subjects are listed and tabulated in Table 1. We observed that trials mostly involve multiple types of cancers, and are also dedicated to specific sites like pancreatic cancer and breast cancer. We provide a brief review of different cancer types covered by neoepitope/neoantigen clinical trials.

3.1 Pancreatic cancer

The ongoing phase 1 clinical trial NCT03122106 of the neoantigen DNA vaccine against pancreatic cancer addresses its safety and immunogenicity in patients with adjuvant chemotherapy

TABLE 1 List of clinical trials using neoantigen vaccine therapy. Data accessed on December 20, 2022.

NCT Number	Conditions	Intervention/ Drug	Formulation	Administration	Sponsor/Collaborators
NCT03122106	Pancreatic Cancer	Biological: Personalized neoantigen DNA vaccine	Neoantigen DNA vaccine	Intramuscular injections using TDS-IM system	Washington University School of Medicine| National Cancer Institute (NCI)
NCT03956056	Pancreatic Cancer	Biological: Neoantigen Peptide Vaccine| Drug: Poly ICLC	Peptides with poly-ICLC	Subcutaneous injection to limb	Washington University School of Medicine| National Institutes of Health (NIH)|National Cancer Institute (NCI)
NCT03645148	Pancreatic Cancer	Biological: iNeo-Vac-P01	iNeo-Vac-P01 (5 – 20 peptides) vaccine with GM-CSF adjuvant	Subcutaneous injections at the dose of 100 µg per peptide	Zhejiang Provincial People's Hospital|Hangzhou Neoantigen Therapeutics Co., Ltd.
NCT04161755	Pancreatic Cancer	Drug: Atezolizumab, mFOLFIRINOX | Biological: RO7198457	RO7198457	Not available	Memorial Sloan Kettering Cancer Center| Genentech, Inc.
NCT04105582	Breast Cancer|Triple Negative Breast Cancer	Biological: Neo-antigen pulsed dendritic cell	Neo-antigen pulsed autologous dendritic cell	Not mentioned	Universidad Nacional de Colombia|FundaciÃ³n Salud de los Andes
NCT04879888	Breast Cancer Female	Biological: Peptide pulsed Dendritic cell	Peptide-pulsed autologous dendritic cells	Intradermal vaccination	Universidad Nacional de Colombia|FundaciÃ³n Salud de los Andes|Instituto Colombiano para el Desarrollo de la Ciencia y la TecnologÃa (COLCIENCIAS)|Subred Integrada de Servicios de Salud Sur ESE - Colombia (South America)
NCT03199040	Triple Negative Breast Cancer	Drug: Durvalumab| Biological: Neoantigen DNA vaccine|	neoantigen DNA vaccine with durvalumab	Two injections using TDS-IM system	Washington University School of Medicine | MedImmune LLC|National Cancer Institute (NCI) |National Institutes of Health (NIH)
NCT02348320	Triple Negative Breast Cancer	Personalized polyepitope DNA vaccine	Naked plasmid DNA vaccine	Intramuscularly using a TriGrid electroporation device	Washington University School of Medicine Susan G. Komen Breast Cancer Foundation
NCT03715985	Melanoma,Non Small Cell Lung Cancer, Bladder Urothelial Cancer	Drug: EVAX-01-CAF09b	Up to 15 peptides with CAF09b as adjuvant.	Intraperitoneal and intramuscular injections	Herlev Hospital
NCT03673020	Solid Tumor, Adult	Biological: ASV® AGEN2017 + QS-21 StimulonÂ® adjuvant	ASV® AGEN2017 with QS-21 Stimulon® adjuvant	Subcutaneous injection	Agenus Inc.
NCT02992977	Advanced Cancer	Biological: AutoSynVax vaccine	AutoSynVax™ vaccine with QS-21 Stimulon® adjuvant	Subcutaneous injection	Agenus Inc.
NCT04509167	Neoplasms	Biological: Neoantigen Peptides	Multi-peptide vaccine with adjuvant Montanide ISA-51 VG	Intradermal injection	Instituto de Medicina Regenerativa
NCT03480152	Melanoma|Colon Cancer|Gastrointestinal Cancer|Genitourinary	Biological: Personalized Cancer Vaccine	Up to 15 peptides using mRNA based vaccine	Intramuscular injection	National Cancer Institute (NCI)|National Institutes of Health Clinical Center (CC)

(Continued)

TABLE 1 Continued

NCT Number	Conditions	Intervention/ Drug	Formulation	Administration	Sponsor/Collaborators
	Cancer|Hepatocellular Cancer				
NCT03568058	Advanced Cancer	Drug: personalized vaccine|Drug: Pembrolizumab	Personalized vaccine	Intravenous infusion	Ezra Cohen|University of California, San Diego
NCT03633110	Cutaneous Melanoma| Non-small Cell Lung Cancer|Head and Neck cancer|Urothelial Cancer|Renal Cell Cancer	Biological: GEN-009 Adjuvanted Vaccine|Drug: Nivolumab, Pembrolizumab	Peptides with poly-ICLC	Subcutaneous injection	Genocea Biosciences, Inc.
NCT03639714	Non Small Cell Lung Cancer|Colorectal Cancer| Gastroesophageal Adenocarcinoma| Urothelial Carcinoma	Biological: GRT-C901, GRT-R902, nivolumab, ipilimumab	20 peptides each having 25 amino acids arranged in a cassette with helper epitopes PADRE and tetanus toxoid. Virus vaccines as vector	Intramuscular injection	Gritstone bio, Inc.|Bristol-Myers Squibb
NCT03662815	Advanced Malignant Solid Tumor	Biological: iNeo-Vac-P01	iNeo-Vac-P01 (5 – 20 peptides) vaccine with GM-CSF adjuvant	Subcutaneous injections at the dose of 100 µg per peptide	Sir Run Run Shaw Hospital|Hangzhou Neoantigen Therapeutics Co., Ltd.
NCT03300843	Melanoma| Gastrointestinal Cancer| Breast Cancer| Ovarian Cancer| Pancreatic Cancer	Biological: Peptide loded dendritic cell vaccine	Autologous mature dendritic cells loaded with long peptides and minimal epitopes	Intravenous and subcutaneous injections	National Cancer Institute (NCI)|National Institutes of Health Clinical Center (CC)
NCT03548467	Locally Advanced or Metastatic Solid Tumours	Biological: VB10.NEO Drug: Bempegaldesleukin	VB10.NEO in with bempegaldesleukin (NKTR-214)	Intravenous injection	Nykode Therapeutics ASA|Nektar Therapeutics| Vaccibody AS
NCT03359239	Urothelial/Bladder Cancer	Drug: Atezolizumab, Poly ICLC | Biological: PGV001	Up to 10 peptides, one teatanus helper peptide mixed with poly-ICLC.	Intravenous infusion	Matthew Galsky|Genentech, Inc.|Icahn School of Medicine at Mount Sinai
NCT03532217	Prostate Cancer	Drug: Nivolumab, Ipilimumab | Biological:: Neoantigen DNA vaccine	Engineered replication-competent vaccinia and Fowlpox virus	Two intramuscular injections using a TriGrid electroporation device	Washington University School of Medicine| Bristol-Myers Squibb|Prostate Cancer Foundation| The Foundation for Barnes-Jewish Hospital| Bavarian Nordic
NCT01970358	Melanoma	Biological: Poly-ICLC, Peptides	Peptides with poly-ICLC	Subcutaneous injection	Dana-Farber Cancer Institute
NCT05309421	Melanoma Stage IVMelanoma Stage III	Drug: EVX-01Drug: Pembrolizumab 25 MG/ML	EVX-01 vaccine	Intramuscular injection	Evaxion Biotech A/S|Merck Sharp & Dohme LLC
NCT04455503	Melanoma Stage IVMelanoma Stage III	Drug: EVX-02A| Drug: EVX-02B| Drug: EVX-02A OR EVX-02B	EVX-02A or EVX-02B vaccine	Intramuscular injection	Evaxion Biotech A/S| Novotech (Australia) Pty Limited
NCT03422094	Glioblastoma	Biological: NeoVax, Nivolumab, Ipilimumab	Up to 20 peptides with poly-ICLC	Subcutaneous injection	Washington University School of Medicine| Bristol-Myers Squibb
NCT02510950	Glioblastoma	Biological: Personalized peptide vaccine| Drug: Poly-ICLC, Temozolomide	Peptide vaccine with poly-ICLC	Not available	Washington University School of Medicine

and surgical resection. The hypothesis is to determine if this neoantigen DNA vaccine is capable of developing CD4+ and CD8+ T cell responses. These vaccines are comprised of prioritized neoantigens together with personalized mesothelin epitopes (79). The clinical trial NCT03956056 is also targeted toward pancreatic cancer patients to evaluate immune cell responses to neoantigen vaccines co-administered with immunostimulant poly-ICLC. Additionally, the clinical trial NCT03645148 is dedicated to pancreatic cancer patients of Chinese origin with a low mutational burden. The vaccine iNeo-Vac-P01 was developed utilizing their in-house pipeline iNeo-Suite. The vaccine contained up to twenty peptides. It was administered to patients having low mutational burden and appeared safe with enhanced effector T cell counts (80). The response of the vaccines also depends on the adjuvant drugs. The ongoing trial NCT04161755 uses the drug atezolizumab along with mFOLFIRINOX in the context of pancreatic cancer patients undergoing neoantigen vaccine therapy.

3.2 Breast cancer

Neoantigen vaccine therapy is being tried in breast cancer patients; specifically, triple negative breast cancers (TNBC) where genetic instability is associated with a high mutational burden. In the clinical trial NCT04105582, up to 25 neopeptides are going to be administered by the autologous dendritic cells over a 16 week span. Another clinical trial NCT04879888 also uses peptide pulsed autologous dendritic cells at six doses on nine TNBC patients. The clinical trial NCT03199040 is designed to evaluate the response of neoantigen vaccines in the presence and absence of the drug durvalumab in triple negative breast cancer patients. The clinical trial, identified as NCT02348320, is an ongoing phase 1 trial of a polyepitope DNA vaccine against triple negative breast cancer. The immunogenicity and safety of the vaccine are being evaluated in the trial.

3.3 Pan-cancer

In a pan-cancer study, researchers are looking for the effects of the EVAX-01-CAF09b vaccine in the metastatic condition of malignant melanoma, NSCLC, and bladder urothelial cancer. The vaccine will be derived using the PIONEER platform and will contain 5-15 peptides (NCT03715985). Agenus Inc. conducted multiple trials on the safety and tolerability of their ASV® AGEN2017 with QS-21 Stimulon® Adjuvant in solid tumors but their enrolled patients were limited to three only (NCT03673020, NCT02992977). The clinical trial NCT04509167 uses Montanide ISA-51 VG as an adjuvant along with 0.5mg of each predicted peptide. The clinical trial NCT03480152 on 4 patients having metastatic melanoma and colon cancer observed enhanced T cell response with no objective response in all patients (81). The anti-PDL1 antibody drug pembrolizumab is being assessed in the neoantigen vaccine trial NCT03568058 in NSCLC, head and neck squamous cell carcinoma (HNSCC), classical Hodgkin lymphoma (cHL) and other solid tumors. This study will observe the immune response when pembrolizumab is administered six weeks before vaccination, at the time of vaccination, and after vaccination. Genocea Biosciences is also conducting a clinical trial (NCT03633110) on 24 participants having different cancers. This trial also uses the drug pembrolizumab along with nivolumab to evaluate the efficacy of vaccine therapy.

A clinical trial with NCT number NCT03639714 assigned to the company Gritstone bio is evaluating the early clinical activity, dose, immunogenicity, and safety of a personalized neoantigen cancer vaccine GRT-C901 and GRT-R902 integrated with the drugs nivolumab and ipilimumab for NSCLC, microsatellite stable colorectal cancer, gastroesophageal adenocarcinoma, and metastatic urothelial cancer patients. The primary objective is to look for any adverse events, serious adverse events (SAEs), and dose-limiting toxicities (DLTs). As well, their objective is to compute Objective Response Rate (ORR) in Phase 2 and identify the recommended Phase 2 dose. Their interim results demonstrate an enhanced overall survival period (82). Gritstone bio is also conducting another clinical trial (NCT03794128) to explore the personalization aspect of neoantigen vaccines. Their objective is to identify personalized and shared vaccines in the context of different cancers involving 93 patients. NCT03662815 refers to a trial on Chinese patients with solid tumors. The outcome shows that of 30 patients, 20 had no adverse effects and 80% of peptides enhanced immune response (83). NCT3300843 was also initiated for pan-cancer study using peptide loaded dendritic cell vaccines but was terminated due to low accrual. Individualized VB10.NEO vaccine and bempegaldesleukin (NKTR-214) are being used in the clinical trial NCT03548467 for patients at the metastatic stage. It plans for 14 vaccinations for each of the 65 patients and bempegaldesleukin (NKTR-214) will be given after at least four doses of vaccinations. The primary goal is to measure the safety and adverse effects of the vaccine. Secondary outcome measurement includes measuring immunogenicity by T cell activity to each neoepitope, ORR, duration of response, progression free survival, and survival at the end of treatment.

3.4 Other cancers

Similar to the trial NCT04161755, clinical trial NCT03359239 aims to determine the effects of atezolizumab in combination with a personalized cancer vaccine, PGV001 (84) for locally advanced or metastatic urothelial cancer patients. A clinical trial is also evaluating the immune response of a shared antigen vaccine PROSTVAC and tumor specific antigens generated DNA vaccine with nivolumab (anti-PD-1), and ipilimumab (anti-CTLA-4) for checkpoint blockade (NCT03532217). The ongoing open label phase 1a/1b clinical trial (NCT03970382) is focusing to evaluate the efficacy, feasibility, and safety of NeoTCR-P1 T cells in subjects with metastatic hormone-sensitive prostate cancer. NCT03040791 is another trial involving pancreatic cancer patients which also utilizes nivolumab to explore DNA repair defects (DRD), mainly in the Homologous Recombination (HR) pathway. The effect of nivolumab is also being investigated with or without ipilimumab in female patients suffering epithelial ovarian, primary peritoneal, or fallopian tube cancer in clinical trial NCT02498600. The outcomes will be measured as per response evaluation criteria in solid tumors, survival periods, and incidence of adverse events in advanced stages of the disease.

Trials are being conducted on skin cancer melanoma which is also characterized by patient specific mutation. Clinical trial with NCT number NCT01970358 enrolled 20 melanoma patients to whom peptide vaccine NeoVax targeting up to twenty peptides was administered starting from day 1 to 162 along with poly-ICLC. It resulted in induced T cell response sustaining over years (85, 86). A clinical trial NCT05309421 is designed to determine the efficacy of EVX-01 vaccine on advanced melanoma patients. The trial will evaluate whether checkpoint inhibitor therapy using pembrolizumab works better when utilized in conjunction with EVX-01 vaccine (87). Clinical trial NCT04455503 also treats advanced melanoma patients but with two types of EVX-02 vaccines with nivolumab in two cohorts. Depending on the study results the third cohort will receive either one of the two types of EVX-02 vaccine. This study will measure safety and tolerability by measuring vital signs like heart rate, blood pressure, and physical examination. Neoepitope-specific T cells will be monitored by ELISPOT. Other pharmacodynamic responses of EVX-02 will be assessed by MHC I multimer analyses detecting neoepitope-recognizing CD8+ T cells and by flow cytometry to detect vaccine induced intracellular cytokine response. Relapse free survival period will be measured as secondary outcomes. A trial (NCT03422094) based on neoantigen vaccine therapy on glioblastoma patients was initiated but later focus was changed to cell therapy. Clinical trial NCT02510950 targeting glioblastoma patients did not proceed due to financial limitations.

We observed variations in the vaccine formulation and administration strategies followed by different trials. The number of chosen peptides varied from 5 - 20 depending on the mutational burden. These peptides are often applied with adjuvants. Poly-ICLC is used as an adjuvant in multiple trials. Poly-ICLC stimulates the release of cytokines and the production of interferon-gamma. The administration process and doses also vary. Intravenous, intramuscular, and subcutaneous injections at limb organs are used for administration. The dose typically remains around 100μg per peptide. The treatment typically continues for several months, depending on its effects. Table 1 lists different formulation and administration strategies observed in the trials.

4 Outcomes

Apart from the ongoing trials, several clinical trials already published their outcomes. In this section, we discuss those outcomes. Mismatch repair (MMR) deficient cells often lead to cancers due to the accumulation of numerous unrepaired mutations like base mismatches, insertions and deletions. This accumulation of mutations may affect cell cycle control genes and promote cancer growth. In this regard, Ott et al. have conducted several studies. In a study conducted on six melanoma patients, the clinicians used up to 20 neoantigens in each patient. They observed no recurrence in 25 months for four patients and for two patients, vaccination followed by anti-PD-1 therapy resulted in complete regression (88). They reported similar observations in glioblastoma patients also (89). Ott et al. also reported a neoantigen-based vaccine NEO-PV-01 along with PD-1 blockade in melanoma, NSCLC or bladder cancer patients. The vaccine showed CD4+ and CD8+ T cell response post vaccination with cytotoxic phenotype which could move to the tumor and mediate the killing of tumor cells. The treatment was found to be safe and no adverse events were reported (NCT02897765) (90). A single mRNA vaccine was presented by Cafri et al. to treat gastrointestinal cancer patients. It was developed by using lymphocytes that infiltrated tumors to detect immunogenic mutations that were expressed in the tumors of the patients. The vaccine (NCT03480152) was found to be safe and generated T cell responses targeting KRAS-G12D mutation. It also exhibited potential to develop vaccines integrated with checkpoint inhibitors or adaptive T cell therapy for common epithelial cancers (81).

Dendritic cells (DC) are often used for administering neoantigens. Carreno et al. vaccinated three melanoma patients with dendritic cell based vaccines and observed enhanced response of T cells (91). Ding et al. also used peptide-pulsed autologous DC vaccine for conducting a clinical trial involving twelve advanced lung cancer patients. They administered 12 – 30 peptides in doses ranging 3 – 14 doses per person. However, the median progression-free survival was limited to 5.5 months (92). In another study, rather than using a set of peptides, researchers used a single peptide targeting only IDH1 mutation in glioma patients (93). Instead of personalized peptides, Mueller et al. used 'shared neoantigen', specific to H3.3K27M mutation among nineteen glioma patients and it was well tolerated with median overall survival of 16.1 months (94). Hilf et al. vaccinated newly diagnosed glioma patients with unmuted antigens first and then with targeted neoepitopes. Unmutated antigens evoked sustained responses of central memory CD8+ T cells and neoepitopes helped to develop CD4+ T cell responses. This combination therapy showed strong immunogenicity (95).

Neoantigen vaccine was tested on ten hepatocellular carcinoma (HCC) patients, and showed no adverse effects with a median recurrence free survival period 7.4 months (96). Kloor et al. performed phase 1 and 2 clinical trials (Micoryx) to evaluate frameshift peptide (FSP) based neoantigen vaccines. This trial is highly relevant in that it demonstrates the possibility of an effective cancer-preventive vaccine which may work among high-risk populations. They selected patients who have completed their chemotherapy and colorectal cancer (stage III or IV) with MMR deficiency. The trial consisted of four subcutaneous vaccination cycles admixed with Montanide ISA-51 VG. Phase I focused on the safety and toxicity of the vaccines, whereas phase II evaluated the cellular and humoral immune response. The results showed humoral and immune responses in all of the patients. Grade 2 injection site reactions were observed in three patients, but no adverse events occurred. Hence, FSP neoantigen based vaccination was observed to be well tolerated with good immune response and may emerge as a promising cancer preventive as well as a treatment for MMR-deficient cancers (97). Kristensen et al. found that only 1.8% of all neopeptides are present within tumor-infiltrating lymphocytes (TILs) infusion products in melanoma. They validated that the presence of neoepitope-specific CD8+ T cells helps in better survival (98). Although an *ex vivo* study but worth mentioning, in the case of breast cancer cells, the co-culture of neoantigen-pulsed DCs and lymphocytes successfully induced cytotoxic T lymphocytes (CTLs) response against cancer cells (99). Holm et al. treated metastatic

urothelial cancer patients with peptides derived from exome sequence data and observed an increase in T cell response after 3 weeks of treatment which also facilitated the activity of immune checkpoint inhibitors (100). Miller et al. correlated somatic mutation and neoantigen burden with survival time from data collected in a clinical trial on 664 myeloma patients. Two-years progression free survival rate reduces from 0.726 to 0.493 and from 0.729 to 0.555 for high somatic mutation and neoantigen burden respectively (86). Palmer et al. reported the interim result of a clinical trial that uses a combinatory approach in colorectal cancer. They have used heterologous chimpanzee adenovirus (ChAd68) and self-amplifying mRNA(samRNA)-based neoantigen vaccine in combination with immune checkpoint inhibitor drugs nivolumab and ipilimumab; and they observed a median OS 8.7 months (82). A comparative study between patients treated with neoantigen specific T cells and anti PD-1 molecules and patients treated with only anti PD-1 molecules revealed patients treated with neoantigen specific T cells have better progression free survival time (13.8 and 4.2 months). However, the overall survival period was the same (101). In a phase 1b study on three pancreatic ductal adenocarcinoma (PDAC) patients, a combination of chemotherapy, dendritic cells with neopeptides and anti PD-1 drug nivolumab was used to enhance the efficacy of the vaccine (102). Clinical trial NCT03645148 reported the outcome observed on seven advanced pancreatic cancer patients. Using the vaccine iNeo-Vac-P01 the mean overall survival period reached 24.1 months whereas progression free survival period was 3.1 months (80). In a case study on a 62 year old pancreatic cancer patient, Sonntag et al. used four peptides derived from two mutations. The vaccination started along with chemotherapy, then chemotherapy stopped, and monthly doses of vaccines continued. The patient had four years of progression free survival, at the time the report was published (103). The clinical trial NCT04688385 published a report on the effect of multi-peptide vaccine on leukemia patients. It developed a workflow for off-the-shelf peptide warehouses which can be applicable for broad personalized therapeutics (104). Overall, we observe that the clinical trials employing neoantigens are showing promising results in terms of immunogenicity and safety. However, on-time delivery of these personalized vaccines to patients remains a challenge.

5 Outlook

Based on our literature review, promising outcomes are observed in the published neoantigen vaccine trials. Neoantigen vaccines are enhancing T cell responses while mitigating other side effects. However, the application is still limited to cases of high mutational load. This limitation can be optimized through rational design. We need a better understanding on the molecular mechanism of the neopeptides. Additionally, neopeptides targeting MHC class II type should be explored to enhance CD4+ T cell responses. Apart from IEDB, a few databases have also been developed that catalog neopeptides that, thus far, have been detected and utilized in preclinical and/or clinical environment. The NeoPeptide database contains characteristics of neoantigens reported in the literature and immunological resources (105). The Cancer Immunome Atlas (TCIA) provides results obtained primarily from TCGA (106). The Cancer Antigenic Peptide Database (CAPED) contains information on peptides, mutations, and associated HLA molecules (107). Tumor-Specific NeoAntigen database (TSNAdb) (108), Cancer Epitope Database and Analysis Resource (CEDAR) (109), and NEPdb (3) are also available. These databases help to find neopeptides whenever a mutation is detected.

We have observed neoantigen vaccines are accompanied by different adjuvant drugs. Among the adjuvant drugs, immune checkpoint blockade drugs are widely used. Drugs like nivolumab, ipilimumab and pembrolizumab are used in multiple types of cancers. Cancer cells express PD-L1 on their surface which binds to PD1 which is present on the surface of the T cells, this results in the inactivation of T cell and the lack of immune response of T cell against cancer cells. Nivolumab blocks PD-L1 binding with PD-1 which results in T cells retaining their immune activity and initiates an immune response against the cancer cells. These active T cells enhance the effectiveness of the treatment. Pembrolizumab also targets PD-1. Ipilimumab targets cytotoxic T-lymphocyte-associated protein 4 (CTLA-4) (110). The combination of nivolumab and ipilimumab is also used (111). Hence, the proper selection of adjuvant drugs at appropriate doses and times plays a crucial role in the success of neoantigen immunotherapy.

We observe that the neoantigen vaccines appear safe with limited side effects. However, the survival period is still not promising. This may be a result of the majority of the trials currently ongoing are conducted on patients who have already reached the metastatic stage or the late stage of the disease. An early intervention with neoantigen vaccines may provide a longer survival period for the patients. It needs to be validated by clinical trials in the future.

The vaccine administration process including the peptide carriers also needs to be more streamlined. Currently, mRNA vaccine, DNA vaccine and pulsed dendritic cells are mostly used as carriers. Compared to TAAs, neoantigens show stronger immunogenicity and binding towards HLAs are not affected by central immunological tolerance (5). Neoantigens are resultant of mutations in tumor cells during tumorigenesis. The mutation landscape also evolves continuously during tumorigenesis and disease progression (5). It makes neoantigens specific to the tumor stage and more trials are needed for exploring patients of different stages. As mentioned in the introductions section and based on the NIH clinical trial website, we noted several clinical trials that are about to initiated. The results from those studies will provide a better landscape on the therapeutic efficacy of neoantigen immunotherapy.

6 Conclusions

Based on the existing circumstances, we conclude neoantigen vaccines are capable of exhibiting tumor-specific immunogenicity in different types of solid tumors. They leverage CD4+ and CD8+ effector T cells across cancer types. However, there is an enormous requirement for improvements in several aspects like the optimized design of neoantigens to ensure the efficacy of the vaccine. Conducting *ex vivo* studies on the effect of peptides on tumor cells

collected from patients will be helpful for a well-defined vaccine design. Further studies are required to evaluate the possibility of the existence of patient subtypes based on the responses to neopeptides. If corroborated, it will make the vaccine production process more economical both in terms of money and time. Researchers and clinicians should explore the possibility of applying vaccines to patients at the earlier stages of the disease which may provide a longer survival period. We are looking forward to improved treatment options for cancer patients.

Author contributions

NB and SC wrote the manuscript. All co-authors have read, revised as required, and agreed with the content of the manuscript.

Conflict of interest

Author's NB, SC and VP were employed by Rhenix Lifesciences.

The remaining authors declare that the research was conducted in the absence of any commercial or financial relationships that could be construed as a potential conflict of interest.

Publisher's note

References

1. Cooper G. *The cell: A molecular approach. 2nd ed.* Sunderland (MA): Sinauer Associates (2000).

2. Ponder BAJ. Molecular genetics of cancer. *Br Med J* (1992) 304(6836):1234–6. doi: 10.1136/bmj.304.6836.1234

3. Xia J, Bai P, Fan W, Li Q, Li Y, Wang D, et al. NEPdb: A database of T-cell experimentally-validated neoantigens and pan-cancer predicted neoepitopes for cancer immunotherapy. *Front Immunol* (2021) 12:992. doi: 10.3389/fimmu.2021.644637

4. Zhang Z, Lu M, Qin Y, Gao W, Tao L, Su W, et al. Neoantigen: A new breakthrough in tumor immunotherapy. *Front Immunol* (2021) 12:672356. doi: 10.3389/fimmu.2021.672356

5. Peng M, Mo Y, Wang Y, Wu P, Zhang Y, Xiong F, et al. Neoantigen vaccine: an emerging tumor immunotherapy. *Mol Cancer.* (2019) 18(1):1–14. doi: 10.1186/s12943-019-1055-6

6. Li L, Goedegebuure SP, Gillanders W. Cancer vaccines: shared tumor antigens return to the spotlight. *Signal Transduct Target Ther* (2020) 5(1):251. doi: 10.1038/s41392-020-00364-8

7. Vigneron N. Human tumor antigens and cancer immunotherapy. *BioMed Res Int* (2015) 2015:1–17. doi: 10.1155/2015/948501

8. Turajlic S, Litchfield K, Xu H, Rosenthal R, McGranahan N, Reading JL, et al. Insertion-and-deletion-derived tumour-specific neoantigens and the immunogenic phenotype: a pan-cancer analysis. *Lancet Oncol* (2017) 18(8):1009–21. doi: 10.1016/S1470-2045(17)30516-8

9. Yang W, Lee KW, Srivastava RM, Kuo F, Krishna C, Chowell D, et al. Immunogenic neoantigens derived from gene fusions stimulate T cell responses. *Nat Med* (2019) 25 (5):767–75. doi: 10.1038/s41591-019-0434-2

10. Duvvuri B, Duvvuri VR, Wang C, Chen L, Wagar LE, Jamnik V, et al. The human immune system recognizes neopeptides derived from mitochondrial DNA deletions. *J Immunol* (2014) 192(10):4581–91. doi: 10.4049/jimmunol.1300774

11. Rosenberg SA, Yang JC, Restifo NP. Cancer immunotherapy: Moving beyond current vaccines. *Nat Med* (2004) 10(9):909–15. doi: 10.1038/nm1100

12. Klebanoff CA, Wolchok JD. Shared cancer neoantigens: Making private matters public. *J Exp Med* (2018) 215(1):7. doi: 10.1084/jem.20172188

13. Zhao W, Wu J, Chen S, Zhou Z. Shared neoantigens: ideal targets for off-the-shelf cancer immunotherapy. *Pharmacogenomics* (2020) 21(9):637–45. doi: 10.2217/pgs-2019-0184

14. Jiang T, Shi T, Zhang H, Hu J, Song Y, Wei J, et al. Tumor neoantigens: from basic research to clinical applications. *J Hematol Oncol* (2019) 12(1):1–13. doi: 10.1186/s13045-019-0787-5

15. Blass E, Ott PA. Advances in the development of personalized neoantigen-based therapeutic cancer vaccines. *Nat Rev Clin Oncol* (2021) 18(4):215–29. doi: 10.1038/s41571-020-00460-2

16. Vita R, Mahajan S, Overton JA, Dhanda SK, Martini S, Cantrell JR, et al. The immune epitope database (IEDB): 2018 update. *Nucleic Acids Res* (2019) 47(Database issue):D339–43. doi: 10.1093/nar/gky1006

17. Wells DK, van Buuren MM, Dang KK, Hubbard-Lucey VM, Sheehan KCF, Campbell KM, et al. Key parameters of tumor epitope immunogenicity revealed through a consortium approach improve neoantigen prediction. *Cell* (2020) 183 (3):818–834.e13. doi: 10.1016/j.cell.2020.09.015

18. Riley TP, Keller GLJ, Smith AR, Davancaze LM, Arbuiso AG, Devlin JR, et al. Structure based prediction of neoantigen immunogenicity. *Front Immunol* (2019) 10 (AUG):2047. doi: 10.3389/fimmu.2019.02047

19. Kim K, Kim HS, Kim JY, Jung H, Sun JM, Ahn JS, et al. Predicting clinical benefit of immunotherapy by antigenic or functional mutations affecting tumour immunogenicity. *Nat Commun* (2020) 11(1):1–11. doi: 10.1038/s41467-020-14562-z

20. Dhanda SK, Mahajan S, Manoharan M. Neoepitopes prediction strategies: an integration of cancer genomics and immunoinformatics approaches. *Brief Funct Genomics* (2022) 18:elac041. doi: 10.1093/bfgp/elac041

21. Hundal J, Kiwala S, McMichael J, Miller CA, Xia H, Wollam AT, et al. pVACtools: A computational toolkit to identify and visualize cancer neoantigens. *Cancer Immunol Res* (2020) 8(3):409–20. doi: 10.1158/2326-6066.CIR-19-0401

22. Rubinsteyn A, Hodes I, Kodysh J, Hammerbacher J. Vaxrank: A computational tool for designing personalized cancer vaccines. *bioRxiv* (2018), 142919. doi: 10.1101/142919

23. Bjerregaard AM, Nielsen M, Hadrup SR, Szallasi Z, Eklund AC. MuPeXI: prediction of neo-epitopes from tumor sequencing data. *Cancer Immunol Immunother* (2017) 66(9):1123–30. doi: 10.1007/s00262-017-2001-3

24. Zhou Z, Lyu X, Wu J, Yang X, Wu S, Zhou J, et al. TSNAD: an integrated software for cancer somatic mutation and tumour-specific neoantigen detection. *R Soc Open Sci* (2017) 4(4):170050. doi: 10.1098/rsos.170050

25. Zhou C, Wei Z, Zhang Z, Zhang B, Zhu C, Chen K, et al. pTuneos: Prioritizing tumor neoantigens from next-generation sequencing data. *Genome Med* (2019) 11(1):67. doi: 10.1186/s13073-019-0679-x

26. Chen S, Zhou Y, Chen Y, Gu J. fastp: An ultra-fast all-in-one FASTQ preprocessor. *Bioinformatics* (2018) 34(17):i884–90. doi: 10.1093/bioinformatics/bty560

27. Bolger AM, Lohse M, Usadel B. Trimmomatic: a flexible trimmer for illumina sequence data. *Bioinformatics* (2014) 30(15):2114–20. doi: 10.1093/bioinformatics/btu170

28. Martin M. Cutadapt removes adapter sequences from high-throughput sequencing reads. *EMBnet.journal* (2011) 17(1):10–2. doi: 10.14806/ej.17.1.200

29. Schmieder R, Edwards R. Quality control and preprocessing of metagenomic datasets. *Bioinformatics* (2011) 27(6):863–4. doi: 10.1093/bioinformatics/btr026

30. Andrews S. FastQC a quality control tool for high throughput sequence data. Available at: https://www.bioinformatics.babraham.ac.uk/projects/fastqc/.

31. Homo_sapiens - ensembl genome browser 107. Available at: https://www.ensembl.org/Homo_sapiens/Info/Index?redirect=no.

32. Li H, Durbin R. Fast and accurate short read alignment with burrows-wheeler transform. *Bioinforma* . (2009) 25(14):1754–60. doi: 10.1093/bioinformatics/btp324

33. NovoAlign. Available at: https://www.novocraft.com/products/novoalign/.

34. McKenna A, Hanna M, Banks E, Sivachenko A, Cibulskis K, Kernytsky A, et al. The genome analysis toolkit: A MapReduce framework for analyzing next-generation DNA sequencing data. *Genome Res* (2010) 20(9):1303. doi: 10.1101/gr.107524.110

35. Dobin A, Davis CA, Schlesinger F, Drenkow J, Zaleski C, Jha S, et al. STAR: ultrafast universal RNA-seq aligner. *Bioinformatics* (2013) 29(1):21. doi: 10.1093/bioinformatics/bts635

36. Wu TD, Watanabe CK. GMAP: a genomic mapping and alignment program for mRNA and EST sequences. *Bioinformatics* (2005) 21(9):1859–75. doi: 10.1093/bioinformatics/bti310

37. Kim D, Pertea G, Trapnell C, Pimentel H, Kelley R, Salzberg SL. TopHat2: Accurate alignment of transcriptomes in the presence of insertions, deletions and gene fusions. *Genome Biol* (2013) 14(4):R36. doi: 10.1186/gb-2013-14-4-r36

38. Langmead B, Salzberg SL. Fast gapped-read alignment with bowtie 2. *Nat Methods* (2012) 9(4):359. doi: 10.1038/nmeth.1923

39. Anders S, Pyl PT, Huber W. HTSeq–a Python framework to work with high-throughput sequencing data. *Bioinformatics* (2015) 31(2):169. doi: 10.1093/bioinformatics/btu638

40. Picard. Available at: https://github.com/broadinstitute/picard/releases/tag/2.27.4.

41. Li H, Handsaker B, Wysoker A, Fennell T, Ruan J, Homer N, et al. The sequence Alignment/Map format and SAMtools. *Bioinformatics* (2009) 25(16):2078–9. doi: 10.1093/bioinformatics/btp352

42. Koboldt DC, Zhang Q, Larson DE, Shen D, McLellan MD, Lin L, et al. VarScan 2: somatic mutation and copy number alteration discovery in cancer by exome sequencing. *Genome Res* (2012) 22(3):568–76. doi: 10.1101/gr.129684.111

43. Mutect2 – GATK. Available at: https://gatk.broadinstitute.org/hc/en-us/articles/360037593851-Mutect2.

44. HaplotypeCaller – GATK. Available at: https://gatk.broadinstitute.org/hc/en-us/articles/360037225632-HaplotypeCaller.

45. Hundal J, Kiwala S, Feng Y-Y, Liu CJ, Govindan R, Chapman WC, et al. Accounting for proximal variants improves neoantigen prediction. *Nat Genet* (2019) 51 (1):175–9. doi: 10.1038/s41588-018-0283-9

46. Resource bundle – GATK. Available at: https://gatk.broadinstitute.org/hc/en-us/articles/360035890811-Resource-bundle.

47. dbSNP. Available at: https://www.ncbi.nlm.nih.gov/snp/.

48. McLaren W, Gil L, Hunt SE, Riat HS, Ritchie GRS, Thormann A, et al. The ensembl variant effect predictor. *Genome Biol* (2016) 17(1):122. doi: 10.1186/s13059-016-0974-4

49. Wang K, Li M, Hakonarson H. ANNOVAR: functional annotation of genetic variants from high-throughput sequencing data. *Nucleic Acids Res* (2010) 38(16):e164. doi: 10.1093/nar/gkq603

50. Cingolani P, Platts A, Wang LL, Coon M, Nguyen T, Wang L, et al. A program for annotating and predicting the effects of single nucleotide polymorphisms, SnpEff: SNPs in the genome of drosophila melanogaster strain w1118; iso-2; iso-3. *Fly (Austin).* (2012) 6 (2):80–92. doi: 10.4161/fly.19695

51. 1000 genomes | a deep catalog of human genetic variation. Available at: https://www.internationalgenome.org/home.

52. O'Donnell TJ, Rubinsteyn A, Laserson U. MHCflurry 2.0: Improved pan-allele prediction of MHC class I-presented peptides by incorporating antigen processing. *Cell Syst* (2020) 11(1):42–8. doi: 10.1016/j.cels.2020.06.010

53. Sarkizova S, Klaeger S, Le PM, Li LW, Oliveira G, Keshishian H, et al. A large peptidome dataset improves HLA class I epitope prediction across most of the human population. *Nat Biotechnol* (2020) 38(2):199–209. doi: 10.1038/s41587-019-0322-9

54. Gfeller D, Guillaume P, Michaux J, Pak H-S, Daniel RT, Racle J, et al. The length distribution and multiple specificity of naturally presented HLA-I ligands. *J Immunol* (2018) 201(12):3705–16. doi: 10.4049/jimmunol.1800914

55. Lundegaard C, Lamberth K, Harndahl M, Buus S, Lund O, Nielsen M. NetMHC-3.0: accurate web accessible predictions of human, mouse and monkey MHC class I affinities for peptides of length 8–11. *Nucleic Acids Res* (2008) 36(Web Server issue):W512. doi: 10.1093/nar/gkn202

56. Reynisson B, Alvarez B, Paul S, Peters B, Nielsen M. NetMHCpan-4.1 and NetMHCIIpan-4.0: improved predictions of MHC antigen presentation by concurrent motif deconvolution and integration of MS MHC eluted ligand data. *Nucleic Acids Res* (2020) 48(W1):W449–54. doi: 10.1093/nar/gkaa379

57. Karosiene E, Lundegaard C, Lund O, Nielsen M. NetMHCcons: a consensus method for the major histocompatibility complex class I predictions. *Immunogenetics* (2012) 64(3):177–86. doi: 10.1007/s00251-011-0579-8

58. Zhang H, Lund O, Nielsen M. The PickPocket method for predicting binding specificities for receptors based on receptor pocket similarities: application to MHC-peptide binding. *Bioinformatics* (2009) 25(10):1299. doi: 10.1093/bioinformatics/btp137

59. Nielsen M, Lundegaard C, Lund O. Prediction of MHC class II binding affinity using SMM-align, a novel stabilization matrix alignment method. *BMC Bioinf* (2007) 8:238. doi: 10.1186/1471-2105-8-238

60. Nielsen M, Andreatta M. NNAlign: a platform to construct and evaluate artificial neural network models of receptor-ligand interactions. *Nucleic Acids Res* (2017) 45(W1): W344–9. doi: 10.1093/nar/gkx276

61. Mei S, Li F, Leier A, Marquez-Lago TT, Giam K, Croft NP, et al. A comprehensive review and performance evaluation of bioinformatics tools for HLA class I peptide-binding prediction. *Brief Bioinform* (2020) 21(4):1119–35. doi: 10.1093/bib/bbz051

62. Wang P, Sidney J, Dow C, Mothé B, Sette A, Peters B. A systematic assessment of MHC class II peptide binding predictions and evaluation of a consensus approach. *PloS Comput Biol* (2008) 4(4):1000048. doi: 10.1371/journal.pcbi.1000048

63. Zhao W, Sher X. Systematically benchmarking peptide-MHC binding predictors: From synthetic to naturally processed epitopes. *PloS Comput Biol* (2018) 14(11): e1006457. doi: 10.1371/journal.pcbi.1006457

64. Oosting LT, Franke K, Martin MV, Kloosterman WP, Jamieson JA, Glenn LA, et al. Development of a personalized tumor neoantigen based vaccine formulation (FRAME-001) for use in a phase II trial for the treatment of advanced non-small cell lung cancer. *Pharmaceutics* (2022) 14(7):1515. doi: 10.3390/pharmaceutics14071515

65. Esprit A, de Mey W, Shahi RB, Thielemans K, Franceschini L, Breckpot K. Neo-antigen mRNA vaccines. *Vaccines* (2020) 8(4):776. doi: 10.3390/vaccines8040776

66. Yang X, Fan J, Wu Y, Ma Z, Huang J, Zhang Y, et al. Synthetic multiepitope neoantigen DNA vaccine for personalized cancer immunotherapy. *Nanomedicine* (2021) 37:102443. doi: 10.1016/j.nano.2021.102443

67. Celluzzi CM, Mayordomo JI, Storkus WJ, Lotze MT, Falo LD. Peptide-pulsed dendritic cells induce antigen-specific CTL-mediated protective tumor immunity. *J Exp Med* (1996) 183(1):283–7. doi: 10.1084/jem.183.1.283

68. Türeci Ö, Löwer M, Schrörs B, Lang M, Tadmor A, Sahin U. Challenges towards the realization of individualized cancer vaccines. *Nat BioMed Eng* (2018) 2(8):566–9. doi: 10.1038/s41551-018-0266-2

69. Guo Y, Lei K, Tang L. Neoantigen vaccine delivery for personalized anticancer immunotherapy. *Front Immunol* (2018) 9(JUL):1499. doi: 10.3389/fimmu.2018.01499

70. Cai L, Yuan W, Zhang Z, He L, Chou KC. In-depth comparison of somatic point mutation callers based on different tumor next-generation sequencing depth data. *Sci Rep* (2016) 6(April):1–9. doi: 10.1038/srep36540

71. Wang Q, Kotoula V, Hsu PC, Papadopoulou K, Ho JWK, Fountzilas G, et al. Comparison of somatic variant detection algorithms using ion torrent targeted deep sequencing data. *BMC Med Genomics* (2019) 12(9):181. doi: 10.1186/s12920-019-0636-y

72. Chun S, Fay JC. Identification of deleterious mutations within three human genomes. *Genome Res* (2009) 19(9):1553–61. doi: 10.1101/gr.092619.109

73. Liu P, Yao M, Gong Y, Song Y, Chen Y, Ye Y, et al. Benchmarking the human leukocyte antigen typing performance of three assays and seven next-generation sequencing-based algorithms. *Front Immunol* (2021) 12:840. doi: 10.3389/fimmu.2021.652258

74. Kiyotani K, Mai TH, Nakamura Y. Comparison of exome-based HLA class I genotyping tools: identification of platform-specific genotyping errors. *J Hum Genet* (2017) 62(3):397–405. doi: 10.1038/jhg.2016.141

75. Burr ML, Sparbier CE, Chan KL, Chan YC, Kersbergen A, Lam EYN, et al. An evolutionarily conserved function of polycomb silences the MHC class I antigen presentation pathway and enables immune evasion in cancer. *Cancer Cell* (2019) 36 (4):385–401. doi: 10.1016/j.ccell.2019.08.008

76. Bremel RD, Homan EJ. Frequency patterns of T-cell exposed amino acid motifs in immunoglobulin heavy chain peptides presented by MHCs. *Front Immunol* (2014) 5 (OCT):541. doi: 10.3389/fimmu.2014.00541

77. Maleki Vareki S. High and low mutational burden tumors versus immunologically hot and cold tumors and response to immune checkpoint inhibitors. *J Immunother Cancer.* (2018) 6(1):157. doi: 10.1186/s40425-018-0479-7

78. Brennick CA, George MM, Corwin WL, Srivastava PK, Ebrahimi-Nik H. Neoepitopes as cancer immunotherapy targets: Key challenges and opportunities. *Immunotherapy* (2017) 9(4):361–71. doi: 10.2217/imt-2016-0146

79. De Mattos-Arruda L, Vazquez M, Finotello F, Lepore R, Porta E, Hundal J, et al. Neoantigen prediction and computational perspectives towards clinical benefit: recommendations from the ESMO precision medicine working group. *Ann Oncol* (2020) 31(8):978–90. doi: 10.1016/j.annonc.2020.05.008

80. Chen Z, Zhang S, Han N, Jiang J, Xu Y, Ma D, et al. A neoantigen-based peptide vaccine for patients with advanced pancreatic cancer refractory to standard treatment. *Front Immunol* (2021) 12:691605. doi: 10.3389/fimmu.2021.691605

81. Cafri G, Gartner JJ, Zaks T, Hopson K, Levin N, Paria BC, et al. mRNA vaccine–induced neoantigen-specific T cell immunity in patients with gastrointestinal cancer. *J Clin Invest.* (2020) 130(11):5976–88. doi: 10.1172/JCI134915

82. Palmer CD, Rappaport AR, Davis MJ, Hart MG, Scallan CD, Hong SJ, et al. Individualized, heterologous chimpanzee adenovirus and self-amplifying mRNA neoantigen vaccine for advanced metastatic solid tumors: phase 1 trial interim results. *Nat Med* (2022) 28(8):1619–29. doi: 10.1038/s41591-022-01937-6

83. Fang Y, Mo F, Shou J, Wang H, Luo K, Zhang S, et al. A pan-cancer clinical study of personalized neoantigen vaccine monotherapy in treating patients with various types of advanced solid tumors. *Clin Cancer Res* (2020) 26(17):4511–20. doi: 10.1158/1078-0432.CCR-19-2881

84. Rubinsteyn A, Kodysh J, Hodes I, Mondet S, Aksoy BA, Finnigan JP, et al. Computational pipeline for the PGV-001 neoantigen vaccine trial. *Front Immunol* (2018) 8:1807. doi: 10.3389/fimmu.2017.01807

85. Hu Z, Leet DE, Allesøe RL, Oliveira G, Li S, Luoma AM, et al. Personal neoantigen vaccines induce persistent memory T cell responses and epitope spreading in patients with melanoma. *Nat Med* (2021) 27(3):515–25. doi: 10.1038/s41591-020-01206-4

86. Miller A, Asmann Y, Cattaneo L, Braggio E, Keats J, Auclair D, et al. High somatic mutation and neoantigen burden are correlated with decreased progression-free survival in multiple myeloma. *Blood Cancer J* (2017) 7(9):e612. doi: 10.1038/bcj.2017.94

87. Long GV, Ferrucci PF, Khattak A, Meniawy TM, Ott PA, Chisamore M, et al. KEYNOTE - D36: personalized immunotherapy with a neoepitope vaccine, EVX-01 and pembrolizumab in advanced melanoma. *Futur Oncol* (2022) 18(31):3473–80. doi: 10.2217/fon-2022-0694

88. Ott PA, Hu Z, Keskin DB, Shukla SA, Sun J, Bozym DJ, et al. An immunogenic personal neoantigen vaccine for melanoma patients. *Nature* (2017) 547(7662):217–21. doi: 10.1038/nature22991

89. Keskin DB, Anandappa AJ, Sun J, Tirosh I, Mathewson ND, Li S, et al. Neoantigen vaccine generates intratumoral T cell responses in phase ib glioblastoma trial. *Nature* (2018) 565(7738):234–9. doi: 10.1038/s41586-018-0792-9

90. Ott PA, Hu-Lieskovan S, Chmielowski B, Govindan R, Naing A, Bhardwaj N, et al. A phase ib trial of personalized neoantigen therapy plus anti-PD-1 in patients with advanced melanoma, non-small cell lung cancer, or bladder cancer. *Cell* (2020) 183 (2):347–362.e24. doi: 10.1016/j.cell.2020.08.053

91. Carreno BM, Magrini V, Becker-Hapak M, Kaabinejadian S, Hundal J, Petti AA, et al. A dendritic cell vaccine increases the breadth and diversity of melanoma neoantigen-specific T cells. *Sci (80-).* (2015) 348(6236):803–8. doi: 10.1126/science.aaa3828

92. Ding Z, Li Q, Zhang R, Xie L, Shu Y, Gao S, et al. Personalized neoantigen pulsed dendritic cell vaccine for advanced lung cancer. *Signal Transduct Target Ther* (2021) 6 (1):26. doi: 10.1038/s41392-020-00448-5

93. Platten M, Bunse L, Wick A, Bunse T, Le Cornet L, Harting I, et al. A vaccine targeting mutant IDH1 in newly diagnosed glioma. *Nature* (2021) 592(7854):463–8. doi: 10.1038/s41586-021-03363-z

94. Mueller S, Taitt JM, Villanueva-Meyer JE, Bonner ER, Nejo T, Lulla RR, et al. Mass cytometry detects H3.3K27M-specific vaccine responses in diffuse midline glioma. *J Clin Invest.* (2020) 130(12):6325–37. doi: 10.1172/JCI140378

95. Hilf N, Kuttruff-Coqui S, Frenzel K, Bukur V, Stevanović S, Gouttefangeas C, et al. Actively personalized vaccination trial for newly diagnosed glioblastoma. *Nat* (2018) 565 (7738):240–5. doi: 10.1038/s41586-018-0810-y

96. Cai Z, Su X, Qiu L, Li Z, Li X, Dong X, et al. Personalized neoantigen vaccine prevents postoperative recurrence in hepatocellular carcinoma patients with vascular invasion. *Mol Cancer.* (2021) 20(1):164. doi: 10.1186/s12943-021-01467-8

97. Kloor M, Reuschenbach M, Pauligk C, Karbach J, Rafiyan MR, Al-Batran SE, et al. A frameshift peptide neoantigen-based vaccine for mismatch repair-deficient cancers: A phase I/IIa clinical trial. *Clin Cancer Res* (2020) 26(17):4503–10. doi: 10.1158/1078-0432.CCR-19-3517

98. Kristensen NP, Heeke C, Tvingsholm SA, Borch A, Draghi A, Crowther MD, et al. Neoantigen-reactive CD8+ T cells affect clinical outcome of adoptive cell therapy with tumor-infiltrating lymphocytes in melanoma. *J Clin Invest.* (2022) 132(2):132. doi: 10.1172/JCI150535

99. Morisaki T, Kubo M, Umebayashi M, Yew PY, Yoshimura S, Park JH, et al. Neoantigens elicit T cell responses in breast cancer. *Sci Rep* (2021) 11(1):13590. doi: 10.1038/s41598-021-91358-1

100. Holm JS, Funt SA, Borch A, Munk KK, Bjerregaard AM, Reading JL, et al. Neoantigen-specific CD8 T cell responses in the peripheral blood following PD-L1 blockade might predict therapy outcome in metastatic urothelial carcinoma. *Nat Commun* (2022) 13(1):1935. doi: 10.1038/s41467-022-29342-0

101. Song Q, Yang B, Sheng W, Zhou Z, Zhang T, Qin B, et al. Safety and efficacy of mutant neoantigen-specific T-cell treatment combined anti-PD-1 therapy in stage IV solid tumors. *Immunotherapy* (2022) 14(7):553–65. doi: 10.2217/imt-2021-0105

102. Bassani-Sternberg M, Digklia A, Huber F, Wagner D, Sempoux C, Stevenson BJ, et al. A phase ib study of the combination of personalized autologous dendritic cell vaccine, aspirin, and standard of care adjuvant chemotherapy followed by nivolumab for resected pancreatic adenocarcinoma–a proof of antigen discovery feasibility in three patients. *Front Immunol* (2019) 10(AUG):1832. doi: 10.3389/fimmu.2019.01832

103. Sonntag K, Hashimoto H, Eyrich M, Menzel M, Schubach M, Döcker D, et al. Immune monitoring and TCR sequencing of CD4 T cells in a long term responsive patient with metastasized pancreatic ductal carcinoma treated with individualized, neoepitope-derived multipeptide vaccines: A case report. *J Transl Med* (2018) 16(1):23. doi: 10.1186/s12967-018-1382-1

104. Nelde A, Maringer Y, Bilich T, Salih HR, Roerden M, Heitmann JS, et al. Immunopeptidomics-guided warehouse design for peptide-based immunotherapy in chronic lymphocytic leukemia. *Front Immunol* (2021) 12:705974. doi: 10.3389/fimmu.2021.705974

105. Zhou WJ, Qu Z, Song CY, Sun Y, Lai AL, Luo MY, et al. NeoPeptide: an immunoinformatic database of T-cell-defined neoantigens. *Database* (2019) 2019:baz128. doi: 10.1093/database/baz128

106. Charoentong P, Finotello F, Angelova M, Mayer C, Efremova M, Rieder D, et al. Pan-cancer immunogenomic analyses reveal genotype-immunophenotype relationships and predictors of response to checkpoint blockade. *Cell Rep* (2017) 18(1):248–62. doi: 10.1016/j.celrep.2016.12.019

107. Cancer antigenic peptide database. Available at: https://caped.icp.ucl.ac.be/about.

108. Wu J, Zhao W, Zhou B, Su Z, Gu X, Zhou Z, et al. TSNAdb: A database for tumor-specific neoantigens from immunogenomics data analysis. *Genomics Proteomics Bioinf* (2018) 16(4):282. doi: 10.1016/j.gpb.2018.06.003

109. Koşaloğlu-Yalçın Z, Blazeska N, Carter H, Nielsen M, Cohen E, Kufe D, et al. The cancer epitope database and analysis resource: A blueprint for the establishment of a new bioinformatics resource for use by the cancer immunology community. *Front Immunol* (2021) 12:3456. doi: 10.3389/fimmu.2021.735609

110. Camacho LH. CTLA-4 blockade with ipilimumab: biology, safety, efficacy, and future considerations. *Cancer Med* (2015) 4(5):661–72. doi: 10.1002/cam4.371

111. Kooshkaki O, Derakhshani A, Hosseinkhani N, Torabi M, Safaei S, Brunetti O, et al. Combination of ipilimumab and nivolumab in cancers: From clinical practice to ongoing clinical trials. *Int J Mol Sci* (2020) 21(12):4427. doi: 10.3390/ijms21124427

frontiers | Frontiers in Immunology

TYPE Original Research
PUBLISHED 24 March 2023
DOI 10.3389/fimmu.2023.1137880

OPEN ACCESS

EDITED BY
Patrick Schmidt,
National Center for Tumor Diseases (NCT), Germany

REVIEWED BY
Jianjun Zhang,
University of Texas MD Anderson Cancer Center, United States
Joshua Ochieng,
University of Texas MD Anderson Cancer Center, United States

*CORRESPONDENCE
Young Wha Koh
youngwha9556@gmail.com

SPECIALTY SECTION
This article was submitted to Cancer Immunity and Immunotherapy, a section of the journal Frontiers in Immunology

RECEIVED 04 January 2023
ACCEPTED 15 March 2023
PUBLISHED 24 March 2023

CITATION
Koh YW, Park B, Jung SH, Han J-H, Haam S and Lee HW (2023) Immune profiles according to EGFR mutant subtypes and correlation with PD-1/PD-L1 inhibitor therapies in lung adenocarcinoma. *Front. Immunol.* 14:1137880. doi: 10.3389/fimmu.2023.1137880

Immune profiles according to EGFR mutant subtypes and correlation with PD-1/PD-L1 inhibitor therapies in lung adenocarcinoma

Young Wha Koh[1]*, Bumhee Park[2,3], Se Hee Jung[3], Jae-Ho Han[1], Seokjin Haam[4] and Hyun Woo Lee[5]

[1]Department of Pathology, Ajou University School of Medicine, Suwon-si, Republic of Korea, [2]Department of Biomedical Informatics, Ajou University School of Medicine, Suwon-si, Republic of Korea, [3]Office of Biostatistics, Medical Research Collaborating Center, Ajou Research Institute for Innovative Medicine, Ajou University Medical Center, Suwon-si, Republic of Korea, [4]Department of Thoracic and Cardiovascular Surgery, Ajou University School of Medicine, Suwon-si, Republic of Korea, [5]Department of Hematology-Oncology, Ajou University School of Medicine, Suwon-si, Republic of Korea

Background: We examined the distributions of 22 immune cell types and the responses to PD-1/PD-L1 inhibitors according to EGFR mutation profile, in three independent datasets of lung adenocarcinoma (LUAD).

Methods: We used CIBERSORTx to analyze the distributions of immune cells, and tumor immune dysfunction and exclusion (TIDE) or tumor mutation burden (TMB) to analyze responses to anti-PD-1/PD-L1 therapy, in two public LUAD datasets. The results were verified with a validation set that included patients treated with PD-1/PD-L1 inhibitors.

Results: Compared to EGFR mutants, EGFR wild-type carcinomas had higher numbers of CD8+ T cells, CD4 memory activated T cells and neutrophils, and lower numbers of resting dendritic cells and resting mast cells, in two of the datasets. In our subgroup analyses, CD8+ T cells and CD4 memory activated T cells were more numerous in EGFR rare variants than in wild-types, L858R mutants, and exon 19 deletion mutants. In our TIDE or TMB analyses, EGFR rare variants were predicted to respond better to PD-1/PD-L1 inhibitors than wild-types, L858R mutants, and exon 19 deletion mutants. In the validation set verified by immunohistochemical staining, levels of CD8+ T cells in the EGFR rare variant or wild-type groups were significantly higher than in the EGFR L858R and exon 19 deletion groups. In patients treated with PD-1/PD-L1 inhibitors, the survival rates of patients with EGFR wild-type and rare mutant carcinomas were higher than those with L858R and exon 19 deletion carcinomas.

Conclusion: The EGFR rare mutation form of LUAD shows a higher immune activation state compared to wild-type, L858R, and exon 19 deletion variants, indicating it as a potential target for PD-1/PD-L1 inhibitor therapy.

KEYWORDS

lung adenocarcinoma, EGFR, PD-L1, PD-1, CD8, CD4

Introduction

Among the adenocarcinomas associated with non-smokers in East Asia, EGFR mutations are the most common driver genes, accounting for approximately 60-78% of driver genes in the group (1). After receiving anti-programmed cell death protein 1/programmed death-ligand 1 (PD-1/PD-L1) treatment, adenocarcinoma patients positive for EGFR mutant show poorer responses than those with the wild-type (2). Because many patients in East Asia have EGFR mutations, they are excluded from treatment with PD-1/PD-L1 inhibitors. NSCLC with mutated EGFR has lower tumor mutation burden (TMB) levels than the wild-type, which may affect PD-1 inhibitor treatment (3). A negative correlation has been found between EGFR mutation and PD-L1 expression (3). Patients with EGFR-mutated NSCLC lack T-cell infiltration and have decreased ratios of PD-L1+/CD8+ tumor-infiltrating T cells (3). Single-cell analysis has reported that CD8+ tissue-resident memory (TRM) cells are deficient in EGFR-mutant forms of LUAD, compared to wild-type forms (4). There are many immune cells other than T cells in the tumor microenvironment that can affect anti-PD-1/PD-L1 treatment, but their effects are poorly understood. Studies of the effects of EGFR mutations in patients receiving anti-PD-1/PD-L1 therapy are rare.

CIBERSORTx is an analytical tool that uses gene expression data to evaluate cell type abundance (5). Tumor immune dysfunction and exclusion (TIDE) is a machine learning tool that uses gene expression data to evaluate T cell dysfunction and exclusion, and to predict tumor responses to anti-PD-1/PD-L1 therapy (6). In this study, we investigated the distributions of 22 immune cells according to the presence or absence of EGFR mutations using two public LUAD gene expression datasets and the CIBERSORTx tool. The response rates to anti-PD-L1/PD-1 treatment according to the presence of EGFR mutation were verified using the TIDE tool or tumor mutation burden (TMB). We also analyzed whether the response varied depending on the presence of EGFR mutation and immune cell type in patients who received anti-PD-L1/PD-1 treatment. Lastly, we investigated differences in the distributions of immune cells and TIDE scores, according to EGFR mutation subtype.

Materials and methods

Study population and EGFR test

Two public gene expression data sets (510 and 110 samples) and one validated data set (203 samples) were studied. We extracted two LUAD mRNA datasets from cBioportal databases (http://cbioportal.org) (7). The first dataset comprised 510 samples (pancancer dataset, wild-type: 444, L858R: 22, exon 19 deletion: 25, rare: 19) (8) and the second dataset (cptac dataset, wild-type: 72, L858R: 16, exon 19 deletion: 16, rare: 6) comprised 110 samples (9). The rare mutations in the first data set consisted of two exon 20 insertions, three G719X mutations, and 14 other mutations. The rare mutations in the second data set consisted of four G719X mutations and two other mutations. We were able to identify EGFR mutation profiles in all datasets. We obtained TMB scores from the cBioportal databases for each case. The demographic and clinical characteristics of validation set are summarized in Table 1. A total of 203 patients were enrolled (wild-type: 84, L858R: 36, exon 19 deletion: 46, rare: 37), 49 were treated with PD-1/PD-L1 inhibitors (wild-type: 31, L858R: 7, exon 19 deletion: 8, rare: 3) and 154 were not (wild-type: 53, L858R: 29, exon 19 deletion: 38, rare: 34). The rare mutations in the treated group consisted of one exon 20 insertion and two G719X mutations, and the rare mutations in the non-treated group consisted of 16 exon 20 insertions, 12 G719X mutations and six other mutations. Ethical approval was granted by the Institutional Review Board of Ajou University School of Medicine (AJOUIRB-KSP-2020-396 and 2020-12-28).

Immunohistochemistry of CD8

Immunochemical staining was performed for surgical resection samples using a tissue microarray, and biopsy samples were performed for whole sections. Anti-CD8 antibodies (clone C8/144B, DAKO) were used in analyses. For evaluation of CD8 immunostaining, membrane-positive cells were measured at three locations and the average value was calculated.

CIBERSORTx and TIDE

We used the CIBERSORTx tool to identify 22 human immune cell subpopulations in lung adenocarcinoma samples (5). We used the TIDE tool to identify four biomarkers: TIDE, interferon gamma gene signature, T-cell-inflamed signature, and PD-L1 (6).

Statistical analyses

We used Spearman's rank coefficient or Kruskal–Wallis H test as nonparametric measures of rank correlation. Pearson's chi-squared test was used for statistical tests on categorical data. Survival analysis was performed using a Kaplan–Meier estimator. IBM SPSS Statistics for Windows, version 25.0 (IGM Inc., Armonk, NY, USA) or R version 3.5.3 (http://www.r-project.org/) were used for all analyses. All p values less than 0.05 were considered statistically significant.

Results

Differences in 22 immune cell components according to EGFR mutation profiles

We confirmed differences in 22 immune cell components according to EGFR mutation profiles in two public LUAD datasets. In the pancancer dataset, CD8+ T cells ($p = 0.001$), CD4 memory activated T cells ($p < 0.001$), follicular helper T cells ($p = 0.012$), resting NK cells ($p = 0.037$), and neutrophils ($p = 0.039$)

TABLE 1 Demographic and clinical characteristics of patients.

Variable	Number (%)
Age, median (range) (years)	64 (35–85)
Male sex	124 (61.1%)
TNM 8th edition	
Stage I	71 (35%)
Stage II	24 (11.8%)
Stage III	55 (27.1%)
Stage IV	53 (26.1%)
EGFR test method	
Real-time PCR	166 (81.8%)
Next-generation sequencing	37 (18.2%)
EGFR results	
Wild	84 (41.4%)
L858R	36 (17.7%)
Exon 19 deletion	46 (22.7%)
Rare	37 (18.2%)
Smoking history	
Presence	96 (59.6%)
Absence	65 (40.4%)
PD-L1/PD-1 inhibitor	
Treatment	49 (24.1%)
No treatment	154 (75.9%)

Smoking history was obtained in 161 patients.

were significantly more abundant in the EGFR wild-type group than in the mutation group. However, CD4 naive T cells ($p = 0.009$), resting dendritic cells ($p = 0.007$), activated dendritic cells ($p = 0.027$), and resting mast cells ($p = 0.029$) were significantly less abundant in the EGFR wild-type group than in the mutation group. In the cptac dataset, naïve B cells ($p = 0.036$), plasma cells ($p = 0.003$), CD8+ T cells ($p = 0.01$), CD4 memory activated T cells ($p = 0.001$), and neutrophils ($p = 0.002$) were significantly more abundant in the EGFR wild-type group than in the mutation group. However, CD4 memory resting T cells ($p = 0.01$), monocytes ($p = 0.015$), M2 macrophages ($p = 0.048$), resting dendritic cells ($p = 0.008$), and resting mast cells ($p = 0.028$) were significantly less abundant in the EGFR wild-type group than in the mutation group. Some common results found between the two datasets were higher levels of CD8+ T cells, CD4 memory activated T cells and neutrophils, and lower levels of resting dendritic cells and resting mast cells in the EGFR wild-type groups versus the mutation groups (Figure 1).

We then performed subgroup analyses according to EGFR mutation subtype for four groups: wild-type, L858R, exon 19 deletion, and rare mutation. Other than L858R and exon 19 deletion, all mutations were classified as rare. Levels of CD8+ T cells, CD4 memory activated T cells, resting dendritic cells, resting mast cells, and neutrophils, which showed significant differences between the two datasets, were included in our subgroup analyses.

In the pancancer dataset, the rare variant had the highest CD8+ T cell and CD4 memory activated T cell levels among the four groups ($p < 0.001$, Figure 1C). Levels of CD8+ T cells and CD4 memory activated T cells were higher in the rare mutant and wild type than in the exon 19 deletion and L858R ($p < 0.001$, Figure 1C). There were no differences in resting dendritic cells, resting mast cells, and neutrophils levels in rare variant, exon 19 deletion, and L858R groups (Figure 1C). In the cptac dataset, the rare variant group also had the highest CD8+ T cell and CD4 memory activated T cell levels among the four (Figure 1D). Levels of CD8+ T cells or CD4 memory activated T cells were also higher in the rare mutant and wild type groups compared to the exon 19 deletion and L858R mutation groups ($p = 0.023$ and $p = 0.002$, respectively, Figure 1D). There were also no differences in resting dendritic cell, resting mast cell, and neutrophil levels in the rare variant, exon 19 deletion, and L858R groups (Figure 1D).

Differences in TIDE score or TMB according to EGFR mutation profile

CD8+ T cells or CD4 memory activated T cells are immune cells closely related to immunotherapy (10, 11). Because the levels of CD8+ T cells and CD4 memory activated T cells were surprisingly high in the rare variant group, we investigated whether the TIDE score was different for each EGFR subtype. We verified differences in four TIDE-associated biomarkers according to EGFR subtype. In previous studies, patients with low TIDE (6), high interferon gamma signature (12), high T cell inflamed signature (13) and high PD-L1 (14) responded better to PD-1/PD-L1 inhibitors. In the pancancer dataset, although not statistically significant, the interferon gamma signature and T cell inflamed signature of the rare variant were the highest among the four groups, and the TIDE score was the lowest among the four groups (Figure 2A). PD-L1 expression in the rare variant group was the second highest after the wild-type group (Figure 2A). In the cptac dataset, although not statistically significant, the interferon gamma signature, T cell inflamed signature, and PD-L1 expression in the rare variant group were also the highest among the four, and the TIDE score was the lowest (Figure 2B). In the pancancer dataset, the TMB score of the rare variant group was the highest among the four ($p < 0.001$, Figure 3A). In the cptac dataset, the TMB score of the rare variant group was the second highest after the wild-type ($p < 0.001$, Figure 3B). The TIDE analysis result was that, of the four group (including the wild-type), the rare variant group was most likely to respond well to PD-L1/PD-1 inhibitor treatment.

Differences in CD8+ T cells according to EGFR mutation profile in the validation set

Because we could not find an immunohistochemical antibody that could clearly detect CD4 memory activated T cells, only CD8+ T cells were re-validated by immunohistochemistry. Levels of CD8+

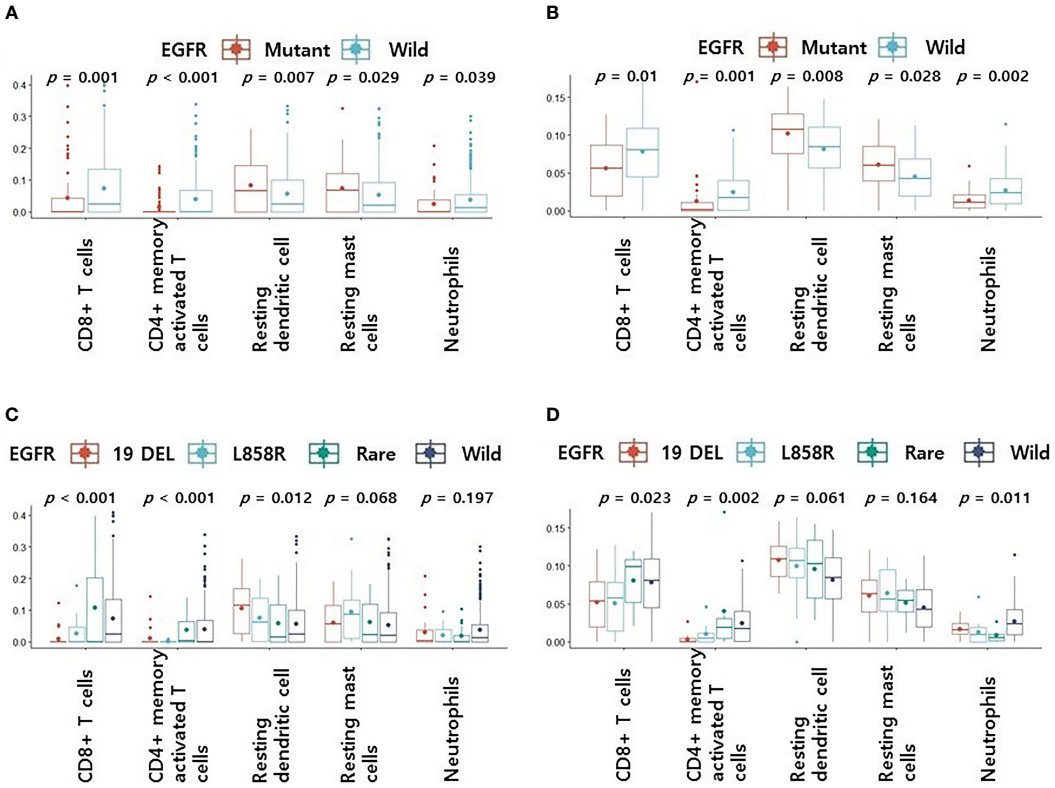

FIGURE 1
Differences in 5 immune cell components according to EGFR mutation profiles. **(A)** Changes in levels of 5 immune cell components according to EGFR mutations in pancancer dataset **(A)** and cptac dataset **(B)**. Changes in levels of CD8+ T cells, CD4 memory activated T cells, resting dendritic cells, resting mast cells and neutrophils according to EGFR mutational subtypes in pancancer dataset **(C)** and cptac dataset **(D)**. The small dot in the boxplot is the mean value. 19 DEL, exon 19 deletion.

T cells were found to be higher in the EGFR wild-type and rare variants groups than in the L858R and exon 19 deletion groups in both tumor and peritumoral regions (Figure 4A, all $p < 0.001$). Representative figures for EGFR wild, L858R, exon 19 deletion, and rare mutation results are summarized in Figure 4B.

Smoking status according to EGFR subtype

Previous studies revealed that patients with smoking histories had high TMB levels and responded well to PD-1 inhibitors (15). Therefore, we examined the relationship between smoking history and EGFR subtype. However, since there was no information on smoking history in the pancancer data set, only the cptac and validation datasets were analyzed. In the cptac dataset, the TMB score was significantly higher for those with a history of smoking than those without a history of smoking (Figure 5A, $p = 0.007$). Smoking history was most frequent in wild-type patients and least frequent in exon 19 deletion patients. (Figure 5B, $p = 0.038$). In the validation dataset, smoking history was also most frequently present in the wild-type group, and least frequent in the exon 19 deletion group (Figure 5C, $p = 0.006$).

Prognostic role of EGFR mutation in patients using PD-L1/PD-1 inhibitors

We investigated the prognostic role of EGFR mutation in patients using PD-L1/PD-1 inhibitors. Although the difference was not statistically significant, the EGFR mutation group had lower overall survival (OS) rates compared to the wild-type (Figure 6A, $p = 0.09$). Although the difference was not statistically significant, groups with EGFR wild type or rare mutations had higher rates of OS compared to groups with L858R or exon 19 deletion mutations (Figure 6B, $p = 0.184$).

Discussion

We found that levels of CD8+ T cells or CD4 memory activated T cells were higher in EGFR wild-type and rare variant cancers than in EGFR L858R and exon 19 deletion types. Among patients using PD-1/PD-L1 inhibitors, those with EGFR wild-type and EGFR rare mutations had better prognoses than those with EGFR L858R and exon 19 deletion mutations. CD8+ T cells are the most potent effectors in the anti-cancer immune response, and serve as the

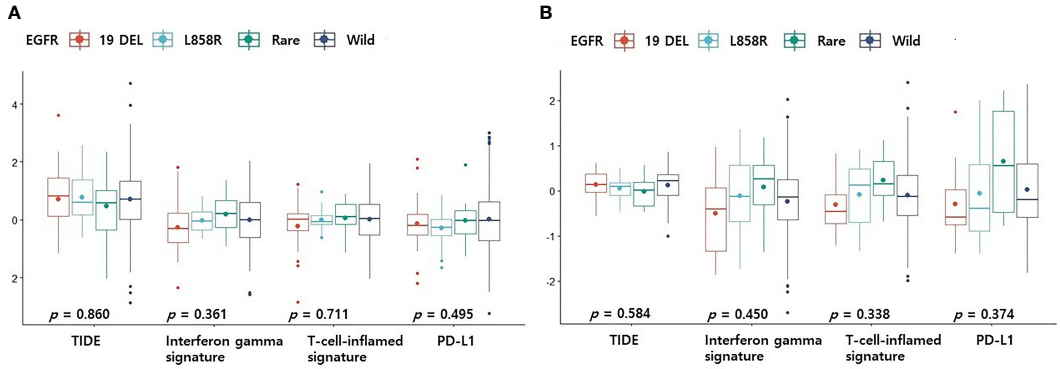

FIGURE 2
Differences in TIDE-related biomarkers according to EGFR mutational subtypes. Changes in levels of TIDE-related biomarkers according to EGFR mutational subtypes in pancancer dataset **(A)** and cptac dataset **(B)**. The small dot in the boxplot is the mean value. 19 DEL, exon 19 deletion.

backbone of cancer immunotherapy (11). Immune checkpoint inhibitors block inhibitory immune receptors and aim to activate dysfunctional CD8+ T cells (11). Immune cold tumor is a common immunotherapy-resistant phenotype observed in solid tumors (16). The definition of hot and cold tumors depends in part on the extent and location of infiltrating CD8+ T cells (17). Therefore, it is predictable that hot tumors respond well to immunotherapy and cold tumors do not. One previous study also reported that EGFR-mutated NSCLC carcinomas were free of T cell infiltration and had decreased proportions of PD-L1+/CD8+ tumor-infiltrating T cells (3). Studies of patients using PD-1/PD-L1 inhibitors have shown that NSCLCs carrying EGFR mutations are associated with poor responses, suggesting that these mutations are associated with a smaller proportion of CD8+ T cells (18). Another study showed that lung cancer patients with the L858R EGFR mutation had more inflammatory tumors with higher CD4 and CD8+ T cell expressions compared to those with the exon 19 deletion mutation (19). However, we found no significant differences in CD4 and CD8+ T cells between L858R and exon 19 deletion groups. Infiltration of CD8+ T cells and neutrophils was observed more frequently in the rare EGFR mutant group than in the L858R and exon 19 deletion groups.

CD4+ T cells have recently been highlighted as playing important roles in regulating the anti-tumor immune response (10). One study found that a higher number of $CD62L^{low}$ CD4+ T cells prior to PD-1 blockade therapy was significantly associated with better responses (20). Laheurte et al. reported that higher levels of anti-TERT $Th1^{high}$ CD4+ T cells in the peripheral blood was correlated with better clinical outcomes in NSCLC patients (21). Activated CD4+ T cells secrete interleukin (IL)-2 to directly activate CD8+ cytotoxic T cells (22). CD4+ T cells can induce antitumor responses by secreting interferon gamma and tumor necrosis factor-α (TNFα) (23). CD4+ T cells also induce humoral responses to tumor antigens on B cells through the interaction of CD40 with CD40 ligands (10). High CD4 memory activated T cells was significantly associated with better overall survival in gastric

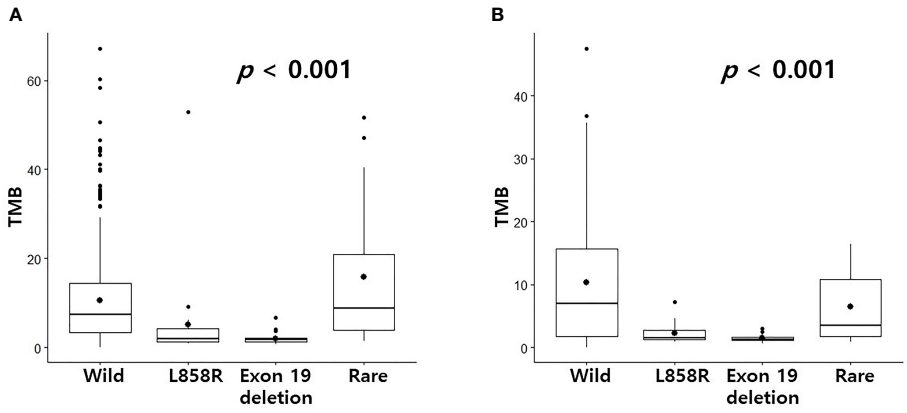

FIGURE 3
Differences in TMB according to EGFR mutational subtypes. Changes in levels of TMB according to EGFR mutational subtypes in pancancer dataset **(A)** and cptac dataset **(B)**. The small dot in the boxplot is the mean value.

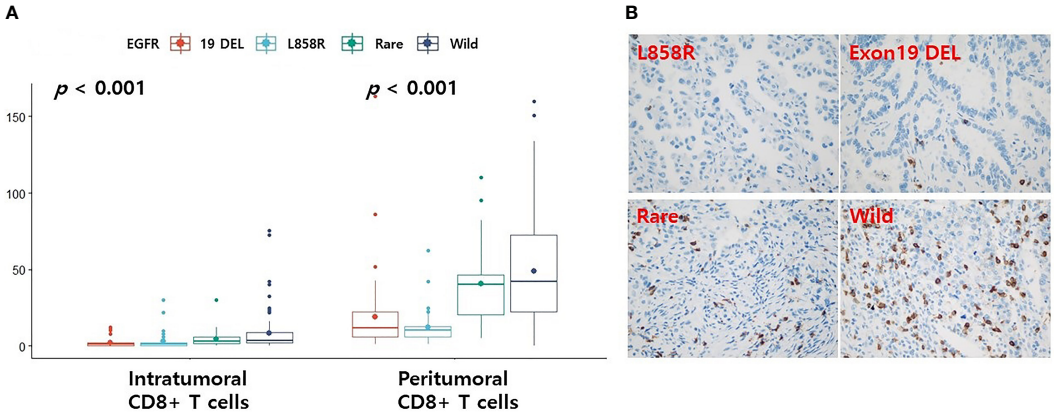

FIGURE 4
Differences in the levels of CD8 according to EGFR mutational subtypes analyzed by immunohistochemistry. **(A)** Changes in levels of CD8 according to EGFR mutational subtypes. Representative immunohistochemical images of CD8 expression. **(B)** Case with EGFR L858R or exon 19 deletion mutation is associated with low CD8+ T cells. Case with EGFR rare variant or wild-type is associated with high CD8+ T cells. The small dot in the boxplot is the mean value. 19 DEL, exon 19 deletion.

cancer (24). In head and neck squamous cell carcinoma, the group with high activated CD4(+)CD69(+) T cells had a better prognosis than the group with low CD4(+)CD69(+) T cells (25).

In our study, the five biomarkers used to predict response to PD-L1/PD-1 inhibitors were TIDE, interferon gamma gene signature, T cell inflammatory signature, PD-L1, and TMB. Ayers et al. found that the interferon gamma gene signature could predict responses to PD-1 inhibitors in 220 patients with nine cancers, including NSCLC (12). The T cell inflammatory signature is a well-known indicator of T cell dysfunction (13). PD-L1 expression is the most frequently used biomarker for the use of PD-L1/PD-1 inhibitors in solid cancers, including NSCLC, in clinical practice (26). Therefore, these four biomarkers are currently the most widely used biomarkers for PD-L1/PD-1 inhibitors. Although not statistically significant, rare variants were predicted to respond best to PD-L1/PD-1 inhibitor treatment in four TIDE biomarkers. It is well known from previous studies that tumors with high TMB have more neoantigens and more immunogenicity (27). Rizvi et al. reported that high TMB levels in tumors of NSCLC patients treated with pembrolizumab had good prognoses (27). Although in our study only TMB was statistically significant and the other factors were not, due to the small number of samples of rare variants, PD-L1/PD-1 inhibitor treatment should be considered for the treatment rare variant NSCLC tumors in the future, as they are expected to respond better than wild-type ones.

Negrao et al. reported that EGFR exon 20 mutations were associated with low expression of PD-L1 (28). Therefore, EGFR exon 20 mutations were also predicted to have less benefit from PD-1 inhibitors. Hastings et al. also reported that the exon 20 insertion mutation was associated with low levels of TMB, whereas the G719X mutation was associated with high TMB levels (15). The G719X mutation was also associated with higher expression of TMB and PD-L1 than the classical EGFR mutation in another study of NSCLC patients (29). In the two public datasets we reviewed, the frequency of exon 20 insertion was relatively low and the frequency of G719X mutation was relatively high (12% vs. 18% in the pancancer dataset and 0% vs 66% in the cptac dataset, respectively). In our survival analysis of our validation dataset, the frequency of the G719X mutation was higher than that of exon 20 insertion (66% vs. 33%). In our dataset, the high frequency of the G719X mutation and the low frequency of the exon 20 insertion mutation may have been the causes of high CD8+ T cell scores and high TMBs.

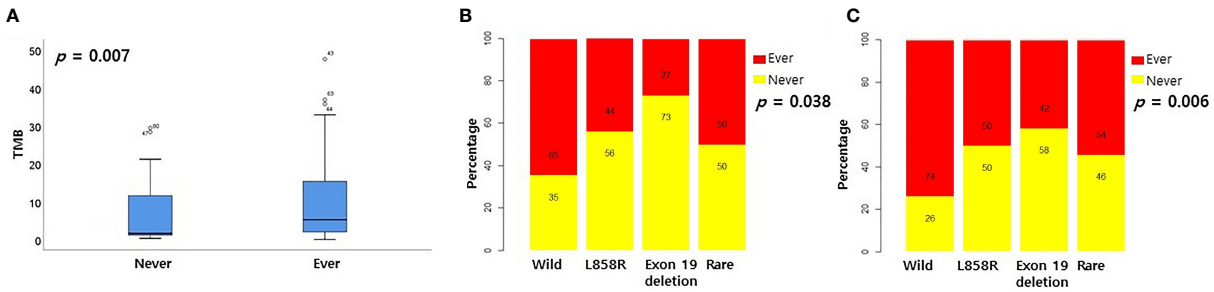

FIGURE 5
Relationship between smoking history and EGFR mutational subtypes. **(A)** Relationship between smoking history and TMB in cptac dataset. Relationship between smoking history and EGFR mutational subtypes in cptac **(B)** and validation **(C)** dataset.

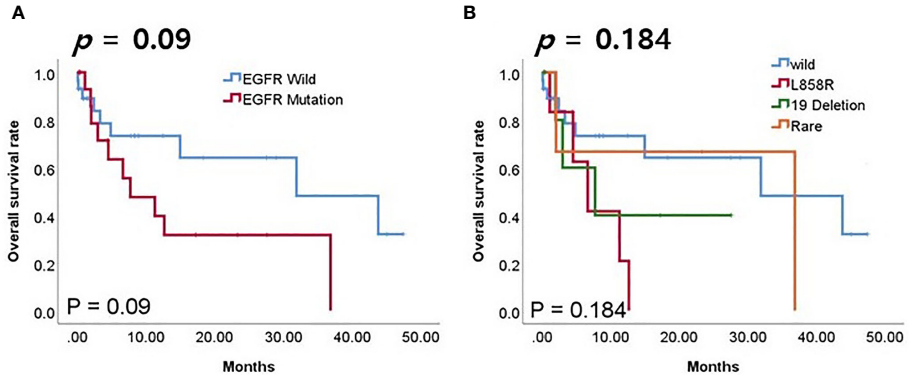

FIGURE 6
Survival analyses according to EGFR mutation in patients receiving PD-1/PD-L1 inhibitors. **(A)** Overall survival (OS) according to EGFR mutation. **(B)** OS according to EGFR mutation subtype.

Hastings et al. reported that a smoking history was associated with a high TMB level and responded well to immune checkpoint inhibitors (15). A positive correlation between smoking history and TMB levels was also identified in our cptac data set. In previous report, smoking history was observed more frequently with the L858R mutation than with the exon 19 deletion (15). In our two data sets, smoking history was also found more frequently with the L858R mutation compared to the exon 19 deletion. Among the four EGFR subtypes of our two data sets, smoking history was most common in the wild type and second most common in rare mutations.

Compared to other studies in the past (15, 28, 30), the sample size of our study is relatively too small. Two studies (Hastings et al's cohort (n=554) (15) and Negrao et al's cohort (n=4189) (28)) reported that EGFR exon 20 mutations were associated with reduced benefit from PD-1 inhibitors. Mazieres et al. found no difference in survival between rare and classical EGFR mutations on PD-1/PD-L1 treatment in 551 NSCLCs (30). However, experiments with a relatively large number of samples also reported that rare mutations in EGFR were associated with high levels of TMB or PD-L1 expression. In an experiment targeting 1,111 NSCLC patients, it was found that the levels of TMB and PD-L1 in the G719X mutation were higher than those in the classical EGFR mutation (29). In 2417 NSCLC patients, PD-L1 high-expression was more likely to shown with G719X/S768I/exon 20 insertion than with classical EGFR /L861Q mutation (31). In 982 NSCLCs, rare EGFR mutations (G719X, L861Q, S768I, exon 20 insertion) showed statistically significantly higher PD-L1 expression than classical EGFR mutations (32). Although our results indicate that patients with rare EGFR mutations are more likely to respond to PD-L1/PD-1 inhibitors in three independent data sets, the prescription of PD-L1/PD-1 inhibitors for rare EGFR mutations needs to be validated with more samples.

Our study had some limitations. First, although numerous EGFR rare mutations have been reported, these were combined and analyzed together in this study. As a result, the immune profiles associated with specific rare mutations or their relationships to PD-1/PD-L1 inhibitors were not examined. Because the number of rare EGFR mutations was small, it was difficult to perform subgroup analysis for rare EGFR mutations. The immune characteristics of specific rare mutations should be investigated in larger-scale studies. Second, our validation set consisted of 203 patients, of which 49 were treated with PD-1/PD-L1 inhibitors. The small number of patients divided into four groups (EGFR wild, L858R, exon 19 deletion, and rare) for analysis may have limited the interpretation of the results. Third, we did not perform CIBERSORTx, TIDE, and immunohistochemistry analyses on the same LUAD dataset. Although similar results were obtained for all three datasets, our results should be validated using the same dataset. Fourth, we could not confirm the distribution of CD4 memory activated T cells in the validation set. Because the level of CD4 memory activated T cells in the two public datasets was the highest in the rare variant, it is thought that CD4 memory activated T cells may affect immunotherapy.

In this study, we investigated differences in 22 immune cell components following EGFR mutation in 620 LUADs in two public databases, for the first time. Subgroup analysis revealed that the rare variant group had the highest CD8+ T cell and CD4 memory activated T cell levels among the four groups, including the wild-type. TIDE and TMB analyses also showed that rare EGFR variants was more likely to respond to PD-L1/PD-1 inhibitors than wild-type, L858R-mutated, and exon 19 deletion-mutated EGFR lung cancers. A validation set using CD8+ T cell immunochemical staining demonstrated an immune profile similar to the previous two data sets for EGFR rare mutations, and a better prognosis for these cancer types than L858R and exon 19 deletions, with PD-1/PD-L1 inhibitor treatment. The results of this study indicate that rare EGFR mutations may be potential targets for PD-1/PD-L1 inhibitors.

Data availability statement

The original contributions presented in the study are included in the article/supplementary materials. Further inquiries can be directed to the corresponding author.

Ethics statement

The studies involving human participants were reviewed and approved by The Institutional Review Board of Ajou University School of Medicine. Written informed consent for participation was not required for this study in accordance with the national legislation and the institutional requirements.

Author contributions

YK designed the study. SH, J-HH, HL, and YK collected the data, SH, J-HH, HL, BP, SJ, and YK performed the experiments and analyzed the data. SH, J-HH, HL, and YK wrote the manuscript. All authors contributed to the article and approved the submitted version.

Funding

This research was supported by the Basic Science Research Program through the National Research Foundation of Korea (NRF) funded by the Ministry of Science, ICT (NRF-2020R1A2C1100568 for Young Wha Koh).

Conflict of interest

The authors declare that the research was conducted in the absence of any commercial or financial relationships that could be construed as a potential conflict of interest.

Publisher's note

All claims expressed in this article are solely those of the authors and do not necessarily represent those of their affiliated organizations, or those of the publisher, the editors and the reviewers. Any product that may be evaluated in this article, or claim that may be made by its manufacturer, is not guaranteed or endorsed by the publisher.

References

1. Zhou F, Zhou C. Lung cancer in never smokers–the East Asian experience. *Trans Lung Cancer Res* (2018) 7(4):450–63. doi: 10.21037/tlcr.2018.05.14

2. Li J, Gu J. PD-L1 expression and EGFR status in advanced non-small-cell lung cancer patients receiving PD-1/PD-L1 inhibitors: a meta-analysis. *Future Oncol* (2019) 15(14):1667–78. doi: 10.2217/fon-2018-0639

3. Dong ZY, Zhang JT, Liu SY, Su J, Zhang C, Xie Z, et al. EGFR mutation correlates with uninflamed phenotype and weak immunogenicity, causing impaired response to PD-1 blockade in non-small cell lung cancer. *Oncoimmunology* (2017) 6(11):e1356145. doi: 10.1080/2162402x.2017.1356145

4. Yang L, He YT, Dong S, Wei XW, Chen ZH, Zhang B, et al. Single-cell transcriptome analysis revealed a suppressive tumor immune microenvironment in EGFR mutant lung adenocarcinoma. *J Immunother Cancer.* (2022) 10(2):e003534. doi: 10.1136/jitc-2021-003534

5. Newman AM, Steen CB, Liu CL, Gentles AJ, Chaudhuri AA, Scherer F, et al. Determining cell type abundance and expression from bulk tissues with digital cytometry. *Nat Biotechnol* (2019) 37(7):773–82. doi: 10.1038/s41587-019-0114-2

6. Jiang P, Gu S, Pan D, Fu J, Sahu A, Hu X, et al. Signatures of T cell dysfunction and exclusion predict cancer immunotherapy response. *Nat Med* (2018) 24(10):1550–8. doi: 10.1038/s41591-018-0136-1

7. Cerami E, Gao J, Dogrusoz U, Gross BE, Sumer SO, Aksoy BA, et al. The cBio cancer genomics portal: an open platform for exploring multidimensional cancer genomics data. *Cancer discovery.* (2012) 2(5):401–4. doi: 10.1158/2159-8290.Cd-12-0095

8. Hoadley KA, Yau C, Hinoue T, Wolf DM, Lazar AJ, Drill E, et al. Cell-of-Origin patterns dominate the molecular classification of 10,000 tumors from 33 types of cancer. *Cell*> (2018) 173(2):291–304.e6. doi: 10.1016/j.cell.2018.03.022

9. Gillette MA, Satpathy S, Cao S, Dhanasekaran SM, Vasaikar SV, Krug K, et al. Proteogenomic characterization reveals therapeutic vulnerabilities in lung adenocarcinoma. *Cell* (2020) 182(1):200–25.e35. doi: 10.1016/j.cell.2020.06.013

10. Tay RE, Richardson EK, Toh HC. Revisiting the role of CD4+ T cells in cancer immunotherapy–new insights into old paradigms. *Cancer Gene Ther* (2021) 28(1):5–17. doi: 10.1038/s41417-020-0183-x

11. Raskov H, Orhan A, Christensen JP, Gögenur I. Cytotoxic CD8(+) T cells in cancer and cancer immunotherapy. *Br J cancer.* (2021) 124(2):359–67. doi: 10.1038/s41416-020-01048-4

12. Ayers M, Lunceford J, Nebozhyn M, Murphy E, Loboda A, Kaufman DR, et al. IFN-γ-related mRNA profile predicts clinical response to PD-1 blockade. *J Clin Invest.* (2017) 127(8):2930–40. doi: 10.1172/jci91190

13. Woo SR, Corrales L, Gajewski TF. The STING pathway and the T cell-inflamed tumor microenvironment. *Trends Immunol* (2015) 36(4):250–6. doi: 10.1016/j.it.2015.02.003

14. Brahmer J, Reckamp KL, Baas P, Crinò L, Eberhardt WE, Poddubskaya E, et al. Nivolumab versus docetaxel in advanced squamous-cell non-Small-Cell lung cancer. *New Engl J Med* (2015) 373(2):123–35. doi: 10.1056/NEJMoa1504627

15. Hastings K, Yu HA, Wei W, Sanchez-Vega F, DeVeaux M, Choi J, et al. EGFR mutation subtypes and response to immune checkpoint blockade treatment in non-small-cell lung cancer. *Ann Oncol* (2019) 30(8):1311–20. doi: 10.1093/annonc/mdz141

16. Trujillo JA, Sweis RF, Bao R, Luke JJ. T Cell-inflamed versus non-T cell-inflamed tumors: A conceptual framework for cancer immunotherapy drug development and combination therapy selection. *Cancer Immunol Res* (2018) 6(9):990–1000. doi: 10.1158/2326-6066.Cir-18-0277

17. Galon J, Bruni D. Approaches to treat immune hot, altered and cold tumours with combination immunotherapies. *Nat Rev Drug discovery.* (2019) 18(3):197–218. doi: 10.1038/s41573-018-0007-y

18. Gainor JF, Shaw AT, Sequist LV, Fu X, Azzoli CG, Piotrowska Z, et al. EGFR mutations and ALK rearrangements are associated with low response rates to PD-1 pathway blockade in non-small cell lung cancer: A retrospective analysis. *Clin Cancer research: an Off J Am Assoc Cancer Res* (2016) 22(18):4585–93. doi: 10.1158/1078-0432.Ccr-15-3101

19. Toki MI, Mani N, Smithy JW, Liu Y, Altan M, Wasserman B, et al. Immune marker profiling and programmed death ligand 1 expression across NSCLC mutations. *J Thorac oncology: Off Publ Int Assoc Study Lung Cancer.* (2018) 13(12):1884–96. doi: 10.1016/j.jtho.2018.09.012

20. Kagamu H, Kitano S, Yamaguchi O, Yoshimura K, Horimoto K, Kitazawa M, et al. CD4(+) T-cell immunity in the peripheral blood correlates with response to anti-PD-1 therapy. *Cancer Immunol Res* (2020) 8(3):334–44. doi: 10.1158/2326-6066.Cir-19-0574

21. Laheurte C, Dosset M, Vernerey D, Boullerot L, Gaugler B, Gravelin E, et al. Distinct prognostic value of circulating anti-telomerase CD4(+) Th1 immunity and exhausted PD-1(+)/TIM-3(+) T cells in lung cancer. *Br J cancer.* (2019) 121(5):405–16. doi: 10.1038/s41416-019-0531-5

22. Borst J, Ahrends T, Bąbała N, Melief CJM, Kastenmüller W. CD4(+) T cell help in cancer immunology and immunotherapy. *Nat Rev Immunol* (2018) 18(10):635–47. doi: 10.1038/s41577-018-0044-0

23. Kennedy R, Celis E. Multiple roles for CD4+ T cells in anti-tumor immune responses. *Immunol Rev* (2008) 222:129–44. doi: 10.1111/j.1600-065X.2008.00616.x

24. Ning ZK, Hu CG, Huang C, Liu J, Zhou TC, Zong Z. Molecular subtypes and CD4(+) memory T cell-based signature associated with clinical outcomes in gastric cancer. *Front Oncol* (2020) 10:626912. doi: 10.3389/fonc.2020.626912

25. Badoual C, Hans S, Rodriguez J, Peyrard S, Klein C, Agueznay Nel H, et al. Prognostic value of tumor-infiltrating CD4+ T-cell subpopulations in head and neck cancers. *Clin Cancer Res* (2006) 12(2):465–72. doi: 10.1158/1078-0432.Ccr-05-1886

26. Yu H, Boyle TA, Zhou C, Rimm DL, Hirsch FR. PD-L1 expression in lung cancer. *J Thorac oncology: Off Publ Int Assoc Study Lung Cancer.* (2016) 11(7):964–75. doi: 10.1016/j.jtho.2016.04.014

27. Rizvi NA, Hellmann MD, Snyder A, Kvistborg P, Makarov V, Havel JJ, et al. Cancer immunology. mutational landscape determines sensitivity to PD-1 blockade in non-small cell lung cancer. *Science* (2015) 348(6230):124–8. doi: 10.1126/science.aaa1348

28. Negrao MV, Skoulidis F, Montesion M, Schulze K, Bara I, Shen V, et al. Oncogene-specific differences in tumor mutational burden, PD-L1 expression, and outcomes from immunotherapy in non-small cell lung cancer. *J Immunother Cancer.* (2021) 9(8):e002891. doi: 10.1136/jitc-2021-002891

29. Ma T, Jiao J, Huo R, Li X, Fang G, Zhao Q, et al. PD-L1 expression, tumor mutational burden, and immune cell infiltration in non-small cell lung cancer patients with epithelial growth factor receptor mutations. *Front Oncol* (2022) 12:922899. doi: 10.3389/fonc.2022.922899

30. Mazieres J, Drilon A, Lusque A, Mhanna L, Cortot AB, Mezquita L, et al. Immune checkpoint inhibitors for patients with advanced lung cancer and oncogenic driver alterations: results from the IMMUNOTARGET registry. *Ann Oncol* (2019) 30 (8):1321–8. doi: 10.1093/annonc/mdz167

31. Liu Y, Quan F, Chen S, Lu G, Yang Y, Deng W, et al. Correlation between PD-L1 high-expression and EGFR variants in non-small cell lung cancer. *J Clin Oncol* (2022) 40(16_suppl):e21062–e. doi: 10.1200/JCO.2022.40.16_suppl.e21062

32. Evans M, O'Sullivan B, Smith M, Hughes F, Trim N, Mullis T, et al. The association between PD-L1 expression, EGFR mutation and ALK translocation in a series of 982 lung cancers. *Ann Oncol* (2017) 28:v29. doi: 10.1093/annonc/mdx363.022

frontiers | Frontiers in Immunology

TYPE Original Research
PUBLISHED 17 May 2023
DOI 10.3389/fimmu.2023.1161718

OPEN ACCESS

EDITED BY
Yun-Fan Sun,
Fudan University, China

REVIEWED BY
Nuria Pardo Aranda,
Vall d'Hebron University Hospital, Spain
Jialei Wang,
Fudan University, China

*CORRESPONDENCE
Wei Zhang
zhwei2002@sjtu.edu.cn
Baohui Han
18930858216@163.com
Yuqing Lou
louyq@hotmail.com

†These authors share first authorship

RECEIVED 08 February 2023
ACCEPTED 28 March 2023
PUBLISHED 17 May 2023

CITATION
Li Y, Jiang H, Qian F, Chen Y, Zhou W, Zhang Y, Lu J, Lou Y, Han B and Zhang W (2023) Efficacy of ICI-based treatment in advanced NSCLC patients with PD-L1≥50% who developed EGFR-TKI resistance. *Front. Immunol.* 14:1161718. doi: 10.3389/fimmu.2023.1161718

Efficacy of ICI-based treatment in advanced NSCLC patients with PD-L1≥50% who developed EGFR-TKI resistance

Yujing Li[1†], Haohua Jiang[1†], Fangfei Qian[1†], Ya Chen[2], Wensheng Zhou[3], Yanwei Zhang[1], Jun Lu[1], Yuqing Lou[1*], Baohui Han[1*] and Wei Zhang[1*]

[1]Department of Respiratory and Critical Care Medicine, Shanghai Chest Hospital, Shanghai Jiao Tong University School of Medicine, Shanghai, China, [2]Department of Respiratory and Critical Care Medicine, The First Affiliated Hospital of University of Science and Technology (USTC), Division of Life Science and Medicine, University of Science and Technology of China, Hefei, China, [3]State Key Laboratory of Respiratory Disease, National Clinical Research Center for Respiratory Disease, Guangzhou Institute of Respiratory Health, The First Affiliated Hospital of Guangzhou Medical University, Guangzhou, China

Introduction: Platinum-based chemotherapy is still the standard of care for Epidermal growth factor receptor (EGFR) mutated non-small cell lung cancer (NSCLC) patients after developing EGFR-TKI resistance. However, no study focusing on the role of immuno checkpoint inhibitor (ICI) based treatments for EGFR mutated NSCLC patients who carried programmed death ligand 1 (PD-L1) tumor proportion score (TPS) greater than 50% progressed after EGFR-TKI therapy. In this study, we retrospectively investigated the outcomes of ICI-based treatments for EGFR mutated NSCLC patients carried PD-L1 TPS≥50% after developing EGFR-TKI resistance and to explore the population that may benefited from ICI-based treatment.

Methods: We retrospectively collected data of advanced NSCLC patients with EGFR mutations and PD-L1 TPS≥50% who have failed prior EGFR-TKI therapies without T790M mutation at Shanghai Chest Hospital between January 2018 and June 2021. Progression-free survival (PFS) and overall survival (OS) were utilized to evaluate the outcomes of this study.

Results: A total of 146 patients were included. Up to June 20th, 2022, median follow-up was 36.7 months (IQR, 12.5-44.2 months). Among the population, 66 patients (45.2%) received chemotherapy, the remaning (54.8%) received ICI-based treatment, including 56 patients(70.0%) received ICI combined with chemotherapy (IC) and 24 patients (30.0%) received ICI monotherapy (IM). In IC group,31 patients received ICI combined with chemotherapy,19 patients received ICI combined with antiangiogenic therapy and remaing received ICI combined with chemotherapy and antiangiogenic therapy. Survival analysis shown that patients who received ICI-based treatment had better progress-free survival (PFS) and overall survival (OS) compared with those treated with other therapy (median PFS, 10.0 vs. 4.0 months, P<0.001; median OS, 39.5 vs. 24.2 months, P<0.001). What's more, patients who treated with IC treatment had a superior survival time than those received IM treatment (median PFS, 10.3 vs. 7.0 months, P<0.001; median OS, 41.6 vs. 32.4 months, P<0.001). Subgroup analysis found that the PFS and OS benefit of IC was evident in all subgroups.

Conclusions: For advanced NSCLC patients with EGFR mutations and PD-L1 TPS≥50% who have failed prior EGFR-TKI therapies without T790M mutation, ICI-based treatment could provide a more favorable survival than classical chemotherapy. What' s more, compared with ICI monotherapy, ICI combined with chemotherapy seems to be the preferred treatment.

KEYWORDS

non-small-cell lung cancer, immunotherapy, drug resistance, epidermal growth factor receptor-tyrosine kinase inhibitor (EGFR-TKI), programmed death ligand 1 (PD-L1)

Introduction

Lung cancer remains the most prevalent malignancy worldwide, with non-small cell lung cancer (NSCLC) accounting for approximately 85% of all newly diagnosed lung cancers (1, 2). For patients with advanced NSCLC harboring epidermal growth factor receptor (EGFR) mutations, EGFR-tyrosine kinase inhibitors (EGFR-TKIs) are usually considered the first-line treatment (3–5). However, drug-acquired resistance is inevitable. Platinum-based chemotherapy remains the standard of care for patients with non-small cell lung cancer (NSCLC) with epidermal growth factor receptor (EGFR) mutations after developing EGFR-TKI resistance without EGFR T790M mutation, while the clinical benefit was limited (6).

In recent years, immune checkpoint inhibitors have dramatically changed the standard of care for patients with advanced NSCLC. Nevertheless, the response to immunotherapy seems to vary depending on the inherent immune microenvironment (7, 8). For example, NSCLC patients with PD-L1 tumor proportion score (TPS) ≥ 50% seem to benefit from immunotherapy, but for those carrying EGFR-sensitive mutations and ALK rearrangements (EGFR+/ALK+), the response to immunotherapy appears to be poor.

Few studies have investigated second-line treatment strategies for EGFR-mutant NSCLC patients carrying PD-L1 TPS greater than 50% who progressed after EGFR-TKI therapy. The possible reason for this is that EGFR-mutated NSCLC usually has a lower level of PD-L1 expression (9, 10), and NSCLC patients carrying EGFR mutations with PD-L1 TPS greater than 50% account for approximately 11.8% of all non-small cell lung cancers. In this study, we retrospectively investigated the outcome of NSCLC patients with EGFR mutations carrying PD-L1 TPS ≥ 50% after developing EGFR-TKI resistance with ICI therapy and explored the population that may benefit from ICI therapy.

Materials and methods

Study design and patients

We retrospectively collected 2037 patients carrying EGFR mutations treated at Shanghai Chest Hospital between January 2018 and June 2021 and identified them from the database. Our inclusion criteria indluding (1): diagnosed with non-small cell lung cancer; (2) carry EGFR mutations; (3) receive EGFR-TKI as first line treatment. Some of these patients were excluded according to the following criteria: (1) other driver mutations; (2) any recent surgery; (3) negative PD-L1 expression or PD-L1 TPS < 50%; (4) diagnosis of other tumors; (5) incomplete clinical information; (6) missed follow-up; (7) receiving chemotherapy or immunotherapy in first-line treatment and (8) carry T790M mutation after developing EGFR-TKI resistance. Also, clinicopathological characteristics such as gender, age, TNM stage, smoking history, histology, and treatment details were recorded. This study was approved by the Institutional Review Board of the Shanghai Chest Hospital and was conducted following the Declaration of Helsinki.

Detection of genes and PD-L1 TPS

Tissue samples were obtained at disease diagnosis before first-line treatment or after developing EGFR-TKI resistance, and EGFR mutations were detected by next-generation sequencing (NGS) or single-gene test (LungCureCDx, Burning Rock, Suzhou, China). Assessment of PD-L1 expression before first-line therapy or or after developing EGFR-TKI resistance by PD-L1 IHC 22C3 pharmDx assay (Agilent Technologies China, Beijing, China)

Assessment and treatment

According to the International Association for the Study of Lung Cancer (IASLC) 8th edition tumor-node-metastasis (TNM) classification, the clinical stage was determined at the time of disease diagnosis. High-resolution chest computed tomography (HRCT) and abdominal ultrasound scans were performed every 6-8 weeks after treatment initiation to assess tumor response. For patients without brain metastases at baseline or without associated symptoms after that, brain magnetic resonance imaging (MRI) was performed every six months. Tumor response was assessed according to the Response Evaluation Criteria in Solid Tumors (RECIST version 1.1).

Experienced physicians completed all evaluations, and therapeutic schedules were decided and adjusted according to the patient's condition and disease progression (including

chemotherapy, anti-angiogenesis treatment, immunotherapy and their combinations).

Follow up

Patients' follow-up data were obtained from regular clinical records. Patients receiving chemotherapy or immunotherapy would be admitted monthly, while other outpatients were required to follow up at least every two months. Telephone interviews were also used to verify the information and to contact patients who were not followed up regularly. The primary endpoints of this study were PFS (from initiation of immunotherapy to disease progression or death; if patients do not receive PD-1 inhibitors, then d0 should be the start of second-line therapy) and OS (from initiation of immunotherapy to death or last follow-up). If the patient died, a date was used as the last follow-up.

Statistical analysis

Categorical variables were compared using the Chi-square and Fisher's exact test (percentage calculated). Median PFS and median OS, and between-group survival differences were determined using the Kaplan-Meier (KM) method and the Log-rank test. Univariate and multivariate analyses were performed using Cox proportional hazards models for significant independent risk factors for PFS and OS. Factors with $P < 0.2$ in univariate analysis were further incorporated into the multivariate analysis. All P values were two-sided, and statistically significant differences were considered when $p < 0.05$. All statistical analyses were performed using SPSS version 28.0 (IBM Corporation, Armonk, NY, USA) and R software (version 4.0.2, R Foundation for Statistical Computing, Vienna, Austria).

Results

Patient characteristics

After screening, 146 patients met the above criteria and were divided into three groups. Patients received either chemotherapy (n=32), anti-angiogenesis(n=11) or both(n=13) were included in the immunotherapy negative (IN) group. Similarly, patients in the IM group received ICI monotherapy (n = 24, 16.4%), and in the IC group received both immunotherapy and anti-angiogenic therapy or chemotherapy (n = 56, 38.35%, Figure 1). Complete baseline characteristics of both groups are shown in Table 1. 78 (53.4%) patients were male, 68 (46.4%) were female, 81 patients were under 65 years of age (55.5%), and most of them were stage IV (91.1%). In addition, 62 (42.5%) were former or current smokers. All variables were balanced between the two groups and did not differ statistically ($p > 0.05$).

Pathological specimens from all patients were tested for EGFR mutations by single-gene test or NGS. 58 (39.7%) patients had EGFR exon 19 deletions, 75 (51.4%) patients had EGFR exon 21 L858R mutations, 13(8.9%) patients carried EGFR T790M mutation and 20 (13.7%) patients had other rare EGFR mutations, such as S768I missense mutation (n=2), C797S cis-mutation (n=3), exon 20ins (n=2), R776X missense mutation (n=5), G719X missense mutation (n=8), G724S missense mutation (n=2) and L861Q missense mutation (N=1). Incidentally, the most common combined mutation was TP53 (n = 72, 49.32%), and various missense mutations (n = 53, 73.61%) were most common among TP53 mutations (Figure 1).

Survival analysis

Until June 20th, 2022, the median follow-up time was 36.7 months (IQR, 12.5-44.2 months). Among a total of 146 patients,

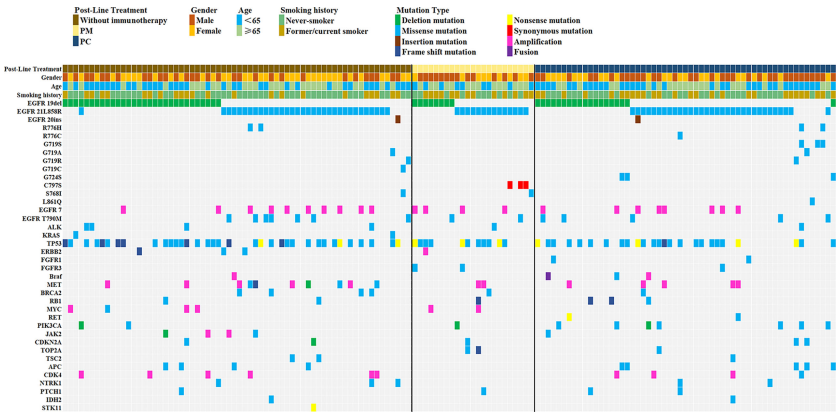

FIGURE 1
Molecular features of the EGFR-mutated NSCLC patients with PD-L1≥50% who developed EGFR-TKI resistance.

10.3389/fimmu.2023.1161718

TABLE 1 Clinical characteristics for all patients.

Characteristics	Total cohort (n=146) (%)	Immunotherapy		*P* value
		Without (n=66) (%)	With (n=80) (%)	
Gender				0.080
Male	78 (53.4)	30 (45.5)	48 (60.0)	
Female	68 (46.6)	36 (54.5)	32 (40.0)	
Age(y)				0.898
<65	81 (55.5)	37 (56.1)	44 (55.0)	
≥65	65 (44.5)	29 (43.9)	36 (45.0)	
Smoking History				0.091
Never-smoker	84 (57.5)	43 (65.2)	41 (51.2)	
Former/current smoker	62 (42.5)	23 (34.8)	39 (48.8)	
TNM stage				0.215
III	13 (8.9)	8 (12.1)	5 (6.3)	
IV	133 (91.1)	58 (87.9)	75 (93.7)	
Histology				0.196
Squamous	2 (1.4)	0 (0.0)	2 (2.5)	
Adenocarcinoma	144 (98.6)	66 (100.0)	78 (97.5)	
ECOG-PS				0.472
0-1	136 (93.2)	63 (95.5)	73 (91.2)	
2	10 (6.8)	3 (4.5)	7 (8.8)	
EGFR mutation type				0.298
19del	59 (40.4)	31 (47.0)	28 (35.0)	
21L858R	75 (51.4)	31 (47.0)	44 (55.0)	
Otders	12 (8.2)	4 (6.0)	8 (10.0)	
Primary brain metastasis				0.210
Yes	43 (29.5)	16 (19.4)	27 (23.6)	
No	103 (70.5)	50 (46.6)	53 (56.4)	
Primary liver metastasis				0.517
Yes	11 (7.5)	6 (9.1)	5 (6.3)	
No	135 (92.5)	60 (90.9)	75 (93.7)	
EGFR-TKI				0.358
Gefitinib	51 (34.9)	21 (31.9)	30 (37.5)	
Icotinib	53 (36.3)	22 (33.3)	31 (38.8)	
Erlotinib	7 (4.8)	5 (7.6)	2 (2.5)	
Afatinib	10 (6.8)	4 (6.1)	6 (7.5)	
Osimertinib	23 (15.8)	13 (19.6)	10 (12.5)	
Dacomitinib	2 (1.4)	1 (1.5)	1 (1.2)	

tumor progression occurred in all patients. 43 (29.5%) patients had brain metastasis, and 16 (11.0%) patients had liver metastasis. Most recurrent sites were in the lungs (42.86%), bones (15.07%), and brain (11.64%).

Survival analysis showed that patients treated with ICIs had better progression-free survival (PFS) and overall survival (OS) compared with those treated with other treatments (median PFS, 10.0 vs. 4.0 months, P < 0.001; median OS, 39.5 vs. 24.2 months, P < 0.001, Figure 2).

Factors affecting PFS and OS were enrolled (Tables 2, 3). Cox proportional-hazards models were used to analyze the factors that might impact PFS and OS. P < 0.2 was considered significant in the univariable analysis. In the univariate analysis, we found that ECOG PS state, EGFR mutation type, primary liver metastasis, and post-line immunotherapy were significant factors affecting PFS (p < 0.001, p = 0.120, p = 0.038, and p < 0.001, respectively) to improve sensitivity. These variables were further incorporated into the multivariate analysis, which showed that poor PS state, primary liver metastasis, and absence of immunotherapy were independent predictors of PFS (p < 0.001, p = 0.044, p < 0.001, respectively; Table 2). In terms of OS, univariate analysis revealed that age, ECOG PS state, primary liver metastasis, and post-line immunotherapy were significant factors for OS (p = 0.122, p = 0.006, p = 0.032, p = 0.012, respectively). Further multivariate analysis showed that all these variables were also independent risk factors for OS (p = 0.008, p = 0.037, p = 0.005, respectively; Table 3).

Immunotherapy

We further analyzed the differences between the IC and IM groups (n = 80). All variants were balanced between IM and IC patients, except for physicians' preference to use combination therapy in second-line treatment rather than further treatment (p = 0.01, Table 4). The objective response rate to immunotherapy reached 41.3% (n = 33), with 39 patients (48.2%) having stable disease and eight patients (11.0%) having progressive disease (Figure 3A).

In our study, subgroup analysis revealed that the PFS and OS benefit of IC was significant in most subgroups, except for patients

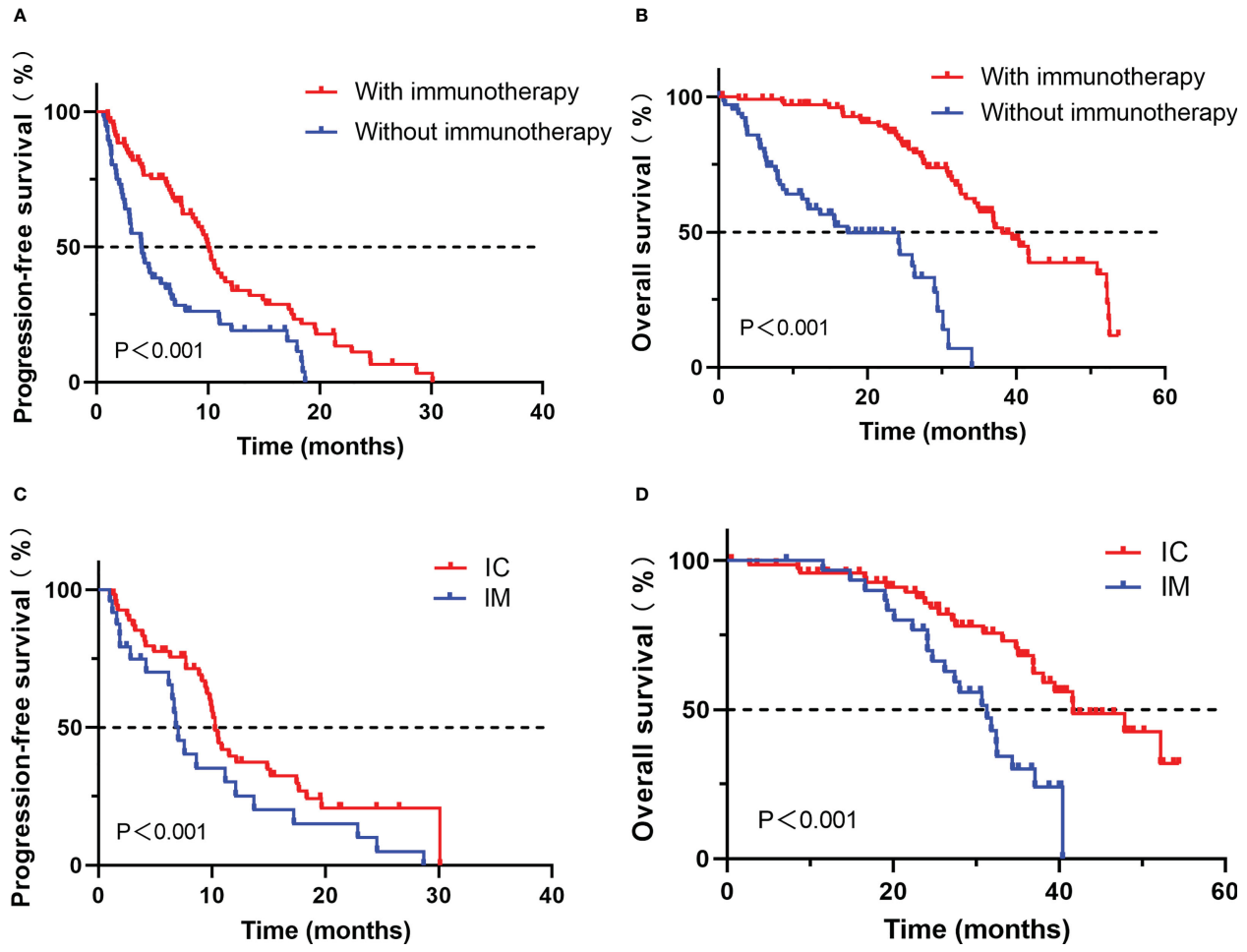

FIGURE 2
Comparison of progression-free survival **(A)** and overall survival **(B)** for advanced NSCLC patients with PD-L1≥50% who developed EGFR-TKI resistance treated with or without immunotherapy; Comparison of progression-free survival **(C)** and overall survival **(D)** for advanced NSCLC patients with PD-L1≥50% who developed EGFR-TKI resistance treated with IC or IM.

10.3389/fimmu.2023.1161718

TABLE 2 Univariable and multivariable analysis for progression-free survival (PFS) in all patients.

Characteristics	Univariable analysis			Multivariable analysis		
	HR	95%CI	*P*	HR	95%CI	*P*
Gender			0.416			
Male	reference					
Female	0.852	0.579-1.254				
Age(y)			0.740			
<65	reference					
≥65	0.937	0.640-1.373				
Smoking History			0.315			
Yes	reference					
No	0.892	0.830-1.782				
TNM stage			0.948			
III	reference					
IV	1.021	0.544-1.917				
Histology			0.676			
Squamous	reference					
Adenocarcinoma	0.741	0.182-3.019				
ECOG-PS			**<0.001**			**<0.001**
0-1	reference			reference		
2	5.675	2.544-7.658		5.363	2.376-12.106	
EGFR mutation type			0.120			0.363
19del	reference			reference		
21L858R	0.764	0.509-1.145	0.192	0.329	0.547-1.257	0.377
Otders	0.908	0.453-1.821	0.074	1.312	0.638-2.699	0.461
Primary brain metastasis			0.901			
Yes	reference					
No	1.027	0.673-1.569				
Primary liver metastasis			**0.038**			**0.044**
Yes	reference			reference		
No	0.481	0.241-0.959		0.572	0.278-0.902	
Post-line immunotderapy			**<0.001**			**<0.001**
Yes	reference			reference		
No	2.183	1.465-3.253		2.201	1.460-3.318	

ECOG-PS, Eastern cooperative oncology group-performance status; EGFR, epidermal growth factor receptor.
The bold values mean these characters are both significant in univariable and multivarible analysis.

with primary liver metastases and other mutations of EGFR, because the sample was too small to calculate HR and 95% CI (Figures 3B, C).

Change in PD-L1 expression

Among 38 patients who underwent PD-L1 immunohistochemical testing after developing EGFR-TKI resistance, we also explored changes in PD-L1 expression in tumor cells between before receiving EGFR-TKI treatment and the development of drug resistance. PD-L1 expression was remarkablely increased after receiving EGFR-TKI treatment (p=0.044, Figure 4A). Then, association of PD-L1 expression postprogression with efficacy of post-line ICI treatment was investigated. among those patients whose PD-L1 expression improved after developing EGFR-TKI resistance, survival analysis showed that treated with ICIs had better progression-free survival

10.3389/fimmu.2023.1161718

TABLE 3 Univariable and multivariable cox regression analysis for overall survival (OS) in all patients.

Characteristics	Univariable analysis			Multivariable analysis		
	HR	95%CI	*P*	HR	95%CI	*P*
Gender			0.322			
Male	reference					
Female	0.767	0.454-1.297				
Age(y)			0.122			0.130
<65	reference			reference		
≥65	1.524	0.894-2.600		1.519	0.885-2.610	
Smoking History			0.734			
Yes	reference					
No	0.915	0.548-1.528				
TNM stage			0.400			
III	reference					
IV	1.441	0.616-3.372				
Histology			0.368			
Squamous	reference					
Adenocarcinoma	0.377	0.195-1.665				
ECOG-PS			**0.006**			**0.008**
0-1	reference			reference		
2	2.210	1.191-3.841		2.270	1.112-3.877	
EGFR mutation type			0.531			
19del	reference					
21L858R	0.789	0.452-1.379	0.406			
Otders	1.231	0.502-3.015	0.650			
Primary brain metastasis			0.745			
Yes	reference					
No	0.912	0.522-1.592				
Primary liver metastasis			**0.032**			**0.037**
Yes	reference			reference		
No	0.457	0.194-0.772		0.550	0.230-0.793	
Post-line immunotderapy			**0.012**			**0.005**
Yes	reference			reference		
No	1.963	1.163-3.314		2.184	1.273-3.746	

ECOG-PS, Eastern cooperative oncology group-performance status; EGFR, epidermal growth factor receptor.
The bold values mean these characters are both significant in univariable and multivarible analysis.

(PFS) and overall survival (OS) compared with those treated with other treatments (PFS, P < 0.005; OS, P < 0.040, Figures 4B, C).

Discussion

The applicability of ICI-based therapies to patients with EGFR-mutated NSCLC who carry PD-L1 TPS > 50% and progress after EGFR-TKI therapy remains controversial. Our investigations suggest that ICI-based treatment may provide more favorable survival for these patients than classical chemotherapy. ICI combined with chemotherapy seems to be the preferred therapy compared to ICI monotherapy.

Previous studies have shown that patients with advanced NSCLC carrying EGFR mutations have a poor response to immunotherapy, and a possible mechanism for this poor

10.3389/fimmu.2023.1161718

TABLE 4 Clinical characteristics for patients with immunotherapy.

Characteristics	Total (n=80) (%)	Immunotherapy (n=80)		*P* value
		IM(n=24)(%)	IC (n=56) (%)	
Gender				0.765
Male	48(60)	15(62.5)	33(58.9)	
Female	32(40)	9(37.5)	23(41.1)	
Age(y)				0.117
<65	44(55)	10(41.7)	34(60.7)	
≥65	36(45)	14(58.3)	22(39.3)	
Smoking History				0.526
Never-smoker	41(51.2)	11(45.8)	30(53.6)	
Former/current smoker	39(48.8)	13(54.2)	26(46.4)	
TNM stage				0.131
III	5(6.2)	0(0)	5(8.9)	
IV	75(93.8)	24(100.0)	51(91.1)	
Histologgy				/
Squamous	0	0	0	
Adenocarcinoma	80(100)	24(100)	56(100)	
ECOG-PS				0.370
0-1	76(95.0)	22(91.7)	54(96.4)	
2	4(5.0)	2(8.3)	2(3.6)	
EGFR mutation type				0.523
19del	28(35.0)	9(37.5)	19(33.9)	
21L858R	44(55.0)	14(58.3)	30(53.6)	
Otders	8(10.0)	1(4.2)	7(12.5)	
Primary brain metastasis				0.327
Yes	27(33.8)	10(41.7)	17(30.4)	
No	53(66.3)	14(58.3)	39(69.6)	
Primary liver metastasis				0.131
Yes	5(6.2)	3(12.5)	2(3.6)	
No	75(93.8)	21(87.5)	54(96.4)	
Treatment line of immunotderapy				**0.010**
Second line	34(42.5)	5(20.8)	29(51.8)	
Third or after line	46(57.5)	19(79.2)	27(48.2)	
Immunotderapy				0.389
Pembrolizumab	39(48.8)	12(50.0)	27(48.2)	
Nivolumab	24(30.0)	9(37.5)	15(26.8)	
Otders	17(21.2)	3(12.5)	14(25.0)	

ECOG-PS, Eastern cooperative oncology group-performance status; EGFR, epidermal growth factor receptor.
The bold values mean these characters are both significant in univariable and multivarible analysis.

10.3389/fimmu.2023.1161718

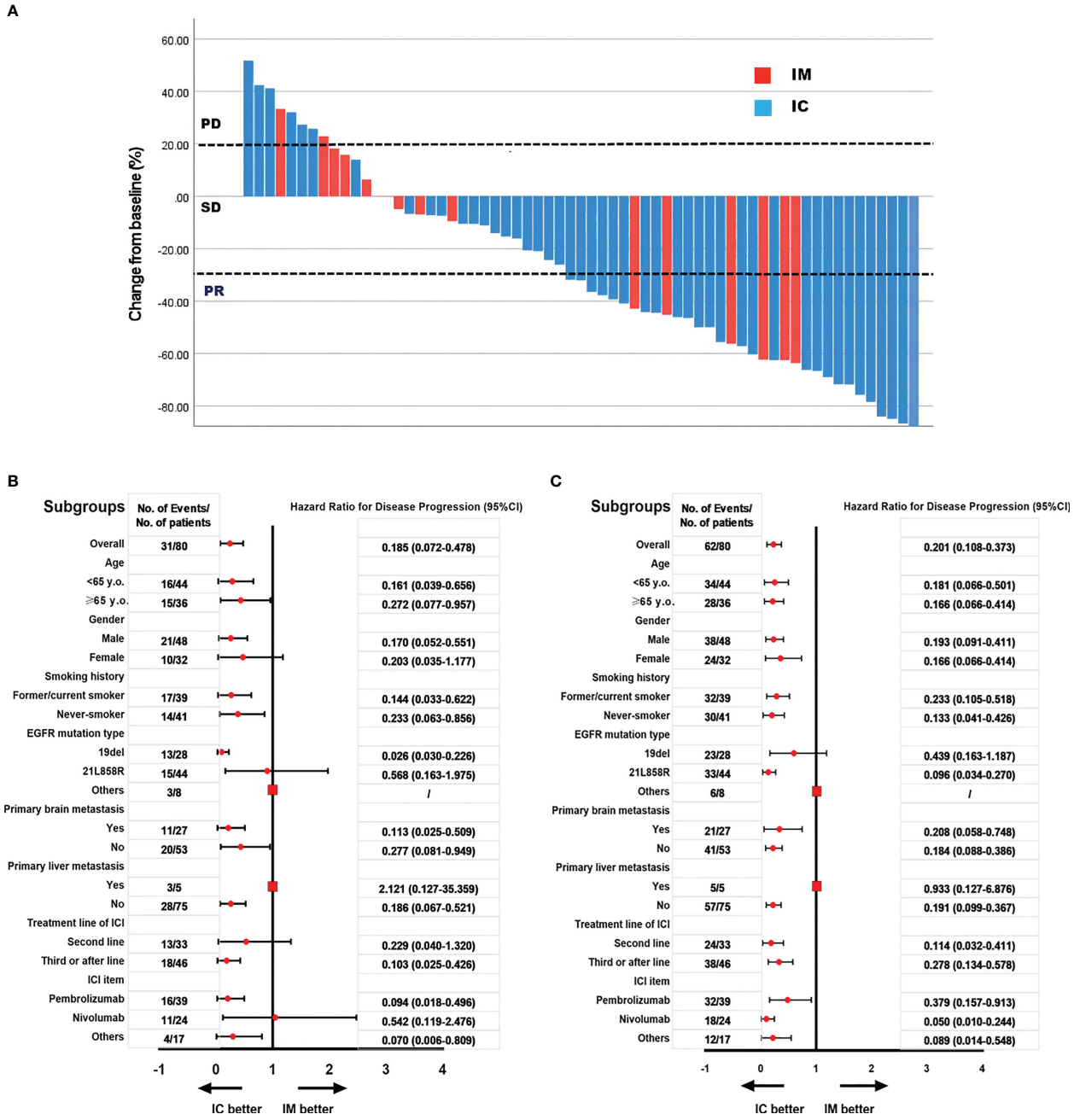

FIGURE 3
The objective response rate is shown as a percent change of target lesions from baseline in IC and IM groups **(A)**; Subgroups analysis of PFS in IC and IM groups **(B)**; Subgroups analysis of OS in IC and IM groups **(C)**.

response is the low expression of PD-L1 or the lack of infiltrating T cells in the tumor microenvironment (TME) (11–14). The TME generalization may change with the progression of the tumor, and therefore, resistance to EGFR-TKI may enhance the response to immunotherapy response (7, 15, 16). As reported in the EGFR +/ALK+ cohort in the ATLANTIC study, if PD-L1 expression is greater than 25%, monotherapy with durvalumab led to favorable outcomes with median PFS and OS of 1.9 and 13.3 months, respectively (17).

Previous studies have reported that chemotherapy alone may be the best option when resistance to EGFR-TKI is present (18). In the present study, we compared the outcomes of ICI-based therapy with chemotherapy alone and found that ICI-based treatment had a significant prognostic advantage.

The combination of chemotherapy and immunotherapy enhances the infiltration of effector T cells and downregulates the expression of immunosuppressive cells (19, 20). Ultimately, the efficacy of immunotherapy may be improved. A critical phase II study showed that in EGFR-TKI-resistant NSCLC, ICI combined with chemotherapy resulted in good objective remission rates (ORR, 50%) and survival time (PFS, 7.0 months; OS, 23.5 months) (21). More importantly, a retrospective study also

10.3389/fimmu.2023.1161718

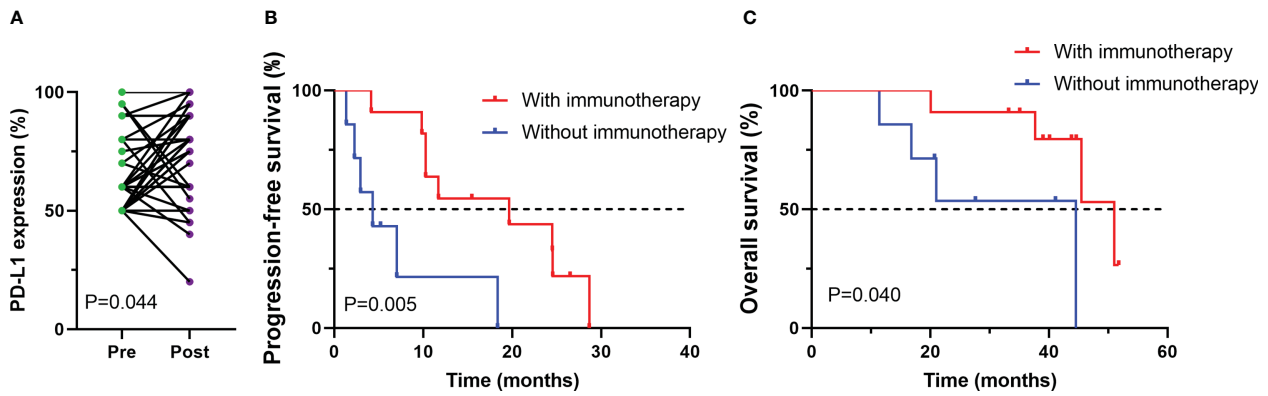

FIGURE 4
Changes in PD-L1 expression between before (pre) and after (post) EGFR-TKI treatment for patients with available paired tumor samples **(A)**; Progression-free survival (PFS) **(B)** and overall survival (OS) **(C)** among patients whose PD-L1 expression improved after developing EGFR-TKI resistance.

showed the value of ICI combination chemotherapy in metastatic NSCLC after EGFR-TKI resistance (22). In our study, ICI combination therapy resulted in PFS of 10.3 months and OS of 41.6 months in NSCLC patients carrying EGFR mutations and PD-L1 TPS ≥ 50% after developing EGFR-TKI resistance without T790M mutations. The survival time in this study was longer than other studies. The possible reason was that the population included in our study had a higher level of PD-L1 expression than other studies, and NSCLC patients with PD-L1 TPS ≥ 50% seemed to benefit from immunotherapy. Subgroup analysis in our study found that the PFS and OS benefit of IC was significant in most subgroups, except for patients with primary liver metastases and other mutations in EGFR, because the sample was too small to calculate HR and 95% CI.

PD-L1 expression is an effective predictor for ICI response in NSCLC (23). Previous study found that targeted therapy was associated with a significant increase in PD-L1 expression in tumor cells in postprogression tumor samples compared with those obtained at baseline, especially in the case of T790M-negative patients (24). Our reseaech also found that PD-L1 expression was remarkablely improved after receiving EGFR-TKI treatment. Among those patients whoso PD-L1 expression improved after developing EGFR-TKI resistance, survival analysis showed that treated with ICIs had better progression-free survival (PFS) and overall survival (OS) compared with those treated with other treatments, which means improved PD-L1 expression after developing EGFR-TKI resistance may indicate a good response to immunotherapy in poster-line treatment.

Several possible limitations can be seen in our study. First, this study is a retrospective single-center study, which inevitably causes selection bias. Secondly, the lack of sufficient tissue samples for exploratory analysis is a limitation of this study. Therefore, we could only perform PD-L1 status testing on a limited number of specimens before ICI treatment. Multicenter prospective and large sample studies are expected to provide more comprehensive insights into EGFR-mutated NSCLC patients carrying PD-L1 TPS > 50%.

In conclusion, our study suggests that for patients with advanced NSCLC with EGFR mutations and PD-L1 TPS ≥ 50% who have failed prior EGFR-TKI therapies without T790M mutation, ICI-based treatment could provide more favorable survival than classical chemotherapy. More importantly, ICI combination therapy was superior to ICI monotherapy.

Data availability statement

The sequencing data presented in the study are deposited in the Figshare repository (https://figshare.com/articles/dataset/Patient_genetic_data_xlsx/22664644).

Ethics statement

The studies involving human participants were reviewed and approved by the Institutional Review Board of the Shanghai Chest Hospital. The patients/participants provided their written informed consent to participate in this study.

Author contributions

WZ, BH, YQL and YJL: study conceptualization and manuscript revision. YJL, HJ and FQ: paper writing. YC, WSZ and YJL: data analysis and figures. YZ and JL: clinical data collection. WZ, BH and YQL: study progress supervision. All authors listed have made a substantial, direct, and intellectual contribution to the work and approved it for publication. All authors contributed to the article and approved the submitted version.

Funding

This research was supported by grants from Shanghai Shen Kang Hospital Development Center Clinical Research Plan of SHDC (SHDC2020CR4017).

Conflict of interest

The authors declare that the research was conducted in the absence of any commercial or financial relationships that could be construed as a potential conflict of interest.

Publisher's note

Supplementary material

The Supplementary Material for this article can be found online at: https://www.frontiersin.org/articles/10.3389/fimmu.2023.1161718/full#supplementary-material

References

1. Chen P, Liu Y, Wen Y, Zhou C. Non-small cell lung cancer in China. *Cancer Commun (Lond)* (2022) 42(10):937–70. doi: 10.1002/cac2.12359

2. Qiu H, Cao S, Xu R. Cancer incidence, mortality, and burden in China: a time-trend analysis and comparison with the united states and united kingdom based on the global epidemiological data released in 2020. *Cancer Commun (Lond)* (2021) 41 (10):1037–48. doi: 10.1002/cac2.12197

3. Tian X, Gu T, Lee MH, Dong Z. Challenge and countermeasures for EGFR targeted therapy in non-small cell lung cancer. *Biochim Biophys Acta Rev Cancer* (2022) 1877(1):188645. doi: 10.1016/j.bbcan.2021.188645

4. Majeed U, Manochakian R, Zhao Y, Lou Y. Targeted therapy in advanced non-small cell lung cancer: current advances and future trends. *J Hematol Oncol* (2021) 14 (1):108. doi: 10.1186/s13045-021-01121-2

5. lanchard D. Adjuvant osimertinib in EGFR-mutated non-Small-Cell lung cancer. *N Engl J Med* (2020) 383(18):1780–2. doi: 10.1056/NEJMe2029532

6. Passaro A, Jänne PA, Mok T, Peters S. Overcoming therapy resistance in EGFR-mutant lung cancer. *Nat Cancer* (2021) 2(4):377–91. doi: 10.1038/s43018-021-00195-8

7. Madeddu C, Donisi C, Liscia N, Lai E, Scartozzi M, Macciò A. EGFR-mutated non-small cell lung cancer and resistance to immunotherapy: Role of the tumor microenvironment. *Int J Mol Sci* (2022) 23(12):6489. doi: 10.3390/ijms23126489

8. Qiao M, Jiang T, Liu X, Mao S, Zhou F, Li X, et al. Immune checkpoint inhibitors in EGFR-mutated NSCLC: Dusk or dawn? *J Thorac Oncol* (2021) 16(8):1267–88. doi: 10.1016/j.jtho.2021.04.003

9. Dong ZY, Zhang JT, Liu SY, Su J, Zhang C, Xie Z, et al. EGFR mutation correlates with uninflamed phenotype and weak immunogenicity, causing impaired response to PD-1 blockade in non-small cell lung cancer. *Oncoimmunology* (2017) 6(11):e1356145. doi: 10.1080/2162402X.2017.1356145

10. Masuda K, Horinouchi H, Tanaka M, Higashiyama R, Shinno Y, Sato J, et al. Efficacy of anti-PD-1 antibodies in NSCLC patients with an EGFR mutation and high PD-L1 expression. *J Cancer Res Clin Oncol* (2021) 147(1):245–51. doi: 10.1007/s00432-020-03329-0

11. Tian T, Yu M, Li J, Jiang M, Ma D, Tang S, et al. Front-line ICI-based combination therapy post-TKI resistance may improve survival in NSCLC patients with EGFR mutation. *Front Oncol* (2021) 11:739090. doi: 10.3389/fonc.2021.739090

12. Mazieres J, Drilon A, Lusque A, Mhanna L, Cortot AB, Mezquita L, et al. Immune checkpoint inhibitors for patients with advanced lung cancer and oncogenic driver alterations: results from the IMMUNOTARGET registry. *Ann Oncol* (2019) 30 (8):1321–8. doi: 10.1093/annonc/mdz167

13. Gao G, Ni J, Wang Y, Ren S, Liu Z, Chen G, et al. Efficacy and safety of camrelizumab plus apatinib in previously treated patients with advanced non-small cell lung cancer harboring EGFR or ALK genetic aberration. *Transl Lung Cancer Res* (2022) 11(6):964–74. doi: 10.21037/tlcr-22-22

14. Zhou F, Zhou C. Chemotherapy should be combined with checkpoint inhibitors in the treatment of patients with stage IV EGFR-mutant NSCLC whose disease has progressed on all available tyrosine kinase inhibitors. *J Thorac Oncol* (2021) 16 (10):1622–6. doi: 10.1016/j.jtho.2021.07.011

15. Han JJ, Kim DW, Koh J, Keam B, Kim TM, Jeon YK, et al. Change in PD-L1 expression after acquiring resistance to gefitinib in EGFR-mutant non-Small-Cell lung cancer. *Clin Lung Cancer* (2016) 17(4):263–70.e2. doi: 10.1016/j.cllc.2015.11.006

16. Haratani K, Hayashi H, Tanaka T, Kaneda H, Togashi Y, Sakai K, et al. Tumor immune microenvironment and nivolumab efficacy in EGFR mutation-positive non-small-cell lung cancer based on T790M status after disease progression during EGFR-TKI treatment. *Ann Oncol* (2017) 28(7):1532–9. doi: 10.1093/annonc/mdx183

17. Garassino MC, Cho BC, Kim JH, Mazières J, Vansteenkiste J, Lena H, et al. Durvalumab as third-line or later treatment for advanced non-small-cell lung cancer (ATLANTIC): an open-label, single-arm, phase 2 study. *Lancet Oncol* (2018) 19 (4):521–36. doi: 10.1016/S1470-2045(18)30144-X

18. Wu SG, Shih JY. Management of acquired resistance to EGFR TKI-targeted therapy in advanced non-small cell lung cancer. *Mol Cancer* (2018) 17(1):38. doi: 10.1186/s12943-018-0777-1

19. Bylicki O, Paleiron N, Margery J, Guisier F, Vergnenegre A, Robinet G, et al. Targeting the PD-1/PD-L1 immune checkpoint in EGFR-mutated or ALK-translocated non-Small-Cell lung cancer. *Target Oncol* (2017) 12(5):563–9. doi: 10.1007/s11523-017-0510-9

20. Liu SY, Dong ZY, Wu SP, Xie Z, Yan LX, Li YF, et al. Clinical relevance of PD-L1 expression and CD8+ T cells infiltration in patients with EGFR-mutated and ALK-rearranged lung cancer. *Lung Cancer* (2018) 125:86–92. doi: 10.1016/j.lungcan.2018.09.010

21. Garassino MC, Cho BC, Kim JH, Mazières J, Vansteenkiste J, Lena H, et al. Final overall survival and safety update for durvalumab in third- or later-line advanced NSCLC: The phase II ATLANTIC study. *Lung Cancer* (2020) 147:137–42. doi: 10.1016/j.lungcan.2020.06.032

22. Cheng Y, Yang B, Ouyang W, Jie C, Zhang W, Chen G, et al. Is ICI-based therapy better than chemotherapy for metastatic NSCLC patients who develop EGFR-TKI resistance? A real-world investigation. *Front Oncol* (2022) 12:920047. doi: 10.3389/fonc.2022.920047

23. Patel SP, Kurzrock R. PD-L1 expression as a predictive biomarker in cancer immunotherapy. *Mol Cancer Ther* (2015) 14(4):847–56. doi: 10.1158/1535-7163.MCT-14-0983

24. Isomoto K, Haratani K, Hayashi H, Shimizu S, Tomida S, Niwa T, et al. Impact of EGFR-TKI treatment on the tumor immune microenvironment in EGFR mutation-positive non-small cell lung cancer. *Clin Cancer Res* (2020) 26(8):2037–46. doi: 10.1158/1078-0432.CCR-19-2027

frontiers | Frontiers in Immunology

TYPE Original Research
PUBLISHED 23 May 2023
DOI 10.3389/fimmu.2023.1185618

OPEN ACCESS

EDITED BY
Patrick Schmidt,
National Center for Tumor Diseases (NCT), Germany

REVIEWED BY
Sjoukje Van Der Stegen,
Memorial Sloan Kettering Cancer Center, United States
Achim Temme,
Technical University Dresden, Germany
Christian J. Buchholz,
Paul-Ehrlich-Institut (PEI), Germany

*CORRESPONDENCE
Dennis Christoph Harrer
dennis.harrer@ukr.de

RECEIVED 13 March 2023
ACCEPTED 15 May 2023
PUBLISHED 23 May 2023

CITATION
Harrer DC, Bezler V, Hartley J, Herr W and Abken H (2023) IRF4 downregulation improves sensitivity and endurance of CAR T cell functional capacities.
Front. Immunol. 14:1185618.
doi: 10.3389/fimmu.2023.1185618

IRF4 downregulation improves sensitivity and endurance of CAR T cell functional capacities

Dennis Christoph Harrer[1,2]*, Valerie Bezler[2], Jordan Hartley[2], Wolfgang Herr[1] and Hinrich Abken[2]

[1]Dept. Hematology and Medical Oncology, Clinic III Internal Medicine, University Hospital Regensburg, Regensburg, Germany, [2]Leibniz Institute for Immunotherapy, Div. Genetic Immunotherapy, Regensburg, Germany

Chimeric antigen receptor (CAR) modified T cells can induce complete remissions in patients with advanced hematological malignancies. Nevertheless, the efficacy is mostly transient and remains so far poor in the treatment of solid tumors. Crucial barriers to long-term CAR T cell success encompass loss of functional capacities known as "exhaustion", among others. To extend CAR T cell functionality, we reduced interferon regulatory factor 4 (IRF4) levels in CAR T cells using a one-vector system encoding a specific short-hairpin (sh) RNA along with constitutive CAR expression. At baseline, CAR T cells with downregulated IRF4 showed equal cytotoxicity and cytokine release compared to conventional CAR T cells. However, under conditions of repetitive antigen encounter, IRF4^{low} CAR T cells displayed enhanced functionality with superior cancer cell control in the long-term compared with conventional CAR T cells. Mechanistically, the downregulation of IRF4 in CAR T cells resulted in prolonged functional capacities and upregulation of CD27. Moreover, IRF4^{low} CAR T cells were more sensitive to cancer cells with low levels of target antigen. Overall, IRF4 downregulation capacitates CAR T cells to recognize and respond to target cells with improved sensitivity and endurance.

KEYWORDS
CAR, IRF4, exhaustion, sensitivity, tumor

1 Introduction

Chimeric antigen receptor (CAR) T cells evolved into a crucial pillar of cancer immunotherapy in recent years (1). Following long-lasting complete remissions in patients with advanced B-cell malignancies, regulatory authorities in the US and Europe issued approval for CAR T cell treatment in patients with refractory or relapsing acute lymphoblastic leukemia and specific lymphoma entities (2). While numerous clinical trials are successfully evaluating CAR T cell therapy in a wide variety of hematological malignancies, a sizable portion of patients does not benefit from CAR T cell therapy. Moreover, CAR T cell therapy of solid tumors showed poor results so far (3, 4). Given these insufficiencies, preclinical refinement of CAR T cell constructs is ongoing to improve and

extend the power of CAR T cell therapy and to overcome T cell dysfunctionality upon repetitive target engagement (5, 6).

T cell dysfunctionality, commonly termed "exhaustion", and entry into cell death are intrinsic barriers limiting T cell activation and finally therapeutic efficacy (7, 8). Hallmarks of T cell exhaustion include differentiation into the effector cell compartment, upregulation of inhibitory receptors, reduced proliferative capacity, lack of IL-2 production, as well as diminished cytotoxicity and reduced release of pro-inflammatory cytokines (9, 10). Based thereon, a plethora of efforts are currently undertaken to prevent or counteract CAR T cell exhaustion once the CAR recognizes its target. These efforts encompass the use of long-lived, self-renewing, multipotent T memory stem cells (TSCMs) (11, 12), the knockdown of inhibitory molecules (13–17), the engraftment of artificial IL-9 signaling (18), and the optimization of co-stimulatory signals to the CAR T cell (19–21). On the other hand, a growing body of evidence implies specific transcription factors, such as BLIMP-1 and TOX, in inducing and maintaining exhaustive phenotypes in CAR T cells (22, 23). Correspondingly, CAR T cells with knockdown of BLIMP-1 or TOX displayed a reduced propensity to exhaustion eventuating in an augmented CAR T cell functionality *in vitro* and superior CAR T cell performance in tumor bearing mice (24, 25).

More recently, the T cell receptor (TCR)-induced transcription factor interferon regulatory factor 4 (IRF4) is gaining attention in the context of T cell exhaustion. Seminal evidence linking IRF4 to T cell exhaustion was derived from mice with chronic lymphocytic choriomeningitis virus (LCMV) infection (26). In these mice, antigen-specific T cells expressed high IRF4 levels associated with upregulated inhibitory receptors, such as PD-1, repressed memory-associated regulators, like TCF1, and triggered metabolic stress reactions. The exhausted stage could be reversed by targeted decrease of IRF4 levels resulting in highly functional antigen-specific T cells with a memory-like phenotype (26). On the other hand, IRF4 was recently found to be upregulated in CARs with artificially high tonic signaling driving T cells into exhaustion (9). Overexpression of the transcription factor c-Jun abrogated T cell exhaustion in tonically signaling CARs. Remarkably, this process was accompanied by the downregulation of IRF4 and other exhaustion-associated genes regulated by IRF4 (9). Taken together, we see a crucial role of IRF4 in establishing and maintaining T cell exhaustion.

We here aimed at improving anti-cancer cell functionality of CAR T cells by reducing IRF4 levels. Given a physiological role for IRF4 in T cell biology, such as activation, expansion and functionality of $CD8^+$ T cells, we did not seek to completely abrogate IRF4 expression in CAR T cells (27, 28), but rather substantially reduce IRF4 levels. With respect to manufacturing, we newly designed a one-vector system that encodes both the shRNA for reducing IRF4 levels and the CAR for constitutive expression. Under conditions of repetitive antigen stimulation, CAR T cells with downregulated IRF4 performed superior with respect to anti-tumor effector functions as compared to conventional CAR T cells. Mechanistically, we observed that the downregulation of IRF4 in CAR T cells resulted in prolonged functionality and upregulation of CD27. Moreover, such CAR T cells were capable of targeting otherwise neglected target cells with low antigen levels demonstrating a strategy to improve CAR T cell sensitivity towards cancer cells.

2 Materials and methods

2.1 Cells and reagents

Peripheral blood mononuclear cells (PBMCs) were obtained by Lymphoprep centrifugation (Axis-Shield, Oslo, Norway) of blood from healthy donors upon informed consent and approval by the institutional review board. Isolated PBMCs were cryopreserved and stored at -80°C until experimental use. T cells were maintained in RPMI 1640 medium, 1% GlutaMAX (Gibco, ThermoFisher, Waltham, MA, USA), 100 IU/mL penicillin, 100 µg/mL streptomycin (Pan-Biotech, Aidenbach, Germany), 2 mM HEPES (PAA, Palo Alto, CA, USA), and 10% (v/v) heat-inactivated fetal calf serum (Pan-Biotech, Aidenbach, Germany). 293T cells are human embryonic kidney cells that express the SV40 large T antigen (ATCC CRL-3216), BxPC-3 (ATCC CRL-1420; American Type Culture Collection, Manassas, VA) and MIA PaCa-2 (ATCC CRL-1687) are human pancreatic cancer cells. Tumor cells were cultured in DMEM, 1% GlutaMAX (Gibco, ThermoFisher), 100 IU/mL penicillin, 100 µg/mL streptomycin (Pan-Biotech), and 10% (v/v) heat-inactivated fetal calf serum (Sigma-Aldrich, St. Louis, USA).

2.2 CAR T cell generation

Cryopreserved PBMCs were thawed and stimulated on the same day with the anti-CD3 monoclonal antibody (mAb) OKT-3, the CD28 mAb 15E8 and IL-2 (1000 IU/mL). Recombinant IL-2 (200 IU/mL) was added on days 2, 3, and 4 after activation (IL-2 was just added without performing a complete medium exchange). Retroviral transduction was performed as previously described in detail (29). Viral particles were added on day +2 and day +3 after activation of PBMCs. Four days after activation (day +4), CAR T cells were enriched by labeling CAR T cells with a biotinylated goat F(ab´)2 anti-human IgG antibody (Southern Biotech, Birmingham, AL, USA) followed by purification with anti-biotin microbeads (Miltenyi Biotec, Bergisch Gladbach, Germany). Following a 24-hour culture period in IL-2 free medium, CAR T cells were used for *in vitro* assays. Untransduced cells were generated by activation of PBMCs and subsequent expansion with IL-2, but without retroviral transduction. The CEA-specific CAR BW431/26scFv-Fc-CD28-ζ expression cassette was previously published (30). The vectors encoding the CEA-specific CAR together with shRNAs either targeting IRF4 (BW431/26scFv-Fc-CD28-ζ-I1, BW431/26scFv-Fc-CD28-ζ-I2) or kanamycin (BW431/26scFv-Fc-CD28-ζ-K) were synthesized by GenScript Biotech (Piscataway, N.J., USA). TRCN0000433892 was used to generate the shRNA for BW431/26scFv-Fc-CD28-ζ-I1. TRCN0000014764 was used to generate the shRNA for BW431/26scFv-Fc-CD28-ζ-I2. A well- characterized control shRNA targeting the kanamycin gene was used to generate BW431/26scFv-Fc-CD28-ζ-K (19). The shRNA

constructs were embedded in a modified miR-30 scaffold as previously described and inserted at the 3' end of the CAR construct (31, 32).

2.3 Flow cytometry

Cells were incubated with antibodies at 4°C for 15 min for surface staining. For intracellular staining, cells were fixed and permeabilized with the "Transcription Buffer" set (BD Biosciences, Franklin Lakes, NJ, USA) for 30 min at 4°C. For STAT5 staining, the "Transcription Factor Phospho Buffer Set" (BD Biosciences, Franklin Lakes, NJ, USA) was used according to the manufacturer´s instructions. The viability dye eFluor 780 (ThermoFisher, Waltham, MA, USA) was employed for live/dead discrimination. Fluorescent-minus-one (FMO) controls were used for gating. The goat F(ab')2 anti-human IgG-PE antibody and the goat F(ab')2 anti-human IgG-FITC antibody were purchased from SouthernBiotech to detect the CAR. The following antibodies were obtained from Miltenyi Biotech: FITC-conjugated anti-CD3 (clone BW 264/56), FITC-conjugated anti-CD8 (clone BW135/80), APC-conjugated anti-CD4 (clone VIT4), PE-conjugated anti-CD25 (clone 4E3), APC-conjugated anti-CD70 (clone REA292), and APC Vio770-conjugated anti-CD66abcde (clone TET2). The following antibodies were purchased from Biolegend (San Diego, CA, USA): PerCP-Cy5.5-conjugated anti-CD27 (clone M-T271), PerCP-Cy5.5-conjugated anti-TIGIT (clone A15153G), BV421-conjugated anti-CD3 (clone OKT3), PerCP-Cy5.5-conjugated anti-CD86 (IT2.2), PE-conjugated anti-41BBL (clone 5F4), PerCP-Cy5.5-conjugated anti-CD28, and PE-conjugated anti-IRF4 (clone IRF4.3E4) together with the corresponding isotype control antibody. The following antibodies were purchased from BD Biosciences: BV421-conjugated anti-TIM3 (clone 7D3), BV421-conjugated anti-CD62L (clone DREG-56), BV605-conjugated anti-CD45RO (clone UCHL1), BV421-conjugated anti-CD8 (clone RPA-T8), FITC-conjugated anti-CD80 (clone L307.4), BV421-conjuagted anti-CD137 (clone 4B4-1), and BV421-conjugated anti-pSTAT5 (clone 47/STAT5 pY694). Immunofluorescence was measured using a BD FACSLyric (BD Biosciences) equipped with FACSuite software (BD Biosciences). Data were analyzed using the FlowJo software version 10.7.1 Express 5 (BD Biosciences).

2.4 Western blot analysis

After a 24-hour co-culture period with BxPC-3 cells, untransduced T cells, CEA-28ζ-K (Ctrl) CAR T cells, and CEA-28ζ-I1 CAR T cells were lysed (3 x 10^6 cells per condition) and lysates were electrophoresed by SDS-PAGE in 4–12% (w/v) Bis-Tris gels under reducing conditions, blotted and probed with the anti–IRF4 mAb (clone IRF4.3E4, BioLegend) at 1:200 and by the peroxidase-labeled anti-rat IgG1 antibody (Sigma-Aldrich) at 1:5,000 dilution. Membranes were stripped and re-probed with peroxidase-labeled anti–β-actin antibody (Santa Cruz Biotechnology) at 1:20,000 dilution. Bands were detected by chemoluminescence (ChemiDoc Imaging System, BioRad).

2.5 Cytokine secretion

Cancer cells were seeded in 96 well round-bottom plates (1 x 10^5 cells/well) overnight, before addition of untransduced T cells or CAR T cells (1 x 10^5 cells/well). Alternatively, the anti-idiotypic monoclonal antibody BW2064/36 was coated overnight on 96 well plates at the indicated concentrations before adding CAR T cells (1 x 10^5 cells/well). After 48 hours of co-culture, IL-2 and IFN-γ in culture supernatants were detected by ELISA as previously described (33). TNF-α was detected using the "human TNF-α Standard ABTS ELISA Development Kit" (PeproTech, Cranbury, NJ, USA) according to the manufacturer´s instructions.

2.6 Cytotoxicity assay

CAR T cells (0.125-10 × 10^4 cells/well) were co-cultivated for 72 hours in 96 well round bottom plates with target cells (each 1 × 10^4 cells/well) at the indicated effector to target ratios. The XTT-based colorimetric assay employing the "Cell Proliferation Kit II" (Roche Diagnostics, Mannheim, Germany) was used to determine specific cytotoxicity. Viability of tumor cells was calculated as mean values of six wells containing only tumor cells subtracted by the mean background level of wells containing medium only. Formation of formazan due to the presence of T cells was determined from triplicate wells containing T cells in the same number as in the corresponding experimental wells. The percentage of viable tumor cells in experimental wells was calculated as follows: viability (%) = [OD(experimental wells - corresponding number of T cells)]/[OD (tumor cells without T cells - medium)] × 100. Cytotoxicity (%) was defined as 100 - viability (%).

2.7 Repetitive stimulation assay

BxPC-3 cells labeled with GFP were seeded in 12 well plates at 0.1 × 10^6 cells per well. After 24 hours, 0.1 × 10^6 CAR T cells were added per well. After three days (Round 1, R1), the wells were resuspended and harvested. Subsequently, the wells were trypsinized, resuspended with T cell medium, and pooled with the initial supernatant. Then, cells were washed with PBS and resuspended in 1 ml T cell medium. Finally, 100 µl were used for cell counting (live GFP^+ tumor cells and live $CD3^+$/CAR^+ CAR T cells) *via* flow cytometry using counting beads ("CountBright", ThermoFisher), and the remaining 900 µl were added to a new 12 well plate with 0.1 × 10^6 BxPC-3 cells for four days (round 2, R2). The procedure was reiterated for round 3 (R3) and round 4 (R4). For flow cytometric analyses, unlabeled BxPC-3 cells were employed, and three rounds (R1-R3) of stimulation were performed.

2.8 CD107a degranulation assay

Degranulation of CAR T cells in response to BxPC-3 cells was measured using a conventional CD107a staining. BxPC-3 cells were seeded overnight in 96 well plates at 0.05 × 10^6 cells per well. At the end of each round (R1-3) of stimulation, CEA-28ζ-K CAR T cells

and CEA-28ζ-I1 CAR T cells were re-stimulated with BxPC-3 cells. Monensin (eBioscience, San Diego, CA, USA) at a final concentration of 1 µM and a FITC-conjugated anti-CD107a antibody (BD Biosciences, San Jose, CA, USA, clone: H4A3) were added at the beginning of co-culture. Four hours later, T cells were stained with the viability dye eFluor 780, the goat F(ab')2 anti-human IgG-PE antibody, a BV421-conjugated anti-CD8 antibody (BD), and an APC-conjugated anti-CD4 antibody (Miltenyi Biotech). Subsequently, degranulation measured as $CD107a^+$ cells was analyzed *via* flow cytometry.

2.9 Phycoerythrin QuantiBRITE antigen density quantitation assay

The density of CEA on the surface of 293T cells, BxPC3-cells and MIA PaCa-2 cells was determined using the QuantiBRITE PE assay (LOT: #60550, BD) according to the manufacturer´s instructions in conjunction with a PE-labeled anti-CEA antibody (clone TET2, Miltenyi) using flow cytometry. The assay is predicated on a pre-calibrated standard bead set involving known numbers of fluorophore molecules bound per bead to calibrate and translate the intensity of fluorescence signals obtained by flow cytometry into the number of fluorophores.

2.10 Statistical analysis

Statistical analysis was performed using GraphPad Prism, Version 9 (GraphPad Software, San Diego, CA, USA). P values were calculated by Student`s t test or paired t test as indicated; ns indicates not significant, * indicates $p \leq 0.05$, ** indicates $p \leq 0.01$, and *** indicates $p \leq 0.001$.

3 Results

3.1 Generation of CAR T cells with reduced IRF4 expression

To generate CAR T cells with reduced IRF4 levels, we engineered a retroviral expression cassette coding for both a CAR (CEA-28ζ) specific for the carcinoembryonic antigen (CEA) and for an IRF4-specific shRNA embedded within the miRNA30 backbone to allow shRNA transcription by the CMV promotor within the LTR (Figure 1A). Two shRNAs targeting IRF4 were designed, CEA-28ζ-I1 and CEA-28ζ-I2. A vector with the well-established shRNA directed against the kanamycin gene (19) served as control construct (CEA-28ζ-K). After retroviral transduction CEA-28ζ-I1 CAR T cells and CEA-28ζ-I2 CAR T cells exhibited similar CAR expression levels (Figure 1B). CEA-28ζ-K CAR T cells displayed a slightly lower transduction rate (Figure 1B). CAR^+ cells were enriched by magnetic-activated cell sorting (MACS) resulting in more than 90% CAR^+ cells without substantial differences in CAR levels (Figures 1B, S1A). Enriched CAR T cell preparations were used in further analyses.

IRF4 is physiologically strongly upregulated after T cell activation (Figure S1B). To verify downregulation in the presence of shRNA, the IRF4 expression by CEA-specific CAR T cells was monitored up to 72 hours after co-culture with CEA^+ BxPC-3

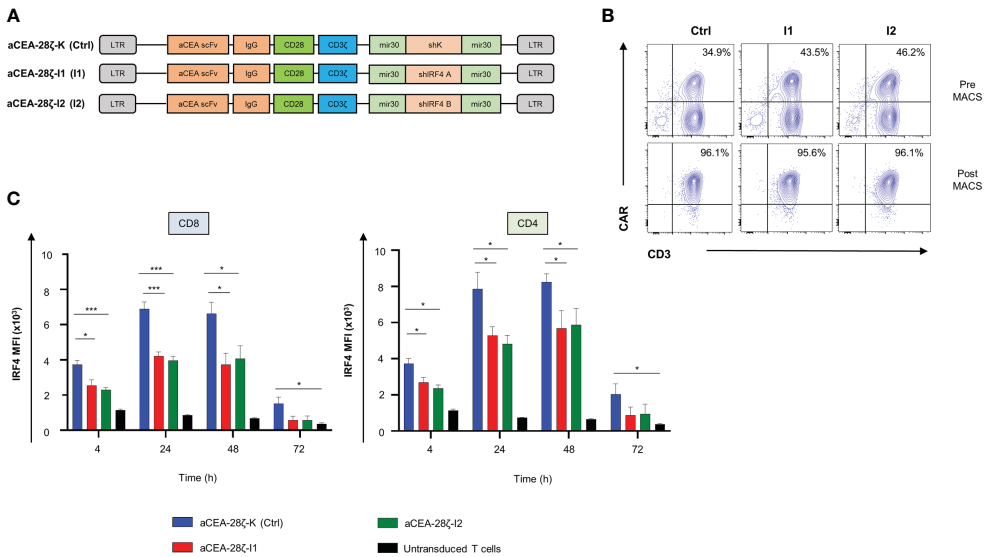

FIGURE 1
Downregulation of IRF4 expression in CAR T cells. **(A)** Schematic of CAR constructs. **(B)** CAR expression in T cells detected by staining with a phycoerythrin (PE)-labeled goat anti-human IgG antibody before (upper panels) and after (lower panels) magnetic cell separation (MACS). One representative donor out of four is shown. **(C)** Intracellular staining of IRF4 after stimulation with CEA^+ BxPC-3 cells at the indicated time points in $CD8^+$ (left panel) and $CD4^+$ CAR T cells (right panel). CAR T cells were generated as described in the materials and methods section by activation of PBMCs followed by retroviral transduction. Untransduced cells were generated by activation of PBMCs and subsequent expansion with IL-2, but without retroviral transduction. Data represent means ± SEM of five donors, p values were calculated by Student´s t test, *indicates $p \leq 0.05$, ***indicates $p \leq 0.001$.

pancreatic cells. Upon CAR stimulation, IRF4 was upregulated after four hours in both $CD8^+$ and $CD4^+$ CAR T cells with IRF4 expression reaching a peak at 24-48 hours followed by a decline to baseline after 72 hours (Figure 1C, Supplementary Figure 1C). In comparison to control CEA-28ζ-K CAR T cells, CAR T cells transduced with the IRF4-specific shRNA showed a significantly reduced IRF4 expression at all time points. Both IRF4 shRNA constructs were similarly efficacious in reducing IRF4 expression. In further analyses, we used the CEA-28ζ-I1 construct. Prior to functional evaluation, we corroborated downregulation of IRF4 in T cells transduced with CEA-28ζ-I1 by Western blot analysis (Supplementary Figure 1D). Taken together, the one-vector retroviral system enabled downregulation of IRF4 by shRNA along with constitutive CAR expression which will facilitate convenient manufacturing of the respective CAR T cells.

3.2 IRF4 downregulation does not impair cytotoxicity of CAR T cells

We recorded CAR-triggered cytotoxicity and cytokine secretion of CEA-28ζ-I1 CAR T cells with downregulated IRF4 in comparison to control CEA-28ζ-K CAR T cells. To this end, CAR T cells were co-cultured with CEA^- 293T cells and CEA^+ BxPC-3 pancreatic cells for 24 hours. Across different effector to target cell ratios, both CEA-28ζ-I1 and CEA-28ζ-K CAR T cells were equally effective in killing of BxPC-3 cells (Figure 2A). No significant background cytotoxicity against 293T cells was recorded (Figure 2B). Furthermore, we interrogated cytokine secretion after 48 hours of co-culture with target cells using ELISA. Upon antigen-triggered stimulation with BxPC-3 cells for 48 hours, CEA-28ζ-I1 and CEA-28ζ-K secreted similar amounts of IL-2, IFN-γ and TNF-α (Figure 2B). Little spontaneous background cytokine release was detected (Figure 2B). Moreover, intracellular staining of IRF4 in untransduced T cells and CAR T cells was performed to assess baseline IRF4 expression at the start of *in vitro* assays. Similar to IRF4 expression after antigen-specific stimulation, baseline IRF4 levels were significantly reduced in CEA-28ζ-I1 CAR T cells as compared to CEA-28ζ-K CAR T cells (Supplementary Figure 2). In aggregate, IRF4 downregulation in CAR T cells did not impair basic cytotoxicity and cytokine release upon activation.

3.3 Downregulation of IRF4 enhances CAR T cell functionality under repetitive stimulatory conditions

We aimed to mitigate CAR T cell exhaustion in the long-term upon repetitive antigen challenge by reducing IRF4 levels in CAR T cells. To address the issue, we assayed CAR T cell effector functions during four consecutive rounds (Round 1–4) of stimulation with GFP-labeled CEA^+ BxPC-3 cells with each round lasting for three to four days. CEA-28ζ-K CAR T cells with physiological IRF4 levels expanded within the first round of stimulation followed by a contraction phase during the following rounds (Figure 3A). Similarly, CAR T cells with reduced IRF4 expression displayed expansion followed by swift contraction without major difference to control CAR T cells. With respect to anti-tumor activity, both CEA-28ζ-K and CEA-28ζ-I1 CAR T cells evinced robust elimination of BxPC-3 cells in the first two rounds of cancer cell challenge while cancer cell elimination declined in round three. However, CAR T cells with reduced IRF4 levels were still capable of eliminating half of seeded BxPC-3 cells in round four whereas the cytotoxic capacity of CEA-28ζ-K control CAR T cells was nearly extinguished (Figure 3A). Data demonstrate that CAR T cells with reduced IRF4 levels retain

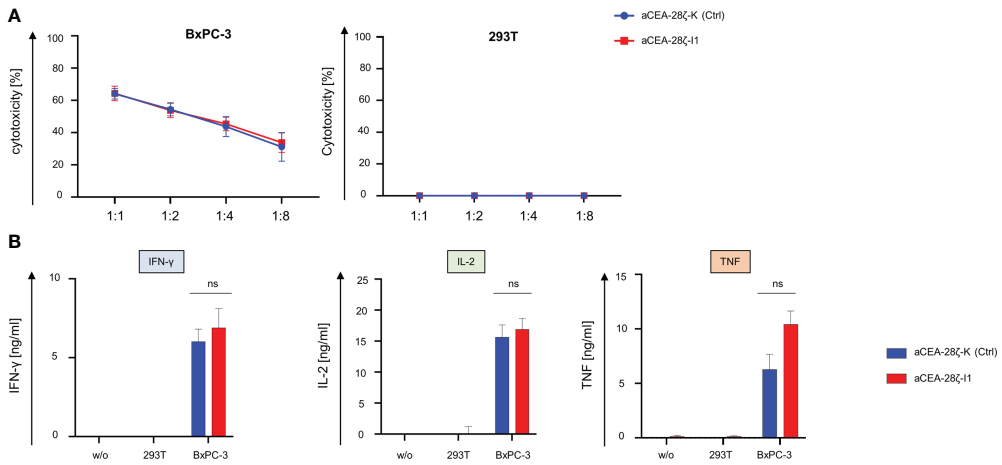

FIGURE 2
Cytotoxicity and cytokine signaling after IRF4 downregulation. **(A)** Cytotoxicity of CAR T cells upon a 24-hour co-culture with CEA^+ BxPC-3 cells (left panel) and CEA^- 293T cells (right panel) was measured at the indicated effector to target ratios by an XTT-based colorimetric assay. Data represent means ± SEM of six donors, p values were calculated by Student´s t test. **(B)** ELISA-based quantification of CAR activation induced IFN-γ (left panel), IL-2 (middle panel), and TNF-α (right panel) in the supernatant after a 48-hour co-culture with medium (w/o), 293T cells, and BxPC-3 cells. Please note the different scales (pg/ml as compared to ng/ml in Figure 2B). Data represent means ± SEM of at least five donors, p values were calculated by Student´s t test, ns indicates not significant.

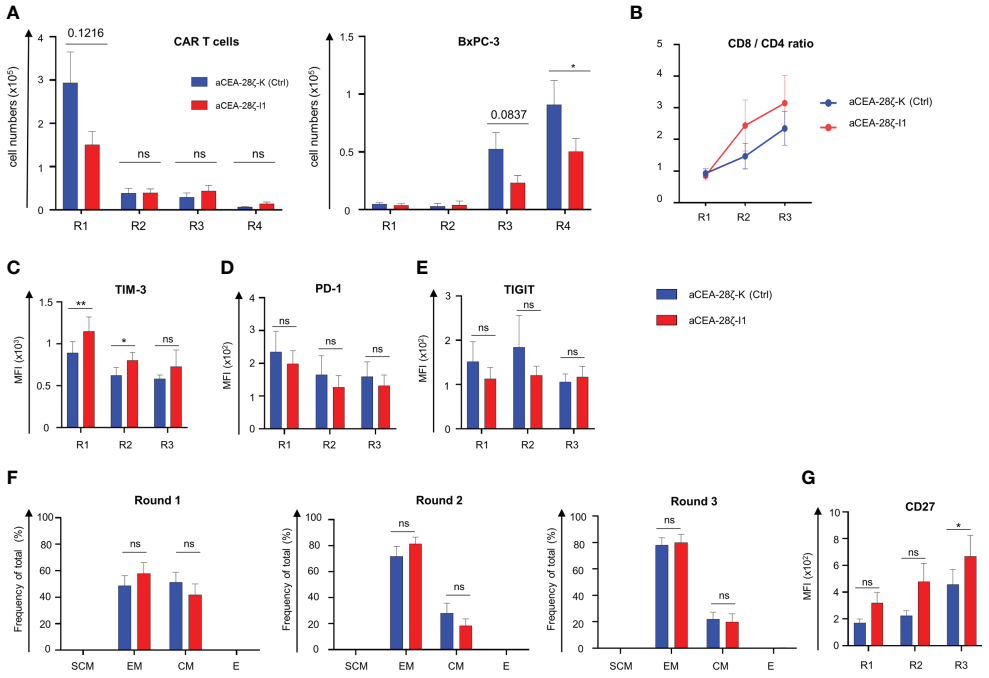

FIGURE 3
Downregulation of IRF4 enhances CAR T cell functionality. **(A)** CAR T cells (starting with 1 x 10^5 CAR T cells) underwent four rounds (R1-R4) of stimulation with GFP-labeled CEA$^+$ BxPC-3 cells (1 x 10^5 tumor cells at the beginning of each round). At the end of each round, CAR T cells (live CD3$^+$ CAR$^+$) (left panel) and BxPC-3 cells (right panel) were quantified by flow cytometry. Data represent means ± SEM of six donors, p values were calculated by Student´s t test, ns indicates not significant, and * indicates p ≤ 0.05. **(B-G)** Phenotypic analysis of CD8$^+$ CAR T cells during repetitive antigen stimulation. CAR T cells underwent three rounds (R1-R3) of antigen-stimulation with unlabeled BxPC-3 cells. At the end of each round, the CD8/CD4 T cell ratio was determined **(B)**. CAR T cells were stained for CD8 and further characterized regarding TIM-3 **(C)**, PD-1 **(D)**, TIGIT **(E)** expression and effector-memory cell differentiation: SCM = T stem-cell-memory (CD45RO$^+$ CD62L$^+$), EM = effector-memory (CD45RO$^+$ CD62L$^-$), CM = central-memory (CD45RO$^+$ CD62L$^+$), E = effector (CD45RO$^-$ CD62L$^-$) **(F)**, and CD27 expression **(G)**. Data represent geometric means of ± SEM of at least four donors, p values were calculated by paired t test, ns indicates not significant, *indicates p ≤ 0.05, **indicates p ≤ 0.01.

anti-cancer cell activity under repetitive challenge conditions for a longer period than conventional CAR T cells.

To elucidate the underlying mechanism, we recorded the CD8/CD4 ratio of CAR T cells, the expression of markers associated with T cell exhaustion, the differentiation state, and the expression of CD27 during repetitive challenge with CEA$^+$ BxPC-3 cells. Starting from a relatively even level of 1 to 1 (no normalization was performed) the CD8/CD4 T cell ratio increased in both CAR T cell sets during repetitive antigen stimulation while IRF4 downregulation favored a higher portion of CD8$^+$ T cells in later rounds (Figure 3B). To investigate whether the improved anti-cancer activity displayed by CEA-28ζ-I1 CAR T cells during repetitive antigen-challenge could derive from the higher frequency of CD8$^+$ T cells, CD107a degranulation with simultaneous detection of CD8$^+$ CAR T cells and CD4$^+$ CAR T cells was recorded upon a short-term re-stimulation with BxPC-3 cells at the end of each round 1-3 (R1-3). Generally, the degranulation capacity of CAR T cells declined during repetitive stimulation, with both CD8$^+$ and CD4$^+$ CEA-28ζ-I1 CAR T cells exhibiting higher degranulation than CEA-28ζ-K control CAR T cells at the end of round three (Supplementary Figures 3A + B). The results are in line with the data obtained from the re-challenge assay (Figure 3A) suggesting an additional improvement of cytotoxicity derived from IRF4 downregulation that is independent from elevated CD8$^+$ CAR T cell frequencies. TIM-3 was expressed at higher levels in CEA-28ζ-I1 CAR T cells as compared to CEA-28ζ-K control CAR T cells during the first two rounds of cancer cell challenge. The upregulation of PD-1 and TIGIT was similar in CEA-28ζ-I1 CAR T cells and CEA-28ζ-K control CAR T cells (Figures 3C-E, Supplementary Figures 3C-E). Starting with a relatively similar distribution of CD45RO$^+$ CD62L$^+$ central memory T cells and CD45RO$^+$ and CD62L$^-$ effector memory cells, both CAR T cells with and without IRF4 down-regulation shifted from central memory to effector memory T cells during the consecutive rounds of cancer cell challenge (Figure 3F, Supplementary Figure 3F). CEA-28ζ-I1 CAR T cells and control CAR T cells did not significantly differ in their effector-memory differentiation (Figure 3F, Supplementary Figure 3F). At the end of round three, the memory-associated molecule CD27 was substantially higher upregulated in CD8$^+$ CEA-28ζ-I1 CAR T cells compared to control CAR T cells (Figure 3G). The effect was restricted to CD8$^+$ T cells and was not recorded in CD4$^+$ CEA-28ζ-I1 CAR T cells (Supplementary Figure 3G). Of note, CD27 upregulation in CD8$^+$ CAR T cells was reported to be associated with enhanced CAR T cell functionality and sustained remissions in patients receiving CAR T cell therapy (34).

Next, we tracked the expression of the co-stimulatory molecules CD137 and CD28 during repetitive challenge. While CD137 was predominately upregulated in CD8$^+$ CAR T cells during the first round of antigen challenge, CD4$^+$ CEA-28ζ-I1 CAR T cells showed

a significantly higher expression of CD137 as compared to CEA-28ζ-K control CAR T cells at end of the first and third round (Supplementary Figure 4A). As for both $CD8^+$ and $CD4^+$ T cells, the upregulation of CD28 was more pronounced in CEA-28ζ-K control CAR T cells as compared to CEA-28ζ-I1 CAR T cells at all time points (Supplementary Figure 4B). Finally, to investigate a potential transactivation of CAR T cells by tumor cells, we checked the expression of co-stimulatory ligands, such as CD70, 41BBL, CD80, and CD86, on BxPC-3 tumor cells by flow cytometry. None of these ligands were detected on BxPC-3 cells (Supplementary Figure 4C).

3.4 Downregulation of IRF4 in CAR T cells enables killing of target cells with low antigen density

Given the significant relevance of cancer cells with low antigen densities evading a CAR T cell attack, we next evaluated the impact of IRF4 downregulation on the killing of targets with low antigen density. To this end, we resorted to MIA PaCa-2 human pancreatic cancer cells that express CEA at low levels (35) (Figure 4A). Using these cells as targets, we compared the CAR-redirected cytotoxicity of CEA-28ζ-I1 CAR T cells with $IRF4^{low}$ levels to CEA-28ζ-K CAR T cells with physiological IRF4 levels in a FACS-based 72-hour killing assay. GFP-labeled MIA PaCa-2 cells were co-cultured with CAR T cells at a 1 to 1 ratio. After 72 hours, the numbers of live GFP^+ MIA PaCa-2 cells and CAR T cells (live $CD3^+$ CAR^+) were analyzed using counting beads. As summarized in Figure 4B, IRF4 downregulation augmented the CAR-triggered elimination of tumor cells with low antigen levels whereas CEA-28ζ-K control CAR T cells did not exhibit significant cytotoxicity towards GFP-labeled MIA PaCa-2 cells. During this period, no substantial expansion of CAR T cells occurred, and absolute CAR T cell numbers did not differ significantly (Figure 4C). In order to confirm the enhanced cytotoxicity of CEA-28ζ-I1 CAR T cells against MIA PaCa-2 cells, a 72-hour XTT-based colorimetric killing assay employing different effector to target ratios was conducted (Figure 4D). No antigen-independent cytotoxicity against CEA^- 293T cells was observed in this assay corroborating an increase of CEA-specific cytotoxicity without raising overall unspecific cytotoxicity.

To address the mechanism of improved functional capacities, we recorded the CAR-triggered cytokine release upon engagement

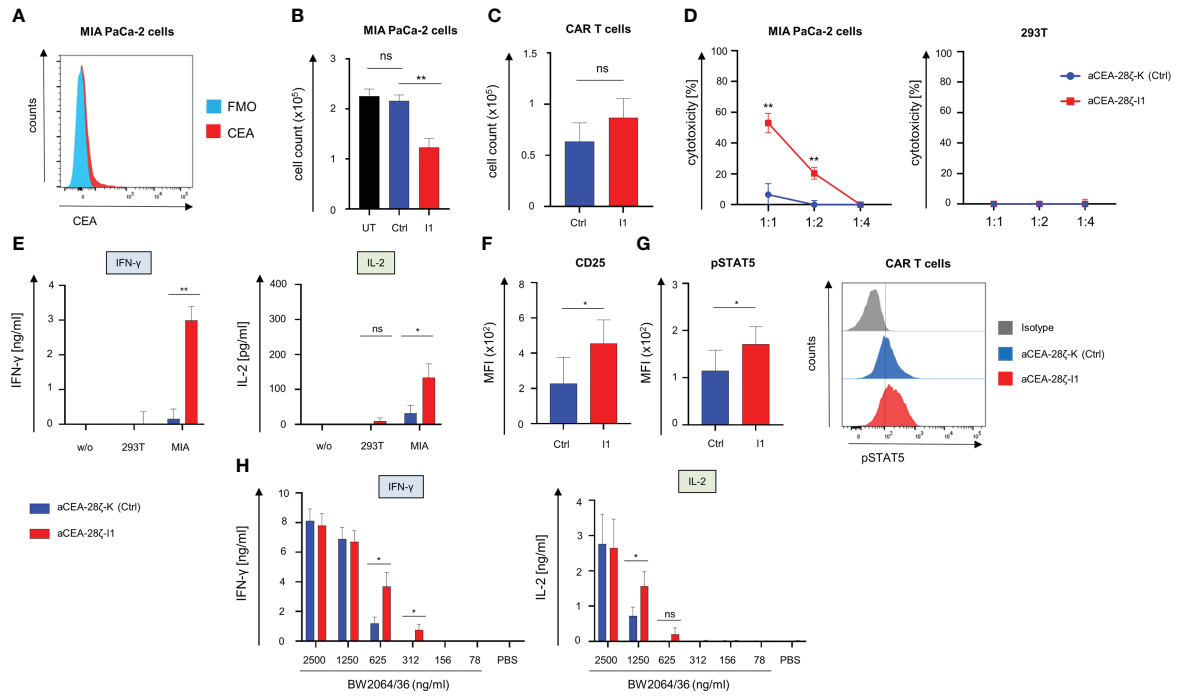

FIGURE 4
Downregulation of IRF4 in CAR T cells enables killing of targets with low antigen density. **(A)** Staining of target cells MIA PaCa-2 for CEA expression using an APC Vio 770-conjugated anti-CEA antibody. One representative staining out of three experiments is shown. **(B)** T cells (1×10^5 T cells) with and without IRF4 downregulation were co-culture with GFP-labeled CEA^+ MIA PaCa-2 cells (1×10^5 tumor cells). After three days, CEA^+ MIA PaCa-2 cells (live GFP^+ cells) and CAR T cells (live $CD3^+$ CAR^+) **(C)** were counted by flow cytometry using counting beads. Data represent means ± SEM of five donors, p values were calculated by Student's t test, ns: not significant, $^{**}p \leq 0.01$. **(D)** Cytotoxicity of CAR T cells upon a 72-hour co-culture with MIA PaCa-2 cells or CEA^- 293T cells was measured at the indicated effector to target cell ratios by an XTT-based colorimetric assay. Data represent means ± SEM of four donors, p values were calculated by Student´s t test. **(E)** IFN-γ and IL-2 in the supernatants after a 48-hour co-culture with medium (w/o), 293T cells, and MIA PaCa-2 cells was recorded by ELISA. Data represent means ± SEM of three donors, p values were calculated by Student´s t test, ns: not significant. **(F)** Staining of CAR T cells for CD25 and for pSTAT5 **(G)** after three days of co-culture with MIA-PaCa-2 cells. Data represent geometric means of ± SEM of three donors, p values were calculated by paired t test, ns indicates not significant, *indicates $p \leq 0.05$. **(H)** ELISA-based quantification of CAR-activation induced IFN-γ and IL-2 in the supernatant after a 48-hour culture on 96 well. plates coated with the anti-idiotypic monoclonal antibody BW2064/36 at the indicated concentrations. Data represent means ± SEM of eight donors, p values were calculated by paired t test, $^*p \leq 0.05$.

of target cells. CEA-28ζ-I1 CAR T cells with reduced IRF4 levels secreted significantly higher quantities of IFN-γ and IL-2 as compared to CEA-28ζ-K control CAR T cells (Figure 4E). High secretion of cytokine levels went along with increased levels of the IL-2 receptor (CD25) on IRF4^{low} CAR T cells after a three-day co-culture with MIA PaCa-2 cells. (Figure 4F). In addition, the downstream signaling mediator phospho-STAT5 is increased in CEA-28ζ-I1 CAR T cells (Figure 4G) reflecting a higher level of activation in response to target cells with low antigen-expression. To further elucidate the sensitivity of CEA-28ζ-I1 CAR T cells, we flow-cytometrically determined the antigen densities of target cells *via* the QuantiBRITE phycoerythrin (PE) assay in conjunction with a PE-labeled anti-CEA antibody. While CEA^{high} BxPC-3 cells expressed an average of 282735 CEA molecules per cell, CEA^{low} MIA PaCa-2 cells showed a more than 100-fold lower CEA expression averaging 602 CEA molecules per cell (Supplementary Figure 5).

To address whether IRF4 downregulation improves sensitivity to antigen by CAR T cells, we stimulated CAR T cells with decrementing concentrations of the anti-idiotypic monoclonal antibody BW2064/36, which acts as surrogate antigen for CEA (36), to provide antigen-specific stimulation through the CEA-specific CAR. Response to CAR-triggered T cell activation was determined by reading IFN-γ and IL-2 release during a 48-hour stimulation period. While both CEA-28ζ-K control CAR T cells and CEA-28ζ-I1 CAR T cells secreted similar amounts of cytokines at high antigen concentrations, CEA-28ζ-I1 CAR T cells with low IRF4 levels released significantly higher amounts of cytokines at low antigen concentrations (Figure 4H). We concluded that IRF4 downregulation resulted in enhanced antigen-sensitivity for CAR T cell activation.

4 Discussion

Evidence indicates that IRF4 plays a crucial role in establishing and maintaining T cell exhaustion during chronic infection (26). To extend a CAR T cell anti-cancer cell response upon repetitive antigen encounter, we reduced IRF4 levels by expressing an IRF4-specific shRNA in CAR T cells. For convenient manufacturing, we designed a retroviral vector that encodes for both the shRNA module targeting the IRF4 gene and the expression of the CEA-specific CAR. The vector allows transduction of T cells to similar rates as canonical vectors encoding exclusively the CAR. ShRNA-mediated IRF4 downregulation did not impair primary cytotoxicity and cytokine secretion of engineered CAR T cells in short-term assays. However, under conditions of repetitive challenge with cognate cancer cells, CEA-28ζ-I1 CAR T cells with IRF4 downregulation showed superior cancer cell elimination compared with conventional CAR T cells. Remarkably, CD8$^+$ CEA-28ζ-I1 CAR T cells with reduced IRF4 levels upregulated CD27 throughout repetitive antigen challenge. Improved CD27 expression has been linked to superior CAR T cell functionality and response to therapy (34). Transcriptome profiling revealed that memory-related genes were enriched in patients attaining complete responses while gene signatures involved in effector cell differentiation, glycolysis, exhaustion, and apoptosis were selectively upregulated in non-responding patients (34). Remarkably, long-lasting complete remissions were associated with enhanced CD27 expression in circulating CD8$^+$ T cells prior to CAR T cell manufacturing. Physiologically, increased CD27 is linked to enhanced T cell functional capacities, survival, and memory formation (37). In sum, we conclude that elevated CD27 expression in CAR T cells may reflect a status of augmented functionality of CEA-28ζ-I1 CAR T cells during repetitive antigen stimulation. In accordance with improved CD27 levels, we did not record major indications for exhaustion since PD1 and TIGIT were not altered. TIM-3 declined after initial increase in early phases of stimulation.

Our analyses also highlight that IRF4 downregulation results in improved antigen sensitivity of CAR T cells to cognate target cells, i.e., decrease in antigen threshold for activation. This enables in successful targeting of antigen-low cells that are neglected by conventional CAR T cells. We assume that this is due to an elevated T cell activation state in response to CD25 and phospho-STAT5 upregulation which both pertain to the IL-2 pathway. Recently, c-Jun overexpression has been shown to eventuate in enhanced antigen-sensitivity by directly augmenting c-Jun-mediated transcriptional activation of target genes, such as IL-2, through displacing AP1-IRF4 complexes from chromatin. AP1-IRF4 complexes induce an exhaustion-related transcriptional program that blunts T cell sensitivity to antigen (9). In the present study, we also observed an elevated activity of the IL-2 pathway in response to IRF4 downregulation, which might also originate from a reduction in chromatin-bound AP-1–IRF4 complexes. Consequently, the enhanced transcriptional access to key T cell effector genes, such as IL-2, might in turn result in enhanced T cell activity particularly visible under conditions of low-antigen density. Nevertheless, extensive chromatin analyses using ATAC-sequencing are required in follow-up studies to thoroughly examine this hypothesis.

Improving antigen sensitivity of CAR T cells has substantial relevance, since tumor evasion of immune cell recognition by low target antigen levels is a leading cause for relapse after CAR T cell therapy (5). Previous strategies to target tumor cells with low antigen density encompass an alternative CAR design, the use of HLA-independent T cell receptors (38) or the co-expression of c-Jun (9). While sensing cancer cells with low antigen levels is beneficial in avoiding tumor relapse, augmenting antigen sensitivity of CAR T cells may raise the risk for on-target/off-tumor toxicities necessitating a careful selection of target antigens with no or limited expression on healthy tissues.

Although the cytokine secretion of conventional CAR T cells and CAR T cells with IRF4 downregulation was not significantly different in our study, the higher activation level of CAR T cells with IRF4 downregulation warrants an enhanced vigilance for cytokine release syndrome (CRS). Moreover, the secretion of central drivers of CRS, such as IL-6 and IL-1β, needs to be determined in future studies. Another potentially lethal side-effect of CAR T cell therapy is constituted by the immune effector cell-associated neurotoxicity syndrome (ICANS). Contrary to CRS, the mechanistic basis for the occurrence of ICANS is still largely unclear and requires further

elucidation (39). In a recent study relying on single-cell RNA sequencing data to identify potential on-target off-tumor expression of the CAR antigen CD19, investigators found low-level expression of CD19 in brain mural cells posing a potential on-target mechanism for neurotoxicity in CD19-directed CAR T cell therapy (40). Against the backdrop of this finding, CD19-specific CAR T cells with enhanced antigen sensitivity should be tightly monitored for potentially causing neurotoxicity. Nevertheless, the majority of patients undergoing CD19-directed CAR T cell therapy do not experience neurotoxicity, and cerebral CD19 expression is not uniform across patients. With the selection of target antigens with no or limited expression on healthy tissues being the most critical step to avoid potentially lethal on-target/off-tumor toxicities (41), suicide genes (42) and initial infusions of CAR T cells with transient CAR expression generated by RNA electroporation should be considered to counteract toxicities (43). For the clinical translation of CAR T cells with enhanced antigen sensitivity, a crucial prerequisite is posed by the selection of safe antigens, the distribution of which has to be checked at the RNA and protein level in all available tissues. Moreover, animal models with orthotopic expression of human antigens, such as exemplified by mice expressing the human mesothelin protein in the lung (44), could be exploited to assess the *in vivo* antigen sensitivity of CAR T cells and the risk for on-target off-tumor toxicity.

In a recent study, IRF4 emerged as crucial regulator of CAR T cell exhaustion upon repetitive encounter of cancer cells (45). Single-cell ATAC-seq analyses identified regulatory networks driving CAR T cell exhaustion with IRF4 as one of the potentially crucial factors. Correspondingly, shRNA-mediated knockdown of IRF4 counteracted exhaustion, inhibited T cell differentiation, improved CAR T cell cytotoxicity, and augmented CAR T cell performance in leukemia bearing mice (45). However, during three rounds of cancer cell challenges we did not detect loss of functional capacities or major differences in effector-memory phenotypes or the expression of exhaustion markers, except transient upregulation of TIM-3, along with IRF4 downregulation. In contrast, we observed augmented anti-cancer cell capacities of CAR T cells after several rounds of repetitive antigen stimulation.

During repetitive antigen challenge we observed phenotypic changes induced by IRF4 downregulation that differed between $CD8^+$ and $CD4^+$ CAR T cells. Most notably, CD27 upregulation was highest in $CD8^+$ CAR T cells with IRF4 downregulation, whereas CD27 upregulation was not significantly different in $CD4^+$ CAR T cells. In T cells, CD27 co-stimulation is known to augment survival and anti-tumor activity (37). In a previous study investigating the impact of IRF4 downregulation on the functionality and expansion of $CD8^+$ T cells during acute viral infections, $CD8^+$ T cells with downregulated IRF4 levels exhibited CD27 upregulation and superior functionality as compared to wild type T cells (46). Especially in $CD8^+$ T cells, direct transcriptional actions of IRF4 on CD27 gene expression could be hypothesized. The preferential upregulation of the survival-promoting molecule CD27 on $CD8^+$ T cells might contribute to the increase in the CD8/CD4 ratio during repetitive antigen stimulation. Published data indicate a role for IRF4 as driver of T cell differentiation (26). Correspondingly, we observed a delayed effector cell differentiation and greater preservation of a central memory phenotype in $CD4^+$ CAR T cells following IRF4 downregulation. Unexpectedly, IRF4 downregulation did not impact effector differentiation in $CD8^+$ CAR T cells during repetitive antigen stimulation which might require even lower IRF4 levels. In contrast to CD27, the expression of CD28 was consistently lower in CAR T cells with IRF4 downregulation and generally higher in $CD4^+$ CAR T cells during the course of repetitive antigen challenge. So far, no reports investigating the connection between IRF4 expression and CD28 expression in T cells have been published. Our data suggest that CD28 is a potential transcriptional target of IRF4.

Taken together, our data highlight downregulation of IRF4 in CAR T cells as a potent tool to augment functional capacities and antigen sensitivity of CAR T cells. Delivery of the IRF4-specific shRNA together with the CAR expression cassette by a one-vector system makes efficient manufacturing of CAR T cells in a GMP conform process feasible suggesting translation to clinical application.

Data availability statement

The raw data supporting the conclusions of this article will be made available by the authors, without undue reservation.

Ethics statement

The studies involving human participants were reviewed and approved by Institutional Review Board of the University of Regensburg (21-2224-101 Regensburg). The patients/participants provided their written informed consent to participate in this study.

Author contributions

The concept of the study was designed by DH, WH, and HA. Experimental design was done by DH, VB, JH, and HA. Experiments were performed by DH. DH and HA wrote the manuscript. The manuscript was reviewed by all co-authors. All authors contributed to the article and approved the submitted version.

Funding

This study was funded in part by the Deutsche Forschungsgemeinschaft (DFG, German Research Foundation) to DH grant 324392634-TRR221, and by the Else-Kröner Fresenius Foundation to DH.

Acknowledgments

The authors would like to thank Charlotte Schenkel for excellent technical assistance.

Conflict of interest

The authors declare that the research was conducted in the absence of any commercial or financial relationships that could be construed as a potential conflict of interest.

Publisher's note

Supplementary material

The Supplementary Material for this article can be found online at: https://www.frontiersin.org/articles/10.3389/fimmu.2023.1185618/full#supplementary-material

SUPPLEMENTARY FIGURE 1
(A-D) CAR T cells were generated as described in the materials and methods section by activation of PBMCs followed by retroviral transduction. Untransduced cells were generated by activation of PBMCs and subsequent expansion with IL-2, but without retroviral transduction. **(A)** Percentage of CAR expressing cells after MACS enrichment (left panel) and CAR MFI after MACS enrichment (right panel). Data represent means ± SEM of four donors, p values were calculated by Student´s t test, ns: not significant. **(B)** Intracellular staining of IRF4 after stimulation of untransduced T cells or CEA-28ζ-K control CAR T cells with coated anti-CD3 mAb OKT-3 (2.5 µg/ml) and anti-CD28 mAb 15E8 (5 µg/ml) after 24 hours in $CD8^+$ (left panel) and $CD4^+$ T cells (right panel). Please note the stimulation with anti-CD3 mAb OKT-3 and anti-CD28 mAb was performed in addition to the standard activation and the transduction procedure. One representative donor out of five donors is shown. **(C)** Histograms showing the intracellular staining of IRF4 in $CD8^+$ (upper panels) and $CD4^+$ CAR T cells (lower panels) after stimulation with CEA^+ BxPC-3 cells at the indicated time points. The values for mean fluorescent intensity (MFI) of IRF4-PE staining are depicted in the histograms. One representative donor out of five donors is shown. **(D)** Western blot showing IRF4 protein expression in untransduced (UT) T cells, CEA-28ζ-K (Ctrl) CAR T cells, and CEA-28ζ-I1 CAR T cells after a 24-hour co-culture period with BxPC-3 cells. One representative donor out of three donors is shown.

SUPPLEMENTARY FIGURE 2
Intracellular staining of IRF4 in untransduced T cells and CAR T cells after a 24-hour culture period in IL-2 free medium to assess IRF4 expression at the start of *in-vitro* assays. CAR T cells were generated as described in the materials and methods section by activation of PBMCs followed by retroviral transduction. Untransduced cells were generated by activation of PBMCs and subsequent expansion with IL-2, but without retroviral transduction. Data represent means ± SEM of four donors, p values were calculated by Student´s t test, ns indicates not significant, and ** indicates $p \leq 0.01$. Additionally, representative histograms are shown (right panel) with values for mean fluorescent intensity of IRF4-PE staining embedded within the histograms. One representative donor out of four donors is shown.

SUPPLEMENTARY FIGURE 3
(A+B) CD107a degranulation assay to separately evaluate the cytotoxic potential of $CD8^+$ and $CD4^+$ CAR T cells during repetitive stimulation using unlabeled BxPC-3 cells. At the end of each round (R1-3), CAR T cells were re-stimulated with unlabeled BxPC-3 cells. After four hours, surface expression of CD107a was measured separately for $CD8^+$ and $CD4^+$ CAR T cells *via* flow cytometry. **(A)** Data represent means of ± SEM of four donors, p values were calculated by Student´s t test, ns: not significant, * $p \leq 0.05$, and ** $p \leq 0.01$. **(B)** Representative dot plots showing degranulation in $CD8^+$ (left panels) and $CD4^+$ (right panels) CAR T cells at the end of round three. One representative donor out of four donors is shown. **(C-G)** Phenotypic analysis of $CD4^+$ CAR T cells during repetitive antigen stimulation. CAR T cells underwent three rounds (R1-R3) of antigen stimulation with unlabeled BxPC-3 cells. At the end of each round, CAR T cells were stained for CD4 and further characterized with respect to TIM-3 **(C)**, PD-1 **(D)**, TIGIT expression **(E)**, and effector-memory cell differentiation: SCM = T stem-cell-memory ($CD45RO^+$ $CD62L^+$), EM = effector-memory ($CD45RO^+$ $CD62L^-$), CM = central-memory ($CD45RO^+$ $CD62L^+$), E = effector ($CD45RO^-$ $CD62L^-$) **(F)**, and CD27 expression **(G)**. Data represent geometric means of ± SEM of at least four donors, p values were calculated by paired t test, ns: not significant, * $p \leq 0.05$.

SUPPLEMENTARY FIGURE 4
(A+B) Phenotypic analysis of CAR T cells during repetitive antigen stimulation. CAR T cells underwent three rounds (R1-R3) of antigen-stimulation with unlabeled BxPC-3 cells. At the end of each round, CAR T cells were stained for CD8 as well as CD4, and further characterized regarding CD137 **(A)** and CD28 **(B)** expression. Data represent geometric means of ± SEM of four donors, p values were calculated by paired t test, ns indicates not significant, * indicates $p \leq 0.05$, ** indicates $p \leq 0.01$. **(C)** Staining of target cells BxPC-3 for the expression of co-stimulatory ligands using an APC -conjugated anti-CD70 antibody, a PE-conjugated anti-41BBL antibody, a FITC-conjugated anti-CD80 antibody, and a PerCPCy5.5-conjugated anti-CD86 antibody. Fluorescent-minus-one (FMO) were used as controls. One representative staining out of three experiments is shown.

SUPPLEMENTARY FIGURE 5
Antigen densities of CEA^- 293T cells, CEA^{low} MIA PaCa-2 cells and CEA^{high} BxPC-3 cells as determined *via* QuantiBRITE phycoerythrin (PE) assay in conjunction with a PE-labeled anti-CEA antibody using flow cytometry. Data represent means (shown on top of bars) ± SEM of three independent experiments.

References

1. June CH, Sadelain M. Chimeric antigen receptor therapy. *N Engl J Med* (2018) 379:64–73. doi: 10.1056/NEJMra1706169

2. Holzinger A, Abken H. Treatment with living drugs: pharmaceutical aspects of CAR T cells. *Pharmacology* (2022) 107:446–63. doi: 10.1159/000525052

3. Ormhøj M, Abken H, Hadrup SR. Engineering T-cells with chimeric antigen receptors to combat hematological cancers: an update on clinical trials. *Cancer Immunol Immunother* (2022) 71:2301–11. doi: 10.1007/s00262-022-03163-y

4. Schaft N. The landscape of CAR-T cell clinical trials against solid tumors-a comprehensive overview. *Cancers (Basel)* (2020) 12. doi: 10.3390/cancers12092567

5. Spiegel JY, Patel S, Muffly L, Hossain NM, Oak J, Baird JH, et al. CAR T cells with dual targeting of CD19 and CD22 in adult patients with recurrent or refractory b cell malignancies: a phase 1 trial. *Nat Med* (2021) 27:1419–31. doi: 10.1038/s41591-021-01436-0

6. Safarzadeh Kozani P, Safarzadeh Kozani P, Ahmadi Najafabadi M, Yousefi F, Mirarefin SM, Rahbarizadeh F. Recent advances in solid tumor CAR-T cell therapy: driving tumor cells from hero to zero? *Front Immunol* (2022) 13:795164. doi: 10.3389/fimmu.2022.795164

7. Sterner RC, Sterner RM. CAR-T cell therapy: current limitations and potential strategies. *Blood Cancer J* (2021) 11:69. doi: 10.1038/s41408-021-00459-7

8. Blank CU, Haining WN, Held W, Hogan PG, Kallies A, Lugli E, et al. Defining 'T cell exhaustion'. *Nat Rev Immunol* (2019) 19:665–74. doi: 10.1038/s41577-019-0221-9

9. Lynn RC, Weber EW, Sotillo E, Gennert D, Xu P, Good Z, et al. C-jun overexpression in CAR T cells induces exhaustion resistance. *Nature* (2019) 576:293–300. doi: 10.1038/s41586-019-1805-z

10. Thommen DS, Schumacher TN. T Cell dysfunction in cancer. *Cancer Cell* (2018) 33:547–62. doi: 10.1016/j.ccell.2018.03.012

11. Sabatino M, Hu J, Sommariva M, Gautam S, Fellowes V, Hocker JD, et al. Generation of clinical-grade CD19-specific CAR-modified CD8+ memory stem cells for the treatment of human b-cell malignancies. *Blood* (2016) 128:519–28. doi: 10.1182/blood-2015-11-683847

12. Gattinoni L, Lugli E, Ji Y, Pos Z, Paulos CM, Quigley MF, et al. A human memory T cell subset with stem cell-like properties. *Nat Med* (2011) 17:1290–7. doi: 10.1038/nm.2446

13. Carnevale J, Shifrut E, Kale N, Nyberg WA, Blaeschke F, Chen YY, et al. RASA2 ablation in T cells boosts antigen sensitivity and long-term function. *Nature* (2022) 609:174–82. doi: 10.1038/s41586-022-05126-w

14. Freitas KA, Belk JA, Sotillo E, Quinn PJ, Ramello MC, Malipatlolla M, et al. Enhanced T cell effector activity by targeting the mediator kinase module. *Science* (2022) 378:eabn5647. doi: 10.1126/science.abn5647

15. Jafarzadeh L, Masoumi E, Mirzaei HR, Alishah K, Fallah-Mehrjardi K, Khakpoor-Koosheh M, et al. Targeted knockdown of Tim3 by short hairpin RNAs improves the function of anti-mesothelin CAR T cells. *Mol Immunol* (2021) 139:1–9. doi: 10.1016/j.molimm.2021.06.007

16. Stadtmauer EA, Fraietta JA, Davis MM, Cohen AD, Weber KL, Lancaster E, et al. CRISPR-engineered T cells in patients with refractory cancer. *Science* (2020) 367. doi: 10.1126/science.aba7365

17. Zhang Y, Zhang X, Cheng C, Mu W, Liu X, Li N, et al. CRISPR-Cas9 mediated LAG-3 disruption in CAR-T cells. *Front Med* (2017) 11:554–62. doi: 10.1007/s11684-017-0543-6

18. Kalbasi A, Siurala M, Su LL, Tariveranmoshabad M, Picton LK, Ravikumar P, et al. Potentiating adoptive cell therapy using synthetic IL-9 receptors. *Nature* (2022) 607:360–5. doi: 10.1038/s41586-022-04801-2

19. Zhao Z, Condomines M, der Stegen v, Sjoukje JC, Perna F, Kloss CC, et al. Structural design of engineered costimulation determines tumor rejection kinetics and persistence of CAR T cells. *Cancer Cell* (2015) 28:415–28. doi: 10.1016/j.ccell.2015.09.004

20. Feucht J, Sun J, Eyquem J, Ho Y-J, Zhao Z, Leibold J, et al. Calibration of CAR activation potential directs alternative T cell fates and therapeutic potency. *Nat Med* (2019) 25:82–8. doi: 10.1038/s41591-018-0290-5

21. Blaeschke F, Ortner E, Stenger D, Mahdawi J, Apfelbeck A, Habjan N, et al. Design and evaluation of TIM-3-CD28 checkpoint fusion proteins to improve anti-CD19 CAR T-cell function. *Front Immunol* (2022) 13:845499. doi: 10.3389/fimmu.2022.845499

22. Khan O, Giles JR, McDonald S, Manne S, Ngiow SF, Patel KP, et al. TOX transcriptionally and epigenetically programs CD8(+) T cell exhaustion. *Nature* (2019) 571:211–8. doi: 10.1038/s41586-019-1325-x

23. Rutishauser RL, Martins GA, Kalachikov S, Chandele A, Parish IA, Meffre E, et al. Transcriptional repressor blimp-1 promotes CD8(+) T cell terminal differentiation and represses the acquisition of central memory T cell properties. *Immunity* (2009) 31:296–308. doi: 10.1016/j.immuni.2009.05.014

24. Seo H, Chen J, González-Avalos E, Samaniego-Castruita D, Das A, Wang YH, et al. TOX and TOX2 transcription factors cooperate with NR4A transcription factors to impose CD8(+) T cell exhaustion. *Proc Natl Acad Sci USA* (2019) 116:12410–5. doi: 10.1073/pnas.1905675116

25. Yoshikawa T, Wu Z, Inoue S, Kasuya H, Matsushita H, Takahashi Y, et al. Genetic ablation of PRDM1 in antitumor T cells enhances therapeutic efficacy of adoptive immunotherapy. *Blood* (2022) 139:2156–72. doi: 10.1182/blood.2021012714

26. Man K, Gabriel SS, Liao Y, Gloury R, Preston S, Henstridge DC, et al. Transcription factor IRF4 promotes CD8(+) T cell exhaustion and limits the development of memory-like T cells during chronic infection. *Immunity* (2017) 47:1129–1141.e5. doi: 10.1016/j.immuni.2017.11.021

27. Lugli E, Brummelman J, Pilipow K, Roychoudhuri R. Paths to expansion: differential requirements of IRF4 in CD8(+) T-cell expansion driven by antigen and homeostatic cytokines. *Eur J Immunol* (2018) 48:1281–4. doi: 10.1002/eji.201847727

28. Yao S, Buzo BF, Pham D, Jiang L, Taparowsky EJ, Kaplan MH, et al. Interferon regulatory factor 4 sustains CD8(+) T cell expansion and effector differentiation. *Immunity* (2013) 39:833–45. doi: 10.1016/j.immuni.2013.10.007

29. Harrer DC, Schenkel C, Bezler V, Kaljanac M, Hartley J, Barden M, et al. CAR triggered release of type-1 interferon limits CAR T-cell activities by an artificial negative autocrine loop. *Cells* (2022) 11. doi: 10.3390/cells11233839

30. Hombach A, Wieczarkowiecz A, Marquardt T, Heuser C, Usai L, Pohl C, et al. Tumor-specific T cell activation by recombinant immunoreceptors: CD3 zeta signaling and CD28 costimulation are simultaneously required for efficient IL-2 secretion and can be integrated into one combined CD28/CD3 zeta signaling receptor molecule. *J Immunol* (2001) 167:6123–31. doi: 10.4049/jimmunol.167.11.6123

31. Chang K, Marran K, Valentine A, Hannon GJ. Creating an miR30-based shRNA vector. *Cold Spring Harb Protoc* (2013) 2013:631–5. doi: 10.1101/pdb.prot075853

32. Choi J-G, Bharaj P, Abraham S, Ma H, Yi G, Ye C, et al. Multiplexing seven miRNA-based shRNAs to suppress HIV replication. *Mol Ther* (2015) 23:310–20. doi: 10.1038/mt.2014.205

33. Hombach AA, Rappl G, Abken H. Blocking CD30 on T cells by a dual specific CAR for CD30 and colon cancer antigens improves the CAR T cell response against CD30(-) tumors. *Mol Ther* (2019) 27:1825–35. doi: 10.1016/j.ymthe.2019.06.007

34. Fraietta JA, Lacey SF, Orlando EJ, Pruteanu-Malinici I, Gohil M, Lundh S, et al. Determinants of response and resistance to CD19 chimeric antigen receptor (CAR) T cell therapy of chronic lymphocytic leukemia. *Nat Med* (2018) 24:563–71. doi: 10.1038/s41591-018-0010-1

35. Girgis MD, Olafsen T, Kenanova V, McCabe KE, Wu AM, Tomlinson JS. Targeting CEA in pancreas cancer xenografts with a mutated scFv-fc antibody fragment. *EJNMMI Res* (2011) 1:24. doi: 10.1186/2191-219X-1-24

36. Hombach A, Koch D, Sircar R, Heuser C, Diehl V, Kruis W, et al. A chimeric receptor that selectively targets membrane-bound carcinoembryonic antigen (mCEA) in the presence of soluble CEA. *Gene Ther* (1999) 6:300–4. doi: 10.1038/sj.gt.3300813

37. Song D-G, Powell DJ. Pro-survival signaling *via* CD27 costimulation drives effective CAR T-cell therapy. *Oncoimmunology* (2012) 1:547–9. doi: 10.4161/onci.19458

38. Mansilla-Soto J, Eyquem J, Haubner S, Hamieh M, Feucht J, Paillon N, et al. HLA-independent T cell receptors for targeting tumors with low antigen density. *Nat Med* (2022) 28:345–52. doi: 10.1038/s41591-021-01621-1

39. Sterner RC, Sterner RM. Immune effector cell associated neurotoxicity syndrome in chimeric antigen receptor-T cell therapy. *Front Immunol* (2022) 13:879608. doi: 10.3389/fimmu.2022.879608

40. Parker KR, Migliorini D, Perkey E, Yost KE, Bhaduri A, Bagga P, et al. Single-cell analyses identify brain mural cells expressing CD19 as potential off-tumor targets for CAR-T immunotherapies. *Cell* (2020) 183:126–142.e17. doi: 10.1016/j.cell.2020.08.022

41. Morgan RA, Yang JC, Kitano M, Dudley ME, Laurencot CM, Rosenberg SA. Case report of a serious adverse event following the administration of T cells transduced with a chimeric antigen receptor recognizing ERBB2. *Mol Ther* (2010) 18:843–51. doi: 10.1038/mt.2010.24

42. Amatya C, Pegues MA, Lam N, Vanasse D, Geldres C, Choi S, et al. Development of CAR T cells expressing a suicide gene plus a chimeric antigen receptor targeting signaling lymphocytic-activation molecule F7. *Mol Ther* (2021) 29:702–17. doi: 10.1016/j.ymthe.2020.10.008

43. Harrer DC, Simon B, Fujii S-I, Shimizu K, Uslu U, Schuler G, et al. RNA-Transfection of γ/δ T cells with a chimeric antigen receptor or an α/β T-cell receptor: a safer alternative to genetically engineered α/β T cells for the immunotherapy of melanoma. *BMC Cancer* (2017) 17:551. doi: 10.1186/s12885-017-3539-3

44. Uslu U, Da T, Assenmacher C-A, Scholler J, Young RM, Tchou J, et al. Chimeric antigen receptor T cells as adjuvant therapy for unresectable adenocarcinoma. *Sci Adv* (2023) 9:eade2526. doi: 10.1126/sciadv.ade2526

45. Jiang P, Zhang Z, Hu Y, Liang Z, Han Y, Li X, et al. Single-cell ATAC-seq maps the comprehensive and dynamic chromatin accessibility landscape of CAR-T cell dysfunction. *Leukemia* (2022) 36:2656–68. doi: 10.1038/s41375-022-01676-0

46. Nayar R, Schutten E, Bautista B, Daniels K, Prince AL, Enos M, et al. Graded levels of IRF4 regulate CD8+ T cell differentiation and expansion, but not attrition, in response to acute virus infection. *J Immunol* (2014) 192:5881–93. doi: 10.4049/jimmunol.1303187

frontiers | Frontiers in Immunology

TYPE Review
PUBLISHED 13 July 2023
DOI 10.3389/fimmu.2023.1216901

OPEN ACCESS

EDITED BY
Yun-Fan Sun,
Fudan University, China

REVIEWED BY
Cun Wang,
Shanghai Cancer Institute, China
Zhang Hongbing,
Chinese Academy of Medical Sciences and Peking Union Medical College, China
Yi Lin,
Shanghai Jiao Tong University, China

*CORRESPONDENCE
Shujie Liao
sjliao@tjh.tjmu.edu.cn
Li Li
lilytjmu@163.com

†These authors have contributed equally to this work

RECEIVED 04 May 2023
ACCEPTED 21 June 2023
PUBLISHED 13 July 2023

CITATION
Wang R, Xiong K, Wang Z, Wu D, Hu B, Ruan J, Sun C, Ma D, Li L and Liao S (2023) Immunodiagnosis — the promise of personalized immunotherapy. *Front. Immunol.* 14:1216901. doi: 10.3389/fimmu.2023.1216901

Immunodiagnosis — the promise of personalized immunotherapy

Renjie Wang[1†], Kairong Xiong[1†], Zhimin Wang[2†], Di Wu[1†], Bai Hu[1], Jinghan Ruan[1], Chaoyang Sun[1], Ding Ma[1], Li Li[1*] and Shujie Liao[1*]

[1]Department of Obstetrics and Gynecology, Cancer Biology Research Center, Tongji Hospital, Tongji Medical College, Huazhong University of Science and Technology, Wuhan, China, [2]Division of Endocrinology and Metabolic Diseases, The First Affiliated Hospital of Zhengzhou University, Zhengzhou, China

Immunotherapy showed remarkable efficacy in several cancer types. However, the majority of patients do not benefit from immunotherapy. Evaluating tumor heterogeneity and immune status before treatment is key to identifying patients that are more likely to respond to immunotherapy. Demographic characteristics (such as sex, age, and race), immune status, and specific biomarkers all contribute to response to immunotherapy. A comprehensive immunodiagnostic model integrating all these three dimensions by artificial intelligence would provide valuable information for predicting treatment response. Here, we coined the term "immunodiagnosis" to describe the blueprint of the immunodiagnostic model. We illustrated the features that should be included in immunodiagnostic model and the strategy of constructing the immunodiagnostic model. Lastly, we discussed the incorporation of this immunodiagnosis model in clinical practice in hopes of improving the prognosis of tumor immunotherapy.

KEYWORDS

immunodiagnosis, cancer, immunotherapy, precision medicine, personalized therapy

1 Introduction

The immune system is an interacting network of immune cells, the molecules they produce, and the lymphoid organs that organize these components (1). Proper immune system function is essential for health, and insufficient immune system activity can lead to different types of diseases included tumor.

In recent years, immunotherapy has yielded new wave in treating tumors with brand-new methods such as immune checkpoint inhibitors (ICIs), adoptive cell therapy (ACT), and therapeutic vaccines. Some patients with tumor types that were previously considered refractory (2) or advanced/metastatic tumors (3) were controlled after receiving ICI treatment. However, most patients do not benefit from immunotherapy (4). In addition, immunotherapy empower immunity against cancer and may lead to immune-related adverse effects (irAEs) such as colitis, dermatitis, pneumonia, and thyroiditis (5). The efficacy and toxicity of immunotherapy remains poorly predictable for given patients till now.

Why do patients with the same disease get dramatically different outcomes when given the same immunotherapy? And how is it possible to tell if a patient might benefit from immunotherapy? Since immunotherapy acts on a strongly heterogeneous immune system of the patient, immune status may be a critical bridge connecting the patient's characteristics to the outcome of immunotherapy. Therefore, it is reasonable to diagnose the immune state of tumor patients before taking immunotherapy - we pioneering name it as immunodiagnosis (ID). We define immunodiagnosis (ID) as systematically, comprehensively, and dynamically evaluating the status of an individual's immune system, to reflect at different disease stages the systemic and local immune status. ID could help clinicians judge the disease phenotypes, evaluate disease activity, and predict the possible progress of disease and then develop a personal treatment plan, rather than directly giving "one-size-fits-all" immunotherapy to patients with very different immune status. With ID, clinicians can qualitatively or quantitatively predict possible immune responses of the local and peripheral immune systems to endogenous and exogenous stimuli, thereby guiding medical decisions. The ID idea has found its way into clinical practice. For example, the FDA has approved the expression of PD-L1 as a biomarker to predict how patients with tumors will respond to ICIs. However, currently used models consist of only a single target or a very small number of targets from a single test sample, which does not fully reflect the complexity of the interaction between the immune system and the host in real-world situations and is therefore less efficient to detect.

Based on the existing research, how should the ID model be constructed? An adult has relatively stable baseline levels of immunity (6), and the composition and function of the immune system are heterogeneous among people of different ages (7), sexes (8), or races etc. As an important guardian of human health, the immune system is continuously stimulated by endogenous and exogenous factors, which can cause fluctuations in the immune status, reflected in the number and composition of immune cell groups, response to stimuli, and cytokine levels. At the same time, the fluctuations of the immune system, stimulated by a diverse array of physiological and pathological processes, should not be neglected. To be more specific, when it comes to certain diseases and treatments, there are certain biomarkers that reflect the relevant immune status. Based on the elaboration of the prognostic factors of immunotherapy in previous literature, we believe that ID models should contain multi-dimensional indicators, including patient demographic characteristics which could basically stratify patients into relatively stable groups, health status which could cause fluctuation of the immune system, and some specific biomarkers that are directly related to the mechanism of disease progression or immunotherapy.

It is difficult for human experts to identify hidden associations from such complex and large datasets. Fortunately, artificial intelligence (AI) has the ability to find unstructured features in such datasets that are large (containing a large number of samples) and complex (each sample has many features). In recent years, AI, especially machine learning and deep learning, has been widely applied in disease clinical research, leading to remarkable predictive performance. Studies have reported that traditional analysis methods, such as statistical analysis and multivariate analysis, are less accurate compared to AI, especially when AI is combined with bioinformatics tools to significantly enhance the accuracy of disease diagnosis and prognosis assessment (9, 10).

In this paper, we present for the first time the important concept of ID, provide a preliminary blueprint for ID systems, analyze what features should be included in ID models, and discuss how to construct ID systems based on existing research (as shown in Figure 1). Furthermore, we look forward to the application of AI in the construction of ID systems, which may shed light on the realization of tumor-precision immunotherapy.

2 Baseline of ID: population stratification of immune status

The immune status can maintain a relatively stable state for several years for an individual (6). However, some intrinsic demographic characteristics are associated with immune status. It is necessary to initially stratify the entire population based on these characteristics and establish a baseline for the ID of different subgroups.

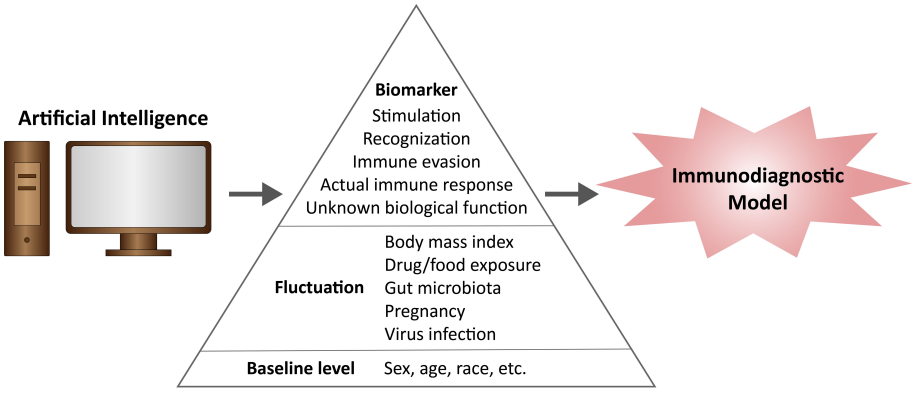

FIGURE 1
The composition of Immunodiagnositic model.

2.1 Sex

The prevalence and types of immune disorders vary significantly between males and females. In general, women tend to have a stronger immune response to external and internal stimuli, and are more susceptible to generating antibodies and suffering adverse side effects (11). Cancer rates in 2018 were approximately 1.15 times higher in men compared to women, and deaths from cancer were higher in men than in women (12).

As a potential prerequisite for ID, the immune status of males and females showed significant differences. The researchers analyzed the global immune cell composition of 49 men and 52 women and found that women had higher naive CD4+T cells, while men had higher activated CD8+T cells (13). Single-cell transcriptome analysis of immune cells from peripheral blood revealed a higher proportion of NK cells in men than in women, while GO analysis revealed higher levels of T and B cell activation signaling in women than in men (14). Therefore, the cut-off for these immunological features in ID should be sex-specific.

While sexual disparities in immune status are widely recognized, little is known about how sex affects the efficacy and toxicity of immunotherapies. A meta-analysis examining 7133 studies found that only 20 randomized controlled trials of ICIs reported an OS relationship with sex (15). Among 11351 pan-cancer patients (with melanoma and non-small cell lung cancer (NSCLC) being the most common types), the hazard ratio (HR) of OS in ICIs groups versus control groups was 0.72 in males and 0.86 in females, revealing a better efficacy of ICIs in males compared to females. Nonetheless, there is potential gender discrimination when patients are enrolled, as the number of female patients is less than half of the male patients, thereby skewing the overall data pool. Consequently, the representation and reliability of female data may be inadequate. The sex disparity in the efficacy of immunotherapy varies with disease type. In NSCLC, anti-PD-1/PD-L1 is more effective in women, whereas in colorectal cancer, it is more effective in men (16).

Sex has also been linked to adverse events (AEs) following immunotherapy. Consistent with higher rates of autoimmune disease, women treated with ICIs had more severe AEs, with a 49 percent higher risk than men (17). As a result, women are more likely to discontinue treatment, resulting in a poorer prognosis. Together, these pieces of evidence support the need for a sex-related ID.

2.2 Age

Aging is associated with several immune pathologies. The incidence of cancer increases with age as the genetic mutation risk accumulates (18). As age increases, the ability of B cells to produce specific antibodies decreases, but their ability to produce autoantibodies increases (19). Immunosenescence, defined as the function of immune system decreases and the composition of immune system remodeling with age (20), includes increased immune memory cells, decreased bone marrow, decreased antigenic diversity of immune cells, decreased co-stimulatory molecules on T cells, and changes of several inflammatory mediators (IL-1a, IL-8, CRP, etc.) (21). However, it is still unclear how immunosenescence affects the efficacy and safety of immunotherapy.

For ICIs, as demonstrated by studies in glioblastoma (22), NSCLC (23), and hepatocellular carcinoma (24, 25), older patients aged 65 to 75 do not respond worse to ICI treatment than younger patients. In other cases, old age has been shown to be a predictor of better efficacy in immunotherapy. In NSCLC, a benefit has been reported in patients over the age of 70 or 75 (26). In metastatic melanoma, a cohort analysis of 538 metastatic melanoma patients found that anti-PD-1 antibodies were more effective in patients over the age of 60 (27). Additionally, researchers have tested this correlation in preclinical models. With transplanted genetically identical tumors, aged mice (52 weeks) performed stronger response to anti-PD-1 than young mice (8 weeks). This phenomenon may be related to the higher Tregs in young mice (27). Fortunately, the toxicity of immunotherapy has not increased in older patients, as supported by anti-PD-1/PD-L1 and anti-CTLA-4 studies (26, 28). For CAR-T, the advantage of immunotherapy in older patients is supported by a clinical trial that in large cell lymphomas patients, the response rates of elders and youngsters are comparable, but the elders have higher rate of complete responses (62% versus 46%) (29).

However, when the age cutoff is reached at 75 years, several studies have reported a trend towards ICI resistance in patients older than 75 years (30). Nonetheless, the age disparity depends on the status of the individual with the disease or on the different types of disease. A retrospectively study collected data from 254 patients with metastatic melanoma, and divided patients into 4 groups by age (≤50, 50-64, 65-74, ≥75 years), revealing no significant difference in median overall survival (mOS), progression-free survival (PFS) and immune-mediated toxicities among these groups (28). Older patients tend to be excluded from the cohort due to higher levels of underlying disease and complications, so data on immunotherapy in older patients is relatively limited.

2.3 Race and ethnicity

Racial ethnical disparities exist in the incidence, mortality, and access to immunotherapy of tumor (31, 32). Furthermore, studies have revealed variations in the normal range of a subset of lymphocytes in people of different races or ethnicities. Indians have higher levels of CD3+ T cells, CD4+ T helper cells, and CD19+ B cells than Chinese or Malays (33). Caucasian Americans have higher levels of γδT cells than African Americans (34). TH17/TH22 is upregulated in Asian patients, while TH17/TH1 is absent in African American patients (35). In addition, signaling activation of immune cells varies across ethnic groups. Single-cell network profiling analysis of a broad panel of immune signaling pathways in peripheral blood mononuclear cell (PBMC) subsets from 60 healthy donors, and found that African Americans had lower B cell anti-IgD-induced pathway activity, including PI3K, MAPK and NF-kB pathway, compared to European Americans (36). These evidences suggest that there are racial differences in immune status and support race as a baseline stratification factor for ID.

There are substantial evidences that race or ethnicity is associated with the outcome of traditional treatments such as chemotherapy for cancers (37), but few studies focused on immunotherapy. It appears that race or ethnicity may be a predictor of efficacy and/or toxicity of immunotherapy, but depends on the treatment strategy.

For ICIs, an observational study enrolled 1,135 patients with unresectable or advanced melanoma treated with anti-PD-1 drugs from 5 institutions in USA, Australia and China, and revealed that white patients have higher overall response rates (ORR) and longer PFS than East Asian, Hispanic, and African (38). As for irAEs, white patients tended to present gastrointestinal irAEs, while other patients had higher rates of endocrine and liver irAEs. Another retrospective cohort of 249 patients with advanced NSCLC treated with anti-PD-1/PD-L1 found that African-American patients had longer treatment discontinuities and longer OS than white patients. The disease control rate was also higher (59.6% versus 56.5%) in African Americans than in white patients (39).

For CAR-T, a retrospective analysis of five Phase I clinical trials involving a total of 139 patients with hematologic malignancies treated with CD19 CAR-T cells found that Hispanic patients were more likely to have severe cytokine release syndrome (40).

For therapeutic vaccines, sipuleucel-T is an autologous cellular vaccine developed for the treatment of asymptomatic/minimally symptomatic metastatic castration-resistant prostate cancer. An observative study involving 1902 patients with prostate cancer treated with sipuleucel-T revealed that the HR of OS between African American and Caucasian is 0.81 (95% CI: 0.68-0.97). African Americans' superior response to immunotherapy may stem from their higher neoepitopes, which can be recognized by the immune system (41).

Still, the disparity appears to vary by disease type and treatment strategy. A study of patients with triple-negative breast cancer treated with anti-PD-L1 combined with neoadjuvant chemotherapy and reported a trend of lower pathologic complete response (43% versus 48%) and lower three-year event-free survival (71.4% versus 78.3%) in African American patients compared with others, although with no statistical significance (42). Together, these pieces of evidence point to the justification of using race and ethnicity as stratification factors in ID. However, the types of diseases and treatment strategies covered by existing studies are insufficient, and most studies only present clinical information without matching serological information to assess immune status.

3 Fluctuations: health states regulate ID

Variant physiological or pathological status can also cause fluctuations in immune status based on baseline immunity levels after stratification of patients by their intrinsic demographic characteristics. We collated the characteristics of immune status and corresponding immunotherapy outcomes in several typical physiological and pathological status.

3.1 Body mass index

Obesity (BMI≥30kg/m2 according to WHO standard definition) can promote inflammation and affect the distribution and abundance of immune cells, and has been validated to relate with the process of malignancy (43). Recently, obesity has been shown to be associated with response to immunotherapy. A meta-analysis of 13 eligible studies involving 5,279 patients with pan-cancer treated with ICIs revealed that high BMI was associated with improved PFS and OS (44), and this finding was also validated in a multi-center clinical trial of patients with NSCLC treated with ICIs (45). In contrast, a study involving 181 patients with advanced NSCLC treated with second-line ICI after first-line chemotherapy had failed found that lower BMI was associated with longer PFS and OS (46). Some studies have found that obesity enhances immunotherapy outcomes only in a subgroup of patients. A randomized controlled trial included 207 melanoma patients treated with anti-CTLA-4 plus chemotherapy, as well as one retrospective cohort with 331 melanoma patients treated with anti-PD-1/PD-L1 monoantibodies, also corroborated the positive correlation between obesity and prolonged PFS and OS, and the association was mainly seen in male patients, while no significant difference was observed in female patients (47). Whether the association varies by sex needs further study. Moreover, treatment settings may affect the benefits of obesity. A multicenter study of NSCLC also found obesity to benefit the efficacy of anti-PD-1/PD-L1 antibodies, but only with the setting of ICI as second- or later-line therapy, with no such difference in the cohort with high PD-L1 expression (≥50%) and treated with ICIs as first-line therapy (48). However, a multi-center trial found the high PD-L1 expression subgroup represent the strongest association between BMI and PFS and OS when received ICI as the first-/second-/later-line therapy (45).

Low BMI may indicate cachexia, defined as a body weight loss >5% over the past 6 months or >2% in patients with a BMI< 20 kg/m2, which was common in advanced cancer (49). Not surprisingly, low BMI was associated with poorer clinical outcomes in several studies involving pan-cancer patients treated with ICIs (50). Consistently, cachexia was also associated with worse outcomes (51).

The correlation between the incidence of treatment-related adverse events and BMI is under debate. A meta-analysis of 20 studies designed to reveal associations between irAEs and BMI in pan-cancer patients treated with immunotherapy found a positive association between BMI and higher risk of irAEs (52), and another multicenter retrospective observational study involving 1,070 patients reported the same propensity (53). Nonetheless, a meta-analysis suggested that there was no significant difference in the incidence of all grades of IAEs among obese, overweight, and normal patients (44), and a clinical trial involving 2,110 patients with advanced NCSLC also supported this view (45). For CAR-T therapy, a study included 64 patients receiving CD-19 CAR-T for relapsed/refractory B cell malignancies and found that patients with ≥2 and earlier stage of cytokine release syndrome possessed a significantly higher BMI (54).

The mechanism explaining the predictive effect of BMI remains unclear, as most studies do not distinguish between the amount of skeletal muscle and the amount of adipose tissue, which have completely different biological functions. A more careful investigation is required. One study involved 74 pre-treated NSCLC patients treated with anti-PD-1 therapy and used CT to assess skeletal muscle, visceral adipose, and subcutaneous adipose (55). They found that neither the visceral-to-subcutaneous ratio of adipose nor the visceral fat area was associated with the efficacy of ICI therapy, suggesting that adipose tissue may not influence clinical outcomes. However, they reported that lower intramuscular adipose tissue content was a prognostic factor of longer OS, but was not significantly associated with PFS. Another retrospective study found a correlation between lower muscle mass and worse OS in NSCLC patients treated with ICIs in combination with chemotherapies (56). The predicted values for the mass and adipose content of skeletal muscles need to be further verified.

3.2 Exposure to drugs and food

Certain drugs have been observed to be associated with immunotherapy outcomes. A classic example is acetaminophen (APAP), which is widely used to manage mild-to-moderate pain caused by advanced tumors, is suggested to have negative immunomodulatory effects. For ICI therapy, a clinical study involving three separate cohorts found that APAP exposure was significantly associated with worse ORR, OS, and PFS in patients treated with ICIs for advanced renal cell carcinoma (57). The underlying mechanism may be that APAP induces Tregs amplification and penetration into the TME and upregulates the expression of the immunosuppressive molecule IL-10, thereby mediating immunosuppressive effects and reducing the efficacy of immunotherapy (57).

Antibiotics have also been reported in relation to immunotherapy. A meta-analysis included 5,560 NSCLC patients treated with ICIs from 23 studies, revealing that the exposure to antibiotics around ICIs initiation (-60 days, +60days) could dramatically decrease the PFS and OS (58). The analysis demonstrated that the median OS decreased by 6.7 months in the patients exposed to antibiotics. However, strong heterogeneity in treatment-line settings and patient clinical data across studies resulted in weak reliability of the analysis. The mechanisms explaining the effects of antibiotics on the efficacy of immunotherapy remain unclear. These drugs should be used with caution in patients receiving immunotherapy. Whether this principle applies to the onset or entire duration of immunotherapy and to all immunotherapy regimens such as therapeutic vaccines and CAR-T requires further study.

Probiotics are a large category of healthcare products and have emerged as a beneficial complement during immunotherapy. A trial surveyed the dietary habits and probiotics intake of 158 patients with late-stage melanoma, 49 of 158 patients reported probiotic usage in 1 month before the initiating of ICI therapy. The study observed a correlation between probiotics and a significantly reduced frequency of tumor-infiltrating IFN-γ positive CD8+ T cells, as well as fewer tumor-infiltrating TH1 cells though not reach significance, revealing a suppression of anti-tumor immunity caused by probiotics (59). In contrast, other previous studies have found that probiotics may benefit the efficacy of immunotherapy in mouse models and clinical patients. Yusuke Tomita and colleagues retrospectively surveyed 118 NSCLC patients treated with ICIs in Japan and found that probiotic Clostridium difficile therapy was associated with prolonged PFS and OS, even in patients with antibiotic exposure (60). To identify whether diet change in the onset of ICI can safely and effectively improve the clinical outcomes, Christine N Spencer and colleagues are performing a phase II trial (NCT04645680).

3.3 Gut microbiota

The gut microbiome can have a systemic effect on the immune system. It has been reviewed that gut microbiome plays an important role in cancer development, anti-tumor immunity, and response to therapy (61). More recently, the gut microbiome has emerged as a predictor of response to immunotherapy. For ICI therapy, studies have shown that specific bacteria can stimulate the immune system and have been demonstrated to augment the efficacy of ICI therapy in mouse models (62, 63). Specifically, Bifidobacterium may improve the activation of DCs and tumor-specific CD8+T cell responses (63), while B fragilis may increase the activation of TH1 cells (62). For adoptive T cell therapy, higher abundance of the Bacteroidales S24-7 family is correlated with higher IL-12 and more CD8α+ DCs in the peripheral blood of mouse model, suggesting that this species could improve anti-tumor immunity (64).

Clinical outcomes also vary depending on the gut microbiome composition. A prospective study enrolled 70 Japanese patients with advanced NSCLC and treated them with anti-PD-1/PD-L1 monoclonal antibodies and performed 16S rRNA sequencing of stool samples. Lower alpha-diversity of gut microbes at baseline was associated with worse OS. Besides, Ruminococcaceae UCG13 and Agathobacter were enriched in patients with reassuring ORR and PFS (65). In contrast, in another clinical trial involved 438 melanoma patients, the alpha and beta diversity of the gut microbiota have no significant differences between ICI responders and nonresponders (66).

Gut microbiome is also associated with toxicity, as supported by an analysis involving 77 patients with advanced melanoma treated with anti-CTLA-4 in combination with anti-PD-1 therapy (66). Moreover, fecal material transplantation may modulate the response to ICI. Preclinical studies have demonstrated that when germ-free mice are treated with fecal microbiome transplants from ICI responders, these mice also respond to ICI therapy. In contrast, the mice did not respond to ICI therapy when the stool material was from patients who did not respond to ICI (67). A Phase I clinical trial evaluating the safety and feasibility of fecal material transplantation in 10 patients with anti-PD-1 refractory metastatic melanoma successfully induced 1 complete response and 2 partial responses (68). The mechanisms underlying the influence of gut microbiota on the efficacy and toxicity of immunotherapy remain to be further demonstrated.

3.4 Pregnancy

Pregnancy can be divided into three trimesters, and the immune state also undergoes three phases. First, there is a pro-inflammatory phase in the first trimester, during which the embryo is implanted and the placenta is formed (69). Second, an anti-inflammatory phase in the second and third trimesters is necessary for fetal tolerance (70). Lastly, the immune state switches back to a pro-inflammatory phase during delivery for uterine contraction and placental expulsion (69).

The local immune status at the mother-fetus interface, or by another name, uterine decidua, is critical for fetal-maternal tolerance. The uterine decidua consists of trophoblasts, decidual stromal cells, and immune cells (71). Throughout pregnancy, the fluctuations and interactions of these cells aid in trophoblast invasion and protect the fetus from rejection by the mother (71). Here we focus on features that are directly related to common immunotherapies. PD-1 and PD-L1 form a co-inhibitory signal that modulates T cell activation and is important for fetal-maternal tolerance (72). PD-1 is primarily expressed by lymphocytes, with levels increasing in deciduous lymphocytes and decreasing in peripheral lymphocytes during the first trimester (72). PD-L1 is expressed by decidual stromal cells and trophoblasts, and the expression levels of PD-L1 increases from the 10-12 weeks after implantation (73). CTLA-4 and CD80/86 are also important inhibitory signals. CTLA-4 is predominantly expressed on Tregs, which show a constant expression during pregnancy (74). CD80/86 are costimulatory molecules on decidual stromal cells, and may contribute to the Th2 propensity of decidual DCs (75). Common ICI drugs target both signaling pathways. Therefore, when pregnant women require immunotherapy, the pregnancy may be disrupted and fluctuations in the expression of target molecules may affect immunotherapy.

Immunotherapy is rarely administered during pregnancy because of concerns about the potential effects on the fetus. For ICIs, seven cases of women becoming pregnant while undergoing ICI treatment have been reported (76–81), and four cases of ICI therapy beginning during pregnancy, with or without chemotherapy (76, 82–84). Three of the melanoma mothers showed disease progression after delivery (80, 82, 83), and one had an emergency Caesarean section at 24 weeks gestation due to tumor progression and died the day after surgery (82). Five placentas were pathologically examined in these studies, including one from a patient with metastatic melanoma that showed several metastases on the maternal side (82). During follow-up, none of the children showed signs of tumor metastasis. Three women developed irAE, one with diarrhea (83) and two with hepatotoxicity (79), and one of the latter discontinued ICIs (80). A case report indicated that exposure to ICIs may cause irAE in newborns (82). For therapeutic vaccines, Calmette-Guerin (BCG) is the tuberculosis vaccine and could be used to treat bladder cancer by injecting it into the bladder. A female was diagnosed with bladder cancer at 36 weeks gestation and treated with BCG. She gave birth to a healthy baby and continued breast-feeding after the baby received the intradermal BCG vaccine (85).

3.5 Virus infection

Approximately 10-12% of all newly diagnosed cancer cases worldwide are associated with viral infections (86). Eight viruses have been found to contribute to cancer development, including human papilloma virus(HPV), hepatitis B and C virus (HBV/HCV) (86). Viruses affect host immunity and cell malignancy through several mechanisms, such as directly increasing genomic instability promoting tumor cells (87), indirectly providing an environment for tumor progression by inducing chronic inflammation (88), and impairing the immune system preventing tumor cells from being excluded (89). Varies immunotherapy methods have been developed based on the association of the virus and the pathological process of cancer. Certain viral proteins are continuously expressed in tumor cells, and tumor cells may be specifically killed by targeting these proteins, known as therapeutic vaccines (90). Several therapeutic vaccines have entered clinical trials (90). Another approach is infusion of T cells carrying native TCR, known as ACT therapy (91). However, whether viral infection status in tumor patients affect immunotherapy has not been fully elucidated.

3.5.1 SARS-CoV-2

The COVID-19 pandemic has and will inevitably have a long-term impact on world health, and it is of interest to see how SARS-CoV-2 infection in cancer patients affects immune status and immunotherapy. SARS-CoV-2 is a single-stranded RNA virus. Its spike protein interacts with ACE2 to facilitate cellular invasion by the virus and stimulate immunity. In the first few days after SARS-CoV-2 infection, innate immune cells identify pathogen associated molecular pattern or damage associated molecular pattern via pattern recognition receptors (PRRs). These PRRs are triggered, causing a substantial release of cytokines that exert direct antiviral effects and activate downstream immune responses (92). The severity of COVID-19 is associated with immune imbalance and sustained release of high levels of cytokines, not viral load (93). Cancer patients are often accompanied by immune balances, weakened immune cells, and destruction of immune-related anatomical structures, making them more vulnerable to SARS-CoV-2 infections. Tumor type, active tumor, and advanced tumor stage are risk factors for death from COVID-19 (94).

SARS-CoV-2 infection can cause long-term perturbations in immune status (95). Notably, change of immune cells, antibody production, and cytokine release due to SARS-CoV-2 infection are influenced by confounding factors such as age, gender, and tumor treatment, which should be taken into consideration comprehensively (96). Tumors and COVID-19 share similar immune processes, such as excessive cytokine release and weakened humoral and cellular immunity. Immunotherapy can elevate IFN-γ expression, thereby increasing ACE2 expression which makes patients receiving immunotherapy more susceptible to SARS-CoV-2 infection (97). This evidence suggests the complexity of the immune status in the coexistence of tumors and SARS-CoV-2, presenting a challenge for immunotherapy and ID.

Vaccination against SARS-CoV-2 is one of the most critical measures to reduce COVID-19 mortality. However, the vaccination efficacy (VE) for tumor patients (62-72%) is lower than that of the normal population (94%), with hematologic tumors demonstrating even lower VE compared to solid tumors (98). The treatment of tumors with chemotherapy, anti-CD20, anti-CD38, and CAR-T has been found to disrupt the humoral immune response induced by SARS-CoV-2 vaccine and impair the VE, while surgery, ICIs, endocrine therapy and radiotherapy did not affect the VE (98, 99). In addition, tumor patients often experience long-term chronic depletion, requiring repeated consolidation of immune memory. A study found that administering a third dose of the SARS-CoV-2 vaccine increased the detection rate of Omicron-specific serum antibodies in tumor patients from 47.8% to 88.9% (100). COVID-19 should be considered a long-term infection and be included in the ID model. Treatment decisions should be based on comprehensive assessment of patients' multiple diseases.

The safety and prognosis of comorbidities with cancer immunotherapy and SARS-CoV-2 infection remain controversial. Several studies have indicated that ICIs may increase the risk of COVID-19-related deaths (101). The mechanism behind this involves over-activation of CD8+ T cells, which not only promotes acute respiratory diseases, but also causes subsequent suppresses of cellular immunity, providing an opportunity for tumor cells to thrive. Severe symptoms and need for hospitalization due to SARS-CoV-2 infection have been reported in 39 - 54% of cancer patients, a higher rate compared to individuals without tumors (102). However, other studies have contradicted these findings, demonstrating that ICIs do not increase mortality due to COVID-19, and can even enhance the immune system's specific response to the virus, which is associated with developed OS (103, 104). These conflicting results may be related to disease type, cancer stage, and immune system status, highlighting the importance of ID.

There are certain commonalities between cancer immunotherapy adverse events and the pathogenesis of COVID-19. For example, the co-occurrence of pulmonary irAEs and COVID-19 pneumonia increases the potential risk of interstitial inflammatory infiltration and diffuse alveolar damage, thereby increasing the likelihood of death from terminal respiratory failure (105). Additionally, there are similarities between the process of acute respiratory distress syndrome caused by SARS-CoV-2 through cytokine storm and cytokine release syndrome after CAR-T treatment (106, 107). Cancer patients treated with CD19 CAR-T therapy may develop B cell aplasia, which impairs the antiviral humoral immune response and puts them at increased risk for complications of SARS-CoV-2 infection (97). In conclusion, there are many interactions of the pathological processes and immune mechanisms between viral infections and cancer. Therefore, the predictive value of including viruses in ID models for cancer and immunotherapy should be appreciated.

3.5.2 HBV/HCV

Recent evidence suggests that HBV/HCV may affect cancer immunotherapy. A multicenter retrospective cohort of 180 patients with advanced CRC treated with anti-PD-1 found that HBV patients had higher mismatch repair defects and fewer cancer metastases than non-HBV patients (108). Nevertheless, there was no statically significant difference in the ORR (both of 39%) between HBV and non-HBV group. Notably, the CR rate in the HBV group (17 CR, 13 PR) was higher than in the non-HBV group (11CR, 19PR). Whether this indicates that HBV infection favors anti-PD-1 therapy remains to be further investigated. Another retrospective study, which included 50 cancer patients with HIV and/or HBV/HCV infection, found no significant association between viral load and anti-tumor immune response (109).

3.5.3 HIV

HIV can damage human T cells and cause acquired immunodeficiency syndrome (AIDS), and there are approximately 3782700 HIV-infected individuals worldwide. However, people with HIV are generally excluded from immunotherapy cohorts, and most studies of HIV and cancer treatment have been conducted in Europe and the United States, rather than in Asia, Africa and Latin America, where 75 percent of HIV patients live (110). Therefore, few clinical trials have provided guidance for personalized treatment of HIV in cancer patients. A phase I clinical trial found that Pembrolizumab is safe for the treatment of advanced cancer in HIV-infected patients with a CD4+ T cell count of greater than 100 cells/μL (111). To recap, all of these evidence supports the inclusion of more virus-infected cancer patients for immunotherapy in the future to further determine the impact of infection on cancer immunotherapy, thereby developing the ID model with the concern of virus infection.

4 Biomarkers: direct predictive factors in ID

The outcome of immunotherapy is highly heterogeneous among individuals. Early practice has demonstrated that when specific therapies are used to treat specific diseases, there are biomarkers that may partially fulfill the function of ID as envisioned. To enumerate all biomarkers and describe them in detail is not the focus of this paper. Instead, we would like to try to discuss the characteristics of ideal biomarkers to provide a reference for the construction of ID systems. Moreover, we will provide some successful cases to illustrate the feasibility of this idea.

An ideal biomarker should be accurate, discriminative between the population of interest and controls, and repeatable. Biomarkers from peripheral blood are an attractive option because they are relatively non-invasive and can be taken multiple times. Biomarkers within imaging methods such as CT/MRI are also worth investigating. Biomarkers should be involved in pathogenesis mechanisms and related to disease activity or therapeutic targets.

Tumor-related biomarkers have been widely discussed. We analyze the role and characteristics of the major biomarkers in the tumor-immune interaction mechanism and summarize these biomarkers into five categories.

Some biomarkers reflect the tumor's ability to stimulate the immune system. Deficient mismatch repair (dMMR) means the loss of expression of mismatch repair proteins that could correct mismatched bases during DNA replication, so the DNA replication errors at microsatellite regions accumulated, causing microsatellite instability-high (MSI-H). Furthermore, patients with MSI-H/dMMR may have more tumor associated antigens (TAAs) and tumor specific antigens (TSAs) that could stimulate the immune system. The tumor mutation burden (TMB) is the genetic mutation rate of tumor cells, and is also associated with the TSAs, also known as neoantigens. The neoantigenic burden is dominated by TSAs targeted by T cells. Recent studies have provided evidence that MSI-H/dMMR (112), TMB (113), and neoantigen burden (114) are emerging as promising biomarkers for clinical outcomes in cancer immunotherapy. Also, Marta and colleagues build a neoantigen fitness model based on immune interactions of neoantigens that could predict survival in melanoma patients and lung cancer patients treated with ICIs. These studies demonstrate the potential of neoantigens and related gene backgrounds as ID models, and suggest that ID may reveal new therapeutic targets.

Another dimension is the immune system's ability to recognize malignant cells. CD8+ T cell dependent killing of cancer cells requires appropriate presentation of tumor antigens by MHC, which in humans is human leukocyte antigen (HLA) molecules, resulting in at least three kinds of biomarkers: specific HLA genotype for certain cancer type (115), some kind of HLA alleles having strong antigen presentation ability (116), and high HLA diversity which could provide a large library and are more likely to have appropriate HLA (117). An exploratory study of multiple myeloma patients treated with bortezomib found some HLA alleles as candidates, as patients carrying HLA-DQB1*03:02, HLA-DQB1*05:01, and HLA-DRB1*01:01 class II alleles are more likely to get a complete response (115). In 1535 advanced cancer patients treated with ICIs, the HLA-B44 supertype is associated with extended survival, whereas the HLA-B62 supertype was associated with poor outcomes (116). In patients with kidney cancer treated with Lenvatinib and Pembrolizumab, it has been found that HLA-I evolutionary divergence is associated with both improved clinical benefit and response durability (117).

Tumors exploit multiple mechanisms to evade immune recognition, and several features associated with immune evasion could be excellent predictors. Overexpression of the PD-L1 protein (a kind of immune checkpoint) on the cancer cells is a major immune evasion mechanism, and antibodies to blockade the PD-1/PD-L1 interaction could normalize anti-tumor immunity. PD-L1 expression levels are the first and most investigated biomarkers to predict prognosis with respect to ICIs for certain cancer types. KEYNOTE-024 provided the highest level of clinical evidence certifying that immunotherapy accompanied with PD-L1 diagnosis could bring nearly clinical cure outcome to advanced non-small cell lung cancer (NSCLC) (118). For solid tumors, CD8+ T cells need to infiltrate into the tumor to contact cancer cells and kill them, but the TME may exclude T cells (119). Levels of intratumoral tumor infiltrating lymphocytes were associated with a better prognosis in epithelial ovarian cancer (120). TME is rich in immunosuppressive cytokines and cells, and may cause T cell depletion and inhibit anti-tumor immunity. Researchers had analyzed the immune cell composition and transcriptomic features of hepatocellular carcinoma samples, and defined a 9-gene signature related to T cell exhaustion, whose expression was higher in responders, and independently predicted better progression free survival (PFS) and overall survival (OS) (121).

Some markers can reflect the actual immune system response to the tumor. For example, peripheral tumor antigen-specific T cell expansion suggests a large therapeutic response. A clinical trial of patients with metastatic urothelial carcinoma treated with anti-PD-L1 demonstrated a higher number of neoantigen-specific CD8+ T cells in the peripheral blood compared to disease progression in patients with control disease (122). Other studies suggest the peripheral blood neutrophil to lymphocyte ratio (NLR) as a negative prognosis predictor of immunotherapy. A phase III trial of advanced gastric cancer patients treated with nivolumab showed that low blood NLR (≤2.9, median) was associated with better PFS and OS (123), as lower blood NLR reflect to higher lymphocytes expansion after immunotherapy.

With the development of sequencing and bioinformatics, a growing number of studies have identified a number of genomic, transcriptomic, or protein signatures associated with immunotherapy outcomes. However, it remains unclear what is the underlying mechanism behind these features affecting immunotherapy. Numerous studies have constructed predictive models by mining public or private databases. For instance, Qing Liu and colleagues screened 1018 differentially expressed immunologic genes (DEGs) of a dataset consisting of 414 bladder cancer samples and 19 normal samples from The Cancer Genome Atlas (TCGA), and constructed a predict risk model consisting of 15 genes (124). They validated the model in another dataset consisting of RNA-seq data from 48 tumor tissues and the relevant clinical information, GSE19423, from the Gene Expression Omnibus (GEO). The proposed model demonstrated good predictive power in predicting OS risk in the validation dataset. They reviewed the literature and found that 10 out of 15 genes are involved in TME, with the mechanism still to be investigated further. Similar studies have sprung up in recent years, but are still far from clinical practice. This type of research is promising as a prototype for an ideal ID system with validation in larger external datasets, including more dimensional variables, combined with a deeper understanding of immune mechanisms.

5 AI helps to construct ID system

AI refers to the use of machines to imitate intelligent behavior for performing complex tasks with minimal human intervention. Machine Learning (ML) is a branch of AI, which involved the use of algorithms such as Logistic Regression, Decision Trees, Random Forests, and Support Vector Machines. Deep Learning (DL) and Artificial Neural Networks represent new frontiers in ML that encompass Convolutional Neural Networks (CNN) and Recurrent

Neural Networks (RNN). CNN offer unique advantages for image processing applications and have been successfully employed for feature extraction in clinical imaging data. RNN is often used for the analysis of time-series data and has shown advantages in dynamic monitoring of disease. Additionally, DL can directly process unstructured data such as images, sounds, and languages, making it particularly suitable for clinical medical record texts, image classification, and tumor diagnosis and treatment (125).The main processes of AI are shown in Figure 2.

AI has been applied to multiple medicine fields such as diabetes (126), including artificial pancreas (calculate and inject insulin dosage automatically) and continuous blood glucose prediction; ophthalmology (127), including detecting diabetic retinopathy and macular oedema. In recent years, significant progress has been made in the research of AI application for early tumor diagnosis. Studies have demonstrated that AI can achieve comparable accuracy and specificity to specialist physicians in diagnosing various cancers, such as breast cancer (128), lung cancer (129), skin tumors (130), and ovarian cancer (131). In addition to accurate identification and early diagnosis of cancer, AI can also assist in long-term follow-up and health management of cancer recurrence (132).

ID is a challenging prediction problem. The input dataset should be large enough and contain enough representative features. An ideal ID system requires simple, inexpensive, and reproducible detection techniques. The rapid development of microfluidic chip platforms in recent years has provided a miniaturized and highly controlled environment for the occurrence of biochemical reactions. It is also compatible with analytical methods, and can give rapid detection results from trace samples (133). Another area that has received a lot of attention is wearable devices. Wearable devices can collect health information noninvasively and continuously, and have shown promising potential to support and implement medical decisions (134). These innovations in detection and monitoring methods, combined with AI, promise to expand the dataset amount.

5.1 Opportunities of AI in precise immunotherapy

5.1.1 Standardizing the diagnostic criteria for existing biomarkers

Currently, immunohistochemistry (IHC) detection of PD-L1 expression as a predictive biomarker for ICIs has been clinically implemented. The staining results are semi-quantitatively evaluated by pathologists. However, due to the heterogeneous expression of PD-L1 in tumor cells and various immune cells, manual interpretation lacks consistency and reproducibility. Moreover, accurate expression values cannot be provided, and manual scoring is subjective, leading to diagnostic bias. To address this issue, several studies have utilized AI for quantitative analysis of digital slides. The established models demonstrated good consistency with human experts' scores and have significantly improved the diagnostic efficiency of untrained pathologists (135–137).

5.1.2 Identify unstructured data

Traditional statistical methods are often insufficient to extract features from high-dimensional clinical images such as CT, MRI, and PET/CT, while subjective interpretation by clinical experts can lead to bias. Recently, advances in AI-based medical image biomarkers have shown great potential for noninvasive characterization of tumors and TME, enabling patient selection and efficacy prediction for immunotherapy. For instance, AI has been utilized to automatically analyze CT features of NSCLC and

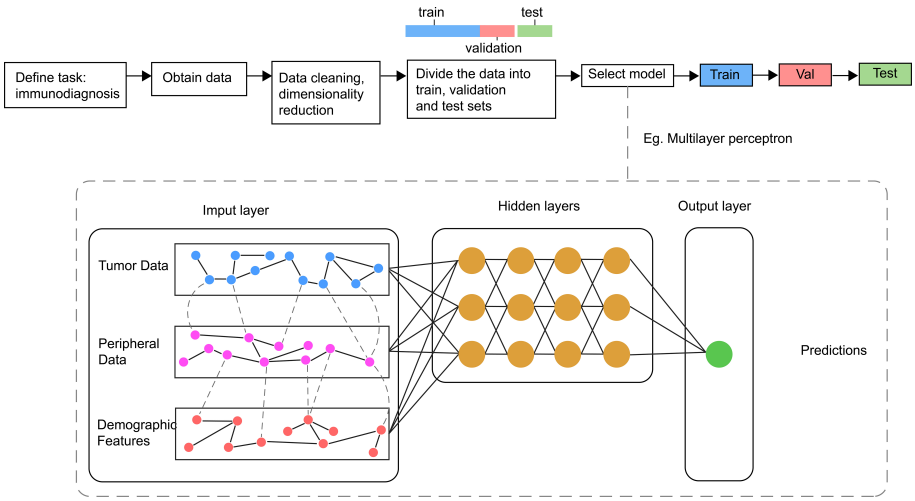

FIGURE 2
Main processes and sample model of AI in Immunodiagnosis. Different data related with immune status are collected and processed before inputted into the model for the training, validating and testing. In general, the model consists of one input layer, many hidden layers and one output layer. The output layer is associated with different labels refer to outcomes of immunotherapy.

melanoma patients, resulting in the development of a noninvasive radiomic biomarker that effectively distinguished immunotherapy responders and non-responders (138). Odors are also unstructured data. Using AI technology, researchers have trained a device called the "electronic nose" to detect volatile organic compound patterns in exhaled breath that were related to the response of NSCLC patients to anti-PD-1, enabling accurate prediction of treatment outcomes (139).

5.1.3 Developing personalized drugs

The combination of AI and multi-omics data holds the potential of developing personalized drugs quickly. Researchers have developed an AI-based platform named PIONER for target discovery that enabled the selection of neoantigens suitable for personalized DNA vaccine EVX-02. The approach involved sequencing both tumor and healthy tissues from cancer patients, identifying genetic mutations in the tumor tissue through comparison with healthy tissue, and utilizing AI to predict which mutations are most likely to generate neoantigens capable of elicitin an immune response in patients. The I/IIa clinical trial of EVX-02 combined with nivolumab achieved good results, with no instances of recurrence observed among the 10 patients enrolled during the trial period (140).

5.1.4 Integrated multidimensional unstructured data to build ID model

The complexity of tumor-immune interactions necessitates a multi-dimensional model for accurate prediction. To this end, Timothy Chan's team has comprehensively integrated multiple biological features relevant to immunotherapy efficacy, including but not limited to TMB, MSI, BMI, sex, NLR, tumor stage/type, and age. They included 1,479 patients across 16 cancer types and established two AI models named RF11 and RF16 that incorporated 11 and 16 biological features, respectively. In the training set, RF16 had an AUC exceeding 0.8 in various cancers, far surpassing the independent predictive efficacy of single indicator (~0.6) (141). Another study found that merely measuring the quantity of TILs cannot accurately reflect the tumor-immune interactions and the functional status of T cells and developed an AI-based PhenoTIL system incorporating multidimensional factors. The PhenoTIL system exhibited a superior AUC (0.738 versus 0.683) compared to TNM staging in NSCLC patients (142).

5.1.5 An ID system in the whole process of tumor diagnosis, treatment, and follow-up

The explosive growth of biology data and the development of portable devices to monitor patients' health state enable the application of AI on generating tumor decision support ID systems. AI can be used to optimize immunotherapy methods in search of a balance between efficacy, adverse reactions, and cost (143). AI could also be used to predict the risk of recurrence. Patients with low recurrence risk can avoid unnecessary radiation exposure and tedious hospital follow-ups, improving their quality of life (132). These findings, along with numerous emerging findings, strongly support the use of AI in facilitating precision immunotherapy.

5.2 Barriers to adopting AI in the clinical transformation

Despite the notable advancements in immune evaluation facilitated by AI, the clinical transformation practice of this technology remains confronted with several challenges that can be categorized into three distinct aspects:

5.2.1 Accessibility of big data

The efficacy of AI is optimized when it is trained and validated on extensive data sets. However, the paucity of publicly available data may be attributed to the imperative of safeguarding patient privacy or commercial conflicts of interest. Consequently, it is imperative to establish a comprehensive public data platform of considerable magnitude. Zlatko and colleagues have created The Cancer Immunome Atlas (https://tcia.at/) to characterize the intratumoral immune landscapes of 20 solid cancers and used machine learning to develop a scoring scheme for the quantification termed immunophenoscore, which showed the predicted value of response to CTLA-4 and PD-1 inhibitors in two independent cohorts (144). In addition, medical records consist of a variety of unstructured data types, including text, images, and voice. In order to enable effective input of this information for use by AI, it is necessary to create a uniform data format.

5.2.2 Open the black box

The nature of AI algorithms is often referred to as 'black box', the output of which is difficult to interpret for the engineers who develop it and for the doctors and patients who use it. Laboratory studies may be required to provide a biological basis, but it may take more time.

5.2.3 What if AI made a mistake?

In situations where AI produces errors, it is essential to determine how to identify and address these inaccuracies. Furthermore, if a mistake made by AI impairs the health or well-being of a patient, it becomes necessary to assign responsibility for the error. A study involving 657 NSCLC patients entered 34 clinical data into an AI model and compared the combination of 8 feature reduction methods and 10 machine learning classification algorithm (145). The researchers discovered notable variances in the AUC among multiple combinations, and the best combinations for predicting RFS, recurrence, and death were different, which suggested us to select appropriate AI approaches for different clinical scenarios. One plausible solution is to incorporate multiple AI algorithms and feature selection methods concurrently. Additionally, a group of human experts should review when different AI models yield conflicting outcomes.

We envisioned the components of an ID model and a blueprint for using AI to establish an ID system for cancer management (Figure 3). The model can diagnose the immune status of patients, determine whether they are suitable for immunotherapy, and even recommend best therapeutic strategies. From the review above, we summarized that the model contains three levels of features: demographic characteristics obtained from the patients' medical

10.3389/fimmu.2023.1216901

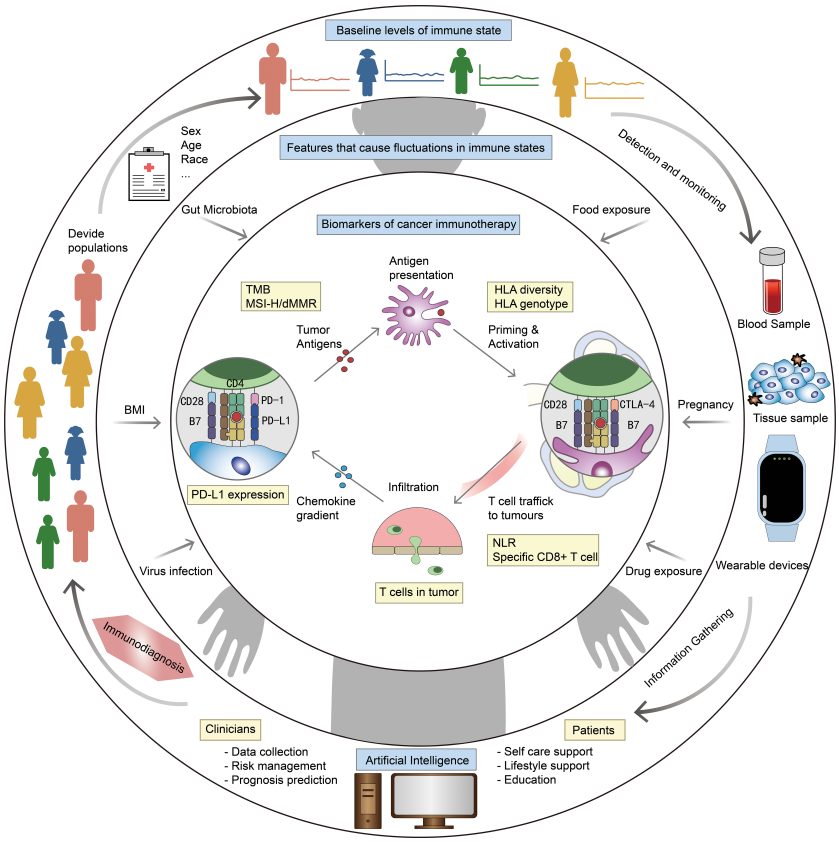

FIGURE 3
Blueprint of ID model and ID system. Outer ring: factors related to baseline level of immune status, eg. sex and age. Middle ring: factors that cause fluctuations in immune status, eg. body mass index (BMI) and gut microbiota. Inner ring: biomarkers for specific diseases and therapies, eg. PD-L1 expression and HLA diversity. The outer ring describes our vision for ID system: stratify patients based on medical record information, get more information from blood/tissue samples and wearable devices, integrate all information by AI to make ID, and optimize the diagnostic model at any time based on clinical feedback.

record to determine a baseline immune level; some variable physiological or pathological factor, reflects the influence of the patient's current health level on immune status; cellular, molecular and genetic characteristics obtained from the patients' tumor histopathologic and blood samples, serve as biomarkers that match the tumor types and therapeutic strategies. By making immunotherapy decision with ID model, and continuously evaluating patients' immune status and immune response through wearable devices and other monitoring methods, it is expected to contribute to the precision of tumor immunotherapy.

6 Conclusion

In this paper, we first present the important concept of ID and describe the method to construct an ID system. There is significant individual heterogeneity in the outcomes of immunotherapy for immune-related diseases and ID should be performed prior to treatment planning. Different demographic characteristics, physiological and pathological conditions have many disturbing effects on the human immune system. As a result, management protocols for patients should be tailored to address their needs at different points in the course of the disease. Depending on the treatment mechanism, there may be some characteristic biomarkers. Combining cutting-edge AI methods to integrate multidimensional information will hopefully build an ideal ID system. Of course, the blueprint of ID system we came up with is just a prototype of an ideal system. With the in-depth research on the mechanism of immune and tumor development and immunotherapy, as well as the continuous iteration of AI, we can expect more accurate and sensitive ID system to be applied to real clinical practice.

Author contributions

RW and KX wrote the initial draft and draw the figures for clear presentation. ZW had a critically overview of the entire manuscript and substantially revised it. DW had a critically overview of the entire manuscript and provided expertise on the machine learning. BH complemented the references and optimized the figures for better presentation. JR and CS provided professional advice on artificial intelligence and complemented cutting-edge research. DM had an editorial overview of the entire manuscript and supervised the whole program. SL and LL did the seminar design and provided scientific expertise, guidance and had and editorial overview of the

entire manuscript. All authors contributed to the article and approved the submitted version.

Funding

This work was supported by the National Natural Science Foundation of China (81672085); The Hubei Provincial Natural Science Foundation of China (2019CFA062); Reproductive Health Fund of Huiling Stem Cell Innovation Institute (FIRMSCOV05); Gynecological tumor special research Fund of Beijing Kanghua Traditional Chinese and Western Medicine Development Foundation (KH-2021-LLZX-074); National Medical Professional Postgraduate Education Steering Committee research topic (B2-YX20190502-01); Open Fund of State Key Laboratory of Reproductive Medicine (SKLRM-K201802).

Conflict of interest

The authors declare that the research was conducted in the absence of any commercial or financial relationships that could be construed as a potential conflict of interest.

Publisher's note

All claims expressed in this article are solely those of the authors and do not necessarily represent those of their affiliated organizations, or those of the publisher, the editors and the reviewers. Any product that may be evaluated in this article, or claim that may be made by its manufacturer, is not guaranteed or endorsed by the publisher.

References

1. Parkin J, Cohen B. An overview of the immune system. *Lancet* (2001) 357 (9270):1777–89. doi: 10.1016/S0140-6736(00)04904-7

2. Zsiros E, Lynam S, Attwood KM, Wang C, Chilakapati S, Gomez EC, et al. Efficacy and safety of pembrolizumab in combination with bevacizumab and oral metronomic cyclophosphamide in the treatment of recurrent ovarian cancer: a phase 2 nonrandomized clinical trial. *JAMA Oncol* (2021) 7(1):78–85. doi: 10.1001/jamaoncol.2020.5945

3. Reckamp KL, Redman MW, Dragnev KH, Minichiello K, Villaruz LC, Faller B, et al. Phase II randomized study of ramucirumab and pembrolizumab versus standard of care in advanced non-Small-Cell lung cancer previously treated with immunotherapy-Lung-MAP S1800A. *J Clin Oncol* (2022) 40(21):2295–306. doi: 10.1200/JCO.22.00912

4. Haslam A, Prasad V. Estimation of the percentage of US patients with cancer who are eligible for and respond to checkpoint inhibitor immunotherapy drugs. *JAMA Netw Open* (2019) 2(5):e192535. doi: 10.1001/jamanetworkopen.2019.2535

5. Sullivan RJ, Weber JS. Immune-related toxicities of checkpoint inhibitors: mechanisms and mitigation strategies. *Nat Rev Drug Discovery* (2022) 21(7):495–508. doi: 10.1038/s41573-021-00259-5

6. Shen-Orr SS, Furman D, Kidd BA, Hadad F, Lovelace P, Huang YW, et al. Defective signaling in the JAK-STAT pathway tracks with chronic inflammation and cardiovascular risk in aging humans. *Cell Syst* (2016) 3(4):374–384.e4. doi: 10.1016/j.cels.2016.09.009

7. Carr EJ, Dooley J, Garcia-Perez JE, Lagou V, Lee JC, Wouters C, et al. The cellular composition of the human immune system is shaped by age and cohabitation. *Nat Immunol* (2016) 17(4):461–8. doi: 10.1038/ni.3371

8. Di Florio DN, Sin J, Coronado MJ, Atwal PS, Fairweather D. Sex differences in inflammation, redox biology, mitochondria and autoimmunity. *Redox Biol* (2020) 31:101482. doi: 10.1016/j.redox.2020.101482

9. Gautier T, Ziegler LB, Gerber MS, Campos-Náñez E, Patek SD. Artificial intelligence and diabetes technology: a review. *Metabolism* (2021) 124:154872. doi: 10.1016/j.metabol.2021.154872

10. Elemento O, Leslie C, Lundin J, Tourassi G. Artificial intelligence in cancer research, diagnosis and therapy. *Nat Rev Canc* (2021) 21(12):747–52. doi: 10.1038/s41568-021-00399-1

11. Wang L, Wang FS, Gershwin ME. Human autoimmune diseases: a comprehensive update. *J Intern Med* (2015) 278(4):369–95. doi: 10.1111/joim.12395

12. Haupt S, Caramia F, Klein SL, Rubin JB, Haupt Y. Sex disparities matter in cancer development and therapy. *Nat Rev Cancer* (2021) 21(6):393–407. doi: 10.1038/s41568-021-00348-y

13. Lakshmikanth T, Muhammad SA, Olin A, Chen Y, Mikes J, Fagerberg L, et al. Human immune system variation during 1 year. *Cell Rep* (2020) 32(3):107923. doi: 10.1016/j.celrep.2020.107923

14. Huang Z, Chen B, Liu X, Li H, Xie L, Gao Y, et al. Effects of sex and aging on the immune cell landscape as assessed by single-cell transcriptomic analysis. *Proc Natl Acad Sci U.S.A.* (2021) 118(33):e2023216118. doi: 10.1073/pnas.2023216118

15. Conforti F, Pala L, Bagnardi V, De Pas T, Martinetti M, Viale G, et al. Cancer immunotherapy efficacy and patients' sex: a systematic review and meta-analysis. *Lancet Oncol* (2018) 19(6):737–46. doi: 10.1016/S1470-2045(18)30261-4

16. Ye Y, Jing Y, Li L, Mills GB, Diao L, Liu H, et al. Sex-associated molecular differences for cancer immunotherapy. *Nat Commun* (2020) 11(1):1779. doi: 10.1038/s41467-020-15679-x

17. Unger JM, Vaidya R, Albain KS, LeBlanc M, Minasian LM, Gotay CC, et al. Sex differences in risk of severe adverse events in patients receiving immunotherapy, targeted therapy, or chemotherapy in cancer clinical trials. *J Clin Oncol* (2022) 40 (13):1474–86. doi: 10.1200/JCO.21.02377

18. Thakkar JP, Villano JL, McCarthy BJ. Age-specific cancer incidence rates increase through the oldest age groups. *Am J Med Sci* (2014) 348(1):65–70. doi: 10.1097/MAJ.0000000000000281

19. Park H, Bourla AB, Kastner DL, Colbert RA, Siegel RM. Lighting the fires within: the cell biology of autoinflammatory diseases. *Nat Rev Immunol* (2012) 12 (8):570–80. doi: 10.1038/nri3261

20. Nikolich-Žugich J. The twilight of immunity: emerging concepts in aging of the immune system. *Nat Immunol* (2018) 19(1):10–9. doi: 10.1038/s41590-017-0006-x

21. Berben L, Floris G, Kenis C, Dalmasso B, Smeets A, Vos H, et al. Age-related remodelling of the blood immunological portrait and the local tumor immune response in patients with luminal breast cancer. *Clin Transl Immunol* (2020) 9(10):e1184. doi: 10.1002/cti2.1184

22. Hu W, Liu H, Li Z, Liu J, Chen L. Impact of molecular and clinical variables on survival outcome with immunotherapy for glioblastoma patients: a systematic review and meta-analysis. *CNS Neurosci Ther* (2022) 28(10):1476–91. doi: 10.1111/cns.13915

23. Rittmeyer A, Barlesi F, Waterkamp D, Park K, Ciardiello F, von Pawel J, et al. Atezolizumab versus docetaxel in patients with previously treated non-small-cell lung cancer (OAK): a phase 3, open-label, multicentre randomised controlled trial. *Lancet* (2017) 389(10066):255–65. doi: 10.1016/S0140-6736(16)32517-X

24. Yau T, Hsu C, Kim TY, Choo SP, Kang YK, Hou MM, et al. Nivolumab in advanced hepatocellular carcinoma: sorafenib-experienced Asian cohort analysis. *J Hepatol* (2019) 71(3):543–52. doi: 10.1016/j.jhep.2019.05.014

25. Finn RS, Ryoo BY, Merle P, Kudo M, Bouattour M, Lim HY, et al. Pembrolizumab as second-line therapy in patients with advanced hepatocellular carcinoma in KEYNOTE-240: a randomized, double-blind, phase III trial. *J Clin Oncol* (2020) 38(3):193–202. doi: 10.1200/JCO.19.01307

26. Spigel DR, McCleod M, Jotte RM, Einhorn L, Horn L, Waterhouse DM, et al. Safety, efficacy, and patient-reported health-related quality of life and symptom burden with nivolumab in patients with advanced non–small cell lung cancer, including patients aged 70 years or older or with poor performance status (CheckMate 153). *J Thorac Oncol* (2019) 14(9):1628–39. doi: 10.1016/j.jtho.2019.05.010

27. Kugel CH III, Douglass SM, Webster MR, Kaur A, Liu Q, Yin X, et al. Age correlates with response to anti-PD1, reflecting age-related differences in intratumoral effector and regulatory T-cell populations. *Clin Cancer Res* (2018) 24(21):5347–56. doi: 10.1158/1078-0432.CCR-18-1116

28. Betof AS, Nipp RD, Giobbie-Hurder A, Johnpulle RAN, Rubin K, Rubinstein SM, et al. Impact of age on outcomes with immunotherapy for patients with melanoma. *Oncologist* (2017) 22(8):963–71. doi: 10.1634/theoncologist.2016-0450

29. Pasquini MC, Locke FL, Herrera AF, Siddiqi T, Ghobadi A, Komanduri KV, et al. Post-marketing use outcomes of an anti-CD19 chimeric antigen receptor (CAR) T cell therapy, axicabtagene ciloleucel (Axi-cel), for the treatment of Large b cell

lymphoma (LBCL) in the united states (US). *Blood* (2019) 134:764. doi: 10.1182/blood-2019-124750

30. Motzer RJ, Tannir NM, McDermott DF, Arén Frontera O, Melichar B, Choueiri TK, et al. Nivolumab plus ipilimumab versus sunitinib in advanced renal-cell carcinoma. *N Engl J Med* (2018) 378(14):1277–90. doi: 10.1056/NEJMoa1712126

31. Siegel RL, Miller KD, Fuchs HE, Jemal A. Cancer statistics, 2022. *CA Cancer J Clin* (2022) 72(1):7–33. doi: 10.3322/caac.21708

32. Zhang C, Zhang C, Wang Q, Li Z, Lin J, Wang H. Differences in stage of cancer at diagnosis, treatment, and survival by race and ethnicity among leading cancer types. *JAMA Netw Open* (2020) 3(4):e202950. doi: 10.1001/jamanetworkopen.2020.2950

33. Chng WJ, Tan GB, Kuperan P. Establishment of adult peripheral blood lymphocyte subset reference range for an Asian population by single-platform flow cytometry: influence of age, sex, and race and comparison with other published studies. *Clin Diagn Lab Immunol* (2004) 11(1):168–73. doi: 10.1128/CDLI.11.1.168-173.2004

34. Cairo C, Armstrong CL, Cummings JS, Deetz CO, Tan M, Lu C, et al. Impact of age, gender, and race on circulating γδ T cells. *Hum Immunol* (2010) 71(10):968–75. doi: 10.1016/j.humimm.2010.06.014

35. Brunner PM, Guttman-Yassky E. Racial differences in atopic dermatitis. *Ann Allergy Asthma Immunol* (2019) 122(5):449–55. doi: 10.1016/j.anai.2018.11.015

36. Longo DM, Louie B, Mathi K, Pos Z, Wang E, Hawtin RE, et al. Racial differences in b cell receptor signaling pathway activation. *J Transl Med* (2012) 10:113. doi: 10.1186/1479-5876-10-113

37. Printz C. Neurotoxicity more likely in Hispanic children treated for acute lymphoblastic leukemia. *Cancer* (2019) 125(4):494–5. doi: 10.1002/cncr.31989

38. Bai X, Shoushtari AN, Betof Warner A, Si L, Tang B, Cui C, et al. Benefit and toxicity of programmed death-1 blockade vary by ethnicity in patients with advanced melanoma: an international multicentre observational study. *Br J Dermatol* (2022) 187 (3):401–10. doi: 10.1111/bjd.21241

39. Ayers KL, Mullaney T, Zhou X, Liu JJ, Lee K, Ma M, et al. Analysis of real-world data to investigate the impact of race and ethnicity on response to programmed cell death-1 and programmed cell death-ligand 1 inhibitors in advanced non-small cell lung cancers. *Oncologist* (2021) 26(7):e1226–39. doi: 10.1002/onco.13780

40. Faruqi AJ, Ligon JA, Borgman P, Steinberg SM, Foley T, Little L, et al. The impact of race, ethnicity, and obesity on CAR T-cell therapy outcomes. *Blood Adv* (2022) 6(23):6040–50. doi: 10.1182/bloodadvances.2022007676

41. Jaratlerdsiri W, Chan EKF, Gong T, Petersen DC, Kalsbeek AMF, Venter PA, et al. Whole-genome sequencing reveals elevated tumor mutational burden and initiating driver mutations in African men with treatment-naïve, high-risk prostate cancer. *Cancer Res* (2018) 78(24):6736–46. doi: 10.1158/0008-5472.CAN-18-0254

42. Foldi J, Kahn A, Silber A, Qing T, Reisenbichler E, Fischbach N, et al. Clinical outcomes and immune markers by race in a phase I/II clinical trial of durvalumab concomitant with neoadjuvant chemotherapy in early-stage TNBC. *Clin Cancer Res* (2022) 28(17):3720–8. doi: 10.1158/1078-0432.CCR-22-0862

43. Rathmell JC. Obesity, immunity, and cancer. *N Engl J Med* (2021) 384(12):1160–2. doi: 10.1056/NEJMcibr2035081

44. An Y, Wu Z, Wang N, Yang Z, Li Y, Xu B, et al. Association between body mass index and survival outcomes for cancer patients treated with immune checkpoint inhibitors: a systematic review and meta-analysis. *J Transl Med* (2020) 18(1):235. doi: 10.1186/s12967-020-02404-x

45. Kichenadasse G, Miners JO, Mangoni AA, Rowland A, Hopkins AM, Sorich MJ. Association between body mass index and overall survival with immune checkpoint inhibitor therapy for advanced non-small cell lung cancer. *JAMA Oncol* (2020) 6 (4):512–8. doi: 10.1001/jamaoncol.2019.5241

46. Roh J, Eom JS, Lee MK, Kim J, Jang T, Yoon SH, et al. Prognostic factors of second-line immune checkpoint inhibitors in patients with advanced-stage non-small cell lung cancer: a multicenter, retrospective study. *Am J Clin Oncol* (2021) 44(7):356–60. doi: 10.1097/COC.0000000000000828

47. McQuade JL, Daniel CR, Hess KR, Mak C, Wang DY, Rai RR, et al. Association of body-mass index and outcomes in patients with metastatic melanoma treated with targeted therapy, immunotherapy, or chemotherapy: a retrospective, multicohort analysis. *Lancet Oncol* (2018) 19(3):310–22. doi: 10.1016/S1470-2045(18)30078-0

48. Ichihara E, Harada D, Inoue K, Sato K, Hosokawa S, Kishino D, et al. The impact of body mass index on the efficacy of anti-PD-1/PD-L1 antibodies in patients with non-small cell lung cancer. *Lung Canc* (2020) 139:140–5. doi: 10.1016/j.lungcan.2019.11.011

49. Biswas AK, Acharyya S. Understanding cachexia in the context of metastatic progression. *Nat Rev Canc* (2020) 20(5):274–84. doi: 10.1038/s41568-020-0251-4

50. Joshi I, Peravali M, Geng X, Rao S, Chen KY, Veytsman I, et al. Impact of baseline clinical biomarkers on treatment outcomes in patients with advanced NSCLC receiving first-line pembrolizumab-based therapy. *Clin Lung Cancer* (2022) 23(5):438–45. doi: 10.1016/j.cllc.2022.03.010

51. Jo H, Yoshida T, Horinouchi H, Yagishita S, Matsumoto Y, Shinno Y, et al. Prognostic significance of cachexia in advanced non-small cell lung cancer patients treated with pembrolizumab. *Cancer Immunol Immunother* (2022) 71(2):387–98. doi: 10.1007/s00262-021-02997-2

52. You Y, Jiang C, Peng K, He W, Wang L, Jin Y, et al. The predictive value of body mass index on prognosis and adverse events of cancers treated with immunotherapy: a systematic review and meta-analysis. *Cancer Immunol Immunother*. (2021) 70 (8):2323–35. doi: 10.1007/s00262-021-02858-y

53. Cortellini A, Bersanelli M, Santini D, Buti S, Tiseo M, Cannita K, et al. Another side of the association between body mass index (BMI) and clinical outcomes of cancer patients receiving programmed cell death protein-1 (PD-1)/Programmed cell death-ligand 1 (PD-L1) checkpoint inhibitors: a multicentre analysis of immune-related adverse events. *Eur J Canc* (2020) 128:17–26. doi: 10.1016/j.ejca.2019.12.031

54. Dos Santos DMC, Rejeski K, Winkelmann M, Liu L, Trinkner P, Günther S, et al. Increased visceral fat distribution and body composition impact cytokine release syndrome onset and severity after CD19 chimeric antigen receptor T-cell therapy in advanced b-cell malignancies. *Haematologica* (2022) 107(9):2096–107. doi: 10.3324/haematol.2021.280189

55. Minami S, Ihara S, Tanaka T, Komuta K. Sarcopenia and visceral adiposity did not affect efficacy of immune-checkpoint inhibitor monotherapy for pretreated patients with advanced non-small cell lung cancer. *World J Oncol* (2020) 11(1):9–22. doi: 10.14740/wjon1225

56. Bolte FJ, McTavish S, Wakefield N, Shantzer L, Hubbard C, Krishnaraj A, et al. Association of sarcopenia with survival in advanced NSCLC patients receiving concurrent immunotherapy and chemotherapy. *Front Oncol* (2022) 12:986236. doi: 10.3389/fonc.2022.986236

57. Bessede A, Marabelle A, Guégan JP, Danlos FX, Cousin S, Peyraud F, et al. Impact of acetaminophen on the efficacy of immunotherapy in cancer patients. *Ann Oncol* (2022) 33(9):909–15. doi: 10.1016/j.annonc.2022.05.010

58. Lurienne L, Cervesi J, Duhalde L, de Gunzburg J, Andremont A, Zalcman G, et al. NSCLC immunotherapy efficacy and antibiotic use: a systematic review and meta-analysis. *J Thorac Oncol* (2020) 15(7):1147–59. doi: 10.1016/j.jtho.2020.03.002

59. Spencer CN, McQuade JL, Gopalakrishnan V, McCulloch JA, Vetizou M, Cogdill AP, et al. Dietary fiber and probiotics influence the gut microbiome and melanoma immunotherapy response. *Science* (2021) 374(6575):1632–40. doi: 10.1126/science.aaz7015

60. Tomita Y, Ikeda T, Sakata S, Saruwatari K, Sato R, Iyama S, et al. Association of probiotic clostridium butyricum therapy with survival and response to immune checkpoint blockade in patients with lung cancer. *Cancer Immunol Res* (2020) 8 (10):1236–42. doi: 10.1158/2326-6066.CIR-20-0051

61. Matson V, Chervin CS, Gajewski TF. Cancer and the microbiome–influence of the commensal microbiota on cancer, immune responses, and immunotherapy. *Gastroenterology* (2021) 160(2):600–13. doi: 10.1053/j.gastro.2020.11.041

62. Vétizou M, Pitt JM, Daillère R, Lepage P, Waldschmitt N, Flament C, et al. Anticancer immunotherapy by CTLA-4 blockade relies on the gut microbiota. *Science* (2015) 350(6264):1079–84. doi: 10.1126/science.aad1329

63. Sivan A, Corrales L, Hubert N, Williams JB, Aquino-Michaels K, Earley ZM, et al. Commensal bifidobacterium promotes antitumor immunity and facilitates anti-PD-L1 efficacy. *Science* (2015) 350(6264):1084–9. doi: 10.1126/science.aac4255

64. Uribe-Herranz M, Bittinger K, Rafail S, Guedan S, Pierini S, Tanes C, et al. Gut microbiota modulates adoptive cell therapy via CD8α dendritic cells and IL-12. *JCI Insight* (2018) 3(4):e94952. doi: 10.1172/jci.insight.94952

65. Hakozaki T, Richard C, Elkrief A, Hosomi Y, Benlaïfaoui M, Mimpen I, et al. The gut microbiome associates with immune checkpoint inhibition outcomes in patients with advanced non–small cell lung cancer. *Cancer Immunol Res* (2020) 8 (10):1243–50. doi: 10.1158/2326-6066.CIR-20-0196

66. Andrews MC, Duong CPM, Gopalakrishnan V, Iebba V, Chen WS, Derosa L, et al. Gut microbiota signatures are associated with toxicity to combined CTLA-4 and PD-1 blockade. *Nat Med* (2021) 27(8):1432–41. doi: 10.1038/s41591-021-01406-6

67. Routy B, Le Chatelier E, Derosa L, Duong CPM, Alou MT, Daillère R, et al. Gut microbiome influences efficacy of PD-1-based immunotherapy against epithelial tumors. *Science* (2018) 359(6371):91–7. doi: 10.1126/science.aan3706

68. Baruch EN, Youngster I, Ben-Betzalel G, Ortenberg R, Lahat A, Katz L, et al. Fecal microbiota transplant promotes response in immunotherapy-refractory melanoma patients. *Science* (2021) 371(6529):602–9. doi: 10.1126/science.abb5920

69. Fuhler GM. The immune system and microbiome in pregnancy. *Best Pract Res Clin Gastroenterol* (2020) 44–45:101671. doi: 10.1016/j.bpg.2020.101671

70. Mor G, Cardenas I, Abrahams V, Guller S. Inflammation and pregnancy: the role of the immune system at the implantation site. *Ann N Y Acad Sci* (2011) 1221 (1):80–7. doi: 10.1111/j.1749-6632.2010.05938.x

71. Yang F, Zheng Q, Jin L. Dynamic function and composition changes of immune cells during normal and pathological pregnancy at the maternal-fetal interface. *Front Immunol* (2019) 10:2317. doi: 10.3389/fimmu.2019.02317

72. Zhao SJ, Muyayalo KP, Luo J, Huang D, Mor G, Liao AH. Next generation of immune checkpoint molecules in maternal-fetal immunity. *Immunol Rev* (2022) 308 (1):40–54. doi: 10.1111/imr.13073

73. Veras E, Kurman RJ, Wang TL, Shih IM. PD-L1 expression in human placentas and gestational trophoblastic diseases. *Int J Gynecol Pathol* (2017) 36(2):146–53. doi: 10.1097/PGP.0000000000000305

74. Wang S, Sun F, Li M, Qian J, Chen C, Wang M, et al. The appropriate frequency and function of decidual Tim-3+CTLA-4+CD8+ T cells are important in maintaining normal pregnancy. *Cell Death Dis* (2019) 10(6):407. doi: 10.1038/s41419-019-1642-x

75. Zhao Y, Zheng Q, Jin L. The role of B7 family molecules in maternal-fetal immunity. *Front Immunol* (2020) 11:458. doi: 10.3389/fimmu.2020.00458

76. Salehi I, Porto L, Elser C, Singh J, Saibil S, Maxwell C. Immune checkpoint inhibitor exposure in pregnancy: a scoping review. *J Immunother* (2022) 45(5):231. doi: 10.1097/CJI.0000000000000418

77. Xu W, Moor RJ, Walpole ET, Atkinson VG. Pregnancy with successful foetal and maternal outcome in a melanoma patient treated with nivolumab in the first trimester: case report and review of the literature. *Melanoma Res* (2019) 29(3):333–7. doi: 10.1097/CMR.0000000000000586

78. Bucheit AD, Hardy JT, Szender JB, Glitza Oliva IC. Conception and viable twin pregnancy in a patient with metastatic melanoma while treated with CTLA-4 and PD-1 checkpoint inhibition. *Melanoma Res* (2020) 30(4):423–5. doi: 10.1097/CMR.0000000000000657

79. Haiduk J, Ziemer M. Pregnancy in a patient with metastatic uveal melanoma treated with nivolumab. *J Dtsch Dermatol Ges.* (2021) 19(5):762–5. doi: 10.1111/ddg.14463

80. Burotto M, Gormaz JG, Samtani S, Valls N, Silva R, Rojas C, et al. Viable pregnancy in a patient with metastatic melanoma treated with double checkpoint immunotherapy. *Semin Oncol* (2018) 45(3):164–9. doi: 10.1053/j.seminoncol.2018.03.003

81. Polnaszek B, Mullen M, Bligard K, Raghuraman N, Massad LS. Term pregnancy after complete response of placental site trophoblastic tumor to immunotherapy. *Obstet Gynecol.* (2021) 138(1):115–8. doi: 10.1097/AOG.0000000000004434

82. Menzer C, Beedgen B, Rom J, Duffert CM, Volckmar AL, Sedlaczek O, et al. Immunotherapy with ipilimumab plus nivolumab in a stage IV melanoma patient during pregnancy. *Eur J Canc* (2018) 104:239–42. doi: 10.1016/j.ejca.2018.09.008

83. Mehta A, Kim KB, Minor DR. Case report of a pregnancy during ipilimumab therapy. *J Glob Oncol* (2018) 4:1–3. doi: 10.1200/JGO.17.00019

84. Stang A, Schwärzler P, Schmidtke S, Tolosa E, Kobbe R. Successful immunochemotherapy for burkitt lymphoma during pregnancy as a bridge to postpartum high-dose methotrexate therapy: a case report and review of the literature. *Clin Lymphoma Myeloma Leukemia* (2020) 20(6):e284–90. doi: 10.1016/j.clml.2019.12.012

85. Barbur E, Doganca T, Obek C. Safe use of intravesical bacillus calmette-guérin immunotherapy for bladder cancer during breastfeeding: a case report. *Immunotherapy* (2022) 14(10):759–64. doi: 10.2217/imt-2021-0203

86. Plummer M, de Martel C, Vignat J, Ferlay J, Bray F, Franceschi S. Global burden of cancers attributable to infections in 2012: a synthetic analysis. *Lancet Glob Health* (2016) 4(9):e609–616. doi: 10.1016/S2214-109X(16)30143-7

87. Mesri EA, Feitelson MA, Munger K. Human viral oncogenesis: a cancer hallmarks analysis. *Cell Host Microbe* (2014) 15(3):266–82. doi: 10.1016/j.chom.2014.02.011

88. Ilhan ZE, Łaniewski P, Thomas N, Roe DJ, Chase DM, Herbst-Kralovetz MM. Deciphering the complex interplay between microbiota, HPV, inflammation and cancer through cervicovaginal metabolic profiling. *EBioMedicine* (2019) 44:675–90. doi: 10.1016/j.ebiom.2019.04.028

89. Moir S, Chun TW, Fauci AS. Pathogenic mechanisms of HIV disease. *Annu Rev Pathol* (2011) 6:223–48. doi: 10.1146/annurev-pathol-011110-130254

90. Wang R, Pan W, Jin L, Huang W, Li Y, Wu D, et al. Human papillomavirus vaccine against cervical cancer: opportunity and challenge. *Cancer Lett* (2020) 471:88–102. doi: 10.1016/j.canlet.2019.11.039

91. Draper LM, Kwong MLM, Gros A, Stevanović S, Tran E, Kerkar S, et al. Targeting of HPV-16+ epithelial cancer cells by TCR gene engineered T cells directed against E6. *Clin Cancer Res* (2015) 21(19):4431–9. doi: 10.1158/1078-0432.CCR-14-3341

92. Magazine N, Zhang T, Wu Y, McGee MC, Veggiani G, Huang W. Mutations and evolution of the SARS-CoV-2 spike protein. *Viruses* (2022) 14(3):640. doi: 10.3390/v14030640

93. Jamal M, Bangash HI, Habiba M, Lei Y, Xie T, Sun J, et al. Immune dysregulation and system pathology in COVID-19. *Virulence* (2021) 12(1):918–36. doi: 10.1080/21505594.2021.1898790

94. Williamson EJ, Walker AJ, Bhaskaran K, Bacon S, Bates C, Morton CE, et al. Factors associated with COVID-19-related death using OpenSAFELY. *Nature* (2020) 584(7821):430–6. doi: 10.1038/s41586-020-2521-4

95. Wu H, Liao S, Wang Y, Guo M, Lin X, Wu J, et al. Molecular evidence suggesting the persistence of residual SARS-CoV-2 and immune responses in the placentas of pregnant patients recovered from COVID-19. *Cell Prolif.* (2021) 54(9):e13091. doi: 10.1111/cpr.13091

96. Lv D, Hu B, Lin X, Wang R, Wu D, Long R, et al. Immunopathogenesis of patients with COVID-19: from the perspective of immune system "evolution" and "revolution" *Expert Rev Mol Med* (2022) 24:e19. doi: 10.1017/erm.2022.12

97. Fathi M, Vakili K, Jazi K, Sadeghi MA, Hajiesmaeili M, Mohamadkhani A, et al. Challenges of cancer immunotherapy and chemotherapy during the COVID-19 pandemic. *Tumori* (2022) 108(5):407–19. doi: 10.1177/03008916211063939

98. Fendler A, de Vries EGE, GeurtsvanKessel CH, Haanen JB, Wörmann B, Turajlic S, et al. COVID-19 vaccines in patients with cancer: immunogenicity, efficacy and safety. *Nat Rev Clin Oncol* (2022) 19(6):385–401. doi: 10.1038/s41571-022-00610-8

99. Houot R, Levy R, Cartron G, Armand P. Could anti-CD20 therapy jeopardise the efficacy of a SARS-CoV-2 vaccine? *Eur J Cancer* (2020) 136:4–6. doi: 10.1016/j.ejca.2020.06.017

100. Zeng C, Evans JP, Chakravarthy K, Qu P, Reisinger S, Song NJ, et al. COVID-19 mRNA booster vaccines elicit strong protection against SARS-CoV-2 omicron variant in patients with cancer. *Cancer Cell* (2022) 40(2):117–9. doi: 10.1016/j.ccell.2021.12.014

101. Dai M, Liu D, Liu M, Zhou F, Li G, Chen Z, et al. Patients with cancer appear more vulnerable to SARS-CoV-2: a multicenter study during the COVID-19 outbreak. *Cancer Discovery* (2020) 10(6):783–91. doi: 10.1158/2159-8290.CD-20-0422

102. von Lilienfeld-Toal M, Vehreschild JJ, Cornely O, Pagano L, Compagno FEHA Infectious Disease Scientific Working Group, et al. Frequently asked questions regarding SARS-CoV-2 in cancer patients-recommendations for clinicians caring for patients with malignant diseases. *Leukemia* (2020) 34(6):1487–94. doi: 10.1038/s41375-020-0832-y

103. Bersanelli M, Buti S, Banna GL, De Giorgi U, Cortellini A, Rebuzzi SE, et al. Impact of influenza syndrome and flu vaccine on survival of cancer patients during immunotherapy in the INVIDIa study. *Immunotherapy* (2020) 12(2):151–9. doi: 10.2217/imt-2019-0180

104. Yatim N, Boussier J, Tetu P, Smith N, Bruel T, Charbit B, et al. Immune checkpoint inhibitors increase T cell immunity during SARS-CoV-2 infection. *Sci Adv* (2021) 7(34):eabg4081. doi: 10.1126/sciadv.abg4081

105. Yarza R, Bover M, Paredes D, López-López F, Jara-Casas D, Castelo-Loureiro A, et al. SARS-CoV-2 infection in cancer patients undergoing active treatment: analysis of clinical features and predictive factors for severe respiratory failure and death. *Eur J Canc* (2020) 135:242–50. doi: 10.1016/j.ejca.2020.06.001

106. Qin C, Zhou L, Hu Z, Zhang S, Yang S, Tao Y, et al. Dysregulation of immune response in patients with coronavirus 2019 (COVID-19) in wuhan, China. *Clin Infect Dis* (2020) 71(15):762–8. doi: 10.1093/cid/ciaa248

107. Lim SY, Lee JH, Gide TN, Menzies AM, Guminski A, Carlino MS, et al. Circulating cytokines predict immune-related toxicity in melanoma patients receiving anti-PD-1-Based immunotherapy. *Clin Cancer Res* (2019) 25(5):1557–63. doi: 10.1158/1078-0432.CCR-18-2795

108. Cheng YK, Chen P, Chen DW, Lin ZS, Ye SB, Lan P. Comparative safety, efficacy and survival outcome of anti-PD-1 immunotherapy in colorectal cancer patients with vs without hepatitis b virus infection: a multicenter cohort study. *Clin Transl Gastroenterol* (2022) 13(5):e00475. doi: 10.14309/ctg.0000000000000475

109. Shah NJ, Al-Shbool G, Blackburn M, Cook M, Belouali A, Liu SV, et al. Safety and efficacy of immune checkpoint inhibitors (ICIs) in cancer patients with HIV, hepatitis b, or hepatitis c viral infection. *J Immunother Canc* (2019) 7(1):353. doi: 10.1186/s40425-019-0771-1

110. Puronen CE, Ford ES, Uldrick TS. Immunotherapy in people with HIV and cancer. *Front Immunol* (2019) 10:2060. doi: 10.3389/fimmu.2019.02060

111. Uldrick TS, Gonçalves PH, Abdul-Hay M, Claeys AJ, Emu B, Ernstoff MS, et al. Assessment of the safety of pembrolizumab in patients with HIV and advanced cancer-a phase 1 study. *JAMA Oncol* (2019) 5(9):1332–9. doi: 10.1001/jamaoncol.2019.2244

112. Le DT, Durham JN, Smith KN, Wang H, Bartlett BR, Aulakh LK, et al. Mismatch repair deficiency predicts response of solid tumors to PD-1 blockade. *Science* (2017) 357(6349):409–13. doi: 10.1126/science.aan6733

113. Chung HC, Ros W, Delord JP, Perets R, Italiano A, Shapira-Frommer R, et al. Efficacy and safety of pembrolizumab in previously treated advanced cervical cancer: results from the phase II KEYNOTE-158 study. *J Clin Oncol* (2019) 37(17):1470–8. doi: 10.1200/JCO.18.01265

114. De Mattos-Arruda L, Vazquez M, Finotello F, Lepore R, Porta E, Hundal J, et al. Neoantigen prediction and computational perspectives towards clinical benefit: recommendations from the ESMO precision medicine working group. *Ann Oncol* (2020) 31(8):978–90. doi: 10.1016/j.annonc.2020.05.008

115. Ri M, Iida S, Maruyama D, Sakabe A, Kamei R, Nakashima T, et al. HLA genotyping in Japanese patients with multiple myeloma receiving bortezomib: an exploratory biomarker study of JCOG1105 (JCOG1105A1). *Cancer Sci* (2021) 112 (12):5011–9. doi: 10.1111/cas.15158

116. Chowell D, Morris LGT, Grigg CM, Weber JK, Samstein RM, Makarov V, et al. Patient HLA class I genotype influences cancer response to checkpoint blockade immunotherapy. *Science* (2018) 359(6375):582–7. doi: 10.1126/science.aao4572

117. Lee CH, DiNatale RG, Chowell D, Krishna C, Makarov V, Valero C, et al. High response rate and durability driven by HLA genetic diversity in patients with kidney cancer treated with lenvatinib and pembrolizumab. *Mol Cancer Res* (2021) 19(9):1510–21. doi: 10.1158/1541-7786.MCR-21-0053

118. Shindo Y, Hazama S, Tsunedomi R, Suzuki N, Nagano H. Novel biomarkers for personalized cancer immunotherapy. *Cancers (Basel).* (2019) 11(9):E1223. doi: 10.3390/cancers11091223

119. Joyce JA, Fearon DT. T Cell exclusion, immune privilege, and the tumor microenvironment. *Science* (2015) 348(6230):74–80. doi: 10.1126/science.aaa6204

120. James FR, Jiminez-Linan M, Alsop J, Mack M, Song H, Brenton JD, et al. Association between tumour infiltrating lymphocytes, histotype and clinical outcome in epithelial ovarian cancer. *BMC Canc* (2017) 17(1):657. doi: 10.1186/s12885-017-3585-x

121. Hsu CL, Ou DL, Bai LY, Chen CW, Lin L, Huang SF, et al. Exploring markers of exhausted CD8 T cells to predict response to immune checkpoint inhibitor therapy for hepatocellular carcinoma. *Liver Canc* (2021) 10(4):346–59. doi: 10.1159/000515305

122. Holm JS, Funt SA, Borch A, Munk KK, Bjerregaard AM, Reading JL, et al. Neoantigen-specific CD8 T cell responses in the peripheral blood following PD-L1 blockade might predict therapy outcome in metastatic urothelial carcinoma. *Nat Commun* (2022) 13(1):1935. doi: 10.1038/s41467-022-29342-0

123. Kim JH, Ryu MH, Park YS, Ma J, Lee SY, Kim D, et al. Predictive biomarkers for the efficacy of nivolumab as ≥ 3rd-line therapy in patients with advanced gastric cancer: a subset analysis of ATTRACTION-2 phase III trial. *BMC Canc* (2022) 22 (1):378. doi: 10.1186/s12885-022-09488-2

124. Liu Q, Wang Y, Gao H, Sun F, Wang X, Zhang H, et al. An individualized prognostic signature for clinically predicting the survival of patients with bladder cancer. *Front Genet* (2022) 13:837301. doi: 10.3389/fgene.2022.837301

125. Huynh E, Hosny A, Guthier C, Bitterman DS, Petit SF, Haas-Kogan DA, et al. Artificial intelligence in radiation oncology. *Nat Rev Clin Oncol* (2020) 17(12):771–81. doi: 10.1038/s41571-020-0417-8

126. Contreras I, Vehi J. Artificial intelligence for diabetes management and decision support: literature review. *J Med Internet Res* (2018) 20(5):e10775. doi: 10.2196/10775

127. Ting DSW, Pasquale LR, Peng L, Campbell JP, Lee AY, Raman R, et al. Artificial intelligence and deep learning in ophthalmology. *Br J Ophthalmol* (2019) 103 (2):167–75. doi: 10.1136/bjophthalmol-2018-313173

128. Akselrod-Ballin A, Chorev M, Shoshan Y, Spiro A, Hazan A, Melamed R, et al. Predicting breast cancer by applying deep learning to linked health records and mammograms. *Radiology* (2019) 292(2):331–42. doi: 10.1148/radiol.2019182622

129. Ardila D, Kiraly AP, Bharadwaj S, Choi B, Reicher JJ, Peng L, et al. End-to-end lung cancer screening with three-dimensional deep learning on low-dose chest computed tomography. *Nat Med* (2019) 25(6):954–61. doi: 10.1038/s41591-019-0447-x

130. Esteva A, Kuprel B, Novoa RA, Ko J, Swetter SM, Blau HM, et al. Dermatologist-level classification of skin cancer with deep neural networks. *Nature* (2017) 542(7639):115–8. doi: 10.1038/nature21056

131. Chen H, Yang BW, Qian L, Meng YS, Bai XH, Hong XW, et al. Deep learning prediction of ovarian malignancy at US compared with O-RADS and expert assessment. *Radiology* (2022) 304(1):106–13. doi: 10.1148/radiol.211367

132. Wang S, Liu Z, Rong Y, Zhou B, Bai Y, Wei W, et al. Deep learning provides a new computed tomography-based prognostic biomarker for recurrence prediction in high-grade serous ovarian cancer. *Radiother Oncol* (2019) 132:171–7. doi: 10.1016/j.radonc.2018.10.019

133. Li B, Qi J, Fu L, Han J, Choo J, deMello AJ, et al. Integrated hand-powered centrifugation and paper-based diagnosis with blood-in/answer-out capabilities. *Biosens Bioelectron.* (2020) 165:112282. doi: 10.1016/j.bios.2020.112282

134. Ahmed A, Aziz S, Abd-Alrazaq A, Farooq F, Sheikh J. Overview of artificial intelligence-driven wearable devices for diabetes: scoping review. *J Med Internet Res* (2022) 24(8):e36010. doi: 10.2196/36010

135. Wu J, Liu C, Liu X, Sun W, Li L, Gao N, et al. Artificial intelligence-assisted system for precision diagnosis of PD-L1 expression in non-small cell lung cancer. *Mod Pathol* (2022) 35(3):403–11. doi: 10.1038/s41379-021-00904-9

136. Shamai G, Livne A, Polónia A, Sabo E, Cretu A, Bar-Sela G, et al. Deep learning-based image analysis predicts PD-L1 status from H&E-stained histopathology images in breast cancer. *Nat Commun* (2022) 13(1):6753. doi: 10.1038/s41467-022-34275-9

137. Kapil A, Meier A, Zuraw A, Steele KE, Rebelatto MC, Schmidt G, et al. Deep semi supervised generative learning for automated tumor proportion scoring on NSCLC tissue needle biopsies. *Sci Rep* (2018) 8(1):17343. doi: 10.1038/s41598-018-35501-5

138. Trebeschi S, Drago SG, Birkbak NJ, Kurilova I, Călin AM, Delli Pizzi A, et al. Predicting response to cancer immunotherapy using noninvasive radiomic biomarkers. *Ann Oncol* (2019) 30(6):998–1004. doi: 10.1093/annonc/mdz108

139. Abbasi J. "Electronic nose" predicts immunotherapy response. *JAMA* (2019) 322(18):1756. doi: 10.1001/jama.2019.18225

140. Kleine-Kohlbrecher D, Petersen NV, Pavlidis MA, Trolle T, Friis S, Kringelum J, et al. Abstract LB199: a personalized neoantigen vaccine is well tolerated and induces specific T-cell immune response in patients with resected melanoma. *Cancer Res* (2023) 83(8_Supplement):LB199. doi: 10.1158/1538-7445.AM2023-LB199

141. Chowell D, Yoo SK, Valero C, Pastore A, Krishna C, Lee M, et al. Improved prediction of immune checkpoint blockade efficacy across multiple cancer types. *Nat Biotechnol* (2022) 40(4):499–506. doi: 10.1038/s41587-021-01070-8

142. Barrera C, Corredor G, Viswanathan VS, Ding R, Toro P, Fu P, et al. Deep computational image analysis of immune cell niches reveals treatment-specific outcome associations in lung cancer. *NPJ Precis Oncol* (2023) 7(1):52. doi: 10.1038/s41698-023-00403-x

143. Houy N, Le Grand F. Optimizing immune cell therapies with artificial intelligence. *J Theor Biol* (2019) 461:34–40. doi: 10.1016/j.jtbi.2018.09.007

144. Charoentong P, Finotello F, Angelova M, Mayer C, Efremova M, Rieder D, et al. Pan-cancer immunogenomic analyses reveal genotype-immunophenotype relationships and predictors of response to checkpoint blockade. *Cell Rep* (2017) 18 (1):248–62. doi: 10.1016/j.celrep.2016.12.019

145. Hindocha S, Charlton TG, Linton-Reid K, Hunter B, Chan C, Ahmed M, et al. A comparison of machine learning methods for predicting recurrence and death after curative-intent radiotherapy for non-small cell lung cancer: development and validation of multivariable clinical prediction models. *EBioMedicine* (2022) 77:103911. doi: 10.1016/j.ebiom.2022.103911

frontiers | Frontiers in Oncology

TYPE Original Research
PUBLISHED 18 July 2023
DOI 10.3389/fonc.2023.1217872

OPEN ACCESS

EDITED BY
Stefan B. Eichmüller,
German Cancer Research Center (DKFZ), Germany

REVIEWED BY
Alberto Pavan,
Azienda ULSS 3 Serenissima, Italy
Theresa Kordaß,
German Cancer Research Center (DKFZ), Germany

*CORRESPONDENCE
Hao Tang
tanghao_0921@126.com

RECEIVED 06 May 2023
ACCEPTED 26 June 2023
PUBLISHED 18 July 2023

CITATION
Wei K, Zhou C, Chen Y, Feng X and Tang H (2023) Real-world study of PD-1/L1 immune checkpoint inhibitors for advanced non-small cell lung cancer after resistance to EGFR-TKIs.
Front. Oncol. 13:1217872.
doi: 10.3389/fonc.2023.1217872

Real-world study of PD-1/L1 immune checkpoint inhibitors for advanced non-small cell lung cancer after resistance to EGFR-TKIs

Kunchen Wei, Chao Zhou, Yang Chen, Xiao Feng and Hao Tang*

Department of Respiratory and Critical Care Medicine, Changzheng Hospital, Navy Medical University, Shanghai, China

Background: Programmed cell death-1 (PD-1) and its ligand 1 (PD-L1) inhibitors have achieved good efficacy and safety in patients with advanced EGFR mutation-negative non-small cell lung cancer (NSCLC), but their efficacy in patients with previous EGFR mutations is limited. The aim of the present study was to explore the efficacy of PD-1/L1 immune checkpoint inhibitors for the treatment of patients with advanced NSCLC who are resistant to EGFR-TKIs

Methods: This retrospective study included 123 patients with stage IV NSCLC who received treatment in Shanghai Changzheng Hospital between January 2019 and January 2022 after failure of first-line EGFR-TKIs. Of them, 39 received ICIs + chemotherapy and anti-angiogenic drugs (ICIs+BCP group), 51 received ICIs monotherapy (ICIs group), and 33 received chemotherapy and anti-angiogenic drugs (BCP group). The gender, age, smoking history, ECOG score, EGFR mutation type, PD-L1 TPS expression, and the first routine blood index before second-line treatment of all enrolled patients were recorded, and their clinical outcomes and prognosis factors were analyzed.

Results: There was no significant difference in the objective response rate (ORR) and disease control rate (DCR) between the three groups. Patients in ICIs+BCP group had better prognosis than those in ICIs monotherapy group (PFS:9.5 *vs.* 4.64 months, p<0.001; OS: 16.97 *vs.* 7.9 months p<0.001) or BCP group (9.5 *vs.* 6.48 months, p<0.005; OS: 16.97 *vs.* 11.39 months p<0.005).

Conclusion: Our findings suggest that in the real-world practice in China, PD-1/L1 immune checkpoint inhibitors combined with chemotherapy and anti-angiogenic drugs are effective for the treatment of patients with advanced NSCLC who are resistant to EGFR-TKIs.

KEYWORDS

non-small cell lung cancer, epidermal growth factor receptor, immune checkpoint inhibitor, nomogram, EGFR TKI resistance

Background

Epidermal growth factor receptor tyrosine kinase inhibitors (EGFR-TKIs) are the first-line standard of care for advanced non-small cell lung cancer (NSCLC) patients with EGFR-sensitive mutations (1, 2). Unfortunately, drug resistance often develops following EGFR-TKIs treatment and the mechanisms of resistance are variable (3). Currently, there are limited follow-up therapies for patients who are resistant to EGFR-TKIs. Programmed cell death 1 (PD-1) and its ligand 1 (PD-L1) inhibitors have achieved good efficacy and safety in some patients with advanced EGFR mutation-negative NSCLC, but their benefits in patients with previous EGFR mutations are limited (4–6). The aim of the present study was to investigate the efficacy of immune checkpoint inhibitors (ICIs) as the second line treatment for stage IV NSCLC patients following failure of first line EGFR-TKIs by retrospectively analyzing the clinicopathological features of patients with advanced NSCLC who were admitted to Changzheng Hospital (Shanghai, China) between January 2019 and January 2022, their progression survival (PFS), overall survival (OS), the objective response rate (ORR), disease control rate (DCR), and EGFR driver mutation.

Patients and methods

Patient selection

The medical records of patients who failed the treatment with first-line EGFR-TKIs were analyzed retrospectively, in whom histological or somatic cytological investigation and second-generation sequencing study were performed to determine the presence or absence of EGFR driver mutations. Patients who met the following criteria were included for further analysis: (1) age ≥ 18 years and ≤ 75 years; (2) with histologically, cytologically or pathologically confirmed stage IV NSCLC in accordance with the TNM criteria specified in the 2017 8th Edition of the International Association for the Study of Lung Cancer (IASLC); (3) with at least one quantifiable lesion in accordance with RECIST 1.1 standards; (4) confirmation by next generation sequencing testing as having EGFR driver gene mutation possibly with another positive driver gene; (5) received first-line targeted therapy with first/second generation EGFR-TKIs, including gefitinib, erlotinib, afatinib, and dacomitinib; (6) disease progression after treatment with first-line EGFR-TKIs; and (7) second-generation sequencing test showing clear negativity for EGFR T790M again after resistance to first-line EGFR-TKIs. The main exclusion criteria were (1) genetic testing suggesting T790M positivity again after resistance to first-line EGFR-TKIs; (2) inability to proceed to second-line treatment due to severe toxic and adverse effects; and (3) pathologically confirmed small cell lung cancer after resistance to first-line EGFR-TKIs. This study was approved by the ethics committee of Shanghai Changzheng hospital (2021SL018). Because this was a retrospective cohort study, informed consent was waived.

Abbreviations: ECOG, Eastern Cooperative Oncology Group performance status; EGFR, Epidermal growth factor receptor; MLR, monocyte-to-lymphocyte ratio; NLR, neutrophil-to-lymphocyte ratio; PLR, platelet-to-lymphocyte ratio; NSCLC, non-small cell lung cancer; PD-1, Programmed Cell Death-1; PD-L1, Programmed Cell Death Ligand-1; RECIST1.1, Response Evaluation Criteria in Solid Tumors RECIST Version 1.1.

Study design

According to their second-line treatment modality, all study participants were given first-line EGFR-TKIs and then divided into three groups: ICIs combined with platinum-containing two-drug chemotherapy and anti-angiogenic drugs (ICIs+BCP group), ICIs monotherapy group (ICIs group), and platinum-containing two-drug chemotherapy combined with anti-angiogenic drugs (BCP group). Gender, age, smoking history, ECOG score, EGFR mutation type, PD-L1 tumor cell proportion score (TPS), first routine blood parameters before second-line treatment including neutrophil, lymphocyte, monocyte count and platelet counts, and serum inflammation-related factors were recorded in all patients. In addition, general information including the neutrophil-to-lymphocyte ratio (NLR), monocyte-to-lymphocyte ratio (MLR) and platelet-to-lymphocyte ratio were measured. All patients were followed up until January 2022, when their PFS, OS, ORR and DCR were calculated to determine the effectiveness of ICIs as the second-line treatment for patients with advanced NSCLC who were resistant to EGFR-TKIs. 20 NSCLC patients meeting inclusion criteria from February 1, 2022 to January 31, 2023 as an external validation set.

Statistical analysis

This study was conducted using STATA (version 16.0), R (version 4.0.3), SPSS (version 26.0) and GraphPad Prism (version 8.0.1) software for statistical analysis and data visualization. Measurement data are expressed as the mean ± standard deviation (SD), and enumeration data are expressed as the percentage (%). Analysis of variance (ANOVA) was used for comparison between groups for measurement data, and $\chi 2$ test was used for comparison between groups for enumeration data. Kaplan-Meier method was used to assess OS and PFS between patient groups, and Log-rank method was used to analyze survival differences. Univariate and multifactorial COX regression analyses were used to screen for independent prognostic factors. R software and associated R package were used to construct Nomogram prediction models. The closer the AUC value to 1 indicates better discrimination. $P < 0.05$ was considered statistically significant.

Results

Patient characteristics

A total of 442 patients diagnosed with stage IV NSCLC were collected in this study, excluding 81 patients whose disease had not

yet progressed after treatment with first-line EGFR-TKIs, and a total of 361 patients showed disease progression requiring second-line treatment, of whom 43 patients received targeted therapy with third-generation EGFR-TKIs, and 123 patients met the inclusion criteria of this study. Analysis of the general data of all enrolled patients revealed 123 patients with advanced NSCLC, who were classified as three groups: 39 in ICIs+BCP group, 51 in ICIs group, and 33 in BCP group. ANOVA analysis showed significant differences in age distribution, ECOG score, EGFR mutation type and PD-L1 TPS expression between the three groups ($p < 0.05$). The details are listed in Table 1.

Therapeutic efficacy

Until January 2022, no patient achieved complete remission (CR) in all three groups. The number of patients who achieved partial remission (PR) was 6 (15.4%) in ICIs+BCP group, 10 (19.6%) in ICIs group, and 4 (12.1%) in BCP group. Stable disease (SD) in 30 (76.9%), 39 (76.5%) and 26 (78.8%) patients of the three groups respectively, 3 (7.7%), 2 (3.9%) and 3 (8.3%) patients demonstrated progressive disease (PD). There were no significant differences in ORR and DCR between the three groups (Table 2). Log-rank test of OS and PFS in 39 cases in ICIs+BCP group and 51 cases in ICIs-alone group showed that the overall prognosis in ICIs+BCP group was significantly better than that in ICIs-alone group [OS: 16.97 months (15.11-18.84 months) *vs.* 7.9 months (7.33-8.55 months), p<0.001; PFS: 64 3.92-5.35 months *vs.* 4 9.5 (8.1-10.91) months, p<0.001] (Figures 1A, B). Log-rank test of OS and PFS of 39 cases in ICIs+BCP group and 33 cases in BCP group showed that the prognosis in ICIs_BCP group was significantly better than that in BCP group [OS: 16.97 (15.11-18.84) months *vs.* 11.39 (9.70-13.08) months, P<0.05; PFS: 9.5 months, (8.1-10.9) months 6.48 (5.36-7.60) months, P<0.05] (Figures 1C, D).

Analysis of prognostic factors

After the occurrence of resistance to first-line EGFR-TKIs in the 123 NSCLC patients, univariate analysis was performed of their age, gender, smoking history, whether or not receiving immunotherapy, driver mutation type, ECOG score, PD-L1 TPS expression, neutrophil count (NEUT), lymphocyte count (LYM), monocyte count (MON), platelet count (PLT) and inflammation-related factors in serum, and neutrophil-lymphocyte ratio (NLR), monocyte/lymphocyte ratio (MLR), and platelet to lymphocyte ratio (PLR). Factors with P<0,05 in univariate analysis were subjected to multivariate analysis. the result of univariate analysis showed that PD-L1 TPS expression, MLR, PLT, whether receiving immunotherapy, and age were significant prognostic

TABLE 1 Patient characteristics (*N* = 123).

Characteristic	ICIs+BCP (*N*=39)	ICIs (*N*=51)	BCP (*N*=33)	*p*
Age (`x ± s)	64.2±11.9	63.5 ± 13.9	60.4 ± 10.8	<0.001
≦65	17 (43.6%)	40 (78.4%)	27 (81.8%)	
>65	22 (56.4%)	11 (21.6%)	6 (18.2%)	
Sex				
Male	24 (61.5%)	25 (49.0%)	15 (45.5%)	0.338
Female	15 (38.5%)	26 (51.0%)	18 (54.5%)	
Smoking history				
No	30 (76.9%)	33 (64.7%)	21 (63.6%)	0.373
Yes	9 (23.1%)	18 (35.3%)	12 (36.4%)	
ECOG score				
0	25 (64.1%)	44 (86.3%)	30 (90.9%)	0.017
1	13 (33.3%)	7 (13.7%)	3 (9.1%)	
2	2(2.6%)	0 (0.0%)	0 (0.0%)	
EGFR mutation				
19del	27 (69.2%)	40 (78.4%)	14 (42.4%)	0.003
21L858R	12 (30.8%)	11 (21.6%)	19 (57.6%)	
PD-L1 TPS				
<1%	27 (69.2%)	42 (82.4%)	18 (54.5%)	0.023
≧1%	12 (30.8%)	9 (17.6%)	15 (45.5%)	

ECOG, Eastern Cooperative Oncology Group; EGFR Epidermal, Growth Factor Receptor; TPS, Tumor cell Proportion Score.

TABLE 2 Overall response to treatment.

Best overall response	ICIs+BCP No.	ICIs No.	BCP No.
Overall	39	51	33
Complete response	0	0	0
Partial response	6	10	4
Stable disease	30	39	26
Progressive disease	3	2	3
Objective Response Rate (%)	15.38%	19.61%	12.12%
Disease Control Rate (%)	92.31%	96.08%	90.91%

factors affecting OS in NSCLC patients after receiving first-line EGFR-TKIs therapy resistance (p<0.05) (Table 3), while gender, smoking history, EGFR driver mutation type, ECOG score, NEUT, LYM, MON, NLR, and PLR had no significant effect on OS of the patients. Among them, the difference between PD-L1 TPS ≥1% and PD-L1 negative patients was statistically significant (HR=0.349, 0.176-0.691, p=0.003); treatment with ICIs after drug resistance had a more significant effect on patient survival (HR=0.533, 0.286-0.991, p=0.047); higher MLR and higher EGFR-TKIs-resistance indicated a worse prognosis (HR=2.66, 1.396-5.070, p=0.003) (Figures 2A, B)

The significant prognostic factors in univariate analysis were subjected to multifactorial COX regression analysis, and the result showed that PD-L1 TPS expression was an independent prognostic factor (HR=0.235, 0.077-0.712, p=0.01), while MLR (HR=1.357, 0.245-7.500, p=0.726), PLT (HR=0.997 0.991-1.002, p=0.256), whether receiving immunotherapy (HR=0.472, 0.163-1.361, p=0.165), and age (HR=0.976, 0.948-1.004, p=0.091) were not statistically significant (Figure 2C).

LASSO Cox regression includes a total of 21 variables including age, gender, smoking history, whether or not receiving immunotherapy, driver mutation type, ECOG score, PD-L1 TPS expression, NEUT, LYM, MON, PLT, NLR, MLR, and PLR. 5-fold cross-validation in our study showed PD-L1 TPS expression, MLR, PLT, whether or not receiving immunotherapy and age remained the five non-zero coefficient variables as OS significant predictors (Figures 2D, E).

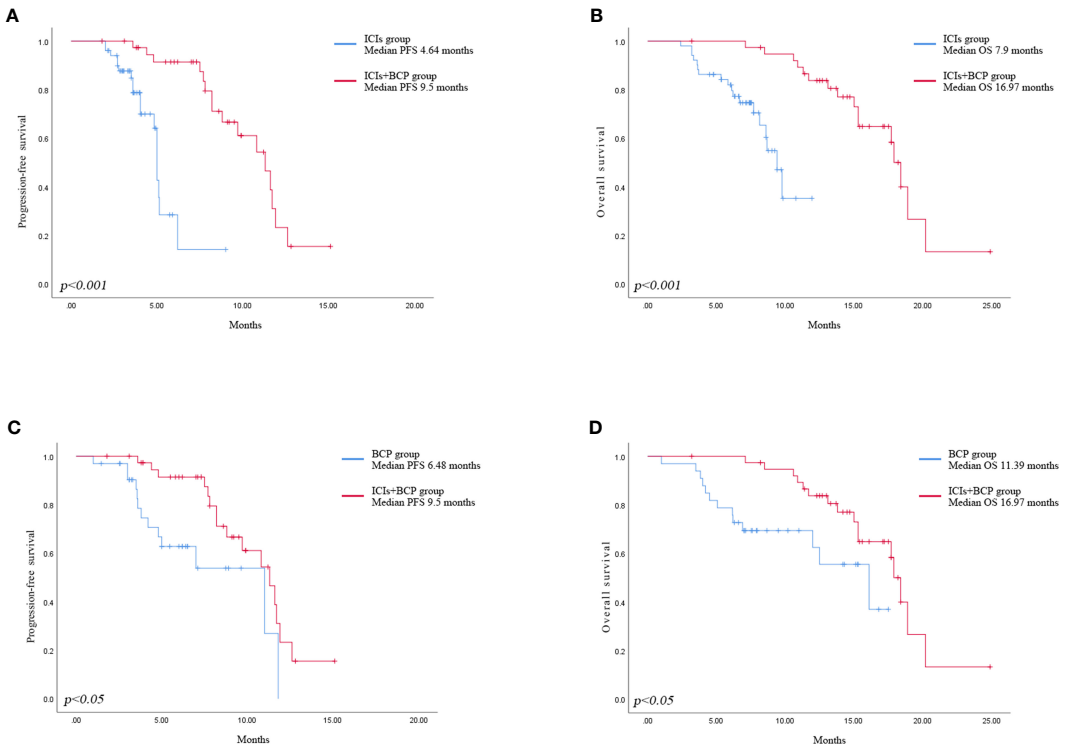

FIGURE 1
Kaplan-Meier analysis of progression-free survival in ICIs group and ICIs+BCP group **(A)**. Overall survival in ICIs group and ICIs+BCP group **(B)**. Progression-free survival in BCP group and ICIs+BCP group **(C)**. Overall survival in BCP group and ICIs+BCP group **(D)**.

TABLE 3 Univariate and multivariate Cox regression analyses.

Characteristics	Univariable Analysis			Multivariate Analysis		
	HR	95% CI	*P*	HR	95% CI	*P*
PD-L1	0.349	0.176-0.691	0.003	0.235	0.077-0.712	0.010
MLR	2.660	1.396-5.070	0.003	1.357	0.245-7.500	0.726
Platelets	0.994	0.990-0.999	0.009	0.997	0.991-1.002	0.256
ICIs	0.533	0.286-0.991	0.047	0.472	0.163-1.361	0.165
Age	0.978	0.956-1.000	0.050	0.976	0.948-1.004	0.091
Monocytes	1.303	0.970-1.750	0.079	–	–	–
NLR	1.131	0.970-1.318	0.116	–	–	–
ECOG	0.597	0.302-1.179	0.137	–	–	–
ALB	1.050	0.976-1.129	0.190	–	–	–
21L858R	1.468	0.821-2.623	0.195	–	–	–
19del	0.681	0.381-1.218	0.195	–	–	–
T790M	1.415	0.658-3.042	0.374	–	–	–
Leukocytes	1.032	0.953-1.117	0.439	–	–	–
Gender	1.229	0.697-2.169	0.476	–	–	–
CAR	0.846	0.436-1.640	0.620	–	–	–
Lymphocytes	1.023	0.926-1.131	0.650	–	–	–
SMOKING	1.127	0.594-2.139	0.714	–	–	–
PLR	1.001	0.997-1.004	0.752	–	–	–
Neutrophils	1.019	0.846-1.227	0.844	–	–	–
CRP	1.000	0.976-1.024	0.975	–	–	–
Eosinophils	0.999	0.283-3.524	0.998	–	–	–

Nomogram of the prediction model

Based on the predictors obtained from the above univariate and multivariate analyses, a prediction model for the probability of patient survival after EGFR-TKIs resistance was constructed. The column line graph prediction model of the probability of survival of patients after EGFR-TKIs resistance was established using R software (Figure 3A). According to the obtained prediction model, each factor could obtain the corresponding score, and the total score was obtained by summing the corresponding scores of each factor, and the total score was projected onto the bottom probability value axis, which could predict the relative survival probability. The differentiation of the constructed Nomogram prediction model was evaluated by plotting the Receiver Operating Characteristic (ROC) based on the Nomogram prediction model and using the magnitude of the Area Under Curve (AUC) of the ROC curve. The AUC value of the EGFR and prediction model for 1- and 2-year survival after TKIs resistance were 0.815 and 0.846, respectively, which showed that the model had a good prediction effect and did not show significant overfitting (Figure 3B). We established an external validation curve using a dataset that consisted of 20 NSCLC patients meeting inclusion criteria from February 1, 2022 to January 31, 2023 to validate the predictive power of the nomogram (Figure 3C). The AUC value was 0.734.

Discussion

Several previous studies have demonstrated the poor efficacy of PD-1/L1 inhibitors in patients resistant to epithelial growth factor receptor- tyrosine-kinase inhibitors (EGFR-TKIs). A KEYNOTE-001 phase II trial reported that 11 of the 25 patients with positive EGFR mutations treated with pembrolizumab monotherapy discontinued the treatment because of failure to respond to the treatment (7). A Checkmate 012 trial used Nivolumab monotherapy in EGFR mutation-positive patients, with unsatisfactory outcomes (ORR=14%; mPFS=1.8 months) (8), suggesting an unclear role of immunotherapy in patients resistant to EGFR-TKIs. Several previous studies have demonstrated that high PD-L1 expression, high TMB expression, and high CD8+ T cell infiltration often suggest good immunotherapy efficacy, especially in NCSCLC patients with high PD-L1 expression. A phase 3 Checkmate 057 clinical trial randomized 582 patients

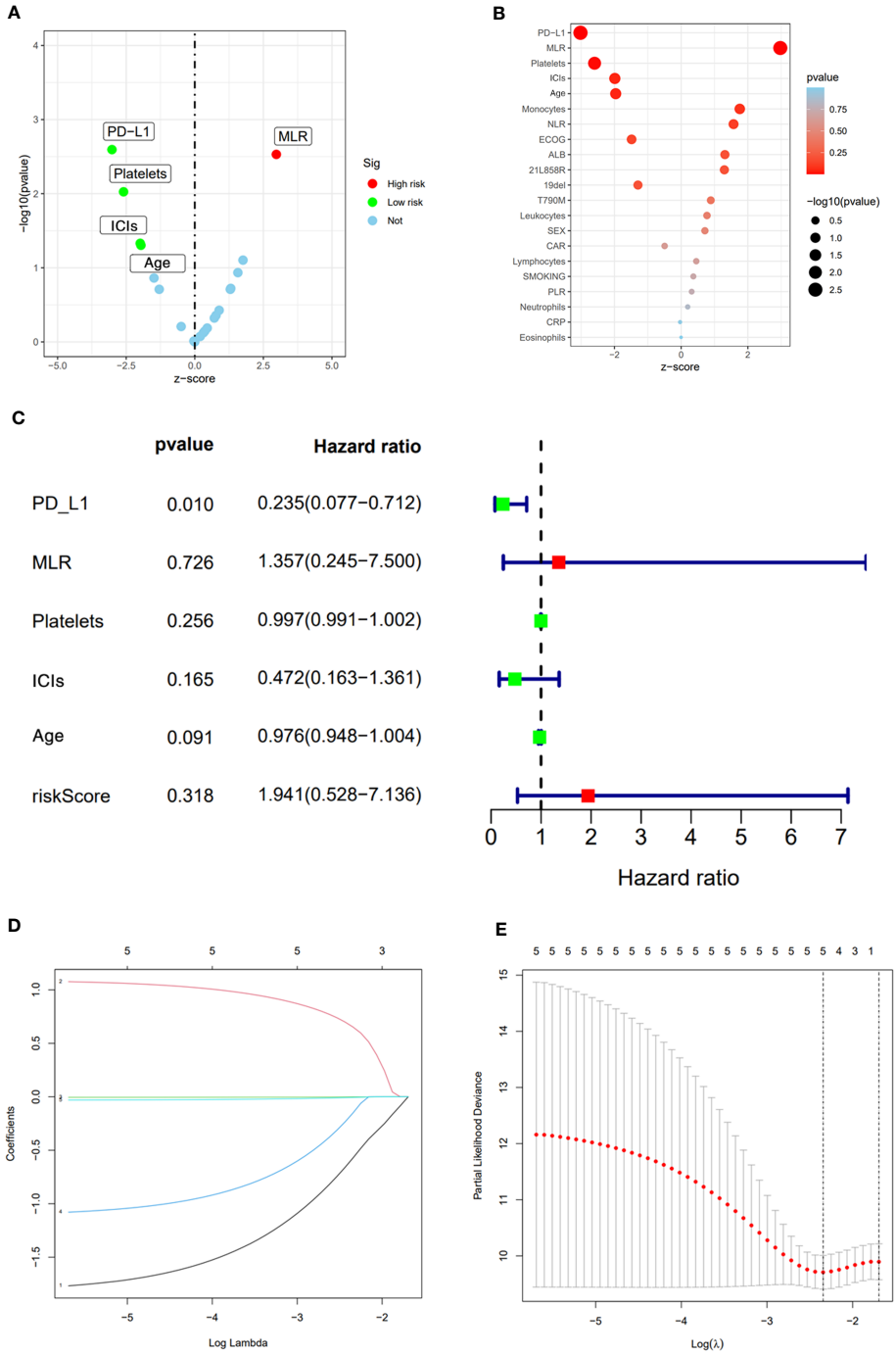

FIGURE 2
Univariate analysis results **(A, B)**. Multivariate analysis results **(C)**. LASSO Cox regression model construction, Processes of LASSO Cox model fitting **(D)**. λ selection by 10-fold cross-validation **(E)**.

with lung adenocarcinoma who failed to respond to first-line chemotherapy into a group receiving docetaxel second-line chemotherapy and a group receiving a second-line chemotherapy. The result of their subgroup analysis based on PD-L1 expression levels (≥1%, ≥5% and ≥10%) showed that the Nivolumab monotherapy group was superior to the docetaxel second-line chemotherapy group in patients with positive PD-L1 expression (9).The level of PD-L1 expression remains unclear in NSCLC patients resistant to EGFR-TKIs therapy. Le et al. (10) showed that the PD-L1 expression, TMB level and CD8+ T cell infiltration were all low in EGFR mutation positive patients with an immune inert phenotype in tumor cells, although this trial demonstrated *in vitro* that cells expressing EGFR mutations could significantly suppress immune cell activity, but the exact mechanism remains unclear. Some studies found that when PD-1/L1 immune checkpoint inhibitors were applied to patients with EGFR

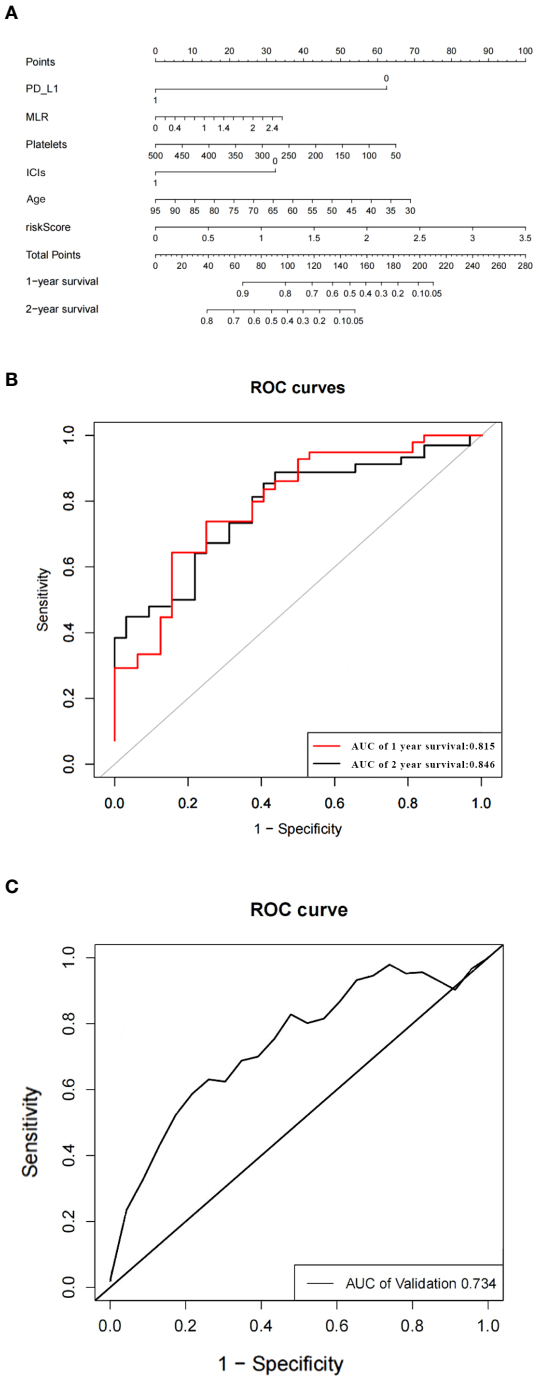

FIGURE 3
The nomogram of the overall survival prediction model **(A)**. The area under the ROC curve (AUC) indicates that the prediction model has good prediction accuracy **(B)**. ROC curve of predictive model from validation set **(C)**.

mutations, some patients showed a robust immune response, while others did not. Kohsuke et al. (11) retrospectively collected 138 EGFR mutation-positive patients who were tested again for PD-L1 expression levels after resistance to EGFR-TKIs. Paired analysis of the pre- and post-progression samples showed a significant increase in PD-L1 expression in tumor samples after EGFRTKI treatment resistance, especially for T790M-negative patients, but they were unsure whether increased PD-L1 expression could provide a survival benefit for patients resistant to EGFR-TKIs treatment.

Several previous studies such as KEYNOTE-010, ATLANTIC, and POPLAR reported their uncertainty about whether ICIs alone could achieve a survival benefit in EGFR mutation-positive patients, because they found that the efficacy of ICIs was not superior to that of conventional platinum-containing two-drug chemotherapy (12–14). ICIs combined with platinum-containing two-drug chemotherapy also failed to achieve survival benefit in patients resistant to EGFR-TKIs (15, 16). In contrast to immune monotherapy, immune combination with platinum-containing

dual-agent chemotherapy and anti-angiogenic drug treatment strategies have yielded good results. Related studies have shown the immunomodulatory effects of vascular endothelial growth factor (VEGF) inhibitors, a highly specific pro-vascular endothelial cell growth factor, and the key role of VEGF in suppressing anti-tumor immune responses, in addition to its angiogenic effects by negatively affecting antigen-presenting cells (APCs) and effector T cells on the one hand, and enhancing the action of immunosuppressive cells such as regulatory T cells (Treg) and myeloid-derived suppressor cells (MDSCs) on the other, which in turn bind to their receptor VEGFR2 to inhibit the differentiation of monocytes to dendritic cells (DCs) and drive immune evasion by reducing DC maturation and antigen presentation. Anti-angiogenic drugs, on the other hand, reverse VEGF-mediated immunosuppression by enhancing the killing capacity of cancer cells by T-cell-mediated checkpoint inhibitors and re-sensitizing this subset of tumors to PD-L1 inhibitors (17, 18).

Several studies have demonstrated that the combination of PD-1/L1 inhibitors, platinum-containing dual-agent chemotherapy and VEGF inhibitors can improve the survival prognosis of patients with EGFR mutation-positive disease. The CT 18 study was designed to explore the efficacy, safety and predictive biomarkers of toripalimab in combination with chemotherapy as second-line therapy for patients with EGFR-mutated advanced NSCLC. The results showed that the use of toripalimab in combination with platinum-containing two-agent chemotherapy in T790M-negative patients after resistance to EGFR-TKIs resulted in an 50% ORR, median PFS of 7 months, and median OS of 23.5 months, which were all better than controls (19, 20). The ORIENT-31 study was the first phase III, double-blind, randomized, controlled study in EGFR-resistant patients, which included 444 patients with nonsquamous, NSCLC with metastatic EGFR. All of them progressed after receiving targeted therapy. Patients were randomized to a four-drug combination group (sintilimab + VEGF inhibitor + pemetrexed + cisplatin), a three-drug combination group (sintilimab + pemetrexed + cisplatin), and a two-drug combination group (pemetrexed + cisplatin), and the results of the first interim analysis showed that the four-drug combination group was superior to the two-drug group (mPFS 6.9m vs. 4.3m, HR=0.46, P<0.0001) (21). The IMpower150 study is a phase III clinical trial exploring atezolizumab in combination with bevacizumab and carboplatin and paclitaxel (ABCP) in the first-line treatment of patients with advanced NSCLC. In patients with EGFR mutations, the efficacy in ABCP group was better than that in bevacizumab combined with carboplatin and paclitaxel group (mOS 29.4m *vs.* 18.1m, HR=0.6, 95% CI:0.31-1.14) (22). In the present study, we retrospectively analyzed 123 NSCLC patients who were previously EGFR mutation positive and resistant to treatment with EGFR-TKIs, the median PFS in the immune four-drug combination group was better than that in the other two treatment regimen groups, which is consistent with the experimental result of the ORIENT-31 study. In addition, the NCT03647956 trial also included patients with EGFR-mutated NSCLC who progressed after treatment with EGFR-TKIs. In patients who received a combination of atezolizumab (1200 mg), bevacizumab (7.5 mg/kg), pemetrexed (500 mg/m2) and carboplatin (AUC 5) every 3 weeks, with maintenance treatment with atezolizumab + bevacizumab + pemetrexed after 6 cycles, the ORR was 62.5%, the median PFS was 9.4 months (95% CI: 7.6-12.1), and the 1-year OS rate was 72.5% (95% CI: 0.56-0.83). in addition, PFS was significantly improved with the four-drug combination regimen compared with PFS with EGFR-TKIs-containing regimen rechallenge (5.8 months [95% CI 3.9-10.0 months]) and PFS with EGFR-TKIs single-drug rechallenge treatment (4.0 months [95% CI: 1.3-4.6 months]).

In this study, we enrolled 123 patients with NSCLC who were resistant to first-line EGFR-TKIs and analyzed the clinical efficacy of PD-1/PD-L1 inhibitors by counting PFS, OS, ORR and DCR of all patients to explore the efficacy of ICIs as second-line treatment in patients with EGFR-TKIs-resistant advanced NSCLC. The results showed that for patients with advanced NSCLC after resistance to EGFR-TKIs, PD-1/L1 immune checkpoint inhibitors combined with bevacizumab in combination with platinum-containing two-drug chemotherapy had some efficacy in terms of patient survival and toxicity tolerance as compared with conventional platinum-containing two-drug chemotherapy.

Conclusions

Our study demonstrated that the PD-1/L1 immune checkpoint inhibitors combined with bevacizumab in combination with platinum-containing two-drug chemotherapy were effective in patients with advanced NSCLC after resistance to EGFR-TKIs, in whom survival was better than that in patients receiving conventional platinum-containing two-drug chemotherapy. Combination of patients' PD-L1 TPS expression, MLR, PLT, whether or not receiving immunotherapy, age and other clinical indicators were used for survival prediction of patients with resistance to EGFR-TKIs, which enables better individualized treatment and prognosis assessment.

Data availability statement

The original contributions presented in the study are included in the article/supplementary material. Further inquiries can be directed to the corresponding author.

Ethics statement

All procedures performed in studies involving human participants were in accordance with the ethical standards of the institutional and/or national research committee and with the 1964 Helsinki Declaration and its later amendments or comparable ethical standards. The study was approved by the institutional review boards of all participating institutions (Approval No. 2021SL018).

Author contributions

KW and HT designed the research study. KW, CZ, YC, and XF collected cases. KW analyzed and interpreted patient data. KW and CZ wrote the manuscript. All authors have read and approved the final manuscript. All authors contributed to the article and approved the submitted version.

Funding

The research was sponsored by "Shuguang Program" supported by Shanghai Education Development Foundation and Shanghai Municipal Education Commission (20SG38); Shanghai Municipal Science and Technology Committee of Shanghai Outstanding Academic Leaders Plan (20XD1423300); and the General Program of National Nature Science Foundation of China (No. 82070036).

Conflict of interest

The authors declare that the research was conducted in the absence of any commercial or financial relationships that could be construed as a potential conflict of interest.

Publisher's note

References

1. Ciardiello F, Tortora G. EGFR antagonists in cancer treatment. *N Engl J Med* (2008) 358:1160–74. doi: 10.1056/NEJMra0707704

2. He M, Capelletti M, Nafa K, Cai-Hong Y, Maria E, Vincent A, et al. EGFR exon 19 insertions: a new family of sensitizing EGFR mutations in lung adenocarcinoma. *Clin Cancer Res* (2012) 18:1790–7. doi: 10.1158/1078-0432.CCR-11-2361

3. Passaro A, Jänne PA, Mok T, Peters S. Overcoming therapy resistance in EGFR-mutant lung cancer. *Nat Cancer* (2021) 2(4):377–91. doi: 10.1038/s43018-021-00195-8

4. Liu B, Song Y, Liu D. Recent development in clinical applications of PD-1 and PD-L1 anti-bodies for cancer immunotherapy. *J Hematol Oncol* (2017) 10:174. doi: 10.1186/s13045-017-0541-9

5. Bhatnagar V, Gormley NJ, Luo L, Shen Y, Sridhara R, Subramaniam S, et al. FDA Approval summary: daratumumab for treatment of multiple myeloma after one prior therapy. *Oncologist* (2017) 22:1347–53. doi: 10.1634/theoncologist.2017-0229

6. Borghaei H, Paz-Ares L, Horn L, Horn L, Spigel D, Steins M, et al. Nivolumab versus docetaxel in advanced nonsquamous non-small-cell lung cancer. *N Engl J Med* (2015) 373:1627–39. doi: 10.1056/NEJMoa1507643

7. Lisberg A, Cummings A, Goldman JW, Bornazyan K, Reese N, Wang T, et al. A phase II study of pembrolizumab in EGFR-mutant, PD-L1+, tyrosine kinase inhibitor naive patients with advanced NSCLC. *J Thorac Oncol* (2018) 13(8):1138–45. doi: 10.1016/j.jtho.2018.03.035

8. Gettinger S, Hellmann MD, Chow LQM, Borghaei H, Antonia S, Brahmer JR, et al. Nivolumab plus erlotinib in patients with EGFR-mutant advanced NSCLC. *J Thorac Oncol* (2018) 13(9):1363–72. doi: 10.1016/j.jtho.2018.05.015

9. Borghaei H, Paz-Ares L, Horn L, Spigel DR, Steins M, et al. Nivolumab versus docetaxel in advanced nonsquamous non-Small-Cell lung cancer. *N Engl J Med* (2015) 373(17):1627–39. doi: 10.1056/NEJMoa1507643

10. Le X, Negrao MV, Reuben A, Federico L, Diao L, McGrail D, et al. Characterization of the immune landscape of EGFR-mutant NSCLC identifies CD73/Adenosine pathway as a potential therapeutic Target. *J Thorac Oncol* (2021) 16(4):583–600. doi: 10.1016/j.jtho.2020.12.010

11. Isomoto K, Haratani K, Hayashi H, Shimizu S, Tomida S, Niwa T, et al. Impact of EGFR-TKI treatment on the tumor immune microenvironment in EGFR mutation–positive non–small cell lung Cancer. *Clin Cancer Res* (2020) 26(8):2037–46.12. doi: 10.1158/1078-0432.CCR-19-2027

12. Herbst RS, Baas P, Kim D-W, Felip E, Pérez-Gracia JL, Han J-Y, et al. Pembrolizumab versus docetaxel for previously treated, PD-L1-positive, advanced non-small-cell lung cancer (KEYNOTE-010): a randomised controlled trial. *Lancet* (2016) 387(10027):1540–50. doi: 10.1016/S0140-6736(15)01281-7

13. Garassino MC, Cho B-C, Kim J-H, Mazières J, Vansteenkiste J, Lena H, et al. Durvalumab as third-line or later treatment for advanced non-small-cell lung cancer (ATLANTIC):an open-label, single-arm, phase 2 study. *Lancet Oncol* (2018) 19(4):521–36. doi: 10.1016/S1470-2045(18)30144-X

14. Lee CK, Man J, Lord S, Links M, Gebski V, Mok T, et al. Check-point inhibitors in metastatic EGFR-mutated non-small cell lung cancer-a meta-analysis. *J Thorac Oncol* (2017) 12(2):403–7. doi: 10.1016/j.jtho.2016.10.007

15. Mok TSK, Nakagawa K, Park K, et al. Nivolumab (NIVO) + chemotherapy (chemo) vs chemo in patients (pts) with EGFR-mutated metastatic non-small cell lung cancer (mNSCLC) with disease progression after EGFR tyrosine kinase inhibitors (TKIs) in CheckMate 722. 2022 ESMO ASIA. *Abs LBA8*. doi: 10.1016/j.annonc.2022.10.350

16. Yang JC, Lee DH, Lee JS, Fan Y, Marinis F, Okamoto I, et al. Pemetrexed and platinum with or without pembrolizumab for tyrosine kinase inhibitor (TKI)-resistant, EGFR-mutant, metastatic nonsquamous NSCLC: phase 3 KEYNOTE-789 study. *2023 ASCO* (2023) LBA9000.

17. Galon J, Bruni D. Approaches to treat immune hot, altered and cold tumours with combination immunotherapies. *Nat Rev Drug Discovery* (2019) 18(3):197–218. doi: 10.1038/s41573-018-0007-y

18. Hegde PS, Karanikas V, Evers S. The where, the when, and the how of immune monitoring for cancer immunotherapies in the era of checkpoint inhibition. *Clin Cancer Res* (2016) 22(8):1865–74. doi: 10.1158/1078-0432.CCR-15-1507

19. Ren S, Zhang J, Zhao Y, Mu X, Zhou J, Bao Z, et al. A multi-center phase II study of toripalimab with chemotherapy in patients with EGFR mutant advanced NSCLC patients resistant to EGFR TKIs: efficacy and biomarker analysis. *J Clin Oncol* (2020) 38 (15_suppl):e21618–e. doi: 10.1200/JCO.2020.38.15_suppl.e21618

20. Zhang J, Zhou C, Zhao Y, Mu X, Zhou J, Bao Z, et al. MA11.06 a PII study of toripalimab, a PD-1 mAb, in combination with chemotherapy in EGFR+ advanced NSCLC patients failed to prior EGFR TKI therapies. *J Thorac Oncol* (2019) 14(10). doi: 10.1016/j.jtho.2019.08.587

21. Lu S, Wu L, Jian H, Chen Y, Wang Q, Fang J, et al. Sintilimab plus bevacizumab biosimilar IBI305 and chemotherapy for patients with EGFR-mutated non-squamous non-small-cell lung cancer who progressed on EGFR tyrosine-kinase inhibitor therapy (ORIENT-31): first interim results from a randomised, double-blind, multicentre, phase 3 trial. *Lancet Oncol* (2022) S1470-2045(22):00382–5. doi: 10.1016/S1470-2045(22)00382-5

22. Reck M, Mok T, Socinski MA, Jotte RM, Lim DWT, Cap-puzzo F, et al. 1293P IMpower150: updated efficacy analysis in patients with EGFR mutations. *Ann Oncol* (2020) 31:S837–S8. doi: 10.1016/j.annonc.2020.08.1607

frontiers | Frontiers in Immunology

TYPE Original Research
PUBLISHED 21 July 2023
DOI 10.3389/fimmu.2023.1219720

OPEN ACCESS

EDITED BY
Stefan B. Eichmüller,
German Cancer Research Center (DKFZ), Germany

REVIEWED BY
Saghar Kaabinejadian,
Pure MHC, LLC, United States
Anthony Wayne Purcell,
Monash University, Australia
Jonas Becker,
German Cancer Consortium, German Cancer Research Center (DKFZ), Germany

*CORRESPONDENCE
Juliane S. Walz
juliane.walz@med.uni-tuebingen.de

†These authors have contributed equally to this work and share first authorship

RECEIVED 09 May 2023
ACCEPTED 05 July 2023
PUBLISHED 21 July 2023

CITATION
Wacker M, Bauer J, Wessling L, Dubbelaar M, Nelde A, Rammensee H-G and Walz JS (2023) Immunoprecipitation methods impact the peptide repertoire in immunopeptidomics.
Front. Immunol. 14:1219720.
doi: 10.3389/fimmu.2023.1219720

Immunoprecipitation methods impact the peptide repertoire in immunopeptidomics

Marcel Wacker[1,2,3†], Jens Bauer[1,2,3†], Laura Wessling[2], Marissa Dubbelaar[1,2,3,4], Annika Nelde[1,2,3], Hans-Georg Rammensee[2,3,5] and Juliane S. Walz[1,2,3,5,6*]

[1]Department of Peptide-based Immunotherapy, University and University Hospital Tübingen, Tübingen, Germany, [2]Institute for Cell Biology, Department of Immunology, University of Tübingen, Tübingen, Germany, [3]Cluster of Excellence iFIT (EXC2180) "Image-Guided and Functionally Instructed Tumor Therapies", University of Tübingen, Tübingen, Germany, [4]Quantitative Biology Center (QBiC), University of Tübingen, Tübingen, Germany, [5]German Cancer Consortium (DKTK) and German Cancer Research Center (DKFZ), partner site Tübingen, Tübingen, Germany, [6]Clinical Collaboration Unit Translational Immunology, German Cancer Consortium (DKTK), Department of Internal Medicine, University Hospital Tübingen, Tübingen, Germany

Introduction: Mass spectrometry-based immunopeptidomics is the only unbiased method to identify naturally presented HLA ligands, which is an indispensable prerequisite for characterizing novel tumor antigens for immunotherapeutic approaches. In recent years, improvements based on devices and methodology have been made to optimize sensitivity and throughput in immunopeptidomics. However, developments in ligand isolation, mass spectrometric analysis, and subsequent data processing can have a marked impact on the quality and quantity of immunopeptidomics data.

Methods: In this work, we compared the immunopeptidome composition in terms of peptide yields, spectra quality, hydrophobicity, retention time, and immunogenicity of two established immunoprecipitation methods (column-based and 96-well-based) using cell lines as well as primary solid and hematological tumor samples.

Results: Although, we identified comparable overall peptide yields, large proportions of method-exclusive peptides were detected with significantly higher hydrophobicity for the column-based method with potential implications for the identification of immunogenic tumor antigens. We showed that column preparation does not lose hydrophilic peptides in the hydrophilic washing step. In contrast, an additional 50% acetonitrile elution could partially regain lost hydrophobic peptides during 96-well preparation, suggesting a reduction of the bias towards the column-based method but not completely equalizing it.

Discussion: Together, this work showed how different immunoprecipitation methods and their adaptions can impact the peptide repertoire of immunopeptidomic analysis and therefore the identification of potential tumor-associated antigens.

KEYWORDS

immunotherapies, HLA peptides, mass spectrometry, immunopeptidomics, immunoprecipitation, hydrophobicity, immunogenicity

1 Introduction

Human leukocyte antigen (HLA)-presented peptides and their T cell recognition play a key role in the immune surveillance of malignant diseases (1, 2). Utilizing the respective tumor antigens to therapeutically induce anti-tumor T cell responses is the aim of various recent T cell-based immunotherapeutic approaches (3–6). Therefore, a critical step of these therapeutic approaches is correctly identifying suitable antigen targets recognized by the immune system and showing natural, high-frequent, and tumor-exclusive presentation on the tumor cell surface (7). Currently, the only methodology suitable for an unbiased identification and characterization of naturally presented HLA class I- and HLA class II-restricted peptides is mass spectrometry (MS)-based immunopeptidomics (8, 9). The three core steps for immunopeptidome analysis are first the co-immunoprecipitation (co-IP) of solubilized HLA-peptide complexes from cell or tissue lysates, followed by the isolation and purification of HLA-restricted peptides and the MS-based peptide sequencing by liquid chromatography-coupled tandem mass spectrometry (LC-MS/MS) (10–12). Finally, the data analysis of acquired peptide spectra is performed by database search tools (13–15) with an applied false discovery rate (FDR) to identify HLA-presented peptides (10, 11, 16). Of note, adjustments or changes in these steps, particularly the preparation method, can lead to methodological biases including altered qualitative and quantitative peptide yields (17–22), which might impact target peptide selection. Recently, a high-throughput co-IP method enabling the isolation of HLA ligands in a 96-well format was developed, which showed, additionally to increased throughput, high reproducibility and sensitivity (12). This method provides various alterations in lysis buffers, purification steps, and 96-well plate format compared to classical column-based methods (10), which could impact the quantitative and qualitative peptide yields. Recently, a modified protocol of a similar, C18-cartridge-based method, has been proposed which used higher percentages of acetonitrile (ACN) (19). Following the example of this publication, higher ACN elution concentrations were examined.

Thus, in this work, we compared cell line- and primary tumor sample-derived immunopeptidome data sets generated either with the column-based (10), the 96-well-based (12), or the modified 96-well-based (19) isolation method by comparing their associated immunopeptidome composition, in terms of peptide yields, spectra quality, retention time, predicted hydrophobicity, and predicted immunogenicity to investigate the influence of the isolation method on target peptide selection for the development of T cell-based immunotherapy approaches.

Abbreviations: ACN, Acetonitrile; CHAPS, 3-[(3-cholamidopropyl) dimethylammonio]-1-propanesulfonate; CLL, Chronic lymphocytic leukemia; co-IP, Co-immunoprecipitation; DCA, deoxycholic acid; DCA, deoxycholic acid; FCS, Fetal calf serum; FDR, False discovery rate; GRAVY, Grand average of hydropathy; HCD, Higher-energy C-trap dissociation; HLA, Human leukocyte antigen; IEDB, The Immune Epitope Database; LC-MS/MS, Liquid chromatography-coupled tandem mass spectrometry; mAb, Monoclonal antibody; MS, Mass spectrometry; OG, glucopyranoside; PBMC, Peripheral blood mononuclear cell; OG, glucopyranoside; PBS, Phosphate-buffered saline; RCC, Renal cell carcinoma; TFA, Trifluoroacetic acid.

2 Materials and methods

2.1 Patient samples

Peripheral blood mononuclear cells (PBMCs) of a chronic lymphocytic leukemia (CLL) patient and solid tumor tissue of a renal cell carcinoma (RCC) patient were used for HLA ligand isolation by a column- and a 96-well-based preparation method and subsequent MS-based immunopeptidome analysis. Blood of the CLL patient was collected at the CCU Translational Immunology, Department of Internal Medicine, University Hospital Tübingen, Germany and PBMCs were isolated by density gradient centrifugation, snap frozen, and stored at -80°C until further use. Primary RCC tumor tissue was collected at the Department of Urology, University Hospital Tübingen, Germany, and stored at -80°C until further use. Informed consent was obtained according to the Declaration of Helsinki protocol. The study was performed according to the guidelines of the local ethics committees (406/2019B02, 424/2007B02). The Department of Hematology and Oncology, Tübingen, Germany and the Stefan Morsch Stiftung, Birkenfeld, Germany carried out HLA typing.

2.2 Cell line

The JY cell line (ECACC 94022533, batch 5070, HLA-A*02:01, -B*07:02, -C*07:02, -DRB1*04:04, -DRB1*13:01, -DQA1*01:03, -DQA1*03:01, -DQB1*03:02, -DQB1*06:03, -DPA1*01:03, -DPB1*02:01, -DPB1*04:01[1]) was cultivated in RPMI 1640 medium with 10% fetal calf serum (FCS) and 1% penicillin-streptomycin, harvested, washed 3x with phosphate-buffered saline (PBS), centrifuged down to pellets of $1x10^8$ cells and stored at -80°C until further us.

2.3 Immunopurification of HLA peptides

HLA immunopurifications were performed either as column-based (10) or 96-well-based (11, 12) preparation using the pan-HLA class I-specific monoclonal antibody (mAb) W6/32, the pan-HLA class II-specific mAb Tü-39, and the HLA-DR-specific mAb L243 (all produced in-house) to extract HLA ligands. All steps were performed at 4°C in a cold room.

2.3.1 Column-based immunopurification of HLA peptides

For the cell lysis, 1.25 ml per $1x10^8$ cells or 7 ml per gram tissue of a 3-[(3-cholamidopropyl)dimethylammonio]-1-propanesulfonate (CHAPS)-based lysis buffer (1.2% (w/v) in PBS (pH 7.2); Panreac AppliChem, Darmstadt, Germany) were used. The masses of the tissue sample were determined and then immediately transferred to a petri dish, covered with lysis buffer, cut into thin slices using a scalpel, and homogenized in a homogenizer. Cell pellets or homogenized

1 https://www.ebi.ac.uk/ipd/imgt/hla/cells/cell/?cellid=10882, 05.06.2023

tissue samples were incubated in lysis buffer shaking for 1 hour, followed by ultra sonification (with at least 150 W of ultrasonic power, 50% pulse length, 2 minutes) and another subsequent incubation of 1 hour. Cell debris was cleared by centrifugation at maximum speed (3100 x g), followed by sterile filtration through a 5 µm filter. The column system consisted of two columns (Econo Column® Chromatography Columns 0.5 cm × 5 cm BioRad, München, Germany) connected by tubing, where the upper column was used for the mAb W6/32 coupled to cyanobromide-activated sepharose beads (1 mg mAb was coupled to 40 mg beads suspended in 1 ml PBS (cyanobromide-activated sepharose 4B, Cytiva Sweden AB, Uppsala, Sweden)), and the lower column was used for the cyanobromide-activated sepharose beads coupled mAbs Tü-39 and L243 (mixture 1:1). The sample was circulated overnight through the column system containing 1 mg antibody per $1x10^8$ cells or per 0.83 gram tissue. Washing with PBS and double distilled water was performed, followed by transiently drying of the matrix. Four times acid elution were performed afterwards with transiently drying of the matrix in between the elution steps. In the first elution, 150 µl of 0.2% (v/v) trifluoro acetic acid (TFA) and 50 µl of 10% (v/v) TFA were used, followed by 150 µl of 0.2% (v/v) TFA in the last 3 repeats. The incubation time of acidic elution was 15 minutes for each of the four elution steps. All four eluates were combined and then filtered with 3 kDa and 10 kDa ultracentrifuge filters (Amicon Ultra 0.5 centrifugal filter unit 3 or 10 kDa, Merck Millipore, Billerica, USA) for HLA class I and HLA class II peptides, respectively. Filtrates were then frozen at -80°C and subsequently concentrated using a lyophilizer, followed by purification and desalting steps using a ZipTip C18 pipette tip (15 µm particle size, 200 Å pore size, 0.6 µl volume, Merck-Milipore, Darmstadt, Germany). After binding of peptides to the C18 ZipTip, the tip was washed in 0.1% (v/v) TFA, and the peptides were subsequently eluted in 32% (v/v) ACN in 0.2% (v/v) TFA. The 0.1% (v/v) TFA washing solution (termed desalting) was also investigated further to determine a potential loss of peptides during washing. The desalting and final sample volumes were reduced with vacuum centrifugation and filled up to a volume of 25 µl with 1% (v/v) ACN in 0.05% (v/v) TFA and subsequently analyzed by LC-MS/MS.

2.3.2 Desalting step

The lyophilized filtrates were desalted with a ZipTip C18 pipette tip during the column-based preparation method. Before the peptides were eluted in 32% (v/v) ACN in 0.2% (v/v) TFA, a washing step was performed in 0.1% (v/v) TFA. The liquid of the washing solution was lyophilized and filled up to a volume of 25 µl with 1% (v/v) ACN in 0.05% (v/v) TFA and separately analyzed by LC-MS/MS.

2.3.3 96-well-based immunopurification of HLA peptides

The 96-well-based preparation lysis buffer consisted of sodium deoxycholate (0.25% (w/v); Sigma-Aldrich, Steinheim am Albuch, Germany) and octyl-beta-D glucopyranoside (1% (w/v); Sigma-Aldrich) in PBS (pH 7.2). 1 ml per 10^8 cells or 9 ml per gram tissue of lysis buffer were used. The masses of the tissue sample were determined and immediately transferred to a petri dish, covered with lysis buffer, cut into thin slices using a scalpel, and homogenized in a homogenizer. Cell pellets or homogenized tissue samples were incubated in lysis buffer shaking for 1 hour, followed by ultra sonification (with at least 150 W of ultrasonic power, 50% pulse length, 2 minutes) and another subsequent incubation of 1 hour. Cell debris was cleared by centrifugation at maximum speed (3100 x g), followed by sterile filtration through a 5 µm filter. An upper 96-well plate (Polypropylene 96-well filter-micro plates, Agilent Technologies, Santa Clara, USA, 3 µm fiberglass, 25 µm polyethylene membrane) was filled with the mAb W6/32 crosslinked to protein A sepharose beads (1 mg mAb was coupled to 200 µl beads (Protein A-Sepharose 4B, Invitrogen Rockford, IL, USA)), and a lower 96-well plate with the mAbs Tü-29 and L243 (1:1 mixture) crosslinked to protein A sepharose beads. For the immunoprecipitation-step, the lysates were loaded on both plates by gravity containing 1 mg antibody per $1x10^8$ cells or per 0.83 gram tissue. Washing of samples followed, where several washing steps with different concentrations of Tris-HCl/NaCl (4x 150 mM sodium chloride (NaCl) in 20 mM Tris-HCl pH 8; 4x 400 mM NaCl in 20 mM Tris-HCl pH 8; 4x 150 mM NaCl in 20 mM Tris-HCl pH 8; 2x 20 mM Tris-HCl pH 8) were done. Acidic elution was performed directly with 500 µl 1% TFA (v/v) onto C18 plates (Sep-Pak® tC18 100 mg, 37-55 µm particle size, 125 Å pore size, 96-Well-plates, Waters, Milford MA, USA), followed by hydrophobic elution with 500 µl 28% (v/v) or 32% (v/v) ACN in 0.1% (v/v) TFA for HLA class I or HLA class II peptides into collection plates, respectively. All eluates were frozen at -80°C, concentrated in a lyophilizer, and filled up to a volume of 25 µl with 1% (v/v) ACN in 0.05% (v/v) TFA and subsequently analyzed by LC-MS/MS.

2.3.4 Adapted 96-well-based immunopurification of HLA peptides with 50% ACN elution step

For the adapted 96-well-based immunopurification of HLA peptides with 50% ACN elution step, another elution from the same C18 plates was performed after the hydrophobic elution of C18-bound peptides with 500 µl 28% (v/v) or 32% (v/v) ACN in 0.1% (v/v) TFA for HLA class I or HLA class II peptides into collection plates. This additional elution was performed with 50% (v/v) ACN in 0.1% (v/v) TFA in a new collection plate for HLA class I or HLA class II, respectively. The sample was frozen at -80°C, concentrated in a lyophilizer, and filled up to a volume of 25 µl with 1% (v/v) ACN in 0.05% (v/v) TFA and subsequently analyzed by LC-MS/MS.

2.4 Mass spectrometry-based analysis

Reversed-phase liquid chromatography (nanoUHPLC, UltiMate 3000 RSLCnano, Thermo Fisher, Waltham, Massachusetts, USA) was used for peptide separation, followed by an on-line coupled Q Exactive HF mass spectrometer (Thermo Fisher). Samples were analyzed in three technical replicates, where 5 µl with shares of 20% were injected onto a 75 µm x 2 cm trapping column (Thermo Fisher, Waltham,

Massachusetts, USA) at 4 µl/min for 5.75 min with 1% (v/v) ACN in 0.05% (v/v) TFA as loading buffer followed by peptide separation at 50° C and a flow rate of 300 nL/min on a 50 µm x 25 cm separation column with 2 µm particle size (PepMap C18, Thermo Fisher) applying a gradient ranging from 2.4% to 32.0% of ACN over 90 min. Ionization of eluting peptides was conducted by a nanospray source and analysis occurred in the on-line coupled mass spectrometer by implementing a top 35 HCD (Higher-energy C-trap dissociation) method generating fragment spectra with a resolution of 30,000, a mass range limited to 400-650 m/z for HLA class I peptides and 400-1000 m/z for HLA class II peptides, and positive charge states 2–3 for HLA class I and 2–5 for HLA class II were selected for fragmentation.

2.5 Data processing

Data processing was performed as described previously (10). Integrating database search results of the SequestHT search engine [University of Washington (14)] against the human proteome (Swiss-Prot database, 20,279 reviewed protein sequences, September 27th, 2013) was performed by the Proteome Discoverer (v1.4, Thermo Fisher), using a precursor mass tolerance of 5 ppm, fragment mass tolerance of 0.02 Da, and allowing oxidized methionine as a dynamic modification. HLA class I and HLA class II peptides for the JY cell line, and primary tumor samples of CLL and RCC patients were co-processed, respectively. 1 co-processed dataset was composed of 1 biological, 1 technical preparation and 3 technical MS replicates, respectively. The false discovery rate (FDR, estimated by the Percolator algorithm 2.04 (23)) was limited to 5% for HLA class I and 1% for HLA class II. Identified peptides were filtered for 8-12 or 12-21 amino acids length for HLA class I or HLA class II. HLA class I binder analysis was performed using SYFPEITHI 1.0 (24) (% of max. score ≥ 60) and NetMHCpan 4.1 (25) (percentile rank ≤ 2). Either one or both of the predictions had to meet the binder criteria for the ligand to be included into the HLA class I data set. HLA class II binder analysis was performed using NetMHCIIpan 4.1[2] (26) where the predictions had to meet the binder criteria of a percentile rank ≤ 5.

2.6 Software and statistical analysis

All figures and statistical analyses were generated using GraphPad Prism 9.4.0 (GraphPad Software). P values of < 0.05 were considered statistically significant. Overlap analyses were performed with InteraciVenn (27). Grand average of hydropathy (GRAVY) scores were calculated with a GRAVY calculator[3] (28).

To analyze previously described tumor-associated antigens, datasets from CLL- (29–31) and RCC-related publications (32–34) were filtered for the HLA class I types of the respective sample. All HLA class II peptides within the length filters of 12-21 amino acids of the mentioned publications were used for the analysis.

The Immune Epitope Database (IEDB) (35) was filtered for linear peptides, MHC ligand (positive) in Homo sapiens (human) (ID:9606) with an MHC restriction for either HLA class I or HLA class II. Human was selected as the host, and either cancer (ID : DOID:162) or healthy (ID : ONTIE:0003423) was used as a filter for disease. Furthermore, peptides > 12 amino acids or < 8 amino acids were excluded for HLA class I as well as peptides > 21 amino acids or < 12 amino acids for HLA class II.

For the predicted immunogenicity calculation, column- or 96-well-based method-exclusive 9-mer peptides were analyzed with the "Class I immunogenicity" prediction tool on the IEDB[4].

2.7 Data availability

The mass spectrometry proteomics data have been deposited to the ProteomeXchange Consortium *via* the PRIDE (36) partner repository with the dataset identifier PXD041804.

3 Results

3.1 Column-based and 96-well-based immunoprecipitation methods show a large proportion of method-exclusive peptides

To investigate the influence on identified HLA-restricted peptides of the column- and 96-well-based co-IP methods, we performed immunopeptidome analysis from biological triplicates of the JY cell line as well as from a primary CLL and RCC sample, respectively. Therefore, immunoprecipitation and MS analyses were performed in technical triplicates, resulting in 27 HLA class I and 27 HLA class II single MS measurements per specimen (Figure 1A, Supplementary Figure 1, Supplementary Table 1). HLA class I peptide yields, in terms of unique identified peptides were significantly higher with the 96-well preparation for the JY sample (median column 2406, 96-well 3918). In contrast, the column preparation revealed significantly higher HLA class I peptide yields for the CLL (median column 4916, 96-well 3259) and RCC (median column 5719, 96-well 4817) specimens (Figure 1B). For HLA class II peptide yields, only for the CLL sample (median column 1964, 96-well 1418), a significantly higher peptide yield was detected with the column preparation. In contrast, for JY (median column 1696, 96-well 3227) and RCC (median column 1651, 96-well 1335), no significant difference was observed between the two methods (Figure 1B). The spectra quality, intensity distribution of the identified HLA class I and HLA class II peptides and reproducibility were similar between the two investigated methods in all three specimens (Figure 1C, Supplementary Figure 2A–C, Supplementary Tables 2, 3). Only minor differences between XCorr values were detected, with no clear trend towards a method. Focusing on the reproducibility of the column-based and the 96-well-based method, a mean of 58.3% and 61.8% of the identified ligands were represented in at least three of the

2 https://services.healthtech.dtu.dk/services/NetMHCIIpan-4.1/

3 http://www.gravy-calculator.de/

4 http://tools.iedb.org/immunogenicity/

10.3389/fimmu.2023.1219720

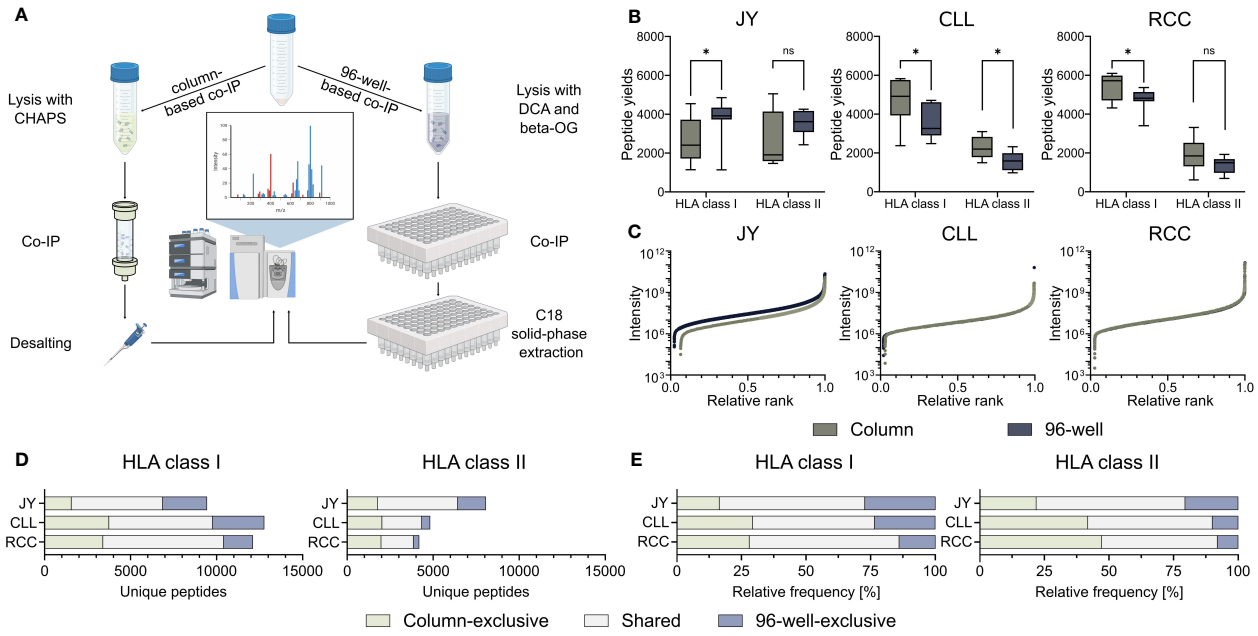

FIGURE 1
Comparison of 96-well- and column-based immunoprecipitation methods. **(A)** Schematic overview of the column- (left) and 96-well-based (right) co-immunoprecipitation (co-IP) methods. For the column-based method, a 3-[(3-cholamidopropyl)dimethylammonio]-1-propanesulfonate (CHAPS) lysis buffer was used, co-IP was performed in columns with cyclic samples overnight, and the eluted samples were finally desalted by a C18 pipet tip filter (ZipTip®). For the 96-well-based method, samples were lysed with a deoxycholic acid (DCA) and octyl-β-D-glucopyranoside (β-OG) buffer, and co-IP was performed in a 96-well system. The eluted samples were bound by C18 columns in a 96-well plate, and the peptides were eluted with acetonitrile (ACN). Samples from both preparation methods were measured using the same mass spectrometer (MS) device and method. Created with BioRender.com. **(B)** HLA class I and HLA class II peptide yields for the JY cell line (left panel), and primary tumor samples of a chronic lymphocytic leukemia (CLL, middle panel) and a renal cell carcinoma (RCC, right panel) patient (n = 9 co-processed datasets for each specimen and HLA class (Supplementary Figure 1, Supplementary Table 1). Green depicts all column-based peptides, light green column-based exclusive peptides; gray-blue depicts all 96-well peptides; light gray-blue depicts 96-well exclusive peptides. Boxes represent the median and 25th to 75th percentiles, whiskers are minimum to maximum. Unpaired t-tests, *p<0.05, ns not significant. **(C)** Relative ranked intensities of MS-acquired data of JY, CLL and RCC derived peptides from the combined HLA class I immunopeptidomes of all samples (n = 9), respectively. **(D, E)** Unique **(D)** absolute and **(E)** relative HLA class I (left panel) and HLA class II (right panel) peptide yields of JY, CLL and RCC identified by the column- and/or the 96-well-based method.

nine technical replicates, respectively. Of note, comparing the identified peptide sequences revealed a high proportion of method-exclusive peptides (Figures 1D, E). For HLA class I, 1553 (16.5%), 3735 (29.3%), and 3389 (28.0%) column-exclusive and 2575 (27.3%), 3003 (23.5%), and 1695 (14.0%) 96-well-exclusive peptides were detected of JY, CLL, and RCC samples, respectively. For HLA class II, there were 1759 (21.8%), 2015 (41.8%), 1969 (47.2%) column-exclusive, and 1649 (20.5%), 480 (10.0%), and 331 (7.9%) 96-well exclusive peptides of JY, CLL, and RCC samples, respectively (Figures 1D, E). In total, up to 47.2% of the identified peptides were method-exclusive.

3.2 Peptides isolated with column-based immunoprecipitation showed overall higher hydrophobicity scores

Further analysis of the method-exclusive peptides revealed a significant increase of peptide sequences with higher predicted hydrophobicity (Figure 2A) and, consequently also a shifted measured retention time (Figure 2B), for the column preparation compared to the 96-well preparation (Supplementary Table 4). The median of the calculated grand average of hydropathy (GRAVY) scores (28) of the column-exclusive HLA class I peptides was 0.8, 0.4, and 0.5 of JY, CLL, and RCC samples, and -0.1, -0.4 and -0.6, for the 96-well-exclusive peptides (Figure 2A). For HLA class II, the median GRAVY scores of the column-exclusive peptides were -0.1, -0.3 and -0.1 and -0.5, -0.7 and -0.9 for the 96-well-exclusive peptides of JY, CLL and RCC samples, respectively (Figure 2A). In line, the measured retention times of the column-exclusive peptides were significantly shifted towards later retention times compared to 96-well-exclusive peptides (Figure 2B). These effects were not only observed for method-exclusive but similarly for the entirety of identified peptides with significant differences in GRAVY scores and retention times for both HLA class I and HLA class II with significantly more hydrophobic peptides obtained with the column preparation (Supplementary Figures 3A, B, Supplementary Tables 2, 3).

Since it is unclear from these data, whether this shift is caused by the absence of hydrophilic peptides in the column-based or the absence of hydrophobic peptides in the 96-well-method, we further investigated the most hydrophilic step of the column-based method and the most hydrophobic step of the 96-well-based process. The most hydrophilic step in the column-based method is the washing step in 0.1% (v/v) TFA during the ZipTip C18-based desalting step (referred to as desalting) (Figure 2C). Only 136 (1.9%), 55 (0.6%),

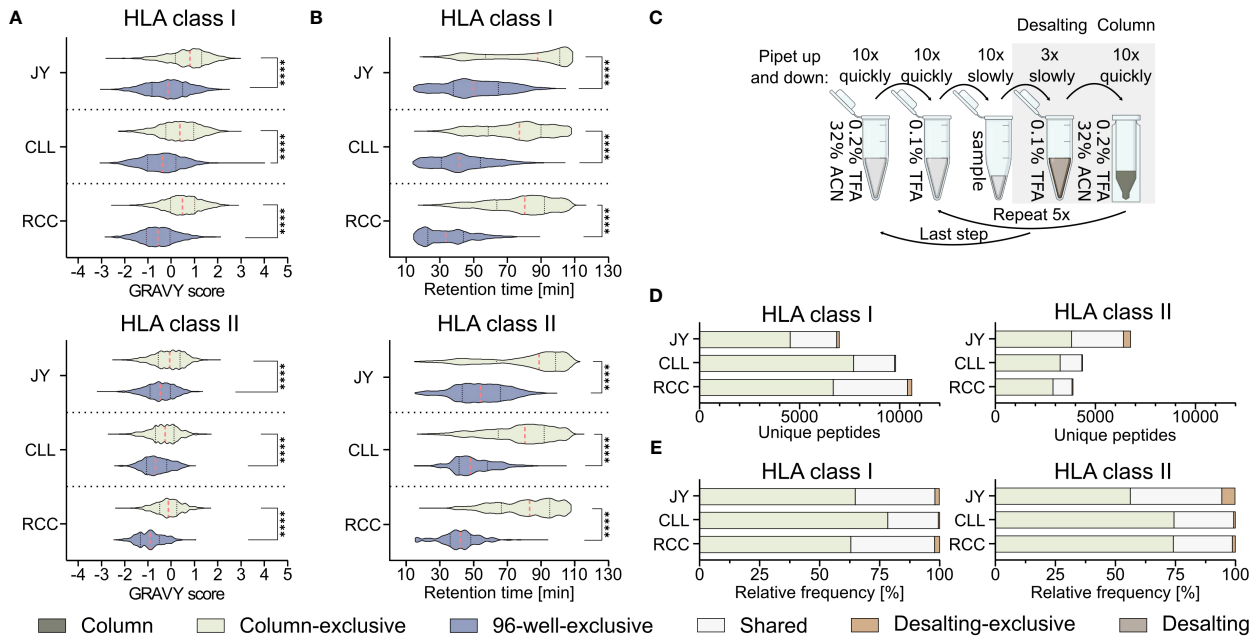

FIGURE 2
Influence of the immunoprecipitation method on the hydrophobicity of isolated peptides. **(A, B)** Violin plots of **(A)** grand average of hydropathy (GRAVY) scores and **(B)** retention times of column and 96-well preparation method-exclusive HLA class I (upper panel) and HLA class II (lower panel) peptides of JY, CLL, and RCC. Red dashed lines show the median, black dotted lines the 25th and 75th percentiles. ****p<0.0001. **(A)** Unpaired t-tests, **(B)** Mann-Whitney tests. **(C)** Schematic illustration of the desalting step during the column-based method, conducted with a C18 pipet filter tip (ZipTip®). Before hydrophobic elution of peptides occurred in 32% ACN (green), the filter tip was washed in 0.1% TFA, (brown, desalting). Immunopeptidome analyses were performed from the two gray underlaid conditions (column-based and desalting). Created with BioRender.com. **(D, E)** Unique peptide identification and frequency bar plots of column-exclusive (light green) or desalting wash step exclusive (light brown) peptides and shared peptides (light gray). Absolute **(D)** and relative **(E)** frequency of unique HLA class I (left panel) and HLA class II (right panel) peptides. Peptides unique to the column-based method are shown in light-green, peptides unique to the 96-well method are in gray-blue, peptides unique to the desalting step are in light brown and peptides found by the column method and the desalting wash step in light gray.

and 213 (2.0%) HLA class I and 370 (5.5%), 25 (0.6%), and 47 (1.2%) HLA class II peptides were exclusively detected in the desalting step of JY, CLL, and RCC samples, respectively. The majority of the peptides identified in the desalting solution were overlapping with the peptides also detected with the column preparation only (Figures 2D, E). The GRAVY scores of these desalting-exclusive peptides were in general lower, thus more hydrophilic (Supplementary Figure 3C). In line, desalting-exclusive peptides elute significantly earlier (Supplementary Figure 3D). Based on the low number of desalting-exclusive peptides, the desalting step of the column-based method did not lead to the loss of hydrophilic peptides and was not responsible for the hydrophobicity shift between the column- and 96-well-based co-IP methods.

3.3 The loss of hydrophobic peptides can partially be restored with higher acetonitrile percentage

To investigate whether the hydrophobicity shift was due to the loss of hydrophobic peptides with the 96-well-based co-IP method, a modified protocol introducing a second elution step of the same C18 plates after the 28/32% ACN elution with 50% ACN was performed as described before (19). This second elution step resulted in up to 26% other HLA class I (JY 18% (1760/9640), CLL 8% (794/9819), RCC 21% (2426/11131)) and HLA class II (JY 13% (956/7254), CLL 2% (51/2853), RCC 5% (127/2332)) peptide identifications compared to the unmodified 96-well method (Figure 3A) and enabled the additional isolation of highly hydrophobic peptides (Figures 3B, C). GRAVY scores referring to the hydrophobicity of the 50% ACN-exclusive peptides, were significantly higher with medians of 0.9, 0.5 and 0.5 for HLA class I peptides and 0.0, -0.1 and 0.2 for HLA class II of JY, CLL and RCC samples, compared to the conventional 96-well preparation-exclusive peptides with medians of -0.3, -0.4 and -0.5 for HLA class I and -0.5, -0.8 and -0.8 for HLA class II (Figure 3B), respectively. In line, the median of the retention times of 50% ACN-exclusive peptides shifted by up to 49 minutes for HLA class I and up to 40 minutes for HLA class II towards later elution times compared to 96-well-exclusive peptides (Figure 3C). The same effects were not only observed for method-exclusive but also the entirety of identified peptides, showing significantly increased GRAVY scores and retention times for the 50% ACN elution compared to the 96-well preparation for both HLA class I and HLA class II (Supplementary Figure 4).

To examine whether a subsequent elution step with 50% ACN in the 96-well method could rescue the missing hydrophobic peptides compared to the column-based method, the 96-well preparation peptides and the peptides found by eluting a second time with 50% ACN (combination further called 96-well 50% ACN) were compared

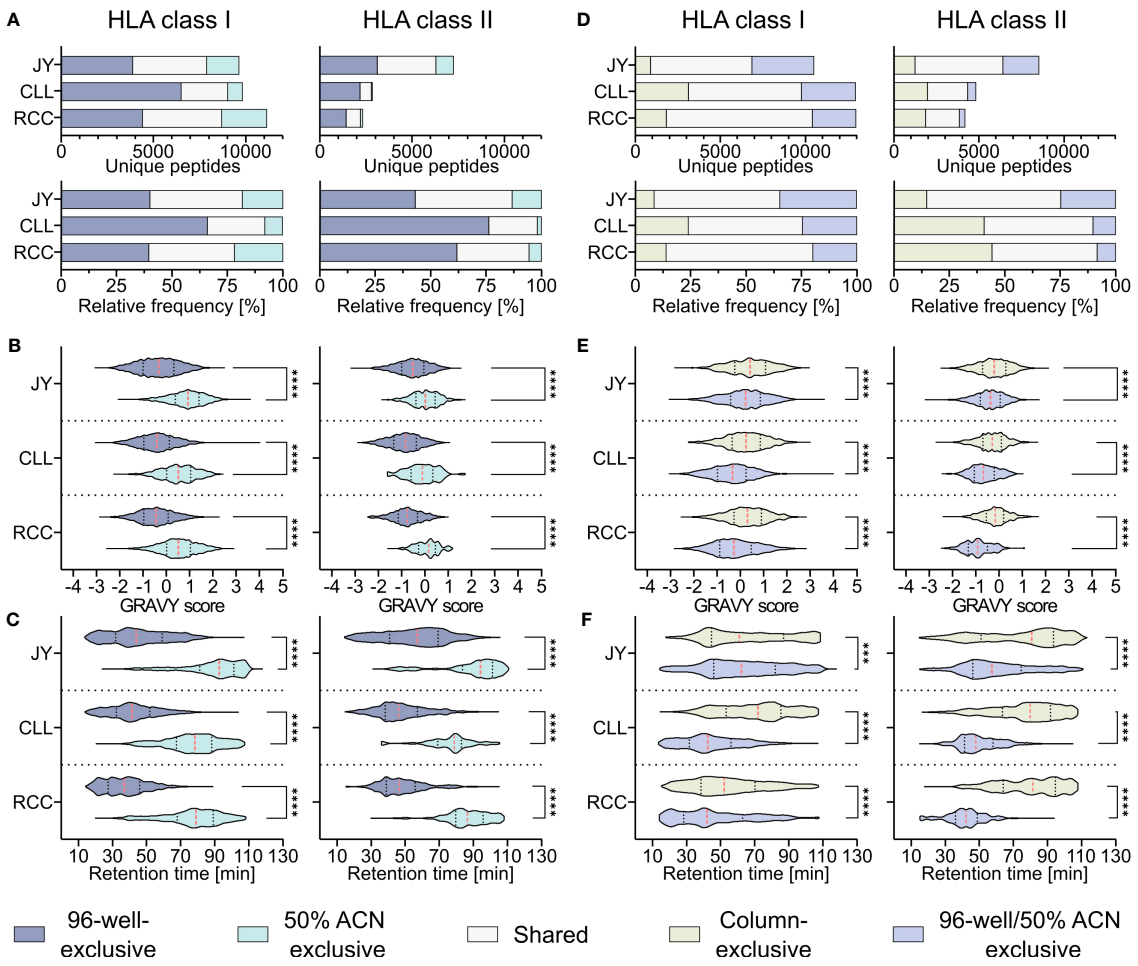

FIGURE 3
Effect of a second elution step with 50% acetonitrile (ACN) in the 96-well method. **(A)** Absolute (upper panels) and relative (lower panels) HLA class I (left panels) and HLA class II (right panels) peptide yields of JY, CLL and RCC samples identified by the 96-well-based method and/or the additional elution step with 50% ACN from the same 96-well plate. **(B, C)** Violin plots of **(B)** GRAVY scores and **(C)** retention times of 96-well-exclusive (gray-blue), 50% ACN-exclusive (turquoise) HLA class I (left panel) and HLA class II (right panel) peptides of JY, CLL, and RCC. Red dashed lines show the median, black dotted lines the 25th and 75th percentiles. ****p<0.0001. **(B)** Unpaired t-tests, **(C)** Mann-Whitney tests. **(D)** Absolute (upper panels) and relative (lower panels) HLA class I (left panels) and HLA class II (right panels) peptides and percentage of JY, CLL and RCC peptide yields identified by the column-based method (light green), or the 96-well method combined with the subsequent elution step with 50% ACN from the same 96-well plate (light gray-blue) or both (light gray). **(E, F)** Violin plots of **(E)** GRAVY scores and **(F)** retention times of column-based method-exclusive (light green), combination of 96-well method and 50% ACN exclusive (light gray-blue) HLA class I (left panel) and HLA class II (right panel) peptides of JY, CLL, and RCC. Red dashed lines show the median and black dotted lines show the 25th and 75th percentiles. ***p<0.001, ****p<0.0001. **(E)** Unpaired t-tests, **(F)** Mann-Whitney tests.

with the column preparation. However, up to 24% and 44% of the identified HLA class I (JY 9% (895/10475), CLL 24% (3108/12931), RCC 14% (1817/12948)) and HLA class II (JY 15% (1255/8509), CLL 41% (1968/4821), RCC 44% (1852/4184)) peptides identified in the column-based method remain exclusive even when the 96-well method is supplemented with the 50% ACN elution step (Figure 3D). Additionally, a significant difference in the hydrophobicity regarding GRAVY score and retention times was still observed for the method-exclusive peptides, albeit reduced compared to the 96-well method without the additional 50% ACN elution (Figures 3E, F) emphasizing the benefit of this method adaption. A global analysis of the researched methods and method adaptions (column, desalting, 96-well, 50% ACN) showed that peptide yields are not influenced by hydrophobic or hydrophilic binding motifs of corresponding HLA allotypes, thus do not influence peptide yields. However, allotypes with more hydrophobic binding motifs tend to present more hydrophobic peptides and vice versa (Supplementary Figures 5A–C).

3.4 Different immunoprecipitation methods show a bias in the identification of tumor-associated antigens

To further investigate the impact of the used co-IP methods on the immunopeptidome-based identification of tumor-associated antigens, a comparative analysis of previously described CLL- (29–31) and RCC-associated TAAs (32–34), the IEDB and the here identified peptides was performed (Supplementary Table 5). Of the HLA-matched previously described CLL-associated HLA class I TAAs, 53% (79/149) could be reidentified in our analysis with at least one of the used

10.3389/fimmu.2023.1219720

methods (column, 96-well, or 50% ACN method), while 7 of the reidentified peptides were shown to be immunogenic in previous publications. Interestingly, 22% (17/79) of the peptides were exclusively identified with the column-based preparation method, whereas only 3% (2/79) and 6% (5/79) were identified solely with the 96-well-preparation method and the 50% ACN elution step, respectively (Figure 4A). Of the previously described CLL-associated HLA class II TAAs, 21% (135/643) could be reidentified with at least one method, and the same bias could be observed with 43% (58/135), 7% (9/135) and 0% (0/135) identified exclusively with the column-based method, the 96- well-based method and the 50% ACN elution step (Figure 4A). 4 of the re-identified peptides were immunogenic in previous publications. Of the HLA-matched previously described RCC-associated HLA class I and HLA class II TAAs, 70% (7/10) and 10% (1/10) could be reidentified in the RCC sample, respectively. None of the HLA class I peptides could be identified exclusively with one method and 3 of the reidentified peptides were immunogenic in previous publications. However, one peptide was reidentified with the column-based method and with 50% ACN elution but not with the 96-well-based method. The one HLA class II peptide could be identified exclusively with the column-based method (Figure 4B).

Furthermore, to examine the characteristics of the column-based or 96-well-based method in terms of the identification of TAAs, we compared the here identified peptides with the benign- and tumor-associated peptides described in the IEDB. Comparing the column and 96-well method-derived peptides with the described benign peptides showed a similar percentage of method-exclusive HLA class I peptides not found within the benign IEDB dataset (Figure 4C). Similarly, comparing the column and 96-well method-derived peptides with the malignant IEDB showed a similar percentage of method-exclusive HLA class I peptides also found in the malignant IEDB and therefore, similar ratios of method-exclusive TAAs (Figure 4D, Supplementary Table 6). For HLA class II, the ratio of the method-exclusive peptides acted similarly to HLA class I peptide rations. However, column-based method-exclusive peptides percentages were larger than those with the 96-well preparation for CLL and RCC. These distributions resemble the original relative distribution (Figure 1E). When these points are taken together, each method shows an equal potential to expand the IEDB database and discover tumor-associated antigens.

To further evaluate the impact of the co-IP methods on the immunogenicity of immunopeptidome-identified peptides, we predicted the immunogenicity of the column- or 96-well method-exclusive 9-mer peptides (Figure 4E, Supplementary Table 7). For all specimens, the median predicted immunogenicity of column preparation exclusive peptides was significantly higher compared to 96-well preparation peptides.

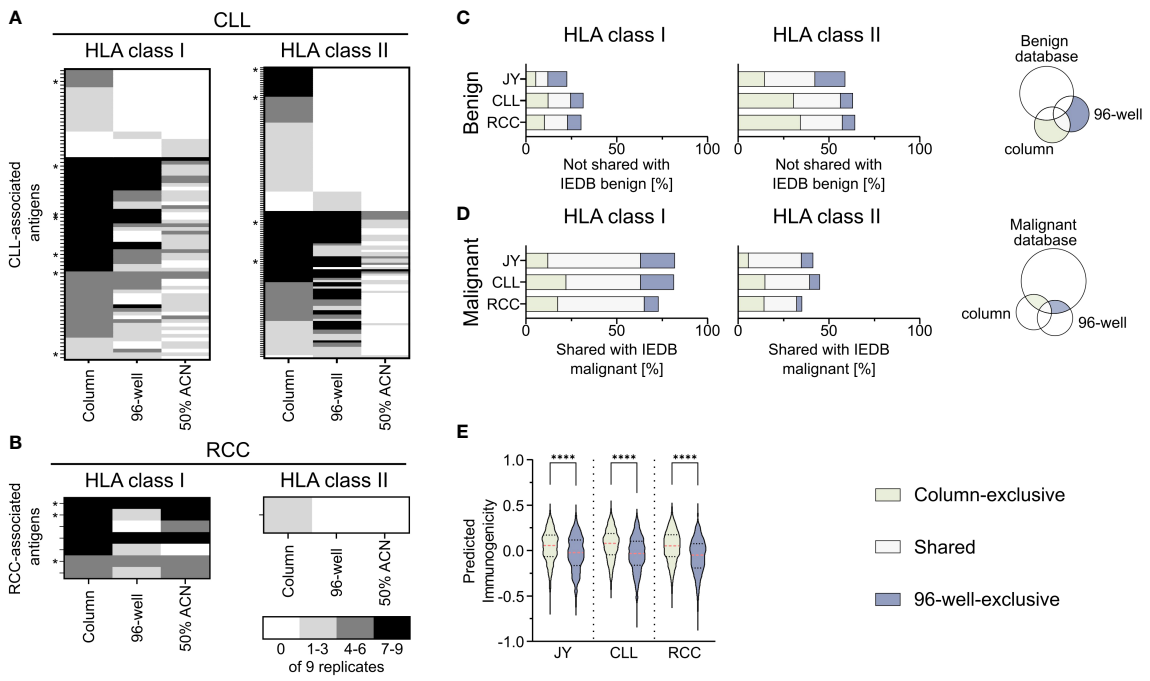

FIGURE 4
Comparison of identified peptides with published databases. **(A, B)** Heat map depicting previously described HLA class I (left panel) and HLA class II (right panel) tumor-associated antigens (TAAs), which were reidentified at least once in the immunopeptidomes of the analyzed **(A)** chronic lymphocytic leukemia (CLL, n = 9) and **(B)** renal cell carcinoma (RCC, n = 9) samples. The gray color intensity indicates the frequency of the respective peptide in the immunopeptidome replicates. * indicates a tumor-associated peptide with proven immunogenicity in the respective publication. **(C, D)** Relative overlaps of the column- or 96-well-exclusive HLA class I (left panel) and HLA class II (middle panel) peptides with **(C)** the benign and **(D)** the cancer-associated IEDB database. Percentages refer to the combined total of the unique column and 96-well peptides. A schematic Venn diagram (right panel) indicates which peptides are depicted in the bar plots. **(E)** Violin plot of predicted immunogenicity scores for 9-mers peptides within the HLA class I column- (light green) and 96-well-exclusive (light gray-blue) peptides. Red dashed lines show the median, black dotted lines the 25th and 75th percentiles. ****p<0.0001. Unpaired t-tests, ****p<0.0001.

4 Discussion

Mass spectrometry-based immunopeptidomics is the only unbiased method to identify naturally presented HLA ligands (8, 9), which is an indispensable prerequisite for the characterization of novel tumor antigens for immunotherapeutic approaches (3–6, 37, 38). Immense improvements based on devices and methodology have been made in recent years to optimize sensitivity and sample throughput (12, 21, 39, 40). However, novel isolation methods, mass spectrometric devices and data processing pipelines and tools can have a marked impact on the quality and quantity of immunopeptidomics data and identified peptides (19, 20, 22, 41).

In this work, we performed a head-to-head comparison of two established immunoprecipitation methods that differ significantly in their purification steps to understand the bias that might be introduced by using these different methods (10, 12). Whereas peptide yields, spectra quality and reproducibility were comparable, a large proportion of method-exclusive peptides were identified with significant differences in their hydrophobicity, which might have potential implications for the identification of immunogenic tumor antigens.

Regarding peptide yields, no general trend towards higher yields of one of the methods was observed between the column-based and the 96-well-based method across all samples. The acquired variation in peptide yields might be due to the usage of different detergents in the lysis buffers of both methods (22). Although no tendency in terms of peptide yields was detected, with the 96-well method showing a trend of higher reproducibility, tremendous fractions of the identified peptides were exclusively detected in one of the methods. This was based on an increased number of hydrophobic peptides identified with the column method, which were not identified by the 96-well-based method. These findings align with previous studies that have reported alterations in peptide composition and/or hydrophobicity with different HLA-peptide isolation methods. Differences in salt concentrations during washing steps, lysis buffers, elution methods, or the use of different C18 based purification methods were described as main sources of method induced biases (19, 21, 22, 42). Specifically, the latter two can have a particular impact on hydrophobicity, as the use of different ACN percentages or different C18 materials have different properties to elute or bind hydrophobic peptides. Interestingly, method-specific peptide yields were not impacted by specific HLA allotypes, despite the allotype-specific hydrophobicity of the corresponding anchor amino acids, however the GRAVY score distribution showed the same method specific bias.

Since the number of open-access immunopeptidomic data is increasingly growing, these alterations in identified peptide repertoire based on different immunoprecipitation methods can have a marked impact on our knowledge about the immunopeptidome. In particular, selecting tumor-exclusive HLA peptides based on the subtraction of benign tissue immunopeptidome repositories could be biased using datasets generated with different immunoprecipitation methods. This becomes even more apparent within a specific search of previously published TAAs (29–34) identified with the column method within our dataset. These TAAs were preferentially detected in samples examined with the column method and were underrepresented in 96-well examined samples. Moreover, as we and others have shown, hydrophobic peptides tend to be more immunogenic (43, 44), and the immunoprecipitation method might also significantly impact the identification of T cell epitopes in individual tumor samples.

With an in-depth analysis of the purification steps, we could show that the shift in hydrophobicity is not caused by a loss of hydrophilic peptides during the hydrophilic washing step of the column preparation but generated by the loss of hydrophobic peptides during 96-well preparation, which can be partially overcome by increased ACN fractions for peptide elution. This underlines the positive effect of an additional elution step with increased ACN percentages, which is in line with previous reports showing that higher ACN proportion can increase peptide yields as well as the hydrophobicity and thus immunogenicity of peptide identifications (19, 21, 22). Nonetheless, we could show that column-based method-exclusive peptides still had significantly higher hydrophobicity, suggesting that 50% ACN elution in the 96-well method could reduce the bias towards the column-based method but not completely equalize it, further underlining the importance of knowing about method-specific biases.

Together, this work showed how different immunoprecipitation methods and their adaptions can impact the immunopeptidome composition in terms of hydrophobicity, retention time and immunogenicity and thus the identification of potential TAA.

Data availability statement

The datasets presented in this study can be found in online repositories. The names of the repository/repositories and accession number(s) can be found below: https://www.ebi.ac.uk/pride/archive/, PXD041804.

Ethics statement

The studies involving human participants were reviewed and approved by the Ethics Committee of the faculty of medicine of the University of Tübingen. The patients/participants provided their written informed consent to participate in this study.

Author contributions

MW, JB, AN, and JSW conceptualized this study. MW, JB, and LW performed immunopeptidome experiments. MD performed bioinformatic analysis. AN, H-GR, and JSW supervised this study. All authors contributed to the article and approved the submitted version.

Funding

This work was supported by the Deutsche Forschungsgemeinschaft under Germany's Excellence Strategy (Grant EXC2180-390900677 (H-GR and JSW), the German Cancer Consortium (DKTK) (H-GR, and JSW), the Deutsche Forschungsgemeinschaft (DFG, German Research Foundation, Grant WA4608/1-2 (JSW), the Wilhelm Sander Stiftung (Grant 2016.177.3 (JSW)), the Deutsche Krebshilfe (German Cancer

Aid, 70114948 (JSW)), the Zentren für Personalisierte Medizin (ZPM, JSW)). We acknowledge support from the Open Access Publication Fund of the University of Tübingen.

Acknowledgments

We thank R. Agrusa, C. Falkenburger, and U. Wulle for their excellent technical support.

Conflict of interest

The authors declare that the research was conducted in the absence of any commercial or financial relationships that could be construed as a potential conflict of interest.

Publisher's note

Supplementary material

The Supplementary Material for this article can be found online at: https://www.frontiersin.org/articles/10.3389/fimmu.2023.1219720/full#supplementary-material

References

1. Ryschich E, Notzel T, Hinz U, Autschbach F, Ferguson J, Simon I, et al. Control of T-cell-mediated immune response by HLA class I in human pancreatic carcinoma. *Clin Cancer Res* (2005) 11(2 Pt 1):498–504. doi: 10.1158/1078-0432.498.11.2

2. Gao Q, Liang WW, Foltz SM, Mutharasu G, Jayasinghe RG, Cao S, et al. Driver fusions and their implications in the development and treatment of human cancers. *Cell Rep* (2018) 23(1):227–38 e3. doi: 10.1016/j.celrep.2018.03.050

3. Loffler MW, Chandran PA, Laske K, Schroeder C, Bonzheim I, Walzer M, et al. Personalized peptide vaccine-induced immune response associated with long-term survival of a metastatic cholangiocarcinoma patient. *J Hepatol* (2016) 65(4):849–55. doi: 10.1016/j.jhep.2016.06.027

4. Ott PA, Hu Z, Keskin DB, Shukla SA, Sun J, Bozym DJ, et al. An immunogenic personal neoantigen vaccine for patients with melanoma. *Nature* (2017) 547 (7662):217–21. doi: 10.1038/nature22991

5. Sahin U, Derhovanessian E, Miller M, Kloke BP, Simon P, Lower M, et al. Personalized rna mutanome vaccines mobilize poly-specific therapeutic immunity against cancer. *Nature* (2017) 547(7662):222–6. doi: 10.1038/nature23003

6. Wick W, Dietrich PY, Kuttruff S, Hilf N, Frenzel K, Admon A, et al. Gapvac-101: first-in-human trial of a highly personalized peptide vaccination approach for patients with newly diagnosed glioblastoma. *J Clin Oncol* (2018) 36(15):2000–. doi: 10.1200/JCO.2018.36.15_suppl.2000

7. Nelde A, Rammensee HG, Walz JS. The peptide vaccine of the future. *Mol Cell Proteomics* (2021) 20:100022. doi: 10.1074/mcp.R120.002309

8. Kote S, Pirog A, Bedran G, Alfaro J, Dapic I. Mass spectrometry-based identification of MHC-associated peptides. *Cancers (Basel)* (2020) 12(3):535. doi: 10.3390/cancers12030535

9. Becker JP, Riemer AB. The importance of being presented: target validation by immunopeptidomics for epitope-specific immunotherapies. *Front Immunol* (2022) 13:883989. doi: 10.3389/fimmu.2022.883989

10. Nelde A, Kowalewski DJ, Stevanovic S. Purification and identification of naturally presented MHC class I and Ii ligands. *Methods Mol Biol* (2019) 1988:123–36. doi: 10.1007/978-1-4939-9450-2_10

11. Bassani-Sternberg M. Mass spectrometry based immunopeptidomics for the discovery of cancer neoantigens. *Methods Mol Biol* (2018) 1719:209–21. doi: 10.1007/978-1-4939-7537-2_14

12. Chong C, Marino F, Pak H, Racle J, Daniel RT, Muller M, et al. High-throughput and sensitive immunopeptidomics platform reveals profound interferongamma-mediated remodeling of the human leukocyte antigen (HLA) ligandome. *Mol Cell Proteomics* (2018) 17(3):533–48. doi: 10.1074/mcp.TIR117.000383

13. Eng JK, Jahan TA, Hoopmann MR. Comet: an open-source Ms/Ms sequence database search tool. *Proteomics* (2013) 13(1):22–4. doi: 10.1002/pmic.201200439

14. Eng JK, McCormack AL, Yates JR. An approach to correlate tandem mass spectral data of peptides with amino acid sequences in a protein database. *J Am Soc Mass Spectrom* (1994) 5(11):976–89. doi: 10.1016/1044-0305(94)80016-2

15. Zhang J, Xin L, Shan B, Chen W, Xie M, Yuen D, et al. Peaks Db: de novo sequencing assisted database search for sensitive and accurate peptide identification. *Mol Cell Proteomics* (2012) 11(4):M111 010587. doi: 10.1074/mcp.M111.010587

16. Falk K, Rötzscheke O, Stevanović S, Jung G, Rammensee HG. Allele-specific motifs revealed by sequencing of self-peptides eluted from MHC molecules. *Nature* (1991) 351:290–6. doi: 10.1038/351290a0

17. Fritsche J, Kowalewski DJ, Backert L, Gwinner F, Dorner S, Priemer M, et al. Pitfalls in HLA ligandomics-how to catch a Li(E)Gand. *Mol Cell Proteomics* (2021) 20:100110. doi: 10.1016/j.mcpro.2021.100110

18. Verheggen K, Raeder H, Berven FS, Martens L, Barsnes H, Vaudel M. Anatomy and evolution of database search engines-a central component of mass spectrometry based proteomic workflows. *Mass Spectrom Rev* (2020) 39(3):292–306. doi: 10.1002/mas.21543

19. Klatt MG, Mack KN, Bai Y, Aretz ZEH, Nathan LI, Mun SS, et al. Solving an MHC allele-specific bias in the reported immunopeptidome. *JCI Insight* (2020) 5(19): e141264 . doi: 10.1172/jci.insight.141264

20. Sturm T, Sautter B, Worner TP, Stevanovic S, Rammensee HG, Planz O, et al. Mild acid elution and MHC immunoaffinity chromatography reveal similar albeit not identical profiles of the HLA class I immunopeptidome. *J Proteome Res* (2021) 20 (1):289–304. doi: 10.1021/acs.jproteome.0c00386

21. Bernhardt M, Cruz-Garcia Y, Rech A, Meierjohann S, Erhard F, Schilling B, et al. Extending the mass spectrometry-detectable landscape of MHC peptides by use of restricted access material. *Anal Chem* (2022) 94(41):14214–22. doi: 10.1021/acs.analchem.2c02198

22. Nicastri A, Liao H, Muller J, Purcell AW, Ternette N. The choice of HLA-associated peptide enrichment and purification strategy affects peptide yields and creates a bias in detected sequence repertoire. *Proteomics* (2020) 20(12):e1900401. doi: 10.1002/pmic.201900401

23. Kall L, Canterbury JD, Weston J, Noble WS, MacCoss MJ. Semi-supervised learning for peptide identification from shotgun proteomics datasets. *Nat Methods* (2007) 4(11):923–5. doi: 10.1038/nmeth1113

24. Schuler MM, Nastke MD, Stevanovic S. Syfpeithi: database for searching and T-cell epitope prediction. *Methods Mol Biol* (2007) 409:75–93. doi: 10.1007/978-1-60327-118-9_5

25. Reynisson B, Alvarez B, Paul S, Peters B, Nielsen M. NetMHCpan-4.1 and netMHCiipan-4.0: improved predictions of MHC antigen presentation by concurrent motif deconvolution and integration of Ms MHC eluted ligand data. *Nucleic Acids Res* (2020) 48(W1):W449–W54. doi: 10.1093/nar/gkaa379

26. Reynisson B, Barra C, Kaabinejadian S, Hildebrand WH, Peters B, Nielsen M. Improved prediction of MHC Ii antigen presentation through integration and motif deconvolution of mass spectrometry MHC eluted ligand data. *J Proteome Res* (2020) 19 (6):2304–15. doi: 10.1021/acs.jproteome.9b00874

27. Heberle H, Meirelles GV, da Silva FR, Telles GP, Minghim R. Interactivenn: A web-based tool for the analysis of sets through venn diagrams. *BMC Bioinf* (2015) 16:169. doi: 10.1186/s12859-015-0611-3

28. Kyte J, Doolittle RF. A simple method for displaying the hydropathic character of a protein. *J Mol Biol* (1982) 157:150–32. doi: 10.1016/0022-2836(82)90515-0

29. Kowalewski DJ, Schuster H, Backert L, Berlin C, Kahn S, Kanz L, et al. HLA ligandome analysis identifies the underlying specificities of spontaneous antileukemia immune responses in chronic lymphocytic leukemia (Cll). *Proc Natl Acad Sci U.S.A.* (2015) 112(2):E166–75. doi: 10.1073/pnas.1416389112

30. Backert L, Kowalewski DJ, Walz S, Schuster H, Berlin C, Neidert MC, et al. A meta-analysis of HLA peptidome composition in different hematological entities_entity-specific dividing lines and "Panleukemia" Antigens. *Oncotarget* (2017) 8 (27):43915–24. doi: 10.18632/oncotarget.14918

31. Nelde A, Maringer Y, Bilich T, Salih HR, Roerden M, Heitmann JS, et al. Immunopeptidomics-guided warehouse design for peptide-based immunotherapy in chronic lymphocytic leukemia. *Front Immunol* (2021) 12:705974. doi: 10.3389/fimmu.2021.705974

32. Klatt MG, Kowalewski DJ, Schuster H, Di Marco M, Hennenlotter J, Stenzl A, et al. Carcinogenesis of renal cell carcinoma reflected in HLA ligands: A novel approach for synergistic peptide vaccination design. *Oncoimmunology* (2016) 5(8):e1204504. doi: 10.1080/2162402X.2016.1204504

33. Reustle A, Di Marco M, Meyerhoff C, Nelde A, Walz JS, Winter S, et al. Integrative -omics and HLA-ligandomics analysis to identify novel drug targets for ccrcc immunotherapy. *Genome Med* (2020) 12(1):32. doi: 10.1186/s13073-020-00731-8

34. Walter S, Weinschenk T, Stenzl A, Zdrojowy R, Pluzanska A, Szczylik C, et al. Multipeptide immune response to cancer vaccine ima901 after single-dose cyclophosphamide associates with longer patient survival. *Nat Med* (2012) 18 (8):1254–61. doi: 10.1038/nm.2883

35. Vita R, Mahajan S, Overton JA, Dhanda SK, Martini S, Cantrell JR, et al. The immune epitope database (Iedb): 2018 update. *Nucleic Acids Res* (2019) 47(D1):D339–D43. doi: 10.1093/nar/gky1006

36. Perez-Riverol Y, Bai J, Bandla C, Garcia-Seisdedos D, Hewapathirana S, Kamatchinathan S, et al. The pride database resources in 2022: A hub for mass spectrometry-based proteomics evidences. *Nucleic Acids Res* (2022) 50(D1):D543–D52. doi: 10.1093/nar/gkab1038

37. Sheikh QM, Gatherer D, Reche PA, Flower DR. Towards the knowledge-based design of universal influenza epitope ensemble vaccines. *Bioinformatics* (2016) 32 (21):3233–9. doi: 10.1093/bioinformatics/btw399

38. Khodadoust MS, Olsson N, Wagar LE, Haabeth OA, Chen B, Swaminathan K, et al. Antigen presentation profiling reveals recognition of lymphoma immunoglobulin neoantigens. *Nature* (2017) 543(7647):723–7. doi: 10.1038/nature21433

39. Purcell AW, Ramarathinam SH, Ternette N. Mass spectrometry-based identification of MHC-bound peptides for immunopeptidomics. *Nat Protoc* (2019) 14(6):1687–707. doi: 10.1038/s41596-019-0133-y

40. Klaeger S, Apffel A, Clauser KR, Sarkizova S, Oliveira G, Rachimi S, et al. Optimized liquid and gas phase fractionation increases HLA-peptidome coverage for primary cell and tissue samples. *Mol Cell Proteomics* (2021) 20:100133. doi: 10.1016/j.mcpro.2021.100133

41. Hoenisch Gravel N, Nelde A, Bauer J, Mühlenbruch L, Schroeder S, Neidert MC, et al. Timstof mass spectrometry-based immunopeptidomics refines tumor antigen identification. *Research Square [Preprint]* (2023). Available at: https://www.researchsquare.com/article/rs-2402111/v1 (Accessed 27.04.2023).

42. Pandey K, Mifsud NA, Lim Kam Sian TCC, Ayala R, Ternette N, Ramarathinam SH, et al. In-depth mining of the immunopeptidome of an acute myeloid leukemia cell line using complementary ligand enrichment and data acquisition strategies. *Mol Immunol* (2020) 123:7–17. doi: 10.1016/j.molimm.2020.04.008

43. Chowell D, Krishna S, Becker PD, Cocita C, Shu J, Tan X, et al. Tcr contact residue hydrophobicity is a hallmark of immunogenic cd8+ T cell epitopes. *Proc Natl Acad Sci U.S.A.* (2015) 112(14):E1754–62. doi: 10.1073/pnas.1500973112

44. Calis JJ, Maybeno M, Greenbaum JA, Weiskopf D, De Silva AD, Sette A, et al. Properties of MHC class I presented peptides that enhance immunogenicity. *PloS Comput Biol* (2013) 9(10):e1003266. doi: 10.1371/journal.pcbi.1003266

frontiers | Frontiers in Immunology

TYPE Original Research
PUBLISHED 04 September 2023
DOI 10.3389/fimmu.2023.1251603

OPEN ACCESS

EDITED BY
Patrick Schmidt,
National Center for Tumor Diseases (NCT), Germany

REVIEWED BY
Ming Yi,
Zhejiang University, China
Ngoc Hieu Tran,
University of Waterloo, Canada

*CORRESPONDENCE
Le Son Tran
leson1808@gmail.com
Hoai-Nghia Nguyen
nhnghia81@gmail.com

†These authors have contributed equally to this work

RECEIVED 02 July 2023
ACCEPTED 17 August 2023
PUBLISHED 04 September 2023

CITATION
Nguyen BQT, Tran TPD, Nguyen HT, Nguyen TN, Pham TMQ, Nguyen HTP, Tran DH, Nguyen V, Tran TS, Pham T-VN, Le M-T, Phan M-D, Giang H, Nguyen H-N and Tran LS (2023) Improvement in neoantigen prediction via integration of RNA sequencing data for variant calling. *Front. Immunol.* 14:1251603. doi: 10.3389/fimmu.2023.1251603

Improvement in neoantigen prediction via integration of RNA sequencing data for variant calling

Bui Que Tran Nguyen[1†], Thi Phuong Diem Tran[1†], Huu Thinh Nguyen[2], Thanh Nhan Nguyen[1], Thi Mong Quynh Pham[1], Hoang Thien Phuc Nguyen[1], Duc Huy Tran[2], Vy Nguyen[1], Thanh Sang Tran[2], Truong-Vinh Ngoc Pham[2], Minh-Triet Le[2], Minh-Duy Phan[1], Hoa Giang[1], Hoai-Nghia Nguyen[1*] and Le Son Tran[1*]

[1]Medical Genetics Institute, Ho Chi Minh, Vietnam, [2]University Medical Center Ho Chi Minh City, Ho Chi Minh, Vietnam

Introduction: Neoantigen-based immunotherapy has emerged as a promising strategy for improving the life expectancy of cancer patients. This therapeutic approach heavily relies on accurate identification of cancer mutations using DNA sequencing (DNAseq) data. However, current workflows tend to provide a large number of neoantigen candidates, of which only a limited number elicit efficient and immunogenic T-cell responses suitable for downstream clinical evaluation. To overcome this limitation and increase the number of high-quality immunogenic neoantigens, we propose integrating RNA sequencing (RNAseq) data into the mutation identification step in the neoantigen prediction workflow.

Methods: In this study, we characterize the mutation profiles identified from DNAseq and/or RNAseq data in tumor tissues of 25 patients with colorectal cancer (CRC). Immunogenicity was then validated by ELISpot assay using long synthesis peptides (sLP).

Results: We detected only 22.4% of variants shared between the two methods. In contrast, RNAseq-derived variants displayed unique features of affinity and immunogenicity. We further established that neoantigen candidates identified by RNAseq data significantly increased the number of highly immunogenic neoantigens (confirmed by ELISpot) that would otherwise be overlooked if relying solely on DNAseq data.

Discussion: This integrative approach holds great potential for improving the selection of neoantigens for personalized cancer immunotherapy, ultimately leading to enhanced treatment outcomes and improved survival rates for cancer patients.

KEYWORDS

neoantigen, colorectal cancer (CRC), RNA sequencing (RNAseq), tumor variant calling, neoantigen identification workflow, Neoantigen prioritization, cancer immunotherapy

Introduction

Colorectal cancer (CRC) is a major global health concern, being the third most common cancer in the world and the fifth leading cause of cancer-related mortality among the Vietnamese population (1, 2). Traditional treatments, such as surgery, chemotherapy, and radiation therapy, have limited efficacy and are poorly tolerant, particularly in advanced stages of CRC (3). Immunotherapy, while not a cure for CRC, has the potential to significantly improve patient survival rates and quality of life (4, 5). In metastatic CRC patients, immunotherapy has demonstrated promise in improving outcomes. Immune checkpoint inhibitors (ICIs), which block negative regulatory pathways in T-cell activation, have been approved by the US Food and Drug Administration (FDA) for the treatment of deficient mismatch repair (dMMR) or high microsatellite instability (MSI-H) CRC patients (6–8). However, alternative immunotherapy strategies are urgently required for CRC patients, as patients with proficient mismatch repair (pMMR) or microsatellite stability (MSS) have not shown significant responses to immune checkpoint inhibitors (6, 9).

Neoantigens (neopeptides) have emerged as potential targets for personalized cancer immunotherapy, including CRC (10–12). Neoantigens are peptides resulting from somatic mutations, capable of being presented by class I human leukocyte antigen (HLA-I) molecules on cancer cell surface and by class II HLA molecules on professional antigen-presenting cells, thereby activating anti-tumor immune responses (13). Recent studies have demonstrated that the presence of neoantigens is associated with better responses to immune checkpoint inhibitor (ICI) therapy in CRC patients (14, 15). A high neoantigen burden has been linked to improved overall survival and progression-free survival in patients with various solid tumors, including CRC (14, 15). Therefore, neoantigen-based immunotherapies are thought to have the potential to significantly improve treatment outcomes for CRC patients.

The identification of neoantigens with strong binding affinity to their respective HLA-I molecules and high immunogenicity is critical for the development of effective neoantigen-based therapies. This process involves the use of next-generation sequencing (NGS) and bioinformatics tools. Initially, DNA sequencing of tumor tissues and paired white blood cells enables the identification of cancer associated genomic mutations, while RNA sequencing is used to determine patient's HLA-I allele profile and to quantify expression levels of genes carrying mutations. Next, tumor somatic variant, HLA-I allele, and gene expression data are analyzed using *in silico* tools based on machine learning algorithms to predict the binding affinity of neoantigens to patients' HLA-I alleles and their potential to activate T cell responses (16–18). This standard workflow has been exploited in numerous studies to identify clinically relevant neoantigens in melanoma, lung cancer, and other malignancies (17, 19).

Despite promising results, only small portions of patients benefit from the current approach due to the limited number of effective immunogenic neoantigens identified for each patient. To maximize the detection of potential neoantigens, whole exosome sequencing (WES) has been employed to comprehensively profile the cancer-specific landscape (20–22). While WES allows a much larger search space for mutations within the genome, it is not a cost- and time-effective approach. Moreover, a significant proportion of identified tumor DNA mutations, especially those which are not actively transcribed or transcribed at very low levels, might not result in the formation of neoantigens (19). Lastly, WES-based mutation calling is inefficient in capturing all tumor somatic mutations, especially clonal mutations with low frequencies and underrepresentation in the sequencing data (23), while targeting combined neoantigens derived from both clonal and subclonal mutations is necessary to evoke efficient immune-mediated cell death in a broader range of tumor cells. Therefore, relying solely on DNAseq data for tumor mutation calling, which has traditionally been the basis for identifying neoantigens, may not capture the full extent of tumor-related mutations, resulting in an incomplete identification of neoantigens.

Genetic variants at the RNA level are frequently excluded from conventional bioinformatic workflows, despite several studies indicating that neoantigens can be derived from RNA mutations, such as splicing, polyadenylation dysregulation, or RNA editing (24, 25). In addition, recent studies have shown that the presence of variant-bearing transcripts is an important factor for accurate identification of immunogenic neoantigen candidates (26, 27). Therefore, integrating RNAseq data into tumor mutation calling holds promise for unveiling a more comprehensive repertoire of neoantigens and, consequently, advancing the development of personalized immunotherapies for cancer. However, the feasibility and effectiveness of this approach require further examination.

To assess the utility of RNAseq analysis for neoantigen identification, we compared the cancer mutation profiles, binding affinity to HLA-I of neoantigens identified from RNAseq and DNAseq, and their predicted immunogenicity across 25 CRC patients. Moreover, we performed experimental validation to assess the effectiveness of utilizing RNAseq for the identification of immunogenic neoantigens. This validation utilized the ELISpot assay to measure the ability of neoantigen candidates, predicted from DNAseq and RNAseq-derived variants, to activate T cells in PBMCs obtained from four CRC patients.

Abbreviations: CRC, colorectal cancer; dMMR, deficient mismatch repair; DNAseq, DNA sequencing; FDA, the US Food and Drug Administration; FPKM, Fragments Per Kilobase of transcript per Million mapped reads; GATK, Genome Analysis Toolkit; HLA, human leukocyte antigens; ICI, immune checkpoint inhibitor; IFN-γ, interferon-gamma; LPs, long peptides; MAF, mutant-allele fraction; MSI-H, high microsatellite instability; MSS, microsatellite stability; NGS, next-generation sequencing;PBMCs, peripheral blood mononuclear cells; pMMR, proficient mismatch repair; RNAseq, RNA sequencing; SNPs, single nucleotide polymorphisms; TCR, T cell receptor; VAF, variant allele frequency; WES, whole exosome sequencing.

Materials and methods

Tumor biopsy and peripheral blood collection

A total of 25 patients diagnosed with colorectal cancer (CRC) were enrolled in this study from the University Medical Center at Ho Chi

Minh city between June 2022 and April 2023. The confirmation of CRC was based on abnormal colonoscopies and histopathological analysis confirming the presence of malignancy. The stages of CRC were determined following the guidelines provided by the American Joint Committee on Cancer and the International Union for Cancer Control. Prior to participation, all patients provided written informed consent for the collection of tumor and whole blood samples. Relevant clinical data, including demographics, cancer stages, and pathology information, were extracted from the medical records of the University Medical Center. Detailed information regarding the clinical factors of the patients can be found in Table S1. The Ethics Committee of The University of Medicine and Pharmacy at Ho Chi Minh City, Vietnam approved this study. Fresh CRC specimens were collected immediately after biopsy or tumor resection and were placed in microtubes containing RNAlater, an RNA stabilization solution (Thermo Fisher Scientific, Japan). For four patients, ten mL of peripheral blood was collected serially before surgery and stored in Heparin tubes.

Targeted DNA and RNA sequencing

The DNA/RNA samples were isolated using either the AllPrep DNA/RNA Mini Kit or the AllPrep DNA/RNA/miRNA Universal Kit (Qiagen, Germany) as per the manufacturer's protocol. In addition, matched genomic DNA from the white blood cells (WBC) of individuals was also extracted from the buffy coat using the GeneJET Whole Blood Genomic DNA Purification Mini kit (ThermoFisher, MA, USA), following the manufacturer's instructions. Genomic DNA samples from the patients's paired tumor tissues and WBCs were used to prepare DNA libraries for DNA sequencing with the ThruPLEX Tag-seq Kit (Takara Bio, USA). The libraries were then pooled and hybridized with pre-designed probes for 95 targeted genes (Integrated DNA Technologies, USA). This gene panel encompasses commonly mutated genes in CRC tumors, as reported in the Catalog of Somatic Mutations in Cancer (COSMIC) database. The DNA libraries were then subjected to massive parallel sequencing on the DNBSEQ-G400 sequencer (MGI, Shenzhen, China) for paired-end reads of 2x100 bp with an average target coverage of 200X (with actual coverage from 89 to 968X).

Isolated total RNA was subjected to a NEBNext Poly(A) mRNA Magnetic Isolation Module (New England Biolabs, MA, USA) to isolate intact poly(A)+ RNA as per manufacturer instructions. RNA libraries were constructed using NEBNext Ultra Directional RNA Library Prep Kit for Illumina (New England Biolabs). These libraries were subsequently sequenced for paired end reads of 2x100 bp on an MGI system at 50X depth coverage.

Variant calling from DNAseq and RNAseq data

To select the optimal variant calling tool for DNAseq data, we evaluated the performance of three different pipelines including Dragen, VarScan and MuTect2, which are commonly used for somatic variant calling (28, 29). Among the three pipelines, Dragen demonstrated superior performance for detecting a set of validated ground truth variants in a standard dataset downloaded from a public repository, NCBI Sequencing Read Archive SRA (ID: SRR7890830) (Figure S1A). Therefore, we utilized Dragen (Illumina) (30) in tumor-normal mode to call somatic mutations from DNAseq data. The default filtering thresholds of Dragen were used to call SNPs and indels. SNPs were further filtered using the dbSNP and 1000 Genome datasets. Germline mutations in tumor tissues were identified by comparing them with matched WBC-DNA samples. Mutations within immunoglobulin and HLA genes were excluded due to alignment difficulties in these highly polymorphic regions that require specialized analysis tools (31). Additionally, synonymous mutations were removed from downstream analysis. Included for analysis were somatic mutations that surpassed a minimum threshold of ≥2% variant allele frequency (VAF) in DNA extracted from fresh frozen tissues.

To identify the most suitable variant calling tools for RNAseq data, we assessed the performance of two different pipelines, VarScan and MuTect2 by comparing the proportions of variants that overlapped with DNA-derived variants. Sequencing reads were trimmed using Trimmomatic (32) and aligned to the human reference genome using STAR (version 2.6.0c) (33). Prior to alignment, the raw sequencing reads underwent quality checks using FastQC version 0.11.9 (34). VarScan 2 (28), which accepts both DNA and RNAseq data, was used to call mutations in paired tumor and WBC samples in 95 cancer-associated genes, again in the tumor-normal mode. Four filtering steps were applied: (i) only calls with a PASS status were used, (ii) population SNPs overlapping with a panel of normal samples from the 1000 Genome dataset were excluded, (iii) somatic mutations included for analysis met a minimum threshold of ≥10× read depth and ≥2% VAF in RNA extracted from FF tissue, and (iv) synonymous mutations and those related to HLA were removed from downstream analysis. The resulting BAM files were sorted and indexed using Samtools version 1.10 (35), and PCR duplicates were eliminated using Picard tools version 2.25.6 (36). The mutations from RNAseq data were also called using MuTect2, a variant caller from the Genome Analysis Toolkit (GATK) pipeline. Like VarScan, the MuTect2 pipeline was run in tumor versus normal mode, utilizing default settings. Following variant calling, a similar variant filtration step was also applied to eliminate potential false positives. Somatic variants from the two pipelines were manually checked using Integrative Genomics Viewer (v2.8.2). The VCF files generated by Dragen (for DNAseq) and by MuTect2 and VarScan (for RNAseq) were subsequently annotated using the Ensembl Variant Effect Predictor (VEP version 105) (37) to extract the potential effect of variants on the phenotypic outcome.

Gene expression quantification and tumor purity estimation

We used the Cufflinks (38) to analyze the tumor RNAseq data using the Ensemble human reference transcriptomes (GRCh38) for assessing gene expression. The expression data was used to calculate the tumor purity via ESTIMATE (v1.0.13) package, (R-v3.6.3) (39).

In silico prediction of HLA binding affinity and immunogenicity

Class I HLA alleles (HLA-A/B/C) with two-digit resolution were identified from patient tumor RNAseq data using OptiType tool (40). The annotated VCF files were analyzed using pVAC-Seq, a tool of pVACtools (v1.5.9) (16, 41, 42) with the default settings, except for disabling the coverage and MAF filters. We used all HLA-I binding algorithms that were implemented in pVAC-Seq to predict 8 to 11-mer epitopes binding to HLA-I (A, B, or C) for downstream analysis. Neoantigen candidates were subjected to MHC binding predictions and subsequent prioritization based on their binding affinity scores (measured in nM) using NetMHCpan-4.1 (18). The prioritization process involved calculating the percentile ranking of each neoantigen's binding affinity score within the distribution of scores for the corresponding HLA allele. Neoantigen candidates with a percentile rank lower than 2% were selected for our immunogenicity analysis.

The immunogenicity of neoantigens was validated by the PRIME tool (43) with default settings. To predict the immunogenicity of neoantigen candidates, a two-step ranking process was employed, involving ranking the neoantigen candidates based on their immunogenicity score and estimating percentiles for each HLA allele. These scores represented the predicted likelihood of a neoantigen being immunogenic. The neoantigens were then ranked in descending order based on their immunogenicity scores, enabling the prioritization of neoantigen candidates with higher predicted immunogenicity for further analysis. A ranking value for immunogenicity was assigned to each neoantigen candidate by determining the percentile rank of its immunogenicity score within the group of neoantigens predicted to bind to the same HLA allele. The percentile rank of binding affinity score in NetMHCpan or immunogenicity score in PRIME for a peptide is the fraction of random peptides that would have a score higher or equal to the peptide given in input. Therefore, a peptide with lower percentile rank value of NetMHCpan or PRIME indicate better binding affinity and immunogenicity, respectively. To identify public neoantigens, we conducted a comprehensive search of several databases, including TSNAdb (44, 45), NeoPeptide (46), dbPepNeo (47, 48), NEPdb (49), TANTIGEN (50, 51), and IEDB (52). All databases contained epitopes from published studies where their immunogenicity was validated by immunological assays.

Isolation, culture, and stimulation of PBMCs with long peptides

Peripheral blood samples from four patients were collected prior to surgery using BD Vacutainer Heparin Tubes (BD Biosciences, NJ, USA). Peripheral blood mononuclear cells (PBMCs) were isolated through gradient centrifugation using Lymphoprep (STEMCELL Technologies) within 4 hours. PBMCs were then resuspended in FBS/10% DMSO solution with a concentration of 7-10x10^6 cells/mL for freezing in liquid nitrogen.

Frozen PBMCs were thawed in AIM-V media (Gibco, Thermo Scientific, MA, USA) supplemented with 10% FBS (Cytiva, USA) and DNase I (Stemcell Technology, Canada) (1 µg/mL) solution. 10^5 PBMCs were allowed to rest in 96-round bottom well-plate containing AIM V media supplemented with 10% FBS, 10 mM HEPES, and 50 µM β-mercaptoethanol overnight before stimulation with synthesized long peptides at a concentration of 5 µM in a humidified incubator at 37°C with 5% CO_2. PBMCs were further stimulated with GM-CSF (2000 IU/mL, Gibco, MT, USA) and IL-4 (1000 IU/mL, Invitrogen, MA, USA) for 24 hours. Following this initial stimulation, LPS (100 ng/mL, Sigma-Aldrich, MA, USA) and IFN-γ (10 ng/mL, Gibco, MT, USA) were added to the PBMCs along with the peptides for an additional 12 hours. On the following day, IL-7, IL-15, and IL-21 (each at a concentration of 10 ng/mL) (Peprotech, NJ, USA) were added to the PBMC culture. The restimulation process involved exposing the peptides to a fresh media containing IL-7, IL-15, and IL-21 every 3 days for a total of 3 times. On day 12, PBMCs were restimulated with peptides and cultured in media without cytokines. ELISpot assays were performed on stimulated PBMCs on day 13.

ELISpot assay on PBMCs stimulated with long peptides

Cultured T cells were transferred to an ELISpot plate (Mabtech, Sweden) and incubated for 20 hours at 37°C. PBMCs cultured with DMSO were used as a negative control group, while PBMCs stimulated with anti-CD3 were used as a positive control group. ELISpot assay was performed on treated PBMCs using ELISpot Pro: Human IFN-γ (ALP) kit (Mabtech, Sweden), following manufacture's protocol. Developed spots on the ELISpot plate were then enumerated using an ELISpot reader (Mabtech, Sweden). The reactivity was determined by measuring the fold increase in the number of spots of PBMCs treated with mutant peptides relative to those treated with wild type peptides. A fold change of two was selected as the cut off for positivity (53).

Flow cytometry intracellular staining for IFN-γ

Cells from ELISpot plate were collected in media supplemented with GolgiStop Protein Transport Inhibitor (BD Biosciences, NJ, USA) and incubated for 6 hr at 37°C. Positive control group was treated with 50 µM PMA (Abcam, UK), 1 mg/mL Ionomycin (Abcam, UK). Cells were then washed, blocked with Fc receptor (Biolegend, CA, USA), and stained with CD3-PE (clone HIT3a, Biolegend), CD4-PE/Cyanine7 (clone RPA-T4, Biolegend), CD8-FITC (clone RPA-T8, Cell Signaling) antibodies for 2 hr at 4°C. Cells were permeabilized for 20 mins at 4°C and then stained overnight with IFN-γ-APC (clone 4S.B3, Biolegend) antibody at 4°C.

Statistical analysis

The Wilcoxon rank-sum test was used to compare the coverage, VAF, and immunogenicity percentile among three groups for three

mutation groups (DNA-unique, RNA-unique and Shared). All statistical analyses were carried out using R (v2.6.3).

Results

Comparison of mutation profiles from DNA sequencing and RNA sequencing data

RNA sequencing (RNAseq) data, which is commonly used for analysis of mutated gene expression in the current standard workflow of neoantigen identification, have been exploited to identify cancer-specific mutations in recent studies (27, 54, 55). However, the properties of RNAseq derived variants and neoantigens have not been fully characterized. To assess the utility of RNAseq in calling cancer-specific somatic mutations for neoantigen prediction, we sought to compare the mutation profiles obtained from RNAseq and DNAseq data across 25 CRC patients (Table S1), with a focus on all single nucleotide variants (SNVs) and indel variants (Figure 1). To achieve a balance between cost and mutation detection efficiency, we used a targeted sequencing panel consisting of 95 commonly mutated cancer-associated genes (Table S2). As a result, our comparison of RNAseq and DNAseq analysis was limited to these genes (Figure 1). The DNAseq and RNAseq data obtained from all 25 CRC patients have successfully met quality metrics, ensuring reliable datasets for mutation calling (Tables S3, S4). To identify mutations in DNAseq data, we used Dragen as our primary tool due to its superior performance in both SNV and indel mutation calling from a reference sample compared to other tools used in the analysis of DNAseq data (Figure S1A) (56).

To determine the most effective tool for calling mutations from RNAseq data, we compared the performance of VarScan and MuTect2. We found that VarScan yielded a higher proportion of variants overlapping with mutations detected from DNAseq compared to MuTect2 (18.3% versus 0.8%, Figure S1B). Furthermore, while MuTect2 tended to call a high percentage of indels with abnormal length, VarScan yielded a higher proportion of SNVs that were comparable to the mutation profiles identified from DNAseq (Figures S1C, D). These data suggested that VarScan exhibited higher sensitivity in detecting SNVs and produced fewer artifact indels. Thus, we decided to use VarScan as the variant calling tool for RNAseq data from the 25 CRC patients.

Out of the total 1,520 variants identified, only 340 (22.4%) were common between the two mutation calling methods, while most variants (77.6%) were exclusively detected by either DNAseq (DNA-unique) or RNAseq (RNA-unique) data. DNA-unique variants were more frequent than RNA-unique variants (56.1% versus 21.5.%, Figure 2A). Shared variants were detected in 16 out of the 25 CRC patients, accounting for 1% to 47% of the total identified variants (Figure 2B, Table S5). Interestingly, we found that RNA-unique variants were the major source of variants in 4 out of 25 (16%) patients (Figure 2B), while DNA-unique variants were identified as the major source of variants in the remaining 21 patients.

When comparing the distribution of variant types between DNAseq and RNAseq, we observed a consistent pattern where missense variants were the most prevalent variant type (>50% of all

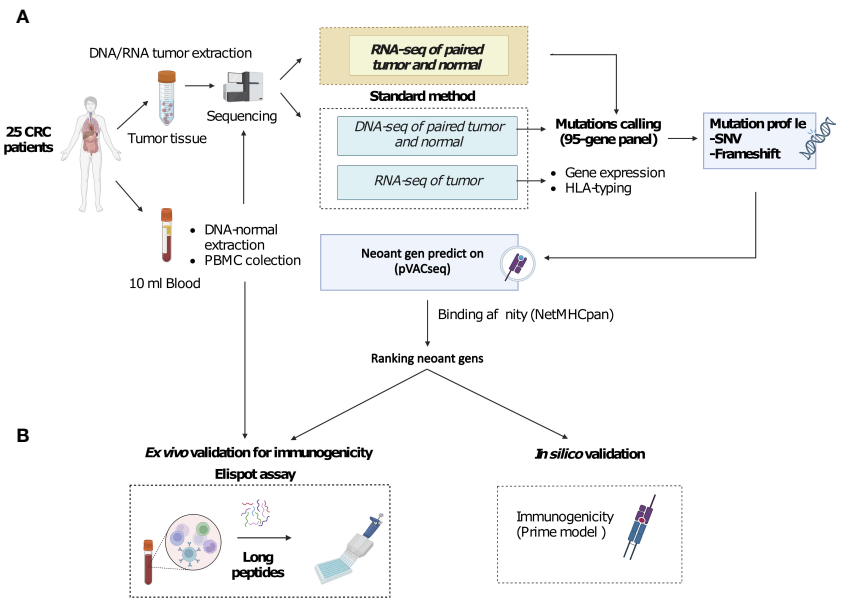

FIGURE 1
A novel workflow for CRC neoantigen identification and validation that integrates RNAseq data into somatic mutation calling. **(A)**. Schematic diagram of the new workflow. Tumor biopsies and blood samples from CRC patients are subjected to targeted DNA and RNA sequencing, which focuses on a panel of 95 genes, for somatic mutation calling. Additionally, RNAseq data is used to determine gene expression and HLA-typing information. pVAC-Seq tool is then utilized for neoantigen prediction using DNA and RNA-derived somatic mutation data, gene expression data, and patient-specific HLA-typing data as inputs. **(B)**. Methods to validate the advantages of the workflow. Predicted neoantigens from the workflow are subsequently validated by *ex vivo* ELISpot assay measuring IFN-γ secretion from PBMCs stimulated with long peptides carrying predicted variants and by *in silico* prediction of immunogenicity by PRIME tool.

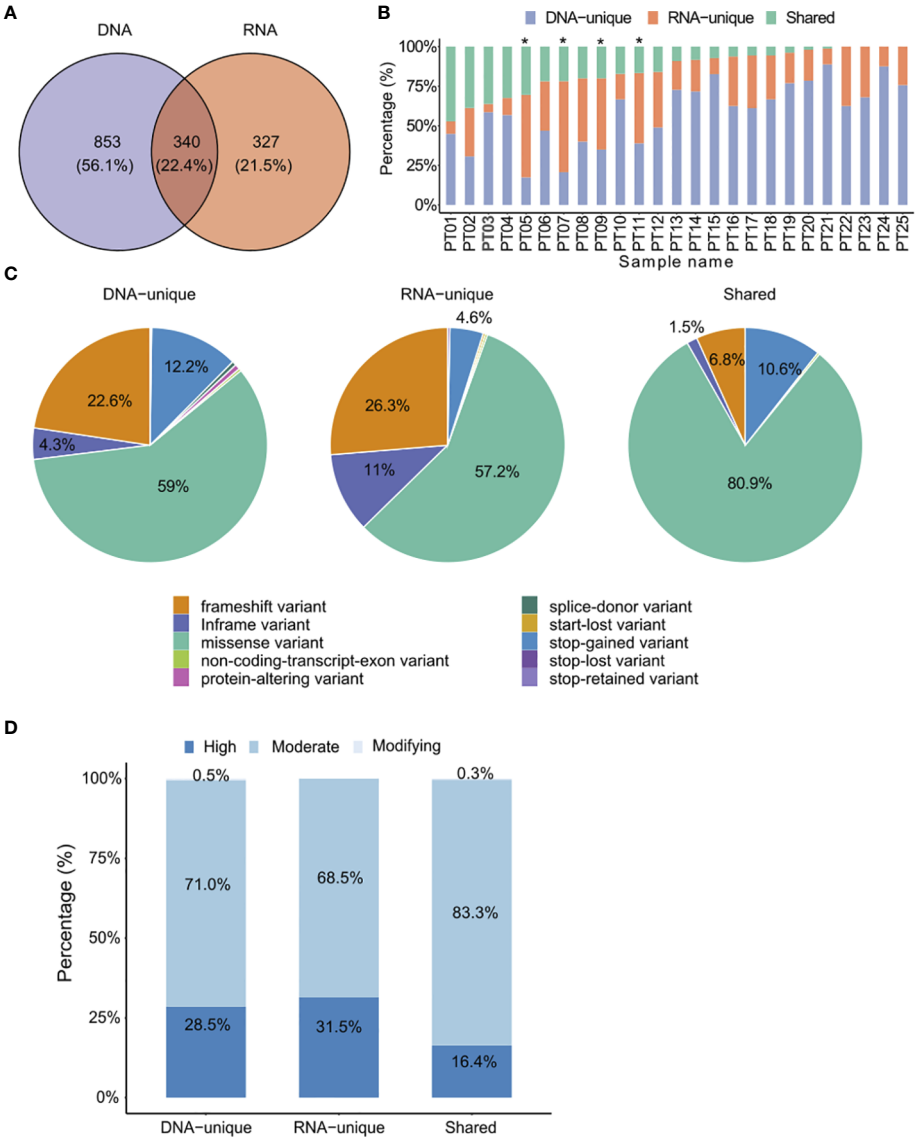

FIGURE 2
Comparison of identified somatic mutations between DNAseq data and RNAseq data. **(A)** Venn diagrams display the numbers of DNA and RNA mutations called by the specified mutation callers on matched tumor-normal DNAseq and RNAseq data from 25 CRC patients. **(B)** Proportions of each type of variants identified from both DNAseq and RNAseq data for each patient. The graph is presented in descending order based on the proportion of shared variants. Patients marked with an asterisk exhibited a higher proportion of RNA-unique variants compared to DNA-unique variants. **(C)** Pie charts presenting the percentages of mutation types. **(D)** The proportions of indicated types of variants in relation to their phenotypic impacts.

variants in each group, Figure 2C). However, we did notice some notable differences. Specifically, RNA-unique variants exhibited a higher frequency of in-frame variants (11% compared to 4.3% in DNAseq, Figure 2C) and frameshift variants (26.3% versus 22.6%, Figure 2C). On the other hand, DNA-unique variants had a higher occurrence of stop-gained variants (12.2% versus 4.6%, Figure 2C). In the shared-variant group, most variants consisted of missense variants (80.9%) and stop-gained variants (10.6%), collectively accounting for approximately 91.5% of all variants. To predict the functional impact of the three variant groups, we employed the Ensembl's Variant Effect Predictor tool (37). Our analysis revealed that the phenotypic outcome was most significantly affected by RNA-unique variants in the high impact category, followed by DNA-unique and shared variants (Figure 2D). These results indicate a clear distinction between the tumor variant landscapes profiled by RNAseq and DNAseq, wherein RNAseq reveals a greater proportion of clinically relevant variants compared to DNAseq. Therefore, RNAseq appears to be particularly valuable in identifying variants with potential clinical significance.

To gain deeper insights into the variants identified by both sequencing methods, we conducted an analysis of their depth coverage and mutation allele frequency (MAF). Despite having lower coverage levels ($P= 9.1x10^{-5}$, Figure 3A), the shared variants exhibited significantly higher MAFs ($P= 2.22x10^{-16}$, Figure 3B) compared to the DNA-unique. This observation suggests that the shared variants are likely derived from major clones of somatic mutation clones, while the

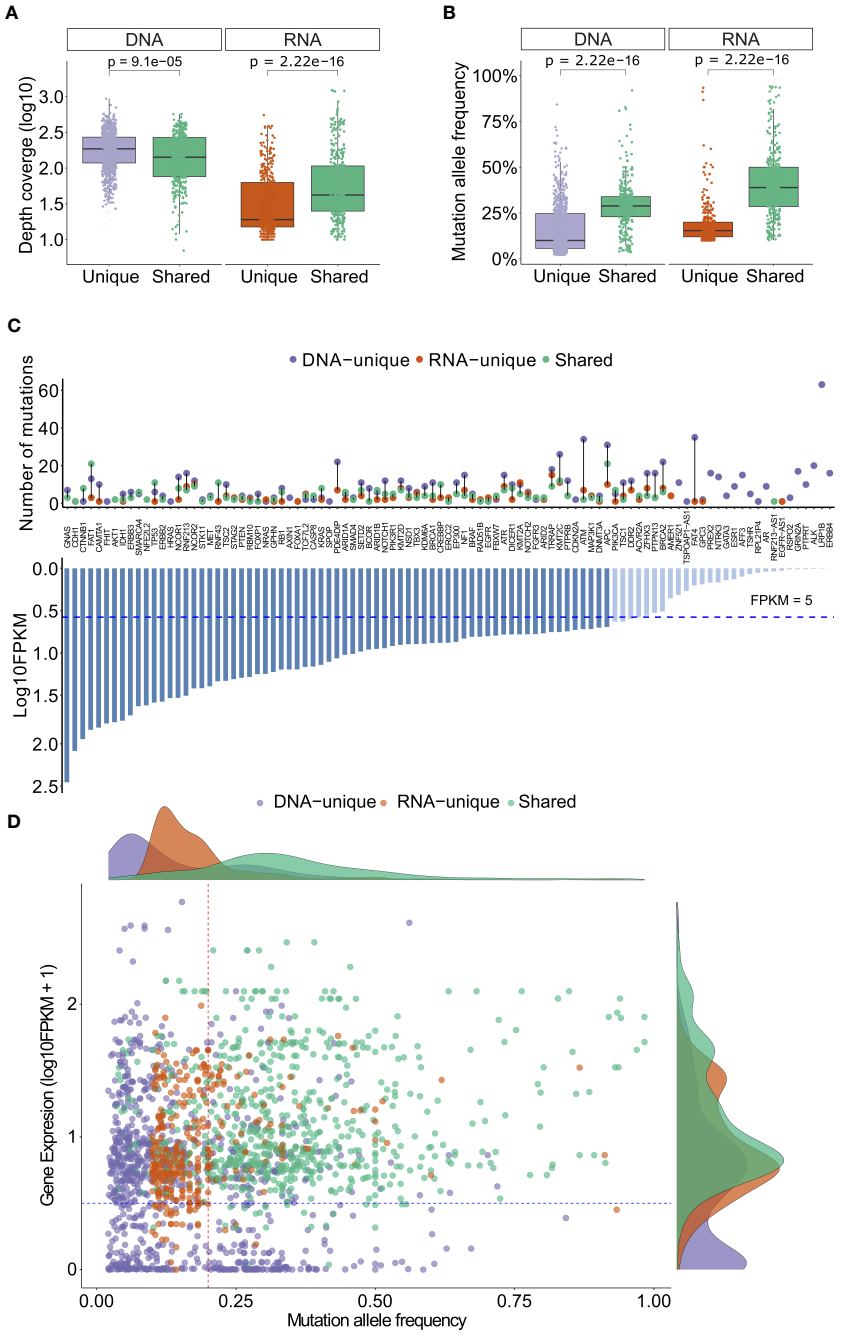

FIGURE 3
Depth coverage, MAFs and gene expression levels of variants from DNAseq and RNAseq data. **(A)** Depth coverage of the indicated groups of variants based on DNAseq and RNAseq data. **(B)** Mutation allele frequency of the indicated groups of variants. **(C)** A list of genes with indicated variants, along with their corresponding FPKM. **(D)** Gene expression levels of different groups of variants in relation to their mutation allele frequency. In **(A, B)**, the boxes represent the median value, as well as the lower and upper quartiles (25th and 75th percentiles). The p-values were obtained from the Wilcoxon rank-sum test.

DNA-unique variants, characterized by significantly lower MAF ($P < 2.22x10^{-16}$, Figure 3B), may originate from minor tumor clones.

RNA-unique variants displayed a notably lower median depth of coverage ($P<2.22x10^{-}16$, Figure 3A) and MAF (20% versus 40%, $p<2.22x10^{-6}$, Figure 3B) compared to the shared variants. These findings suggest that RNA-unique variants may originate from genes with low expression levels, resulting in a smaller number of variant transcripts. It is notable that the majority of shared variants and RNA-unique variants were identified in genes with high expression levels (FPKM >5, dashed line, Figure 3C), while unique variants identified through DNAseq (494/853, 58%, Table S5) were more commonly found in genes with low expression levels (FPKM <5, Figure 3C). Furthermore, when examining the MAF of variants in relation to their gene expression levels, shared variants (green dots, Figure 3D) exhibited higher levels of gene expression (FPKM >5) and MAF (> 24%) compared to other mutation types. In contrast, RNA-unique variants

(orange dots, Figure 3D) tended to have similar gene expression levels but lower MAF, while a substantial number of DNA-unique variants (purple dots, Figure 3D) displayed both low gene expression and MAF. These observations strongly suggest that the MAF and transcriptional activity of mutated genes are significant factors contributing to the disparities observed between RNAseq and DNAseq. Notably, shared variants with high numbers of MAF may arise from dominant tumor clones and are highly expressed, making them potential neoantigen candidates. On the other hand, unique variants displaying low MAFs may be derived from subclonal mutations or poorly expressed mutations, further emphasizing the influence of MAF and gene expression on the distinct characteristics of the identified variants.

In silico analysis of HLA-I binding affinity and immunogenicity of neoantigens derived from DNAseq and RNAseq

To identify neoantigen candidates, we utilized the pVAC-Seq pipeline, a well-established computation tool, to predict the binding affinity of 8-13 mer peptides generated from DNA or RNA variants to patient-specific HLA class I molecules (42). The HLA-I allele profiles of 25 patients were presented in Table S6. Through our analysis, we identified a total of 48,155 DNA-unique variants derived neoantigen candidates (61.7%), 15,584 shared-variant derived neoantigen candidates (20%), and 14,532 RNA-unique derived neoantigen candidates (18.4%) (Figure 4A, Table S7). As expected, the proportions of candidates from each group showed a significant correlation with the proportions of nucleotide mutations (Figure S2A).

It is well established that effective activation of T cell responses relies on the presentation of neoantigens on the patient's HLA-I molecules (57). Here, we assessed the binding affinity of predicted neoantigen candidates from each group of tumor variants to HLA-I using NetMHCpan 4.1 (18). For this analysis, only neoantigen candidates with predicted percentile ranks of less than 2% were considered, in accordance with the recommendations provided by NetMHCpan. We further considered 0.5 and 2 as percentile rank cutoffs to identify strong binding and weak binding epitopes, respectively. In Figure 4B, we presented the density distribution of

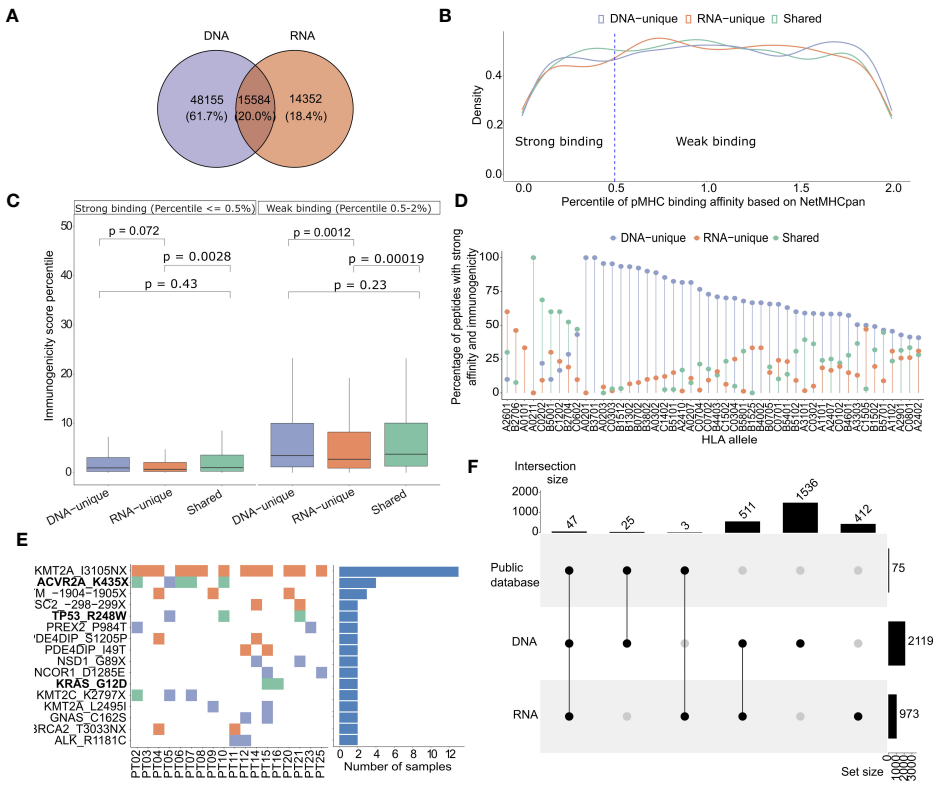

FIGURE 4
HLA-I binding affinity and immunogenicity of predicted neoantigens derived from DNAseq and RNAseq data. **(A)** A Venn diagram illustrates the proportion of each type of neoantigens identified from DNAseq and RNAseq data. **(B)** Histograms showing the density distribution of neoantigens with percentile ranks for HLA-I binding affinity calculated by NetMHCpan, that fall below 2%. The threshold value of 0.5% rank, designated for distinguishing strong and weak binders, is indicated by dashed lines. This distinction aligns with the recommendation provided by NetMHCpan. **(C)** Predicted immunogenicity, as calculated by the PRIME tool, for both strong binding and weak binding neoantigens. The box plot represents the median value, along with the lower and upper quartiles (25th and 75th percentiles). Outliers are not displayed for clarity of visualization. The p-values were estimated using the Wilcoxon rank-sum test. **(D)** A Lollipop plot depicts the distribution of specific groups of neoantigens based on their percentage, focusing on indicated HLA-I alleles. These plots highlight neoantigens that fall within the top 2% in terms of strong binding affinity to HLA-I and demonstrate high immunogenicity. **(E)** A map illustrates the frequency of indicated mutations on 25 CRC patients. The ones highlighted in bold have been previously validated as highly immunogenic through immunological assays in previous studies. **(F)** An UpSet plot illustrates the frequency distribution of the indicated groups of variants identified from public datasets.

predicted neoantigen candidates originating from DNA-unique, RNA-unique, or shared variants based on their percentile ranks of HLA-I binding affinity as predicted by NetMHCpan 4.1 (18). We observed that neoantigen candidates from RNA-unique variants exhibited a lower proportion a lower proportion of strong binding neoantigen (< 0.5%rank) compared to those from shared and DNA-unique variants (Figure 4B). This suggests that, in comparison to neoantigen candidates derived from DNA-unique variants, those originating from RNA-unique variants exhibited lower HLA-I binding affinity, as indicated by the NetMHCpan predictions. It has been reported that the binding affinity to HLA-I is determined by specific anchor residues in neopeptides (58). When comparing DNA-unique and shared neoantigens with RNA-unique neoantigens, it was observed that the latter exhibited a reduced proportion of mutations at P2 (Figure S2B). Notably, P2 serves as a crucial anchor residue involved in the primary interactions between the peptide and HLA-I molecule, and mutations occured within this position increase the binding affinity to HLA-I. This observation suggests that the decreased frequency of RNA-unique derived neoantigens carrying mutations at this anchor site, in comparison to other sources of neoantigens, may account for their lower binding affinity.

To assess the immunogenicity of the predicted candidates, we employed the PRIME tool which captures biophysical properties of both antigen presentation and TCR recognition to evaluate their potential to elicit a $CD8^+$ T cell-specific immune response (43). The predicted immunogenicity of neoantigen candidates was evaluated in relation to their predicted binding affinity to HLA-I (Figure 4C). We observed a positive correlation between the predicted binding affinity to HLA-I using NetMHCpan and the predicted immunogenicity assessed by the PRIME tool, irrespective of the neoantigen candidate class. Notably, strong binding neoantigen candidates exhibited lower percentile ranks of immunogenicity (Figure 4C). However, among the neoantigen candidates with strong HLA-I binding affinity, the RNA-unique neoantigen candidates showed significantly lower percentiles of immunogenicity compared to both DNA-unique (P=0.0075, Figure 4C) and shared neoantigen candidates (P= 0.0045, Figure 4C). Within the weak binding neoantigen candidates, RNA-unique neoantigen candidates consistently demonstrated lower percentiles of immunogenicity compared to DNA-unique (P=0.0012, Figure 4C) and shared neoantigen candidates (P=0.0011, Figure 4C). Subsequently, neoantigen candidates meeting the criteria for predicted binding affinity and immunogenicity within the top two percentile for both parameters were profiled based on the specific HLA-I alleles identified in our cohort of 25 CRC patients. As shown in Figure 4D, we observed that the binding affinity of predicted neoantigen candidates to HLA-I was influenced by both the specific neoantigen candidate's sequence and the HLA-I allele. For instance, we observed that the HLA-I allele A02011 exhibited a higher binding affinity to shared neoantigen candidates, as this allele showed the highest proportion of detected neoantigen candidates in this group. Similarly, the HLA-I allele A2601 displayed a stronger binding affinity for RNA-unique derived neoantigen candidates; while the HLA-I allele A0201 showed a stronger binding affinity for DNA-unique derived neoantigen candidates, in comparison to shared and RNA-unique neoantigen candidates (Figure 4D). Among the neoantigen candidates displaying strong predicted affinity and immunogenicity, a noteworthy subset of 16 neoantigen candidates was consistently identified in at least two patients (Figure 4E). Of those, neoantigen candidates derived from three shared mutations (ACVR2A_K435X, TP53_R428W, and KRAS_G12D) have been experimentally validated in previous studies and reported in public databases of immunogenic neoantigens. Notably, the KMT2A_IN3105X neoantigen candidate predicted from an RNA-unique variant, exhibited the highest frequency among these frequently detected neoantigen candidates, being present in 13 out of 25 (52%) patients. This suggests that this neoantigen candidate has the potential to serve as a public neoantigen, capable of eliciting immune responses across multiple individuals. Additionally, a total of 75 strong affinity and immunogenic neoantigen candidates were previously reported in public databases of immunogenic peptides. Among these, the majority (47/75, 62.7%%) could be found from shared variants, while 25 and 3 neoantigens were predicted from DNA-unique and RNA-unique variants, respectively (Figure 4F). These findings underscore the presence of both shared and unique neoantigen candidates with strong binding and immunogenicity in 25 analyzed patients, further highlighting the importance of considering different sources of NGS data for mutation identification in neoantigen-based immunotherapy approaches.

Taken together, these findings emphasize the distinct binding affinity and immunogenic potential of neoantigen candidates originating from different variant groups. Particularly, our data suggests that despite their low predicted binding affinity, neoantigen candidates derived from RNA somatic mutations still exhibit high immunogenicity, indicating their potential to elicit an immune response for immunotherapy. These observations underscore the importance of considering not only DNAseq but also RNAseq derived variants for selecting candidate neoantigens.

Experimental validation of predicted neoantigen candidates by ELISpot

To evaluate the effectiveness of integrating RNAseq variant calling into the current standard method, we conducted ELISpot assay on four CRC patients using autologous PBMCs following the procedure outlined in Figure 5A. Initially, we identified 431 nonsynonymous variants from both DNAseq and RNAseq data, resulting in a total of 18,479 predicted neoantigen candidates using the pVAC-Seq tool. To accommodate the limited availability of PBMCs, only the top ten mutations resulting in neoantigen candidates with the highest predicted binding affinity to HLA-I were chosen for each patient. As a result, a total of 40 synthesized long peptides (LPs) carrying the corresponding mutations were synthesized and used in an *ex vivo* ELISpot assay to measure the release of IFN-γ from patients' PBMCs (Figure 5A, Table S8).

Among the 40 designed LPs, those originating from shared neoantigen candidates were detected in all patients, whereas LPs derived from DNA-unique or RNA-unique variants were only detected in three out of four patients (Figure 5B). However, no LPs were identified within the DNA-unique group for patient PT10 and within the RNA-unique group for patient PT03 (Figure 5B). When

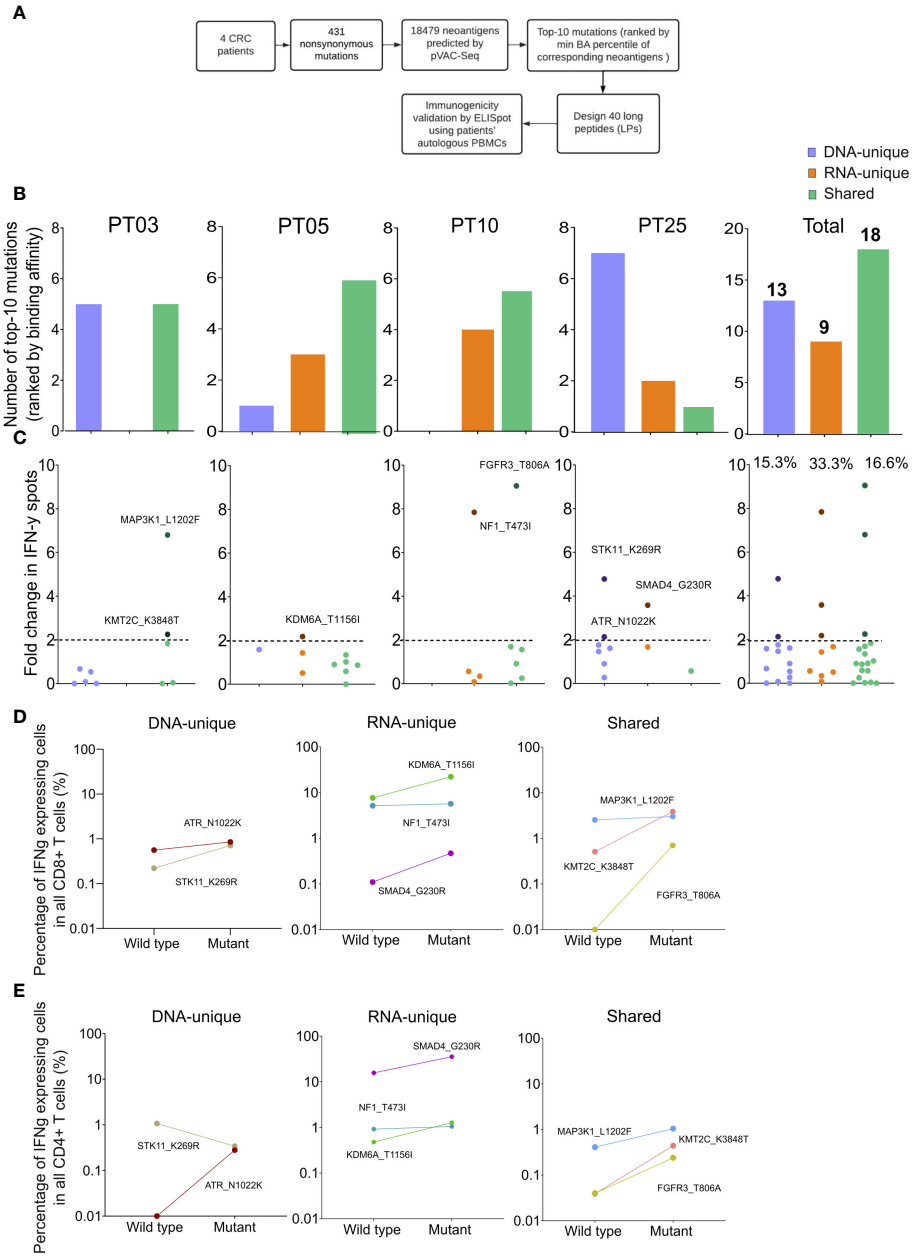

FIGURE 5
Validation of neoantigens *in silico* identified from the modified workflow by ELISpot assays on four CRC patients. **(A)** A schematic diagram illustrates the procedural steps of neoantigen prioritization and the ELISpot assay. **(B)** The number of each type of neoantigens identified from each CRC patient. **(C)** The fold change in IFN-γ spots, relative to the wildtype peptides, for 40 long peptides. Note: only the mutants that result in a positive value in ELISpot are depicted with their corresponding amino acid change. **(D)** The percentage of IFN-γ expressing CD4+ T cells induced by indicated long peptides. Note: these long peptides induce a more than 2-fold change in IFN-γ spots as observed in the ELISpot assay. **(E)** The percentage of IFN-γ expressing CD8+ T cells induced by indicated long peptides.

considering the cumulative number of LPs across all patients, it was observed that shared-variants yielded the highest number (18 out of 40), while RNA-unique variants yielded the fewest (9 out of 40, Figure 5B).

The PBMCs from four patients were subjected to three rounds of stimulation with 40 LPs carrying mutations or their corresponding wildtype counterparts to measure the secretion of IFN-γ. The ELISpot results for the 40 tested LPs were presented in Figure 5C and Table S8. A fold change of two in the number of IFN-γ spots from LPs relative to their corresponding wildtype peptides was chosen as the positivity cutoff, with LPs resulting in an ELISpot fold change value of two or higher considered as immunogenic (53). Among 40 tested LPs, we identified eight immunogenic LPs, with three originating from RNA-unique variants, three from shared variants, and two from DNA-unique variants (Figures 5C, S3). Notably, all four patients had at least one LP capable of inducing IFN-γ production by PBMCs. Among the LPs derived from RNA-

unique variants, three out of nine (33.3%) were positive for IFN-γ activation, while the proportions of positive LPs were lower for those derived from shared variants (three out of 18, 16.7%, Figure 5C) or DNA-unique variants (two out of 13, 15.4%, Figure 5C). The findings suggest that RNA-unique variants may result in fewer neoantigen candidates with strong binding affinity to HLA-I, but they are more likely to activate T cells compared to shared or DNA-unique neoantigen candidates.

Intracellular flow cytometry staining of IFN-γ in T cells further demonstrated that all LPs showing positive results in the ELISpot assay effectively activated CD8+ T cells. This activation led to a significant increase in the percentage of IFN-γ positive cells, with a fold increase greater than 1 compared to their corresponding wildtype peptides (Figures 5D, S4). Moreover, consistent with the activation of $CD8^+$ T cells, all LPs exhibited increased production of IFN-γ by $CD4^+$T cells, except for the LP carrying STK11_K269R, which originated from a DNA-unique variant (Figure 5E). Although this LP did not exhibit detectable changes in intracellular IFN- γ levels in $CD4^+$ T cells, it still demonstrated $CD8^+$ T cell activation. Overall, these findings suggested that the integration of RNAseq data for variant calling into the current neoantigen prediction workflow could enhance the identification of effective and immunogenic neoantigen candidates for the development of cancer immunotherapies.

Discussion

The identification of highly immunogenic neoantigens capable of eliciting T-cell-mediated responses is essential for the development of effective personalized immunotherapies for cancer. However, the current challenge lies in accurately identifying these neoantigens due to the limited number of highly immunogenic neopeptides predicted by conventional bioinformatic workflows. These workflows solely rely on genomic sequencing data for tumor mutation calling, overlooking the potential contribution of transcriptomic variants in generating neoantigens. To address this limitation, we aimed to enhance the identification of highly immunogenic neoantigens by integrating RNA sequencing data into the conventional bioinformatic workflow (Figure 1). By considering tumor mutations at the transcriptional level, we sought to expand the pool of valuable immunogenic neopeptides for colorectal cancer (CRC) patients. In our study, we successfully demonstrated that integrating RNAseq data into the conventional workflow for variant calling significantly increased the number of valuable immunogenic neopeptides for CRC patients. This improvement provides a promising avenue for the development of more effective cancer treatments.

Our analysis of tumor variants using DNAseq and RNAseq data obtained from 25 CRC patients identified a moderate proportion (22.4%) of shared somatic variants (Figure 2A). This finding is consistent with a previous study that reported a similar trend in two datasets (59). The differences in variants identified by DNAseq and RNAseq could be attributed to variations in sequencing technologies or variant calling tools, as reported in previous studies (60). To mitigate the impact of differences in sequencing technology and *in silico* tools on mutation results, we conducted both DNAseq and RNAseq on the same sequencing platform and selected the optimal variant calling tools for RNAseq data that exhibit the highest concordance with the DNAseq mutation profile (Figure S1A). However, we believe that more validation studies are required to improve the variant calling tools and standardize their use for RNA sequencing data. In addition to these technical factors, it has been reported that RNA mutations could be generated from a post-transcriptional modification process known as RNA editing (61, 62). Such mutations exclusively occur in transcribed RNA and have been shown to result in a new source of neoantigens in cancer patients (63, 64).

Additionally, the proportions of shared mutations exhibited significant variation among patients (Figure 2B), highlighting the intrinsic diversity of cancer mutations and the heterogeneity of clonal expansion within each patient. Furthermore, different variant groups displayed distinct characteristics, with RNA-variants showing an enrichment for frameshift and inframe variants and displaying more profound impact on the phenotypic outcome (Figures 2C, D). Neoantigens derived from frameshift or indel variants, which are greatly distinct from self peptides, have been shown to generate highly immunogenic tumor neoantigens and thereby expand the pool of ideal candidates for immunotherapy (65, 66).

Both DNA-unique and RNA-unique variants displayed significantly lower MAFs compared to shared variants (Figure 3B). This observation implies that these unique variants likely originated from tumor clones with low frequencies, which might not be consistently detected at both genomic and transcriptomic levels due to the limited sensitivity of sequencing methods. Notably, our analysis revealed that DNA-unique variants were more frequently associated with genes characterized by low FPKMs, unlike shared or RNA-unique variants (Figures 3C, D). These findings suggest that DNA-unique variants may arise from genes with low expression or those displaying mono-allelic expression of the wild-type allele. Conversely, RNA-unique or shared variants tend to occur in genes exhibiting high expression levels, implying their abundant transcription. Previous studies have demonstrated a correlation between the expression levels of neoantigens and their likelihood of being presented by HLA-I on the surface of tumor cells, which can trigger immune responses leading to the eradication of tumor cells (67, 68). Hence, neoantigens arising from RNA-unique or shared variants might be superior, as they are more likely to be presented and recognized by the immune system. The discrepancies in mutation profiles between RNAseq and DNAseq could be attributed to the low MAFs, low quantities of transcripts harboring variants, and/or insufficient sequencing coverage.

The proportions of neoantigens predicted by the pVAC-Seq tool are similar to those of nucleotide variants (Figures 3A, 4A). Currently, the prediction of peptide binding affinity for HLA-I is a pivotal criterion in the selection of neoantigens for experimental validation (18). Employing NetMHCpan 4.1, we discovered that neoantigen candidates originating from RNA-unique variants exhibited lower percentile ranks of binding affinity compared to those derived from shared or DNA-unique variants (Figure 4B). This finding suggests that neoantigen candidates resulting from

RNA variants tend to display reduced levels of HLA-I binding affinity in comparison to those arising from DNA variants. Prior research has indicated that the position of mutations within mutant peptides can influence their binding affinity to HLA-I molecules, with specific residues in the peptides, known as anchor residues, serving as key determinants of binding affinity (69). Therefore, it is plausible that amino acid changes in neoantigen candidates predicted from RNA mutations may arise from positions that do not lead to enhanced binding affinity, in contrast to those arising from DNA mutations. Interestingly, our findings revealed a lower proportion of RNA-derived neoantigen candidates with mutations occurring at the primary anchor site P2, which is recognized as a critical factor influencing peptide affinity for various HLA-I types. This distinction was observed when comparing RNA-derived neoantigen candidates with both shared and DNA-unique derived ones (Figure S2B) (70). Another possible explanation for the lower binding affinity of RNA-unique neoantigen candidates could be attributed to the fact that current prediction tools have not been specifically trained on this particular group of candidates (71).

While predicted HLA-I binding affinity serves as a crucial indicator for the presentation of neoantigens on tumor cells, it is not the sole determinant of neoantigen immunogenicity. The immunogenicity of neoantigens is also influenced by the interaction between peptide-HLA complexes and T cell receptors (TCR) (43, 72, 73). Therefore, in our study, we initially selected neopeptides with strong binding affinity (< 2% percentile rank). Subsequently, we employed the PRIME tool (43), which captures molecular properties related to both antigen presentation and TCR recognition, to estimate the immunogenicity of these selected peptides. Interestingly, we observed that neoantigen candidates derived from RNA-unique mutations or shared mutations exhibited significantly higher immunogenicity compared to those derived from DNA-unique mutations (Figure 4C). Schmidt et al. have identified specific amino acid positions within the neopeptide sequence, known as minimally impacting on HLA-I affinity positions. These positions have been found to have significant roles in binding to the T cell receptor (TCR) (43). Therefore, it is plausible that amino acid changes in neopeptides derived from RNA mutations may occur at such positions, resulting in enhanced TCR affinity and consequently explaining their stronger immunogenicity. Analysis of neoantigen candidates' immunogenicity, considering the HLA-I allele panels obtained from our CRC patient cohort, revealed a notable dependence on specific HLA-I alleles, thereby emphasizing the significance of profiling the HLA-I genotype of cancer patients for personalized immunotherapy (Figure 4D). The notable immunogenicity scores of neoantigen candidates derived from RNA variants suggest their potential to effectively activate T cell-mediated immune responses, rendering them valuable candidates for clinical evaluation. Our *in silico* analysis successfully identified a recurrent RNA-derived neoantigen candidate (KMT2A_IN3105X) in 25 CRC patients. Additionally, we discovered three shared candidates (ACVR2A_K435X, TP53_R428W, and KRAS_G12D) that have been experimentally validated as highly immunogenic in publicly available databases (Figures 4E, F). These neopeptides hold potential as public neoantigens, making them suitable candidates for an off-the-shelf vaccine strategy. Thus, we speculate that incorporating RNA-unique variants, which exhibit strong binding affinity and higher transcription abundance, can serve as a strategy to identify more effective targets for neoantigen-based vaccination.

To validate our hypothesis regarding the effectiveness of neoantigen candidates derived from RNA variants compared to DNA-derived candidates, we conducted *ex vivo* ELISpot assays on four patients with available blood samples for PBMC collection. The purpose was to assess the immunogenicity of predicted neoantigen candidates originating from different mutation sources. For each patient, we selected the top 10 mutations based on the predicted binding affinity of the corresponding neopeptides to the patients' HLA-I profile. To evaluate immunogenicity, we designed LPs incorporating these mutations (Figure 5A). Consistent with our analysis on 25 CRC patients, the proportion of LPs derived from RNA-unique mutations with strong binding affinity was lower compared to those derived from DNA-unique or shared mutations (Figure 5B). However, in the *ex vivo* ELISpot assays, three out of nine LPs (33.3%) carrying RNA-unique variants triggered IFN-γ production in PBMCs of three out of four patients, while only two out of 13 LPs (15.3%) carrying DNA-unique variants induced IFN-γ production in a single patient (Figure 5C). In line with the ELISpot data, we detected IFN-γ activation not only in $CD8^+$ T cells but also in $CD4^+$ T cells for most of the tested long peptides. However, one LP derived from a DNA-unique mutation exclusively activated $CD8^+$ T cells (Figures 5D, E). Our selection and design of LPs was based on the rank of neopeptide candidates' HLA-I binding affinity, aiming to specifically activate $CD8^+$ T cells. However, our findings align with a previous study demonstrating that LPs covering target mutations could be intracellularly processed to peptides of differrent lengths and subsequenty presented to both $CD4^+$ and $CD8^+$ T cells (74). Our *ex vivo* validation of neoantigens' immunogenicity using patients' PBMCs provides compelling experimental evidence that relying solely on DNAseq data for tumor mutation calling would overlook valuable neoantigen candidates derived from RNA variants and that integrating variant calling by RNAseq into this process significantly enhances the likelihood of detecting immunogenic neoantigens.

This study has several limitations that should be acknowledged. Firstly, in order to develop a cost-effective workflow for neoantigen identification, the analysis was focused on SNV and indel variants within only 95 cancer-associated genes. Consequently, other types of mutations, such as gene fusions and alternative splicing, and other genes were not explored (75, 76). Secondly, while RNAseq holds the potential to identify mutations on a genome-wide scale, its sensitivity and specificity are influenced by many factors such as sequencing depth, tumor purity, and the variant calling pipeline. To mitigate the potential impact of these biases, we carefully selected the optimal mutation caller for RNAseq data, VarScan, after comparing its performance with MuTect2. However, more validation studies are necessary to

improve the variant calling tools for RNAseq data and standardize their use. Thirdly, the study was conducted with a limited sample size of 25 CRC patients, and the experimental validation of predicted neoantigens through *ex-vivo* ELISpot assays was performed on only four patients due to the availability of blood samples. As a result, the generalizability of the findings may be constrained. Finally, the assessment of the immunogenicity of candidate LPs relied exclusively on *ex-vivo* stimulation of patients' PBMCs, which may not accurately reflect the natural presentation of neoantigens by HLA-I molecules expressed in patients' tumor cells. Therefore, additional experimental validation using liquid chromatography mass spectrometry-based immunopeptidomics may be required to confirm the presentation of predicted neoantigens on HLA-I molecules in tumor cells.

Taken together, in this proof-of concept study, we provide compelling evidence for the benefits of utilizing RNAseq-guided mutations for neoantigen prediction, as it allows for the identification of a larger pool of potential and highly immunogenic neoantigens by leveraging additional information from RNAseq data beyond conventional gene expression levels.

Data availability statement

The datasets presented in this study can be found in online repositories. The names of the repository/repositories and accession number(s) can be found below: BioProject via accession ID PRJNA1005034.

Ethics statement

This study was approved by the Ethics Committee of University of Medicine and Pharmacy at Ho Chi Minh City, Vietnam. The patients/participants provided written informed consent for the collection of tumor and whole blood samples.

Author contributions

BN and TPDT conduct experiments, perform formal analysis, curate data, and develop methodologies. HTN is responsible for patient recruitment and conceptualization. TN specializes in data curation and formal analysis. TP conducts experiments and performs formal analysis. HTPN and V.N conduct experiments, perform formal analysis, and curate data. DT, TST, TP, and ML recruit patients and analyze data. MP, HG, and HNN conceptualize the study and edit writings. LT conceptualizes the study, writes the original manuscript, and edits the final document. All authors contributed to the article and approved the submitted version.

Funding

This research was funded by a NexCalibur Therapeutic grant.

Acknowledgments

The authors thank all participants who agreed to take part in this study. We thank Dr. Kien Nguyen for proofreading our manuscript.

Conflict of interest

The authors declare that the research was conducted in the absence of any commercial or financial relationships that could be construed as a potential conflict of interest.

Publisher's note

Supplementary material

The Supplementary Material for this article can be found online at: https://www.frontiersin.org/articles/10.3389/fimmu.2023.1251603/full#supplementary-material

SUPPLEMENTARY FIGURE 1
Evaluation of mutation calling tools for DNAseq and RNAseq data **(A)** Comparison of performance of three indicated mutation callers on a reference DNAseq dataset. **(B)** A Venn diagram illustrates the number of mutations identified by Dragen and two RNA mutation callers, VarScan and MuTect2. **(C)** Proportions of SNV and indel mutations called by indicated tools. **(D)** Length distribution of INDEL mutations called by indicated tools

SUPPLEMENTARY FIGURE 2
Distribution of mutation positions of DNAseq and RNAseq derived neoantigen **(A)** Correlation between the numbers of variants and neoantigens within the indicated groups. **(B)** A lollipop plot displays the percentage of neoantigens from the indicated groups that contain mutations at positions 1 to 12. The blue box represents the anchor site of the peptide and HLA-I molecule.

SUPPLEMENTARY FIGURE 3
ELISpot assays on eight long peptides which result in 2-fold change of IFN-γ spots.

SUPPLEMENTARY FIGURE 4
Gating strategy for detecting IFN-γ production from $CD4^+$ and $CD8^+$ T cells in LP-stimulated PBMCs of 4 CRC patients.

References

1. Bray F, Ferlay J, Soerjomataram I, Siegel RL, Torre LA, Jemal A. Global cancer statistics 2018: GLOBOCAN estimates of incidence and mortality worldwide for 36 cancers in 185 countries. *CA Cancer J Clin* (2018) 68:394–424. doi: 10.3322/caac.21492

2. Ferlay J, Colombet M, Soerjomataram I, Parkin DM, Piñeros M, Znaor A, et al. Cancer statistics for the year 2020: An overview. *Int J Cancer* (2021) 149:778–89. doi: 10.1002/ijc.33588

3. Biller LH, Schrag D. Diagnosis and treatment of metastatic colorectal cancer: A review. *JAMA* (2021) 325:669–85. doi: 10.1001/jama.2021.0106

4. Ciardiello D, Vitiello P P, Cardone C, Martini G, Troiani T, Martinelli E, et al. Immunotherapy of colorectal cancer: Challenges for therapeutic efficacy. *Cancer Treat Rev* (2019) 76:22–32. doi: 10.1016/j.ctrv.2019.04.003

5. Overman MJ, Ernstoff MS, Morse MA. Where we stand with immunotherapy in colorectal cancer: deficient mismatch repair, proficient mismatch repair, and toxicity management. *Am Soc Clin Oncol Educ Book* (2018) 38:239–47. doi: 10.1200/EDBK_200821

6. Dudley JC, Lin MT, Le DT, Eshleman JR. Microsatellite instability as a biomarker for PD-1 blockade. *Clin Cancer Res* (2016) 22:813–20. doi: 10.1158/1078-0432.CCR-15-1678

7. Le DT, Uram JN, Wang H, Bartlett BR, Kemberling H, Eyring AD, et al. PD-1 blockade in tumors with mismatch-repair deficiency. *N Engl J Med* (2015) 372:2509–20. doi: 10.1056/NEJMoa1500596

8. Overman MJ, McDermott R, Leach JL, Lonardi S, Lenz HJ, Morse MA, et al. Nivolumab in patients with metastatic DNA mismatch repair-deficient or microsatellite instability-high colorectal cancer (CheckMate 142): an open-label, multicentre, phase 2 study. *Lancet Oncol* (2017) 18:1182–91. doi: 10.1016/S1470-2045(17)30422-9

9. Le DT, Durham JN, Smith KN, Wang H, Bartlett BR, Aulakh LK, et al. Mismatch repair deficiency predicts response of solid tumors to PD-1 blockade. *Science* (2017) 357:409–13. doi: 10.1126/science.aan6733

10. Yu Y, Zhang J, Ni L, Zhu Y, Yu H, Teng Y, et al. Neoantigen-reactive T cells exhibit effective anti-tumor activity against colorectal cancer. *Hum Vaccin Immunother* (2022) 18:1–11. doi: 10.1080/21645515.2021.1891814

11. Kim VM, Pan X, Soares KC, Azad NS, Ahuja N, Gamper CJ, et al. Neoantigen-based EpiGVAX vaccine initiates antitumor immunity in colorectal cancer. *JCI Insight* (2020) 5(9):e136368. doi: 10.1172/jci.insight.136368

12. Yi M, Qin S, Zhao W, Yu S, Chu Q, Wu K. The role of neoantigen in immune checkpoint blockade therapy. *Exp Hematol Oncol* (2018) 7:28. doi: 10.1186/s40164-018-0120-y

13. Blass E, Ott PA. Advances in the development of personalized neoantigen-based therapeutic cancer vaccines. *Nat Rev Clin Oncol* (2021) 18:215–29. doi: 10.1038/s41571-020-00460-2

14. Miao D, Margolis CA, Gao W, Voss MH, Li W, Martini DJ, et al. Genomic correlates of response to immune checkpoint therapies in clear cell renal cell carcinoma. *Science* (2018) 359:801–6. doi: 10.1126/science.aan5951

15. Yarchoan M, Hopkins A, Jaffee EM. Tumor mutational burden and response rate to PD-1 inhibition. *N Engl J Med* (2017) 377:2500–1. doi: 10.1056/NEJMc1713444

16. Hundal J, Kiwala S, McMichael J, Miller CA, Xia H, Wollam AT, et al. pVACtools: A computational toolkit to identify and visualize cancer neoantigens. *Cancer Immunol Res* (2020) 8:409–20. doi: 10.1158/2326-6066.CIR-19-0401

17. Chheda ZS, Kohanbash G, Okada K, Jahan N, Sidney J, Pecoraro M, et al. Novel and shared neoantigen derived from histone 3 variant H3.3K27M mutation for glioma T cell therapy. *J Exp Med* (2018) 215:141–57. doi: 10.1084/jem.20171046

18. Reynisson B, Alvarez B, Paul S, Peters B, Nielsen M. NetMHCpan-4.1 and NetMHCIIpan-4.0: improved predictions of MHC antigen presentation by concurrent motif deconvolution and integration of MS MHC eluted ligand data. *Nucleic Acids Res* (2020) 48:W449–54. doi: 10.1093/nar/gkaa379

19. Schumacher TN, Schreiber RD. Neoantigens in cancer immunotherapy. *Science* (2015) 348:69–74. doi: 10.1126/science.aaa4971

20. Yadav M, Jhunjhunwala S, Phung QT, Lupardus P, Tanguay J, Bumbaca S, et al. Predicting immunogenic tumour mutations by combining mass spectrometry and exome sequencing. *Nature* (2014) 515:572–6. doi: 10.1038/nature14001

21. Tran E, Turcotte S, Gros A, Robbins PF, Lu YC, Dudley ME, et al. Cancer immunotherapy based on mutation-specific CD4+ T cells in a patient with epithelial cancer. *Science* (2014) 344:641–5. doi: 10.1126/science.1251102

22. van Rooij N, van Buuren MM, Philips D, Velds A, Toebes M, Heemskerk B, et al. Tumor exome analysis reveals neoantigen-specific T-cell reactivity in an ipilimumab-responsive melanoma. *J Clin Oncol* (2013) 31:e439–442. doi: 10.1200/JCO.2012.47.7521

23. Gerlinger M, Rowan AJ, Horswell S, Larkin J, Endesfelder D, Gronroos E, et al. Intratumor heterogeneity and branched evolution revealed by multiregion sequencing. *N Engl J Med* (2012) 366:883–92. doi: 10.1056/NEJMoa1113205

24. Yang HD, Nam SW. Pathogenic diversity of RNA variants and RNA variation-associated factors in cancer development. *Exp Mol Med* (2020) 52:582–93. doi: 10.1038/s12276-020-0429-6

25. Obeng EA, Stewart C, Abdel-Wahab O. Altered RNA processing in cancer pathogenesis and therapy. *Cancer Discovery* (2019) 9:1493–510. doi: 10.1158/2159-8290.CD-19-0399

26. Borden ES, Ghafoor S, Buetow KH, LaFleur BJ, Wilson MA, Hastings KT. NeoScore integrates characteristics of the neoantigen : MHC class I interaction and expression to accurately prioritize immunogenic neoantigens. *J Immunol* (2022) 208:1813–27. doi: 10.4049/jimmunol.2100700

27. Hashimoto S, Noguchi E, Bando H, Miyadera H, Morii W, Nakamura T, et al. Neoantigen prediction in human breast cancer using RNA sequencing data. *Cancer Sci* (2021) 112:465–75. doi: 10.1111/cas.14720

28. Koboldt DC, Zhang Q, Larson DE, Shen D, McLellan MD, Lin L, et al. VarScan 2: somatic mutation and copy number alteration discovery in cancer by exome sequencing. *Genome Res* (2012) 22:568–76. doi: 10.1101/gr.129684.111

29. Zhao S, Agafonov O, Azab A, Stokowy T, Hovig E. Accuracy and efficiency of germline variant calling pipelines for human genome data. *Sci Rep* (2020) 10:20222. doi: 10.1038/s41598-020-77218-4

30. Severine Catreux VJ, Murray L, Mehio R, Parnaby G, Roddey C, Ruehle M, et alAvailable at: https://www.illumina.com/science/genomics-research/articles/dragen-shines-again-precisionfda-truth-challenge-v2.html

31. Richards NM. Secretary upholds FDA on generics. *Pa Med* (1990) 93:28.

32. Bolger AM, Lohse M, Usadel B. Trimmomatic: a flexible trimmer for Illumina sequence data. *Bioinformatics* (2014) 30:2114–20. doi: 10.1093/bioinformatics/btu170

33. Dobin A, Davis CA, Schlesinger F, Drenkow J, Zaleski C, Jha S, et al. STAR: ultrafast universal RNA-seq aligner. *Bioinformatics* (2013) 29:15–21. doi: 10.1093/bioinformatics/bts635

34. FastQC, A. Quality control tool for high throughput sequence data. *BibSonomy* (2015). Available online: https://www. bibsonomy. org/bibtex/f230a919c34360709aa298734d63dca3. (Accessed March 17, 2022).

35. Li H, Handsaker B, Wysoker A, Fennell T, Ruan J, Homer N, et al. The sequence alignment/map format and SAMtools. *Bioinformatics* (2009) 25:2078–9. doi: 10.1093/bioinformatics/btp352

36. Available at: http://broadinstitute.github.io/picard.

37. McLaren W, Gil L, Hunt SE, Riat HS, Ritchie GR, Thormann A, et al. The ensembl variant effect predictor. *Genome Biol* (2016) 17:122. doi: 10.1186/s13059-016-0974-4

38. Trapnell C, Williams BA, Pertea G, Mortazavi A, Kwan G, van Baren MJ, et al. Transcript assembly and quantification by RNA-Seq reveals unannotated transcripts and isoform switching during cell differentiation. *Nat Biotechnol* (2010) 28:511–5. doi: 10.1038/nbt.1621

39. Available at: https://www.R-project.org/.

40. Szolek A, Schubert B, Mohr C, Sturm M, Feldhahn M, Kohlbacher O. OptiType: precision HLA typing from next-generation sequencing data. *Bioinformatics* (2014) 30:3310–6. doi: 10.1093/bioinformatics/btu548

41. Hundal J, Kiwala S, Feng YY, Liu CJ, Govindan R, Chapman WC, et al. Accounting for proximal variants improves neoantigen prediction. *Nat Genet* (2019) 51:175–9. doi: 10.1038/s41588-018-0283-9

42. Hundal J, Carreno BM, Petti AA, Linette GP, Griffith OL, Mardis ER, et al. pVAC-Seq: A genome-guided in silico approach to identifying tumor neoantigens. *Genome Med* (2016) 8:11. doi: 10.1186/s13073-016-0264-5

43. Schmidt J, Smith AR, Magnin M, Racle J, Devlin JR, Bobisse S, et al. Prediction of neo-epitope immunogenicity reveals TCR recognition determinants and provides insight into immunoediting. *Cell Rep Med* (2021) 2:100194. doi: 10.1016/j.xcrm.2021.100194

44. Wu J, Zhao W, Zhou B, Su Z, Gu X, Zhou Z, et al. TSNAdb: A database for tumor-specific neoantigens from immunogenomics data analysis. *Genomics Proteomics Bioinf* (2018) 16:276–82. doi: 10.1016/j.gpb.2018.06.003

45. Wu J, Chen W, Zhou Y, Chi Y, Hua X, Wu J, et al. TSNAdb v2.0: the updated version of tumor-specific neoantigen database. *Genomics Proteomics Bioinf* (2022) S1672-0229(22)00128-0. doi: 10.1016/j.gpb.2022.09.012

46. Zhou WJ, Qu Z, Song CY, Sun Y, Lai AL, Luo MY, et al. NeoPeptide: an immunoinformatic database of T-cell-defined neoantigens. *Database* (2019) 2019: baz128. doi: 10.1093/database/baz128

47. Lu M, Xu L, Jian X, Tan X, Zhao J, Liu Z, et al. dbPepNeo2.0: A database for human tumor neoantigen peptides from mass spectrometry and TCR recognition. *Front Immunol* (2022) 13:855976. doi: 10.3389/fimmu.2022.855976

48. Tan X, Li D, Huang P, Jian X, Wan H, Wang G, et al. dbPepNeo: a manually curated database for human tumor neoantigen peptides. *Database* (2020) 2020: baaa004. doi: 10.1093/database/baaa004

49. Xia J, Bai P, Fan W, Li Q, Li Y, Wang D, et al. NEPdb: A database of T-cell experimentally-validated neoantigens and pan-cancer predicted neoepitopes for cancer immunotherapy. *Front Immunol* (2021) 12:644637. doi: 10.3389/fimmu.2021.644637

50. Zhang G, Chitkushev L, Olsen LR, Keskin DB, Brusic V. TANTIGEN 2.0: a knowledge base of tumor T cell antigens and epitopes. *BMC Bioinf* (2021) 22:40. doi: 10.1186/s12859-021-03962-7

51. Olsen LR, Tongchusak S, Lin H, Reinherz EL, Brusic V, Zhang GL. TANTIGEN: a comprehensive database of tumor T cell antigens. *Cancer Immunol Immunother* (2017) 66:731–5. doi: 10.1007/s00262-017-1978-y

52. Vita R, Mahajan S, Overton JA, Dhanda SK, Martini S, Cantrell JR, et al. The immune epitope database (IEDB): 2018 update. *Nucleic Acids Res* (2019) 47:D339–43. doi: 10.1093/nar/gky1006

53. Moodie Z, Price L, Gouttefangeas C, Mander A, Janetzki S, Löwer M, et al. Response definition criteria for ELISPOT assays revisited. *Cancer Immunol Immunother* (2010) 59:1489–501. doi: 10.1007/s00262-010-0875-4

54. Chepelev I, Wei G, Tang Q, Zhao K. Detection of single nucleotide variations in expressed exons of the human genome using RNA-Seq. *Nucleic Acids Res* (2009) 37: e106. doi: 10.1093/nar/gkp507

55. Katzir R, Rudberg N, Yizhak K. Estimating tumor mutational burden from RNA-sequencing without a matched-normal sample. *Nat Commun* (2022) 13:3092. doi: 10.1038/s41467-022-30753-2

56. Fang LT, Zhu B, Zhao Y, Chen W, Yang Z, Kerrigan L, et al. Establishing community reference samples, data and call sets for benchmarking cancer mutation detection using whole-genome sequencing. *Nat Biotechnol* (2021) 39:1151–60. doi: 10.1038/s41587-021-00993-6

57. Xie N, Shen G, Gao W, Huang Z, Huang C, Fu L. Neoantigens: promising targets for cancer therapy. *Signal Transduct Target Ther* (2023) 8:9. doi: 10.1038/s41392-022-01270-x

58. Nguyen AT, Szeto C, Gras S. The pockets guide to HLA class I molecules. *Biochem Soc Trans* (2021) 49:2319–31. doi: 10.1042/BST20210410

59. Tretter C, de Andrade Kraetzig N, Pecoraro M, Lange S, Seifert P, von Frankenberg C, et al. Proteogenomic analysis reveals RNA as an important source for tumor-agnostic neoantigen identification correlating with T-cell infiltration. *bioRxiv* (2022) 14(1):4632. doi: 10.1101/2022.09.17.508207

60. Koboldt DC. Best practices for variant calling in clinical sequencing. *Genome Med* (2020) 12:91. doi: 10.1186/s13073-020-00791-w

61. Guo Y, Yu H, Samuels DC, Yue W, Ness S, Zhao YY. Single-nucleotide variants in human RNA: RNA editing and beyond. *Brief Funct Genomics* (2019) 18:30–9. doi: 10.1093/bfgp/ely032

62. O'Brien TD, Jia P, Xia J, Saxena U, Jin H, Vuong H, et al. Inconsistency and features of single nucleotide variants detected in whole exome sequencing versus transcriptome sequencing: A case study in lung cancer. *Methods* (2015) 83:118–27. doi: 10.1016/j.ymeth.2015.04.016

63. Komatsu Y, Shigeyasu K, Yano S, Takeda S, Takahashi K, Hata N, et al. RNA editing facilitates the enhanced production of neoantigens during the simultaneous administration of oxaliplatin and radiotherapy in colorectal cancer. *Sci Rep* (2022) 12:13540. doi: 10.1038/s41598-022-17773-0

64. Wang W, Zhou W, Lu Q, Ding T, Fan L. Investigating the clinical relevance of RNA editing events and their derived neoantigens in patients with melanoma treated with immunotherapy. *J Clin Oncol* (2023) 41:e21580–0.

65. Mattos-Arruda L, Vazquez M, Finotello F, Lepore R, Porta E, Hundal J, et al. Neoantigen prediction and computational perspectives towards clinical benefit: recommendations from the ESMO Precision Medicine Working Group. *Ann Oncol* (2020) 31:978–90. doi: 10.1016/j.annonc.2020.05.008

66. Turajlic S, Litchfield K, Xu H, Rosenthal R, McGranahan N, Reading JL, et al. Insertion-and-deletion-derived tumour-specific neoantigens and the immunogenic phenotype: a pan-cancer analysis. *Lancet Oncol* (2017) 18:1009–21. doi: 10.1016/S1470-2045(17)30516-8

67. Lo AA, Wallace A, Oreper D, Lounsbury N, Havnar C, Pechuan-Jorge X, et al. Indication-specific tumor evolution and its impact on neoantigen targeting and biomarkers for individualized cancer immunotherapies. *J Immunother Cancer* (2021) 9(10):e003001. doi: 10.1101/2021.03.15.434617

68. Yi M, Dong B, Chu Q, Wu K. Immune pressures drive the promoter hypermethylation of neoantigen genes. *Exp Hematol Oncol* (2019) 8:32. doi: 10.1186/s40164-019-0156-7

69. Capietto AH, Jhunjhunwala S, Pollock SB, Lupardus P, Wong J, Hänsch L, et al. Mutation position is an important determinant for predicting cancer neoantigens. *J Exp Med* (2020) 217(4):e20190179. doi: 10.1084/jem.20190179

70. Sidney J, Assarsson E, Moore C, Ngo S, Pinilla C, Sette A, et al. Quantitative peptide binding motifs for 19 human and mouse MHC class I molecules derived using positional scanning combinatorial peptide libraries. *Immunome Res* (2008) 4:2. doi: 10.1186/1745-7580-4-2

71. Richters MM, Xia H, Campbell KM, Gillanders WE, Griffith OL, Griffith M. Best practices for bioinformatic characterization of neoantigens for clinical utility. *Genome Med* (2019) 11:56. doi: 10.1186/s13073-019-0666-2

72. Montemurro A, Schuster V, Povlsen HR, Bentzen AK, Jurtz V, Chronister WD, et al. NetTCR-2.0 enables accurate prediction of TCR-peptide binding by using paired TCRalpha and beta sequence data. *Commun Biol* (2021) 4:1060. doi: 10.1038/s42003-021-02610-3

73. Pham MN, Nguyen TN, Tran LS, Nguyen QTB, Nguyen TPH, Pham TMQ, et al. epiTCR: a highly sensitive predictor for TCR-peptide binding. *Bioinformatics* (2023) 39 (5):btad284. doi: 10.1093/bioinformatics/btad284

74. Chen X, Yang J, Wang L, Liu B. Personalized neoantigen vaccination with synthetic long peptides: recent advances and future perspectives. *Theranostics* (2020) 10:6011–23. doi: 10.7150/thno.38742

75. Yang W, Lee KW, Srivastava RM, Kuo F, Krishna C, Chowell D, et al. Immunogenic neoantigens derived from gene fusions stimulate T cell responses. *Nat Med* (2019) 25:767–75. doi: 10.1038/s41591-019-0434-2

76. Slansky JE, Spellman PT. Alternative splicing in tumors - A path to immunogenicity? *N Engl J Med* (2019) 380:877–80. doi: 10.1056/NEJMcibr1814237

frontiers | Frontiers in Immunology

TYPE Review
PUBLISHED 06 September 2023
DOI 10.3389/fimmu.2023.1248867

OPEN ACCESS

EDITED BY
Patrick Schmidt,
National Center for Tumor Diseases (NCT), Germany

REVIEWED BY
Dipendra Khadka,
Wonkwang University School of Medicine, Republic of Korea
Yan-Ruide Li,
University of California, Los Angeles, United States

*CORRESPONDENCE
Niels Schaft
niels.schaft@uk-erlangen.de

†These authors share first authorship

‡These authors share senior authorship

RECEIVED 27 June 2023
ACCEPTED 11 August 2023
PUBLISHED 06 September 2023

CITATION
Schaft N, Dörrie J, Schuler G, Schuler-Thurner B, Sallam H, Klein S, Eisenberg G, Frankenburg S, Lotem M and Khatib A (2023) The future of affordable cancer immunotherapy. *Front. Immunol.* 14:1248867. doi: 10.3389/fimmu.2023.1248867

The future of affordable cancer immunotherapy

Niels Schaft[1,2,3,4*†], Jan Dörrie[1,2,3,4†], Gerold Schuler[1,2,3], Beatrice Schuler-Thurner[1,2,3], Husam Sallam[5], Shiri Klein[6], Galit Eisenberg[6], Shoshana Frankenburg[6], Michal Lotem[6,7‡] and Areej Khatib[8‡]

[1]Department of Dermatology, Friedrich-Alexander-Universität Erlangen-Nürnberg, Universitätsklinikum Erlangen, Erlangen, Germany, [2]Comprehensive Cancer Center Erlangen European Metropolitan Area of Nuremberg (CCC ER-EMN), Erlangen, Germany, [3]Deutsches Zentrum Immuntherapie (DZI), Erlangen, Germany, [4]Bavarian Cancer Research Center (BZKF), Erlangen, Germany, [5]Molecular Genetics and Genetic Toxicology, Health Science Department, American Arab University, Ramallah, Palestine, [6]Sharett Institute of Oncology, Hadassah Hebrew University Hospital, Jerusalem, Israel, [7]Hadassah Cancer Research Institute, Hadassah Hebrew University Hospital, Jerusalem, Israel, [8]Women's Health Research Unit, The Research Institute of the McGill University Health Centre, Montreal, QC, Canada

The treatment of cancer was revolutionized within the last two decades by utilizing the mechanism of the immune system against malignant tissue in so-called cancer immunotherapy. Two main developments boosted cancer immunotherapy: 1) the use of checkpoint inhibitors, which are characterized by a relatively high response rate mainly in solid tumors; however, at the cost of serious side effects, and 2) the use of chimeric antigen receptor (CAR)-T cells, which were shown to be very efficient in the treatment of hematologic malignancies, but failed to show high clinical effectiveness in solid tumors until now. In addition, active immunization against individual tumors is emerging, and the first products have reached clinical approval. These new treatment options are very cost-intensive and are not financially compensated by health insurance in many countries. Hence, strategies must be developed to make cancer immunotherapy affordable and to improve the cost-benefit ratio. In this review, we discuss the following strategies: 1) to leverage the antigenicity of "cold tumors" with affordable reagents, 2) to use microbiome-based products as markers or therapeutics, 3) to apply measures that make adoptive cell therapy (ACT) cheaper, e.g., the use of off-the-shelf products, 4) to use immunotherapies that offer cheaper platforms, such as RNA- or peptide-based vaccines and vaccines that use shared or common antigens instead of highly personal antigens, 5) to use a small set of predictive biomarkers instead of the "sequence everything" approach, and 6) to explore affordable immunohistochemistry markers that may direct individual therapies.

KEYWORDS

immunotherapy, affordable, adoptive cell therapy, microbiome, RNA-based vaccines, biomarkers, immunohistochemistry

1 Introduction

Immunotherapy has changed the cancer treatment scenario and revolutionized tumor immunology. Immunotherapy treatments, such as adoptive T-cell therapy (ACT) or the use of immune checkpoint inhibitors (ICIs), are now well-established components of the toolbox of cancer treatments, significantly improving longevity in a substantial proportion of patients (1–3). The vast amount of ongoing research in the field is expected to enhance the essential role of immunotherapy in cancer treatment.

However, with the advancing success of cancer immunotherapy, it is becoming clear that a significant drawback of current immunotherapies is their high expense. To enable the wide usage of immunotherapy, efforts will eventually have to be centered on developing immunotherapy treatments that are significantly cheaper and affordable to larger populations worldwide.

Getting a cancer immunotherapy treatment costs more than a house in many cities in the US and is more expensive than putting a few children through private college. The average cost of cancer drugs increased from $50,000 per patient in the mid-1990s to $250,000. That is four times the median US household annual income. Immunotherapies often cost more than $100,000 per patient. For some of the newest immunotherapies, the price tag is even steeper: When including the value of the medical support necessary to deliver these treatments, a price tag of $850,000 per patient is not unheard of (4). For example, although the wholesale acquisition cost of CAR-T-cell therapies to treat B-cell lymphoma is $373,000, a new study by Prime Therapeutics of real-world data found that the total cost averages more than $700,000 and can exceed $1 million in some cases (5).

Increasingly, approaches to treat solid tumors and hematological malignancies involve the concurrent administration of several products with distinct but complementary mechanisms of action in combination or close sequence as part of a regimen that also seeks to minimize the development of drug resistance (6–8). The use of combined immunotherapies means that costs can quickly double or triple. Some recent examples include the addition of pertuzumab to trastuzumab for the treatment of human epidermal growth factor receptor-2 (HER-2)-positive breast cancer and the use of programmed cell death protein (PD-1) and programmed cell death ligand (PD-L1) inhibitors in combination with anti-cytotoxic T-lymphocyte-associated protein 4 (CTLA-4) therapies in metastatic melanoma. This trend presents serious challenges for Health Technology Assessment (HTA) bodies and payers. Combination regimens are expected to increase over the next few years (7, 9). Almost all information regarding the costs of immunotherapy is based on data from OECD countries; however, access to oncology medicines remains unequal across OECD/EU countries. The charges in non-OECD countries will probably be higher and may enjoy less support from health or insurance institutions or drug companies. Additionally, there is little doubt that the population of third-world countries will mostly be unable to cope with such expenses.

The future of cancer immunotherapy will largely depend on the ability of researchers to make it affordable to larger populations. This review summarizes some scientific suggestions for making this happen (Figure 1).

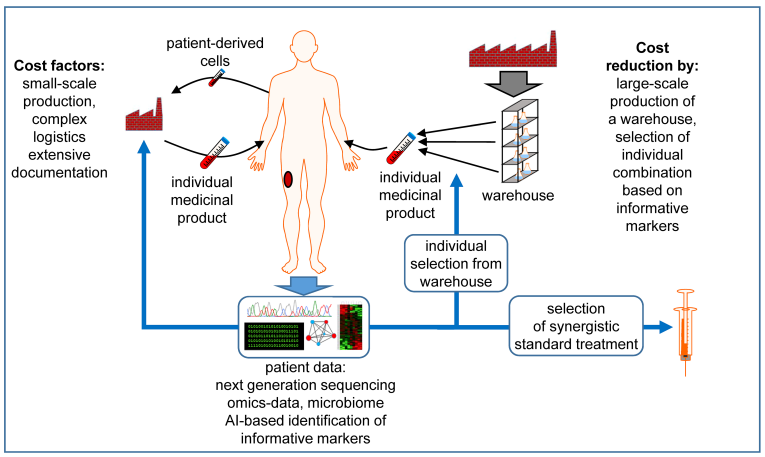

FIGURE 1
Factors that contribute to the high costs of individualized medicinal products and possibilities for cost reduction. The production of cellular therapeutics usually takes place on a per-patient basis, i.e. each patient requires a personal small-scale production of the individualized medicinal product in a specialized facility under labor-intensive documentation. Source materials are usually patient-derived living cells, which increases the logistic effort. Next generation sequencing and other omics data are exploited to define individual antigens, which are synthesized in a personalized manner. Alternatively, therapeutic components could be produced at larger scale, increasing the economic efficiency, creating a warehouse of constituents. Using individual patient data, possibly exploited with the help of Artificial Intelligence (AI) to identify a manageable set of informative markers, an individual combination of these elements is selected to generate the individualized product. When possible, truly individual components are avoided or reduced to a minimum, including patient-derived cells. To improve the efficiency of the treatment further, the in depth data analysis can propose the use of established thus cheaper drugs in combination with the advanced individualized medicinal products. See the main text for further details. The Motifolio Scientific Illustration Toolkit was used for the generation of this figure.

2 Leverage the antigenicity of "cold tumors" with affordable reagents

One of the most consistent predictors for the success of immune checkpoint inhibitors (ICI) in metastatic patients is the general load of missense mutations and the density of lymphocytic infiltrate in the tumors (10–12). The accepted paradigm for the contribution of non-synonymous mutations or frameshifts is that they generate altered peptide epitopes that work as neo-antigens (13–15). Unlike wild-type sequences, these neo-antigens have not induced a tolerizing mechanism. Consequently, T-cell clones can emerge, which recognize these neo-epitopes with high affinity and effectively destroy cancer cells (16, 17). The power of neo-antigen-cognate T cells in the clinic was shown in several pioneering works by Rosenberg et al., targeting four mutant proteins in a patient with breast cancer (NCT01174121), and by Tran et al., targeting mutant KRAS G12 (18–20).

The situation is very different in cancers referred to as "cold tumors" or "immune deserts," two descriptions relating to the scarcity of immune targets and effector T cells. Among these are uveal melanoma, pancreatic cancer, ovarian and breast cancers, and any cancer with loss of HLA class I, mutations in β2 microglobulin, and defects in antigen presentation (21–24).

Neo-epitopes are not solely generated by mutations. In the absence of genomic-encoded antigens, the mRNA transcript, or the actual protein product itself, is sought as a source for immunogenic neo-epitopes. The concept that defects in any of the ribosomal proteins (DRiPs) will yield impaired peptides and enrich the immune-peptidome to be detected by the immune system was described by Yewdell et al. but was not leveraged towards a therapy (25). Admon et al. described that, following viral infection, large numbers of HLA class I peptides derive from DRiPs (26). Thus, it was proposed that damaging ribosomal proteins will enhance the anti-viral immune response; this may also apply to cancers (27).

A renewed interest in this approach was evoked by Abdel-Wahab and colleagues, showing that in blood malignancies with mutant splicing factors, novel splicing-derived proteins may appear (28). Similarly, Oka et al. show in lung cancer cell lines that ablations of the nonsense-mediated mRNA decay (NMD) factor UPF1, and a splicing factor, SF3B1, are found to increase the proportion of aberrant transcripts (29). Taking one further step forwards, Lu et al. used a pharmacological compound, indisulam, which enhances the degradation of the RNA-binding motif protein 39 (RBM39), which often is upregulated in cancers (30). Indisulam and other sulfonamides can affect splicing in tumor cells at a concentration that may be safe to use in the clinic. Most intriguingly is the demonstration that true neo-epitopes emerged by clinical-grade pharmaceutics, primarily due to intron retention.

In summary, DriPs and peptide products of splice-disrupted mRNA can be induced in cancer cells. This especially applies to cancers harboring oncogenic splicing factor mutations, which have limited benefit from ICI: acute myeloid leukemias, uveal melanoma, myelodysplastic syndrome, and non-small-cell lung cancer. Rapid screens of small molecule libraries and antitumor antibiotics are highly encouraged. If issues of patenting and IP are put aside, these compounds may be cheap to produce and replace the expensive cell therapies that are among the few options for these "cold" tumors.

3 Microbiome-based products

There is growing evidence that gut microbiota is related to immunotherapy outcomes. For example, it has been shown that transcriptionally expressed metagenomic pathways in the gut microbiome are related to progression-free survival in melanoma (31). Results from a study by Nomura et al. suggest that fecal short-chain fatty acid (SCFA) concentrations may be associated with PD-1 inhibitor efficacy; thus, SCFAs may be the link between the gut microbiota and PD-1 inhibitor treatment outcome. Because fecal examinations are entirely non-invasive, they may be applicable for routine monitoring of patients (32). Recently, a correlation between gut bacterial composition and prognosis in hepatocellular carcinoma patients suggested a potential role for the gut microbiome as a prognostic marker for the response to nivolumab (33) and the response to anti-CD19 CAR-T-cell therapy in patients with B-cell malignancies (34). Another study demonstrated that secondary resistance and immune-related adverse events are related to longitudinal dynamics of the intestinal microbiota in patients with advanced malignancies (35).

That the gut microbiome can affect the immune response was already shown by Gur et al. in 2015. They found that a bacterium from the oral cavity directly interacted with TIGIT to diminish NK- and T-cell functionality (36). Since then, an emerging body of evidence has implicated host-intrinsic microorganisms in influencing the response to cancer immunotherapy (37). Attempts to translate microbiome-based therapies, e.g., in melanoma patients, have mild success (NCT03353402) (38, 39). Still, the gut microbiota diversity in individuals of different ethnicities and geographic areas makes it difficult to standardize therapeutic formulations. Despite these problems, techniques of fecal transplantation will remain cheap and accessible and are currently being tested in several clinical trials (NCT05502913 (40), NCT05286294, NCT04975217). The potential synergy between gut bacteria and ICI will not only increase the response rate but may shorten the time to achieve these benefits, which is also tested in many clinical trials, e.g., in liver cancer (NCT05750030, NCT05690048) (41), lung cancer (NCT05669846, NCT04924374), colorectal cancer (NCT05279677, NCT04729322) (42), melanoma (NCT05251389 (43), NCT04988841, NCT04577729, NCT03341143) (44), kidney cancer (NCT04758507) (45), gastrointestinal cancer (NCT04130763) (46), prostate cancer (NCT04116775), and mesothelioma (NCT04056026) (47).

4 Can adoptive cell therapy be made affordable?

Cell therapy consists of cellular "drugs" prepared mostly in local production facilities. The long manufacturing time, complex delivery systems, and discrete and per-patient production are only

some of the hurdles affecting the time-to-market and manufacturing costs of cell-based therapeutics.

Most cell therapies developed in recent years, approved and in clinical pipelines, use autologous cell products. The personalized generation of cellular products tailored to fit a specific antigen or disease condition has advanced immensely, with feasible applications. Although autologous cells benefit from the advantage of avoiding rejection, using allogeneic cells offers scalable production from abundant cell sources. Therefore, significantly simplifying and expediting manufacturing turns the product more affordable and thus allows many more patients to be treated. Albeit these advantages, allogeneic cells trigger graft versus host disease (GvHD) or vice versa- host versus grafted lymphocytes, due to HLA mismatched α/β T cells.

Using allogeneic cell sources that elicit minimal immunogenic reactions is one approach for reducing GvHD. NK cells are one of the options for this type of cell source. Pioneering work from the Ruggeri group shows that KIR-mismatched alloreactive donor NK cells protected patients from AML relapse with no GvHD (48). NK cells also do not produce IL-1 and IL-6, the main cytokines involved in cytokine release syndrome (CRS), minimizing one of the main adverse events of current cell therapy (49). Allogeneic NK CD19 chimeric antigen receptor (CAR) cells derived from cord blood have a 73% response rate without significant toxic effects in lymphoma and chronic lymphatic leukemia (CLL) patients (50). Many ongoing clinical trials use CAR-NK targeting various antigens, including CD19 (e.g., NCT05487651, NCT05410041), EGFR, EpCAM, GD2, mesothelin (NCT03692637), and HSP70 (51).

The ability of iNKT cells to rapidly respond to lipid antigens and secrete a wide variety of cytokines has placed these cells at the frontlines of many types of immune responses (52), including cytotoxic responses, which can lead to tumor lysis, recruitment of other innate- and adaptive-related immune cells, and regulation of immunosuppression (53). These responses, robust in mouse models and humans, are problematic in cancer patients since their number in the peripheral blood of these patients is significantly decreased (54–56). In addition, their functionality is hampered in these patients, as shown by their lower secretion of IFNγ and a tendency to a Th2 phenotype. These facts make their potential application for human immunotherapy problematic (52, 54).

Alternatively, γδ T cells can be used as an allogenic source since they do not recognize MHC molecules and are hence not alloreactive (57–59). It was shown that γδ T cells – retrovirally transduced or RNA-transfected with an αβ TCR against, e.g., cytomegalovirus (CMV) or a tumor antigen – were highly functional *in vitro* (60, 61) and in mice (62, 63). Also, CARs were functionally introduced into γδ T cells (61) and are even tested in clinical trials (NCT04107142, NCT04735471 (64), NCT05302037). An additional advantage of CAR-transfected γδ T cells is that they produce lower quantities of cytokines compared to CAR-transfected αβ T cells, reducing the risks of CRS (61).

Recently, a population of unconventional innate-like T cells, mucosal-associated invariant (MAIT) cells, has elicited hopes for efficient off-the-shelf, allogeneic immunotherapy for two main reasons. First, their semi-invariant αβ T-cell receptor recognizes small-molecule biosynthetic derivatives of riboflavin synthesis presented on the restriction molecule major histocompatibility complex (MHC)-related protein-1 (MR1). As a result, MAIT cells do not recognize autoantigens or induce graft-versus-host disease (GvHD). Second, MAIT cells are strong cytotoxic cells that secrete pro-inflammatory cytokines and lyse infected cells using granzyme B and perforin. Taken together, these characteristics justify the efforts and enthusiasm that are being invested in this population to achieve a new approach to immunotherapy (65).

Mesenchymal stem cells (MSCs) are also considered a source of evasive immune cells. They are highly immunosuppressive, diminishing T-cell activation and antigen-presenting cell maturation and, in this way, they delay allo-rejection (66). However, since MSCs have been used to deliver cytotoxic reagents into tumors with limited efficacy (67), further studies are needed to exploit their therapeutic potential.

A different approach for generating universal cell sources exploits the vast advances in cell engineering, turning allogeneic cellular products into less immunogenic ones. Genome editing using CRISPR-Cas9 or similar editing systems targeting the β2-microglobulin HLA class I molecule and the T-cell receptor (TCR) in combination with CAR expression has been used to create universal CAR-T cells that are less prone to attack autologous T cells (68). These combined efforts reduce GvHD but also host versus graft (HvG), allowing for a broader therapeutic window for CAR-T cells. The CAR construct is often introduced into the TRAC, TRBC1, or TRBC2 locus to create TCR knockout cells and regulate the CAR expression through the TCR promoter (69). A retrospective comparison between auto-CD19 CARs and allo-CD19 CARs showed only minor GvHD in allo-CARs. Nonetheless, the response rate was favorable toward the allo-CAR with 100% at nine months follow-up compared to 88% in the auto-CAR. This advantage was attributed to the combined signals in allo-CAR of TCR and CAR (70). Clinical testing of allogeneic CAR-T trials directed at hematological and solid tumors is ongoing in many centers. Targets for these CAR-T trials include CD19, BCMA (71), and CD20 in hematological tumors, and GD2, mesothelin (NCT03545815), CD70 (NCT05795595, NCT04438083, NCT04696731), MUC1-C [NCT05239143 (72)], and NKG2DL in solid tumors.

Another option for producing off-the-shelf cell products is performing genetic editing on induced pluripotent stem cells (iPSCs) before cellular differentiation. Following manipulation, these cells can be differentiated into many types, including T cells, NK cells, and dendritic cells. Allo-iPSCs can be used from either a matched homogenous genetic background individual or following allele-specific editing. These cells can be manipulated to avoid GvHD and HvG by HLA pseudo-homozygosity, escaping recognition by both T and NK cells (73). Further manipulations, such as the expression of CD47 and HLA-G, can mediate escape from NK and macrophages, creating 'universal' iPSCs (74). Clinical trials using NK derived from iPSCs were completed or are ongoing in solid tumors and hematological malignancies (NCT03841110, NCT04630769, NCT05182073).

Hematopoietic stem cells (HSCs) possess unlimited expansion capacity and can differentiate into multiple cell types. Conventional sources of HSCs include adult bone marrow and the umbilical cord of

newborns. An additional method to achieve a high number of HSCs uses iPS cells, which have high scalability due to the robustness of their cell culture conditions. HSCs derived from cord blood or bone marrow are currently being evaluated to manufacture CAR-HSCs, which can differentiate into effector cells, including CAR-T and CAR-NK cells. Interestingly, stem cell-derived T cells have a unique cytokine profile with fewer safety risks (75, 76).

The production costs of TCR-T or CAR-T cells can be reduced by transfection of mRNA encoding the receptors into T cells instead of using viral transduction for receptor transfer. In addition to being an easier process than viral transduction, receptor-RNA transfection of T cells (or any other cells) can even be performed decentralized with, e.g., closed electroporation systems, making local and cheaper production possible (77). Another advantage is that CAR-RNA transfection has a favorable toxicity profile considering possible on-target/off-tumor reactions due to its transient effects. Two clinical studies showed that on-target/off-tumor toxicity could cause severe problems and even death if the receptor is introduced by stable viral transduction (78, 79). By transient transfection of T cells, the receptor expression is temporarily restricted, rendering potential off-target and on-target/off-tumor toxicity also transient. The CAR-RNA transfer strategy is especially attractive in preclinical and phase I clinical trials exploring new tumor antigens for CAR-T-cell therapy with an unknown clinical safety profile. The mRNA transfection strategy for CARs was proposed by us some time ago (80) and has, in the meantime, been applied in several clinical trials in patients with breast cancer and melanoma (NCT01837602 NCT03060356; targeting c-MET) (81) and mesothelioma, pancreatic cancer, and ovarian cancer (NCT03608618, NCT01897415, NCT01355965 targeting mesothelin) (82–84). RNA transfection was even explored with non-solid tumors using CD19 and CD123 as target antigens (NCT02277522, NCT02624258, NCT02623582) (85). The mRNA-CAR-T cells in these studies were well tolerated, migrated to primary and metastatic tumor sites, showed clinical antitumor activity, and showed no evidence of on-target/off-tumor toxicity against normal tissues (81, 82). However, the transient receptor expression *per se* necessitates repetitive injections. Unlike virally transduced cells, which have to be given only once and proliferate in the patient's body, RNA-transfected cells will lose CAR expression and must be replenished to maintain cytolytic pressure on the tumor. This might, in turn, increase the treatment costs if many more cells need to be produced.

The significant number of approaches being actively evaluated to make adoptive cell therapy affordable, only some of which are described here, point toward the high expectations of the scientific community and overall raise hopes for widespread immunotherapy, which may be shortly more than a wishful dream.

5 RNA-based therapeutic cancer vaccines

In the past decade, RNA therapeutics have witnessed a true revolution. Several RNA-based therapies have been approved by the FDA for treating genetic diseases, with unprecedented success, as in spinal muscular atrophy (86–88). Moreover, recent years showed the world that RNA-based therapies, specifically mRNA vaccines, can be the answer to a pandemic and save the lives of millions.

However, in the field of cancer treatments, RNA therapies are lagging. The rapidly adaptable mRNA vaccines against Covid-19 ended years of concerns regarding the large-scale feasibility of RNA-based therapeutics. In addition to a vast amount of clinical data on safety and efficacy, pharmaceutical companies augmented their production capabilities, and new solutions to incurable diseases, mainly cancer, can now be sought.

However, due to its high antigen heterogeneity, cancer represents a significant challenge in the design of therapeutic cancer vaccines. RNA-based cancer vaccines can encode individually mutated neo-antigens, resulting in their presentation, which is a very personalized medicinal product, and, therefore, very cost intensive. Finding these mutations involves high costs for the sequencing of the tumor, usually also involving challenging logistics and centralized sequencing facilities. A possibility to reduce this expense may be the use of new decentralized 3rd-generation sequencing technologies which offer much better cost efficiency. Very recently, Moderna and Merck announced that mRNA-4157/V940, an investigational personalized mRNA cancer vaccine, in combination with Keytruda® (Pembrolizumab), was approved as a breakthrough therapy by the FDA for adjuvant treatment of patients with high-risk melanoma following complete resection (NCT03897881) (89, 90). Several other clinical trials, both in the adjuvant and metastatic setting, are running (e.g., NCT04161755 in pancreatic cancer (91), NCT02316457 in triple-negative breast cancer, NCT03815058 in melanoma, NCT04486378 in colorectal cancer, NCT03480152 in gastrointestinal cancer (92), NCT05761717 in hepatocellular carcinoma, and NCT03289962 in several solid tumors).

Alternatively, an off-the-shelf approach can also be chosen if the vaccines are based on prepared mRNAs encoding non-mutated antigens often expressed in the tumor, reducing costs. Examples of this exist for ovarian carcinoma treated with a liposome-formulated mRNA vaccine encoding three ovarian carcinoma tumor-associated antigens (TAA) (NCT04163094), melanoma treated with a liposome-formulated mRNA vaccine encoding four selected malignant melanoma-associated antigens: New York-ESO 1 (NY-ESO-1), tyrosinase, melanoma-associated antigen A3 (MAGE-A3), and trans-membrane phosphatase with tensin homology (TPTE) (NCT02410733) (93), prostate cancer (NCT04382898 (targeting five different antigens), NCT00831467), and non-small cell lung cancer (NCT05142189, NCT03164772 (with six target antigens), NCT00923312 (with five target antigens). However, a "one size fits all"-tumor vaccine formulation does not exist. Since individual tumors from even a narrowly defined cancer type still vary substantially in their antigen expression even at different sites, any pre-selection of defined antigens will always be a compromise between comprehensiveness and cost efficiency. Here, an individually defined cocktail prepared from an off-the-shelf tumor antigen warehouse could be a more cost-efficient solution (94). Although this requires determining the individual tumor's antigen expression again, decentral field sequencing technologies like the Oxford Nanopore™ platform could offer a cheaper option.

Adding an adjuvant is beneficial to achieve an effective immune response against a cancer vaccine antigen. Several approaches are followed to reduce costs for such adjuvants. For example, one can re-purpose effective immune adjuvants with no intellectual property (e.g., Freund's, BCG, Alum). Moreover, one can also combine the RNA-based vaccines described above with a fraction of double-stranded (ds)RNA resulting in an adjuvant-like stimulus through NFκB activation by Toll-like receptor 3 (TLR3), which binds to the dsRNA (95), or by complexing a fraction of the mRNA with protamine, which then acts as an adjuvant that induces an effective immune response through TLR7-mediated signaling (96, 97).

Over the last 20 years, a well-established approach was to transfect dendritic cells (DCs) with mRNA *ex-vivo* and inject those cells to induce antitumor immune responses. Although a slow but constant improvement concerning immunologic activity was achieved during this period, this technology never made it to a broader clinical application. The *ex-vivo* production of such an individualized cellular product never met a sufficient cost-effectivity ratio to be commercially attractive. The only DC-based cancer vaccine that received clinical approval was sipuleucel-T (Provenge™) produced by Dendreon Corporation, which consisted of a DC-enriched PBMC fraction pulsed with a GM-CSF/PAP fusion molecule and was discontinued for commercial reasons (98, 99). Performed under the required high standards of good manufacturing practice (GMP), the production costs to treat one patient are within the range of ten thousands of dollars without any revenues. Retail prices would be significantly higher if a customary profit margin was intended. Nevertheless, the highly controlled surrounding of the large number of trials provided a cornucopia of valuable information and insights translated into vaccination approaches (100, 101), in which the antigen was given to target APCs *in vivo* for expression of the antigen (102). The rapid implementation of mRNA-based vaccines against Covid-19 would not have been possible without all the existing data generated in the field of mRNA-based tumor vaccination both with *ex-vivo* transfected DCs and via the application of mRNA-based formulations *in vivo*.

The following hurdles must be tackled to facilitate affordable mRNA-based cancer vaccines: 1) Tumor sequencing must be fast and cheap to allow a tailored individual selection of antigens from a pre-produced warehouse of mRNAs, possibly via panel sequencing on decentralized field sequencing devices. 2) RNA production must be economical. The production of large batches of mRNA can achieve this. However, producing individual mRNAs for only one patient will not be feasible. 3) RNA must be formulated to be stable at -20°C to circumvent excessively complex transport and storage logistics. 4) The other components of the vaccine formulation must be affordable. 5) The additional expenses for GMP compliance must be limited. While safety must be maintained, bureaucracy must be reduced.

The last section focused on RNA-based cancer vaccines, although there are other formats in which antigens may be provided. Specific epitopes can be delivered as synthetic peptides (101, 103), and whole tumor antigens as full-length proteins. Even complete tumor cells can be lysed and used as antigen source. All these approaches have been tested in humans, while peptides appear to be the most promising competitor of RNA (103). Although we focused on RNA-based strategies in the section above, all limitations, lines of reasoning, and rationales discussed more or less apply to the latter approaches of cancer vaccination as well.

6 A small set of predictive biomarkers instead of the "sequence everything" approach

Currently, the most applied approach in cancer immunotherapy is targeting immune checkpoints or immune regulatory molecules, which have shown high success rates in several clinical trials. Melanoma is a highly mutated cancer with a wide frequency range, of 0.1-100 somatic mutations per Megabase (MB). In a study on 3083 matched tumor-normal pairs from 27 different tumor types, melanoma was found to have the highest mutational frequency of all cancers analyzed (104). Two studies that performed whole-exome sequencing on tumor samples of melanoma patients showed improved clinical outcomes after being treated with checkpoint inhibitors in patients with a high mutational burden (105, 106). Therefore, whole-exome sequencing is being used by some groups to identify mutational load as a biomarker to give patients the advantage of immunotherapy.

On the other hand, studies using smaller gene panels (170-500 genes) have shown that the total exomic mutational burden can be extrapolated, and, more important, also the response to immunotherapy can be predicted. In a study with 65 melanoma patients, the mutational burden calculated using FoundationOne (315 genes) was found to be significantly associated with treatment response and survival, particularly at >20 mutations/MB) (107). Therefore, determining mutational load using smaller panels may also be a biomarker of response to immunotherapy with much lower costs. An additional benefit of such sequencing panels may lie in a better selection of therapeutic alternatives besides immunotherapy. Regulatory pathology and oncology bodies such as the College of American Pathologists (CAP) have adopted this minimalistic approach and recommend a panel of BRAF, NRAS, and KIT mutations as a routine in melanoma patients (108). The identification of mutations in tumor samples of melanoma patients can even be customized in simple multiplex PCR assays for labs with limited resources. Our group has tested tumor samples of a small cohort of cutaneous melanoma patients using the Trusight Oncology 500 panel. The analysis showed that all samples had a high mutational burden, ranging from ~5-48 mutations per MB. All samples were found to have one or more mutations in BRAF, NRAS, and/or KIT that could be used in targeted therapy.

In conclusion, genomic tests on tumor samples can be run with a small, cost-effective panel to identify the mutational burden and to allow decisions regarding treatment with targeted therapy and immunotherapy.

7 Exploring affordable immunohistochemistry markers that may direct individual therapies

Traditionally, immunohistochemistry (IHC) is used as a tool to help the pathologist confirm the cancer diagnosis. Thus the method is routinely established in oncologic centers worldwide, and the required equipment is available. While targeted therapies and immune checkpoint inhibitors have demonstrated remarkable efficacy, these drugs do not show uniform responses in all patients. Immunohistochemistry has emerged as a promising tool for assessing the expression of specific proteins within tumor samples that may predict response. Among those proteins, programmed death ligand 1 (PD-L1), T-cell markers, and mitotic index markers are used the most.

Immunohistochemical analysis of PD-L1 expression in melanoma samples has shown correlations with response to immune checkpoint inhibitors such as Pembrolizumab (Keytruda) and Nivolumab (Opdivo) (109). High PD-L1 expression is associated with improved response rates and increased overall survival in some studies, suggesting PD-L1 as a potential predictive biomarker (110).

Furthermore, tumor-infiltrating lymphocytes (TILs) within the tumor microenvironment have been linked to better treatment outcomes in cancer, especially melanoma (111). Objective assessment of TILs has traditionally been performed by flow cytometry to derive T-cell lineage (112). However, immunohistochemistry can also quantify TIL subsets, including $CD8^+$ cytotoxic T cells and $CD4^+$ helper T cells (113). In addition, IHC staining of FoxP3 can help evaluate the presence and density of Tregs within the tumor microenvironment (114).

Many studies tried to connect one or more other IHC stainings with prognosis and response to therapy, such as mitotic index and angiogenesis markers (115). Additionally, BAP1 (BRCA1-associated protein 1) and MITF (microphthalmia-associated transcription factor) expression were linked to poor prognosis (116, 117).

Thus, using IHC of a limited set of markers can be a cost-efficient tool to direct clinical treatment decisions.

8 Conclusions

Cancer is a common disease that affects many humans. New technologies helped to understand the molecular basis of the different malignancies and their interplay with the human immune system. They led to new treatment strategies, some turning a previously fatal diagnosis into a treatable and even curable condition. However, in many cases, this comes with a price tag of several hundred thousand dollars. Even in developed countries, this is a financial burden that is hard to bear for society and unbearable for most individuals. Hence, economic considerations are crucial for the general use of the new drugs. The biggest cost drivers are, on the one hand, the high grade of personalization, often involving the individual production of cellular products, and on the other hand the successive administration of the different advanced medicinal products, due to the nescience, which product is clinically effective. The first could be addressed by an individualized combination of components from a warehouse of products, thus allowing a more economic production. The use of *in-vivo*-targeted substances like mRNA can help to reduce or avoid the cost-intensive employment of living cells. The second could be tackled by implementing new kinds of patient data, while narrowing the information from established technologies to an informative set of markers, which aid in treatment selection, thus avoiding the trial and error principle. In addition, supportive therapies, which are *per se* inexpensive, but increase the response rate to the advanced treatments can decrease overall costs. Hopefully, the ideas and proposals mentioned above will raise awareness of this dilemma and contribute to developing cost-efficient and clinically effective treatment strategies.

Author contributions

NS, JD, SF, and ML contributed to the conception and design of the review. NS, JD, SK, SF, ML, and AK wrote the first draft of the manuscript. All authors contributed to the article and approved the submitted version.

Funding

This study was funded by the Deutsche Forschungsgemeinschaft (DFG, German Research Foundation) through the trilateral grant SCHA 1247/3-1 to NS, JD, GS, BS-T, AK, GE, SF, and ML, and a Dr. Miriam and Sheldon G Adelson Medical Research Foundation grant to ML. This work was also supported by funding from the European Unions' Horizon Europe research and innovation programme under grant agreement number 101057250 (CANCERNA) to NS, JD, and ML on behalf of the CANCERNA Consortium. We acknowledge financial support by Deutsche Forschungsgemeinschaft and Friedrich-Alexander-Universität Erlangen-Nürnberg within the funding programme "Open Access Publication Funding" to NS and JD.

Conflict of interest

The authors declare that the research was conducted in the absence of any commercial or financial relationships that could be construed as a potential conflict of interest.

Publisher's note

References

1. Yang L, Ning Q, Tang S-s. Recent advances and next breakthrough in immunotherapy for cancer treatment. *J Immunol Res* (2022) 2022:8052212. doi: 10.1155/2022/8052212

2. Filin IY, Solovyeva VV, Kitaeva KV, Rutland CS, Rizvanov AA. Current trends in cancer immunotherapy. *Biomedicines* (2020) 8(12):621. doi: 10.3390/biomedicines8120621

3. Darvishi M, Tosan F, Nakhaei P, Manjili DA, Kharkouei SA, Alizadeh A, et al. Recent progress in cancer immunotherapy: Overview of current status and challenges. *Pathol - Res Practice* (2023) 241:154241. doi: 10.1016/j.prp.2022.154241

4. Belluz J. *The Nobel Prize is a reminder of the outrageous cost of curing cancer* (2018). Available at: https://www.vox.com/science-and-health/2018/10/1/17923720/immunotherapy-cancer-cost.

5. Antrim A. *Study finds total cost of care for CAR-T, post-treatment events can exceed $1 million*. Cranbury, NJ, USA: Pharmacy Times (2021). Available at: https://www.pharmacytimes.com/view/study-finds-total-cost-of-care-for-car-t-post-treatment-events-can-exceed-1-million.

6. Zhu S, Zhang T, Zheng L, Liu H, Song W, Liu D, et al. Combination strategies to maximize the benefits of cancer immunotherapy. *J Hematol Oncol* (2021) 14(1):156. doi: 10.1186/s13045-021-01164-5

7. Murciano-Goroff YR, Warner AB, Wolchok JD. The future of cancer immunotherapy: microenvironment-targeting combinations. *Cell Res* (2020) 30 (6):507–19. doi: 10.1038/s41422-020-0337-2

8. Hoteit M, Oneissi Z, Reda R, Wakim F, Zaidan A, Farran M, et al. Cancer immunotherapy: A comprehensive appraisal of its modes of application (Review). *Oncol Lett* (2021) 22(3):655. doi: 10.3892/ol.2021.12916

9. OECD. *Addressing challenges in access to oncology medicines Analytical Report* (2020). Available at: https://www.oecd.org/health/health-systems/Addressing-Challenges-in-Access-to-Oncology-Medicines-Analytical-Report.pdf.

10. Sade-Feldman M, Yizhak K, Bjorgaard SL, Ray JP, de Boer CG, Jenkins RW, et al. Defining T cell states associated with response to checkpoint immunotherapy in melanoma. *Cell* (2019) 176(1-2):404. doi: 10.1016/j.cell.2018.12.034

11. Freeman SS, Sade-Feldman M, Kim J, Stewart C, Gonye ALK, Ravi A, et al. Combined tumor and immune signals from genomes or transcriptomes predict outcomes of checkpoint inhibition in melanoma. *Cell Rep Med* (2022) 3(2):100500. doi: 10.1016/j.xcrm.2021.100500

12. Kim JY, Kronbichler A, Eisenhut M, Hong SH, van der Vliet HJ, Kang J, et al. Tumor mutational burden and efficacy of immune checkpoint inhibitors: A systematic review and meta-analysis. *Cancers (Basel)* (2019) 11(11):1798. doi: 10.3390/cancers11111798

13. Leidner R, Sanjuan Silva N, Huang H, Sprott D, Zheng C, Shih YP, et al. Neoantigen T-cell receptor gene therapy in pancreatic cancer. *N Engl J Med* (2022) 386 (22):2112–9. doi: 10.1056/NEJMoa2119662

14. Chan TA, Yarchoan M, Jaffee E, Swanton C, Quezada SA, Stenzinger A, et al. Development of tumor mutation burden as an immunotherapy biomarker: utility for the oncology clinic. *Ann Oncol* (2019) 30(1):44–56. doi: 10.1093/annonc/mdy495

15. Shen L, Zhang J, Lee H, Batista MT, Johnston SA. RNA transcription and splicing errors as a source of cancer frameshift neoantigens for vaccines. *Sci Rep* (2019) 9(1):14184. doi: 10.1038/s41598-019-50738-4

16. Verdegaal EM, de MIranda NF, Visser M, Harryvan T, van Buuren MM, Andersen RS, et al. Neoantigen landscape dynamics during human melanoma-T cell interactions. *Nature* (2016) 536(7614):91–5. doi: 10.1038/nature18945

17. Rizvi NA, Hellmann MD, Snyder A, Kvistborg P, Makarov V, Havel JJ, et al. Cancer immunology. Mutational landscape determines sensitivity to PD-1 blockade in non-small cell lung cancer. *Science* (2015) 348(6230):124–8. doi: 10.1126/science.aaa1348

18. Sim MJW, Lu J, Spencer M, Hopkins F, Tran E, Rosenberg SA, et al. High-affinity oligoclonal TCRs define effective adoptive T cell therapy targeting mutant KRAS-G12D. *Proc Natl Acad Sci U S A* (2020) 117(23):12826–35. doi: 10.1073/pnas.1921964117

19. Zacharakis N, Chinnasamy H, Black M, Xu H, Lu YC, Zheng Z, et al. Immune recognition of somatic mutations leading to complete durable regression in metastatic breast cancer. *Nat Med* (2018) 24(6):724–30. doi: 10.1038/s41591-018-0040-8

20. Zacharakis N, Huq LM, Seitter SJ, Kim SP, Gartner JJ, Sindiri S, et al. Breast cancers are immunogenic: immunologic analyses and a phase II pilot clinical trial using mutation-reactive autologous lymphocytes. *J Clin Oncol* (2022) 40(16):1741–54. doi: 10.1200/JCO.21.02170

21. Zhang J, Huang D, Saw PE, Song E. Turning cold tumors hot: from molecular mechanisms to clinical applications. *Trends Immunol* (2022) 43(7):523–45. doi: 10.1016/j.it.2022.04.010

22. Benoit A, Vogin G, Duhem C, Berchem G, Janji B. Lighting up the fire in the microenvironment of cold tumors: A major challenge to improve cancer immunotherapy. *Cells* (2023) 12(13):1787. doi: 10.3390/cells12131787

23. Galon J, Bruni D. Approaches to treat immune hot, altered and cold tumours with combination immunotherapies. *Nat Rev Drug Discovery* (2019) 18(3):197–218. doi: 10.1038/s41573-018-0007-y

24. Bonaventura P, Shekarian T, Alcazer V, Valladeau-Guilemond J, Valsesia-Wittmann S, Amigorena S, et al. Cold tumors: A therapeutic challenge for immunotherapy. *Front Immunol* (2019) 10:168. doi: 10.3389/fimmu.2019.00168

25. Wei J, Kishton RJ, Angel M, Conn CS, Dalla-Venezia N, Marcel V, et al. Ribosomal proteins regulate MHC class I peptide generation for immunosurveillance. *Mol Cell* (2019) 73(6):1162–73.e5. doi: 10.1016/j.molcel.2018.12.020

26. Bourdetsky D, Schmelzer CE, Admon A. The nature and extent of contributions by defective ribosome products to the HLA peptidome. *Proc Natl Acad Sci U S A* (2014) 111(16):E1591–9. doi: 10.1073/pnas.1321902111

27. Yewdell JW, Holly J. DRiPs get molecular. *Curr Opin Immunol* (2020) 64:130–6. doi: 10.1016/j.coi.2020.05.009

28. Stanley RF, Abdel-Wahab O. Dysregulation and therapeutic targeting of RNA splicing in cancer. *Nat Cancer* (2022) 3(5):536–46. doi: 10.1038/s43018-022-00384-z

29. Oka M, Xu L, Suzuki T, Yoshikawa T, Sakamoto H, Uemura H, et al. Aberrant splicing isoforms detected by full-length transcriptome sequencing as transcripts of potential neoantigens in non-small cell lung cancer. *Genome Biol* (2021) 22(1):9. doi: 10.1186/s13059-020-02240-8

30. Lu SX, De Neef E, Thomas JD, Sabio E, Rousseau B, Gigoux M, et al. Pharmacologic modulation of RNA splicing enhances anti-tumor immunity. *Cell* (2021) 184(15):4032–47.e31. doi: 10.1016/j.cell.2021.05.038

31. Peters BA, Wilson M, Moran U, Pavlick A, Izsak A, Wechter T, et al. Relating the gut metagenome and metatranscriptome to immunotherapy responses in melanoma patients. *Genome Med* (2019) 11(1):61. doi: 10.1186/s13073-019-0672-4

32. Nomura M, Nagatomo R, Doi K, Shimizu J, Baba K, Saito T, et al. Association of short-chain fatty acids in the gut microbiome with clinical response to treatment with nivolumab or pembrolizumab in patients with solid cancer tumors. *JAMA Netw Open* (2020) 3(4):e202895. doi: 10.1001/jamanetworkopen.2020.2895

33. Chung MW, Kim MJ, Won EJ, Lee YJ, Yun YW, Cho SB, et al. Gut microbiome composition can predict the response to nivolumab in advanced hepatocellular carcinoma patients. *World J Gastroenterol* (2021) 27(42):7340–9. doi: 10.3748/wjg.v27.i42.7340

34. Smith M, Dai A, Ghilardi G, Amelsberg KV, Devlin SM, Pajarillo R, et al. Gut microbiome correlates of response and toxicity following anti-CD19 CAR T cell therapy. *Nat Med* (2022) 28(4):713–23. doi: 10.1038/s41591-022-01702-9

35. Zeng Y, Shi Q, Liu X, Tang H, Lu B, Zhou Q, et al. Dynamic gut microbiota changes in patients with advanced Malignancies experiencing secondary resistance to immune checkpoint inhibitors and immune-related adverse events. *Front Oncol* (2023) 13:1144534. doi: 10.3389/fonc.2023.1144534

36. Gur C, Ibrahim Y, Isaacson B, Yamin R, Abed J, Gamliel M, et al. Binding of the Fap2 protein of Fusobacterium nucleatum to human inhibitory receptor TIGIT protects tumors from immune cell attack. *Immunity* (2015) 42(2):344–55. doi: 10.1016/j.immuni.2015.01.010

37. Fidelle M, Rauber C, Alves Costa Silva C, Tian A-L, Lahmar I, de la Varende A-LM, et al. A microbiota-modulated checkpoint directs immunosuppressive intestinal T cells into cancers. *Science* (2023) 380(6649):eabo2296. doi: 10.1126/science.abo2296

38. Baruch EN, Youngster I, Ben-Betzalel G, Ortenberg R, Lahat A, Katz L, et al. Fecal microbiota transplant promotes response in immunotherapy-refractory melanoma patients. *Science* (2021) 371(6529):602–9. doi: 10.1126/science.abb5920

39. Gopalakrishnan V, Spencer CN, Nezi L, Reuben A, Andrews MC, Karpinets TV, et al. Gut microbiome modulates response to anti-PD-1 immunotherapy in melanoma patients. *Science* (2018) 359(6371):97–103. doi: 10.1126/science.aan4236

40. Massalha I, Segal A, Moskovitz MT, Yakobson A, Zabit R, Stemmer SM, et al. 76TiP Fecal microbiota transplantation to improve efficacy of immune checkpoint inhibitors in metastatic lung cancer. *J Thorac Oncol* (2023) 18(4, Supplement):S84. doi: 10.1016/S1556-0864(23)00330-1

41. Rodríguez-Lara A, Rueda-Robles A, Sáez-Lara MJ, Plaza-Diaz J, Álvarez-Mercado AI. From non-alcoholic fatty liver disease to liver cancer: microbiota and inflammation as key players. *Pathogens* (2023) 12(7):940. doi: 10.3390/pathogens12070940

42. Conti G, D'Amico F, Fabbrini M, Brigidi P, Barone M, Turroni S. Pharmacomicrobiomics in anticancer therapies: why the gut microbiota should be pointed out. *Genes (Basel)* (2022) 14(1):55. doi: 10.3390/genes14010055

43. Borgers JSW, Burgers F, Terveer EM, van Leerdam M, Korse TM, Kessels R, et al. 120TiP Conversion of response to immune checkpoint inhibition by fecal microbiota transplantation in patients with metastatic melanoma: A randomized phase Ib/IIa trial. *Immuno-Oncol Technol* (2022) 16:100224. doi: 10.1016/j.iotech.2022.100224

44. Davar D, Dzutsev AK, McCulloch JA, Rodrigues RR, Chauvin JM, Morrison RM, et al. Fecal microbiota transplant overcomes resistance to anti-PD-1 therapy in melanoma patients. *Science* (2021) 371(6529):595–602. doi: 10.1126/science.abf3363

45. Porcari S, Ciccarese C, Pinto F, Quaranta G, Giorgi SD, Rondinella D, et al. Fecal microbiota transplantation to improve efficacy of immune checkpoint inhibitors in renal cell carcinoma (TACITO trial). *J Clin Oncol* (2022) 40(6_suppl):TPS407–TPS. doi: 10.1200/JCO.2022.40.6_suppl.TPS407

46. Peng Z, Zhang X, Xie T, Cheng S, Han Z, Wang S, et al. Efficacy of fecal microbiota transplantation in patients with anti-PD-1–resistant/refractory

gastrointestinal cancers. *J Clin Oncol* (2023) 41(4_suppl):389–. doi: 10.1200/JCO.2023.41.4_suppl.389

47. Zhou Y, Liu Z, Chen T. Gut microbiota: A promising milestone in enhancing the efficacy of PD1/PD-L1 blockade therapy. *Front Oncol* (2022) 12. doi: 10.3389/fonc.2022.847350

48. Ruggeri L, Capanni M, Casucci M, Volpi I, Tosti A, Perruccio K, et al. Role of natural killer cell alloreactivity in HLA-mismatched hematopoietic stem cell transplantation. *Blood* (1999) 94(1):333–9. doi: 10.1182/blood.V94.1.333.413a31_333_339

49. Shin MH, Kim J, Lim SA, Kim J, Kim SJ, Lee KM. NK cell-based immunotherapies in cancer. *Immune Netw* (2020) 20(2):e14. doi: 10.4110/in.2020.20.e14

50. Liu E, Marin D, Banerjee P, Macapinlac HA, Thompson P, Basar R, et al. Use of CAR-transduced natural killer cells in CD19-positive lymphoid tumors. *N Engl J Med* (2020) 382(6):545–53. doi: 10.1056/NEJMoa1910607

51. Bashiri Dezfouli A, Yazdi M, Pockley AG, Khosravi M, Kobold S, Wagner E, et al. NK cells armed with chimeric antigen receptors (CAR): roadblocks to successful development. *Cells* (2021) 10(12):3390. doi: 10.3390/cells10123390

52. Nair S, Dhodapkar MV. Natural killer T cells in cancer immunotherapy. *Front Immunol* (2017) 8:1178. doi: 10.3389/fimmu.2017.01178

53. Look A, Burns D, Tews I, Roghanian A, Mansour S. Towards a better understanding of human iNKT cell subpopulations for improved clinical outcomes. *Front Immunol* (2023) 14:1176724. doi: 10.3389/fimmu.2023.1176724

54. Tahir SM, Cheng O, Shaulov A, Koezuka Y, Bubley GJ, Wilson SB, et al. Loss of IFN-gamma production by invariant NK T cells in advanced cancer. *J Immunol* (2001) 167(7):4046–50. doi: 10.4049/jimmunol.167.7.4046

55. Giaccone G, Punt CJ, Ando Y, Ruijter R, Nishi N, Peters M, et al. A phase I study of the natural killer T-cell ligand alpha-galactosylceramide (KRN7000) in patients with solid tumors. *Clin Cancer Res* (2002) 8(12):3702–9.

56. Molling JW, Kolgen W, van der Vliet HJ, Boomsma MF, Kruizenga H, Smorenburg CH, et al. Peripheral blood IFN-gamma-secreting Valpha24+Vbeta11+ NKT cell numbers are decreased in cancer patients independent of tumor type or tumor load. *Int J Cancer* (2005) 116(1):87–93. doi: 10.1002/ijc.20998

57. Oevermann L, Lang P, Feuchtinger T, Schumm M, Teltschik HM, Schlegel P, et al. Immune reconstitution and strategies for rebuilding the immune system after haploidentical stem cell transplantation. *Ann N Y Acad Sci* (2012) 1266:161–70. doi: 10.1111/j.1749-6632.2012.06606.x

58. Morita CT, Beckman EM, Bukowski JF, Tanaka Y, Band H, Bloom BR, et al. Direct presentation of nonpeptide prenyl pyrophosphate antigens to human gamma delta T cells. *Immunity* (1995) 3(4):495–507. doi: 10.1016/1074-7613(95)90178-7

59. Tanaka Y, Morita CT, Tanaka Y, Nieves E, Brenner MB, Bloom BR. Natural and synthetic non-peptide antigens recognized by human gamma delta T cells. *Nature* (1995) 375(6527):155–8. doi: 10.1038/375155a0

60. van der Veken LT, Hagedoorn RS, van Loenen MM, Willemze R, Falkenburg JH, Heemskerk MH. Alphabeta T-cell receptor engineered gammadelta T cells mediate effective antileukemic reactivity. *Cancer Res* (2006) 66(6):3331–7. doi: 10.1158/0008-5472.CAN-05-4190

61. Harrer DC, Simon B, Fujii SI, Shimizu K, Uslu U, Schuler G, et al. RNA-transfection of gamma/delta T cells with a chimeric antigen receptor or an alpha/beta T-cell receptor: a safer alternative to genetically engineered alpha/beta T cells for the immunotherapy of melanoma. *BMC Cancer* (2017) 17(1):551. doi: 10.1186/s12885-017-3539-3

62. van der Veken LT, Coccoris M, Swart E, Falkenburg JH, Schumacher TN, Heemskerk MH. Alpha beta T cell receptor transfer to gamma delta T cells generates functional effector cells without mixed TCR dimers in vivo. *J Immunol* (2009) 182 (1):164–70. doi: 10.4049/jimmunol.182.1.164

63. Hanagiri T, Shigematsu Y, Kuroda K, Baba T, Shiota H, Ichiki Y, et al. Antitumor activity of human gammadelta T cells transducted with CD8 and with T-cell receptors of tumor-specific cytotoxic T lymphocytes. *Cancer Sci* (2012) 103(8):1414–9. doi: 10.1111/j.1349-7006.2012.02337.x

64. Nishimoto KP, Barca T, Azameera A, Makkouk A, Romero JM, Bai L, et al. Allogeneic CD20-targeted γδ T cells exhibit innate and adaptive antitumor activities in preclinical B-cell lymphoma models. *Clin Transl Immunol* (2022) 11(2):e1373. doi: 10.1002/cti2.1373

65. Li YR, Zhou K, Wilson M, Kramer A, Zhu Y, Dawson N, et al. Mucosal-associated invariant T cells for cancer immunotherapy. *Mol Ther* (2023) 31(3):631–46. doi: 10.1016/j.ymthe.2022.11.019

66. Ankrum JA, Ong JF, Karp JM. Mesenchymal stem cells: immune evasive, not immune privileged. *Nat Biotechnol* (2014) 32(3):252–60. doi: 10.1038/nbt.2816

67. Schweizer MT, Wang H, Bivalacqua TJ, Partin AW, Lim SJ, Chapman C, et al. A phase I study to assess the safety and cancer-homing ability of allogeneic bone marrow-derived mesenchymal stem cells in men with localized prostate cancer. *Stem Cells Transl Med* (2019) 8(5):441–9. doi: 10.1002/sctm.18-0230

68. Ren J, Liu X, Fang C, Jiang S, June CH, Zhao Y. Multiplex genome editing to generate universal CAR T cells resistant to PD1 inhibition. *Clin Cancer Res* (2017) 23 (9):2255–66. doi: 10.1158/1078-0432.CCR-16-1300

69. Schober K, Muller TR, Gokmen F, Grassmann S, Effenberger M, Poltorak M, et al. Orthotopic replacement of T-cell receptor alpha- and beta-chains with preservation of near-physiological T-cell function. *Nat BioMed Eng* (2019) 3 (12):974–84. doi: 10.1038/s41551-019-0409-0

70. Hu Y, Wang J, Wei G, Yu J, Luo Y, Shi J, et al. A retrospective comparison of allogenic and autologous chimeric antigen receptor T cell therapy targeting CD19 in patients with relapsed/refractory acute lymphoblastic leukemia. *Bone Marrow Transpl* (2019) 54(8):1208–17. doi: 10.1038/s41409-018-0403-2

71. Mohammed T, Mailankody S. "Off-the-shelf" immunotherapies for multiple myeloma. *Semin Oncol* (2022) 49(1):60–8. doi: 10.1053/j.seminoncol.2022.01.001

72. Zhang Y, Kozlowska A, Fritz J, Zhao Y, Torre CPL, Cranert S, et al. 123 P-MUC1C-ALLO1: A fully allogeneic stem cell memory T cell (TSCM) CAR-T therapy with broad potential in solid tumor. *J Immunother Cancer* (2021) 9(Suppl 2):A132–A. doi: 10.1136/jitc-2021-SITC2021.123

73. Xu H, Wang B, Ono M, Kagita A, Fujii K, Sasakawa N, et al. Targeted Disruption of HLA Genes via CRISPR-Cas9 Generates iPSCs with Enhanced Immune Compatibility. *Cell Stem Cell* (2019) 24(4):566–78.e7. doi: 10.1016/j.stem.2019.02.005

74. Deuse T, Hu X, Gravina A, Wang D, Tediashvili G, De C, et al. Hypoimmunogenic derivatives of induced pluripotent stem cells evade immune rejection in fully immunocompetent allogeneic recipients. *Nat Biotechnol* (2019) 37 (3):252–8. doi: 10.1038/s41587-019-0016-3

75. Arias J, Yu J, Varshney M, Inzunza J, Nalvarte I. Hematopoietic stem cell- and induced pluripotent stem cell-derived CAR-NK cells as reliable cell-based therapy solutions. *Stem Cells Transl Med* (2021) 10(7):987–95. doi: 10.1002/sctm.20-0459

76. Li YR, Dunn ZS, Yu Y, Li M, Wang P, Yang L. Advancing cell-based cancer immunotherapy through stem cell engineering. *Cell Stem Cell* (2023) 30(5):592–610. doi: 10.1016/j.stem.2023.02.009

77. Ran T, Eichmüller SB, Schmidt P, Schlander M. Cost of decentralized CAR T-cell production in an academic nonprofit setting. *Int J Cancer* (2020) 147(12):3438–45. doi: 10.1002/ijc.33156

78. Lamers CH, Sleijfer S, Vulto AG, Kruit WH, Kliffen M, Debets R, et al. Treatment of metastatic renal cell carcinoma with autologous T-lymphocytes genetically retargeted against carbonic anhydrase IX: first clinical experience. *J Clin Oncol* (2006) 24(13):e20–e2. doi: 10.1200/JCO.2006.05.9964

79. Morgan RA, Yang JC, Kitano M, Dudley ME, Laurencot CM, Rosenberg SA. Case report of a serious adverse event following the administration of T cells transduced with a chimeric antigen receptor recognizing ERBB2. *Mol Ther* (2010) 18 (4):843–51. doi: 10.1038/mt.2010.24

80. Birkholz K, Hombach A, Krug C, Reuter S, Kershaw M, Kampgen E, et al. Transfer of mRNA encoding recombinant immunoreceptors reprograms CD4+ and CD8+ T cells for use in the adoptive immunotherapy of cancer. *Gene Ther* (2009) 16 (5):596–604. doi: 10.1038/gt.2008.189

81. Tchou J, Zhao Y, Levine BL, Zhang PJ, Davis MM, Melenhorst JJ, et al. Safety and efficacy of intratumoral injections of chimeric antigen receptor (CAR) T cells in metastatic breast cancer. *Cancer Immunol Res* (2017) 5(12):1152–61. doi: 10.1158/2326-6066.CIR-17-0189

82. Beatty GL, Haas AR, Maus MV, Torigian DA, Soulen MC, Plesa G, et al. Mesothelin-specific Chimeric Antigen Receptor mRNA-Engineered T cells Induce Anti-Tumor Activity in Solid Malignancies. *Cancer Immunol Res* (2014) 2(2):112–20. doi: 10.1158/2326-6066.CIR-13-0170

83. Beatty GL, O'Hara MH, Lacey SF, Torigian DA, Nazimuddin F, Chen F, et al. Activity of mesothelin-specific chimeric antigen receptor T cells against pancreatic carcinoma metastases in a phase 1 trial. *Gastroenterology* (2018) 155(1):29–32. doi: 10.1053/j.gastro.2018.03.029

84. Maus MV, Haas AR, Beatty GL, Albelda SM, Levine BL, Liu X, et al. T cells expressing chimeric antigen receptors can cause anaphylaxis in humans. *Cancer Immunol Res* (2013) 1(1):26–31. doi: 10.1158/2326-6066.CIR-13-0006

85. Svoboda J, Rheingold SR, Gill SI, Grupp SA, Lacey SF, Kulikovskaya I, et al. Nonviral RNA chimeric antigen receptor-modified T cells in patients with Hodgkin lymphoma. *Blood* (2018) 132(10):1022–6. doi: 10.1182/blood-2018-03-837609

86. De Vivo DC, Bertini E, Swoboda KJ, Hwu WL, Crawford TO, Finkel RS, et al. Nusinersen initiated in infants during the presymptomatic stage of spinal muscular atrophy: Interim efficacy and safety results from the Phase 2 NURTURE study. *Neuromuscul Disord* (2019) 29(11):842–56. doi: 10.1016/j.nmd.2019.09.007

87. Darras BT, Farrar MA, Mercuri E, Finkel RS, Foster R, Hughes SG, et al. An integrated safety analysis of infants and children with symptomatic spinal muscular atrophy (SMA) treated with nusinersen in seven clinical trials. *CNS Drugs* (2019) 33 (9):919–32. doi: 10.1007/s40263-019-00656-w

88. FDA. *FDA approves first drug for spinal muscular atrophy* (2016). Available at: https://www.fda.gov/news-events/press-announcements/fda-approves-first-drug-spinal-muscular-atrophy.

89. Moderna. *Moderna and Merck announce mRNA-4157/V940, an investigational personalized mRNA cancer vaccine, in combination with KEYTRUDA(R) (Pembrolizumab), was granted breakthrough therapy desination by the FDA for adjuvant treatment of patients with high-risk melanoma following complete resection* (2023). Available at: https://news.modernatx.com/news/news-details/2023/Moderna-and-Merck-Announce-mRNA-4157V940-an-Investigational-Personalized-mRNA-Cancer-Vaccine-in-Combination-With-KEYTRUDAR-pembrolizumab-was-Granted-Breakthrough-Therapy-Designation-by-the-FDA-for-Adjuvant-Treatment-of-Patients-With-High-Risk-Melanom/defaultaspx.

90. Sava J. *FDA Greenlights BTD of a Personalized mRNA Vaccine for High-Risk Melanoma* (2023). Available at: https://www.targetedonc.com/view/fda-greenlights-btd-of-a-personalized-mrna-vaccine-for-high-risk-melanoma.

91. Rojas LA, Sethna Z, Soares KC, Olcese C, Pang N, Patterson E, et al. Personalized RNA neoantigen vaccines stimulate T cells in pancreatic cancer. *Nature* (2023) 618 (7963):144–50. doi: 10.1038/s41586-023-06063-y

92. Cafri G, Gartner JJ, Zaks T, Hopson K, Levin N, Paria BC, et al. mRNA vaccine-induced neoantigen-specific T cell immunity in patients with gastrointestinal cancer. *J Clin Invest* (2020) 130(11):5976–88. doi: 10.1172/JCI134915

93. Sahin U, Oehm P, Derhovanessian E, Jabulowsky RA, Vormehr M, Gold M, et al. An RNA vaccine drives immunity in checkpoint-inhibitor-treated melanoma. *Nature* (2020) 585(7823):107–12. doi: 10.1038/s41586-020-2537-9

94. Koch EAT, Schaft N, Kummer M, Berking C, Schuler G, Hasumi K, et al. A one-armed phase I dose escalation trial design: personalized vaccination with IKKβ-matured, RNA-loaded dendritic cells for metastatic uveal melanoma. *Front Immunol* (2022) 13. doi: 10.3389/fimmu.2022.785231

95. Alexopoulou L, Holt AC, Medzhitov R, Flavell RA. Recognition of double-stranded RNA and activation of NF-kappaB by Toll-like receptor 3. *Nature* (2001) 413 (6857):732–8. doi: 10.1038/35099560

96. Kallen KJ, Heidenreich R, Schnee M, Petsch B, Schlake T, Thess A, et al. A novel, disruptive vaccination technology: self-adjuvanted RNActive(®) vaccines. *Hum Vaccin Immunother* (2013) 9(10):2263–76. doi: 10.4161/hv.25181

97. Kallen KJ, Theß A. A development that may evolve into a revolution in medicine: mRNA as the basis for novel, nucleotide-based vaccines and drugs. *Ther Adv Vaccines* (2014) 2(1):10–31. doi: 10.1177/2051013613508729

98. EMA. *Provenge; autologous peripheral-blood mononuclear cells activated with prostatic acid phosphatase granulocyte-macrophage colony-stimulating factor (sipuleucel-T)* (2013). Available at: https://www.emaeuropaeu/en/medicines/human/EPAR/provenge.

99. EMA. *Provenge; Withdrawal of the marketing authorisation in the European Union* (2015). Available at: https://www.emaeuropaeu/en/documents/public-statement/public-statement-provenge-withdrawal-marketing-authorisation-european-union_en.pdf.

100. Dorrie J, Schaft N, Schuler G, Schuler-Thurner B. Therapeutic cancer vaccination with ex vivo RNA-transfected dendritic cells-an update. *Pharmaceutics* (2020) 12(2):92. doi: 10.3390/pharmaceutics12020092

101. Laureano RS, Sprooten J, Vanmeerbeerk I, Borras DM, Govaerts J, Naulaerts S, et al. Trial watch: Dendritic cell (DC)-based immunotherapy for cancer. *Oncoimmunology* (2022) 11(1):2096363. doi: 10.1080/2162402X.2022.2096363

102. Vishweshwaraiah YL, Dokholyan NV. mRNA vaccines for cancer immunotherapy. *Front Immunol* (2022) 13:1029069. doi: 10.3389/fimmu.2022.1029069

103. Nelde A, Rammensee HG, Walz JS. The peptide vaccine of the future. *Mol Cell Proteomics* (2021) 20:100022. doi: 10.1074/mcp.R120.002309

104. Alexandrov LB, Nik-Zainal S, Wedge DC, Aparicio SA, Behjati S, Biankin AV, et al. Signatures of mutational processes in human cancer. *Nature* (2013) 500 (7463):415–21. doi: 10.1038/nature12477

105. Hugo W, Zaretsky JM, Sun L, Song C, Moreno BH, Hu-Lieskovan S, et al. Genomic and transcriptomic features of response to anti-PD-1 therapy in metastatic melanoma. *Cell* (2016) 165(1):35–44. doi: 10.1016/j.cell.2016.02.065

106. Riaz N, Havel JJ, Makarov V, Desrichard A, Urba WJ, Sims JS, et al. Tumor and microenvironment evolution during immunotherapy with nivolumab. *Cell* (2017) 171 (4):934–49.e16. doi: 10.1016/j.cell.2017.09.028

107. Roszik J, Haydu LE, Hess KR, Oba J, Joon AY, Siroy AE, et al. Novel algorithmic approach predicts tumor mutation load and correlates with immunotherapy clinical outcomes using a defined gene mutation set. *BMC Med* (2016) 14(1):168. doi: 10.1186/s12916-016-0705-4

108. Sholl LM, Andea A, Bridge JA, Cheng L, Davies MA, Ehteshami M, et al. Template for reporting results of biomarker testing of specimens from patients with melanoma. *Arch Pathol Lab Med* (2016) 140(4):355–7. doi: 10.5858/arpa.2015-0278-CP

109. Larkin J, Hodi FS, Wolchok JD. Combined nivolumab and ipilimumab or monotherapy in untreated melanoma. *N Engl J Med* (2015) 373(13):1270–1. doi: 10.1056/NEJMoa1504030

110. Parvini S, Majidpoor J, Mortezaee K. The impact of PD-L1 as a biomarker of cancer responses to combo anti-PD-1/CTLA-4. *Pathol Res Pract* (2023) 247:154583. doi: 10.1016/j.prp.2023.154583

111. Galon J, Pagès F, Marincola FM, Thurin M, Trinchieri G, Fox BA, et al. The immune score as a new possible approach for the classification of cancer. *J Transl Med* (2012) 10:1. doi: 10.1186/1479-5876-10-1

112. Gros A, Robbins PF, Yao X, Li YF, Turcotte S, Tran E, et al. PD-1 identifies the patient-specific $CD8^+$ tumor-reactive repertoire infiltrating human tumors. *J Clin Invest* (2014) 124(5):2246–59. doi: 10.1172/JCI73639

113. Tumeh PC, Harview CL, Yearley JH, Shintaku IP, Taylor EJ, Robert L, et al. PD-1 blockade induces responses by inhibiting adaptive immune resistance. *Nature* (2014) 515(7528):568–71. doi: 10.1038/nature13954

114. Fridman WH, Galon J, Pagès F, Tartour E, Sautès-Fridman C, Kroemer G. Prognostic and predictive impact of intra- and peritumoral immune infiltrates. *Cancer Res* (2011) 71(17):5601–5. doi: 10.1158/0008-5472.CAN-11-1316

115. Mihic-Probst D, Ikenberg K, Tinguely M, Schraml P, Behnke S, Seifert B, et al. Tumor cell plasticity and angiogenesis in human melanomas. *PloS One* (2012) 7(3): e33571. doi: 10.1371/journal.pone.0033571

116. Koopmans AE, Verdijk RM, Brouwer RW, van den Bosch TP, van den Berg MM, Vaarwater J, et al. Clinical significance of immunohistochemistry for detection of BAP1 mutations in uveal melanoma. *Mod Pathol* (2014) 27(10):1321–30. doi: 10.1038/modpathol.2014.43

117. Carreira S, Goodall J, Denat L, Rodriguez M, Nuciforo P, Hoek KS, et al. Mitf regulation of Dia1 controls melanoma proliferation and invasiveness. *Genes Dev* (2006) 20(24):3426–39. doi: 10.1101/gad.406406

frontiers | Frontiers in Immunology

TYPE Review
PUBLISHED 27 September 2023
DOI 10.3389/fimmu.2023.1258013

OPEN ACCESS

EDITED BY
Yun-Fan Sun,
Fudan University, China

REVIEWED BY
Ghanbar Mahmoodi Chalbatani,
Tehran University of Medical Sciences, Iran
Zaixiang Tang,
Soochow University Medical College, China

*CORRESPONDENCE
Barbara Seliger
Barbara.seliger@uk-halle.de

RECEIVED 13 July 2023
ACCEPTED 05 September 2023
PUBLISHED 27 September 2023

CITATION
Massa C and Seliger B (2023) Combination of multiple omics techniques for a personalized therapy or treatment selection. *Front. Immunol.* 14:1258013. doi: 10.3389/fimmu.2023.1258013

Combination of multiple omics techniques for a personalized therapy or treatment selection

Chiara Massa[1] and Barbara Seliger[1,2,3]*

[1]Institute for Translational Immunology, Brandenburg Medical School Theodor Fontane, Brandenburg an der Havel, Germany, [2]Institute of Medical Immunology, Martin Luther University Halle-Wittenberg, Halle, Germany, [3]Fraunhofer Institute for Cell Therapy and Immunology, Leipzig, Germany

Despite targeted therapies and immunotherapies have revolutionized the treatment of cancer patients, only a limited number of patients have long-term responses. Moreover, due to differences within cancer patients in the tumor mutational burden, composition of the tumor microenvironment as well as of the peripheral immune system and microbiome, and in the development of immune escape mechanisms, there is no "one fit all" therapy. Thus, the treatment of patients must be personalized based on the specific molecular, immunologic and/or metabolic landscape of their tumor. In order to identify for each patient the best possible therapy, different approaches should be employed and combined. These include (i) the use of predictive biomarkers identified on large cohorts of patients with the same tumor type and (ii) the evaluation of the individual tumor with "omics"-based analyses as well as its *ex vivo* characterization for susceptibility to different therapies.

KEYWORDS

high throughput technologies, biomarker, cancer, patient stratification, personalized therapy

1 Introduction

Cancer is one of the major causes of death worldwide and despite the development of many novel targeted therapies, a high number of patients either do not respond or develop resistance to the treatment. Similar holds true for tumor immunotherapeutic approaches including the treatment with immune checkpoint inhibitors (ICPi), which induce a complete tumor regression, but only in a small number of patients, whose characteristics have not yet been completely understood. Thus, there is an urgent need to determine for each patient the best possible therapy either by identifying biomarkers that can predict response to an available "off the shelf" therapy or by creating an individually-tailored (immune-based) therapy (Figure 1). Due to the availability of different high throughput technologies, which are currently also used in clinical research and practice, there exist currently efforts to integrate different omics technologies to advance not only the understanding of the biology of each individual tumor specimen, but also to implement this information e.g. for patients' stratification and treatment decisions.

In the following paragraphs, we will report on the recent developments in the setting of genomics, transcriptomics, proteomics, microbiomics, metabolomics and immunomics and how they have been beneficial for the management of tumors by providing some examples of clinically relevant discoveries.

2 Search for biomarkers for patient stratification

Based on the improvements over the last decade in different "omics" technologies, a huge amount of data was generated from large cohorts of patients with tumors of different histological origin and (sub)types. Large scale genomics, transcriptomics and proteomics analyses have increased our understanding of the (genetic) drivers of cancer and also helped to identify new clinically relevant disease subtypes (1, 2). All these data could be correlated with patients' clinical characteristics, age, sex, outcome and therapy response in order to identify novel diagnostic, prognostic and predictive markers that will help patients' stratification to the different therapies currently available.

For example, the improvement in genomic and gene sequencing techniques together with their reduced costs allows deep sequencing not only of different sample types from each patient, including next to tumor lesions also liquid biopsies and stool, but also of multiple types of nucleic acid species, such as DNA and coding as well as non-coding RNA. Moreover, the development of single cell RNA sequencing (scRNAseq) technologies has highlighted a high level of intra-tumoral heterogeneity that was not detected by previous bulk RNA sequence evaluations (3). Sequencing has also been used to identify regulating mechanisms, not only in the form of non-coding RNA species, but also by determining the genome 3D organization, in particular the accessibility of genetic loci to transcription (4).

Furthermore, standard immunohistochemistry (IHC) used for the "pathological/diagnostic" evaluation of tumor samples has been upgraded by different technical approaches, such as the conjugation of antibodies (Ab) with metals or barcodes versus the use of sequential cycles of staining and elution, to multiplex IHC. In such settings, a high number of different Ab can be used on the same tissue slide thereby enabling a deep characterization of the different cell types present within the tumor tissue, which can also be evaluated for their localization and relative spatial distribution and thus their possibility to interact.

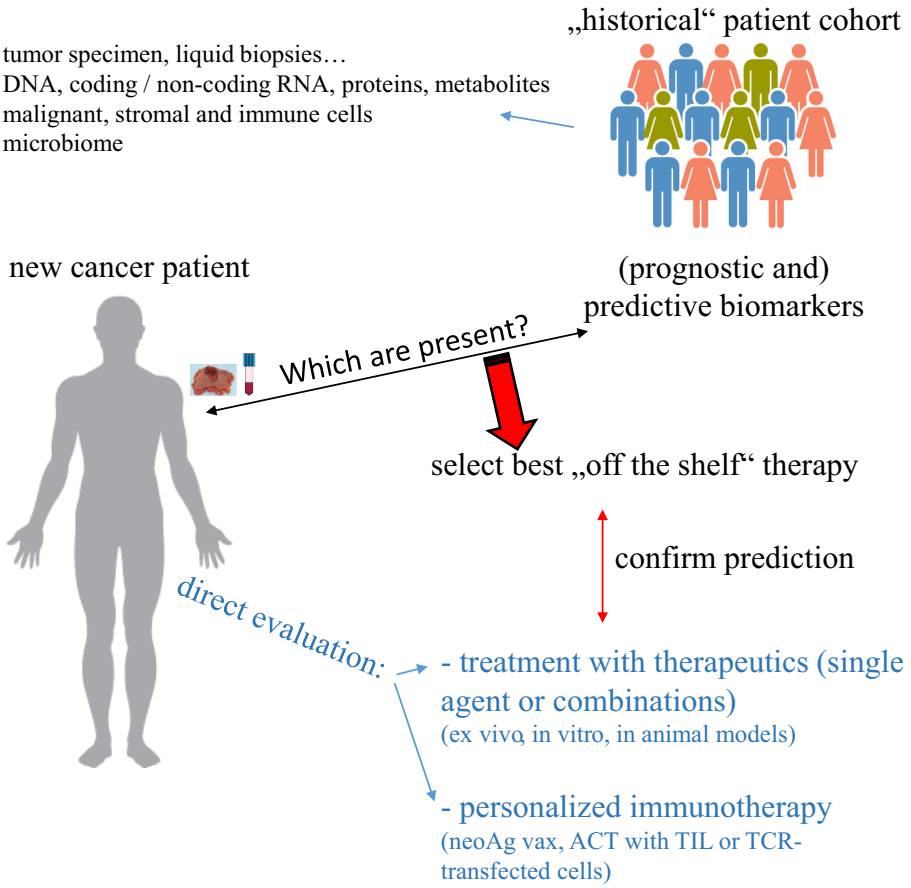

FIGURE 1
Strategies to select an individually-tailored cancer therapy. Specimen from "new" cancer patients can be evaluated for the expression of biomarkers previously identified to predict response to therapy and/or directly tested *ex vivo* for responsiveness to such therapy. In the case of neoAg as a biomarker, a personalized immunotherapeutic approach can be created.

The multiplicity of detection has further been extended also to RNA species with different forms of fluorescence *in situ* hybridization (FISH) that allows the identification of more than hundreds of mRNA transcripts/slide at the single cell or almost single cell level (5).

Employing one or a combination of these techniques, a number of "biological read outs" have been evaluated in the search of biomarkers that would allow patients' stratification with respect to risk and probability to respond to different therapies, thus leading to the selection of an individually tailored therapeutic approach. These biological read outs represent all major hallmarks of cancer (6), ranging from the intrinsic capacity of the transformed cells to proliferate, migrate, survive and rewire their metabolism to the composition of the tumor microenvironment (TME) and the interactions among its different cellular components, namely stromal and immune cells.

2.1 Tumor signatures

Neoplastic transformation is mediated by an accumulation of mutations in oncogenes or tumor suppressor genes (7), some of which are shared within the particular tumor type or subtype, whereas others are individual, which might be e.g. the reason, why many patients do not respond to "general tumor type-selected" targeted therapies.

In addition to such inter-patient heterogeneity, therapy resistance is also related to the intra-patient heterogeneity of the tumor. Since a long time it is known that there exists a niche of tumor stem cells with a higher resistance to therapy. Recently, a stemness signature correlating to patients' risk and low response to ICPi therapy across many tumor types has been described (8). Similarly, a pan-cancer evaluation for prediction of resistance to ICPi identified a malignant cell signature centered on the CDK4/6 pathway, which was associated with the induction of a T cell excluded phenotype (9).

The complexity of the intra-patient heterogeneity of the tumor has been further highlighted by the widespread application of multiplex IHC and scRNAseq, which can identify within the "bulk" tumor mass individual cells expressing characteristics of a tumor subtype distinct from the bulk tumor (10). Such intra-tumor heterogeneity has important consequences in patients with metastatic disease. Indeed, the evaluation of paired samples from primary and lymph node (LN) metastases of breast cancer (BC) patients highlighted discrepancies in the prevalent "molecular subset" between the two locations suggesting that for optimal therapy not only the knowledge of the presence of LN metastases, but also the characterization of their molecular features are required (11).

In addition to bioinformatics analyses of available patients´ data from large cohorts and evaluation of their response to therapy to identify predictive gene signatures, databanks of cell lines and their *in vitro* tested sensitivity to chemotherapeutic drugs are also used to create predicting algorithms of responsiveness [reviewed in (12)]. For example, Geeleher and co-workers employed whole genome expression data obtained from multiple tumor cell lines with known sensitivity to selected drugs to generate a prediction tool allowing the identification of drug sensitivity of tumor from patients in a clinical trial (13). Despite the analyses at the proteomic level are for now far from clinical translation, Tognetti and co-authors were able to identify different signaling pathways in BC cell lines that were able to predict response to specific drugs of patient-derived xenografts (PDX) (14).

2.2 Neoantigens

Due to their high proliferation rate, malignant cells accumulate mutations that can lead to the generation of neoantigens (neoAg), i.e. immunogenic peptides encompassing a tumor specific mutation, against which no central tolerance has been created and thus representing optimal targets for immunotherapy (15).

In order to be implemented for therapy, such neoAg have to be identified, which is currently performed by two complementary strategies: (i) at the protein level by elution of peptides associated with the HLA class I and class II molecules on the surface of tumor cell (lines) followed by their identification via mass spectrometry, which leads to the generation of different databanks (16, 17). This approach has been recently expanded to healthy tissue in order to create a reference for a more precise identification of "real" tumor associated neoAg (18). (ii) At the genetic level by comparison of the genomic sequences between malignant and normal cells, which allows the identification of somatic mutations and translocations within the tumor cells. Peptides encompassing such mutations are then subjected to "*in silico*" analysis for the possibility to give rise to epitopes presented via the HLA alleles expressed by the patient (19). In recent years, next to "standard" HLA class I-restricted peptides, these strategies have identified many neoAg-restricted to HLA class II molecules (20, 21) or derived from non-coding sequences (22) leading to the development of new algorithms for their improved identification from sequencing data (23–25). Continuous progresses in artificial intelligence approaches are further improving the capabilities to identify neoAg for clinical application (26).

Some of the identified neoAg are "public" or shared, corresponding to hotspot of mutations present in many tumors within and among different histotypes or derived from viral antigens in viral-driven cancers. In some cases, "off the shelf" therapeutics have been generated for such neoAg, such as transgenic T cell receptors (TCR) or TCR mimics against shared mutations of KRAS (27) and p53 (28) as well as against human papillomavirus (HPV) antigens (29).

However, in most cases, neoAg are private, i.e. specific for each individual tumor, and therefore a personalized vaccine has to be created for each patient. Many different strategies can be implemented, ranging from their direct use as a vaccine in the form of synthetic peptides or of the coding mRNA to their *in vitro* use to load dendritic cells (DC) that will then be employed for vaccination or for *in vitro* expansion of autologous tumor infiltrating lymphocytes (TIL) (30, 31). Such *in vitro* T cell restimulation with the neoAg peptides can be implemented as a screening tool to test the immunogenicity of the predicted epitopes as well as to isolate neoAg-specific T cell clones and their TCR (32).

Those TCR sequences could then be cloned and transfected into autologous peripheral T cells to provide a non-exhausted source of neoAg-specific TCR-transgenic effector cells.

Next to the improved identification of possible neoAg, there are also studies to improve their clinical implementation with better strategies for loading DC with polypeptides (33) or optimal spacers for multi-epitope constructs to allow processing into the single peptides (34). Moreover, a genetic and proteomic signature for neoAg-specific $CD4^+$ and $CD8^+$ T cells has been identified, which could allow the isolation of neoAg-specific T cells from patients' TIL without the need of previous *in vitro* expansion (35).

2.3 Non-coding RNA species

Deep sequencing techniques have identified an array of non-coding RNA species, such as microRNA (miRNA), long non-coding RNA (lncRNA) and circular RNA (circRNA), which are all involved in the regulation of different aspects of malignant transformation (36).

MiRNA are short 20-22 nucleotide RNA sequences that upon binding to complementary regions (seeds) on target mRNA molecules affect their transcription leading in the majority of cases to its inhibition by inducing RNA degradation or inhibiting its translation. Sequencing of patients derived material highlighted multiple miRNA, which could serve as prognostic markers and/or predict treatment response, for example to radiotherapy (RT) and/or tamoxifen in BC patients (37), to RT in prostate cancer (38) and to cisplatin in lung cancer (39).

LncRNA are categorized into different subtypes depending on the chromosomal region from which they are translated and can exert different functions depending on their cellular sublocalization (40). While nuclear located lncRNA are involved in the genomic organization, such as e.g. the inactivation of the second X chromosome in female cells (41), the cytoplasmic lncRNA are involved in post-transcriptional regulation either by acting as a miRNA sponge or by directly interacting with the transcript or with RNA-binding proteins (RBP) (42). Functionally, lncRNA could be involved in all hallmarks of cancer and can therefore be used both as prognostic markers and as therapeutic targets. In multiple myeloma (MM), an array of lncRNA have been associated with resistance to chemotherapy (43). In colorectal cancer (CRC) a lncRNA signature can also predict response to immunotherapy as well as to chemotherapy (44), while in BC linc00665 has been demonstrated to predict response to cisplatin-paclitaxel (45). Evaluation of glioblastoma multiforme identified different immune related lncRNA signatures characterizing different disease subtypes driven by distinct genes and displaying discordant sensitivity to multiple treatments (46).

CircRNA regulates protein translation by different mechanisms, e.g. acting as a sponge for miRNA or protein, but also by interacting with proteins involved in transcription or splicing. In addition, some circRNA can also be translated into proteins (47). Next to being established as diagnostic and prognostic markers in different tumor settings, their use as predictive tool is currently investigated. For example, circ_0026652 could predict response to different targeted treatments in MM (48), whereas in glioblastoma circ-METRN was involved in RT resistance (49). As potential therapeutic target, studies performed with ovarian cancer cell lines indicated a role for circ_0025033 in the resistance to paclitaxel due to the expression of FOXM1 upon inhibition of mir-532-3p (50), whereas circPVT1 protects osteosarcoma from doxorubicin and cisplatin (51, 52) and gastric cancer from paclitaxel (53).

Since both lncRNA and circRNA can compete with miRNA for binding to target mRNA, different studies are currently performed to identify competitive endogenous RNA (ceRNA) networks composed of mRNA, miRNA, lncRNA and circRNA. This will allow to determine the overall effect of all regulatory components at the level of mRNA transcription to improve their diagnostic and/or prognostic value. For example, a prognostic network was identified in acute myeloid leukemia (AML) (54), whereas a ceRNA network was involved in predicting the efficacy of interferon (IFN)-α treatment in hepatocellular carcinoma (55, 56). Similarly, in CRC, a ceRNA signature identified high risk patients, who had also an enhanced sensitivity to different drugs and immunotherapies (57).

Genetic material can also be released by (tumor) cells into the circulation, not only within extracellular vesicles (EV), but also as free molecules. Changes in the repertoire of circulating free DNA (cfDNA) as well as RNA are associated with disease progression and thus studied as diagnostic, prognostic as well as predictive markers (58). For example, serum levels of miR-10b and soluble E-cadherin can predict BC metastases (59), whereas a ceRNA signature in the exosome has been shown to predict response to neoadjuvant chemotherapy in patients with advanced gastric cancer (60).

2.4 3D genomic organization

Evaluation of the 3D organization of the genome of transformed cells can provide information on the existence of chromosomal fusion or translocation, which can lead not only to driver mutations and neoAg, but also to changes in the regulation of gene transcription that could affect therapy response. Indeed, mutations in genes such as histone 1 (61) and STAG2 (62) have profound consequences on the 3D genome landscape of the cells by affecting important signaling pathways in tumors. In addition, screening of glioblastoma stem cells from different patients highlighted differences in their 3D genome leading to different signatures and targetable pathways (63). In BC cell lines, changes in the genomic 3D structure during drug treatment or upon acquired resistance were identified, which could possibly help to define new targets for therapy or reversal of resistance (64–66).

Employing "older techniques", such as FISH and 3D-FISH, differences identified in the translocation between chromosome 9 and 22 in Brc-Abl chronic myeloid leukemia (CML) were associated with the responsiveness to tyrosine kinase inhibitors (TKI), thus correlating the level of nearby chromosome disruption to chemotherapy-responsiveness (67). In a murine BC model, genes in different 3D conformation had a prognostic value for response to endocrine therapy (68)

2.5 Metabolism

Alterations in the tumor metabolism are one hallmark of cancer that not only intrinsically allow malignant cells to proliferate and survive, but also help to establish an immunosuppressive TME, thus further favoring tumor development through immune escape (69). The tumor associated metabolism has been characterized at the level of the mutational profile and the expression of metabolic genes within tumor specimens, by the characterization of metabolites in liquid biopsies via mass spectrometry or directly within the patients by using specific reagents for PET-CT (70) as well as other emerging techniques (71).

General differences in the expression of metabolic genes allowed to stratify patients with ovarian cancer into high and low risk patients and could also predict an enhanced response to different chemotherapies (72). In addition, a 7 metabolism-gene signature identified in BC and further validated in melanoma and urothelial epithelial cancer was stratifying patients for outcome and therapy response (73). Enhanced biosynthesis of nicotinamide adenine dinucleotide (NAD^+), an abundant metabolite that plays a key role in cellular homeostasis, stemness and immune response (74), not only discriminates healthy versus BC tissue, but can also identify a subgroup of patients with a worse prognosis (75). Moreover, since patients with a high NAD^+ biosynthesis have a higher immunogenicity as well as an increased immune suppression, this score might be implemented to select patients with enhanced responsiveness to immunotherapies, such as ICPi (75).

Other studies focused on specific metabolic pathways in order to stratify patients. The most known alteration in the tumor metabolism is the Warburg effect, namely the prevalent usage of anaerobic glycolysis to degrade glucose even in the presence of oxygen (76). In such context, Sun and co-authors identified a lactate related signature in renal cell carcinoma (RCC) patients, which can predict overall survival (OS) (77).

In light of the important role of lipids for signaling as well as for membrane formation, Zhu and coauthor analyzed specimens from bladder cancer identifying a gene signature with 11 lipid-related genes that was able not only to stratify patients better than the currently used system based on clinical characteristics, but also to predict response to immunotherapy (78). In cervical cancer, a signature based more specifically on fatty acid metabolism identified high risk patients (79), whereas the sphingolipid metabolism in association with hypoxia stratified patients with pancreatic ductal adenocarcinoma (80).

Amino acids and their metabolism have also been evaluated. In different tumor histotypes, the presence of specific free amino acids in biological fluids can be used as an early diagnostic marker for tumor development as well as for more subtle patients' stratification regarding grading and outcome (81, 82). In ovarian cancer, a score based on the expression of genes associated with the adenosine metabolism was able to identify patients with a shorter survival and with a (predicted) lower sensitivity to different chemotherapeutics (83), while in lung adenocarcinoma, a signature associated with a low glutamine metabolism identified low-risk patients, which respond to immunotherapy (84)

2.6 Microbiome

The studies performed during the last decade demonstrated that the different host-intrinsic microorganisms composing the microbiome are an important component of the human body, which influence many different functions, ranging from the cellular metabolism to the immune response (85). Thus, alterations in the microbiome composition can have consequences on disease development and therapy response. With the widespread implementation of shotgun metagenomics or 16S rRNA sequencing to evaluate the different species composing the microbiota, a huge amount of information on the microbiome of patients with different tumor types and responding or not to different therapies has been generated and investigated for biomarkers, which could be used for patient stratification as well as for possible therapeutic approaches to improve treatment outcomes in cancer (86).

Whereas the first studies analyzed the gut microbiome, which is the most abundant in the host and easy to sample, the focus has now also moved to the investigation of the intra-tumoral microbiota. Indeed, for all the major tumor types, also from soft tissue with no direct contact with the outer world (87), the presence of intra-tumoral bacteria, viruses and archea has been demonstrated, which is different to the corresponding normal tissue microbiome, indicating a "non-random" mechanism of accumulation. Indeed, evaluation of the spatial distribution of the microorganisms within the tumor lesions indicated a specific accumulation into niches enriched of immunosuppressive cells and depleted of T cells, thus underlying an active interaction with the components of the TME (88). Also for the intra-tumoral microbiome, there is a high level of inter-patient heterogeneity (89).

The determination of the composition of the gut microbiota was used for general prognosis as well as for the prediction of patients' responsiveness to systemic therapies, such as chemotherapies and immunotherapy, thereby linking the response to treatment with the presence or absence of different species (90–92). In contrast, the response to local therapy, such as RT, has been associated with the intra-tumoral, but not with the gut microbiome (87)

In some cases, the mechanisms responsible for the correlation with the patients' outcome were also identified. For example, different gamma-proteobacteria strains can protect CRC from gemcitabine chemotherapeutics by directly metabolizing it into its inactive form (93), whereas *Fusobacterium nucleatum* promotes chemo-resistance in this disease by activating the autophagy pathway of tumor cells and thus protecting them from apoptosis induction (94). The opposite mechanism, a reduction of tumor autophagy due to accumulation of reactive oxygen species, is responsible for the protective role of the microbiota metabolite indole-3-acetic acid in pancreatic cancer (95). Instead, the promotion of tumor cell death by pyroptosis is responsible for the enhanced response to immunotherapy of triple negative breast cancer (TNBC) patients with higher intra-tumoral levels of the microbial metabolite trimethylamine N-oxide (96). Another mechanism, by which the microbiota can influence tumor development, is the neoAg presentation via HLA surface antigens.

Indeed, characterization of peptides eluted from melanoma metastasis identified many HLA class I as well as class II epitopes derived from intracellular pathogens, which could also be recognized by the patients´ TIL (97).

In addition to its prognostic and predictive role, the microbiota could also be used therapeutically to improve therapy response via fecal transfer from healthy donors or from patients responding to the same therapy (98).

2.7 Immunomonitoring

Due to the central role of the immune system not only in the natural immune-surveillance against malignant transformation, but also as a target and mode of therapy, a large array of comparison of the immune system in cancer patients versus healthy individuals as well as in responder and non-responder patients was performed using different technologies and different biomaterials. Immune cells have been identified at the protein level by direct staining with Ab using flow cytometry and (multiplex) IHC or identified within bulk transcriptomic data using different algorithms, such as CIBERSORT (99) or directly by scRNAseq.

Screening can be done on both tumor and liquid biopsies. The first has the advantage of representing the site of the disease and thus the presence and location of the immune cells is highly informative. Since it requires surgery, it is mainly used for diagnostic purposes and not for longitudinal evaluation, whereas liquid biopsies, such as blood samples or lavages, are easier to obtain at multiple time points, but only represent the systemic and not the local composition, spatial distribution and status of the immune system.

Initial markers for patients' stratification using tumor tissues were the evaluation of TIL numbers followed by the development of the immunoscore, where the cell subtypes and their broad location (margin versus tumor center) acquired importance (100). With the improvement of multiplex IHC and of software for data analysis, the spatial distance between different cell types (101, 102), their organization in particular cellular neighborhoods (103), TME archetypes (104) or tertiary lymphoid structure (TLS) (105) could be determined and correlated with response to therapy. Since PD-L1 expression within the tumor is not a good predictor for response to ICPi, many evaluations have focused on its receptor. Due to the opposing effects of PD1 signaling in $CD8^+$ effector T cells and in regulatory T cells (Treg), the relative frequency of $CD8^+$ T cells and Treg expressing PD1 within the TME was found to affect response to ICPi (106). Moreover, high levels of $PD1^+$ Treg were correlated with the hyper-progressor phenotype of patients treated with anti-PD1 Ab (107).

Analysis of the immune cell repertoire in peripheral blood by multicolor flow cytometry or mass cytometry (CyTOF) allow to detect the phenotype of effector cells or the presence of immunosuppressive populations as well as their function/activity. Regarding immunosuppressive subsets and their soluble mediators, a score based on the presence of different myeloid cells identifies melanoma patients with a worse prognosis (108), whereas the amount of IL-13 in the sera of patients with diffuse large B cell lymphoma lesions represents a signature of Treg and is associated with a poor OS (109). An enhanced neutrophil to lymphocyte ratio, which since long time is correlated with a worse patients' prognosis (110), is accompanied by a reduced response to anti-PD1 in non-small lung cell cancer (111). Similarly, higher basophil counts in gastric cancer are associated with a low response to anti-PD1 Ab in combination to chemotherapy, but not to chemotherapy alone (112). In contrast, enhanced starting levels of "immunostimulatory" monocytes (113) and a functional $CD4^+$ T cell compartment (114) predict therapy response. In addition to these "baseline" markers, which are needed for initial patient stratification to therapy, there is also the need of markers during treatment that confirm response or indicate the requirement of a therapy change or optimization due to unresponsiveness or resistance development. In addition to blood evaluation at patient´s first presentation for therapy stratification, immunomonitoring can also be performed longitudinally, during therapy, in order to determine responsiveness to the therapy. For example, the presence of proliferating T cells (i.e. expressing Ki-67) is predictive for a good clinical outcome and therapy response in lung cancer patients (115), whereas in melanoma T cell proliferation has to be normalized to the tumor burden in order to significantly discriminate responding patients (116). Similar discrepancies among different tumor types were found regarding the clonality of the immune response, with a more clonal or a more diverse TCR repertoire correlating with response to ICPi in different tumor types (117).

Based on the availability of databases with clinical as well as RNAseq data from cancer patients undergoing immunotherapy with ICPi, many different immune-related genetic signatures have been identified that correlated with the response, such as the T cell-inflamed signature (118), the adaptive immune response associated with a pro-tumorigenic inflammation ratio (119) and an ICPi responsive B cell cluster signature (120). Moreover, additional signatures focusing on all aspects of the TME have been generated for better patients' stratification (121). A different strategy used tumor cells obtained from patients' material co-cultured *in vitro* with limiting dilution of the autologous, *in vitro* expanded TIL in order to identify a "tumor undergoing T cell attack" signature, which included many components involved in IFNγ signaling and allowed the prediction of the clinical outcome to ICPi in multiple tumor types (122).

Biomarkers predicting response to therapy are required also for other immunotherapeutic interventions, such as for example adoptive cell therapy (ACT). Indeed, due to its personalized nature, implementing autologous TIL expanded *in vitro* or the autologous T cells transfected with chimeric antigen receptor (CAR), the therapeutic agent of ACT is a variable on its own, which has to be optimized for optimal usage. To this aim, the final expanded cell products have been characterized in depth and correlated to the patients' outcome in order to identify T cell phenotypes and subpopulations (123–125) or expression pattern (126, 127), which are positively or negatively associated with the clinical response and could thus be implemented to improve the efficacy of future preparations. In line with the longitudinal evaluation of response to ICPi, also blood samples from patients

undergoing ACT have been analyzed to identify (early) predictive markers of response that might allow possible therapy changes or improvement by e.g. implementing combinations with other treatments. Upon CAR T cell transfer, expansion of the injected cells did not correlate with response (128, 129), while enhanced levels of different subsets such as $CD4^+$ and $CD8^+$ CAR cells expressing CD57 and T-bet (129), or $CD4^+$ CAR T cells expressing PD1 and LAG3 as well as lower levels of $CD8^+$ CAR T expressing CD107 (128) did predict response.

3 Patient derived material for therapy selection

Whereas most of the approaches described above aim to identify biomarker(s)/signature(s) able to predict the responsiveness of a tumor specimen to different treatments in order to select the optimal therapy or combination thereof, tumor cells from the patient specimen can also be directly tested *ex vivo* to evaluate or confirm the predicted susceptibility to available treatments. The experimental settings, which have been implemented to study the tumor development and therapy response with established tumor cell lines, have been adapted for the use of patient derived material. In the following paragraphs, we present those different approaches together with their advantages and limitations for the implementation in personalized medicine and provide some examples of their clinical application.

3.1 Culture of tissue slices/pieces

For the development of slice cultures, tumor material derived from surgical resection is directly cut into pieces or slices, which are then cultured in the presence or absence of the different treatments to be evaluated. These include not only chemotherapeutics or targeted drugs, but also immune-based therapies, such as ICPi, since the full cellular repertoire with its local distribution is preserved within the slice for at least a few days up to 2 weeks without undergoing (excessive) spontaneous cell death (130, 131).

This procedure has been successfully applied to tumors from the liver (132), pancreas (133, 134), stomach and gastroesophageal junction (135), lung (130), prostate and bladder (131) and from hepatic metastasis of CRC (136). At different time points, the slices can be evaluated to determine the level of tumor cell death and when immunotherapeutics were applied to investigate the proliferation and/or relocalization of immune cells (130, 132). Despite the short turn-around time required for the read out and the retention of the tumor composition and structure, a strong limitation of this technique is associated to its low throughput, since the number of conditions that can be evaluated is restricted by the size of the resection specimen and thus the amount of slices, which could be generated.

3.2 *In vitro* culture of tissue digested material

In order to obtain a "never ending source" of malignant cells, tumor specimens have been mechanically and enzymatically digested in order to obtain tumor cell lines that could be then tested *in vitro*. Whereas in the last century, pure tumor cell lines have been obtained and used for drug susceptibility screening in 2D monolayer, nowadays the attempt is to grow tumor cells in 3D spheroids, which better resemble the *in vivo* situation with the formation of concentration gradients and the presence of the physical restrain of a solid tumor mass (137). To mimic more the *in vivo* situation, 3D organoids are currently generated, which include tumor cells as well as stromal cells, like cancer associated fibroblasts (CAF), which might be involved in therapy resistance of the tumor *in vivo*. Different protocols have been established for organoid cultures of different tumor histotypes (138), which were also improved to allow high throughput analysis (139–141). Despite such organoids do not retain the immune cell infiltrate, autologous peripheral blood mononuclear cells (PBMC) as well as TIL can be co-cultured with the organoids in order to evaluate responsiveness to different (immuno)therapeutic approaches (142).

Different cases of highly successful selection of therapy upon screening with organoid have been recently reported in patients with ovarian and lung cancer (143, 144).

3.3 Xenograft setting

In order to physiologically reproduce the *in vivo* conditions of tumor growth, human tumors have been transplanted into immune-deficient mice as PDX, which could be evaluated in an *in vivo* setting for susceptibility to chemotherapy. In order to be able to evaluate also immunotherapeutic approaches, new strains of immune-deficient mice have been developed in order to allow a better engraftment of human immune cells, such as hematopoietic $CD34^+$ stem cells (145, 146) and autologous PBMC (147), or to promote the survival of TIL present within the tumor specimen (148).

Despite being highly relevant, these murine models are more prone to be used for mechanistic and functional studies and retrospective analysis to understand why cancer patients are therapy responders or developed resistances than for direct selection of personalized therapy. Indeed, the time length required for their establishment is an obstacle to their implementation for high risk patients and highly aggressive tumors. Despite that, a combination of organoid and PDX was successfully used for personalized therapy selection for a patient with gallbladder cancer (149). Similarly, for a patient with an urothelial bladder cancer with HRAS mutation, a combination of scRNAseq and PDX identified an upregulation of PD-L1 on chemoresistant cells, thus leading to the treatment of this patient with the anti PD-L1 Ab atezolizumab (150).

Zebrafish has mainly been used as a model to study tumor development but is currently also implemented in the context of personalized therapy. It has many advantages over the conventional murine models including a shorter time required for generation of results and of genetically modified species, lower costs and due to the transparency of its cells an easier evaluation of growing tumor cells than in murine models (151). Establishment of a high throughput system to image and quantify tumor growth further amplify the potential usefulness of this model system (152).

Not only solid tumors, such as melanoma (153), BC (154) and gastric cancer (155), but also different hematopoietic malignancies, such as B cell precursor acute lymphoblastic leukemia (156), CML and AML (157), have been successfully transplanted into zebrafish giving rise to zebrafish PDX (zPDX). The system does not only allow evaluation of responsiveness to chemotherapy, but has also been evaluated to test sensitivity to radiotherapy (158) and its possible enhancement by combination with other drugs, such as metformin (159). Moreover, zPDX are also being implemented to evaluate susceptibility to immunotherapy either in the form of CAR T cells (160, 161) or of retargeting bispecific antibodies, which are injected together with autologous PBMC (162). In this context, it is noteworthy that currently two clinical trials in patients with pancreatic ductus adenocarcinoma (PDAC) (163) and CRC (164) are performed using the zPDX setting for the selection of the patients' optimal therapy.

4 Outlook

As described above many progresses have been made in the identification of blood- and tissue-based biomarkers either for patients' stratification to therapy or to determine their responsiveness to it. In addition, new possible therapeutic targets have also been characterized. Despite most of the approaches reported used only one "omic" technique, there is increasing evidence that for the selection of the best possible therapeutic option for each individual patient, multiple features of the tumor have to be evaluated since its development is influenced by genetic, epigenetic and environmental factors. Combination of data from multiple "omics" profile from a single patient will provide powerful tool to generate a holistic view of molecular, metabolic and immunological effects, which can be used to predict response to therapy. Different strategies based on machine learning have been developed during the last years to perform data integration and have recently been reviewed in various articles (165–168). However, it is noteworthy and has to be taken into account that "omics" data are fundamentally different. While genetic variation data are discrete and static, RNAseq measurements, metabolic profiling or immuno-monitoring are continuous, time dependent, but on the other hand could provide longitudinal information.

Despite all these difficulties, preliminary studies have demonstrated the feasibility to integrate data obtained from different techniques in order to identify the best possible therapy for the patients within a clinical timeframe (169).

Author contributions

CM: Writing – original draft, Writing – review & editing. BS: Writing – review & editing.

Funding

The authors declare financial support was received for the research, authorship, and/or publication of this article. This work was supported from Integrate (the German Cancer Aid, grant #70113450 to BS).

Acknowledgments

We would like to thank Maria Heise for excellent secretarial assistance.

Conflict of interest

The authors declare that the research was conducted in the absence of any commercial or financial relationships that could be construed as a potential conflict of interest.

Publisher's note

References

1. Lawrence MS, Stojanov P, Polak P, Kryukov GV, Cibulskis K, Sivachenko A, et al. Mutational heterogeneity in cancer and the search for new cancer-associated genes. *Nat* (2013) 499(7457):214–8. doi: 10.1038/nature12213

2. Vogelstein B, Papadopoulos N, Velculescu VE, Zhou S, Diaz LA Jr., Kinzler KW. Cancer genome landscapes. *Sci* (2013) 339(6127):1546–58. doi: 10.1126/science.1235122

3. Gonzalez-Silva L, Quevedo L, Varela I. Tumor functional heterogeneity unraveled by scRNA-seq technologies. *Trends Cancer* (2020) 6(1):13–9. doi: 10.1016/j.trecan.2019.11.010

4. Tjalsma SJ, de Laat W. Novel orthogonal methods to uncover the complexity and diversity of nuclear architecture. *Curr Opin Genet Dev* (2021) 67:10–7. doi: 10.1016/j.gde.2020.10.002

5. Wang YS, Guo J. Multiplexed single-cell in *situ* RNA profiling. *Front Mol Biosci* (2021) 8:775410. doi: 10.3389/fmolb.2021.775410

6. Hanahan D. Hallmarks of cancer: new dimensions. *Cancer Discovery* (2022) 12 (1):31–46. doi: 10.1158/2159-8290.CD-21-1059

7. Bashyam MD, Animireddy S, Bala P, Naz A, George SA. The Yin and Yang of cancer genes. *Gene* (2019) 704:121–33. doi: 10.1016/j.gene.2019.04.025

8. Zhang Z, Wang ZX, Chen YX, Wu HX, Yin L, Zhao Q, et al. Integrated analysis of single-cell and bulk RNA sequencing data reveals a pan-cancer stemness signature predicting immunotherapy response. *Genome Med* (2022) 14(1):45. doi: 10.1186/s13073-022-01050-w

9. Jerby-Arnon L, Shah P, Cuoco MS, Rodman C, Su MJ, Melms JC, et al. Regev A. *A Cancer Cell Program Promotes T Cell Exclusion Resistance to Checkpoint Blockade Cell* (2018) 175(4):984–97 e24. doi: 10.1016/j.cell.2018.09.006

10. Patel AP, Tirosh I, Trombetta JJ, Shalek AK, Gillespie SM, Wakimoto H, et al. Single-cell RNA-seq highlights intratumoral heterogeneity in primary glioblastoma. *Sci* (2014) 344(6190):1396–401. doi: 10.1126/science.1254257

11. Fischer JR, Jackson HW, de Souza N, Varga Z, Schraml P, Moch H, et al. Multiplex imaging of breast cancer lymph node metastases identifies prognostic single-cell populations independent of clinical classifiers. *Cell Rep Med* (2023) 4(3):100977. doi: 10.1016/j.xcrm.2023.100977

12. Partin A, Brettin TS, Zhu Y, Narykov O, Clyde A, Overbeek J, et al. Deep learning methods for drug response prediction in cancer: Predominant and emerging trends. *Front Med (Lausanne)* (2023) 10:1086097. doi: 10.3389/fmed.2023.1086097

13. Geeleher P, Cox NJ, Huang RS. Clinical drug response can be predicted using baseline gene expression levels and *in vitro* drug sensitivity in cell lines. *Genome Biol* (2014) 15(3):R47. doi: 10.1186/gb-2014-15-3-r47

14. Tognetti M, Gabor A, Yang M, Cappelletti V, Windhager J, Rueda OM, et al. Deciphering the signaling network of breast cancer improves drug sensitivity prediction. *Cell Syst* (2021) 12(5):401–18 e12. doi: 10.1016/j.cels.2021.04.002

15. Xie N, Shen G, Gao W, Huang Z, Huang C, Fu L. Neoantigens: promising targets for cancer therapy. *Signal Transduct Target Ther* (2023) 8(1):9. doi: 10.1038/s41392-022-01270-x

16. Rammensee H, Bachmann J, Emmerich NP, Bachor OA, Stevanovic S. SYFPEITHI: database for MHC ligands and peptide motifs. *Immunogenetics* (1999) 50(3-4):213–9. doi: 10.1007/s002510050595

17. Cai Y, Lv D, Li D, Yin J, Ma Y, Luo Y, et al. IEAtlas: an atlas of HLA-presented immune epitopes derived from non-coding regions. *Nucleic Acids Res* (2023) 51(D1): D409–D17. doi: 10.1093/nar/gkac776

18. Marcu A, Bichmann L, Kuchenbecker L, Kowalewski DJ, Freudenmann LK, Backert L, et al. HLA Ligand Atlas: a benign reference of HLA-presented peptides to improve T-cell-based cancer immunotherapy. *J Immunother Cancer* (2021) 9(4). doi: 10.1136/jitc-2020-002071

19. Boegel S, Castle JC, Kodysh J, O'Donnell T, Rubinsteyn A. Bioinformatic methods for cancer neoantigen prediction. *Prog Mol Biol Transl Sci* (2019) 164:25–60. doi: 10.1016/bs.pmbts.2019.06.016

20. Veatch JR, Lee SM, Fitzgibbon M, Chow IT, Jesernig B, Schmitt T, et al. Tumor-infiltrating BRAFV600E-specific CD4+ T cells correlated with complete clinical response in melanoma. *J Clin Invest* (2018) 128(4):1563–8. doi: 10.1172/JCI98689

21. Linnemann C, van Buuren MM, Bies L, Verdegaal EM, Schotte R, Calis JJ, et al. High-throughput epitope discovery reveals frequent recognition of neo-antigens by CD4+ T cells in human melanoma. *Nat Med* (2015) 21(1):81–5. doi: 10.1038/nm.3773

22. Laumont CM, Perreault C. Exploiting non-canonical translation to identify new targets for T cell-based cancer immunotherapy. *Cell Mol Life Sci* (2018) 75(4):607–21. doi: 10.1007/s00018-017-2628-4

23. Chen B, Khodadoust MS, Olsson N, Wagar LE, Fast E, Liu CL, et al. Predicting HLA class II antigen presentation through integrated deep learning. *Nat Biotechnol* (2019) 37(11):1332–43. doi: 10.1038/s41587-019-0280-2

24. Tan X, Xu L, Jian X, Ouyang J, Hu B, Yang X, et al. PGNneo: A proteogenomics-based neoantigen prediction pipeline in noncoding regions. *Cells* (2023) 12(5):782. doi: 10.3390/cells12050782

25. Reynisson B, Barra C, Kaabinejadian S, Hildebrand WH, Peters B, Nielsen M. Improved prediction of MHC II antigen presentation through integration and motif deconvolution of mass spectrometry MHC eluted ligand data. *J Proteome Res* (2020) 19 (6):2304–15. doi: 10.1021/acs.jproteome.9b00874

26. Cai Y, Chen R, Gao S, Li W, Liu Y, Su G, et al. Artificial intelligence applied in neoantigen identification facilitates personalized cancer immunotherapy. *Front Oncol* (2022) 12:1054231. doi: 10.3389/fonc.2022.1054231

27. Poole A, Karuppiah V, Hartt A, Haidar JN, Moureau S, Dobrzycki T, et al. Therapeutic high affinity T cell receptor targeting a KRAS(G12D) cancer neoantigen. *Nat Commun* (2022) 13(1):5333. doi: 10.1038/s41467-022-32811-1

28. Kim SP, Vale NR, Zacharakis N, Krishna S, Yu Z, Gasmi B, et al. Adoptive cellular therapy with autologous tumor-infiltrating lymphocytes and T-cell receptor-engineered T cells targeting common p53 neoantigens in human solid tumors. *Cancer Immunol Res* (2022) 10(8):932–46. doi: 10.1158/2326-6066.CIR-22-0040

29. Doran SL, Stevanovic S, Adhikary S, Gartner JJ, Jia L, Kwong MLM, et al. T-cell receptor gene therapy for human papillomavirus-associated epithelial cancers: A first-in-human, phase I/II study. *J Clin Oncol* (2019) 37(30):2759–68. doi: 10.1200/JCO.18.02424

30. Niemi JVL, Sokolov AV, Schioth HB. Neoantigen vaccines; clinical trials, classes, indications, adjuvants and combinatorial treatments. *Cancers (Basel)* (2022) 14 (20):5163. doi: 10.3390/cancers14205163

31. Lybaert L, Thielemans K, Feldman SA, van der Burg SH, Bogaert C, Ott PA. Neoantigen-directed therapeutics in the clinic: where are we? *Trends Cancer* (2023) 9 (6):503–19. doi: 10.1016/j.trecan.2023.02.004

32. Xu R, Du S, Zhu J, Meng F, Liu B. Neoantigen-targeted TCR-T cell therapy for solid tumors: How far from clinical application. *Cancer Lett* (2022) 546:215840. doi: 10.1016/j.canlet.2022.215840

33. Kiessling A, Ramanathan K, Nilsson OB, Notari L, Renken S, Kiessling R, et al. Generation of tumor-specific cytotoxic T cells from blood via *in vitro* expansion using autologous dendritic cells pulsed with neoantigen-coupled microbeads. *Front Oncol* (2022) 12:866763. doi: 10.3389/fonc.2022.866763

34. Aguilar-Gurrieri C, Barajas A, Rovirosa C, Ortiz R, Urrea V, de la Iglesia N, et al. Alanine-based spacers promote an efficient antigen processing and presentation in neoantigen polypeptide vaccines. *Cancer Immunol Immunother* (2023) 72(7):2113–2125. doi: 10.1007/s00262-023-03409-3

35. Hanada KI, Zhao C, Gil-Hoyos R, Gartner JJ, Chow-Parmer C, Lowery FJ, et al. A phenotypic signature that identifies neoantigen-reactive T cells in fresh human lung cancers. *Cancer Cell* (2022) 40(5):479–93 e6. doi: 10.1016/j.ccell.2022.03.012

36. Yan H, Bu P. Non-coding RNA in cancer. *Essays Biochem* (2021) 65(4):625–39. doi: 10.1042/EBC20200032

37. Karkkainen E, Heikkinen S, Tengstrom M, Kosma VM, Mannermaa A, Hartikainen JM. Expression profiles of small non-coding RNAs in breast cancer tumors characterize clinicopathological features and show prognostic and predictive potential. *Sci Rep* (2022) 12(1):22614. doi: 10.1038/s41598-022-26954-w

38. Konoshenko MY, Bryzgunova OE, Laktionov PP. miRNAs and radiotherapy response in prostate cancer. *Andrology* (2021) 9(2):529–45. doi: 10.1111/andr.12921

39. Konoshenko M, Lansukhay Y, Krasilnikov S, Laktionov P. MicroRNAs as predictors of lung-cancer resistance and sensitivity to cisplatin. *Int J Mol Sci* (2022) 23(14):7594. doi: 10.3390/ijms23147594

40. Sang L, Yang L, Ge Q, Xie S, Zhou T, Lin A. Subcellular distribution, localization, and function of noncoding RNAs. *Wiley Interdiscip Rev RNA* (2022) 13(6):e1729. doi: 10.1002/wrna.1729

41. Loda A, Collombet S, Heard E. Gene regulation in time and space during X-chromosome inactivation. *Nat Rev Mol Cell Biol* (2022) 23(4):231–49. doi: 10.1038/s41580-021-00438-7

42. Statello L, Guo CJ, Chen LL, Huarte M. Gene regulation by long non-coding RNAs and its biological functions. *Nat Rev Mol Cell Biol* (2021) 22(2):96–118. doi: 10.1038/s41580-020-00315-9

43. Saltarella I, Apollonio B, Lamanuzzi A, Desantis V, Mariggio MA, Desaphy JF, et al. The landscape of lncRNAs in multiple myeloma: implications in the "Hallmarks of cancer", clinical perspectives and therapeutic opportunities. *Cancers (Basel)* (2022) 14(8):1963. doi: 10.3390/cancers14081963

44. Song W, Ren J, Xiang R, Yuan W, Fu T. Cross-Talk Between m(6)A- and m(5)C-Related lncRNAs to Construct a Novel Signature and Predict the Immune Landscape of Colorectal Cancer Patients. *Front Immunol* (2022) 13:740960. doi: 10.3389/fimmu.2022.740960

45. Dai H, Sheng X, Sha R, Peng J, Yang F, Zhou L, et al. Linc00665 can predict the response to cisplatin-paclitaxel neoadjuvant chemotherapy for breast cancer patients. *Front Oncol* (2021) 11:604319. doi: 10.3389/fonc.2021.604319

46. Yu W, Ma Y, Hou W, Wang F, Cheng W, Qiu F, et al. Identification of immune-related lncRNA prognostic signature and molecular subtypes for glioblastoma. *Front Immunol* (2021) 12:706936. doi: 10.3389/fimmu.2021.706936

47. Su M, Xiao Y, Ma J, Tang Y, Tian B, Zhang Y, et al. Circular RNAs in Cancer: emerging functions in hallmarks, stemness, resistance and roles as potential biomarkers. *Mol Cancer* (2019) 18(1):90. doi: 10.1186/s12943-019-1002-6

48. Li L, Liu J, Du J, Jiang H, He H, Lu J, et al. Dysregulated circular RNAs are closely linked to multiple myeloma prognosis, with circ_0026652 predicting bortezomib –based treatment response and survival via the microRNA–608–mediated Wnt/beta –catenin pathway. *Oncol Rep* (2022) 48(5):195. doi: 10.3892/or.2022.8410

49. Wang X, Cao Q, Shi Y, Wu X, Mi Y, Liu K, et al. Identification of low-dose radiation-induced exosomal circ-METRN and miR-4709-3p/GRB14/PDGFRalpha pathway as a key regulatory mechanism in Glioblastoma progression and radioresistance: Functional validation and clinical theranostic significance. *Int J Biol Sci* (2021) 17(4):1061–78. doi: 10.7150/ijbs.57168

50. Huang H, Yan L, Zhong J, Hong L, Zhang N, Luo X. Circ_0025033 deficiency suppresses paclitaxel resistance and Malignant development of paclitaxel-resistant ovarian cancer cells by modulating the miR-532-3p/FOXM1 network. *Immunopharmacol Immunotoxicol* (2022) 44(2):275–86. doi: 10.1080/08923973.2022.2038194

51. Kun-Peng Z, Xiao-Long M, Chun-Lin Z. Overexpressed circPVT1, a potential new circular RNA biomarker, contributes to doxorubicin and cisplatin resistance of osteosarcoma cells by regulating ABCB1. *Int J Biol Sci* (2018) 14(3):321–30. doi: 10.7150/ijbs.24360

52. Li D, Huang Y, Wang G. Circular RNA circPVT1 Contributes to Doxorubicin (DXR) Resistance of Osteosarcoma Cells by Regulating TRIAP1 via miR-137. *BioMed Res Int* (2021) 2021:7463867. doi: 10.1155/2021/7463867

53. Liu YY, Zhang LY, Du WZ. Circular RNA circ-PVT1 contributes to paclitaxel resistance of gastric cancer cells through the regulation of ZEB1 expression by sponging miR-124-3p. *Biosci Rep* (2019) 39(12). doi: 10.1042/BSR20193045

54. Cheng Y, Su Y, Wang S, Liu Y, Jin L, Wan Q, et al. Identification of circRNA-lncRNA-miRNA-mRNA competitive endogenous RNA network as novel prognostic markers for acute myeloid leukemia. *Genes (Basel)* (2020) 11(8):868. doi: 10.3390/genes11080868

55. Zhu WP, He XG, Zhu HX, Wang LR, Lin ZH, Wang M, et al. Identification of miRNAs, mRNAs, lncRNAs, and circRNAs associated with hepatocellular carcinoma recurrence after interferon treatment. *J Biol Regul Homeost Agents* (2021) 35(4). doi: 10.23812/21-173-A

56. Wu Y, Wang L, Wang X, Zhao Y, Mao A, Zhang N, et al. RNA sequencing analysis reveals the competing endogenous RNAs interplay in resected hepatocellular carcinoma patients who received interferon-alpha therapy. *Cancer Cell Int* (2021) 21(1):464. doi: 10.1186/s12935-021-02170-w

57. Chen Q, Tang P, Huang H, Qiu X. Establishment of a circular RNA regulatory stemness-related gene pair signature for predicting prognosis and therapeutic response in colorectal cancer. *Front Immunol* (2022) 13:934124. doi: 10.3389/fimmu.2022.934124

58. Chen M, Zhao H. Next-generation sequencing in liquid biopsy: cancer screening and early detection. *Hum Genomics* (2019) 13(1):34. doi: 10.1186/s40246-019-0220-8

59. Dwedar FI, Shams-Eldin RS, Nayer Mohamed S, Mohammed AF, Gomaa SH. Potential value of circulatory microRNA10b gene expression and its target E-cadherin as a prognostic and metastatic prediction marker for breast cancer. *J Clin Lab Anal* (2021) 35(8):e23887. doi: 10.1002/jcla.23887

60. Guo T, Tang XH, Gao XY, Zhou Y, Jin B, Deng ZQ, et al. A liquid biopsy signature of circulating exosome-derived mRNAs, miRNAs and lncRNAs predict therapeutic efficacy to neoadjuvant chemotherapy in patients with advanced gastric cancer. *Mol Cancer* (2022) 21(1):216. doi: 10.1186/s12943-022-01684-9

61. Yusufova N, Kloetgen A, Teater M, Osunsade A, Camarillo JM, Chin CR, et al. Histone H1 loss drives lymphoma by disrupting 3D chromatin architecture. *Nat* (2021) 589(7841):299–305. doi: 10.1038/s41586-020-3017-y

62. Chu Z, Gu L, Hu Y, Zhang X, Li M, Chen J, et al. STAG2 regulates interferon signaling in melanoma via enhancer loop reprogramming. *Nat Commun* (2022) 13(1):1859. doi: 10.1038/s41467-022-29541-9

63. Johnston MJ, Nikolic A, Ninkovic N, Guilhamon P, Cavalli FMG, Seaman S, et al. High-resolution structural genomics reveals new therapeutic vulnerabilities in glioblastoma. *Genome Res* (2019) 29(8):1211–22. doi: 10.1101/gr.246520.118

64. Zhou Y, Gerrard DL, Wang J, Li T, Yang Y, Fritz AJ, et al. Temporal dynamic reorganization of 3D chromatin architecture in hormone-induced breast cancer and endocrine resistance. *Nat Commun* (2019) 10(1):1522. doi: 10.1038/s41467-019-09320-9

65. Achinger-Kawecka J, Valdes-Mora F, Luu PL, Giles KA, Caldon CE, Qu W, et al. Epigenetic reprogramming at estrogen-receptor binding sites alters 3D chromatin landscape in endocrine-resistant breast cancer. *Nat Commun* (2020) 11(1):320. doi: 10.1038/s41467-019-14098-x

66. Yang Y, Choppavarapu L, Fang K, Naeini AS, Nosirov B, Li J, et al. The 3D genomic landscape of differential response to EGFR/HER2 inhibition in endocrine-resistant breast cancer cells. *Biochim Biophys Acta Gene Regul Mech* (2020) 1863(11):194631. doi: 10.1016/j.bbagrm.2020.194631

67. Fabian-Morales E, Vallejo-Escamilla D, Gudino A, Rodriguez A, Gonzalez-Barrios R, Rodriguez Torres YL, et al. Large-scale topological disruption of chromosome territories 9 and 22 is associated with nonresponse to treatment in CML. *Int J Cancer* (2022) 150(9):1455–70. doi: 10.1002/ijc.33903

68. Li J, Fang K, Choppavarapu L, Yang K, Yang Y, Wang J, et al. Hi-C profiling of cancer spheroids identifies 3D-growth-specific chromatin interactions in breast cancer endocrine resistance. *Clin Epigenetics* (2021) 13(1):175. doi: 10.1186/s13148-021-01167-6

69. Pavlova NN, Zhu J, Thompson CB. The hallmarks of cancer metabolism: Still emerging. *Cell Metab* (2022) 34(3):355–77. doi: 10.1016/j.cmet.2022.01.007

70. Lewis DY, Soloviev D, Brindle KM. Imaging tumor metabolism using positron emission tomography. *Cancer J* (2015) 21(2):129–36. doi: 10.1097/PPO.0000000000000105

71. Ntziachristos V, Pleitez MA, Aime S, Brindle KM. Emerging technologies to image tissue metabolism. *Cell Metab* (2019) 29(3):518–38. doi: 10.1016/j.cmet.2018.09.004

72. Zhang H, Chi M, Su D, Xiong Y, Wei H, Yu Y, et al. A random forest-based metabolic risk model to assess the prognosis and metabolism-related drug targets in ovarian cancer. *Comput Biol Med* (2023) 153:106432. doi: 10.1016/j.compbiomed.2022.106432

73. Li C, Tao Y, Chen Y, Wu Y, He Y, Yin S, et al. Development of a metabolism-related signature for predicting prognosis, immune infiltration and immunotherapy response in breast cancer. *Am J Cancer Res* (2022) 12(12):5440–61.

74. Navas LE, Carnero A. NAD(+) metabolism, stemness, the immune response, and cancer. *Signal Transduct Target Ther* (2021) 6(1):2. doi: 10.1038/s41392-020-00354-w

75. Yang Y, Wang Z, He M, Diao L, Yu B, Li D. NAD+ biosynthesis metabolism predicts prognosis and indicates immune microenvironment for breast cancer. *Pathol Oncol Res* (2023) 29:1610956. doi: 10.3389/pore.2023.1610956

76. Bononi G, Masoni S, Di Bussolo V, Tuccinardi T, Granchi C, Minutolo F. Historical perspective of tumor glycolysis: A century with Otto Warburg. *Semin Cancer Biol* (2022) 86:325–333. doi: 10.1016/j.semcancer.2022.07.003

77. Sun Z, Tao W, Guo X, Jing C, Zhang M, Wang Z, et al. Construction of a lactate-related prognostic signature for predicting prognosis, tumor microenvironment, and immune response in kidney renal clear cell carcinoma. *Front Immunol* (2022) 13:818984. doi: 10.3389/fimmu.2022.818984

78. Zhu K, Xiaoqiang L, Deng W, Wang G, Fu B. Development and validation of a novel lipid metabolism-related gene prognostic signature and candidate drugs for patients with bladder cancer. *Lipids Health Dis* (2021) 20(1):146. doi: 10.1186/s12944-021-01554-1

79. Zhou Y, Zhu J, Gu M, Gu K. Prognosis and characterization of microenvironment in cervical cancer influenced by fatty acid metabolism-related genes. *J Oncol* (2023) 2023:6851036. doi: 10.1155/2023/6851036

80. Li Y, Liang X, Che G, Chen Y, Luo L, Liu K, et al. Molecular classification of genes associated with hypoxic lipid metabolism in pancreatic cancer. *Biomolecules* (2022) 12(10):1533. doi: 10.3390/biom12101533

81. Siminska E, Koba M. Amino acid profiling as a method of discovering biomarkers for early diagnosis of cancer. *Amino Acids* (2016) 48(6):1339–45. doi: 10.1007/s00726-016-2215-2

82. Cadoni G, Giraldi L, Chiarla C, Gervasoni J, Persichilli S, Primiano A, et al. Prognostic role of serum amino acids in head and neck cancer. *Dis Markers* (2020) 2020:2291759. doi: 10.1155/2020/2291759

83. Liang W, Zhou C, Wang J, Zhao J, Liu F, Wang G, et al. A prognostic signature based on adenosine metabolism related genes for ovarian cancer. *Front Oncol* (2022) 12:1003512. doi: 10.3389/fonc.2022.1003512

84. Liu J, Shen H, Gu W, Zheng H, Wang Y, Ma G, et al. Prediction of prognosis, immunogenicity and efficacy of immunotherapy based on glutamine metabolism in lung adenocarcinoma. *Front Immunol* (2022) 13:960738. doi: 10.3389/fimmu.2022.960738

85. Zheng D, Liwinski T, Elinav E. Interaction between microbiota and immunity in health and disease. *Cell Res* (2020) 30(6):492–506. doi: 10.1038/s41422-020-0332-7

86. Park EM, Chelvanambi M, Bhutiani N, Kroemer G, Zitvogel L, Wargo JA. Targeting the gut and tumor microbiota in cancer. *Nat Med* (2022) 28(4):690–703. doi: 10.1038/s41591-022-01779-2

87. Perry LM, Cruz SM, Kleber KT, Judge SJ, Darrow MA, Jones LB, et al. Human soft tissue sarcomas harbor an intratumoral viral microbiome which is linked with natural killer cell infiltrate and prognosis. *J Immunother Cancer* (2023) 11(1). doi: 10.1136/jitc-2021-004285

88. Galeano Nino JL, Wu H, LaCourse KD, Kempchinsky AG, Baryiames A, Barber B, et al. Effect of the intratumoral microbiota on spatial and cellular heterogeneity in cancer. *Nat* (2022) 611(7937):810–7. doi: 10.1038/s41586-022-05435-0

89. Yuan D, Tao Y, Wang H, Wang J, Cao Y, Cao W, et al. A comprehensive analysis of the microbiota composition and host driver gene mutations in colorectal cancer. *Invest New Drugs* (2022) 40(5):884–94. doi: 10.1007/s10637-022-01263-1

90. Derosa L, Routy B, Thomas AM, Iebba V, Zalcman G, Friard S, et al. Intestinal Akkermansia muciniphila predicts clinical response to PD-1 blockade in patients with advanced non-small-cell lung cancer. *Nat Med* (2022) 28(2):315–24. doi: 10.1038/s41591-021-01655-5

91. Matson V, Fessler J, Bao R, Chongsuwat T, Zha Y, Alegre ML, et al. The commensal microbiome is associated with anti-PD-1 efficacy in metastatic melanoma patients. *Sci* (2018) 359(6371):104–8. doi: 10.1126/science.aao3290

92. Yang X, An H, He Y, Fu G, Jiang Z. Comprehensive analysis of microbiota signature across 32 cancer types. *Front Oncol* (2023) 13:1127225. doi: 10.3389/fonc.2023.1127225

93. Geller LT, Barzily-Rokni M, Danino T, Jonas OH, Shental N, Nejman D, et al. Potential role of intratumor bacteria in mediating tumor resistance to the chemotherapeutic drug gemcitabine. *Sci* (2017) 357(6356):1156–60. doi: 10.1126/science.aah5043

94. Yu T, Guo F, Yu Y, Sun T, Ma D, Han J, et al. Fusobacterium nucleatum promotes chemoresistance to colorectal cancer by modulating autophagy. *Cell* (2017) 170(3):548–63 e16. doi: 10.1016/j.cell.2017.07.008

95. Tintelnot J, Xu Y, Lesker TR, Schonlein M, Konczalla L, Giannou AD, et al. Microbiota-derived 3-IAA influences chemotherapy efficacy in pancreatic cancer. *Nat* (2023) 615(7950):168–74. doi: 10.1038/s41586-023-05728-y

96. Wang H, Rong X, Zhao G, Zhou Y, Xiao Y, Ma D, et al. The microbial metabolite trimethylamine N-oxide promotes antitumor immunity in triple-negative breast cancer. *Cell Metab* (2022) 34(4):581–94 e8. doi: 10.1016/j.cmet.2022.02.010

97. Kalaora S, Nagler A, Nejman D, Alon M, Barbolin C, Barnea E, et al. Identification of bacteria-derived HLA-bound peptides in melanoma. *Nat* (2021) 592(7852):138–43. doi: 10.1038/s41586-021-03368-8

98. Daillere R, Derosa L, Bonvalet M, Segata N, Routy B, Gariboldi M, et al. Trial watch: the gut microbiota as a tool to boost the clinical efficacy of anticancer immunotherapy. *Oncoimmunology* (2020) 9(1):1774298. doi: 10.1080/2162402X.2020.1774298

99. Newman AM, Liu CL, Green MR, Gentles AJ, Feng W, Xu Y, et al. Robust enumeration of cell subsets from tissue expression profiles. *Nat Methods* (2015) 12(5):453–7. doi: 10.1038/nmeth.3337

100. Pages F, Kirilovsky A, Mlecnik B, Asslaber M, Tosolini M, Bindea G, et al. *In situ* cytotoxic and memory T cells predict outcome in patients with early-stage colorectal cancer. *J Clin Oncol* (2009) 27(35):5944–51. doi: 10.1200/JCO.2008.19.6147

101. Moldoveanu D, Ramsay L, Lajoie M, Anderson-Trocme L, Lingrand M, Berry D, et al. Spatially mapping the immune landscape of melanoma using imaging mass cytometry. *Sci Immunol* (2022) 7(70):eabi5072. doi: 10.1126/sciimmunol.abi5072

102. Feng Z, Bethmann D, Kappler M, Ballesteros-Merino C, Eckert A, Bell RB, et al. Multiparametric immune profiling in HPV- oral squamous cell cancer. *JCI Insight* (2017) 2(14). doi: 10.1172/jci.insight.93652

103. Schurch CM, Bhate SS, Barlow GL, Phillips DJ, Noti L, Zlobec I, et al. Coordinated cellular neighborhoods orchestrate antitumoral immunity at the colorectal cancer invasive front. *Cell* (2020) 182(5):1341–59 e19. doi: 10.1016/j.cell.2020.07.005

104. Xiao X, Guo Q, Cui C, Lin Y, Zhang L, Ding X, et al. Multiplexed imaging mass cytometry reveals distinct tumor-immune microenvironments linked to immunotherapy responses in melanoma. *Commun Med (Lond)* (2022) 2:131. doi: 10.1038/s43856-022-00197-2

105. Xia J, Xie Z, Niu G, Lu Z, Wang Z, Xing Y, et al. Single-cell landscape and clinical outcomes of infiltrating B cells in colorectal cancer. *Immunology* (2023) 168 (1):135–51. doi: 10.1111/imm.13568

106. Kumagai S, Togashi Y, Kamada T, Sugiyama E, Nishinakamura H, Takeuchi Y, et al. The PD-1 expression balance between effector and regulatory T cells predicts the clinical efficacy of PD-1 blockade therapies. *Nat Immunol* (2020) 21(11):1346–58. doi: 10.1038/s41590-020-0769-3

107. Kamada T, Togashi Y, Tay C, Ha D, Sasaki A, Nakamura Y, et al. PD-1(+) regulatory T cells amplified by PD-1 blockade promote hyperprogression of cancer. *Proc Natl Acad Sci U S A* (2019) 116(20):9999–10008. doi: 10.1073/pnas.1822001116

108. Huber V, Di Guardo L, Lalli L, Giardiello D, Cova A, Squarcina P, et al. Back to simplicity: a four-marker blood cell score to quantify prognostically relevant myeloid cells in melanoma patients. *J Immunother Cancer* (2021) 9(2). doi: 10.1136/jitc-2020-001167

109. Li X, Liu M, Shi Q, Fang Y, Fu D, Shen ZX, et al. Elevated serum IL-13 level is associated with increased Treg cells in tumor microenvironment and disease progression of diffuse large B-cell lymphoma. *Hematol Oncol* (2023) 41(2):230–8. doi: 10.1002/hon.2993

110. Guthrie GJ, Charles KA, Roxburgh CS, Horgan PG, McMillan DC, Clarke SJ. The systemic inflammation-based neutrophil-lymphocyte ratio: experience in patients with cancer. *Crit Rev Oncol Hematol* (2013) 88(1):218–30. doi: 10.1016/j.critrevonc.2013.03.010

111. Alessi JV, Ricciuti B, Alden SL, Bertram AA, Lin JJ, Sakhi M, et al. Low peripheral blood derived neutrophil-to-lymphocyte ratio (dNLR) is associated with increased tumor T-cell infiltration and favorable outcomes to first-line pembrolizumab in non-small cell lung cancer. *J Immunother Cancer* (2021) 9(11). doi: 10.1136/jitc-2021-003536

112. Wu C, Qiu Y, Zhang R, Li X, Liang H, Wang M, et al. Association of peripheral basophils with tumor M2 macrophage infiltration and outcomes of the anti-PD-1 inhibitor plus chemotherapy combination in advanced gastric cancer. *J Transl Med* (2022) 20(1):386. doi: 10.1186/s12967-022-03598-y

113. Krieg C, Nowicka M, Guglietta S, Schindler S, Hartmann FJ, Weber LM, et al. High-dimensional single-cell analysis predicts response to anti-PD-1 immunotherapy. *Nat Med* (2018) 24(2):144–53. doi: 10.1038/nm.4466

114. Zuazo M, Arasanz H, Fernandez-Hinojal G, Garcia-Granda MJ, Gato M, Bocanegra A, et al. Functional systemic CD4 immunity is required for clinical responses to PD-L1/PD-1 blockade therapy. *EMBO Mol Med* (2019) 11(7):e10293. doi: 10.15252/emmm.201910293

115. Kamphorst AO, Pillai RN, Yang S, Nasti TH, Akondy RS, Wieland A, et al. Proliferation of PD-1+ CD8 T cells in peripheral blood after PD-1-targeted therapy in lung cancer patients. *Proc Natl Acad Sci U S A* (2017) 114(19):4993–8. doi: 10.1073/pnas.1705327114

116. Huang AC, Postow MA, Orlowski RJ, Mick R, Bengsch B, Manne S, et al. T-cell invigoration to tumour burden ratio associated with anti-PD-1 response. *Nat* (2017) 545(7652):60–5. doi: 10.1038/nature22079

117. Naidus E, Bouquet J, Oh DY, Looney TJ, Yang H, Fong L, et al. Early changes in the circulating T cells are associated with clinical outcomes after PD-L1 blockade by durvalumab in advanced NSCLC patients. *Cancer Immunol Immunother* (2021) 70 (7):2095–102. doi: 10.1007/s00262-020-02833-z

118. Ayers M, Lunceford J, Nebozhyn M, Murphy E, Loboda A, Kaufman DR, et al. IFN-gamma-related mRNA profile predicts clinical response to PD-1 blockade. *J Clin Invest* (2017) 127(8):2930–40. doi: 10.1172/JCI91190

119. Wang L, Sfakianos JP, Beaumont KG, Akturk G, Horowitz A, Sebra RP, et al. Myeloid cell-associated resistance to PD-1/PD-L1 blockade in urothelial cancer revealed through bulk and single-cell RNA sequencing. *Clin Cancer Res* (2021) 27 (15):4287–300. doi: 10.1158/1078-0432.CCR-20-4574

120. Wu Z, Zhou J, Xiao Y, Ming J, Zhou J, Dong F, et al. CD20(+)CD22(+) ADAM28(+) B cells in tertiary lymphoid structures promote immunotherapy response. *Front Immunol* (2022) 13:865596. doi: 10.3389/fimmu.2022.865596

121. Bagaev A, Kotlov N, Nomie K, Svekolkin V, Gafurov A, Isaeva O, et al. Conserved pan-cancer microenvironment subtypes predict response to immunotherapy. *Cancer Cell* (2021) 39(6):845–65 e7. doi: 10.1016/j.ccell.2021.04.014

122. Gokuldass A, SChina A, Lauss M, Harbst K, Chamberlain CA, Draghi A, et al. Transcriptomic signatures of tumors undergoing T cell attack. *Cancer Immunol Immunother* (2022) 71(3):553–63. doi: 10.1007/s00262-021-03015-1

123. Martinez-Usatorre A, Carmona SJ, Godfroid C, Yacoub Maroun C, Labiano S, Romero P. Enhanced phenotype definition for precision isolation of precursor exhausted tumor-infiltrating CD8 T cells. *Front Immunol* (2020) 11:340. doi: 10.3389/fimmu.2020.00340

124. Deng Q, Han G, Puebla-Osorio N, Ma MCJ, Strati P, Chasen B, et al. Characteristics of anti-CD19 CAR T cell infusion products associated with efficacy and toxicity in patients with large B cell lymphomas. *Nat Med* (2020) 26(12):1878–87. doi: 10.1038/s41591-020-1061-7

125. Krishna S, Lowery FJ, Copeland AR, Bahadiroglu E, Mukherjee R, Jia L, et al. Stem-like CD8 T cells mediate response of adoptive cell immunotherapy against human cancer. *Sci* (2020) 370(6522):1328–34. doi: 10.1126/science.abb9847

126. Galore-Haskel G, Greenberg E, Yahav I, Markovits E, Ortenberg R, Shapira-Fromer R, et al. microRNA expression patterns in tumor infiltrating lymphocytes are strongly associated with response to adoptive cell transfer therapy. *Cancer Immunol Immunother* (2021) 70(6):1541–55. doi: 10.1007/s00262-020-02782-7

127. Lu YC, Jia L, Zheng Z, Tran E, Robbins PF, Rosenberg SA. Single-cell transcriptome analysis reveals gene signatures associated with T-cell persistence following adoptive cell therapy. *Cancer Immunol Res* (2019) 7(11):1824–36. doi: 10.1158/2326-6066.CIR-19-0299

128. Garcia-Calderon CB, Sierro-Martinez B, Garcia-Guerrero E, Sanoja-Flores L, Munoz-Garcia R, Ruiz-Maldonado V, et al. Monitoring of kinetics and exhaustion markers of circulating CAR-T cells as early predictive factors in patients with B-cell Malignancies. *Front Immunol* (2023) 14:1152498. doi: 10.3389/fimmu.2023.1152498

129. Good Z, Spiegel JY, Sahaf B, Malipatlolla MB, Ehlinger ZJ, Kurra S, et al. Post-infusion CAR T(Reg) cells identify patients resistant to CD19-CAR therapy. *Nat Med* (2022) 28(9):1860–71. doi: 10.1038/s41591-022-01960-7

130. Junk D, Kramer S, Broschewitz J, Laura H, Massa C, Moulla Y, et al. Human tissue cultures of lung cancer predict patient susceptibility to immune-checkpoint inhibition. *Cell Death Discovery* (2021) 7(1):264. doi: 10.1038/s41420-021-00651-5

131. van de Merbel AF, van der Horst G, van der Mark MH, van Uhm JIM, van Gennep EJ, Kloen P, et al. An *ex vivo* Tissue Culture Model for the Assessment of Individualized Drug Responses in Prostate and Bladder Cancer. *Front Oncol* (2018) 8:400. doi: 10.3389/fonc.2018.00400

132. Sivakumar R, Chan M, Shin JS, Nishida-Aoki N, Kenerson HL, Elemento O, et al. Organotypic tumor slice cultures provide a versatile platform for immuno-oncology and drug discovery. *Oncoimmunology* (2019) 8(12):e1670019. doi: 10.1080/2162402X.2019.1670019

133. Braun R, Lapshyna O, Eckelmann S, Honselmann K, Bolm L, Ten Winkel M, et al. Organotypic slice cultures as preclinical models of tumor microenvironment in primary pancreatic cancer and metastasis. *J Vis Exp* (2021)(172). doi: 10.3791/62541

134. Jiang X, Seo YD, Chang JH, Coveler A, Nigjeh EN, Pan S, et al. Long-lived pancreatic ductal adenocarcinoma slice cultures enable precise study of the immune microenvironment. *Oncoimmunology* (2017) 6(7):e1333210. doi: 10.1080/2162402X.2017.1333210

135. Husstegge M, Hoang NA, Rebstock J, Monecke A, Gockel I, Weimann A, et al. PD-1 inhibition in patient derived tissue cultures of human gastric and gastroesophageal adenocarcinoma. *Oncoimmunology* (2021) 10(1):1960729. doi: 10.1080/2162402X.2021.1960729

136. Martin SZ, Wagner DC, Horner N, Horst D, Lang H, Tagscherer KE, et al. *Ex vivo* tissue slice culture system to measure drug-response rates of hepatic metastatic colorectal cancer. *BMC Cancer* (2019) 19(1):1030. doi: 10.1186/s12885-019-6270-4

137. Ravi M, Paramesh V, Kaviya SR, Anuradha E, Solomon FD. 3D cell culture systems: advantages and applications. *J Cell Physiol* (2015) 230(1):16–26. doi: 10.1002/jcp.24683

138. Driehuis E, Kretzschmar K, Clevers H. Establishment of patient-derived cancer organoids for drug-screening applications. *Nat Protoc* (2020) 15(10):3380–409. doi: 10.1038/s41596-020-0379-4

139. Li NT, Wu NC, Cao R, Cadavid JL, Latour S, Lu X, et al. An off-the-shelf multi-well scaffold-supported platform for tumour organoid-based tissues. *Biomaterials* (2022) 291:121883. doi: 10.1016/j.biomaterials.2022.121883

140. Boehnke K, Iversen PW, Schumacher D, Lallena MJ, Haro R, Amat J, et al. Assay establishment and validation of a high-throughput screening platform for three-dimensional patient-derived colon cancer organoid cultures. *J Biomol Screen* (2016) 21 (9):931–41. doi: 10.1177/1087057116650965

141. Du Y, Li X, Niu Q, Mo X, Qui M, Ma T, et al. Development of a miniaturized 3D organoid culture platform for ultra-high-throughput screening. *J Mol Cell Biol* (2020) 12(8):630–43. doi: 10.1093/jmcb/mjaa036

142. Magre L, Verstegen MMA, Buschow S, van der Laan LJW, Peppelenbosch M, Desai J. Emerging organoid-immune co-culture models for cancer research: from oncoimmunology to personalized immunotherapies. *J Immunother Cancer* (2023) 11 (5). doi: 10.1136/jitc-2022-006290

143. Gray HJ, Chatterjee P, Rosati R, Appleyard LR, Durenberger GJ, Diaz RL, et al. Extraordinary clinical response to ibrutinib in low-grade ovarian cancer guided by organoid drug testing. *NPJ Precis Oncol* (2023) 7(1):45. doi: 10.1038/s41698-023-00379-8

144. Pan Y, Cui H, Song Y. Organoid drug screening report for a non-small cell lung cancer patient with EGFR gene mutation negativity: A case report and review of the literature. *Front Oncol* (2023) 13:1109274. doi: 10.3389/fonc.2023.1109274

145. Choi B, Lee JS, Kim SJ, Hong D, Park JB, Lee KY. Anti-tumor effects of anti-PD-1 antibody, pembrolizumab, in humanized NSG PDX mice xenografted with dedifferentiated liposarcoma. *Cancer Lett* (2020) 478:56–69. doi: 10.1016/j.canlet.2020.02.042

146. Rosato RR, Davila-Gonzalez D, Choi DS, Qian W, Chen W, Kozielski AJ, et al. Evaluation of anti-PD-1-based therapy against triple-negative breast cancer patient-derived xenograft tumors engrafted in humanized mouse models. *Breast Cancer Res* (2018) 20(1):108. doi: 10.1186/s13058-018-1037-4

147. Suto H, Funakoshi Y, Nagatani Y, Imamura Y, Toyoda M, Kiyota N, et al. Microsatellite instability-high colorectal cancer patient-derived xenograft models for cancer immunity research. *J Cancer Res Ther* (2021) 17(6):1358–69. doi: 10.4103/jcrt.JCRT_1092_20

148. Ny L, Rizzo LY, Belgrano V, Karlsson J, Jespersen H, Carstam L, et al. Supporting clinical decision making in advanced melanoma by preclinical testing in personalized immune-humanized xenograft mouse models. *Ann Oncol* (2020) 31(2):266–73. doi: 10.1016/j.annonc.2019.11.002

149. Tan D, An J, Gong M, Wang H, Li H, Meng H, et al. Screening of an individualized treatment strategy for an advanced gallbladder cancer using patient-derived tumor xenograft and organoid models. *Front Oncol* (2022) 12:1043479. doi: 10.3389/fonc.2022.1043479

150. Lee HW, Chung W, Lee HO, Jeong DE, Jo A, Lim JE, et al. Single-cell RNA sequencing reveals the tumor microenvironment and facilitates strategic choices to circumvent treatment failure in a chemorefractory bladder cancer patient. *Genome Med* (2020) 12(1):47. doi: 10.1186/s13073-020-00741-6

151. Li X, Li M. The application of zebrafish patient-derived xenograft tumor models in the development of antitumor agents. *Med Res Rev* (2023) 43(1):212–36. doi: 10.1002/med.21924

152. Sturtzel C, Grissenberger S, Bozatzi P, Scheuringer E, Wenninger-Weinzierl A, Zajec Z, et al. Refined high-content imaging-based phenotypic drug screening in zebrafish xenografts. *NPJ Precis Oncol* (2023) 7(1):44. doi: 10.1038/s41698-023-00386-9

153. Waster P, Orfanidis K, Eriksson I, Rosdahl I, Seifert O, Ollinger K. UV radiation promotes melanoma dissemination mediated by the sequential reaction axis of cathepsins-TGF-beta1-FAP-alpha. *Br J Cancer* (2017) 117(4):535–44. doi: 10.1038/bjc.2017.182

154. Mercatali L, La Manna F, Groenewoud A, Casadei R, Recine F, Miserocchi G, et al. Development of a patient-derived xenograft (PDX) of breast cancer bone metastasis in a zebrafish model. *Int J Mol Sci* (2016) 17(8):1375. doi: 10.3390/ijms17081375

155. Wu JQ, Zhai J, Li CY, Tan AM, Wei P, Shen LZ, et al. Patient-derived xenograft in zebrafish embryos: a new platform for translational research in gastric cancer. *J Exp Clin Cancer Res* (2017) 36(1):160. doi: 10.1186/s13046-017-0631-0

156. Gauert A, Olk N, Pimentel-Gutierrez H, Astrahantseff K, Jensen LD, Cao Y, et al. Fast, *in vivo* model for drug-response prediction in patients with B-cell precursor acute lymphoblastic leukemia. *Cancers (Basel)* (2020) 12(7):1883. doi: 10.3390/cancers12071883

157. Somasagara RR, Huang X, Xu C, Haider J, Serody JS, Armistead PM, et al. Targeted therapy of human leukemia xenografts in immunodeficient zebrafish. *Sci Rep* (2021) 11(1):5715. doi: 10.1038/s41598-021-85141-5

158. Costa B, Ferreira S, Povoa V, Cardoso MJ, Vieira S, Stroom J, et al. Developments in zebrafish avatars as radiotherapy sensitivity reporters - towards personalized medicine. *EBioMedicine* (2020) 51:102578. doi: 10.1016/j.ebiom.2019.11.039

159. Costa B, Fernandez LM, Pares O, Rio-Tinto R, Santiago I, Castillo-Martin M, et al. Zebrafish Avatars of rectal cancer patients validate the radiosensitive effect of metformin. *Front Oncol* (2022) 12:862889. doi: 10.3389/fonc.2022.862889

160. Pascoal S, Salzer B, Scheuringer E, Wenninger-Weinzierl A, Sturtzel C, Holter W, et al. A preclinical embryonic zebrafish xenograft model to investigate CAR T cells *in vivo*. *Cancers (Basel)* (2020) 12(3):567. doi: 10.3390/cancers12030567

161. Zhou Z, Li J, Hong J, Chen S, Chen M, Wang L, et al. Interleukin-15 and chemokine ligand 19 enhance cytotoxic effects of chimeric antigen receptor T cells using zebrafish xenograft model of gastric cancer. *Front Immunol* (2022) 13:1002361. doi: 10.3389/fimmu.2022.1002361

162. Yan C, Yang Q, Zhang S, Millar DG, Alpert EJ, Do D, et al. Single-cell imaging of T cell immunotherapy responses in *vivo*. *J Exp Med* (2021) 218(10). doi: 10.1084/jem.20210314

163. Usai A, Di Franco G, Piccardi M, Cateni P, Pollina LE, Vivaldi C, et al. Zebrafish patient-derived xenografts identify chemo-response in pancreatic ductal adenocarcinoma patients. *Cancers (Basel)* (2021) 13(16):4131. doi: 10.3390/cancers13164131

164. Di Franco G, Usai A, Piccardi M, Cateni P, Palmeri M, Pollina LE, et al. Zebrafish patient-derived xenograft model to predict treatment outcomes of colorectal cancer patients. *Biomedicines* (2022) 10(7):1474. doi: 10.3390/biomedicines10071474

165. He X, Liu X, Zuo F, Shi H, Jing J. Artificial intelligence-based multi-omics analysis fuels cancer precision medicine. *Semin Cancer Biol* (2023) 88:187–200. doi: 10.1016/j.semcancer.2022.12.009

166. Adossa N, Khan S, Rytkonen KT, Elo LL. Computational strategies for single-cell multi-omics integration. *Comput Struct Biotechnol J* (2021) 19:2588–96. doi: 10.1016/j.csbj.2021.04.060

167. Cai Z, Poulos RC, Liu J, Zhong Q. Machine learning for multi-omics data integration in cancer. *iSci* (2022) 25(2):103798. doi: 10.1016/j.isci.2022.103798

168. Juan H-F, Huang H-C. Quantitative analysis of high-throughput biological data. *WIREs Comput Mol Science* (2023) 13(4):e1658. doi: 10.1002/wcms.1658

169. Irmisch A, Bonilla X, Chevrier S, Lehmann KV, Singer F, Toussaint NC, et al. The Tumor Profiler Study: integrated, multi-omic, functional tumor profiling for clinical decision support. *Cancer Cell* (2021) 39(3):288–93. doi: 10.1016/j.ccell.2021.01.004

Glossary

Adoptive cell therapy	ACT
acute myeloid leukemia	AML
antibody	Ab
breast cancer	BC
cancer associated fibroblast	CAF
chimeric antigen receptor	CAR
circulating free DNA	cfDNA
chronic myeloid leukemia	CML
circular RNA	circRNA
colorectal cancer	CRC
dendritic cell	DC
extracellular vesicle	EV
fluorescence *in situ* hybridization	FISH
immune checkpoint inhibitor	ICPi
interferon	IFN
immunohistochemistry	IHC
lymph node	LN
long non-coding RNA	lncRNA
microRNA	miRNA
multiple myeloma	MM
neoantigen	neoAg
pancreatic ductus adenocarcinoma	PDAC
patient-derived xenograft	PDX
peripheral blood mononuclear cell	PBMC
radiotherapy	RT
renal cell carcinoma	RCC
RNA-binding protein	RBP
single cell RNA sequencing	scRNAseq
T cell receptor	TCR
tertiary lymphoid structure	TLS
triple negative breast cancer	TNBC
tumor infiltrating lymphocyte	TIL
tumor microenvironment	TME
tumor mutational burden	TMB
regulatory T cell	Treg
tyrosine kinase inhibitor	TKI
zebrafish PDX	zPDX

frontiers | Frontiers in Immunology

TYPE Review
PUBLISHED 21 November 2023
DOI 10.3389/fimmu.2023.1292861

OPEN ACCESS

EDITED BY
Patrick Schmidt,
National Center for Tumor Diseases (NCT), Germany

REVIEWED BY
Veronika Vymetalkova,
Institute of Experimental Medicine (ASCR), Czechia
Pasquale Pisapia,
University of Naples Federico II, Italy

*CORRESPONDENCE
Ketao Jin
jinketao2001@zju.edu.cn
Huanrong Lan
lanhr2018@163.com

†These authors have contributed equally to this work

RECEIVED 12 September 2023
ACCEPTED 03 November 2023
PUBLISHED 21 November 2023

CITATION
Yao S, Han Y, Yang M, Jin K and Lan H (2023) Integration of liquid biopsy and immunotherapy: opening a new era in colorectal cancer treatment. *Front. Immunol.* 14:1292861. doi: 10.3389/fimmu.2023.1292861

Integration of liquid biopsy and immunotherapy: opening a new era in colorectal cancer treatment

Shiya Yao[1†], Yuejun Han[1†], Mengxiang Yang[1†], Ketao Jin[1*] and Huanrong Lan[2*]

[1]Department of Colorectal Surgery, Affiliated Jinhua Hospital, Zhejiang University School of Medicine, Jinhua, Zhejiang, China, [2]Department of Surgical Oncology, Hangzhou Cancer Hospital, Hangzhou, Zhejiang, China

Immunotherapy has revolutionized the conventional treatment approaches for colorectal cancer (CRC), offering new therapeutic prospects for patients. Liquid biopsy has shown significant potential in early screening, diagnosis, and postoperative monitoring by analyzing circulating tumor cells (CTC) and circulating tumor DNA (ctDNA). In the era of immunotherapy, liquid biopsy provides additional possibilities for guiding immune-based treatments. Emerging technologies such as mass spectrometry-based detection of neoantigens and flow cytometry-based T cell sorting offer new tools for liquid biopsy, aiming to optimize immune therapy strategies. The integration of liquid biopsy with immunotherapy holds promise for improving treatment outcomes in colorectal cancer patients, enabling breakthroughs in early diagnosis and treatment, and providing patients with more personalized, precise, and effective treatment strategies.

KEYWORDS

liquid biopsy, immunotherapy, circulating tumor DNA (ctDNA), Circulating tumor cells (CTC), colorectal cancer, neoantigen, mass spectrometry, flow cytometry

1 Introduction

Colorectal cancer (CRC) ranks as the second leading cause of cancer-related mortality worldwide (1), with increasing incidence and mortality rates. Most patients with metastatic CRC receive systemic drug therapy, which can prolong survival and improve symptoms but generally falls short of achieving a cure, making long-term survival challenging (2). In recent years, immunotherapy, represented by immune checkpoint inhibitors (ICIs), has revolutionized the traditional treatment approaches for CRC (3–5).

Immunotherapy has emerged as a promising approach for treating various cancers, including CRC. However, a challenge in the field of immunotherapy is the accurate assessment of treatment response and monitoring the effectiveness of immune interventions. Some biomarkers have been identified as predictors of the anti-tumor

efficacy of ICIs, but there remains a need for clinically useful biomarkers. Traditional response assessment criteria, such as tissue biopsies, fail to capture the complex dynamics of the immune system and tumor microenvironment(TME) (6, 7), highlighting the urgent need for novel detection methods to monitor the efficacy of immunotherapy in real time and enable timely treatment adjustments (8–10).

With the rapid advancements in cell isolation and genetic testing technologies, liquid biopsy, which involves minimally invasive acquisition of tumor material, has gained recognition for its importance in precision oncology (11–13). It allows real-time monitoring of tumor progression, recurrence, or treatment response at the molecular level (14, 15). Circulating tumor cells (CTCs) and circulating tumor DNA (ctDNA) have emerged as representative liquid biopsy biomarkers (16).

In this review, we will first discuss the current biomarkers used for immune monitoring in CRC. Secondly, we will analyze the recent research progress in liquid biopsy, specifically focusing on ctDNA and CTCs, as adjuncts for CRC treatment. Finally, we will discuss the potential of novel technologies to address the challenges of immune therapy monitoring by providing solutions for liquid biopsy in the context of adjuvant immunotherapy.

2 Biomarkers currently used for immunotherapy monitoring in CRC

Currently, the treatment modalities for CRC include endoscopic and surgical resection, systemic adjuvant chemotherapy, radiotherapy, targeted therapy, and immunotherapy (1, 17). Over the past five years, the discovery of ICIs and the successful use of ICIs have revolutionized the treatment paradigm for CRC. ICIs have brought new opportunities for the treatment of CRC (18–21). In 2017, the U.S. Food and Drug Administration (FDA) approved the use of immune therapy drugs for the treatment of metastatic colorectal cancer (mCRC) (22–25). Pembrolizumab, an anti- programmed death receptor 1(PD-1) monoclonal antibody, has been established as the first-line treatment standard for microsatellite-high/deficient mismatch repair (MSI-H/dMMR) mCRC (5). Immunotherapy is gradually becoming an essential component of precision treatment for mCRC.

With the continuous development of medical science and technological advancements, biomarkers play an increasingly important role in clinical applications. These biomarkers provide crucial information to assist physicians in the diagnosis, treatment, and monitoring of diseases. Some biomarkers, such as programmed cell death ligand 1 (PD-L1), tumor mutational burden (TMB), and microsatellite stability, have been identified as predictors of the anti-tumor efficacy of ICIs. However, there remains a gap in the clinical demand for effective biomarkers (26).

Microsatellite stability is currently the most relevant biomarker for immunotherapy sensitivity in CRC and is typically evaluated through solid tissue specimens (27, 28). MSI is a condition of genetic instability caused by defects in DNA repair mechanisms and is commonly observed in a subset of CRC patients. However, despite the promising prospects of MSI-H/dMMR as a biomarker for immunotherapy in CRC, there is variability in the reported overall response rates (ORR) in MSI-H mCRC patients, ranging from 30% to 70% (29–32). This suggests that a significant number of MSI-H mCRC patients do not benefit from immunotherapy (33). Conversely, a small subset of microsatellite-stable (MSS) CRC patients exhibit a response to immunotherapy. One contributing factor to this phenomenon is diagnostic errors caused by the detection methods (34).

Currently available methods for detecting microsatellite instability include immunohistochemistry (IHC), polymerase chain reaction (PCR), and next-generation sequencing (NGS). Immunohistochemistry detects the expression of four mismatch repair genes (MLH1, MSH2, MSH6, and PMS2) in the nuclei of tumor cells, and the absence of one or more of these proteins is defined as dMMR, otherwise known as proficient mismatch repair (pMMR) (35). Detection of MSI status is accomplished through immunohistochemistry on tissue specimens, which has the limitations of subjectivity and a lack of uniform standards (36).

TMB is associated with the treatment response to immunotherapy, and elevated plasma TMB levels (≥28 Mut/Mb) have shown predictable responses to the combination therapy of PD-L1 inhibitor durvalumab and CTLA4 inhibitor tremelimumab in MSS CRC patients (37). TMB has been approved by the U.S. FDA as a diagnostic biomarker for the use of pembrolizumab or dostarlimab in cancer immunotherapy (38, 39). Furthermore, studies have shown that high TMB (TMB ≥8 Mut/Mb) in CRC patients is associated with longer overall survival (OS) and better prognosis compared to low TMB (34, 40). However, the use of TMB as a sole predictor of immunotherapy response in CRC remains controversial. Limitations of using TMB as a predictive biomarker for immunotherapy response in CRC were observed in the KEYNOTE 177 trial (41). TMB assessment requires tumor tissue specimens as the gold standard, and tumor heterogeneity poses limitations to its precise estimation (42). Additionally, similar to any other gene or genomic biomarker, TMB may undergo changes in CRC following standard cytotoxic drug treatments (43).

Moreover, PD-L1 expression levels serve as important indicators of the immune status in cancer patients, which reflects the tumor's response to immunotherapy (44–46). In certain solid tumors such as non-small cell lung cancer, melanoma, and renal cell carcinoma, PD-L1 expression has been proposed as a predictive biomarker for immunotherapy response (47–49). High PD-L1 expression is associated with a better response to immunotherapy. Tumor cells induce immune evasion by upregulating the expression of PD-L1, which binds to PD-1 on the surface of T cells, leading to T cell inactivation (Figure 1). ICIs block the interaction between PD-1 and PD-L1, thereby reactivating the body's anti-tumor immune response (47). CRC patients have been reported to exhibit positive PD-L1 expression (50, 51). Although high PD-L1 expression is associated with a favorable prognosis in CRC patients (52–54), current clinical data suggest that the use of PD-L1 expression alone cannot accurately predict the immunotherapy response in CRC (55).

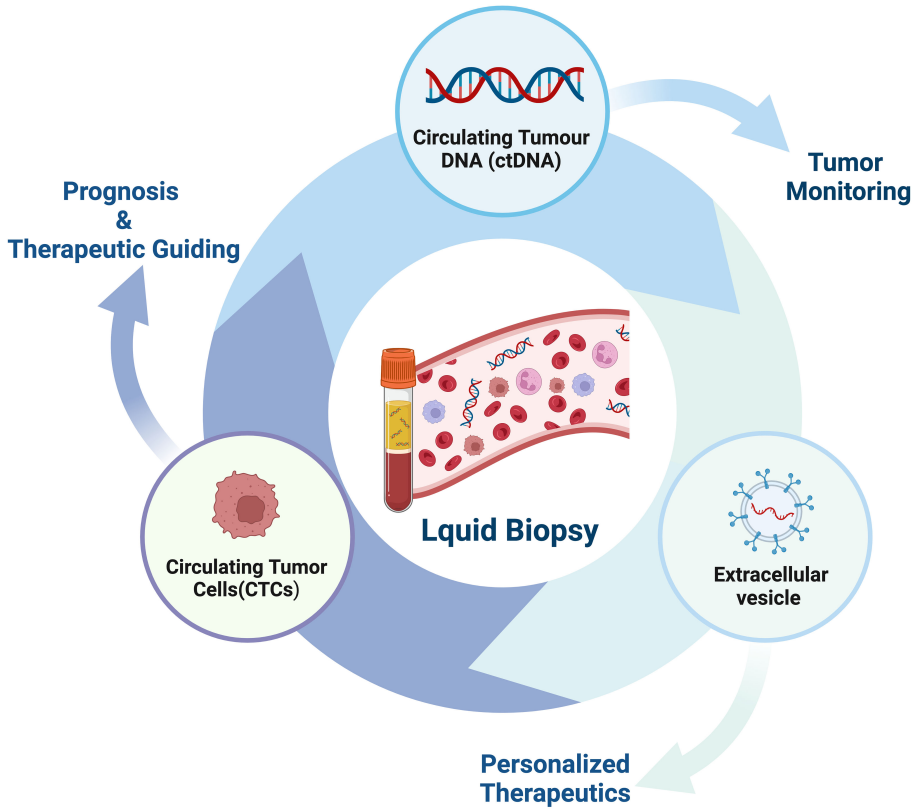

FIGURE 1
Programmed cell death protein 1 (PD-1) plays a crucial role in the initiation and effector phases of the anti-tumor immune response. T cell activation is a fundamental process in immune response, involving antigen presentation by dendritic cells and recognition by the T cell receptor (TCR). Once activated, T cells migrate to the tumor site to eliminate malignant cells. However, the tumor or bystander cells such as macrophages may upregulate PD-L1, which hinders T cell function by inducing inhibitory intracellular signaling.

However, despite the widespread application of certain biomarkers, we still face various challenges and limitations. To overcome these limitations, researchers are actively searching for more suitable detection methods and therapies to enhance the reliability and effectiveness of biomarkers in clinical practice. Through continuous exploration and innovation, we hope to open up new fields and approaches that will bring greater breakthroughs in disease prevention, diagnosis, and treatment. Therefore, the quest for more accurate and reliable biomarkers has become a hot topic in medical research, offering new opportunities and hopes for improving patient health outcomes.

3 Application of liquid biopsy in adjuvant therapy for CRC

Liquid biopsy has opened up a new avenue for cancer patients in terms of prognostic evaluation, detection of minimal residual disease (MRD), treatment selection, resistance mechanisms and monitoring, as well as early cancer diagnosis (56–61) (Figure 2). The fundamental principle of liquid biopsy is the non-invasive detection and assessment of tumors using circulating cell-free DNA (cfDNA), RNA, or tumor cells present in bodily fluids such as blood, urine, and cerebrospinal fluid (62–66). CTCs and ctDNA are important components and are generally considered the foundation of liquid biopsy. ctDNA is formed by apoptotic and necrotic tumor cells, which release fragmented DNA into the bloodstream and harbor genetic alterations of the original tumor cells (67, 68). CTCs are cancer cells that spontaneously detach from primary or metastatic tumors and circulate in the bloodstream (69). They serve as “seeds” of the tumor and can contribute to recurrence through liver metastasis, lymphatic dissemination, and angiogenesis (Figure 3).

Certain characteristics of CTCs, such as the expression of surface markers or genetic mutations, are associated with the prognosis of cancer patients. Changes in CTC counts are correlated with shortened disease-free survival (DFS), progression-free survival (PFS) and OS (70, 71). Increased levels of ctDNA may indicate disease progression (72, 73). By regularly monitoring changes in CTCs and ctDNA, the effectiveness of treatment and the dynamic changes of the tumor can be assessed (59).

MRD refers to the presence of extremely low levels of cancer cells or cancer-associated genetic material after completion of treatment (74). Early detection of MRD can be achieved through the detection of CTCs and ctDNA (75–77). According to the latest results from the GALAXY observational study presented at the 2023 ASCO conference, the detection of MRD through ctDNA testing at

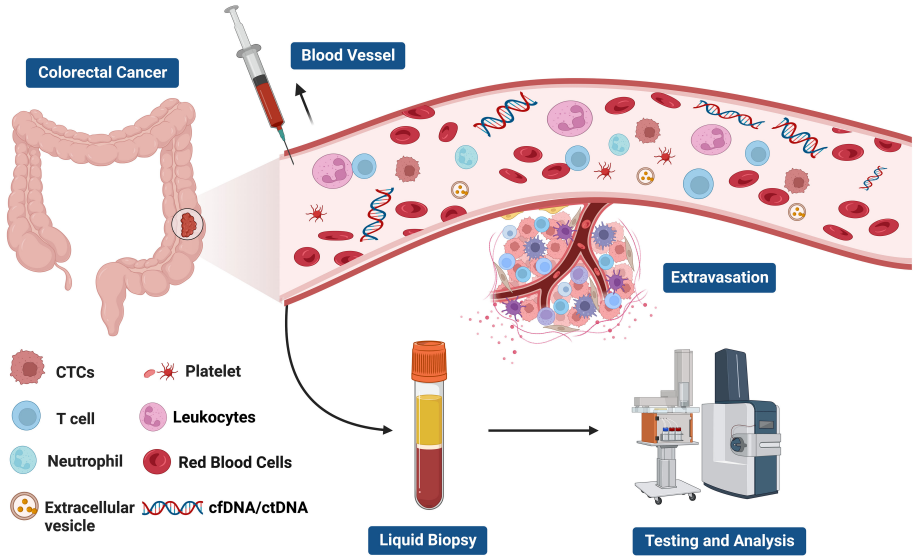

FIGURE 2
The current clinical applications of liquid biopsy. Liquid biopsy provides a non-invasive approach to assess the dynamic changes and treatment response of tumors by analyzing components such as circulating tumor DNA (ctDNA), circulating tumor cells (CTCs), and extracellular vesicles. These components can be obtained from blood samples and detected using highly sensitive analytical techniques. The information derived from liquid biopsy aids in guiding personalized treatment strategies, including the selection of appropriate drugs, monitoring treatment efficacy, and providing treatment guidance. Liquid biopsy holds promising applications in tumor management, offering patients more accurate and effective treatment choices.

4 weeks post-surgery is the strongest prognostic risk factor for DFS in stage II to IV CRC patients, regardless of BRAF ^{V600E} or MSI status (78, 79).

In early-stage CRC patients, the presence of ctDNA positivity after curative surgery is associated with a higher risk of disease recurrence (74, 80–85). A study demonstrated that ctDNA positivity after adjuvant chemotherapy is associated with poorer DFS, and ctDNA detection precedes radiological relapse by a median of 11.5 months (86). The DYNAMIC trial (87) investigated whether a ctDNA-guided approach could reduce the use of adjuvant therapy without compromising the risk of recurrence compared to the standard approach in stage II CRC. Among the 455 randomly assigned patients, 302 were assigned to the ctDNA-guided management group, and 153 were assigned to the standard management group. The median follow-up time was 37 months. The proportion of patients receiving adjuvant chemotherapy was lower in the ctDNA-guided group compared to the standard management group (15% vs. 28%). The ctDNA-

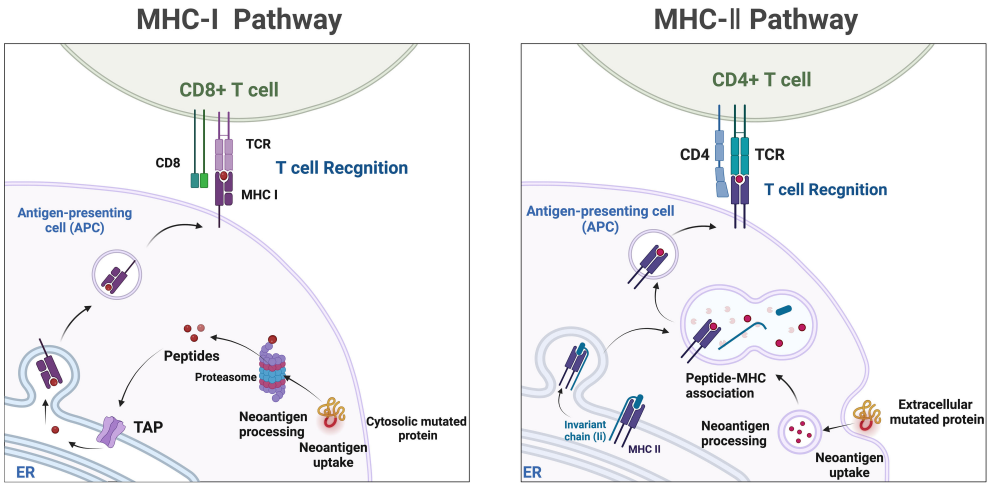

FIGURE 3
The components of liquid biopsy in colorectal cancer(CRC). circulating tumor cells (CTCs) and Circulating tumor DNA (ctDNA) are the main constituents of current liquid biopsy approaches. ctDNA, extracellular vesicle, and CTCs are shed directly from tumor masses or metastatic lesions into the bloodstream. After collection of blood samples, further analysis of these components provides a comprehensive tumor characterization.

guided management was non-inferior to standard management in terms of 2-year disease-free survival rates (93.5% vs. 92.4%). The 3-year disease-free survival rate was 86.4% in ctDNA-positive patients receiving adjuvant chemotherapy and 92.5% in ctDNA-negative patients not receiving adjuvant chemotherapy. The ctDNA-guided approach can reduce the use of adjuvant chemotherapy without compromising disease-free survival in the treatment of stage II CRC. In various cohorts of non-mCRC and resected colorectal liver metastasis patients, the proportion of disease recurrence has consistently exceeded 80% in patients with detectable ctDNA who did not receive adjuvant therapy (74, 88, 89). A study (90) demonstrated that preoperative ctDNA could be detected in 108 out of 122 (88.5%) patients with stage I to III CRC. Longitudinal ctDNA analysis identified 14 out of 16 (87.5%) recurrences after definitive treatment. Furthermore, at postoperative day 30, ctDNA-positive patients were more likely to experience recurrence compared to ctDNA-negative patients. Another study (91) evaluated the prognostic impact of postoperative ctDNA in stage I-III CRC patients and found that ctDNA status was the most significant and independent factor in predicting recurrence-free survival (RFS). Postoperative plasma samples from 108 patients underwent NGS quality control, with 17 (15.7%) classified as ctDNA-positive and 91 classified as ctDNA-negative. Among these 17 ctDNA-positive patients, 2 were stage II, and 15 were stage III. The recurrence rate for ctDNA-positive patients was 76.5% (13/17), significantly higher than the 16.5% (15/91) in ctDNA-negative patients. Kaplan-Meier survival curves showed significantly poorer recurrence-free survival (RFS) for ctDNA-positive patients compared to ctDNA-negative patients. The study results also demonstrated a sensitivity of 49.6% and specificity of 94.7% for ctDNA alone in predicting 2-year RFS. A predictive model combining ctDNA with clinical-pathological risk factors, referred to as CTCP prediction model, exhibited better RFS predictive value than ctDNA alone in stage I-III CRC patients and increased the sensitivity for 2-year RFS to 87.5%. The predictive value of this model was also externally validated. Additionally, ctDNA can be utilized for monitoring locally advanced rectal cancer (LARC) patients who achieve complete response after neoadjuvant therapy and adopt an "watch-and-wait" strategy (92, 93).

Precision therapy involves customizing drug treatments based on the individual characteristics of tumors (94). Liquid biopsy provides molecular profiling information of tumors, such as gene mutations and chromosomal rearrangements, to select appropriate targeted therapy drugs. In CRC, analysis of the molecular features of individual CTCs has revealed significant heterogeneity in the presence of EGFR mutations and other genetic mutations associated with EGFR inhibition (such as KRAS and PIK3CA mutations) among patients and between patients, which explains the different response rates to EGFR-targeted therapy (95). By analyzing mutations in ctDNA, patients who may benefit from targeted EGFR therapy or BRAF and MEK inhibitors can be identified (96–98). In ctDNA-positive CRC patients, plasma testing for RAS status demonstrated a sensitivity of 92.9% and specificity of 87.7% (99). The CHRONOS trial confirmed the importance of evaluating RAS status using ctDNA in metastatic CRC patients (100, 101). The study found that patients who were mutation-negative in ctDNA had good clinical responses to anti-EGFR retreatment. An ongoing randomized Phase III trial (102) is expected to reveal that liquid biopsy-based retreatment with anti-EGFR monoclonal antibodies achieves approximately one-third objective responses in mCRC patients, prospectively demonstrating the effective management of patients through genetic profiling using liquid biopsy.

Similar to predicting response to chemotherapy and/or targeted therapy, liquid biopsy based on ctDNA can guide immunotherapy. While immune therapy has prolonged PFS in patients with MSI-H CRC, it is interesting to note that in the KEYNOTE-177 study, approximately 30% of patients showed no response to pembrolizumab (32). Using ctDNA monitoring to identify non-responders at an early stage can provide an opportunity for physicians to switch to chemotherapy or consider the addition of anti-CTLA-4 agents (103). The mutational burden in ctDNA is associated with the efficacy of immunotherapy and serves as a direct reflection of tumor burden (104–110). Liquid biopsy utilizes ctDNA released into the bloodstream, providing a non-invasive alternative. However, similar to TMB, the MSI status is also influenced by spatial and temporal heterogeneity, making it challenging to monitor its therapeutic value through liquid biopsy (111). A study used liquid biopsy to detect the MSI status in ctDNA and found a high concordance with results from traditional tissue biopsy, effectively predicting immunotherapy sensitivity and clinical outcomes in patients (112). Another study demonstrated that liquid biopsy could monitor changes in MSI status at different time points, providing important information on treatment response and disease progression in patients (74). Furthermore, recent studies have proposed that the concentration of cfDNA can serve as a predictive biomarker for immune therapy response (113–116). cfDNA can be detected in MSI-H CRC patients who respond well to immunotherapy (117, 118). Moreover, dynamic changes in ctDNA have been shown to predict the efficacy of other immunotherapies, including chimeric antigen receptor T-cell (CAR-T) therapy (119, 120). Analysis of tumor-derived structural alterations through shallow whole-genome sequencing revealed a decrease in ctDNA levels in patients who responded well to CAR-T cell therapy, while an increase was observed in patients who did not achieve a treatment response. The abundance of CAR-T cell construct-derived DNA in peripheral blood may be correlated with the dynamic changes in ctDNA and can be used in combination (121).

Several clinical trials focusing on liquid biopsy in the context of immunotherapy are currently underway. The ongoing ARETHUSA trial (NCT03519412) is investigating the use of ctDNA-based TMB assessment as a predictive marker for immunotherapy response following pretreatment with temozolomide in MGMT-methylated mCRC (122). It is worth noting that there are ongoing efforts to identify the optimal approach for TMB analysis (123). The use of ctDNA for predicting response to immunotherapy has shown promise in the INSPIRE study, a prospective Phase II trial that conducted serial ctDNA assessments in 94 patients with advanced solid tumors receiving pembrolizumab (124). It was found that in 42% of patients, an increase in ctDNA and tumor volume was observed at 6 weeks, accurately predicting lack of response with

100% specificity. During immunotherapy, 16% of patients exhibited ctDNA clearance, with a median follow-up exceeding 25 months and an OS of 100%. At the start of the third treatment cycle, 98% of patients had an increase in ctDNA, indicating lack of objective response. This may enable the avoidance of ineffective treatment in a subset of patients. Zhang et al. characterized the prognostic and predictive impact of ctDNA in patients with 16 different solid tumor types enrolled in Phase I/II trials of single-agent durvalumab or combination therapy with tremelimumab (125). Higher pretreatment variant allele frequency (VAF) was associated with poorer survival but not with ORR. In contrast, reductions in VAF during treatment were associated with prolonged PFS, OS, and ORR, suggesting the predictive benefit of ctDNA during the treatment course. In ongoing clinical trials across various tumor types, including CRC, the dynamics of ctDNA, as measured by changes in VAF percentage and/or ctDNA clearance, have emerged as important biomarkers.

The application of liquid biopsy-guided adjuvant therapy for CRC is still in the research stage and requires further clinical validation and optimization. However, it has the advantages of non-invasiveness, repeatability, and real-time monitoring, and is expected to become one of the important auxiliary tools for personalized treatment of CRC.

4 Opportunities and breakthroughs of liquid biopsy in the era of immunotherapy

Significant progress has been made in the study of CTCs and ctDNA using traditional liquid biopsy methods, which have played a powerful auxiliary role in tumor treatment (126–128). Immunotherapy has shown remarkable efficacy in various types of cancer, but it may impact the results of liquid biopsy. Therefore, it is necessary to reassess the traditional liquid biopsy criteria to accommodate the needs of immunotherapy (129, 130). Emerging detection technologies have provided support for liquid biopsy in optimizing treatment strategies, thus contributing to further advancements in the field of immunotherapy.

4.1 T Cell sorting: liquid detection based on flow cytometry

T-cell subset isolation is a method used to separate and purify T cells from a mixed population of cells. Flow cytometry can analyze various indicators such as T-cell subgroups, functional status, and expression of immune checkpoint molecules in blood samples. It can aid in evaluating a patient's immune status and predicting the response to immune therapy (131–135).

The peripheral blood TCR repertoire serves as an important biomarker for the selection of ICIs therapy (136). TCR sequencing enables the study of the immune response mechanism of T cells. Longitudinal monitoring of the dynamic therapeutic evaluation of the TCR repertoire in ctDNA in peripheral blood provides insights into the co-evolution of tumors and immune components during ICIs treatment. TCR repertoire diversity, early conversion of peripheral T cells, and overall remodeling of the T-cell repertoire are associated with clonal regulation during ICIs treatment and are linked to anti-tumor immune responses. The presence of persistently exhausted TCR clones in peripheral blood is associated with adverse reactions to immune therapy (137–142). By combining flow cytometry and gene sequencing techniques, TCR sequences can be rapidly and accurately detected to understand T-cell clonal expansion and diversity.

Peripheral blood immune cell biomarkers, as one of the easily accessible biomarkers, can assess treatment response in the early stages and facilitate adjustments in early management (143–145). Studies have shown that the quantity and function of Tregs cells change in patients receiving immune therapy and are associated with poor prognosis (146–150). Studies using flow cytometry and RNA analysis have found that the percentage of circulating CD4+ and CD8+ T cells is associated with inflammatory tumors, indicating the significant role of these biomarkers in anti-tumor responses (151). Additionally, circulating T-cell lymphocyte subpopulations have been identified as biomarkers for mCRC (152). Decreased proportions of CD4+ cells and Tregs during treatment with folinic acid, 5-fluorouracil, and irinotecan (FOLFIRI) plus bevacizumab are associated with improved survival rates (153). Systemic immune inflammation index, ratios of different immune cells, and ratios of immune cells to platelets are also biomarkers for prognosis and prediction in CRC patients, including platelet-to-lymphocyte ratio (PLR) and neutrophil-to-lymphocyte ratio (NLR) (154–156). Recent studies have discovered novel circulating non-tumor cells and their biomarkers and extracellular matrix components, which have clinical application value in diagnosis, prognosis, and treatment response (157). Some studies suggest that circulating tumor endothelial cells (CTECs) from the tumor may play a prognostic role in CRC, with higher predictive value than CTCs (158–160). Similarly, in patients with mCRC receiving treatment with bevacizumab and chemotherapy, CECs and CD276-positive CTECs based on flow cytometry significantly increase (161). Studies have also shown that CXCR4-positive CECs are associated with longer PFS and OS, providing predictive value for mCRC patients receiving bevacizumab treatment (162–164).

Furthermore, single-cell sequencing technology (scRNA-seq) allows the study of gene expression and genetic variations at the individual cell level (165). The first immunotranscriptomic study based on scRNA-seq was conducted on CD4+ T cells infiltrating CRC. In this study, the impact of the tumor immune microenvironment (TIME) on specific gene expression (LAYN, MAGEH1, and CCR8) in tumor-infiltrating Tregs cells was confirmed, and these gene expressions were found to be correlated with immune therapy response, tumor-suppressive activity, and prognosis (166).

The gene characteristics of peripheral blood immune cells have received attention in the field of immune therapy and precision medicine. By combining T-cell subset isolation and liquid biopsy, comprehensive monitoring tools for immune therapy can be obtained, leading to a better understanding of tumor immune response and treatment outcomes, as well as optimization of treatment strategies.

4.2 Mass spectrometry techniques: unveiling the immunotherapeutic potential of neoantigens and non-mutated neoantigens

Mass spectrometry-based liquid-phase detection is a novel technique that allows for the molecular-level monitoring of chemical components within cells and organisms, providing deeper insights into biological information. Neoantigens are novel antigenic epitopes generated by genetic mutations and serve as important targets in personalized immunotherapy (129). Neoantigens can be produced through proteasome-mediated endogenous protein degradation, and the resulting mutated peptides are subsequently transported to the endoplasmic reticulum (ER) via antigen processing-associated transporter (TAP), where they may be loaded onto MHC-I. MHC-II dimers assemble in the ER and associate with the invariant chain (Ii). The Ii-MHC-II complex can be transported directly from the cell surface or, at times, indirectly endocytosed into the MHC-II compartment (MIIC). Within the MIIC, a series of endolysosomal proteases degrade Ii, releasing it and enabling MHC-II to bind specific peptide segments derived from mutated proteins within the endocytic pathway. These peptide-MHC (pMHC) complexes are subsequently transported to the cell surface, where they are recognized by T cells (167) (Figure 4). Neoantigens possess potential high specificity and targeting, but they are predominantly patient-specific, making it challenging to categorize their utility, and they are often prominent in cancer patient populations. Currently, immune therapies, ICIs, tumor-specific vaccines, and neoantigen-based tumor-infiltrating lymphocytes (TILs) play increasingly important roles in cancer treatment (168). Studies have observed that certain CRC patients with MSI-H may benefit from ICIs treatment due to the presence of neoantigens (169). One of the main obstacles faced in personalized neoantigen immunotherapy is the accessibility of tumor biopsies. Thus far, the identification of neoantigens has typically involved genomic analysis of various tumor biopsies (170). Although this approach is time-consuming, invasive, and has a low positivity rate, it is more common in challenging cases requiring repeated sampling or when samples are limited, particularly in cases of frequent occurrence and metastatic cancers. Specifically, the presence of natural neoantigens at the top of immune checkpoints can enhance the effectiveness of significant inhibitors (171, 172). Given the current situation, liquid biopsies can serve as a viable alternative approach to identify potential neoantigens as immune therapeutic targets, applicable to numerous cancers. Although the limitations of detecting genomic mutations in plasma samples lie in detecting low allele frequencies, the reliability of genetic information obtained from liquid biopsies has been demonstrated (173). Therefore, based on current research on liquid biopsies, valuable insights can be provided for the use of neoantigens in treatment selection. Mass spectrometry-based liquid-phase detection allows for efficient identification and quantification of protein compositions within tumor cells, enabling the discovery of novel tumor-specific antigens by monitoring neoantigens in serum (174). Neoantigen-based immunotherapeutic approaches, such as ICIs, tumor-specific vaccines, and TILs, have become increasingly important in cancer treatment (168). Not all MSI-H CRC patients benefit from ICIs treatment; however, certain MSI-H colorectal cancer patients may benefit from ICIs treatment due to the presence of highly immunogenic neoantigens (169, 173).

Non-mutated neoantigens (NM-neoAgs) are immunogenic protein fragments generated through translational modifications or protein degradation of apoptotic tumor cells (175–181). These unique fragments do not exist in normal cells and are more easily processed and cross-presented by antigen-presenting cells (182). Studies utilizing mass spectrometry techniques and memory T cells as probes have identified NM-neoAgs in serum and found a strong correlation between high levels of NM-neoAgs and the efficacy of immunotherapy. Following induction chemotherapy, the response of NM-neoAgs-specific effector T cells (CD4+ and CD8+ T cells) increases and is further enhanced after immunotherapy, closely associated with patients' survival rates and decreased expression levels of PD-1 (182). NM-neoAgs can target tumors with lower mutational burdens, contributing to the development of effective T cell-based immunotherapies for various cancer patients (182), and expanding the potential targets of liquid biopsy.

In summary, neoantigens and NM-neoAgs are tumor cell-specific antigens with tremendous potential in personalized immunotherapy. New detection methods such as flow cytometry and mass spectrometry techniques provide powerful tools for evaluating the efficacy of immunotherapy, thereby offering more effective treatment strategies for patients.

5 Conclusion

Liquid biopsy, as a non-invasive detection method, has emerged as a promising approach for early screening, diagnosis, postoperative monitoring, treatment response assessment, and evaluation of tumor resistance (183). With advancements in mass spectrometry-based detection of neoantigens and T cell sorting techniques such as flow cytometry, liquid biopsy has gained support as an adjunctive tool in the field of immunotherapy, providing opportunities for optimizing treatment strategies. However, despite significant progress, liquid biopsy remains in the exploratory and developmental stage, facing various challenges and complexities.

These include issues including the typically low concentrations of analytes collected from samples (184, 185), lack of standardization and uniformity for liquid biopsy biomarkers, and a dearth of widely accepted clinical practice guidelines (186, 187),related to false-positive results (188), variations in sensitivity among studies (82, 189), limitations in detection sensitivity and specificity (186, 190), and susceptibility to interference (184, 189, 191, 192). Overcoming these challenges and advancing liquid biopsy requires the development of highly sensitive and specific detection methods, standardization of experimental procedures and validation methods, and the application of artificial intelligence and machine learning algorithms for data analysis and interpretation. Additionally, the exploration of new biomarkers and the conduct of large-scale multicenter studies and clinical trials are essential to enhance the accuracy of early diagnosis and treatment prediction (193–196).

Despite the challenges that remain, the potential of liquid biopsy-assisted immunotherapy in transforming the field of immunotherapy

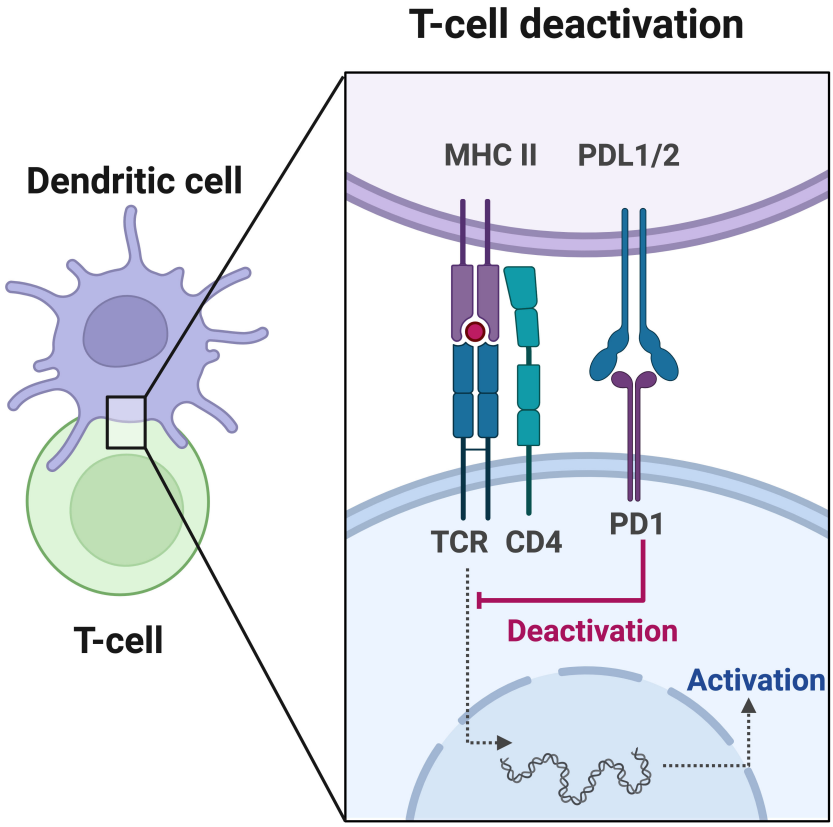

FIGURE 4
Neoantigens, which are mutated peptides generated through proteasome-mediated endogenous protein degradation, can subsequently be transported to the endoplasmic reticulum (ER) via antigen processing-associated transporter (TAP) and may be loaded onto MHC-I. In the ER, MHC-II dimers assemble and associate with the invariant chain (Ii). The Ii-MHC-II complex can be transported directly from the cell surface or, in some cases, indirectly endocytosed into the MHC-II compartment (MIIC). Within the MIIC, a series of endolysosomal proteases degrade Ii, releasing it and enabling MHC-II to bind specific peptide segments derived from mutated proteins within the endocytic pathway. These pMHC complexes are subsequently transported to the cell surface, where they are recognized by T cells.

is undeniable. Looking ahead, in the era of immunotherapy, liquid biopsy-assisted immunotherapy has the potential to fundamentally change the field and provide patients with more precise, effective, and personalized treatment strategies. Continued research, clinical trials, and technological advancements will play a crucial role in fully harnessing liquid biopsy as a valuable tool for guiding immunotherapy and improving future patient outcomes.

Author contributions

SY: Conceptualization, Data curation, Formal analysis, Writing – original draft. YH: Investigation, Methodology, Writing – review & editing. MY: Resources, Software, Writing – original draft. KJ: Conceptualization, Data curation, Writing – original draft, Writing – review & editing. HL: Investigation, Software, Validation, Writing – review & editing.

Funding

The author(s) declare financial support was received for the research, authorship, and/or publication of this article. This work was supported by National Natural Science Foundation of China [grant no. 82104445 to HRL], Zhejiang Provincial Science and Technology Projects (grant no. LGF22H160046 to HRL), Jinhua Municipal Science and Technology Projects (grants no. 2021-3-040 to KTJ, and 2021-3-046 to HRL).

Conflict of interest

The authors declare that the research was conducted in the absence of any commercial or financial relationships that could be construed as a potential conflict of interest.

Publisher's note

References

1. Sung H, Ferlay J, Siegel RL, Laversanne M, Soerjomataram I, Jemal A, et al. Global cancer statistics 2020: GLOBOCAN estimates of incidence and mortality worldwide for 36 cancers in 185 countries. *CA Cancer J Clin* (2021) 71:209–49. doi: 10.3322/caac.21660

2. Pitroda SP, Chmura SJ, Weichselbaum RR. Integration of radiotherapy and immunotherapy for treatment of oligometastases. *Lancet Oncol* (2019) 20:e434–42. doi: 10.1016/s1470-2045(19)30157-3

3. Schmidt C. The benefits of immunotherapy combinations. *Nature* (2017) 552: S67–s69. doi: 10.1038/d41586-017-08702-7

4. Yao S, Lan H, Han Y, Mao C, Yang M, Zhang X, et al. From organ preservation to selective surgery: How immunotherapy changes colorectal surgery? *Surg Open Sci* (2023) 15:44–53. doi: 10.1016/j.sopen.2023.07.024

5. André T, Shiu K-K, Kim TW, Jensen BV, Jensen LH, Punt C, et al. Pembrolizumab in microsatellite-instability–high advanced colorectal cancer. *New Engl J Med* (2020) 383:2207–18. doi: 10.1056/NEJMoa2017699

6. Raza A, Khan AQ, Inchakalody VP, Mestiri S, Yoosuf Z, Bedhiafi T, et al. Dynamic liquid biopsy components as predictive and prognostic biomarkers in colorectal cancer. *J Exp Clin Cancer Res* (2022) 41:99. doi: 10.1186/s13046-022-02318-0

7. Lokhandwala T, Bittoni MA, Dann RA, D'Souza AO, Johnson M, Nagy RJ, et al. Costs of diagnostic assessment for lung cancer: A medicare claims analysis. *Clin Lung Cancer* (2017) 18:e27–34. doi: 10.1016/j.cllc.2016.07.006

8. Marron TU, Ryan AE, Reddy SM, Kaczanowska S, Younis RH, Thakkar D, et al. Considerations for treatment duration in responders to immune checkpoint inhibitors. *J Immunother Cancer* (2021) 9. doi: 10.1136/jitc-2020-001901

9. Meric-Bernstam F, Larkin J, Tabernero J, Bonini C. Enhancing anti-tumour efficacy with immunotherapy combinations. *Lancet* (2021) 397:1010–22. doi: 10.1016/s0140-6736(20)32598-8

10. Ott PA, Hodi FS, Kaufman HL, Wigginton JM, Wolchok JD. Combination immunotherapy: a road map. *J Immunother Cancer* (2017) 5:16. doi: 10.1186/s40425-017-0218-5

11. Ye Q, Ling S, Zheng S, Xu X. Liquid biopsy in hepatocellular carcinoma: circulating tumor cells and circulating tumor DNA. *Mol Cancer* (2019) 18:114. doi: 10.1186/s12943-019-1043-x

12. Diaz LA Jr., Bardelli A. Liquid biopsies: genotyping circulating tumor DNA. *J Clin Oncol* (2014) 32:579–86. doi: 10.1200/jco.2012.45.2011

13. Alix-Panabières C, Pantel K. Clinical applications of circulating tumor cells and circulating tumor DNA as liquid biopsy. *Cancer Discovery* (2016) 6:479–91. doi: 10.1158/2159-8290.Cd-15-1483

14. Heidrich I, Ačkar L, Mossahebi Mohammadi P, Pantel K. Liquid biopsies: Potential and challenges. *Int J Cancer* (2021) 148:528–45. doi: 10.1002/ijc.33217

15. Saini A, Pershad Y, Albadawi H, Kuo M, Alzubaidi S, Naidu S, et al. Liquid biopsy in gastrointestinal cancers. *Diagnostics (Basel)* (2018) 8. doi: 10.3390/diagnostics8040075

16. Ivanova E, Ward A, Wiegmans AP, Richard DJ. Circulating tumor cells in metastatic breast cancer: from genome instability to metastasis. *Front Mol Biosci* (2020) 7:134. doi: 10.3389/fmolb.2020.00134

17. Arnold M, Sierra MS, Laversanne M, Soerjomataram I, Jemal A, Bray F. Global patterns and trends in colorectal cancer incidence and mortality. *Gut* (2017) 66:683–91. doi: 10.1136/gutjnl-2015-310912

18. Pardoll DM. The blockade of immune checkpoints in cancer immunotherapy. *Nat Rev Cancer* (2012) 12:252–64. doi: 10.1038/nrc3239

19. Hodi FS, Chiarion-Sileni V, Gonzalez R, Grob JJ, Rutkowski P, Cowey CL, et al. Nivolumab plus ipilimumab or nivolumab alone versus ipilimumab alone in advanced melanoma (CheckMate 067): 4-year outcomes of a multicentre, randomised, phase 3 trial. *Lancet Oncol* (2018) 19:1480–92. doi: 10.1016/s1470-2045(18)30700-9

20. Reck M, Rodríguez-Abreu D, Robinson AG, Hui R, Csőszi T, Fülöp A, et al. Updated analysis of KEYNOTE-024: pembrolizumab versus platinum-based chemotherapy for advanced non-small-cell lung cancer with PD-L1 tumor proportion score of 50% or greater. *J Clin Oncol* (2019) 37:537–46. doi: 10.1200/jco.18.00149

21. Motzer RJ, Rini BI, McDermott DF, Arén Frontera O, Hammers HJ, Carducci MA, et al. Nivolumab plus ipilimumab versus sunitinib in first-line treatment for advanced renal cell carcinoma: extended follow-up of efficacy and safety results from a randomised, controlled, phase 3 trial. *Lancet Oncol* (2019) 20:1370–85. doi: 10.1016/s1470-2045(19)30413-9

22. Le DT, Uram JN, Wang H, Bartlett BR, Kemberling H, Eyring AD, et al. PD-1 blockade in tumors with mismatch-repair deficiency. *N Engl J Med* (2015) 372:2509–20. doi: 10.1056/NEJMoa1500596

23. Overman MJ, Lonardi S, Wong KYM, Lenz HJ, Gelsomino F, Aglietta M, et al. Durable clinical benefit with nivolumab plus ipilimumab in DNA mismatch repair-deficient/microsatellite instability-high metastatic colorectal cancer. *J Clin Oncol* (2018) 36:773–9. doi: 10.1200/jco.2017.76.9901

24. Overman MJ, McDermott R, Leach JL, Lonardi S, Lenz HJ, Morse MA, et al. Nivolumab in patients with metastatic DNA mismatch repair-deficient or microsatellite instability-high colorectal cancer (CheckMate 142): an open-label, multicentre, phase 2 study. *Lancet Oncol* (2017) 18:1182–91. doi: 10.1016/s1470-2045(17)30422-9

25. Marcus L, Lemery SJ, Keegan P, Pazdur R. FDA approval summary: pembrolizumab for the treatment of microsatellite instability-high solid tumors. *Clin Cancer Res* (2019) 25:3753–8. doi: 10.1158/1078-0432.Ccr-18-4070

26. Xu Y, Fu Y, Zhu B, Wang J, Zhang B. Predictive biomarkers of immune checkpoint inhibitors-related toxicities. *Front Immunol* (2020) 11:2023. doi: 10.3389/fimmu.2020.02023

27. Yoshino T, Arnold D, Taniguchi H, Pentheroudakis G, Yamazaki K, Xu RH, et al. Pan-Asian adapted ESMO consensus guidelines for the management of patients with metastatic colorectal cancer: a JSMO-ESMO initiative endorsed by CSCO, KACO, MOS, SSO and TOS. *Ann Oncol* (2018) 29:44–70. doi: 10.1093/annonc/mdx738

28. Benson AB, Venook AP, Al-Hawary MM, Arain MA, Chen YJ, Ciombor KK, et al. Colon cancer, version 2.2021, NCCN clinical practice guidelines in oncology. *J Natl Compr Canc Netw* (2021) 19:329–59. doi: 10.6004/jnccn.2021.0012

29. Lenz HJ, Van Cutsem E, Luisa Limon M, Wong KYM, Hendlisz A, Aglietta M, et al. First-line nivolumab plus low-dose ipilimumab for microsatellite instability-high/mismatch repair-deficient metastatic colorectal cancer: the phase II checkMate 142 study. *J Clin Oncol* (2022) 40:161–70. doi: 10.1200/jco.21.01015

30. Cohen R, Bennouna J, Meurisse A, Tournigand C, de la Fouchardière C, Tougeron D, et al. RECIST and iRECIST criteria for the evaluation of nivolumab plus ipilimumab in patients with microsatellite instability-high/mismatch repair-deficient metastatic colorectal cancer: the GERCOR NIPICOL phase II study. *J Immunother Cancer* (2020) 8. doi: 10.1136/jitc-2020-001499

31. Asaoka Y, Ijichi H, Koike K. PD-1 blockade in tumors with mismatch-repair deficiency. *N Engl J Med* (2015) 373:1979. doi: 10.1056/NEJMc1510353

32. Le DT, Kim TW, Van Cutsem E, Geva R, Jäger D, Hara H, et al. Phase II open-label study of pembrolizumab in treatment-refractory, microsatellite instability-high/mismatch repair-deficient metastatic colorectal cancer: KEYNOTE-164. *J Clin Oncol* (2020) 38:11–9. doi: 10.1200/jco.19.02107

33. Huyghe N, Baldin P, Van den Eynde M. Immunotherapy with immune checkpoint inhibitors in colorectal cancer: what is the future beyond deficient mismatch-repair tumours? *Gastroenterol Rep (Oxf)* (2020) 8:11–24. doi: 10.1093/gastro/goz061

34. Cohen R, Hain E, Buhard O, Guilloux A, Bardier A, Kaci R, et al. Association of primary resistance to immune checkpoint inhibitors in metastatic colorectal cancer with misdiagnosis of microsatellite instability or mismatch repair deficiency status. *JAMA Oncol* (2019) 5:551–5. doi: 10.1001/jamaoncol.2018.4942

35. Ganesh K, Stadler ZK, Cercek A, Mendelsohn RB, Shia J, Segal NH, et al. Immunotherapy in colorectal cancer: rationale, challenges and potential. *Nat Rev Gastroenterol Hepatol* (2019) 16:361–75. doi: 10.1038/s41575-019-0126-x

36. Amato M, Franco R, Facchini G, Addeo R, Ciardiello F, Berretta M, et al. Microsatellite instability: from the implementation of the detection to a prognostic and predictive role in cancers. *Int J Mol Sci* (2022) 23:23. doi: 10.3390/ijms23158726

37. Chen EX, Jonker DJ, Loree JM, Kennecke HF, Berry SR, Couture F, et al. Effect of combined immune checkpoint inhibition vs best supportive care alone in patients with advanced colorectal cancer: the canadian cancer trials group CO.26 study. *JAMA Oncol* (2020) 6:831–8. doi: 10.1001/jamaoncol.2020.0910

38. Passaro A, Stenzinger A, Peters S. Tumor mutational burden as a pan-cancer biomarker for immunotherapy: the limits and potential for convergence. *Cancer Cell* (2020) 38:624–5. doi: 10.1016/j.ccell.2020.10.019

39. Sha D, Jin Z, Budczies J, Kluck K, Stenzinger A, Sinicrope FA. Tumor mutational burden as a predictive biomarker in solid tumors. *Cancer Discovery* (2020) 10:1808–25. doi: 10.1158/2159-8290.Cd-20-0522

40. Innocenti F, Ou FS, Qu X, Zemla TJ, Niedzwiecki D, Tam R, et al. Mutational analysis of patients with colorectal cancer in CALGB/SWOG 80405 identifies new roles of microsatellite instability and tumor mutational burden for patient outcome. *J Clin Oncol* (2019) 37:1217–27. doi: 10.1200/jco.18.01798

41. Bortolomeazzi M, Keddar MR, Montorsi L, Acha-Sagredo A, Benedetti L, Temelkovski D, et al. Immunogenomics of colorectal cancer response to checkpoint blockade: analysis of the KEYNOTE 177 trial and validation cohorts. *Gastroenterology* (2021) 161:1179–93. doi: 10.1053/j.gastro.2021.06.064

42. Gandara DR, Paul SM, Kowanetz M, Schleifman E, Zou W, Li Y, et al. Blood-based tumor mutational burden as a predictor of clinical benefit in non-small-cell lung cancer patients treated with atezolizumab. *Nat Med* (2018) 24:1441–8. doi: 10.1038/s41591-018-0134-3

43. Pich O, Muiños F, Lolkema MP, Steeghs N, Gonzalez-Perez A, Lopez-Bigas N. The mutational footprints of cancer therapies. *Nat Genet* (2019) 51:1732–40. doi: 10.1038/s41588-019-0525-5

44. Peng QH, Wang CH, Chen HM, Zhang RX, Pan ZZ, Lu ZH, et al. CMTM6 and PD-L1 coexpression is associated with an active immune microenvironment and a

favorable prognosis in colorectal cancer. *J Immunother Cancer* (2021) 9. doi: 10.1136/jitc-2020-001638

45. Omura Y, Toiyama Y, Okugawa Y, Yin C, Shigemori T, Kusunoki K, et al. Prognostic impacts of tumoral expression and serum levels of PD-L1 and CTLA-4 in colorectal cancer patients. *Cancer Immunol Immunother* (2020) 69:2533–46. doi: 10.1007/s00262-020-02645-1

46. Masugi Y, Nishihara R, Yang J, Mima K, da Silva A, Shi Y, et al. Tumour CD274 (PD-L1) expression and T cells in colorectal cancer. *Gut* (2017) 66:1463–73. doi: 10.1136/gutjnl-2016-311421

47. Hou W, Zhou X, Yi C, Zhu H. Immune check point inhibitors and immune-related adverse events in small cell lung cancer. *Front Oncol* (2021) 11:604227. doi: 10.3389/fonc.2021.604227

48. Chen G, Huang AC, Zhang W, Zhang G, Wu M, Xu W, et al. Exosomal PD-L1 contributes to immunosuppression and is associated with anti-PD-1 response. *Nature.* (2018) 560:382–6. doi: 10.1038/s41586-018-0392-8

49. Wang X, Teng F, Kong L, Yu J. PD-L1 expression in human cancers and its association with clinical outcomes. *Onco Targets Ther* (2016) 9:5023–39. doi: 10.2147/ott.S105862

50. Patel SP, Kurzrock R. PD-L1 expression as a predictive biomarker in cancer immunotherapy. *Mol Cancer Ther* (2015) 14:847–56. doi: 10.1158/1535-7163.Mct-14-0983

51. Ahn AR, Kim KM, Jang KY, Moon WS, Ha GW, Lee MR, et al. Correlation of PIK3CA mutation with programmed death ligand-1 (PD-L1) expression and their clinicopathological significance in colorectal cancer. *Ann Transl Med* (2021) 9:1406. doi: 10.21037/atm-21-2315

52. Yang L, Xue R, Pan C. Prognostic and clinicopathological value of PD-L1 in colorectal cancer: a systematic review and meta-analysis. *Onco Targets Ther* (2019) 12:3671–82. doi: 10.2147/ott.S190168

53. Li Y, He M, Zhou Y, Yang C, Wei S, Bian X, et al. The prognostic and clinicopathological roles of PD-L1 expression in colorectal cancer: A systematic review and meta-analysis. *Front Pharmacol* (2019) 10:139. doi: 10.3389/fphar.2019.00139

54. Wang S, Yuan B, Wang Y, Li M, Liu X, Cao J, et al. Clinicopathological and prognostic significance of PD-L1 expression in colorectal cancer: a meta-analysis. *Int J Colorectal Dis* (2021) 36:117–30. doi: 10.1007/s00384-020-03734-4

55. Hou W, Yi C, Zhu H. Predictive biomarkers of colon cancer immunotherapy: Present and future. *Front Immunol* (2022) 13:1032314. doi: 10.3389/fimmu.2022.1032314

56. Pantel K, Alix-Panabières C. Circulating tumour cells in cancer patients: challenges and perspectives. *Trends Mol Med* (2010) 16:398–406. doi: 10.1016/j.molmed.2010.07.001

57. Ignatiadis M, Sledge GW, Jeffrey SS. Liquid biopsy enters the clinic - implementation issues and future challenges. *Nat Rev Clin Oncol* (2021) 18:297–312. doi: 10.1038/s41571-020-00457-x

58. Bidard FC, Peeters DJ, Fehm T, Nolé F, Gisbert-Criado R, Mavroudis D, et al. Clinical validity of circulating tumour cells in patients with metastatic breast cancer: a pooled analysis of individual patient data. *Lancet Oncol* (2014) 15:406–14. doi: 10.1016/s1470-2045(14)70069-5

59. Alix-Panabières C, Pantel K. Challenges in circulating tumour cell research. *Nat Rev Cancer* (2014) 14:623–31. doi: 10.1038/nrc3820

60. Alix-Panabières C, Pantel K. Liquid biopsy: from discovery to clinical application. *Cancer Discovery* (2021) 11:858–73. doi: 10.1158/2159-8290.Cd-20-1311

61. Markou A, Tzanikou E, Lianidou E. The potential of liquid biopsy in the management of cancer patients. *Semin Cancer Biol* (2022) 84:69–79. doi: 10.1016/j.semcancer.2022.03.013

62. Diehl F, Schmidt K, Durkee KH, Moore KJ, Goodman SN, Shuber AP, et al. Analysis of mutations in DNA isolated from plasma and stool of colorectal cancer patients. *Gastroenterology* (2008) 135:489–98. doi: 10.1053/j.gastro.2008.05.039

63. De Mattos-Arruda L, Mayor R, Ng CKY, Weigelt B, Martínez-Ricarte F, Torrejon D, et al. Cerebrospinal fluid-derived circulating tumour DNA better represents the genomic alterations of brain tumours than plasma. *Nat Commun* (2015) 6:8839. doi: 10.1038/ncomms9839

64. Kimura H, Fujiwara Y, Sone T, Kunitoh H, Tamura T, Kasahara K, et al. EGFR mutation status in tumour-derived DNA from pleural effusion fluid is a practical basis for predicting the response to gefitinib. *Br J Cancer* (2006) 95:1390–5. doi: 10.1038/sj.bjc.6603428

65. Wang Y, Springer S, Mulvey CL, Silliman N, Schaefer J, Sausen M, et al. Detection of somatic mutations and HPV in the saliva and plasma of patients with head and neck squamous cell carcinomas. *Sci Transl Med* (2015) 7:293ra104. doi: 10.1126/scitranslmed.aaa8507

66. Mouliere F, El Messaoudi S, Pang D, Dritschilo A, Thierry AR. Multi-marker analysis of circulating cell-free DNA toward personalized medicine for colorectal cancer. *Mol Oncol* (2014) 8:927–41. doi: 10.1016/j.molonc.2014.02.005

67. Muluhngwi P, Valdes R Jr., Fernandez-Botran R, Burton E, Williams B, Linder MW. Cell-free DNA diagnostics: current and emerging applications in oncology. *Pharmacogenomics* (2019) 20:357–80. doi: 10.2217/pgs-2018-0174

68. Spindler KG. Methodological, biological and clinical aspects of circulating free DNA in metastatic colorectal cancer. *Acta Oncol* (2017) 56:7–16. doi: 10.1080/0284186x.2016.1253861

69. Alix-Panabières C, Pantel K. Circulating tumor cells: liquid biopsy of cancer. *Clin Chem* (2013) 59:110–8. doi: 10.1373/clinchem.2012.194258

70. Qi Y, Wang W. Clinical significance of circulating tumor cells in squamous cell lung cancer patients. *Cancer biomark* (2017) 18:161–7. doi: 10.3233/cbm-160090

71. Castello A, Carbone FG, Rossi S, Monterisi S, Federico D, Toschi L, et al. Circulating tumor cells and metabolic parameters in NSCLC patients treated with checkpoint inhibitors. *Cancers (Basel)* (2020) 12. doi: 10.3390/cancers12020487

72. Yu H, Han L, Yuan J, Sun Y. Circulating tumor cell free DNA from plasma and urine in the clinical management of colorectal cancer. *Cancer biomark* (2020) 27:29–37. doi: 10.3233/cbm-182344

73. Kobayashi S, Nakamura Y, Taniguchi H, Odegaard JI, Nomura S, Kojima M, et al. Impact of preoperative circulating tumor DNA status on survival outcomes after hepatectomy for resectable colorectal liver metastases. *Ann Surg Oncol* (2021) 28:4744–55. doi: 10.1245/s10434-020-09449-8

74. Tie J, Wang Y, Tomasetti C, Li L, Springer S, Kinde I, et al. Circulating tumor DNA analysis detects minimal residual disease and predicts recurrence in patients with stage II colon cancer. *Sci Transl Med* (2016) 8:346ra92. doi: 10.1126/scitranslmed.aaf6219

75. Mauri G, Vitiello PP, Sogari A, Crisafulli G, Sartore-Bianchi A, Marsoni S, et al. Liquid biopsies to monitor and direct cancer treatment in colorectal cancer. *Br J Cancer* (2022) 127:394–407. doi: 10.1038/s41416-022-01769-8

76. Montagut C, Vidal J. Liquid biopsy for precision adjuvant chemotherapy in colon cancer. *N Engl J Med* (2022) 386:2330–1. doi: 10.1056/NEJMe2204625

77. McDonald BR, Contente-Cuomo T, Sammut SJ, Odenheimer-Bergman A, Ernst B, Perdigones N, et al. Personalized circulating tumor DNA analysis to detect residual disease after neoadjuvant therapy in breast cancer. *Sci Transl Med* (2019) 11. doi: 10.1126/scitranslmed.aax7392

78. Kotani D, Oki E, Nakamura Y, Yukami H, Mishima S, Bando H, et al. Molecular residual disease and efficacy of adjuvant chemotherapy in patients with colorectal cancer. *Nat Med* (2023) 29:127–34. doi: 10.1038/s41591-022-02115-4

79. Coombes RC, Page K, Salari R, Hastings RK, Armstrong A, Ahmed S, et al. Personalized detection of circulating tumor DNA antedates breast cancer metastatic recurrence. *Clin Cancer Res* (2019) 25:4255–63. doi: 10.1158/1078-0432.Ccr-18-3663

80. Kasi PM, Fehringer G, Taniguchi H, Starling N, Nakamura Y, Kotani D, et al. Impact of circulating tumor DNA-based detection of molecular residual disease on the conduct and design of clinical trials for solid tumors. *JCO Precis Oncol* (2022) 6:e2100181. doi: 10.1200/po.21.00181

81. Tie J, Cohen JD, Wang Y, Christie M, Simons K, Lee M, et al. Circulating tumor DNA analyses as markers of recurrence risk and benefit of adjuvant therapy for stage III colon cancer. *JAMA Oncol* (2019) 5:1710–7. doi: 10.1001/jamaoncol.2019.3616

82. Diehl F, Schmidt K, Choti MA, Romans K, Goodman S, Li M, et al. Circulating mutant DNA to assess tumor dynamics. *Nat Med* (2008) 14:985–90. doi: 10.1038/nm.1789

83. Faulkner LG, Howells LM, Pepper C, Shaw JA, Thomas AL. The utility of ctDNA in detecting minimal residual disease following curative surgery in colorectal cancer: a systematic review and meta-analysis. *Br J Cancer* (2023) 128:297–309. doi: 10.1038/s41416-022-02017-9

84. Reinert T, Henriksen TV, Christensen E, Sharma S, Salari R, Sethi H, et al. Analysis of plasma cell-free DNA by ultradeep sequencing in patients with stages I to III colorectal cancer. *JAMA Oncol* (2019) 5:1124–31. doi: 10.1001/jamaoncol.2019.0528

85. Tie J, Cohen JD, Lo SN, Wang Y, Li L, Christie M, et al. Prognostic significance of postsurgery circulating tumor DNA in nonmetastatic colorectal cancer: Individual patient pooled analysis of three cohort studies. *Int J Cancer* (2021) 148:1014–26. doi: 10.1002/ijc.33312

86. Tarazona N, Gimeno-Valiente F, Gambardella V, Zuñiga S, Rentero-Garrido P, Huerta M, et al. Targeted next-generation sequencing of circulating-tumor DNA for tracking minimal residual disease in localized colon cancer. *Ann Oncol* (2019) 30:1804–12. doi: 10.1093/annonc/mdz390

87. Tie J, Cohen JD, Lahouel K, Lo SN, Wang Y, Kosmider S, et al. Circulating tumor DNA analysis guiding adjuvant therapy in stage II colon cancer. *N Engl J Med* (2022) 386:2261–72. doi: 10.1056/NEJMoa2200075

88. Tie J, Cohen JD, Wang Y, Li L, Christie M, Simons K, et al. Serial circulating tumour DNA analysis during multimodality treatment of locally advanced rectal cancer: a prospective biomarker study. *Gut* (2019) 68:663–71. doi: 10.1136/gutjnl-2017-315852

89. Parikh AR, Van Seventer EE, Siravegna G, Hartwig AV, Jaimovich A, He Y, et al. Minimal residual disease detection using a plasma-only circulating tumor DNA assay in patients with colorectal cancer. *Clin Cancer Res* (2021) 27:5586–94. doi: 10.1158/1078-0432.Ccr-21-0410

90. Taniguchi H, Nakamura Y, Kotani D, Yukami H, Mishima S, Sawada K, et al. CIRCULATE-Japan: Circulating tumor DNA-guided adaptive platform trials to refine adjuvant therapy for colorectal cancer. *Cancer Sci* (2021) 112:2915–20. doi: 10.1111/cas.14926

91. Gao Z, Huang D, Chen H, Yang Y, An K, Ding C, et al. Development and validation of postoperative circulating tumor DNA combined with clinicopathological risk factors for recurrence prediction in patients with stage I-III colorectal cancer. *J Transl Med* (2023) 21:63. doi: 10.1186/s12967-023-03884-3

92. Habr-Gama A, Perez RO, Nadalin W, Sabbaga J, Ribeiro U Jr., Silva e Sousa AH Jr., et al. Operative versus nonoperative treatment for stage 0 distal rectal cancer

following chemoradiation therapy: long-term results. *Ann Surg* (2004) 240:711–7; discussion 717-8. doi: 10.1097/01.sla.0000141194.27992.32

93. Habr-Gama A, Sabbaga J, Gama-Rodrigues J, São Julião GP, Proscurshim I, Bailão Aguilar P, et al. Watch and wait approach following extended neoadjuvant chemoradiation for distal rectal cancer: are we getting closer to anal cancer management? *Dis Colon Rectum* (2013) 56:1109–17. doi: 10.1097/DCR.0b013e3182a25c4e

94. Singh T, Fatehi Hassanabad M, Fatehi Hassanabad A. Non-small cell lung cancer: Emerging molecular targeted and immunotherapeutic agents. *Biochim Biophys Acta Rev Cancer* (2021) 1876:188636. doi: 10.1016/j.bbcan.2021.188636

95. Gasch C, Bauernhofer T, Pichler M, Langer-Freitag S, Reeh M, Seifert AM, et al. Heterogeneity of epidermal growth factor receptor status and mutations of KRAS/PIK3CA in circulating tumor cells of patients with colorectal cancer. *Clin Chem* (2013) 59:252–60. doi: 10.1373/clinchem.2012.188557

96. Li W, Liu JB, Hou LK, Yu F, Zhang J, Wu W, et al. Liquid biopsy in lung cancer: significance in diagnostics, prediction, and treatment monitoring. *Mol Cancer* (2022) 21:25. doi: 10.1186/s12943-022-01505-z

97. Cremolini C, Rossini D, Dell'Aquila E, Lonardi S, Conca E, Del Re M, et al. Rechallenge for patients with RAS and BRAF wild-type metastatic colorectal cancer with acquired resistance to first-line cetuximab and irinotecan: A phase 2 single-arm clinical trial. *JAMA Oncol* (2019) 5:343–50. doi: 10.1001/jamaoncol.2018.5080

98. Martinelli E, Martini G, Famiglietti V, Troiani T, Napolitano S, Pietrantonio F, et al. Cetuximab rechallenge plus avelumab in pretreated patients with RAS wild-type metastatic colorectal cancer: the phase 2 single-arm clinical CAVE trial. *JAMA Oncol* (2021) 7:1529–35. doi: 10.1001/jamaoncol.2021.2915

99. Bachet JB, Bouché O, Taieb J, Dubreuil O, Garcia ML, Meurisse A, et al. RAS mutation analysis in circulating tumor DNA from patients with metastatic colorectal cancer: the AGEO RASANC prospective multicenter study. *Ann Oncol* (2018) 29:1211–9. doi: 10.1093/annonc/mdy061

100. Sartore-Bianchi A, Pietrantonio F, Lonardi S, Mussolin B, Rua F, Fenocchio E, et al. Phase II study of anti-EGFR rechallenge therapy with panitumumab driven by circulating tumor DNA molecular selection in metastatic colorectal cancer: The CHRONOS trial. *J Clin Oncol* (2021) 39:3506–6. doi: 10.1200/JCO.2021.39.15_suppl.3506

101. Parseghian CM, Loree JM, Morris VK, Liu X, Clifton KK, Napolitano S, et al. Anti-EGFR-resistant clones decay exponentially after progression: implications for anti-EGFR re-challenge. *Ann Oncol* (2019) 30:243–9. doi: 10.1093/annonc/mdy509

102. *Metastatic Colorectal Cancer (RAS-wildtype) After Response to First-line Treatment With FOLFIR Plus Cetuximab (AIO-KRK-0114)*. Available at: https://clinicaltrials.gov/study/NCT02934529.

103. Kasi PM, Budde G, Krainock M, Aushev VN, Koyen Malashevich A, Malhotra M, et al. Circulating tumor DNA (ctDNA) serial analysis during progression on PD-1 blockade and later CTLA-4 rescue in patients with mismatch repair deficient metastatic colorectal cancer. *J Immunother Cancer* (2022) 10. doi: 10.1136/jitc-2021-003312

104. Lee JH, Menzies AM, Carlino MS, McEvoy AC, Sandhu S, Weppler AM, et al. Longitudinal monitoring of ctDNA in patients with melanoma and brain metastases treated with immune checkpoint inhibitors. *Clin Cancer Res* (2020) 26:4064–71. doi: 10.1158/1078-0432.Ccr-19-3926

105. Lee JH, Long GV, Boyd S, Lo S, Menzies AM, Tembe V, et al. Circulating tumour DNA predicts response to anti-PD1 antibodies in metastatic melanoma. *Ann Oncol* (2017) 28:1130–6. doi: 10.1093/annonc/mdx026

106. Braune J, Keller L, Schiller F, Graf E, Rafei-Shamsabadi D, Wehrle J, et al. Circulating tumor DNA allows early treatment monitoring in BRAF- and NRAS-mutant Malignant melanoma. *JCO Precis Oncol* (2020) 4:20–31. doi: 10.1200/po.19.00174

107. Valpione S, Gremel G, Mundra P, Middlehurst P, Galvani E, Girotti MR, et al. Plasma total cell-free DNA (cfDNA) is a surrogate biomarker for tumour burden and a prognostic biomarker for survival in metastatic melanoma patients. *Eur J Cancer* (2018) 88:1–9. doi: 10.1016/j.ejca.2017.10.029

108. Wong SQ, Raleigh JM, Callahan J, Vergara IA, Ftouni S, Hatzimihalis A, et al. Circulating tumor DNA analysis and functional imaging provide complementary approaches for comprehensive disease monitoring in metastatic melanoma. *JCO Precis Oncol* (2017) 1:1–14. doi: 10.1200/po.16.00009

109. Chang GA, Tadepalli JS, Shao Y, Zhang Y, Weiss S, Robinson E, et al. Sensitivity of plasma BRAFmutant and NRASmutant cell-free DNA assays to detect metastatic melanoma in patients with low RECIST scores and non-RECIST disease progression. *Mol Oncol* (2016) 10:157–65. doi: 10.1016/j.molonc.2015.09.005

110. Ito K, Schöder H, Teng R, Humm JL, Ni A, Wolchok JD, et al. Prognostic value of baseline metabolic tumor volume measured on (18)F-fluorodeoxyglucose positron emission tomography/computed tomography in melanoma patients treated with ipilimumab therapy. *Eur J Nucl Med Mol Imaging* (2019) 46:930–9. doi: 10.1007/s00259-018-4211-0

111. He WZ, Hu WM, Wang F, Rong YM, Yang L, Xie QK, et al. Comparison of mismatch repair status between primary and matched metastatic sites in patients with colorectal cancer. *J Natl Compr Canc Netw* (2019) 17:1174–83. doi: 10.6004/jnccn.2019.7308

112. Diaz LA Jr., Williams RT, Wu J, Kinde I, Hecht JR, Berlin J, et al. The molecular evolution of acquired resistance to targeted EGFR blockade in colorectal cancers. *Nature* (2012) 486:537–40. doi: 10.1038/nature11219

113. Chan TA, Yarchoan M, Jaffee E, Swanton C, Quezada SA, Stenzinger A, et al. Development of tumor mutation burden as an immunotherapy biomarker: utility for the oncology clinic. *Ann Oncol* (2019) 30:44–56. doi: 10.1093/annonc/mdy495

114. Goodman AM, Kato S, Bazhenova L, Patel SP, Frampton GM, Miller V, et al. Tumor mutational burden as an independent predictor of response to immunotherapy in diverse cancers. *Mol Cancer Ther* (2017) 16:2598–608. doi: 10.1158/1535-7163.Mct-17-0386

115. Rizvi NA, Hellmann MD, Snyder A, Kvistborg P, Makarov V, Havel JJ, et al. Cancer immunology. Mutational landscape determines sensitivity to PD-1 blockade in non-small cell lung cancer. *Science* (2015) 348:124–8. doi: 10.1126/science.aaa1348

116. Cabel L, Riva F, Servois V, Livartowski A, Daniel C, Rampanou A, et al. Circulating tumor DNA changes for early monitoring of anti-PD1 immunotherapy: a proof-of-concept study. *Ann Oncol* (2017) 28:1996–2001. doi: 10.1093/annonc/mdx212

117. Willis J, Lefterova MI, Artyomenko A, Kasi PM, Nakamura Y, Mody K, et al. Validation of microsatellite instability detection using a comprehensive plasma-based genotyping panel. *Clin Cancer Res* (2019) 25:7035–45. doi: 10.1158/1078-0432.Ccr-19-1324

118. Tieng FYF, Abu N, Lee LH, Ab Mutalib NS. Microsatellite instability in colorectal cancer liquid biopsy-current updates on its potential in non-invasive detection, prognosis and as a predictive marker. *Diagnostics (Basel)* (2021) 11. doi: 10.3390/diagnostics11030544

119. Goodman AM, Holden KA, Jeong AR, Kim L, Fitzgerald KD, Almasri E, et al. Assessing CAR T-cell therapy response using genome-wide sequencing of cell-free DNA in patients with B-cell lymphomas. *Transplant Cell Ther* (2022) 28:30.e1–7. doi: 10.1016/j.jtct.2021.10.007

120. Frank MJ, Hossain NM, Bukhari A, Dean E, Spiegel JY, Claire GK, et al. Monitoring of circulating tumor DNA improves early relapse detection after axicabtagene ciloleucel infusion in large B-cell lymphoma: results of a prospective multi-institutional trial. *J Clin Oncol* (2021) 39:3034–43. doi: 10.1200/jco.21.00377

121. Mika T, Thomson J, Nilius-Eliliwi V, Vangala D, Baraniskin A, Wulf G, et al. Quantification of cell-free DNAfor the analysis of CD19-CAR-T cells during lymphoma treatment. *Mol Ther Methods Clin Dev* (2021) 23:539–50. doi: 10.1016/j.omtm.2021.10.009

122. Crisafulli G, Sartore-Bianchi A, Lazzari L, Pietrantonio F, Amatu A, Macagno M, et al. Temozolomide treatment alters mismatch repair and boosts mutational burden in tumor and blood of colorectal cancer patients. *Cancer Discovery* (2022) 12:1656–75. doi: 10.1158/2159-8290.Cd-21-1434

123. Stenzinger A, Allen JD, Maas J, Stewart MD, Merino DM, Wempe MM, et al. Tumor mutational burden standardization initiatives: Recommendations for consistent tumor mutational burden assessment in clinical samples to guide immunotherapy treatment decisions. *Genes Chromosomes Cancer* (2019) 58:578–88. doi: 10.1002/gcc.22733

124. Bratman SV, Yang SYC, Iafolla MAJ, Liu Z, Hansen AR, Bedard PL, et al. Personalized circulating tumor DNA analysis as a predictive biomarker in solid tumor patients treated with pembrolizumab. *Nat Cancer* (2020) 1:873–81. doi: 10.1038/s43018-020-0096-5

125. Zhang Q, Luo J, Wu S, Si H, Gao C, Xu W, et al. Prognostic and predictive impact of circulating tumor DNA in patients with advanced cancers treated with immune checkpoint blockade. *Cancer Discovery* (2020) 10:1842–53. doi: 10.1158/2159-8290.Cd-20-0047

126. Abbosh C, Birkbak NJ, Wilson GA, Jamal-Hanjani M, Constantin T, Salari R, et al. Phylogenetic ctDNA analysis depicts early-stage lung cancer evolution. *Nature* (2017) 545:446–51. doi: 10.1038/nature22364

127. Malla M, Loree JM, Kasi PM, Parikh AR. Using circulating tumor DNA in colorectal cancer: current and evolving practices. *J Clin Oncol* (2022) 40:2846–57. doi: 10.1200/jco.21.02615

128. Stadler JC, Belloum Y, Deitert B, Sementsov M, Heidrich I, Gebhardt C, et al. Current and future clinical applications of ctDNA in immuno-oncology. *Cancer Res* (2022) 82:349–58. doi: 10.1158/0008-5472.Can-21-1718

129. Mirza S, Bhadresha K, Mughal MJ, McCabe M, Shahbazi R, Ruff P, et al. Liquid biopsy approaches and immunotherapy in colorectal cancer for precision medicine: Are we there yet? *Front Oncol* (2022) 12:1023565. doi: 10.3389/fonc.2022.1023565

130. Oshi M, Katsuta E, Yan L, Ebos JML, Rashid OM, Matsuyama R, et al. A novel 4-gene score to predict survival, distant metastasis and response to neoadjuvant therapy in breast cancer. *Cancers (Basel)* (2020) 12. doi: 10.3390/cancers12051148

131. Perfetto SP, Ambrozak D, Nguyen R, Chattopadhyay PK, Roederer M. Quality assurance for polychromatic flow cytometry using a suite of calibration beads. *Nat Protoc* (2012) 7:2067–79. doi: 10.1038/nprot.2012.126

132. Wei C, Wang M, Gao Q, Yuan S, Deng W, Bie L, et al. Dynamic peripheral blood immune cell markers for predicting the response of patients with metastatic cancer to immune checkpoint inhibitors. *Cancer Immunol Immunother* (2023) 72:23–37. doi: 10.1007/s00262-022-03221-5

133. Nixon AB, Schalper KA, Jacobs I, Potluri S, Wang IM, Fleener C. Peripheral immune-based biomarkers in cancer immunotherapy: can we realize their predictive potential? *J Immunother Cancer* (2019) 7:325. doi: 10.1186/s40425-019-0799-2

134. Maecker HT, McCoy JP, Nussenblatt R. Standardizing immunophenotyping for the human immunology project. *Nat Rev Immunol* (2012) 12:191–200. doi: 10.1038/nri3158

135. Wu Q, Liu Z, Gao Z, Luo Y, Li F, Yang C, et al. KLF5 inhibition potentiates anti-PD1 efficacy by enhancing CD8(+) T-cell-dependent antitumor immunity. *Theranostics* (2023) 13:1381–400. doi: 10.7150/thno.82182

136. Rossi G, Russo A, Tagliamento M, Tuzi A, Nigro O, Vallome G, et al. Precision medicine for NSCLC in the era of immunotherapy: new biomarkers to select the most suitable treatment or the most suitable patient. *Cancers (Basel)* (2020) 12. doi: 10.3390/cancers12051125

137. Hogan SA, Courtier A, Cheng PF, Jaberg-Bentele NF, Goldinger SM, Manuel M, et al. Peripheral blood TCR repertoire profiling may facilitate patient stratification for immunotherapy against melanoma. *Cancer Immunol Res* (2019) 7:77–85. doi: 10.1158/2326-6066.Cir-18-0136

138. Valpione S, Galvani E, Tweedy J, Mundra PA, Banyard A, Middlehurst P, et al. Immune-awakening revealed by peripheral T cell dynamics after one cycle of immunotherapy. *Nat Cancer* (2020) 1:210–21. doi: 10.1038/s43018-019-0022-x

139. Poran A, Scherer J, Bushway ME, Besada R, Balogh KN, Wanamaker A, et al. Combined TCR repertoire profiles and blood cell phenotypes predict melanoma patient response to personalized neoantigen therapy plus anti-PD-1. *Cell Rep Med* (2020) 1:100141. doi: 10.1016/j.xcrm.2020.100141

140. Wang X, Muzaffar J, Kirtane K, Song F, Johnson M, Schell MJ, et al. T cell repertoire in peripheral blood as a potential biomarker for predicting response to concurrent cetuximab and nivolumab in head and neck squamous cell carcinoma. *J Immunother Cancer* (2022) 10. doi: 10.1136/jitc-2022-004512

141. Huang AC, Postow MA, Orlowski RJ, Mick R, Bengsch B, Manne S, et al. T-cell invigoration to tumour burden ratio associated with anti-PD-1 response. *Nature* (2017) 545:60–5. doi: 10.1038/nature22079

142. Oliveira G, Stromhaug K, Klaeger S, Kula T, Frederick DT, Le PM, et al. Phenotype, specificity and avidity of antitumour CD8(+) T cells in melanoma. *Nature* (2021) 596:119–25. doi: 10.1038/s41586-021-03704-y

143. Relecom A, Merhi M, Inchakalody V, Uddin S, Rinchai D, Bedognetti D, et al. Emerging dynamics pathways of response and resistance to PD-1 and CTLA-4 blockade: tackling uncertainty by confronting complexity. *J Exp Clin Cancer Res* (2021) 40:74. doi: 10.1186/s13046-021-01872-3

144. Kim KH, Cho J, Ku BM, Koh J, Sun JM, Lee SH, et al. The first-week proliferative response of peripheral blood PD-1(+)CD8(+) T cells predicts the response to anti-PD-1 therapy in solid tumors. *Clin Cancer Res* (2019) 25:2144–54. doi: 10.1158/1078-0432.Ccr-18-1449

145. Li S, Zhang C, Pang G, Wang P. Emerging blood-based biomarkers for predicting response to checkpoint immunotherapy in non-small-cell lung cancer. *Front Immunol* (2020) 11:603157. doi: 10.3389/fimmu.2020.603157

146. Kavanagh B, O'Brien S, Lee D, Hou Y, Weinberg V, Rini B, et al. CTLA4 blockade expands FoxP3+ regulatory and activated effector CD4+ T cells in a dose-dependent fashion. *Blood* (2008) 112:1175–83. doi: 10.1182/blood-2007-11-125435

147. Long SA, Buckner JH. CD4+FOXP3+ T regulatory cells in human autoimmunity: more than a numbers game. *J Immunol* (2011) 187:2061–6. doi: 10.4049/jimmunol.1003224

148. Deng L, Zhang H, Luan Y, Zhang J, Xing Q, Dong S, et al. Accumulation of foxp3+ T regulatory cells in draining lymph nodes correlates with disease progression and immune suppression in colorectal cancer patients. *Clin Cancer Res* (2010) 16:4105–12. doi: 10.1158/1078-0432.Ccr-10-1073

149. Wolf D, Wolf AM, Rumpold H, Fiegl H, Zeimet AG, Muller-Holzner E, et al. The expression of the regulatory T cell-specific forkhead box transcription factor FoxP3 is associated with poor prognosis in ovarian cancer. *Clin Cancer Res* (2005) 11:8326–31. doi: 10.1158/1078-0432.Ccr-05-1244

150. Farinha P, Al-Tourah A, Gill K, Klasa R, Connors JM, Gascoyne RD. The architectural pattern of FOXP3-positive T cells in follicular lymphoma is an independent predictor of survival and histologic transformation. *Blood* (2010) 115:289–95. doi: 10.1182/blood-2009-07-235598

151. Manjarrez-Orduño N, Menard LC, Kansal S, Fischer P, Kakrecha B, Jiang C, et al. Circulating T cell subpopulations correlate with immune responses at the tumor site and clinical response to PD1 inhibition in non-small cell lung cancer. *Front Immunol* (2018) 9:1613. doi: 10.3389/fimmu.2018.01613

152. Roselli M, Formica V, Cereda V, Jochems C, Richards J, Grenga I, et al. The association of clinical outcome and peripheral T-cell subsets in metastatic colorectal cancer patients receiving first-line FOLFIRI plus bevacizumab therapy. *Oncoimmunology* (2016) 5:e1188243. doi: 10.1080/2162402x.2016.1188243

153. Bencsikova B, Budinska E, Selingerova I, Pilatova K, Fedorova L, Greplova K, et al. Circulating T cell subsets are associated with clinical outcome of anti-VEGF-based 1st-line treatment of metastatic colorectal cancer patients: a prospective study with focus on primary tumor sidedness. *BMC Cancer* (2019) 19:687. doi: 10.1186/s12885-019-5909-5

154. Passardi A, Scarpi E, Cavanna L, Dall'Agata M, Tassinari D, Leo S, et al. Inflammatory indexes as predictors of prognosis and bevacizumab efficacy in patients with metastatic colorectal cancer. *Oncotarget*. (2016) 7:33210–9. doi: 10.18632/oncotarget.8901

155. Chang J, Lin G, Ye M, Tong D, Zhao J, Zhu D, et al. Decreased mean platelet volume predicts poor prognosis in metastatic colorectal cancer patients treated with first-line chemotherapy: results from mCRC biomarker study. *BMC Cancer* (2019) 19:15. doi: 10.1186/s12885-018-5252-2

156. Dell'Aquila E, Cremolini C, Zeppola T, Lonardi S, Bergamo F, Masi G, et al. Prognostic and predictive role of neutrophil/lymphocytes ratio in metastatic colorectal cancer: a retrospective analysis of the TRIBE study by GONO. *Ann Oncol* (2018) 29:924–30. doi: 10.1093/annonc/mdy004

157. Galindo-Pumariño C, Collado M, Herrera M, Peña C. Tumor microenvironment in metastatic colorectal cancer: the arbitrator in patients' Outcome. *Cancers (Basel)* (2021) 13. doi: 10.3390/cancers13051130

158. Manzoni M, Comolli G, Torchio M, Mazzini G, Danova M. Circulating endothelial cells and their subpopulations: role as predictive biomarkers in antiangiogenic therapy for colorectal cancer. *Clin Colorectal Cancer* (2015) 14:11–7. doi: 10.1016/j.clcc.2014.12.002

159. Rahbari NN, Schölch S, Bork U, Kahlert C, Schneider M, Rahbari M, et al. Prognostic value of circulating endothelial cells in metastatic colorectal cancer. *Oncotarget* (2017) 8:37491–501. doi: 10.18632/oncotarget.16397

160. Cima I, Kong SL, Sengupta D, Tan IB, Phyo WM, Lee D, et al. Tumor-derived circulating endothelial cell clusters in colorectal cancer. *Sci Transl Med* (2016) 8:345ra89. doi: 10.1126/scitranslmed.aad7369

161. Gootjes EC, Kraan J, Buffart TE, Bakkerus L, Zonderhuis BM, Verhoef C, et al. CD276-positive circulating endothelial cells do not predict response to systemic therapy in advanced colorectal cancer. *Cells* (2020) 9. doi: 10.3390/cells9010124

162. Ronzoni M, Manzoni M, Mariucci S, Loupakis F, Brugnatelli S, Bencardino K, et al. Circulating endothelial cells and endothelial progenitors as predictive markers of clinical response to bevacizumab-based first-line treatment in advanced colorectal cancer patients. *Ann Oncol* (2010) 21:2382–9. doi: 10.1093/annonc/mdq261

163. Malka D, Boige V, Jacques N, Vimond N, Adenis A, Boucher E, et al. Clinical value of circulating endothelial cell levels in metastatic colorectal cancer patients treated with first-line chemotherapy and bevacizumab. *Ann Oncol* (2012) 23:919–27. doi: 10.1093/annonc/mdr365

164. Matsusaka S, Mishima Y, Suenaga M, Terui Y, Kuniyoshi R, Mizunuma N, et al. Circulating endothelial progenitors and CXCR4-positive circulating endothelial cells are predictive markers for bevacizumab. *Cancer* (2011) 117:4026–32. doi: 10.1002/cncr.25977

165. Tieng FYF, Lee LH, Ab Mutalib NS. Deciphering colorectal cancer immune microenvironment transcriptional landscape on single cell resolution - A role for immunotherapy. *Front Immunol* (2022) 13:959705. doi: 10.3389/fimmu.2022.959705

166. De Simone M, Arrigoni A, Rossetti G, Gruarin P, Ranzani V, Politano C, et al. Transcriptional landscape of human tissue lymphocytes unveils uniqueness of tumor-infiltrating T regulatory cells. *Immunity* (2016) 45:1135–47. doi: 10.1016/j.immuni.2016.10.021

167. Xie N, Shen G, Gao W, Huang Z, Huang C, Fu L. Neoantigens: promising targets for cancer therapy. *Signal Transduct Target Ther* (2023) 8:9. doi: 10.1038/s41392-022-01270-x

168. Klebanoff CA, Rosenberg SA, Restifo NP. Prospects for gene-engineered T cell immunotherapy for solid cancers. *Nat Med* (2016) 22:26–36. doi: 10.1038/nm.4015

169. Dudley JC, Lin MT, Le DT, Eshleman JR. Microsatellite instability as a biomarker for PD-1 blockade. *Clin Cancer Res* (2016) 22:813–20. doi: 10.1158/1078-0432.Ccr-15-1678

170. Yarchoan M, Johnson BA 3rd, Lutz ER, Laheru DA, Jaffee EM. Targeting neoantigens to augment antitumour immunity. *Nat Rev Cancer* (2017) 17:209–22. doi: 10.1038/nrc.2016.154

171. Le DT, Durham JN, Smith KN, Wang H, Bartlett BR, Aulakh LK, et al. Mismatch repair deficiency predicts response of solid tumors to PD-1 blockade. *Science* (2017) 357:409–13. doi: 10.1126/science.aan6733

172. Kreiter S, Vormehr M, van de Roemer N, Diken M, Löwer M, Diekmann J, et al. Mutant MHC class II epitopes drive therapeutic immune responses to cancer. *Nature* (2015) 520:692–6. doi: 10.1038/nature14426

173. Parkhurst MR, Robbins PF, Tran E, Prickett TD, Gartner JJ, Jia L, et al. Unique neoantigens arise from somatic mutations in patients with gastrointestinal cancers. *Cancer Discovery* (2019) 9:1022–35. doi: 10.1158/2159-8290.Cd-18-1494

174. Sellars MC, Wu CJ, Fritsch EF. Cancer vaccines: Building a bridge over troubled waters. *Cell* (2022) 185:2770–88. doi: 10.1016/j.cell.2022.06.035

175. Hanada K, Yewdell JW, Yang JC. Immune recognition of a human renal cancer antigen through post-translational protein splicing. *Nature* (2004) 427:252–6. doi: 10.1038/nature02240

176. Cobbold M, de la Peña H, Norris A, Polefrone JM, Qian J, English AM, et al. MHC class I-associated phosphopeptides are the targets of memory-like immunity in leukemia. *Sci Transl Med* (2013) 5:203ra125. doi: 10.1126/scitranslmed.3006061

177. Malaker SA, Penny SA, Steadman LG, Myers PT, Loke JC, Raghavan M, et al. Identification of glycopeptides as posttranslationally modified neoantigens in leukemia. *Cancer Immunol Res* (2017) 5:376–84. doi: 10.1158/2326-6066.Cir-16-0280

178. Oliveira-Ferrer L, Legler K, Milde-Langosch K. Role of protein glycosylation in cancer metastasis. *Semin Cancer Biol* (2017) 44:141–52. doi: 10.1016/j.semcancer.2017.03.002

179. Brentville VA, Metheringham RL, Gunn B, Symonds P, Daniels I, Gijon M, et al. Citrullinated vimentin presented on MHC-II in tumor cells is a target for CD4+ T-cell-mediated antitumor immunity. *Cancer Res* (2016) 76:548–60. doi: 10.1158/0008-5472.Can-15-1085

180. Marijt KA, Blijleven L, Verdegaal EME, Kester MG, Kowalewski DJ, Rammensee HG, et al. Identification of non-mutated neoantigens presented by TAP-deficient tumors. *J Exp Med* (2018) 215:2325–37. doi: 10.1084/jem.20180577

181. Yewdell JW, Nicchitta CV. The DRiP hypothesis decennial: support, controversy, refinement and extension. *Trends Immunol* (2006) 27:368–73. doi: 10.1016/j.it.2006.06.008

182. Grimaldi A, Cammarata I, Martire C, Focaccetti C, Piconese S, Buccilli M, et al. Combination of chemotherapy and PD-1 blockade induces T cell responses to tumor non-mutated neoantigens. *Commun Biol* (2020) 3:85. doi: 10.1038/s42003-020-0811-x

183. Mehnert JM, Monjazeb AM, Beerthuijzen JMT, Collyar D, Rubinstein L, Harris LN. The challenge for development of valuable immuno-oncology biomarkers. *Clin Cancer Res* (2017) 23:4970–9. doi: 10.1158/1078-0432.Ccr-16-3063

184. Kilgour E, Rothwell DG, Brady G, Dive C. Liquid biopsy-based biomarkers of treatment response and resistance. *Cancer Cell* (2020) 37:485–95. doi: 10.1016/j.ccell.2020.03.012

185. Biswas D, Ganeshalingam J, Wan JCM. The future of liquid biopsy. *Lancet Oncol* (2020) 21:e550. doi: 10.1016/s1470-2045(20)30687-2

186. Neumann MHD, Bender S, Krahn T, Schlange T. ctDNA and CTCs in liquid biopsy - current status and where we need to progress. *Comput Struct Biotechnol J* (2018) 16:190–5. doi: 10.1016/j.csbj.2018.05.002

187. Ding Y, Li W, Wang K, Xu C, Hao M, Ding L. Perspectives of the application of liquid biopsy in colorectal cancer. *BioMed Res Int* (2020) 2020:6843180. doi: 10.1155/2020/6843180

188. Morganti S, Tarantino P, Ferraro E, D'Amico P, Duso BA, Curigliano G. Next generation sequencing (NGS): A revolutionary technology in pharmacogenomics and personalized medicine in cancer. *Adv Exp Med Biol* (2019) 1168:9–30. doi: 10.1007/978-3-030-24100-1_2

189. Schøler LV, Reinert T, Ørntoft MW, Kassentoft CG, Árnadóttir SS, Vang S, et al. Clinical implications of monitoring circulating tumor DNA in patients with colorectal cancer. *Clin Cancer Res* (2017) 23:5437–45. doi: 10.1158/1078-0432.Ccr-17-0510

190. Cabel L, Proudhon C, Gortais H, Loirat D, Coussy F, Pierga JY, et al. Circulating tumor cells: clinical validity and utility. *Int J Clin Oncol* (2017) 22:421–30. doi: 10.1007/s10147-017-1105-2

191. Reinert T, Schøler LV, Thomsen R, Tobiasen H, Vang S, Nordentoft I, et al. Analysis of circulating tumour DNA to monitor disease burden following colorectal cancer surgery. *Gut* (2016) 65:625–34. doi: 10.1136/gutjnl-2014-308859

192. Zhou H, Zhu L, Song J, Wang G, Li P, Li W, et al. Liquid biopsy at the frontier of detection, prognosis and progression monitoring in colorectal cancer. *Mol Cancer* (2022) 21:86. doi: 10.1186/s12943-022-01556-2

193. Liu Y, Zugazagoitia J, Ahmed FS, Henick BS, Gettinger SN, Herbst RS, et al. Immune cell PD-L1 colocalizes with macrophages and is associated with outcome in PD-1 pathway blockade therapy. *Clin Cancer Res* (2020) 26:970–97. doi: 10.1158/1078-0432.Ccr-19-1040

194. Lin SY, Chang SC, Lam S, Irene Ramos R, Tran K, Ohe S, et al. Prospective molecular profiling of circulating tumor cells from patients with melanoma receiving combinatorial immunotherapy. *Clin Chem* (2020) 66:169–77. doi: 10.1373/clinchem.2019.307140

195. Dou X, Hua Y, Chen Z, Chao F, Li M. Extracellular vesicles containing PD-L1 contribute to CD8+ T-cell immune suppression and predict poor outcomes in small cell lung cancer. *Clin Exp Immunol* (2022) 207:307–17. doi: 10.1093/cei/uxac006

196. Ma S, Zhou M, Xu Y, Gu X, Zou M, Abudushalamu G, et al. Clinical application and detection techniques of liquid biopsy in gastric cancer. *Mol Cancer* (2023) 22:7. doi: 10.1186/s12943-023-01715-z

Glossary

CRC	Colorectal cancer
ICIs	immune checkpoint inhibitors
CTCs	circulating tumor cells
ctDNA	circulating tumor DNA
cfDNA	circulating cell-free DNA
MRD	minimal residual disease
mCRC	metastatic colorectal cancer
DFS	disease-free survival
PFS	progression-free survival
OS	overall survival
LARC	locally advanced rectal cancer
MSI-H	MSI-H microsatellite instability
CAR-T	chimeric antigen receptor T
TCR	T cell receptor
PLR	platelet-to-lymphocyte ratio
NLR	neutrophil-to-lymphocyte ratio
CTECs	circulating tumor endothelial cells
scRNA-seq	single-cell sequencing technology
TILs	tumor-infiltrating lymphocytes
TIME	tumor immune microenvironment
NM-neoAgs	Non-mutated neoantigens
neoAgs	Neoantigens
FDA	Food and Drug Administration
MSI-H	microsatellite-high
dMMR	deficient mismatch repair
PD-L1	programmed cell death ligand 1
PD-1	programmed death receptor 1
RFS	recurrence-free survival
NGS	next-generation sequencing
RFS	recurrence-free survival
IHC	immunohistochemistry
PCR	polymerase chain reaction
ORR	overall response rates
TME	tumor microenvironment
TMB	tumor mutational burden
MSS	microsatellite-stable
IHC	immunohistochemistry
PCR	polymerase chain reaction

(Continued)

Continued

pMMR	proficient mismatch repair
ER	endoplasmic reticulum
TAP	processing-associated transporter
Ii	invariant chain
MIIC	MHC-II compartment
pMHC	peptide-MHC

frontiers | Frontiers in Immunology

TYPE Original Research
PUBLISHED 04 January 2024
DOI 10.3389/fimmu.2023.1294565

OPEN ACCESS

EDITED BY
Madiha Derouazi,
Speransa Therapeutics GmbH, Germany

REVIEWED BY
Paul Walker,
University of Geneva, Switzerland
Susan Klaeger,
Genentech Inc., United States

*CORRESPONDENCE
Frank Momburg
f.momburg@dkfz-heidelberg.de
Marten Meyer
marten.meyer@dkfz-heidelberg.de

†These authors have contributed equally to this work

RECEIVED 14 September 2023
ACCEPTED 28 November 2023
PUBLISHED 04 January 2024

CITATION
Meyer M, Parpoulas C, Barthélémy T, Becker JP, Charoentong P, Lyu Y, Börsig S, Bulbuc N, Tessmer C, Weinacht L, Ibberson D, Schmidt P, Pipkorn R, Eichmüller SB, Steinberger P, Lindner K, Poschke I, Platten M, Fröhling S, Riemer AB, Hassel JC, Roberti MP, Jäger D, Zörnig I and Momburg F (2024) MediMer: a versatile do-it-yourself peptide-receptive MHC class I multimer platform for tumor neoantigen-specific T cell detection. *Front. Immunol.* 14:1294565. doi: 10.3389/fimmu.2023.1294565

MediMer: a versatile do-it-yourself peptide-receptive MHC class I multimer platform for tumor neoantigen-specific T cell detection

Marten Meyer[1,2,3*], Christina Parpoulas[1†], Titouan Barthélémy[1†], Jonas P. Becker[4,5], Pornpimol Charoentong[2,3,6], Yanhong Lyu[2], Selina Börsig[1,3], Nadja Bulbuc[1], Claudia Tessmer[1,2], Lisa Weinacht[1], David Ibberson[7], Patrick Schmidt[3,8], Rüdiger Pipkorn[8], Stefan B. Eichmüller[8], Peter Steinberger[9], Katharina Lindner[10,11], Isabel Poschke[10,11], Michael Platten[10,11,12,13,14,15], Stefan Fröhling[12,16,17], Angelika B. Riemer[4,5], Jessica C. Hassel[18], Maria Paula Roberti[2,3], Dirk Jäger[2,3], Inka Zörnig[2,3] and Frank Momburg[1,3*]

[1]Antigen Presentation and T/NK Cell Activation Group, German Cancer Research Center (DKFZ), Heidelberg, Germany, [2]Clinical Cooperation Unit Applied Tumor Immunity, DKFZ, Heidelberg, Germany, [3]Department of Medical Oncology, National Center for Tumor Diseases (NCT) Heidelberg, Heidelberg University Hospital, Heidelberg, Germany, [4]Division of Immunotherapy and Immunoprevention, DKFZ, Heidelberg, Germany, [5]German Center for Infection Research (DZIF) Partner Site Heidelberg, Heidelberg, Germany, [6]Center for Quantitative Analysis of Molecular and Cellular Biosystems (Bioquant), Heidelberg University, Heidelberg, Germany, [7]Deep Sequencing Core Facility, Heidelberg University, Heidelberg, Germany, [8]GMP and T Cell Therapy, DKFZ, Heidelberg, Germany, [9]Division of Immune Receptors and T Cell Activation, Center for Pathophysiology, Infectiology, Medical University of Vienna, Vienna, Austria, [10]Clinical Cooperation Unit Neuroimmunology and Brain Tumor Immunology, DKFZ, Heidelberg, Germany, [11]Immune Monitoring Unit, NCT Heidelberg and DKFZ, Heidelberg, Germany, [12]German Cancer Consortium (DKTK), DKFZ, Core Center, Heidelberg, Germany, [13]Department of Neurology, Medical Faculty Mannheim, Mannheim Center for Translational Neuroscience (MCTN), Heidelberg University, Mannheim, Germany, [14]DKFZ Hector Cancer Institute at the University Medical Center, Mannheim, Germany, [15]Helmholtz Institute for Translational Oncology, Mainz (HI-TRON Mainz), Mainz, Germany, [16]Division of Translational Medical Oncology, NCT Heidelberg and DKFZ, Heidelberg, Germany, [17]Institute of Human Genetics, Heidelberg University, Heidelberg, Germany, [18]Section of DermatoOncology, Department of Dermatology and NCT, Heidelberg University Hospital, Heidelberg, Germany

Peptide-loaded MHC class I (pMHC-I) multimers have revolutionized our capabilities to monitor disease-associated T cell responses with high sensitivity and specificity. To improve the discovery of T cell receptors (TCR) targeting neoantigens of individual tumor patients with recombinant MHC molecules, we developed a peptide-loadable MHC class I platform termed MediMer. MediMers are based on soluble disulfide-stabilized β_2-microglobulin/heavy chain ectodomain single-chain dimers (dsSCD) that can be easily produced in large quantities in eukaryotic cells and tailored to individual patients' HLA allotypes with only little hands-on time. Upon transient expression in CHO-S cells together with ER-targeted BirA biotin ligase, biotinylated dsSCD are purified from the cell

supernatant and are ready to use. We show that CHO-produced dsSCD are free of endogenous peptide ligands. Empty dsSCD from more than 30 different HLA-A,B,C allotypes, that were produced and validated so far, can be loaded with synthetic peptides matching the known binding criteria of the respective allotypes, and stored at low temperature without loss of binding activity. We demonstrate the usability of peptide-loaded dsSCD multimers for the detection of human antigen-specific T cells with comparable sensitivities as multimers generated with peptide-tethered β_2m-HLA heavy chain single-chain trimers (SCT) and wild-type peptide-MHC-I complexes prior formed in small-scale refolding reactions. Using allotype-specific, fluorophore-labeled competitor peptides, we present a novel dsSCD-based peptide binding assay capable of interrogating large libraries of *in silico* predicted neoepitope peptides by flow cytometry in a high-throughput and rapid format. We discovered rare T cell populations with specificity for tumor neoepitopes and epitopes from shared tumor-associated antigens in peripheral blood of a melanoma patient including a so far unreported HLA-C*08:02-restricted NY-ESO-1-specific $CD8^+$ T cell population. Two representative TCR of this T cell population, which could be of potential value for a broader spectrum of patients, were identified by dsSCD-guided single-cell sequencing and were validated by cognate pMHC-I multimer staining and functional responses to autologous peptide-pulsed antigen presenting cells. By deploying the technically accessible dsSCD MHC-I MediMer platform, we hope to significantly improve success rates for the discovery of personalized neoepitope-specific TCR in the future by being able to also cover rare HLA allotypes.

KEYWORDS

T cells, tumor immunotherapy, peptide-MHC class I multimer, neoepitope screening, T cell receptor discovery, tumor neoantigen, personalized medicine

1 Introduction

Detection of antigen-specific T cells labeled by recombinantly produced soluble peptide-loaded MHC-I (pMHC-I) molecules using flow cytometry represents to date one of the most sensitive techniques for identifying, monitoring and quantifying T cell responses against well-defined antigens. The pioneering work by Altman and colleagues demonstrated that insufficient binding affinities and high off-rates of soluble monomeric pMHC-I complexes for T cell receptor labeling can be overcome by streptavidin-mediated multimerization of biotinylated MHC-I heavy ectodomains assembled with β_2-microglobulin (β_2m) and an appropriate peptide ligand (1). Soluble pMHC-I multimer staining reagents have since undergone an evolutionary process regarding their production process, multimer valency and methods of peptide loading as well as strategies that allow multiplex detection of various T cell specificities within one labeling reaction by combinatorial color encoding and DNA barcoding of multimers (2–6).

Interrogation of large numbers of potential shared or individual T cell antigens across the human population with pMHC-I multimer reagents however remains a challenging issue and is often limited by the capacity to manufacture individualized pMHC-I multimer libraries and to cover a broad spectrum of HLA allotypes, which is addressed by virtue of a pMHC-I platform.

Originally, bacterially expressed soluble MHC-I heavy chains and β_2m were combined in rather inefficient *in vitro* pMHC-I folding reactions in the presence of a chemically synthesized peptide ligand leading to the necessity of size exclusion chromatography for each individual pMHC-I followed by enzymatic BirA biotin ligase-mediated biotinylation and multimer formation with fluorochrome-conjugated streptavidin (1). This widely used method has been optimized and miniaturized by firstly purifying correctly oxidized heavy chains of *in vivo* biotinylated MHC-I ectodomains isolated from *E. coli* inclusion bodies leading to higher *in vitro* folding efficiencies when combined with synthetic peptides and β_2m in small-scale refolding reactions, which can be

Abbreviations: β2m, β2-microglobulin; CHO-S, Chinese hamster ovary cells growing in suspension; dsSCD, disulfide-stabilized single-chain dimers; dtSCT, disulfide-trapped single-chain trimer; FITC, fluorescein-5-isothiocyanate; MFI, median fluorescence intensity; pMHC-I, peptide-loaded/associated major histocompatibility complex class I; RT, room/ambient temperature; scRNA-Seq, single-cell mRNA sequencing; SAv, streptavidin; SD, standard deviation; TCR, T cell receptor; TAA, non-mutant tumor-associated antigen.

directly multimerized without further purification steps (7), and has recently been used for the identification of immunogenic glioblastoma-specific T cell epitopes derived from transposable elements (8).

By introducing an additional disulfide bond locking the C-terminal end of the peptide binding cleft in MHC-I molecules, Springer and coworkers achieved peptide-independent stabilization of the MHC-I heavy chain (9). Disulfide-stabilized A*02:01 heavy chains molecules showed an unaltered structure of the peptide-binding groove in the peptide-bound and peptide-free states as well as unaffected recognition by an A*02:01-restricted TCR (10–12). Here, *E. coli*-derived disulfide-stabilized MHC-I heavy chains were refolded in the presence of a dipeptide and β_2m to subsequently purify soluble peptide-free MHC-I molecules that are highly peptide-receptive (10). Alternatively, various peptide exchange-based pMHC-I platforms have been proposed, including temperature-induced exchange (13) and a widely used peptide exchange system, utilizing the *in vitro* refolding of MHC-I with β_2m and a conditional placeholder peptide ligand, that are cleaved upon exposure to ultraviolet light (14). Decomposed placeholder peptides rapidly dissociate from the peptide binding groove, thus allowing any other suitable peptide ligand of interest to rescue the heterotrimeric complex. This platform has been successfully applied for the generation of larger pMHC-I libraries (15–17) but is yet commercially available for only a very limited number of HLA alleles.

A different strategy pioneered by Hansen and colleagues makes use of fusion proteins that genetically encode the entire heterotrimeric peptide–β_2m–heavy chain complex linking the components through flexible glycine-serine sequences (18). Such MHC-I single-chain trimers (SCT) have been optimized for peptide binding stability and linker accommodation by introduction of a disulfide trap between a cysteine-substituted conserved tyrosine residue at the C-terminal end of the MHC-I α1 helix with another cysteine in the peptide–β_2m linker (19–21). Disulfide-trapped SCT (dtSCT) feature functionally correct folding, improved thermal stability and complete exclusion of competitor peptides when produced as soluble molecules in bacteria or expressed in the natural membrane-bound form in cell lines and perform excellently in pMHC-I multimers (19, 22). Dimeric SCT tethered to the heavy chain of IgG were successfully used to detect antigen-specific T cells (23, 24). We have previously reported soluble dimeric dtSCT fused to the Fc portion of IgG that are efficiently producible in suspension-adapted Chinese Hamster Ovary (CHO-S) cells (25). While stable peptide binding in SCT is advantageous for their use as vaccines (26–28), the generation of larger SCT libraries for the screening of pMHC-I reactive T cells is technically demanding since each SCT needs to be genetically engineered separately (29, 30).

In screening campaigns for tumor neoepitope-reactive T cells with peptide-loaded MHC multimers we encountered the need to cover a variety of rare HLA-A, -B, and -C allotypes that are presently not commercially available as recombinant MHC-I molecules. In order to fully exploit the tumor patients' T cell repertoire directed against all six HLA-A,B,C allotypes, we developed a new platform termed MediMer (MHC-I, empty, single-chain dimer) based on disulfide-stabilized peptide-free β_2m–MHC-I heavy chain single-chain dimers (dsSCD) that are produced in metabolically biotinylated form by CHO-S producer cells without the need of additional steps such as *in vitro* refolding. The MediMer production system can be easily adapted and allows fast do-it-yourself tailoring of required HLA allotypes for a given patient cohort. Purified dsSCD representing a so far unrestricted number of HLA-A,B,C allotypes, are highly stable and peptide-receptive, making them highly suitable for the screening of individualized neoepitope large peptide libraries. Furthermore, we show that multimerized peptide-loaded dsSCD perform efficiently to label and isolate antigen-specific T cells and can be combined in a single experiment in a complementary manner with other commercial pMHC-I platforms and multiplex labeling strategies such as DNA-barcoding for single cell RNA sequencing. In addition, we present a dsSCD-based peptide binding assay for the fast high-throughput binding validation of *in silico* predicted HLA ligands.

2 Materials and methods

2.1 Cloning of dsSCD and dtSCT expression plasmids

Disulfide-stabilized human β_2-microglobulin (β_2m)-HLA-A,B,C single-chain dimers were cloned by assembling:

1. the modified influenza A virus hemagglutinin H1N1 leader sequence (MAKANLLVLLCALAAADALGS),
2. the leader-less human β_2-microglobulin sequence (accession no. AK315776, Ile_{21}-Met_{119}),
3. a glycine-serine linker sequence (SGGS[GGGGS]$_3$ASGGG),
4. leader-less ectodomains of various HLA-A,B,C alleles (Supplementary Table 4), Gly_1-Pro_{283} containing Tyr_{84} to Cys and Ala_{139} to Cys mutations), forming an additional disulfide bond between α1 and α2 domains (9, 31),
5. the tag-linker sequence including a His_8-tag (**bold**, *italics*), a BirA biotin ligase recognition site (**bold**) and a double thrombin protease cleavage site (*italics*) (32) (TSTGQL***HHHHHHHH***QL**GLNDIFEAQKIEWHE** *LVPRSLVPRS*TS),
6. the Fc portion of mouse IgG2a (BC031479; Glu_{215}-Lys_{447}, Cys_{224}/Ser), and
7. a C-terminal StrepTag-II (**bold**) with adapter sequences (DPG**WSHPQFEK**SR) by restriction enzyme cloning and PCR mutagenesis. In Fc-free dsSCD constructs the tag-linker sequence was terminated with 2 stop codons after the BirA biotin ligase recognition site. Assembled cDNA sequence were cloned between the *Nhe*I and *Xba*I sites of expression vector pcDNA3.1(+) (Invitrogen).

Disulfide-trapped single-chain trimer (dtSCT) constructs were cloned by assembling:

a. the leader sequence MAKANLLVLLCALAAAQPAMA,
b. a sequence encoding an 8-11-mer peptide of choice,
c. glycine-serine linker #1 containing a cysteine residue at position 2 (G**C**GSGGGGAPGSGGGS),
d. the leader-less β_2m sequence,
e. glycine-serine linker #2 (SGGS[GGGGS]$_3$ASGGG),
f. leader-less ectodomains of various HLA-A,B,C alleles containing a Tyr_{84} to Cys mutation to form the disulfide trap with Cys_2 in linker #1 (19) followed by the tag-linker and mIgG2a-Fc as described above and as previously described for dtSCT in (25, 32).

In the HLA-A*02:01 dsSCD with cleavable β_2m linker, the human rhinovirus (HRV) type 14 3C protease cleavage site (bold) was inserted in a modified glycine-serine linker (SGGS[GGGGS]$_3$AS**LEVLFQGP**SGAS). *E. coli* BirA biotin ligase (accession no. M15820) was cloned by PCR from genomic DNA isolated *E. coli* XL1-Blue and the coding sequence except for Met_1 was cloned at the 3' end of an Igk leader sequence in the expression vector pcDNA3.1 (–). The KDEL motif coding for an ER retention/recycling signal was cloned at the C-terminal end of the open reading frame after Glu_{270}.

2.2 Soluble dsSCD and dtSCT synthesis in mammalian cell transient gene expression systems

Expression of dsSCD and dtSCT was tested in suspension-adapted FreeStyle™ Chinese hamster ovary cell (CHO-S, Gibco) as previously described (25, 33) and FreeStyle™ 293-F (293-F, Gibco) transient gene expression systems (32). CHO-S were routinely cultured in PowerCHO-2 CD (Lonza), supplemented with 8 mM GlutaMAX™ (Gibco) and 0.5x Antibiotic Antimycotic solution (Anti-Anti, Sigma-Aldrich) at 37°C, 8% CO_2 and 100 rpm with a 50 mm shaking diameter. 293-F cells were routinely cultured in FreeStyle™ 293 Expression Medium (293-F medium, Gibco) at 37°C, 8% CO_2 and 100 rpm. For protein production in CHO-S, CHO-S cells were resuspended at $3x10^6$ cells/ml in ProCHO4 medium (Lonza) supplemented with 4 mM GlutaMAX™ (Gibco), 4 µg/ml D-biotin (Sigma-Aldrich) and 0.5x Anti-Anti followed by the sequential addition per $1x10^6$ cells of 2.5 µg 25-kDa linear polyethyleneimine (PEI; Polysciences), 0.32 µg plasmid DNA encoding for a dsSCD or dtSCT and 0.32 µg plasmid DNA encoding for an ER-retained BirA ligase ($BirA_{KDEL}$). Co-transfected CHO-S were maintained at 37°C, 8% CO_2 and 100 rpm for 6 hours followed by supplementation with 1 mM valproic acid (VPA, Sigma-Aldrich) and maintenance for 6 days under hypothermic conditions at 32°C, 5% CO2 and 100 rpm. For protein production in 293-F cells, 293-F cells were resuspended at $1x10^6$ cells/ml in 293-F medium supplemented with 4 mM GlutaMAX™, 4 µg/ml D-biotin following co-transfection with dsSCD or dtSCT encoding plasmids and $BirA_{KDEL}$ plasmid using the 293-free transfection reagent (Sigma-Aldrich) according to the manufacturer's protocols. The next day, VPA was added to the 293-F transfected culture to a final concentration of 4 mM as well as 0.5x anti-anti. The supplemented 293-F culture was further maintained for 6 days at 37°C, 8% CO_2 and 100 rpm. On day 6 post transfection, cell-free CHO-S or 293-F supernatants of dsSCD-Fc or dtSCT-Fc transfections were supplemented with 0.1 volumes of 10x Dulbecco's PBS (DPBS) (Sigma-Aldrich) and 2 IU thrombin (Merck) per mg dsSCD-Fc or dtSCT-Fc, quantified by a mouse-IgG-Fc-based sandwich ELISA, followed by an overnight incubation at 37°C. Soluble monomeric Fc-free dtSCT from 293-F cultures or dsSCD from CHO-S cultures were further purified by immobilized metal affinity chromatography (IMAC) using Ni-INDIGO MagBeads (Cube Biotech) or column-packed Ni Sepharose Excel resin (Cytiva), respectively, according to the manufacturers' instructions. Eluted proteins were finally dialyzed against PBS (pH 7.4) and their purity and metabolic biotinylation were verified by a non-reducing 10% SDS-PAGE (Invitrogen) in the presence of streptavidin. Purified dsSCT and dsSCD were stored in PBS at 4°C throughout the study unless otherwise stated. In one experiment purified dsSCD was supplemented with 5% glycerol (v/v) and 0.5% bovine serum albumin (BSA) (w/v) in PBS and stored at -20°C prior to its usage for cell stainings. For expression analysis of CHO-S and 293-F cells by intracellular staining, an aliquot of cells was taken 48 h post transfection and washed once with DPBS followed by labeling with the Zombie Aqua™ Fixable Viability Kit (BioLegend, 1:300) to exclude dead cells. Cells were fixed and permeabilized for 10 min at 4°C and were then stained intracellularly for 30 min with anti-HLA-A2-APC (BB7.2, BioLegend, 343308) using the Cytofix/Cytoperm™ Fixation/Permeabilization Kit (BD Bioscience) according to the manufacturer's instructions. Stained cells were washed once with DPBS + 2% fetal calf serum (FCS) and acquired on a FACSCanto™ II flow cytometer (BD Bioscience). Analysis was done using the FlowJo Software (BD Bioscience). Single living (ZombieAqua$^-$) cells were gated and anti-HLA-A2-APC signals visualized.

2.3 Peptide synthesis

For the fast and reliable peptide binding validation of freshly produced dsSCD of various HLA-A, B, C allotypes, a set of peptide sequences of known HLA-I ligands (Supplementary Table 1) were rationally modified to incorporate a fluorescein-5-isothiocyanate (FITC)-conjugated lysine residue (K^{FITC}/K*) at a selected non-anchor residue.

Chemical peptide synthesis was performed employing the Fmoc strategy (34, 35) in a fully automated multiple synthesizer Syro II (MultiSyn Tech, Germany). The synthesis was carried out on preloaded 2-CT-polystyrene resin (Rapp Polymere GmbH, Germany). As coupling agent 2-(1H-benzotriazole-1-yl)-1,1,3,3-tetramethyluronium hexafluorophosphate (HBTU) was used. For the FITC-conjugated peptides we used Fmoc-Lys(5-FITC)-OH

(Biomol GmbH, Germany). The synthesized peptides were cleaved and deprotected from the solid support by treatment with 90% trifluoroacetic acid, 8% tri-isopropylsilane, and 2% water (v/v/v) for 2.5 h at room temperature. The products were precipitated in ether and checked by analytical LC/MS (Thermo Finnigan LCQ). When necessary, peptides were purified by preparative HPLC on a Kromasil 100–10C 10 µm 120A reverse phase column (20 x 150 mm) using an eluent of 0.1% trifluoroacetic acid in water (A) and 80% acetonitrile in water (B). The peptide was eluted with a successive linear gradient of 10% B to 80% B in 30 min at a flow rate of 17 ml/min. The fractions corresponding to the purified peptide were lyophilized. The purified material was characterized by analytical LC/MS (Thermo Finnigan LCQ).

K^{FITC}-containing peptides as well as selected unlabeled peptides were dissolved to 10 mM and 50 mM in dimethyl sulfoxide (DMSO), respectively. In addition, peptides employed for immunogenicity screening of predicted neoepitopes of the melanoma patient were purchased from JPT Peptide Technologies GmbH (Berlin, Germany).

2.4 DsSCD peptide-binding assays

To verify binding of selected ^{FITC}peptides to dsSCD, dsSCD were diluted to 33 nM in 30 µl DPBS supplemented with 5% glycerol (v/v) and 0.5% BSA (w/v) and 1 µl streptavidin-conjugated beads (Spherotech, SVP-60-05) followed by the addition of 1 µM ^{FITC}peptide. ^{FITC}peptide-pulsed dsSCD-loaded beads were incubated overnight in the dark at room temperature (RT) under shaking conditions in V-bottom 96-well plates. After the incubation, beads were washed twice with DPBS + 0.5% BSA (w/v) + 0.1% Tween-20 (v/v) and once with DPBS + 2% FCS prior their acquisition on a LSRFortessa™ flow cytometer (BD Bioscience). In some experiments, the ^{FITC}peptide concentration or pulse duration or incubation temperature was varied as indicated in the figure legends. To assess the binding of a given unlabeled test peptide to a dsSCD, the selected dsSCD was immobilized at 33 nM on beads as described above and pulsed overnight (ca. 18 h) with 10 µM of the test peptide or were left empty serving as maximum ^{FITC}peptide loading control ("median fluorescence intensity (MFI) Max") in the next step. After the overnight incubation, 1 µM of an established dsSCD binding ^{FITC}peptide was added for 10 min as a competitor directly to the dsSCD-beads in the presence of 10 µM test peptide as well as to dsSCD-beads lacking a prior peptide pulse. dsSCD-beads were washed immediately after the 10min ^{FITC}peptide pulse and subjected to flow cytometric analysis. Unlabeled test peptide occupancy of dsSCD-beads was assessed based on FITC MFI values after ^{FITC}peptide pulse ("MFI Test") relative to dsSCD-beads that had been loaded with ^{FITC}peptide in the absence of a test peptide. For normalization, background MFI of empty beads was subtracted. % MFI reduction was calculated according the following equation:

$$\%\ MFI\ \ reduction = \frac{(Normalized\ \ MFI\ \ Max - Normalized\ \ MFI\ \ Test)}{(Normalized\ \ MFI\ \ Max)}\ x\ 100$$

2.5 EasYmer peptide-HLA-I complex formation assay

HLA-A*01:01, HLA-A*02:01, HLA-A*68:01, HLA-B*08:01, HLA-B*14:01, HLA-C*05:01 and HLA-C*07:01 easYmer® kits were purchased from immunAware ApS (Horsholm, Denmark). Peptide interaction with a given easYmer composed of soluble biotinylated MHC-I heavy chain and non-covalently associated β_2m (7) was detected by a flow cytometry-based peptide-HLA-I complex formation assay according to the manufacturer's protocol. Briefly, easYmers were diluted to 0.5 µM in provided folding buffer and a library of peptides including a designated positive-binding control peptide per HLA allotype was added at a final concentration of 3 µM, or diluted easYmers were left in the absence of peptide as negative control for 2-3 days at RT. The folding reaction was diluted to 5 nM in a final volume of 60 µl DPBS + 5% glycerol and supplemented with streptavidin-conjugated beads (Spherotech, SVP-60-05) (finally diluted 1:135), following an incubation for 1 h at 37°C under constant shaking. EasYmer-loaded beads were washed three times with FACS Buffer (DPBS + 2% FCS) and were stained with anti-β2m-PE (clone BBM.1, Santa Cruz sc-13565 PE) for 30 min at 4°C. Beads were again washed three times with FACS buffer and acquired on a LSRFortessa (BD Bioscience) flow cytometer. Successful peptide-HLA-I complex formation was assessed as an approximation by using the bead-immobilized median fluorescence intensity (MFI) of β2m after addition of a positive control peptide relative to the MFI value of a given test peptide according to the following equation:

$$\%\ easYmer\ \ formation = \frac{MFI\ \ value\ \ of\ \ easYmer\ \ folding\ \ reaction\ \ with\ \ test\ \ peptide}{MFI\ \ value\ \ of\ \ easYmer\ \ folding\ \ reaction\ \ with\ \ positive\ \ ctrl.\ \ peptide}\ x\ 100$$

2.6 Data-independent acquisition mass spectrometry of empty and peptide-loaded dsSCD

CHO cell-derived HLA-A*02:01 dsSCD diluted to 0.18 µg/µL (3 µM) in DPBS was loaded overnight at room temperature with 100 µM of a peptide pool comprising the known HLA-A*02:01 binder NLVPMVATV, VLEETSVML, GLCTLVAML, GILGFVFTL, YLQPRTFLL, ELAGIGILTV and HLA-A*02:01 non-binder CTELKLSDY (Supplementary Table 3) or the diluted HLA-A*02:01 dsSCD was left overnight without external peptide addition. HLA-A*02:01 dsSCD samples were mixed with 1 ml lysis buffer (0.25% sodium deoxycholate, 1% N-octyl-β-D-glucopyranoside, 1 mM PMSF, 1 mM EDTA, 0.2 mM iodoacetamide, 1 cOmplete™ Protease Inhibitor Cocktail Mini tablet (Roche) per 5 ml of lysis buffer) and directly used for immunoprecipitation with an HLA-A2-specific antibody (clone BB7.2) as previously described with minor modifications (36). Lyophilized peptides were dissolved in 12 µl of 5% acetonitrile (ACN) in 0.1% trifluoroacetic acid (TFA) and spiked with 100 fmol Peptide Retention Time Calibration (PRTC) Mixture (Pierce) and transferred to QuanRecovery Vials with MaxPeak HPS

(Waters, Milford, MA, USA). All samples were analyzed using an UltiMate 3000 RSLCnano system coupled to an Orbitrap Exploris 480 equipped with a FAIMS Pro Interface (Thermo Fisher Scientific). For chromatographic separation, peptides were first loaded onto a trapping cartridge (Acclaim PepMap 100 C18 µ-Precolumn, 5 µm, 300 µm i.d. x 5 mm, 100 Å; Thermo Fisher Scientific) and then eluted and separated using a nanoEase M/Z Peptide BEH C18 130A 1.7µm, 75µm x 200mm (Waters). Total analysis time was 120 min and separation was performed using a flow rate of 0.3 µl/min with a gradient starting from 1% solvent B (100% ACN, 0.1% TFA) and 99% solvent A (0.1% formic acid (FA) in H_2O) for 0.5 min. Concentration of solvent B was increased to 2.5% in 12.5 min, to 28.6% in 87 min and then to 38.7% in 1.4 min. Subsequently, concentration of solvent B was increased to 80% in 2.6 min and kept at 80% solvent B for 5 min for washing. Finally, the column was re-equilibrated at 1% solvent B for 11 min. The LC system was coupled on-line to the mass spectrometer using a Nanospray-Flex ion source (Thermo Fisher Scientific), a SimpleLink Uno liquid junction (FossilIonTech) and a CoAnn ESI Emitter (Fused Silica 20 µm ID, 365 µm OD with orifice ID 10 µm; CoAnn Technologies). The mass spectrometer was operated in positive mode and a spray voltage of 2500 V was applied for ionization with an ion transfer tube temperature of 300°C. For ion mobility separation, the FAIMS module was operated with standard resolution and a total carrier gas flow of 4.6 l/min. Each sample was injected twice using either a compensation voltage of -50 V or -70 V for maximal orthogonality and thus increased immunopeptidome coverage. Full Scan MS spectra were acquired for a range of 300 – 1650 m/z with a resolution of 120.000 (RF Lens 50%, AGC Target 300%). MS/MS spectra were acquired in data-independent mode for a cycle time of 3s using 44 previously determined dynamic mass windows optimized for HLA class I peptides with an overlap of 0.5 m/z. HCD collision energy was set to 28% and MS/MS spectra were recorded with a resolution of 30.000 (normalized AGC target 3000%).

MS raw data was analyzed using the directDIA workflow of the Spectronaut software [version 17; Biognosys (37)] and searched against the UniProtKB/TrEMBL database for *Cricetulus griseus* (Chinese hamster) (retrieved: 12.09.2022, 78117 entries) and a database containing the seven peptides used for external loading of the dsSCD. Search parameters were set to non-specific digestion and a peptide length of 7-15 amino acids. Carbamidomethylation of cysteine and oxidation of methionine were included as variable modifications. Additionally, MS raw data were manually searched using Skyline (version 22) (38). Spectral libraries for peptides originating from the peptide pool used for loading were *in silico* generated using PROSIT (39). Spectral angles were calculated as described previously (40). All results were visualized using in-house developed R scripts.

2.7 TCR cloning and generation of stably recombinant TCR expressing CD8$^+$ Jurkat 76 T cell lines

Sequences of published T cell receptors (TCR) were cloned as chimeric human (h) TRVB–mouse (m) TRBC and hTRAV–mTRAC sequences in bicistronic open reading frames containing a P2A or T2A ribosomal skipping sequence between TCRβ and TCRα chains. The HCMV pp65$_{495\text{-}503}$/HLA-A*02:01 specific TCR RA14 (41), the MART1$_{27\text{-}35}$/HLA-A*02:01 specific TCR DMF5 (42), the KRAS$^{G12V}{}_{8\text{-}16}$/HLA-A*11:01 specific TCR Ry-4148-G12V-9mer (43), the KRAS$^{G12D}{}_{10\text{-}18}$/HLA-C*08:02 specific TCR TCR4(G12D) (44), the NY-ESO-1$_{157\text{-}165}$/HLA-A*02:01 specific TCR 1G4 (45), and the NY-ESO-1$_{96\text{-}104}$/HLA-C*03:04 specific TCR 3C7 (46) have been described previously. For this study, 5 additional TCRs following the cloning strategy mentioned above (MM-01 – MM-05) were cloned using sequence information from the vloupe.vloupe output file of a 10x Genomics-based single-cell sequencing data set of pMHC-I multimer$^+$ CD8$^+$ T cell populations that have been cell sorted from peripheral blood of a melanoma patient. All TCR sequences were subcloned in the transposon expression vector pSBbi-pur (47) (addgene plasmid #60523) together with pcDNA3.1(+) expression vector encoding SB100 Sleeping Beauty transposase (48) subcloned from pCMV(CAT) T7-SB100 (addgene plasmid #34879). To test the recombinant TCRs for pMHC-I multimer binding, a J76 Jurkat E6.1 subline expressing CD8 and lacking endogenous TCRα and β chains [J76^{CD8+}, generated as described (49)] was electroporated with 2 µg endotoxin-free TCR plasmid and 2 µg transposase plasmid per 2x10^6 J76^{CD8+} cells using the P3 primary cell 4D-Nucleofector X Kit S (Lonza) according to the manufacturer's recommended protocol. TCR and CD8 expression was monitored by flow cytometry using antibodies against murine TCR-Cβ-APC (clone H57-597, BioLegend 109212) and CD8-PacificBlue (Clone SK1, BioLegend 344718). TCR-transfected J76^{CD8} cells were maintained for one week in RPMI supplemented with 10% FCS, 10 µg/ml gentamycin and 2 mM GlutaMAX at 37°C, 5% CO_2, followed by enrichment for TCR-expressing J76^{CD8} cells using CD3-MicroBead-based (Miltenyi) magnetic cell sorting (MACS) according to the manufacture's protocol prior to their usage in pMHC-I multimer stainings.

2.8 Functional validation of TAA-specific TCRs using autologous expanded B cells

Primary human B cells were magnetically isolated from peripheral blood of a melanoma patient using CD19-MicroBeads (Miltenyi). Isolated B cells expanded over the course of 6 days using StemMACS^{TM} HSC medium supplemented with 0.5 µg/ml multimerized soluble human CD40L, 50 IU/ml IL-4, 10 IU/ml IL-2, 10 ng/ml IL-21 (all from Miltenyi), 40 ng/ml BAFF (BioLegend) and 0.625 µg/ml cyclosporin A (Sigma-Aldrich) at 37°C, 5% CO_2. Expanded B cells were washed three times with DPBS and were co-cultured in a 1:1 ratio with TCR$^+$ J76^{CD8} cells in RPMI supplemented with 10% FCS, 10 µg/ml gentamycin and 2 mM GlutaMAX in the presence of cognate and control peptides at various concentrations. After 18 h of co-culture, activation of TCR$^+$ J76^{CD8} cells was analyzed by flow cytometry for CD69 upregulation by anti-CD69-PE (FN50, BioLegend 310906)

staining combined with anti-murine TCR-Cβ-APC (H57-597) and anti-CD8-Pacific Blue (SK1).

2.9 Isolation of primary CD8$^+$ T cells from PBMC of healthy donors and a melanoma patient

PBMCs of healthy donors HD-01–HD-07 and an advanced-stage melanoma patient were isolated from blood samples using 1.077 g/ml density gradient centrifugation (Pancoll human, PAN Biotech) and cryopreserved in 90% FCS (Gibco) supplemented with 10% dimethyl sulfoxide (DMSO). Blood samples from healthy donors were collected according to the principles of the Declaration of Helsinki and were obtained from the Deutsches Rotes Kreuz (DRK) Blutspendedienst Baden-Württemberg-Hessen gGmbH, Mannheim, Germany. HLA-A*02:01 expression of HD-01, HD-02 and HD-07 was determined by flow cytometry using an anti-HLA-A2-APC (BB7.2, BioLegend 343308) staining. For HD-03–HD-07 and the melanoma patient a 4-digit NGS-based HLA-typing was performed by the DKMS Life Science Lab gGmbH, Dresden, Germany.

Blood samples from the patient with metastasized melanoma (male, age 47) were obtained by the Section of DermatoOncology (NCT), Heidelberg University Hospital. Tumor lymph node metastases were resected in 08/2021 and subjected to whole exome sequencing and mRNA sequencing in the MASTER program. For all conducted pMHC-I multimer binding analysis of primary human material, PBMCs were thawed and rested overnight in AIM-V^{TM} (Gibco) supplemented with 2% human male AB serum (PAN Biotech) and 1 unit/ml Benzonase$^{®}$ nuclease (Sigma-Aldrich) followed by a magnetic CD8$^+$ cell sorting using the REAlease$^{®}$ CD8 MicroBead Kit (Miltenyi) according to the manufacturer's recommended protocol.

2.10 Preparation of single color, dual color-encoded and DNA-barcoded pMHC-I multimer libraries

For multimerization, dsSCD were diluted to 2 µM in DPBS and loaded overnight at RT with indicated peptides at 25 µM. EasYmers$^{®}$ (immunAware) were folded at 2 µM for 2-3 days before multimerization by the addition of 6 µM peptide according to the manufacturer's protocol. Monomeric dtSCT, folded easYmer at 2 µM and peptide-loaded dsSCD were mixed with different streptavidin (SAv)-fluorochrome combinations as detailed below at a 4:1 molar (pMHC-I monomer:SAv) ratio. Following multimerization, individual pMHC-I multimers were supplemented with 25 µM D-biotin (Sigma-Aldrich) to block free binding sites, 2 mM EDTA (Sigma-Aldrich), 2% FCS (Gibco), 5% Horizon^{TM} Brilliant Stain Buffer Plus (BD Bioscience) and 100 nM dasatinib (Sigma-Aldrich) and were incubated for 20 min at 4°C.

pMHC-I multimer binding to TCR$^+$ J76^{CD8} cells was analyzed by dsSCD and dtSCT multimerized through addition of SAv-R-phycoerythrin (SAv-PE, Miltenyi 130-106-790). Dual color-encoded pMHC-I libraries for the parallel interrogation of multiple CD8$^+$ T cell epitopes in one staining experiment were prepared as described previously (3) with modifications. Defined pMHC-I monomers were multimerized with a unique SAv dual color combination and were finally pooled into a single pMHC-I library comprising SAv-PE (Miltenyi), SAv-allophycocyanin (SAv-APC, BioLegend 405207), SAv-Brilliant Violet (BV421, BD Bioscience 563259), SAv-BV711 (BD Bioscience 563262) and SAv-Brilliant Ultra Violet 395 (SAv-BUV395, BD Bioscience 564176) for the analysis of up to 10 antigen-specific T cell populations. For the multiplex analysis of up to 60 antigen-specific T cell populations at once, pMHC-I libraries were prepared using additionally SAv-BUV661 (BD 612979), SAv-BUV737 (BD 612775), SAv-PE-CF594 (BD 562284), SAv-PE-Cy5 (BioLegend 405205), SAv-PE-Cy7 (BioLegend 405206), SAv-BV785 (BioLegend 405249) and SAv-KIRAVIA Blue 520 (BioLegend 405172) omitting PE, PE-CF594, PE-Cy5 and PE-Cy7 dual color combinations.

For subsequent single-cell RNA sequencing (scRNA-Seq) analysis of DNA-barcoded cells, all identified pMHC-I multimer$^+$ populations from the dual-color encoded analysis were pre-clustered into one of three groups for cell sorting depending on their frequencies (low (< 0.1%), intermediate (0.1%–1.0%) or high (>1%)) and associated with the fluorochromes APC, BV421 or BUV395, respectively, and then pooled in a defined ratio (also see Supplementary Figure 2C and Supplementary Table 4) to ensure that also populations of very low frequency were still detectable by the scRNA-Seq sample processing procedure with a limited targeted cell recovery of up to 10,000 cells.

A combined dual-colored and DNA-barcoded pMHC-I multimer library was generated compatible with 10x Genomics 5' Single Cell RNA sequencing protocols with feature barcode technology, by adding 1.2 µl DNA-barcoded, SAv-PE-conjugated dextran polymer backbone (U-Load dCODE Dextramer$^{®}$, Immudex$^{®}$) to 3 µl of dtSCT, easYmer or peptide-loaded dsSCD diluted to 2 µM and was further supplemented with 1 µl U-Load dCODE Dilution Buffer (Immudex$^{®}$). The same pMHC-I monomer was conjugated in parallel either with SAv-APC, SAv-BV421 or SAv-BUV395 based on the previously determined frequencies of dual-color encoded pMHC-I multimer$^+$ CD8$^+$ T cells from the melanoma patient. DNA-barcoded PE-pMHC-I multimer and corresponding pMHC-I multimer based on SAv-APC, SAv-BV421 or SAv-BUV395 were subsequently pooled into a single pMHC-I library before cell labeling and cell sorting.

2.11 pMHC-I multimer cell staining and cell sorting

Cultured TCR$^+$ J76^{CD8} cells were washed once with pMHC staining buffer (DPBS supplemented with 2% FCS, 2 mM EDTA, 100 nM dasatinib) and were then stained with PE-labeled pMHC-I multimers diluted to approximately 50 nM in pMHC staining buffer at RT for 25 min. After pMHC-I multimer staining, TCR$^+$ J76^{CD8} cells were washed once with pMHC staining buffer followed by

labeling with murine TCR-Cβ-APC (clone H57-597, BioLegend) and CD8-PacificBlue (Clone SK1, BioLegend).

Cultured *ex vivo* CD8$^+$ T cells were washed once with DPBS/100 nM dasatinib and were then labeled with the Zombie Aqua™ Fixable Viability Kit (BioLegend 423102) 1:300 for 10 min at RT in DPBS + 100 nM dasatinib. Next, one volume of pMHC staining buffer + Human TruStain FcX (Fc receptor blocking solution, BioLegend 422302) was added 1:50 (v/v) following an incubation for 5 min at RT. Cells were then stained with prepared pMHC-I multimer libraries at RT for 25 min. After one wash, cells were stained using a cocktail containing optimally titrated antibodies (all from BioLegend) against human CD14 (M5E2, Cat. No. 301842), CD16 (3G8, 302048), CD19 (H1B19, 302242), and CD335 (9E2, 331924) (all Brilliant Violet 510-conjugated, defined as dump channel); CD8 (SK1, BioLegend 344714) APC-Cy7, and CD3 (UCHT-1) Alexa Fluor 700 (BioLegend 300424).

For the labeling of CD8$^+$ T cells in freshly isolated PBMC with a DNA-barcoded pMHC-I multimer library, 0.1 µg/ml herring sperm DNA (Invitrogen™) was additionally added to the pMHC-I staining buffer and the above-mentioned antibody panel was appended by an antibody mix containing 30 DNA-barcoded TotalSeq™-C antibodies (BioLegend) as listed in Supplementary Table 4.

Finally, the stained TCR$^+$ J76^{CD8} cells or PBMC-derived CD8$^+$ T cells were stored in DPBS supplemented with 2.5% (v/v) paraformaldehyde and 1% FCS before flow cytometry measurement on a LSRFortessa flow cytometer and analyzed according to the gating strategy shown in Supplementary Figure 2 using FlowJo (BD Biosciences) v.10.9.0. In the dual color-encoded pMHC-I multimer-binding data shown, pMHC-I multimer binding CD8$^+$ T cells were identified by a Boolean gating strategy as live CD8$^+$ T cells stained positive in two pMHC multimer channels and negative in all other pMHC multimer color channels, as previously described (50, 51).

CD8$^+$ T cells labeled with the DNA-barcoded pMHC-I multimer library were kept in pMHC staining buffer and pMHC-I multimer positive cells were sorted with a FACSAria™ Fusion cell sorter (BD Biosciences) according to the gating strategy shown in Supplementary Figure 2 into tubes containing 200 µl pMHC staining buffer.

2.12 Single-cell RNA sequencing of pMHC-I multimer$^+$ CD8$^+$ T cells

Sorted DNA-barcoded pMHC-I multimer$^+$ CD8$^+$ T cells of the melanoma patient were analyzed by single cell RNA sequencing (scRNA-Seq) utilizing the Chromium NEXT GEM Single Cell 5′ TCR profiling and Feature Barcode Technology v2 (dual index) reagent kit (10x Genomics), which enables the combined interrogation of cell surface protein expression including pMHC-I multimer binding (CSP), TCR (VDJ) and gene expression (GEX). Cells were processed according to instructions by 10x Genomics (Protocol CG000330 Rev D). Fourteen cycles of initial cDNA amplification were used for all sets and single-cell sequencing libraries for whole-transcriptome analysis (GEX), TCR profiling (VDJ), and combined cell-surface protein and dCODE Dextramers detection (CSP) were generated. Libraries were quality controlled by automated gel electrophoresis (Agilent TapeStation) and quantified using a Qubit Fluorometer (Thermo Scientific), and finally pooled in a ratio of 4:1:1 (GEX:VDJ:CSP) and sequenced on a NextSeq 550 system (Illumina) using 150 cycles on the basis of sequencing by synthesis (SBS) chemistry with cycle configuration (read 1: 26 bp; index read 1: 10 bp; read 2: 90 bp), with a sequencing depths of at least 20000, 5000, 5000 reads pairs per cell for the GEX, VDJ, CSP libraries, respectively.

Raw scRNA-seq FASTQ files were aligned to the human GRCh38 genome with Cell Ranger version 7.1.0 with default settings for the 'cellranger multi' pipeline (10x Genomics) for combined V(D)J, gene expression and antibody capture (cell surface protein) analysis and GEX:VDJ:CSP libraries were paired for downstream assessment of the data set. The Loupe Cell Browser version 7.0.0 (10x Genomics) software was used for data analysis including cell clustering and data visualization.

2.13 Mutation identification and neoepitope prediction

A tumor biopsy sample of lymph node metastasis of a melanoma patient and matching PBMC sample was sequenced by the DKFZ GPCF as part of the MASTER program (52) to identify expressed somatic nucleotide variants (SNV), genetic insertions and deletions (InDels) and gene fusion events. Whole exome sequencing (WES) of DNA libraries was done using a on a NovaSeq 6000 system (Illumina) (2x 100 bp) and demultiplexing of the sequencing reads was performed with Illumina bcl2fastq (2.20). Adapters were trimmed with Skewer (version 0.2.2) (53). Alignment of sequencing reads was done by the DKFZ alignment workflow from the ICGC Pan-Cancer Analysis of Whole Genome projects (DKFZ AlignmentAndQCWorkflows v1.2.73, (https://github.com/DKFZ-ODCF/AlignmentAndQCWorkflows). The human reference genome version GRCh37/hg19 was used. RNA libraries from the tumor biopsy were prepared using the Kapa RNA HyperPrep Kit with RiboErase (Roche) and subjected to a NovaSeq 6000 system for RNA sequencing (RNA-Seq). RNA-Seq reads were aligned and gene expression quantified using the DKFZ RNA-Seq (v1.2.22-6, https://github.com/DKFZ-ODCF/RNAseqWorkflow). For total library abundance calculations, during TPM and FPKM expression values estimation, genes on chromosomes X, Y, MT, and rRNA and tRNA were omitted to avoid library size estimation biases as previously described (54, 55). SNV and InDel mutation calling was done using DKFZ in-house piplines (SNVCallingWorkflow v1.2.166-1, https://github.com/DKFZ-ODCF/SNVCallingWorkflow); IndelCallingWorkflow v1.2.177, https://github.com/DKFZ-ODCF/IndelCallingWorkflow) as previously described (56). Raw calls for InDels were obtained from Platypus (57). The proteins coding effect of SNVs and InDels were annotated using ANNOVAR according to GENCODE gene annotation (version 19) (58) and overlapped with variants from dbSNP10 (build 141) and the 1000 Genomes Project database. Mutations of interest were defined as somatic SNV and InDels that were predicted to cause protein coding changes (non-synonymous SNVs, gain or loss of stop codons, splice site mutations, frameshift and non-frameshift indels) (55). Gene fusion events were

detected by applying the Arriba algorithm (59) on the RNA-Seq data set. Neoepitopes were predicted from raw sequencing data by a comprehensive and fully automated DKFZ in-house pipeline (60), which is implemented in an Anaconda environment to ensure easy usage and reproducibility. The pipeline integrates previously identified SNVs, InDels, gene fusion events as well as the gene expression level and generates mutations sequences that are flanked by 10 wildtype amino acids upstream and downstream for an SNV mutation and 10 wildtype amino acids upstream of frameshift mutations. Mutated protein sequences were finally queried by the netMHCpan 4.1 algorithm (61) to predict potential binding and presentation by patient's HLA-I alleles. 166 unique peptide/HLA neoepitope candidates with a predicted %Rank_EL > 2.5 spanning 49 SNV and 2 gene fusion events were selected for dsSCD and easYmer binding analysis and subsequent immunogenicity screening.

2.14 Statistical analysis

Unless otherwise stated, all results are expressed as mean ± SD. Analysis and graphical representations were conducted using GraphPad Prism 8 software (GraphPad Software Inc.). Experiments containing more than 2 experimental groups were analyzed using a one- or two-way analysis of variance (ANOVA) with Tukey's multiple comparison test. The number of donors and experiments, as well as the statistical analysis is stated in the respective figure legends with p values <0.05 considered statistically significant (ns, $p>0.05$; *, $p<0.05$; **, $p<0.01$; ***, $p<0.001$; ****, $p<0.0001$).

3 Results

3.1 Peptide-receptive empty MHC-I dsSCD produced in mammalian cells

For the generation and purification of monomeric pMHC-I dtSCT that can be multimerized by streptavidin (SAv) we modified our previously reported Fc-tagged dtSCT format (25) by introducing a His_8 tag, a biotin acceptor peptide, and a tandem thrombin cleavage site between the MHC-I ectodomain and mIgG2a Fc portion (Figure 1A). Fc-tagged dtSCT were produced in HEK293 cells co-transfected with secretory BirA biotin ligase retained by a C-terminal KDEL ER retention signal (62). Treatment of cell supernatants with thrombin liberated biotinylated dtSCT monomers (ca. 57 kDa) as shown exemplarily in Figure 1C for a $MART1_{26-35}$/HLA-A*02:01 dtSCT, that produced a gel shift after incubation with streptavidin indicating SDS-stable complex formation with 2-4 streptavidin monomers of ~15 kDa.

To generate a dsSCD, the peptide sequence and first flexible linker was omitted and in addition to the mutation Y84C present in dtSCT, the mutation A139C was introduced in the MHC-I α2 domain to enable the formation of an artificial intramolecular disulfide bond stabilizing the C-terminal end of the peptide binding groove (9, 10). In contrast to dtSCT that were efficiently produced, HLA-A*02:01 dsSCD were not secreted in detectable amounts by HEK293-F cells albeit being expressed intracellularly (Figures 1B, D). Therefore, we replaced HEK293-F cells by CHO-S producer cells leading to satisfying yields of secreted dsSCD in the range of 10 mg/l culture volume (Figure 1D). DsSCD produced in CHO-S cells were, however, only partially biotinylated by co-expressed BirA ligase as indicated by partial gel shifts (dsSCD: ca. 55 kDa after thrombin cleavage, Figure 1C). With similar production yields, a large series of dsSCD allotypes lacking the thrombin cleavage site and Fc portion were produced in CHO-S cells (Supplementary Figure 1A, Supplementary Table 1). These shortened variants avoid the potential problem of incomplete thrombin cleavage.

We next analyzed the capacity of bead-immobilized HLA-A*02:01 dsSCD to bind three known HLA-A*02:01 ligands and one predicted non-binder by flow cytometry using fluorescently modified variants thereof containing a Lys^{FITC} residue (Figure 1E). While two peptides (NLVPK^{FITC}VATV and NLVPK^{FITC}VATA), *in silico* predicted in their non-FITC-conjugated forms to be high affinity binders, reached saturation plateau signals at 1 µM, at least 10 µM were required for a predicted low affinity binder (QLAK^{FITC}TCPVQL), while the predicted non-binder (CTELK^{FITC}LSDY) only showed minimal binding at 100 µM after incubating for 18 h at ambient temperature. To allow low affinity peptides to occupy dsSCD at least partially, 10 µM or higher was chosen as the standard concentration for overnight loading of unlabeled test peptides. Figure 1F shows the association kinetics of the Lys^{FITC}-substituted high affinity binder, HCMV $pp65_{495-503}$, at 1 µM concentration to bead-immobilized HLA-A*02:01 dsSCD at ambient temperature in comparison to a non-binder, a known HLA-A*01:01 ligand. Between 12 and 24 h of incubation, binding of a the Lys^{FITC}-substituted NLV peptide reached saturating levels.

Mass-spectrometry (MS) was used to examine whether HLA-A*02:01 dsSCD produced in CHO-S cells were loaded with endogenous peptides or not, and whether peptide ligands loaded as positive controls could be re-identified. No peptides of hamster origin could be identified using data-independent acquisition MS, indicating that dsSCD molecules were *bona fide* free of peptide after purification. After loading with a peptide pool of known high-affinity A*02:01 ligands, acid-eluted peptides corresponding to expected binders could be re-identified by MS, e.g. HCMV $pp65_{495-503}$ (NLVPMVATV) (Figure 1G, left panels), while the data generated from untreated dsSCD was devoid of a corresponding peptide signal at the respective retention time window (Figure 1G, right panels and data not shown).

To obtain more information about the binding properties of Lys^{FITC} substituted peptides, we compared the HCMV $pp65_{495-503}$ high-affinity peptide, NLVPMVATV (N9V), substituted in all 9 positions for Lys^{FITC}, for binding to bead-immobilized HLA-A*02:01 dsSCD (Supplementary Figure 1B). Equilibrium dissociation constants (K_D values) that were calculated for observed binding curves show that the bulky Lys^{FITC} side chain was not tolerated at the major anchor positions P2 and P9 and to a minor extent also at positions P4 and P6. For comparison we show the NetMHCpan motif for HLA-A*02:01 and *in silico* predicted relative binding probabilities for Lys-substituted N9V homologs with predicted strong binders ≤ 0.5% Rank_EL and weak binders ≤

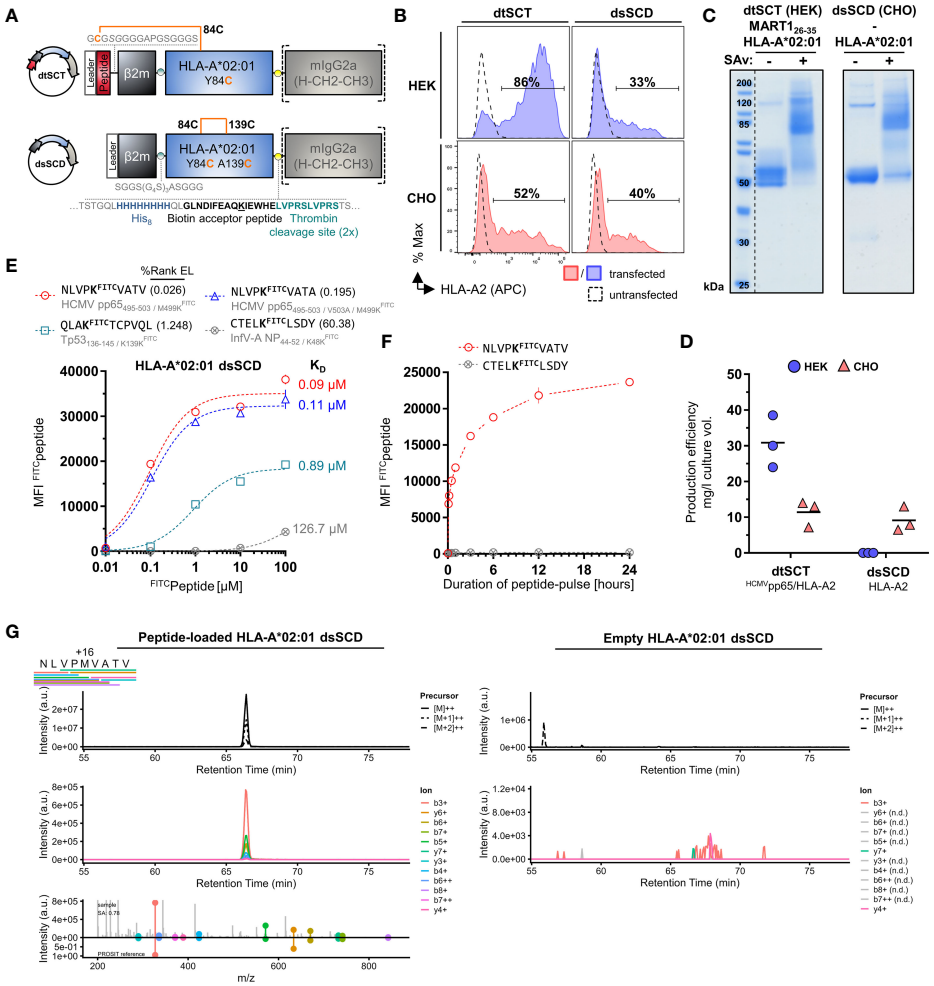

FIGURE 1
Successful CHO cell-based production of *in vivo* biotinylated, empty, peptide-receptive, disulfide-stabilized β_2m-HLA-A*02:01 single-chain dimers (dsSCD). **(A)** Schematic representation of soluble disulfide-trapped peptide-β_2m-HLA-A*02:01 single-chain trimer (dtSCT) (upper panel) and dsSCD (lower panel). dtSCT consist of a single polypeptide chain comprising a peptide ligand, human β_2-microglobulin (β_2m) and MHC-I ectodomain that are covalently linked via flexible glycine-serine-rich linkers (GSL). The SCT intramolecular disulfide trap is generated between a cysteine [C] in the first GSL and a C residue replacing a conserved MHC-I tyrosine [Y] residue at position 84. In dsSCD, β_2m is fused *via* a GSL to the MHC-I ectodomain that harbors an additional alanine [A] A139C, Y84C disulfide bridge that stabilizes the β_2m-MHC-I complex also in the absence of a peptide ligand. dtSCT and dsSCD are C-terminally fused to an octa-histidine tag (His_8), a biotin acceptor peptide that is followed by two consecutive (2x) thrombin cleavage sites fused to a murine IgG2a Fc part. All constructs are designed for mammalian cell expression and were always transiently co-transfected with ER-retained $Ig\kappa_{SP}$-$BirA_{KDEL}$ biotin ligase to allow for site-specific biotinylation during dsSCD/dtSCT expression. **(B)** Representative intracellular HLA-A*02:01 dtSCT and dsSCD expression analysis by flow cytometry 48 hours post plasmid (filled lines) and mock (dotted line) transfection of HEK293-F (HEK) and CHO-S (CHO) cells using anti-HLA-A2 antibody BB7.2. **(C)** SDS-PAGE analysis of affinity chromatography-purified monomeric dtSCT and dsSCD from HEK and CHO cell supernatants, respectively, that have been treated with thrombin to cleave the Fc portion. DtSCT and dsSCD biotinylation is confirmed by equimolar addition of streptavidin prior to SDS-PAGE analysis leading to a gel shift. **(D)** Production efficiencies of dtSCT and dsSCD expressed in HEK or CHO. Values were calculated using the yield in mg of the final protein yield divided by the culture supernatant volume in liters used for affinity chromatography. Dots represent three independent cell transfections for the conditions shown. **(E, F)** Flow cytometry-based FITC-conjugated peptide (^{FITC}peptide) binding assay for bead-immobilized dsSCD. FITC median fluorescence intensities (MFI) of ^{FITC}peptide-loaded dsSCD immobilized on streptavidin-conjugated beads in triplicates are shown. HLA-A*02:01 dsSCD beads were pulsed with the indicated concentrations of ^{FITC}peptides **(E)**, or by a ^{FITC}peptide pulse at 1 µM for the indicated time periods starting with 5, 10, 30 and 60 minutes and ending with 24 hours (h) **(F)**. HLA-A*02:01 %Rank EL prediction values are shown for the indicated peptides with K substitution and their binding levels as putative strong binders (SB, %Rank EL <0.5), weak binders (WB, %Rank EL <2) and non-binders (nonB, %Rank >2) according to the NetMHCpan 4.1 algorithm. The FITC conjugation of the peptide is neglected in this assessment. **(E)** Non-linear regression (one-site specific binding) of the FITC MFI values from means of triplicates (± SD) against the peptide concentration and calculated K_D values in µM are shown. **(F)** Non-linear regression of the FITC MFI from means of triplicates (± SD) against the incubation time is shown. **(G)** Data-independent acquisition mass spectrometry (DIA-MS) of NLVPMVATV loaded (left panels) and empty (right panels) HLA-A*02:01 dsSCD. Left panels show the manual detection of the NLVPMVATV peptide eluted from the externally peptide-loaded HLA-A*02:01 dsSCD. Bars below the NLVPMVATV sequence indicate detected fragment ions in peptide-loaded sample. Top panels show extracted ion chromatograms (XICs) of the precursor and its isotopes, middle panels shows XICs of fragment ions. The top half of the bottom panel shows the MS2 spectra extracted at the highest point of the MS2 XIC, while the bottom half shows the mirrored spectrum as *in silico* predicted by PROSIT. The spectral angle (SA) was calculated and is indicated. Right panels show the lack of matching precursor and fragment ions for the empty dsSCD molecule within a 25 min window centered around the retention time of NLVPMVATV peptide. n.d, not detected.

2.0% Rank_EL. We conclude that Lys^{FITC}-modified indicator peptides mirror the peptide binding properties of known HLA-A*02:01 ligands sufficiently well and can be used as competitors in peptide binding assays with dsSCD if non-anchor positions are substituted. In a similar fashion we rationally designed Lys^{FITC}-modified indicator peptides, based on known strong binders and considering only non-anchor positions for substitution, for a total of 32 dsSCD HLA-A,B,C allotypes presented in this work. We demonstrate successful binding to bead-immobilized respective dsSCD by flow cytometry (Figure 2, Supplementary Table 1).

3.2 Antigen-specific T cell detection with dsSCD-based multimers

We examined the capacity of biotinylated peptide-loaded dsSCD to assemble with fluorochrome-labeled streptavidin (SAv) as MHC-I multimers and stain antigen-specific T cells. To form pMHC-I multimer reagents, monomeric dsSCD were loaded with appropriate peptides for 18-24 h and subsequently multimerized with fluorochrome-labeled streptavidin (Figure 3A). As proof of concept, HLA-A*02:01 dsSCD were loaded with peptides HCMV pp65$_{495\text{-}503}$ or MART1$_{26\text{-}35}$, complexed with PE-conjugated SAv and used for the staining of CD8$^+$ Jurkat 76 cells transfected with TCRs RA14 or DMF5, respectively. For comparison, multimers of biotinylated dtSCT containing the same peptides in tethered form were used in parallel. Both peptide-loaded dsSCD and dtSCT homogenously stained Jurkat 76/CD8 transfectants with equal efficiencies (Figure 3B). A titration of peptides used for the loading of HLA-A*02:01 dsSCD showed that 25 µM is a suitable concentration to achieve maximal labeling of TCR-transfected Jurkat cells (Figure 3B). In Figure 3C we show the comparative stainings of TCR-transfected Jurkat cells with peptide-loaded dsSCD and dtSCT multimers representing complexes of HLA-A*11:01 or HLA-C*08:02 with mutant KRAS peptides, as well as HLA-C*03:04 presenting an NY-ESO-1 peptide. Again, peptide-loaded dsSCD and dtSCT performed equally well. The labeling was highly efficient and peptide-specific, as TCR Ry-4148 did not bind dsSCD and dtSCT loaded with a KRAS wild-type control peptide. Since the KRAS G12D mutation in peptide GA**D**GVGKSA represents a neo-anchor for HLA-C*08:02 and the respective wild-type peptide did not bind to dsSCD nor allowed the production of a respective dtSCT, an unrelated EBNA6 peptide was used as negative control.

To compare the staining performances of the peptide-loadable dsSCD (MediMer) and peptide-tethered dtSCT platforms with the commercially available easYmer platform (immunAware) based on *in vitro* folding of wild-type MHC heavy chain into a stable peptide–β_2m–MHC-I complex (7), the individual platforms were multimerized in parallel and applied in dual-color encoded pMHC-I multimer stainings for the detection of HCMV pp65, EBV BMLF1, Influenza-A MP and MART1 antigen-specific CD8$^+$ T cells

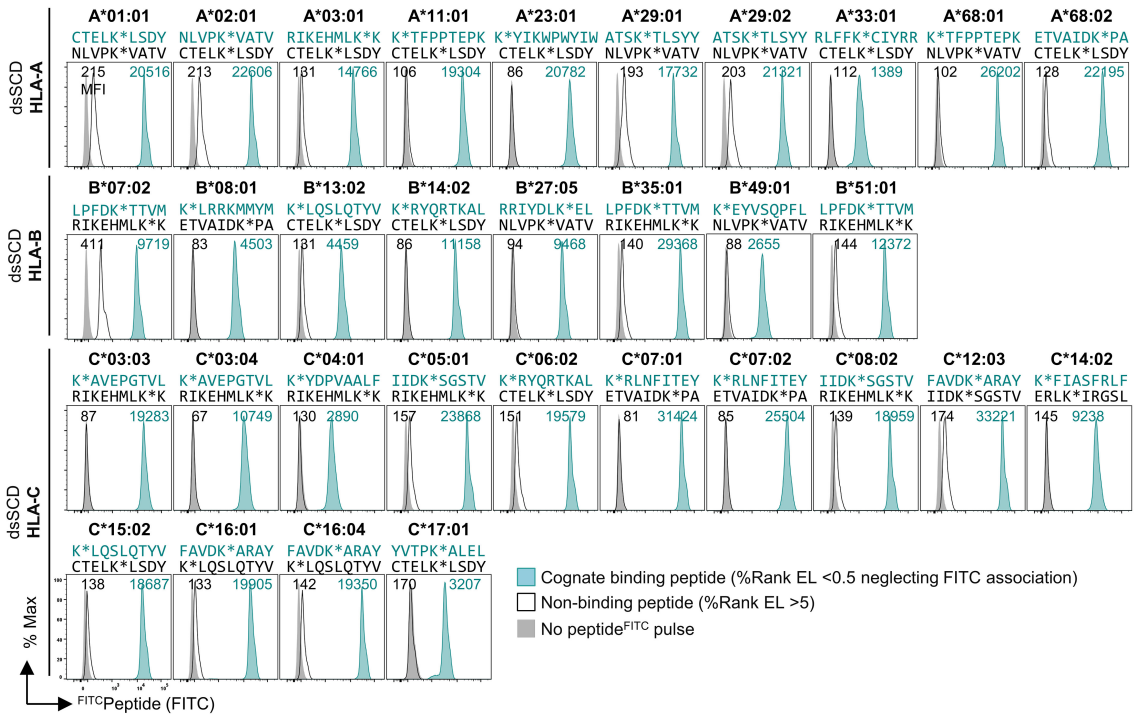

FIGURE 2
Validation of 32 produced HLA-A, -B and -C dsSCD by ^{FITC}peptide binding assay. Individual production yields of dsSCD allotypes and used ^{FITC}peptides are listed in Supplementary Table 1. For dsSCD testing, a set of peptides were rationally designed to have at a selected non-anchor residue a K^{FITC} substitution (K*) based on known ligands, the NetMHCpan 4.1 binding motif viewer and %Rank EL values for the indicated HLA allotype. FACS histograms are shown for bead-immobilized dsSCD pulsed for 18 h with 1 µM of a binding ^{FITC}peptide (peptide sequence and plot shown in teal) and non/poor binding ^{FITC}peptide (black line) and bead background MFI (gray filled) for the indicated HLA allotypes.

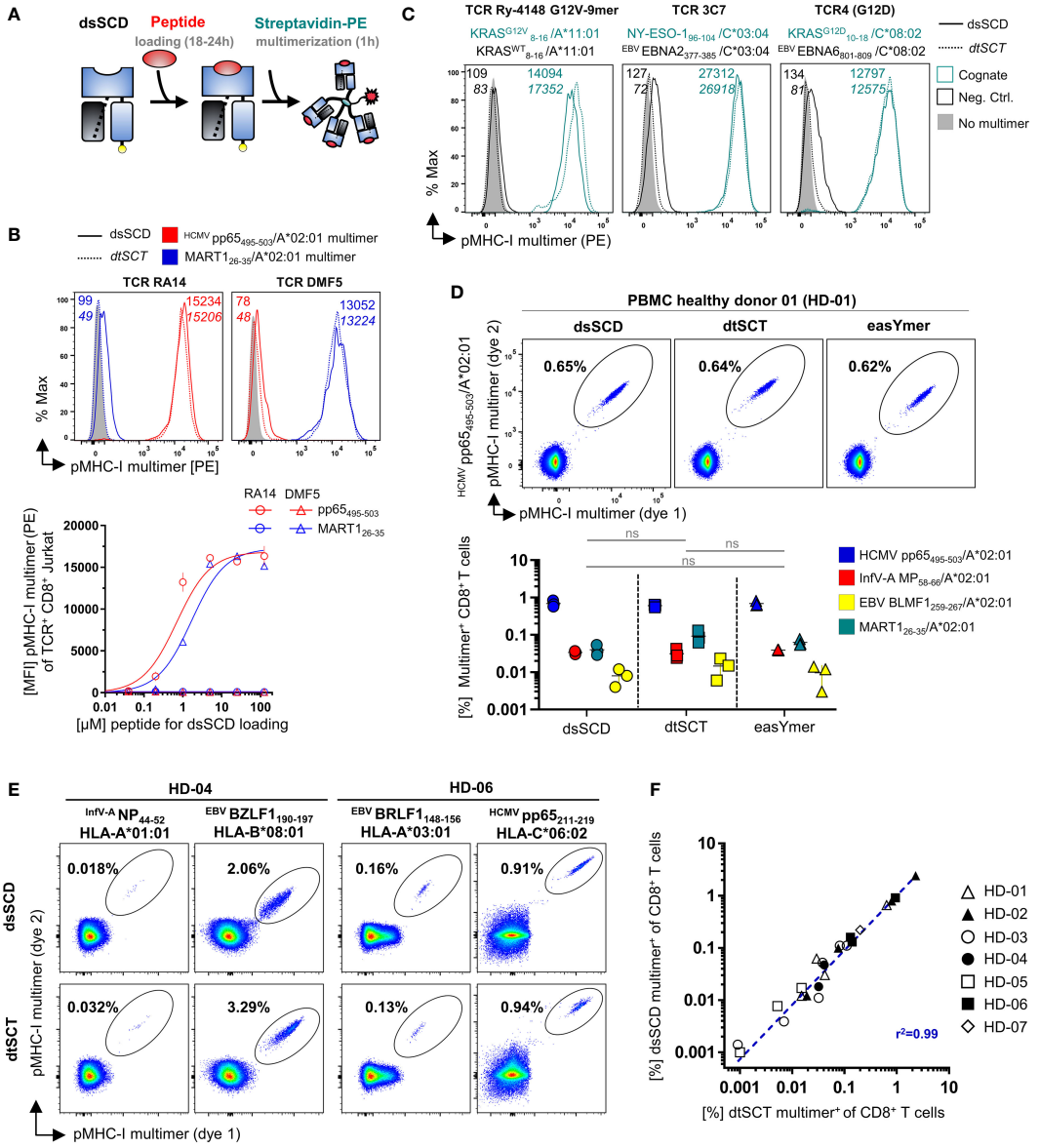

FIGURE 3
Comparable antigen-specific labeling of TCR-transgenic CD8$^+$ Jurkat and healthy donor-derived viral epitope-specific CD8$^+$ T cell populations with peptide-loaded dsSCD and dtSCT multimers. **(A)** Schematic representation of dsSCD for the usage as antigen-specific labeling reagent for defined CD8$^+$ T cell populations. Following an overnight peptide pulse, the biotinylated dsSCD are multimerized by the addition of a fluorochrome-labeled streptavidin. **(B, C)** Cognate dtSCD and dsSCD multimer labeling of CD8$^+$ Jurkat 76 (J76^{CD8+}) stably expressing various published TCR as recombinant chimeric TCR containing murine Cβ and Cα domains. **(B)** J76^{CD8+} cells stably expressing RA14 TCR recognizing HLA-A*02:01/^{HCMV}pp65$_{495-503}$ or DMF5 TCR recognizing HLA-A*02:01/MART-1$_{26-35}$ were labeled with HLA-A*02:01 dsSCD previously loaded at varying concentrations with peptide ^{HCMV}pp65$_{495-503}$ (red symbols) or MART-1$_{26-35}$ (blue symbols), respectively, for 18 h followed by multimerization. The upper panel shows representative histograms of RA14 and DMF5 J76^{CD8+} labeled with dsSCD multimers loaded with 25 µM peptide (filled line, MFI values in plain font) or dtSCT multimers (dotted line, MFI values in *italics*). PE fluorescence-minus-one (FMO) controls of J76^{CD8+} are shown in filled gray. The lower panel shows RA14 (circles) and DMF5 (triangles) J76^{CD8+} staining efficiencies at varying peptide loading concentrations used for dsSCD loading in triplicates and fitting using non-linear regression. For control, RA14 and DMF5 J76^{CD8+} cells were stained with dsSCD loaded with the non-cognate peptide. **(C)** Antigen-specific staining of published neoepitope or tumor-associated antigen-specific HLA-A*11:01, HLA-C*03:04 and HLA-C*08:02-restricted TCR with multimerized dtSCT and dsSCD harboring the cognate peptide (teal) or a dsSCD/dtSCT-binding control peptide (black). **(D, E)** Detection of virus-specific human CD8$^+$ T cell populations in healthy donors with dsSCD and dtSCT multimers using combinatorial dual-fluorochrome encoding. **(D)** Labeling of HLA-A*02:01$^+$ healthy donor 01 (HD-01) CD8$^+$ T cells from PBMC with HLA-A*02:01 multimers generated on the basis of dsSCD, dtSCT or the commercial easYmer. The upper panel shows a representative dot plot of a ^{HCMV}pp65$_{495-503}$/HLA-A*02:01-specific CD8$^+$ T cell population. The lower panel shows the identification of four different HLA-A*02:01-restricted multimer$^+$ populations found in three independent experiments across all three tested pMHC-I multimer platforms. The data set was statistically analyzed by two-way ANOVA followed by Tukey's multiple comparison test and no significant (ns) differences between the platforms were found. **(E)** Labeling of multiple HLA-typed healthy donors with pairs of dtSCT and dsSCD multimers representing 16 known viral and tumor-associated epitopes. Multimer$^+$ populations using HLA-A*01:01, A*03:01, B*08:01 or C*06:02 dtSCT and dsSCD in HD-04 and HD-06 are exemplarily shown. **(F)** Correlation analysis of antigen-specific T cell frequencies detected by HLA-A*01:01, A*02:01, A*03:01 or C*06:02 dsSCD and dtSCT multimers in PBMC-derived CD8$^+$ T cells of HD-01–07. The individual T cell frequencies and specificities are listed in Supplementary Table 2.

population of a HLA-A*02:01 positive healthy donor (Figure 3D). In the top panel, analysis of pMHC-I multimer stainings of pp65-specific T cells from donor HD-01 are exemplarily shown based on a Boolean gating strategy as explained in Supplementary Figure 2. Detected population frequencies of HD-01 determined in three independent experiments using the three pMHC-I platforms (bottom panel) revealed equal efficacies to detect the 4 analyzed T cell populations ranging between 0.01% and 1% in size. Proof-of-concept stainings with HLA-A*02:01 dsSCD multimers were then extended to various additional viral T cell epitopes restricted by HLA-A*01:01, HLA-A*03:01 and HLA-B*08:01 and HLA-C*06:02 detected in the peripheral blood of HLA-typed healthy donors as exemplarily shown for HD-04 and HD-06 (Figure 3E). Respective dsSCD allotypes were loaded with synthetic peptides and compared with dtSCT carrying the same peptides in tethered form. Again, similar frequencies of multimer-stained T cells were detected with both reagents across various HLA-A, -B, -C allotypes. The results from comparative dsSCD and dtSCT multimer stainings addressing 16 viral and tumor-associated epitopes recognized by $CD8^+$ T cells in peripheral blood from 7 different healthy donors are summarized in the correlation plot of Figure 3F, showing a highly consistent detection of T cell populations by both multimer tools over a large range of frequencies (see Supplementary Table 2 for details of peptides and restricted HLA-I allotypes).

3.3 Empty and peptide-loaded dsSCD are functionally stable due to tethered β_2m

To validate the robustness of peptide-receptive dsSCD for the laboratory praxis, we next analyzed the stability of peptide-free and peptide-loaded dsSCD. Purified HLA-A*02:01 dsSCD were stored empty under sterile conditions for the indicated time periods up to one week at 4, 22 or 37°C and were left loaded with 10 µM $MART1_{26-35}$ peptide for the remaining time at the indicated temperatures before being finally used for the staining of TCR DMF5-transfected Jurkat 76/CD8 cells (Figure 4A). After keeping empty or peptide-loaded dsSCD at 4°C for one week the staining capacity was unaltered and very similar to a MART1/A*02:01 dtSCT-based staining. After storing empty dsSCD longer than 120 h at ambient temperature, the staining capacity was slightly diminished, while after storage at 37°C for up to one week the

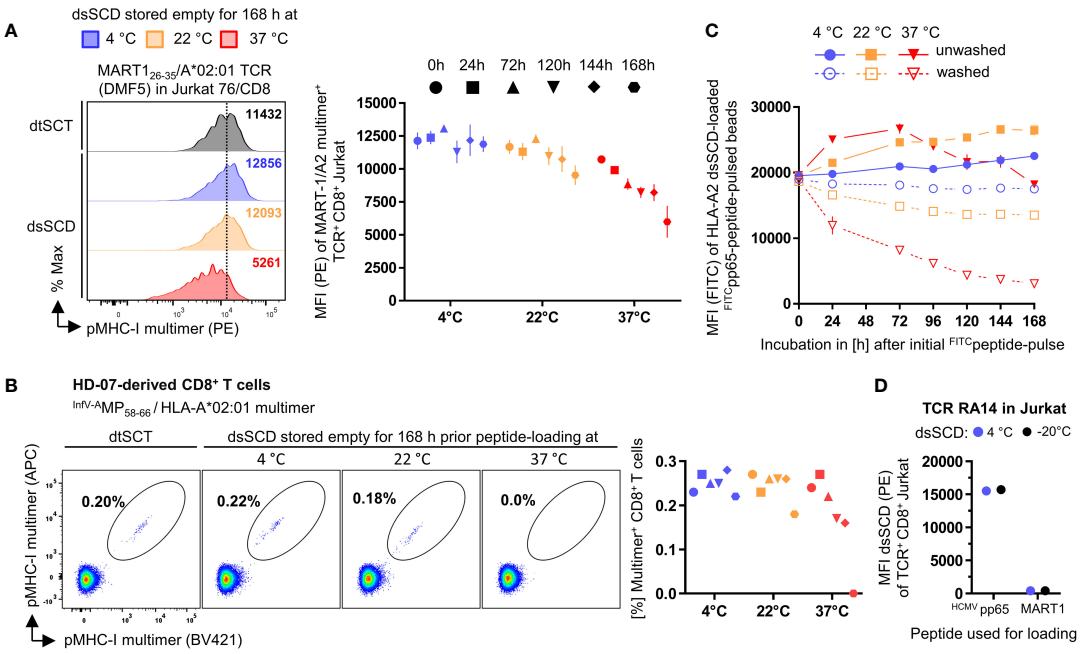

FIGURE 4
Stability assessment of empty and peptide-loaded dsSCD. **(A, B)** Empty dsSCD were stored for up to one week at 4°C, 22°C or 37°C followed by a peptide pulse with MART-1_{26-35} or $^{InfV-A}MP_{58-66}$ peptide and multimerization with streptavidin-PE. The shown durations and storage temperatures indicate conditions used for empty dsSCDs storage before dsSCD were finally loaded with 10 µM peptide and then kept at the indicated temperature peptide-loaded until 168 h were completed. To this add ~3 h incubation time until multimerization was accomplished and samples were analyzed by flow cytometry. Temperature-challenged dsSCD multimers, and dtSCT-based multimers serving as positive controls, were used to stain DMF5 TCR-transfected $J76^{CD8+}$ **(A)** and healthy donor 07 (HD-07)-derived $CD8^+$ T cells **(B)**. **(A)** Representative histogram of DMF5 TCR $J76^{CD8+}$ labeled with multimerized dsSCD that have been stored empty for 168 h at various temperatures (left panel) and MFI values of the entire experiment (right panel). **(B)** Staining of HD-07 $CD8^+$ T cells with multimerized $^{InfV-A}MP_{58-66}$/HLA-A*02:01 dsSCD stored empty for 168 h at various temperatures (left panel) and MFI values of the entire experiment (right panel). Data represent single values. **(C)** Dissociation analysis of ^{FITC}peptide-loaded dsSCD. Beads with immobilized HLA-A*02:01 dsSCD were pulsed overnight with 1 µM NLVPK^{FITC}VATV at 4°C in PBS and were washed with PBS (dotted line) or left unwashed (solid line) at the indicated temperatures and incubation times followed by flow cytometric analysis of the remaining FITC MFI. The 0 h values represent the MFI baseline measured after the initial 24 h peptide pulse. **(D)** Analysis of the freezing compatibility of dsSCD. Empty HLA-A*02:01 dsSCD were stored in the presence of glycerol and BSA at -20°C (black dots) or left in PBS at 4°C (blue dots) for 3 weeks before usage as cognate or control peptide-loaded dsSCD multimers for the staining of HCMV pp65-reactive RA14 TCR-transfected $J76^{CD8+}$ cells. In **(A, C, D)**, the shown data represent the MFI values ± SD of the means of 3 technical replicates.

staining was reduced to about 50% suggesting that dsSCD molecules had slowly deteriorated leading to reduced peptide receptivity. In a parallel experiment, influenzavirus A matrix protein$_{58-66}$ peptide-loaded HLA-A*02:01 dsSCD stored at various conditions were used to detect a small population of MP-reactive T cells in the peripheral blood of a healthy donor (Figure 4B). In accordance with previous results, storage of empty dsSCD for one week at 37°C led to a complete loss of multimer staining while storage of empty or peptide-loaded dsSCD at 4°C did not impair peptide receptivity or subsequent pMHC-I multimer stainings, respectively. While a systematic stability analysis of empty dsSCD was only conducted with the HLA-A*02:01 allotype, here we report the observation that empty dsSCD of various HLA-A,B,C allotypes exhibited unimpaired peptide receptivity after storage at 4°C for 3-12 months (data not shown).

We also assessed the stability of peptide association with dsSCD at various temperatures. To this end, bead-immobilized dsSCD were initially loaded overnight with 1 µM HCMV pp65 N9V [M>K^{FITC}] peptide at 4°C before incubating the peptide-loaded dsSCD for different time periods up to one week at 4, 22 or 37°C and measuring fluorescence by flow cytometry (Figure 4C). After the initial overnight peptide pulse, beads were either washed to remove unbound peptide or kept in the presence of peptide to keep peptide binding at equilibrium. In the presence of excess peptide, dsSCD continued to slowly take up additional peptide which was favored by incubation at ambient temperature, whereas the peptide receptivity of dsSCD incubated at 37°C began to slowly decay after 3 days. Washed dsSCD-N9V^{FITC} complexes bound to beads were fully stable at 4°C, slightly decayed at 22°C, yet rapidly dissociated when incubated at 37°C.

For routine usage it would be useful if dsSCD can be stored frozen without loss of function. To analyze this question, HLA-A*02:01 dsSCD were frozen in glycerol-containing buffer at -20°C for 3 weeks before thawing and charging with unlabeled HCMV pp65$_{495-503}$ peptide or MART1$_{26-35}$ control peptide (Figure 4D). Respective pMHC-I multimers were used to stain TCR RA14-transfected J76^{CD8+} cells in comparison to multimers formed with dsSCD that had been stored at 4°C. Defrozen empty dsSCD molecules fully retained their capacity to load peptide, form multimers and stain peptide-specific T cells, yet also did not gain unspecific binding due to aggregation when loaded with the irrelevant MART1 peptide.

In contrast to soluble disulfide-stabilized MHC-I heavy chains that were refolded *in vitro* in the presence of an excess of free β_2m (10), here we studied single-chain dimers in which the C-terminus of the β_2m open reading frame is tethered to the N-terminus of a disulfide-stabilized MHC-I α1 domain through a 24 amino acid long flexible linker. Tethering is conceived to facilitate the re-assembly of dissociated β_2m since interaction partners remain in close vicinity due to the linker. To study the influence of tethered β_2m on the peptide receptivity of dsSCD, we introduced the human rhinovirus (HRV) 3C protease cleavage sequence (LEVLFN|GP) in an extended linker sequence between β_2m and disulfide-stabilized HLA-A*02:01 heavy chain (Figure 5A). As intended, by addition of 3C protease to the β_2m-cleavable dsSCD*, a dissociation of β_2m from the MHC heavy chain could be visualized by SDS-PAGE analysis, whereas 3C protease treatment did not affect the apparent molecular weight of the non-cleavable dsSCD (Figure 5B). First we studied the staining capacity of pMHC-I multimers loaded with MART1 and NY-ESO-1 peptides for TCR-transfected Jurkat 76/CD8 cells. Peptide-loaded, HRV 3C-cleaved dsSCD* stained antigen-specific TCR as efficiently as non-cleaved dsSCD*, dsSCD or dtSCT-based multimers (Figure 5C), suggesting that a potential loss of peptide receptivity due to β_2m cleavage remained below the threshold of detection. Alternatively, dsSCD with and without HRV 3C cleavage sequence were incubated for 18 h in the absence or presence of 3C protease and with or without a 4.6-fold molar excess of free human β_2m. Treated dsSCD were then immobilized and loaded overnight with 1 µM N9V^{FITC} peptide (Figure 5D). Here, cleavage by 3C in the absence of additional β_2m resulted in a significant reduction of the FITC signal suggesting a partial loss of the peptide receptivity after irreversible dissociation of cleaved β_2m. An excess of free β_2m rescued loading with N9V^{FITC} peptide to the full extent and even slightly enhanced peptide uptake, suggesting a slightly greater functionality of free β_2m replacing tethered β_2m, while addition of free β_2m had no significant effect on non-cleavable dsSCD nor on uncleaved, cleavable dsSCD.

Taken together, biotinylated dsSCD that are purified from supernatants of CHO-S producer cells can be stably charged with synthetic peptides and used as MHC-I multimer tools similar to the established easYmer platform and biotinylated dtSCT. DsSCD are *bona fide* empty after purification, highly peptide-receptive and show a remarkable thermal stability that in part could involve the covalently tethered β_2m molecule.

3.4 Development of a dsSCD-based peptide binding assay and application for tumor patient epitope discovery

We developed a novel dsSCD-based peptide binding assay using high affinity Lys^{FITC}-substituted competitor peptides for individual dsSCD HLA-A,B,C allotypes (see Supplementary Table 1) based on experimental parameters delineated in Figure 1 and optimization of incubation time and concentration of the competitor peptide (data not shown). In the binding assay, bead-immobilized dsSCD were pulsed with unlabeled peptides at 10 µM concentration for 18 h before addition of competitor peptide at 1 µM for 10 min, washing and analyzing the bead-associated fluorescence by flow cytometry. As depicted in the schematic drawing of Figure 6A, a pre-bound high-affinity peptide will prevent the binding of the FITC-labeled competitor and lead to a strong reduction of the maximal achievable fluorescence intensity, while a pre-bound peptide of very low affinity and thus considered as non-binder will be almost completely replaced by the competitor peptide resulting in a strong FITC signal. To validate the binding competition assay, a set of 12 HLA-A*02:01 peptide ligands derived from viral proteins and 8 known peptide ligands from tumor-associated antigens as well as 7 non-A*02:01 binders was then tested with pp65 N9V^{FITC} competitor peptide (Figure 6B, see Supplementary Table 3 for predicted %Rank EL values). HLA-A*02:01 binders produced 85-100% reduction of the median fluorescence intensity (MFI) by

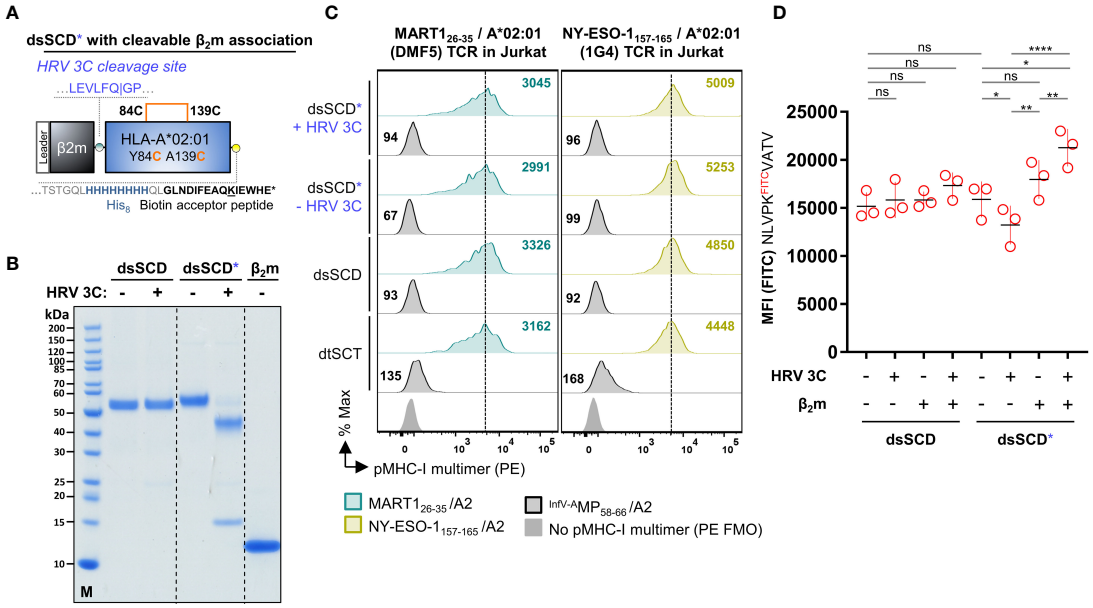

FIGURE 5
Analysis of HLA-A*02:01 dsSCD with cleavable β2m linker. **(A)** Schematic representation of a disulfide-stabilized β_2m-HLA-A*02:01 single-chain dimer with an additional HRV 3C cleavage site at the C-terminal end of the glycine-serine linker between β2m and MHC-I ectodomain (dsSCD*). **(B)** SDS-PAGE analysis of affinity chromatography-purified monomeric HLA-A*02:01 with (dsSCD*) and without (dsSCD) HRV 3C cleavage site incubated overnight in the presence (+) or absence (–) of HRV 3C protease. After dsSCD* cleavage with HRV 3C, free linker-extended β2m is visible. For comparison human β_2-microglobulin isolated from urine is shown. **(C)** Antigen-specific labeling of DMF5 and 1G4-TCR transgenic J76^{CD8+} cells with multimerized peptide-loaded dsSCD* with non-covalent β_2m association (+ HRV 3C) and covalent β_2m association (- HRV 3C). Here, dsSCD* were incubated with HRV 3C overnight followed by a consecutive peptide pulse (25 µM) and multimerization. A corresponding pMHC-I multimer staining using peptide-loaded dsSCD without HRV 3C cleavage site and dtSCT carrying the same peptides is additionally shown. **(D)** Analysis of the ^{FITC}peptide-loading capacity of bead-immobilized dsSCD* and dsSCD treated with HRV 3C. HLA-A*02:01 dsSCD and dsSCD* were incubated overnight in the presence (+) or absence (–) of HRV 3C protease and additional supplementation with a 4.6-fold molar excess of free β2m (+) or no β2m (–) during this incubation step. Treated dsSCD and dsSCD* were immobilized on streptavidin beads and loaded with 1 µM NLVPK^{FITC}VATV peptide overnight followed by flow cytometric analysis. Data represent mean values from 3 independent experiments in triplicates with statistical analysis by one-way ANOVA test followed by Tukey's multiple comparison test. Error bars show the standard deviation. ns, not significant; *p< 0.05; **p< 0.01; ****p< 0.0001.

directly loaded N9V^{FITC} and thus confirmed the informative value of the assay. In Figure 6C we show a comparative analysis of 20 published viral HLA-A*02:01 ligands and 7 non-binders using the dsSCD-based competition assay and the commercial easYmer-based peptide–β_2m–HLA heavy chain complex stabilization assay that is read out by binding of an anti-β_2m antibody. All binders (red circles) cluster with a few outliers around the diagonal at 95-100% N9V^{FITC} MFI reduction while non-binders (blue triangles) cluster around 0-5% MFI reduction, yielding a correlation coefficient of 0.83. Interestingly, two binders, HPV E7$_{11-19}$ and NY-ESO-1$_{93-102}$ relatively weakly stabilized HLA-A*02:01 easYmers whereas the dsSCD competition assay indicated strong binding.

Next, we set out to apply the MediMer peptide binding assay to the six HLA-A,B,C allotypes and 166 unique tumor neoepitope peptides predicted by NetMHCpan 4.1 (61) after whole exome sequencing of tumor cells from a lymph node metastasis of an advanced-stage melanoma patient (Supplementary Table 3). Individual binding data of predicted tumor neoepitope peptides to HLA-A*01:01, A*68:02, B*08:01, B*14:02, C*07:01 and C*08:02 dsSCD, respectively, is shown in Supplementary Figure 3A. In this figure we also show dsSCD binding values for several published allotype-specific peptide ligands derived from non-mutated tumor-associated antigens (TAA) and from viral proteins (see Supplementary Table 3 for details of peptides and predicted binding values). For the same panel of peptides we conducted easYmer complex formation assays in parallel. In lack of an HLA-C*08:02 easYmer, the HLA-C*05:01 easYmer was used instead because it has a very similar peptide binding motif, and the HLA-B*14:01 easYmer was used as a surrogate for the patient's B*14:02 allotype. Binding values in dsSCD and easYmer assays were relatively consistent with correlation coefficients of 0.61-0.88 across all allotypes studied (Figure 6D). We conclude that, although the novel MediMer peptide binding competition assay and the easYmer pMHC-I complex formation assay are obviously different in biochemical terms, results seem to be sufficiently consistent to be combined if required by the availability of reagents.

3.5 dsSCD multimer-based screening for T cells recognizing tumor neoepitopes

Using the peptide binding data obtained in the MediMer screening of the melanoma patient we endeavored to identify neoepitope-reactive T cell populations in the peripheral blood of the melanoma patient. pMHC-I multimers were assembled for each of the 107 selected neoepitopes accompanied by screening for 24 epitopes derived from

10.3389/fimmu.2023.1294565

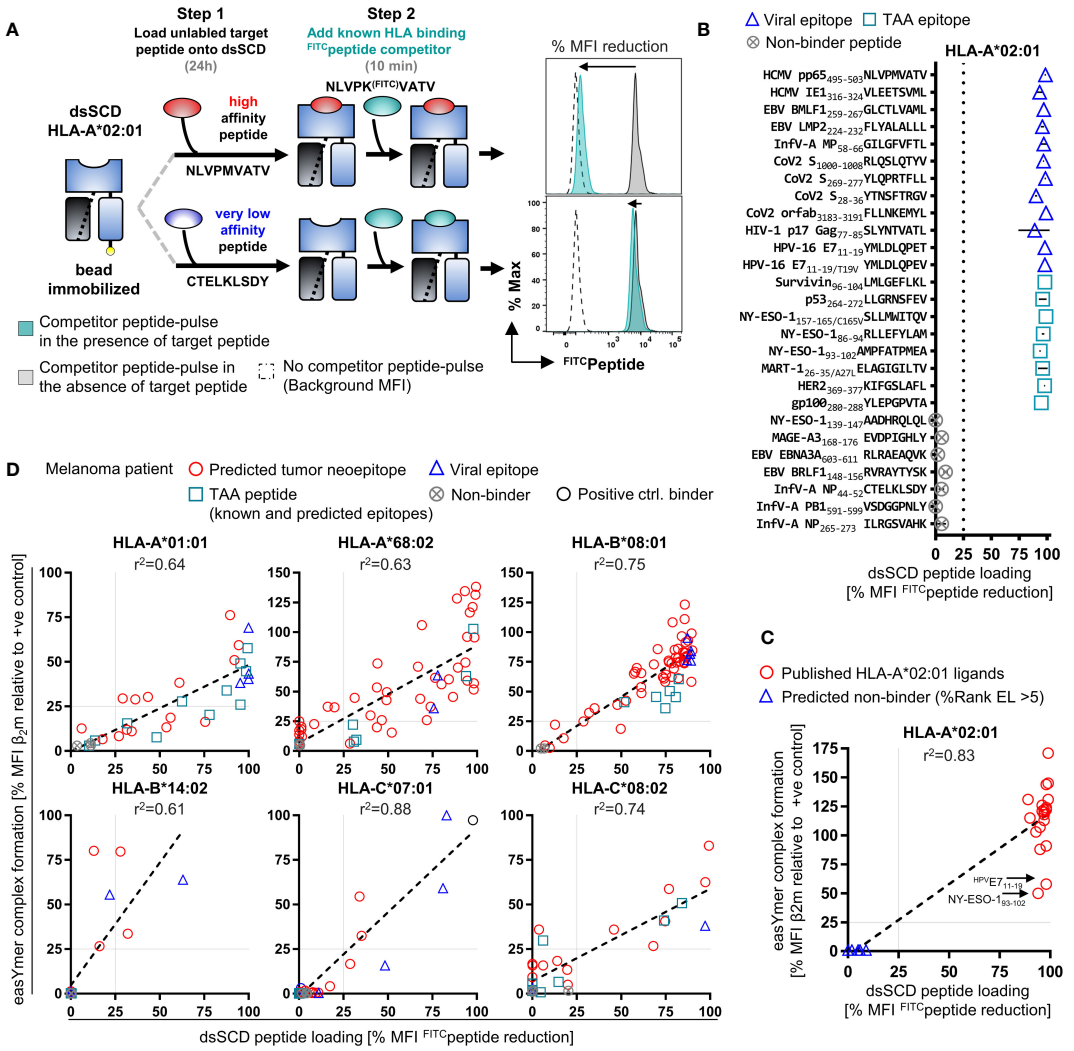

FIGURE 6
High-throughput dsSCD-based screening assay of peptide binding to HLA-I for *in silico* tumor neoepitope prediction validation. **(A)** Principle of a fast, flow cytometry-based assay for the reliable interrogation of large unlabeled peptide libraries for dsSCD binding exemplarily shown for HLA-A*02:01. As a first step, bead-immobilized dsSCD are loaded overnight with an unlabeled peptide at 10 µM followed by a 10 min pulse with a known FITC-labeled competitor peptide at 1 µM concentration. dsSCD occupancy by an unlabeled high-affinity target peptide, or high dsSCD receptivity to the competitor peptide due to prior loading with a very low-affinity peptide, is indicated by a low ^{FITC}peptide signal (i.e. major reduction *vs.* +ve control signal) or a high ^{FITC}peptide signal (i.e. minor reduction *vs.* +ve control signal) on the dsSCD-loaded bead, respectively. **(B)** Binding analysis of a panel of 20 known viral and tumor-associated (TAA) HLA-A*02:01 ligands and 7 predicted HLA-A*02:01 non-binding peptides by the dsSCD-based peptide screening assay. The MFI signal reduction in [%] relative to dsSCD-beads that have been loaded with ^{FITC}peptide in the absence of a target peptide is shown. 100% MFI reduction indicates an approximation of the complete dsSCD occupancy by a target peptide. **(C)** Comparative peptide binding analysis by HLA-A*02:01 dsSCD peptide binding and easYmer complex formation (ECF) assay using known HLA-A*02:01 ligands. Shown is the dsSCD-bead MFI ^{FITC}peptide signal reduction in [%] from Figure 6B in correlation with the bead-immobilized HLA-A*02:01 ECF displayed as MFI value of β_2M in [%] of an ECF performed in the presence of a target peptide relative to an ECF using a designated positive (+ve) control peptide. **(D)** Comparative binding interrogation by ECF and dsSCD-binding assay covering all six HLA-I allotypes of the melanoma patient for *in silico* predicted tumor neoepitopes based on whole-exome sequencing and RNA-Seq data sets of the melanoma patient's lymph node metastasis as well as selected TAA and viral epitopes. Individual peptides analyzed and peptide dsSCD-binding assay data are listed in Supplementary Table 3 and Supplementary Figure 3A, respectively. **(C, D)** Peptides that display a relative MFI lower than 25% (gray dotted lines) have been empirically determined as poor/non-binders. In all assays shown, the easYmers HLA-B*14:01 and HLA-C*05:01 were used as a surrogate for the patient's HLA-B*14:02 and HLA-C*08:02 allotypes, respectively, displaying highly similar peptide binding motifs.

tumor-associated antigens and 17 epitopes from viral peptides predicted to be presented by any of the patient's six HLA-A,B,C allotypes (Figure 7A). By staining CD8$^+$ T cells from PBMC using multimerized easYmers and dsSCD in a complementary manner that were color-coded with streptavidin-fluorochrome conjugates in a 60-fold matrix, we detected 3 HLA-B*08:01- and HLA-C*08:02-restricted T cell populations reactive with tumor-specific point mutations and a neo-sequence resulting from an out-of-frame gene fusion event. In addition, MAGE-A3/A*01:01 and NY-ESO-1/C*08:02 antigen-reactive T cell specificities were detected as well as seven T cell populations specific for known EBV- and influenzavirus-derived epitopes that we had selected for the six HLA allotypes. Exemplarily, color-coded 10-plex multimer stainings are presented in Supplementary Figure 3B, demonstrating the existence of CD8$^+$ T cells subpopulations

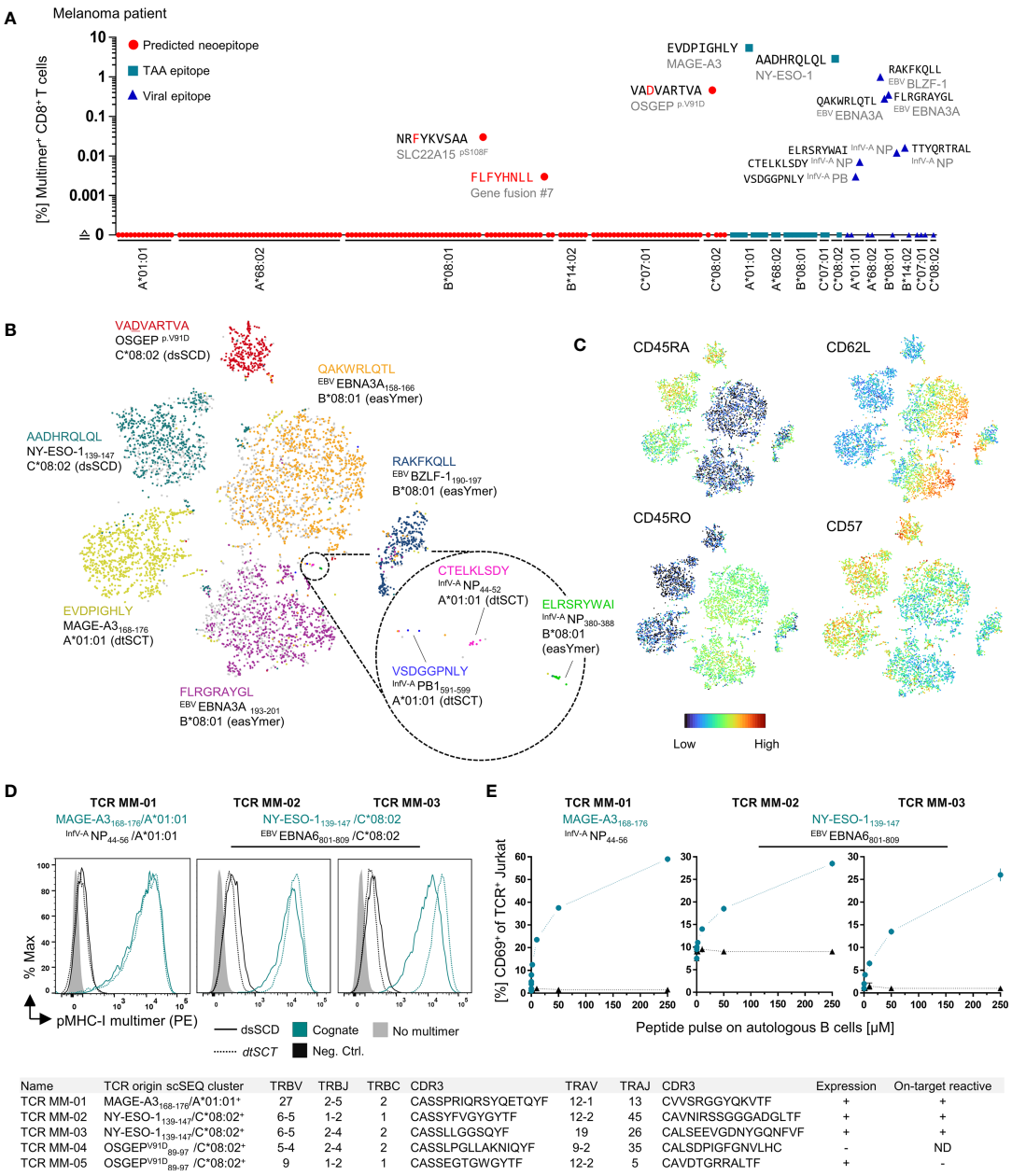

Name	TCR origin scSEQ cluster	TRBV	TRBJ	TRBC	CDR3	TRAV	TRAJ	CDR3	Expression	On-target reactive
TCR MM-01	MAGE-A3$_{168-176}$/A*01:01^{+}	27	2-5	2	CASSPRIQRSYQETQYF	12-1	13	CVVSRGGYQKVTF	+	+
TCR MM-02	NY-ESO-1$_{139-147}$/C*08:02^{+}	6-5	1-2	1	CASSYFVGYGYTF	12-2	45	CAVNIRSSGGGADGLTF	+	+
TCR MM-03	NY-ESO-1$_{139-147}$/C*08:02^{+}	6-5	2-4	2	CASSLLGGSQYF	19	26	CALSEEVGDNYGQNFVF	+	+
TCR MM-04	OSGEP$^{V91D}_{89-97}$ /C*08:02^{+}	5-4	2-4	2	CASSLPGLLAKNIQYF	9-2	35	CALSDPIGFGNVLHC	-	ND
TCR MM-05	OSGEP$^{V91D}_{89-97}$ /C*08:02^{+}	9	1-2	1	CASSEGTGWGYTF	12-2	5	CAVDTGRRALTF	+	-

FIGURE 7
Detection of neoepitope- and TAA-specific CD8^{+} T cell populations in the peripheral blood of melanoma patient using multimerized easYmers, dtSCTs and dsSCD (MediMers) in a complementary manner. **(A)** Identified antigen-specific CD8^{+} T cell populations in the patient's peripheral blood by dual color-encoded pMHC-I multimer staining covering all six HLA alleles of a melanoma patient. In total, 148 pMHC-I multimers were generated (107 predicted neoepitopes, 24 non-mutant tumor-associated antigens (TAA) and 17 viral epitopes) on the basis of a dsSCD for HLA-C*08:02 and easYmers covering the remaining five HLA-I allotypes. EasYmer HLA-B*14:01 was used as a surrogate for the patient's HLA-B*14:02 allotype. For the initial cell staining up to 60 dual color-encoded pMHC-I multimer pairs were used in one single pMHC-I library and detected pMHC-I multimer^{+} populations were verified afterwards by at least two additional independent stainings with up to 10 dual color-encoded pMHC-I multimer pairs. Representative dot plots are shown in Supplementary Figure 3D. Zero values were converted to 0.0001 to allow for plotting on a log scale. **(B, C)** pMHC-I multimer-guided single-cell TCR repertoire and cell surface protein expression analysis. pMHC-I multimer^{+} CD8^{+} T cells were cell sorted using a pMHC-I multimer library comprising uniquely DNA-barcoded and population size-dependent dual color-encoded pMHC-I multimer pairs (see Supplementary Figure 2C) combined with a panel of 30 DNA-barcoded cell phenotyping antibodies (Supplementary Table 4). Multimerized dsSCD, easYmer and dtSCT were used in combination. An experimentally obtained 10x scSeq data set is shown as tSNE plot based on surface marker expression including the pMHC-I multimer labeling of a total of 3236 individual cells represented by dots. Cell clustering based on pMHC-I multimer barcode detection **(B)** and cell surface expression of selected T cell memory markers **(C)** is shown. **(D, E)** Validation of cloned MAGE-A3 and NY-ESO-1-specific TCR from the 10x scSEQ data set. TRBV/TRBJ and TRAV/TRAJ subtypes and respective CDR3 sequences are displayed in the table at the bottom. **(D)** Antigen-specific staining of a MAGE-A3$_{168-176}$/A*01:01-specific TCR (MM-01) and two NY-ESO-1$_{139-147}$/HLA-C*08:02-specific TCR (MM-02 and MM-03) expressed in J76^{CD8+} cells with multimerized dtSCT and dsSCD representing the cognate (teal lines) or a viral control (black lines) epitope. **(E)** Co-culture of TCR-expressing J76^{CD8+} cells with autologous peptide-pulsed B cells. The expression of early T cell activation marker CD69 ± SD in [%] of TCR^{+} J76^{CD8+} cells after 18h co-culture in triplicates in presence of cognate (teal) or a control (black) peptide at various concentrations. Two cloned dominant TCRs (MM-04 and MM-05) derived from the OSGEP^{V91D}/HLA-C*08:02 multimer scSEQ cluster lacked expression in J76^{CD8+} cells or were not stained by corresponding the pMHC-I multimer, respectively. ND, not determined.

recognizing the tumor neoepitopes, $OSGEP_{V91D}$/HLA-C*08:02 (0.46%), $SLC22A15_{S108F}$/HLA-B*08:01 (0.028%) and fusion #7 neo-sequence/HLA-B*08:01 (0.002%). For the two identified neo-epitopes based on single nucleotide variations we conducted peptide binding assays including the corresponding wild-type peptides (Supplementary Figure 3C). Interestingly, in both the $OSGEP_{V91D}$ (VA**D**VARTVA) and the $SLC22A15_{S108F}$ (NR**F**YKVSAA) neoepitope peptides the mutation created a *de novo* anchor residue enabling binding to HLA-C*08:02 and HLA-B*08:01, respectively, while wild-type variants did not bind.

To identify sequences of TCRs recognizing neo-epitopes by single RNA cell sequencing, epitopes from shared tumor-associated antigens as well as viral epitopes, $CD8^+$ T cells from the peripheral blood of the melanoma patient were labeled with pools of peptide-loaded MHC-I molecules multimerized with DNA-barcoded PE-conjugated dCODE Dextramer® reagents (Figure 7B, Supplementary Figure 2C, Supplementary Table 4). Relying on equal labeling performances of the three types of multimers (see Figure 3D), we combined the multimer labeling of the patient's T cells, peptide-loaded dsSCD, peptide-loaded easYmers and dtSCTs due to varying availabilities of the multimer reagents at the time of the experiment (Figure 7B). To increase the likelihood to detect small subpopulations, dual color-coded T cell populations occurring at high (>1%, PE^+ $BUV395^+$), intermediate (~0.1%-1%, PE^+ $BV421^+$) and low (~0.005-0.1% PE^+ APC^+) frequency were separately FACS-sorted and mixed in adjusted numbers under-representing T cell specificities of high and intermediate frequencies (Supplementary Figure 2C). A pool of 30 antibodies reacting with T cell lineage and differentiation markers and labeled with Total SeqC® DNA feature barcodes were used simultaneously in order to phenotype antigen-specific T cells on the single cell level. After scRNA-Seq of pMHC-I multimer$^+$ T cells accomplished by the 10x Genomics platform, we obtained 180 TCRα/β clonotypes, antibody-based phenotypes and gene expression data from 3236 barcoded cells that are depicted in the feature barcode-based t-SNE plot of Figure 7B. T cell specificities defined by respective pMHC-multimers are shown in differently colored t-SNE clusters of greatly varying sizes. Unfortunately, we were unable to retrieve $SLC22A15_{S108F}$/B*08:01 and Fusion#7/B*08:01 labeled populations after scRNA-Seq, which was likely due to insufficient B*08:01 easYmer formation and a too low cell population frequency, respectively, for those two epitopes. Surface marker expression analysis of the identified pMHC-I multimer$^+$ populations clearly characterized the NY-ESO-$1_{139\text{-}147}$, MAGE-$A3_{168\text{-}176}$ and $OSGEP_{89\text{-}97/V91D}$ reactive populations as belonging to the $CD57^+CD45RA^+$ exhausted effector memory T_{EMRA} subset, while $EBNA3A_{158\text{-}166}$ and $EBNA3A_{193\text{-}201}$ clustered to both the $CD45RO^+/CD62L^+$ central and $CD45RO^+/CD62L^-$ effector memory (T_{CM}/T_{EM}) subsets (Figure 7C).

One MAGE-$A3_{168\text{-}176}$/A*01:01 and two NY-ESO-$1_{139\text{-}147}$/C*08:02-reactive TCR, the latter being of a so far unreported specificity, were cloned, expressed in Jurkat 76/CD8 cells and validated by successful staining with dsSCD and dtSCT loaded with the respective peptides (Figure 7D). These TCR-transfected Jurkat 76/CD8 cells were also activated by peptide-pulsed autologous CD40L-expanded B cells showing different sensitivities with regard to CD69 early activation marker upregulation in a peptide titration (Figure 7E). Two putative $OSGEP_{89\text{-}97/V91D}$/C*08:02 reactive TCR were cloned, however, unfortunately either failed to be expressible or could not be labeled by cognate pMHC-I multimer after expression in Jurkat 76/CD8.

To further substantiate the usefulness of the MediMer platform for the screening of peptide binding to various HLA-C allotypes, we interrogated the NY-ESO-1 epitopes 139-147 (AADHRQLQL) and 96-104 (FATPMEAEL) in a binding assay with a library of 14 HLA-C dsSCD allotypes (Supplementary Figure 3D). Clearly, the binding NY-ESO-$1_{139\text{-}147}$ was restricted to HLA-C*05:01, C*08:02 and C*15:02, while NY-ESO-$1_{96\text{-}104}$ binding was more promiscuous among the tested HLA-C allotypes.

Taken together, dsSCD can be manufactured matching all six allotypic HLA-A,B,C molecules of an individual tumor patient, can be used as a high-throughput screening platform for allotype-specific peptide ligand validation and for pMHC-I multimer-guided scRNA-Seq for comprehensive TCR discovery combined with immune cell phenotyping.

4 Discussion

In the emerging field that is dedicated to the discovery of T cells with specificity for tumor-associated peptide antigens there is a high need for specific and highly sensitive tools capable of high throughput screening in order to detect rare T cell populations in the peripheral blood and tumor infiltrate (63, 64). The MHC-I multimer technology has overcome the problem of low affinity interactions between monomeric MHC-I molecules and antigen-specific T cell receptors that are typically 3–4 orders of magnitude lower than antibody–protein antigen interactions (65). Multimerization of biotinylated peptide-loaded MHC-I heavy chain/β_2-microglobulin complexes on fluorochrome-conjugated streptavidin has been shown to sufficiently improve binding avidities to enable flow-cytometric detection of various T cell populations of greatly varying frequencies and has been ever since a valuable assay tool that is subjected to a constant evolution (66–68). Furthermore, the simultaneous usage of multiple fluorochrome-streptavidin variants complexed with individual pMHC-I complexes facilitates in one staining a high-dimensional multiplex analysis (2, 3). Moreover, the MHC-I multimer technology has been combined with DNA barcoding and subsequent pMHC-multimer-guided single-cell TCR sequencing and in-depth gene signature analysis of antigen-specific populations as shown recently (69).

As a major advantage, pMHC multimer stainings can be applied independently of the naïve, memory or exhausted functional status of the analyzed T cell population and no preparation of antigen-presenting cells is required. Furthermore, pMHC multimer stainings often show higher sensitivities compared to most other functional assays, such as ELISpot and intracellular cytokine staining (70). This is important since typically tumor-neoantigen-specific T cells occur in *ex vivo* peripheral blood lymphocytes at frequencies of only 0.02% (1 in 5000 T cells) to 0.0007% (1 in about 150,000 T cells) and lower (71, 72) making it often a necessity to perform *in vitro* stimulations with peptide pools combined with pMHC-I multimer stainings in order to detect neoantigen-specific T cell populations in peripheral blood on a regular basis (73).

A limitation of the pMHC multimer technology is that the MHC allotypes of the patient need to be known and the many potential antigenic epitopes need to be accurately predicted to limit pMHC multimers libraries to reasonable workloads and at the same time also match the often limited availability of tumor patients' blood samples and the urgent medical need.

To manufacture soluble MHC-I molecules, recombinant MHC-I heavy chain molecules lacking transmembrane and intracytoplasmic domains and recombinant β_2m were conventionally produced in *E. coli* by a laborious procedure (74). Inclusion bodies containing expressed proteins need to be harvested, washed and solubilized in urea-containing buffer. Refolding of the denatured heavy chain and β_2m is performed in folding buffers under reducing conditions at pH 8 for several days in the presence of final peptide ligands for the production of a particular peptide-loaded MHC-I monomer (1), or in the presence of UV-cleavable conditional peptide ligands, for the purpose of generating pMHC-I multimer libraries by peptide exchange (3, 4, 10, 14, 75–77). After refolding, pMHC-I complexes are usually enzymatically biotinylated by BirA biotin ligase at a biotin acceptor tag sequence (AviTag™) at the C-terminus of the heavy chain, followed by purification through size exclusion chromatography.

Although a larger panel of 26 HLA-A,B,C allotypes endowed with conditional ligands have been reported (14, 76, 78, 79), up to date there is only the limited number of 8 HLA-A,B,C UV-exchangeable allotypes commercially available as Flex-T™ reagents (BioLegend). This small selection does not satisfy the needs of immune oncologists who intend to screen neoepitope-specific T cells reactive against the entirety of HLA allotypes of all patients.

Other experimental methods described for only a small collection of recombinant MHC-I molecules (HLA-A*02:01, H-2K^b) utilized temperature-dependent peptide exchange of low-affinity placeholder peptides in conventionally refolded, recombinant bacterial MHC-I proteins (13, 80) or tapasin-mediated exchange of pMHC-I (HLA-A*02:01, H-2L^d, H-2D^d) refolded in the presence of truncated low affinity peptides (81).

Recently, disulfide-stabilized MHC-I heavy chains have been used for refolding with β_2m and a stabilizing dipeptide (10). After purification, these molecules are empty and highly receptive for conventional MHC-I peptide ligands, and thus represent ideal tools for the generation of pMHC-I libraries. Peptide-receptive empty MHC-I molecules appear to be superior to systems utilizing peptide exchange of soluble heterotrimers preloaded with endogenous ligands (82) because the efficiencies of peptide exchange by new ligands of low and intermediate affinity is unpredictable. However, so far only a small number of disulfide-stabilized allotypes are commercially available which might be due to technical difficulties associated with the refolding of various disulfide-stabilized HLA-A,B,C heavy chains with β_2m that, except for HLA-A*02:01, A*24:02 and H-2K^b molecules that refold in the presence of dipeptides, required the use of UV-cleavable placeholder peptides during *in vitro* refolding (77).

A successful alternative strategy employs pre-oxidized, bacterially produced heavy chains that can be efficiently biotinylated by BirA overexpressed in *E. coli* co-transformed with the MHC-I plasmid (7, 83). Resulting oxidized, denatured heavy chain can be easily refolded with an excess of β_2m and suitable peptide and form tetramers with fluorochrome-labeled streptavidin in one-pot reactions at miniature scale. While the purification of correctly oxidized MHC-I isoforms appears to be demanding (84), the downstream application is easy, flexible and capable of high-throughput screening of antigen-specific T cells. A large number of HLA-A [25], HLA-B [45] and HLA-C [12] allotypes are presently available as peptide-refoldable easYmers® for flow cytometry (immunAware/Immudex). Due to their good performance, in this work easYmers have been used as benchmark for our own dsSCD. Notably, however, until recently only ca. 80% of the MHC-I allotypes expressed by 23 tumor patients included in neoepitope screening campaigns in our laboratory were covered by the easYmer platform. Moreover, the routine use of commercially available pMHC-I multimer platforms is fraught with a considerable financial burden.

With the development of the herein reported MediMer platform utilizing disulfide-stabilized peptide-receptive recombinant MHC-I molecules produced in mammalian cells we fill the gap of patient-tailored production of recombinant rare HLA-A,B,C allotypes. As we demonstrate in the present work, these can be used in TCR discovery pipelines including a bead-based screening assay for libraries of individual putative neoepitope peptide ligands and the formation of sensitive dsSCD-based pMHC-I multimers usable for the *ex vivo* staining of antigen-specific T cells in peripheral blood, for the isolation of multimer-binding T cells by flow cytometry or magnetic beads, and finally for the validation of cloned TCR expressed as transgenes in T cells.

Except for the cloning of new HLA-A,B,C allotypes harboring the Y84C and A139C mutations that form the stabilizing disulfide, little hands-on time is required after purification via a C-terminal histidine tag. Due to their metabolic biotinylation by co-expressed BirA ligase, peptide-receptive dsSCD molecules are ready to be loaded to streptavidin-coated beads or to be incorporated into pMHC-I multimers based on streptavidin molecules conjugated to a large variety of fluorophores enabling combinatorial color coding. As an obvious advantage, the production of SCT in mammalian producer cells (25, 29, 30, 85, 86) and with this work also of dsSCD is circumventing the limitations of the technically demanding *in vitro* refolding of proteins obtained from *E. coli* inclusion bodies requiring the skills of specialized biochemists. We demonstrate superior thermal stability of empty dsSCD that can be stored frozen as well as peptide-loaded at 4°C and thus represent a versatile off-the-shelf tool.

The principle of tethering β_2m via flexible linker to the C-terminus of soluble mouse MHC-I heavy chains to render peptide-receptive single-chain MHC-I molecules has initially been described about thirty years ago (87). Toshitani and colleagues first reported a membrane-bound HLA-A2 single-chain dimer with N-terminally tethered β_2m (88). A recent study employed His-tagged, affinity-maturated HLA-K^b chimeric ectodomains in peptide exchange assays for the mapping tumor-associated epitopes (82). In another study, soluble single-chain dimers of β_2m and various wild-type HLA-A,B,C allotypes were employed for a detailed

mass spectrometric analysis of HLA peptide ligands (89). Both groups used HEK293 as producer cells. For still unclear reasons we failed to produce Fc-tagged single-chain dimers in HEK293 cells, neither as wild-type HLA-A*02:01 SCD-Fc (data not shown), nor as SCD-Fc containing the groove-opening mutation Y84A (21) (data not shown) nor as dsSCD-Fc (see Figure 1). Since respective molecules were detected by an intracellular staining using BB7.2, an antibody recognizing folded HLA-A2 molecules (Figure 1B), as well as by anti-mouse IgG, we suppose that metabolically biotinylated dsSCD were retained by ER quality control mechanisms that were apparently not active in CHO-S cells since the latter secreted significant amounts of dsSCD-Fc (see Figure 1D). It seems possible that a partial or complete inability of soluble dsSCD to interact with the TAP-tapasin loading peptide complex, due to the mutation of the tapasin-interacting Tyr84 residue (90), contributed to the intracellular retention of dsSCD-Fc in HEK293 cells as the lack of peptide cargo might have been sensed by ER or cis-Golgi quality control mechanisms of HEK293 cells. On the other hand, H-2K^b molecules harboring the same Y84C/A139C disulfide bridge were reported to overcome intracellular retention in peptide loading complex-deficient mouse fibroblasts (9). Alternatively, the production of dsSCD in CHO-S cells at 32°C might have facilitated escape from quality control and subsequent secretion, in line with older reports showing that in peptide transporter-deficient cells, membrane-bound peptide-free MHC-I molecules are efficiently cell surface-expressed at reduced temperatures of 19-33°C (91, 92). Nevertheless, the observation that no endogenous peptide ligands could be detected by mass spectrometry in CHO-S-produced HLA-A*02:01 dsSCD (see Figure 1G) is in our opinion of great practical value since empty dsSCD should be more easily loadable with peptides of low and intermediate affinity thereby expanding the screening space for potential neoepitope ligands.

As previously reported for membrane-bound H-2K^b molecules harboring the peptide binding groove-stabilizing Cys84-Ala139 disulfide bond, the affinity of disulfide-stabilized heavy chains for β_2m is remarkably increased (9). Hence is not surprising that cleavage of the flexible linker between β_2m and heavy chain using an artificially introduced HRV 3C site had no major influence on the peptide receptivity of dsSCD (see Figure 5). Nevertheless, we assume that the presence of tethered β_2m in single-chain dimers is of benefit for the long-term stability of empty dsSCD *in vitro*, as in contrast to non-covalent complexes of free heavy chain and β_2m, tethered β_2m can be conceived to quickly reassemble after occasional partial or complete dissociation, thereby impeding denaturation of the empty heavy chain. We have shown that the time- and temperature-dependent deterioration of the peptide binding capacity of dsSCD is almost completely prevented in the continuous presence of an excess of exogenous peptide even at elevated temperature (see Figure 4C), reaffirming the known importance of peptide for the stability of the heterotrimeric complex (91, 92).

Using empty dsSCD as peptide receptors, the determination of K_D dissociation constants is straightforward for peptides harboring fluorochrome-tagged amino acids such as lysine^{FITC} by extrapolating saturation binding in titration curved (see Figure 1E; Supplementary Figure 1B, while analysis of binding affinities of unlabeled peptides does not appear trivial. A previous study employing preincubation of unlabeled ligand for periods up to 24 h followed by competition with radioactively labeled competitor ligand for 15-30 min (93), suggests that the 'preincubation endpoint approach' resembling the conditions of the dsSCD competiton assay used herein, could enable the estimation of K_D values of unlabeled peptides by simply determining their IC_{50} values for inhibition of binding of FITC-labeled index peptides to a given dsSCD.

By co-expression of an ER-targeted *E. coli* BirA biotin ligase possessing a C-terminal ER retention signal (62), we facilitate metabolic biotinylation of the soluble ds-SCD molecules tagged with BirA ligase recognition sequence (AviTag) circumventing the need for enzymatic biotinylation of purified pMHC-I molecules (86). While metabolic biotinylation appeared to be sufficient to induce a streptavidin-mediated gel shift of a major proportion of all tested HLA-A,B,C allotype monomers and for the loading of streptavidin beads as well as for the formation of streptavidin-based pMHC-I multimers conducted in this work, metabolic biotinylation in CHO-S cells was not as efficient as metabolic biotinylation in BirA-overexpressing *E. coli* for which biotinylation efficiencies of 85-100% were reported for >40 HLA-A and HLA-B alleles (7), or as metabolic biotinylation of dtSCT in 293-F cells conducted in this study. It is possible that insufficient quantities of ER-retained BirA ligase were co-translationally introduced into ER subcompartments where nascent dsSCD molecules were inserted, or that the kinetics of ER-translocated BirA ligase was too slow to completely biotinylate all dsSCD molecules probably leaving the ER and ER-recycling compartments rapidly. In future experiments it will be attempted to improve metabolic biotinylation by generating a CHO-S producer line stably transfected with ER-resident BirA ligase and analyze the option of co-translational biotinylation of nascent dsSCD molecules by over-expression of cytoplasmic BirA ligase.

As shown in this work the newly established MediMer peptide binding assay that is based on equilibrium phase loading with unlabeled test peptides followed by a flow cytometry read-out using a fluorescently labeled competitor peptide, is capable to be conducted in a high-throughput fashion similar to the easYmer complex formation assay that measures the stable association of free β_2m to free biotinylated heavy chains in the presence of stabilizing peptides. These assays are based on different biochemical principles and it is therefore not surprising that we observed minor differences in the binding values obtained for individual members of large panels of peptides, that were only *in silico* predicted to be ligands for an HLA-A,B,C allotype of choice but had not been validated before. Since the overall performance of the two binding assays appear to be sufficiently consistent, they could be used in a combinatorial manner to arrive at a selection of peptides that is subsequently used for pMHC-I multimer formation with the goal of identifying respective CD8$^+$ T cell populations in peripheral blood or tumor infiltrates directly *ex vivo*, or after *in vitro* peptide restimulations.

Undoubtedly, peptide-loaded dsSCD representing various MHC-I allotypes performed equally well in pMHC-I multimers as

compared to pMHC-I multimers formed with easYmers or disulfide-trapped single-chain trimers with regard to the simultaneous discrimination of T cell populations of greatly different frequencies by combinatorial color coding (see Figure 3). We conclude from the very slow peptide dissociation of peptide-loaded dsSCD at 4°C and ambient temperature (see Figure 4), that peptide-dsSCD complexes appear to be highly stable once formed, and due to the high specificity of T cell labeling, suited to be used for the search for very small T cell population below 0.1% frequency that are often encountered when analyzing T cell specificities directly *ex vivo*.

Up to the present time we have been able to successfully produce by transient gene expression in CHO-S producer cells more than 10 HLA-A, 8 HLA-B and 14 HLA-C metabolically biotinylated dsSCD allotypes (Figure 2, Supplementary Figure 1 and data not shown). This success prompted us to screen T cells from an HLA-C*08:02-expressing melanoma patient for tumor-antigen reactive T cells with the herein reported HLA-C*08:02 dsSCD that is not available as easYmer. We first produced 6 dsSCDs matching the HLA-A,B,C allotypes of that patient and employed them in the newly developed MediMer peptide binding assay to screen a large panel of potential neoepitope peptides, peptides derived from shared tumor-associated antigens as well as known viral epitopes for *in vitro* binding to dsSCD and easYmers (see Figure 6D). This screening campaign revealed a large number of confirmed binders that were subsequently incorporated in individual dual color-coded pMHC-I multimers and used in multiplex labeling reactions of peripheral blood $CD8^+$ T cells from the patient (Figure 7A). Using HLA-C*08:02 dsSCD we detected two T cell populations recognizing tumor-derived peptides, one directed against a tumor neoepitope and the other specific for a novel NY-ESO-1 epitope. Using peptide-loaded dsSCD and dtSCT representing A*01:01, B*08:01, and B*14:01 allotypes, we were able to label small neo-epitope specific T cell populations and larger populations reactive with epitopes derived from viral recall antigens that are expected to exist in greater frequencies (Supplementary Figure 3). Enabled by DNA-barcoded pMHC-I multimers representing a combination of peptide-loaded dsSCDs, easYmers and peptide-tethered dtSCTs, we successfully conducted scRNA-Seq of the melanoma patient-derived pMHC-I $multimer^+$ $CD8^+$ T cell population leading to the discovery of novel MAGE-A1/A*01:01 and NY-ESO-1/C*08:02 T cell receptors that could be functionally validated by recombinant expression in Jurkat reporter cells and that could be useful for other patients sharing these HLA-I alleles.

Taken together, we herein presented that the technically easily accessible MediMer platform of peptide-receptive disulfide-stabilized single-chain dimers can be rapidly deployed to screen a large panel of potential tumor-associated peptides in a binding assay, facilitate the detection of antigen-specific T cell populations even at very low frequencies in the peripheral blood of patients and enables pMHC-I multimer-guided scRNA-Seq for the identification and cloning of respective TCR receptors that can be potentially used in adoptive transfer regimens with TCR-transgenic autologous T cells.

Data availability statement

The whole-genome sequencing, RNA sequencing and single-cell RNA sequencing datasets presented in the study are deposited in the European Genome Archive (EGA) repository, accession number EGAS50000000065. The study contains the sequencing datasets EGAD50000000092 (DAC: Momburg/Meyer) and EGAD50000000093 (DAC: HIPO DACO). Additional supporting data are available from the corresponding authors upon reasonable request.

Ethics statement

Blood samples from healthy donors were collected according to the principles of the Declaration of Helsinki and were obtained from the Deutsches Rotes Kreuz (DRK) Blutspendedienst Baden-Württemberg-Hessen gGmbH, Mannheim, Germany. All experiments with patient-derived material were conducted in accordance with the Declaration of Helsinki and a written informed consent was obtained from the patient, approved by ethics votes S-022/2013, S-206/2011 (MASTER trial) and S-207/2005 (NCT Biobank), renewed on 10 September 2018, Ethics Committee of the Medical Faculty of Heidelberg University, Heidelberg, Germany.

Author contributions

Conceptualization: MM, FM; Methodology: MM, CP, TB, JB, SB, DI; Software: PC, YL; Validation: MM, CP, TB, JB, PC; Formal analysis: MM, CP, TB, JB, PC, YL, AR, MR, IZ, FM. Investigation: MM, CP, TB, JB, SB, NB, CT, LW, RP, DI, PaS, KL, AR, JH, MR IZ, FM. Resources: DI, PaS, SE, PeS, IP, MP, SF, AR, JH, DJ, IZ, FM; Data curation: MM, PC; Writing – original draft: MM, FM; Writing – review and editing: All authors; Visualization: MM, CP, TB, JB, FM; Supervision: MM, FM; Project administration: MR, IZ; Funding acquisition: MM, SBE, MP, IP, SF, AR, IZ, DJ, FM. All authors contributed to the article and approved the submitted version.

Funding

The author(s) declare financial support was received for the research, authorship, and/or publication of this article. This research was partially funded by the NCT 3.0 Immunotherapy Program, "Identification of neoepitope-specific T cell receptors – Proof of Concept" and the Dietmar Hopp Foundation (Pilot project for the development of personalized cellular immunotherapies targeting solid cancers). Sequencing data were kindly provided by the NCT Molecular Precision Oncology Program (MASTER). In addition, this work was supported by the Health + Life Science Alliance Heidelberg Mannheim Explore!Tech grant approved by the State Parliament of Baden-Württemberg, Germany. JB was supported by the DKFZ Postdoctoral Fellowship.

Acknowledgments

We are thankful for the excellent technical assistance of Iris Kaiser, Annette Köster, Rosa Eurich and Jasmin Roth (biobanking, sample processing), Mario Koch and Andrea Breuer (peptide synthesis) as well as Rebecca Köhler and Sophia Föhr (DIA-MS). We thank the Flow Cytometry and Genomics & Proteomics core facilities at the German Cancer Research Center (DKFZ) for their excellent support and services.

Conflict of interest

The authors declare that the research was conducted in the absence of any commercial or financial relationships that could be construed as a potential conflict of interest.

The author(s) declared that they were an editorial board member of Frontiers, at the time of submission. This had no impact on the peer review process and the final decision.

Publisher's note

Supplementary material

The Supplementary Material for this article can be found online at: https://www.frontiersin.org/articles/10.3389/fimmu.2023.1294565/full#supplementary-material

SUPPLEMENTARY FIGURE 1
Production of various dsSCD allotypes and positional analysis of lysine^{FITC} substituted peptides. **(A)** Exemplary SDS-PAGE analysis of affinity chromatography-purified dsSCD produced as Fc-free variants in CHO cells. dsSCD biotinylation was confirmed by gel shift upon equimolar addition (+) of streptavidin prior to the gel electrophoresis. **(B)** Systematic binding analysis of FITC-lysine (K^{FITC})-substituted NLVPMVATV peptides towards bead-immobilized HLA-A*02:01 dsSCD. Beads were pulsed with the indicated concentrations of ^{FITC}peptides for 18 hours. Non-linear regression (one-site specific binding) of the FITC MFI against the peptide concentration and calculated K_D values in µM are shown. For comparison, the NetMHCpan 4.1-based binding motif of naturally bound, eluted ligands (EL) of HLA-A*02:01 is shown above the lysine-substituted NLVPMVATV sequence (https://services.healthtech.dtu.dk/services/NetMHCpan-4.1/). HLA-A*02:01 %Rank EL prediction values are shown for the indicated peptides with K substitution and their classified binding levels as putative strong binders (SB, %Rank EL <0.5), weak binders (WB, %Rank EL <2) and non-binders (nonB, %Rank EL >2). The FITC conjugation is neglected by this prediction.

SUPPLEMENTARY FIGURE 2
Flow cytometry gating strategies. **(A)** Antigen-specific TCR validation of stably transfected Jurkat 76 CD8$^+$ (J76^{CD8+}) exemplary shown for the NY-ESO-$1_{139-147}$/HLA-C*08:02-specific TCR MM-03 (see Figure 7). pMHC-I multimer binding (left histograms) or CD69 upregulation in the presence of stimulation (right histograms) is always shown for the TCR$^+$/CD8$^+$ J76^{CD8+} fraction. **(B)** Dual color-encoded pMHC-I multimer analysis of healthy donor (HD-01) and patient-derived CD8$^+$ T cells is exemplary shown for one dual-color encoded pMHC-I multimer$^+$ population of HD-01. HD-01 CD8$^+$ T cells were stained with a pool of three dual-color pMHC-I multimer pairs, each pair associated with a different peptide and a unique dual color combination on the basis of streptavidin-conjugated fluorochromes APC, PE and BV421 used in this experiment for the pMHC-I multimer preparation. For analysis, single, living CD3$^+$ CD8$^+$ T cells were identified following the definition of positive events in each pMHC-I multimer channel as well as the generation of respective NOT gates thereof. To display a single dual color pMHC-I multimer population using Boolean gating, two positive gates (APC, PE) and here one NOT gate (BV421) are combined as a single AND gate (i.e., APC+ AND PE+ AND BV421–). Finally, the APC+ AND PE+ AND BV421– gate is combined as an OR gate with [APC– AND PE– AND BV421–] as shown for the ^{HCMV}pp65/A*02:02-specific CD8$^+$ T cell population of HD-01. **(C)** Used gating strategy for cell sorting of dual color and DNA-barcoded (dCODE dextramers®) pMHC-I multimer$^+$ CD8$^+$ T cells of the melanoma patient for subsequent single-cell sequencing (scSEQ). Based on prior dual-color encoded pMHC-I multimer analysis of CD8$^+$ T cells *ex vivo* from the patient, all identified pMHC-I multimer$^+$ populations were pre-clustered for cell sorting depending on their frequency as low (< 0.1%), intermediate (0.1%–1.0%) or high (>1%) frequent and associated with the fluorochromes APC, BV421 or BUV395, respectively, to ensure that also populations of very low frequency were included in the scSEQ. For the dual-color and DNA-barcoded pMHC-I multimer library generation, each epitope was encoded by a uniquely DNA-barcoded, PE-conjugated dextramer as well as paired with the same pMHC-I multimerized with streptavidin APC, BV421 or BUV395 depending on the frequency (see also Supplementary Table 4). For the sorting, single living CD3$^+$ CD8$^+$ T cells and pMHC-I dextramer-PE$^+$ were selected following the separation of the respective dual-color positive pMHC-I multimer$^+$ populations. Finally, individual, separated pMHC-I multimer$^+$ populations of low, intermediate or high frequency were mixed for the scSEQ in a defined ratio favoring small populations.

SUPPLEMENTARY FIGURE 3
dsSCD peptide binding validation of *in silico* predicted neoepitopes of a melanoma patient's lymph node metastasis and identification of three neoepitope-specific and two TAA-specific CD8$^+$ T cell populations in autologous peripheral blood. **(A)** HLA binding analysis of *in silico* predicted tumor neoepitopes and selected known and predicted tumor-associated non-mutated epitopes (TAA) using dsSCD-based peptide binding assays covering all six HLA-I allotypes of the patient. Shown is the MFI signal reduction ± SD in [%] relative to dsSCD-beads that have been loaded with ^{FITC}peptide in the absence of a target peptide. Individual peptides are listed in top-down order according to their *in silico* binding prediction score (%Rank EL) for the respective HLA allotypes (also see Supplementary Table 3). Peptides are considered as HLA binders if they display a relative MFI reduction higher than 25% (dashed horizontal lines). **(B)** Labeling of the melanoma patient's autologous peripheral CD8$^+$ T cells *ex vivo* with dual-color encoded HLA-I multimers generated on the basis of dsSCD, dtSCT or commercial easYmer®. Representative dot plot of selected pMHC-I multimer$^+$ populations that have been detected in three or more independent experiments are shown. **(C)** Comparative peptide-HLA binding analysis of predicted neoepitopes SLC22A15$^{p.S108F}$ and OSGEP$^{p.V91D}$ and their wild-type counterparts using an HLA-B*08:01 easYmer complex formation assay and HLA-C*08:02 dsSCD peptide binding assay, respectively. **(D)** Binding analysis of the NY-ESO-$1_{139-147}$ (magenta) and NY-ESO-1_{96-104} (black) peptide towards various HLA-C dsSCD allotypes. The experiments shown in **(A, C, D)** were conducted in technical triplicates. SD, Standard deviation of the mean.

References

1. Altman JD, Moss PAH, Goulder PJR, Barouch DH, McHeyzer-Williams MG, Bell JI, et al. Phenotypic analysis of antigen-specific T lymphocytes. *Science* (1996) 274:94–6. doi: 10.1126/science.274.5284.94

2. Newell EW, Klein LO, Yu W, Davis MM. Simultaneous detection of many T-cell specificities using combinatorial tetramer staining. *Nat Methods* (2009) 6:497–9. doi: 10.1038/nmeth.1344

3. Hadrup SR, Bakker AH, Shu CJ, Andersen RS, van Veluw J, Hombrink P, et al. Parallel detection of antigen-specific T-cell responses by multidimensional encoding of MHC multimers. *Nat Methods* (2009) 6:520–6. doi: 10.1038/nmeth.1345

4. Bentzen AK, Marquard AM, Lyngaa R, Saini SK, Ramskov S, Donia M, et al. Large-scale detection of antigen-specific T cells using peptide-MHC-I multimers labeled with DNA barcodes. *Nat Biotechnol* (2016) 34:1037–45. doi: 10.1038/nbt.3662

5. Dolton G, Lissina A, Skowera A, Ladell K, Tungatt K, Jones E, et al. Comparison of peptide-major histocompatibility complex tetramers and dextramers for the identification of antigen-specific T cells. *Clin Exp Immunol* (2014) 177:47–63. doi: 10.1111/cei.12339

6. Huang J, Zeng X, Sigal N, Lund PJ, Su LF, Huang H, et al. Detection, phenotyping, and quantification of antigen-specific T cells using a peptide-MHC dodecamer. *Proc Natl Acad Sci* (2016) 113:E1890–7. doi: 10.1073/pnas.1602488113

7. Leisner C, Loeth N, Lamberth K, Justesen S, Sylvester-Hvid C, Schmidt EG, et al. One-pot, mix-and-read peptide-MHC tetramers. *PloS One* (2008) 3:e1678. doi: 10.1371/journal.pone.0001678

8. Bonté PE, Arribas YA, Merlotti A, Carrascal M, Zhang JV, Zueva E, et al. Single-cell RNA-seq-based proteogenomics identifies glioblastoma-specific transposable elements encoding HLA-I-presented peptides. *Cell Rep* (2022) 39:110916. doi: 10.1016/j.celrep.2022.110916

9. Hein Z, Uchtenhagen H, Abualrous ET, Saini SK, Janssen L, Van Hateren A, et al. Peptide-independent stabilization of MHC class I molecules breaches cellular quality control. *J Cell Sci* (2014) 127:2885–97. doi: 10.1242/jcs.145334

10. Saini SK, Tamhane T, Anjanappa R, Saikia A, Ramskov S, Donia M, et al. Empty peptide-receptive MHC class I molecules for efficient detection of antigen-specific T cells. *Sci Immunol* (2019) 4:eaau9039. doi: 10.1126/sciimmunol.aau9039

11. Moritz A, Anjanappa R, Wagner C, Bunk S, Hofmann M, Pszolla G, et al. High-throughput peptide-MHC complex generation and kinetic screenings of TCRs with peptide-receptive HLA-A*02:01 molecules. *Sci Immunol* (2019) 4:eaav0860. doi: 10.1126/sciimmunol.aav0860

12. Anjanappa R, Garcia-Alai M, Kopicki J-D, Lockhauserbäumer J, Aboelmagd M, Hinrichs J, et al. Structures of peptide-free and partially loaded MHC class I molecules reveal mechanisms of peptide selection. *Nat Commun* (2020) 11:1314. doi: 10.1038/s41467-020-14862-4

13. Luimstra JJ, Garstka MA, Roex MCJ, Redeker A, Janssen GMC, van Veelen PA, et al. A flexible MHC class I multimer loading system for large-scale detection of antigen-specific T cells. *J Exp Med* (2018) 215:1493–504. doi: 10.1084/jem.20180156

14. Toebes M, Coccoris M, Bins A, Rodenko B, Gomez R, Nieuwkoop NJ, et al. Design and use of conditional MHC class I ligands. *Nat Med* (2006) 12:246–51. doi: 10.1038/nm1360

15. van Rooij N, van Buuren M, Philips D, Velds A, Toebes M, Heemskerk B, et al. Tumor exome analysis reveals neoantigen-specific T-cell reactivity in an ipilimumab-responsive melanoma. *J Clin Oncol* (2013) 31:e439–442. doi: 10.1200/JCO.2012.47.7521

16. Bliskovsky VV, Parkhurst MR, Gartner JJ, Rosenberg SA, Horovitz-Fried M, Ankri C, et al. Isolation of neoantigen-specific T cells from tumor and peripheral lymphocytes. *J Clin Invest* (2015) 125:3981–91. doi: 10.1172/jci82416

17. McGranahan N, Furness A, Rosenthal R, Ramskov S, Lyngaa R, Saini S, et al. Clonal neoantigens elicit T cell immunoreactivity and sensitivity to immune checkpoint blockade. *Science* (2016) 351:1463–9. doi: 10.1126/science.aaf1490

18. Hansen TH, Connolly JM, Gould KG, Fremont DH. Basic and translational applications of engineered MHC class I proteins. *Trends Immunol* (2010) 31:363–9. doi: 10.1016/j.it.2010.07.003

19. Mitaksov V, Truscott SM, Lybarger L, Connolly JM, Hansen TH, Fremont DHH. Structural engineering of pMHC reagents for T cell vaccines and diagnostics. *Chem Biol* (2007) 14:909–22. doi: 10.1016/j.chembiol.2007.07.010

20. Truscott SM, Lybarger L, Martinko JM, Mitaksov VE, Kranz DM, Janet M, et al. Disulfide bond engineering to trap peptides in the MHC class I binding groove. *J Immunol* (2007) 178:6280–9. doi: 10.4049/jimmunol.178.10.6280

21. Lybarger L, Lawrence Yu YY, Miley MJ, Fremont DH, Myers N, Primeau T, et al. Enhanced immune presentation of a single-chain major histocompatibility complex class I molecule engineered to optimize linkage of a C-terminally extended peptide. *J Biol Chem* (2003) 278:27105–11. doi: 10.1074/jbc.M303716200

22. Truscott SM, Wang X, Lybarger L, Biddison WE, McBerry C, Martinko JM, et al. Human major histocompatibility complex (MHC) class I molecules with disulfide traps secure disease-related antigenic peptides and exclude competitor peptides. *J Biol Chem* (2008) 283:7480–90. doi: 10.1074/jbc.M709935200

23. Greten TF, Korangy F, Neumann G, Wedemeyer H, Schlote K, Heller A, et al. Peptide-β2-microglobulin-MHC fusion molecules bind antigen-specific T cells and can be used for multivalent MHC-Ig complexes. *J Immunol Methods* (2002) 271:125–35. doi: 10.1016/S0022-1759(02)00346-0

24. Oelke M, Schneck JP. Overview of a HLA-Ig based "lego-like system" for T cell monitoring, modulation and expansion. *Immunol Res* (2010) 47:248–56. doi: 10.1007/s12026-009-8156-z

25. Rölle A, Meyer M, Calderazzo S, Jäger D, Momburg F. Distinct HLA-E peptide complexes modify antibody-driven effector functions of adaptive NK cells. *Cell Rep* (2018) 24:1967–76. doi: 10.1016/j.celrep.2018.07.069

26. Huang CH, Peng S, He L, Tsai YC, Boyd DAK, Hansen TH, et al. Cancer immunotherapy using a DNA vaccine encoding a single-chain trimer of MHC class I linked to an HPV-16 E6 immunodominant CTL epitope. *Gene Ther* (2005) 12:1180–6. doi: 10.1038/sj.gt.3302519

27. Peng S, Trimble C, He L, Tsai YC, Lin CT, Boyd DAK, et al. Characterization of HLA-A2-restricted HPV-16 E7-specific CD8+ T-cell immune responses induced by DNA vaccines in HLA-A2 transgenic mice. *Gene Ther* (2006) 13:67–77. doi: 10.1038/sj.gt.3302607

28. Kim S, Li L, McMurtrey CP, Hildebrand WH, Weidanz JA, Gillanders WE, et al. Single-chain HLA-A2 MHC trimers that incorporate an immundominant peptide elicit protective T cell immunity against lethal west nile virus infection. *J Immunol* (2010) 184:4423–30. doi: 10.4049/jimmunol.0903955

29. Foy SP, Jacoby K, Bota DA, Hunter T, Pan Z, Stawiski E, et al. Non-viral precision T cell receptor replacement for personalized cell therapy. *Nature* (2022) 615:687–96. doi: 10.1038/s41586-022-05531-1

30. Puig-Saus C, Sennino B, Peng S, Wang CL, Pan Z, Yuen B, et al. Neoantigen-targeted CD8+ T cell responses with PD-1 blockade therapy. *Nature* (2023) 615:697–704. doi: 10.1038/s41586-023-05787-1

31. Saini SK, Ostermeir K, Ramnarayan VR, Schuster H, Zacharias M, Springer S. Dipeptides promote folding and peptide binding of MHC class I molecules. *Proc Natl Acad Sci U.S.A.* (2013) 110:15383–8. doi: 10.1073/pnas.1308672110

32. Momburg F, Meyer M, Zoernig I, Jäger D, Halama N, Kaiser I. Artificial antigen presenting molecules and their uses. Heidelberg University. Patent Application Publication US 2022/0381770 A1. (2020).

33. Warwas KM, Meyer M, Gonçalves M, Moldenhauer G, Bulbuc N, Knabe S, et al. Co-stimulatory bispecific antibodies induce enhanced T cell activation and tumor cell killing in breast cancer models. *Front Immunol* (2021) 12:719116. doi: 10.3389/fimmu.2021.719116

34. Merrifield RB. Solid phase peptide synthesis. I. The synthesis of a tetrapeptide. *J Am Chem Soc* (1963) 85:2149–54. doi: 10.1021/j00897025

35. Carpino LA, Han GY. 9-Fluorenylmethoxycarbonyl amino-protecting group. *J Org Chem* (1972) 37:3404–9. doi: 10.1021/jo00795a005

36. Chong C, Marino F, Pak H, Racle J, Daniel RT, Müller M, et al. High-throughput and sensitive immunopeptidomics platform reveals profound interferonγ-mediated remodeling of the human leukocyte antigen (HLA) ligandome. *Mol Cell Proteomics* (2018) 17:533–48. doi: 10.1074/mcp.TIR117.000383

37. Bruderer R, Bernhardt OM, Gandhi T, Miladinović SM, Cheng L-Y, Messner S, et al. Extending the limits of quantitative proteome profiling with data-independent acquisition and application to acetaminophen-treated three-dimensional liver microtissues. *Mol Cell Proteomics* (2015) 14:1400–10. doi: 10.1074/mcp.M114.044305

38. Pino LK, Searle BC, Bollinger JG, Nunn B, MacLean B, MacCoss MJ. The Skyline ecosystem: Informatics for quantitative mass spectrometry proteomics. *Mass Spectrom Rev* (2020) 39:229–44. doi: 10.1002/mas.21540

39. Gessulat S, Schmidt T, Zolg DP, Samaras P, Schnatbaum K, Zerweck J, et al. Prosit: proteome-wide prediction of peptide tandem mass spectra by deep learning. *Nat Methods* (2019) 16:509–18. doi: 10.1038/s41592-019-0426-7

40. Toprak UH, Gillet LC, Maiolica A, Navarro P, Leitner A, Aebersold R. Conserved peptide fragmentation as a benchmarking tool for mass spectrometers and a discriminating feature for targeted proteomics. *Mol Cell Proteomics* (2014) 13:2056–71. doi: 10.1074/mcp.O113.036475

41. Gras S, Saulquin X, Reiser J-B, Debeaupuis E, Echasserieau K, Kissenpfennig A, et al. Structural bases for the affinity-driven selection of a public TCR against a dominant human cytomegalovirus epitope. *J Immunol* (2009) 183:430–7. doi: 10.4049/jimmunol.0900556

42. Borbulevych OY, Santhanagopolan SM, Hossain M, Baker BM. TCRs used in cancer gene therapy cross-react with MART-1/melan-A tumor antigens via distinct mechanisms. *J Immunol* (2011) 187:2453–63. doi: 10.4049/jimmunol.1101268

43. Levin N, Paria BC, Vale NR, Yossef R, Lowery FJ, Parkhurst MR, et al. Identification and validation of T-cell receptors targeting RAS hotspot mutations in human cancers for use in cell-based immunotherapy. *Clin Cancer Res* (2021) 27:5084–95. doi: 10.1158/1078-0432.CCR-21-0849

44. Tran E, Robbins PF, Lu Y-C, Prickett TD, Gartner JJ, Jia L, et al. T-cell transfer therapy targeting mutant KRAS in cancer. *New Engl J Med* (2016) 375:2255–62. doi: 10.1056/NEJMoa1609279

45. Robbins PF, Li YF, El-Gamil M, Zhao Y, Wargo JA, Zheng Z, et al. Single and dual amino acid substitutions in TCR CDRs can enhance antigen-specific T cell functions. *J Immunol* (2008) 180:6116–31. doi: 10.4049/jimmunol.180.9.6116

46. Bethune MT, Li XH, Yu J, McLaughlin J, Cheng D, Mathis C, et al. Isolation and characterization of NY-ESO-1-specific T cell receptors restricted on various MHC molecules. *Proc Natl Acad Sci U.S.A.* (2018) 115:E10702–11. doi: 10.1073/pnas.1810653115

47. Kowarz E, Löscher D, Marschalek R. Optimized Sleeping Beauty transposons rapidly generate stable transgenic cell lines. *Biotechnol J* (2015) 10:647–53. doi: 10.1002/biot.201400821

48. Mátés L, Chuah MKL, Belay E, Jerchow B, Manoj N, Acosta-Sanchez A, et al. Molecular evolution of a novel hyperactive Sleeping Beauty transposase enables robust stable gene transfer in vertebrates. *Nat Genet* (2009) 41:753–61. doi: 10.1038/ng.343

49. Rosskopf S, Leitner J, Paster W, Morton LT, Hagedoorn RS, Steinberger P, et al. A Jurkat 76 based triple parameter reporter system to evaluate TCR functions and adoptive T cell strategies. *Oncotarget* (2018) 9:17608–19. doi: 10.18632/oncotarget.24807

50. Philips D, van den Braber M, Schumacher TN, Kvistborg P. pMHC multiplexing strategy to detect high numbers of T cell responses in parallel. *Methods Mol Biol* (2017) 1514:93–101. doi: 10.1007/978-1-4939-6548-9_7

51. Andersen RS, Kvistborg P, Mørch Frøsig T, Pedersen NW, Lyngaa R, Bakker AH, et al. Parallel detection of antigen-specific T cell responses by combinatorial encoding of MHC multimers. *Nat Protoc* (2012) 7:891–902. doi: 10.1038/nprot.2012.037

52. Jahn A, Rump A, Widmann TJ, Heining C, Horak P, Hutter B, et al. Comprehensive cancer predisposition testing within the prospective MASTER trial identifies hereditary cancer patients and supports treatment decisions for rare cancers. *Ann Oncol* (2022) 33:1186–99. doi: 10.1016/j.annonc.2022.07.008

53. Jiang H, Lei R, Ding SW, Zhu S. Skewer: a fast and accurate adapter trimmer for next-generation sequencing paired-end reads. *BMC Bioinf* (2014) 15:182. doi: 10.1186/1471-2105-15-182

54. Paramasivam N, Hübschmann D, Toprak UH, Ishaque N, Neidert M, Schrimpf D, et al. Mutational patterns and regulatory networks in epigenetic subgroups of meningioma. *Acta Neuropathol* (2019) 138:295–308. doi: 10.1007/s00401-019-02008-w

55. Radke J, Ishaque N, Koll R, Gu Z, Schumann E, Sieverling L, et al. The genomic and transcriptional landscape of primary central nervous system lymphoma. *Nat Commun* (2022) 13:2558. doi: 10.1038/s41467-022-30050-y

56. Ishaque N, Abba ML, Hauser C, Patil N, Paramasivam N, Huebschmann D, et al. Whole genome sequencing puts forward hypotheses on metastasis evolution and therapy in colorectal cancer. *Nat Commun* (2018) 9:4782. doi: 10.1038/s41467-018-07041-z

57. Rimmer A, Phan H, Mathieson I, Iqbal Z, Twigg SRFWGS500 Consortium, et al. Integrating mapping-, assembly- and haplotype-based approaches for calling variants in clinical sequencing applications. *Nat Genet* (2014) 46:912–8. doi: 10.1038/ng.3036

58. Harrow J, Frankish A, Gonzalez JM, Tapanari E, Diekhans M, Kokocinski F, et al. GENCODE: the reference human genome annotation for The ENCODE Project. *Genome Res* (2012) 22:1760–74. doi: 10.1101/gr.135350.111

59. Uhrig S, Ellermann J, Walther T, Burkhardt P, Fröhlich M, Hutter B, et al. Accurate and efficient detection of gene fusions from RNA sequencing data. *Genome Res* (2021) 31:448–60. doi: 10.1101/gr.257246.119

60. Koşaloğlu Z, Zörnig I, Halama N, Kaiser I, Buchhalter I, Grabe N, et al. Identification of immunotherapeutic targets by genomic profiling of rectal NET metastases. *Oncoimmunology* (2016) 5:e1213931. doi: 10.1080/2162402X.2016.1213931

61. Reynisson B, Alvarez B, Paul S, Peters B, Nielsen M. NetMHCpan-4.1 and NetMHCIIpan-4.0: improved predictions of MHC antigen presentation by concurrent motif deconvolution and integration of MS MHC eluted ligand data. *Nucleic Acids Res* (2020) 48:W449–54. doi: 10.1093/nar/gkaa379

62. Barat B, Wu AM. Metabolic biotinylation of recombinant antibody by biotin ligase retained in the endoplasmic reticulum. *Biomol Eng* (2007) 24:283–91. doi: 10.1016/j.bioeng.2007.02.003.Metabolic

63. Garcia-Garijo A, Fajardo CA, Gros A. Determinants for neoantigen identification. *Front Immunol* (2019) 10:1392. doi: 10.3389/fimmu.2019.01392

64. Kast F, Klein C, Umaña P, Gros A, Gasser S. Advances in identification and selection of personalized neoantigen/T-cell pairs for autologous adoptive T cell therapies. *Oncoimmunology* (2021) 10:1869389. doi: 10.1080/2162402X.2020.1869389

65. Davis MM, Altman JD, Newell EW. Interrogating the repertoire: broadening the scope of peptide-MHC multimer analysis. *Nat Rev Immunol* (2011) 11:551–8. doi: 10.1038/nri3020

66. Bentzen A, Hadrup S. Evolution of MHC-based technologies used for detection of antigen-responsive T cells. *Cancer Immunology Immunotherapy* (2017) 66:657–66. doi: 10.1007/s00262-017-1971-5

67. Schmidt J, Dojcinovic D, Guillaume P, Luescher I. Analysis, isolation, and activation of antigen-specific CD4+ and CD8+ T cells by soluble MHC-peptide complexes. *Front Immunol* (2013) 4:218. doi: 10.3389/fimmu.2013.00218

68. Dolton G, Zervoudi E, Rius C, Wall A, Thomas HL, Fuller A, et al. Optimized peptide-MHC multimer protocols for detection and isolation of autoimmune T-cells. *Front Immunol* (2018) 9:1378. doi: 10.3389/fimmu.2018.01378

69. Adamo S, Michler J, Zurbuchen Y, Cervia C, Taeschler P, Raeber ME, et al. Signature of long-lived memory CD8+ T cells in acute SARS-CoV-2 infection. *Nature* (2022) 602:148–55. doi: 10.1038/s41586-021-04280-x

70. Maecker HT, Hassler J, Payne JK, Summers A, Comatas K, Ghanayem M, et al. Precision and linearity targets for validation of an IFNγ ELISPOT, cytokine flow cytometry, and tetramer assay using CMV peptides. *BMC Immunol* (2008) 9:9. doi: 10.1186/1471-2172-9-9

71. Zacharakis N, Chinnasamy H, Black M, Xu H, Lu YC, Zheng Z, et al. Immune recognition of somatic mutations leading to complete durable regression in metastatic breast cancer. *Nat Med* (2018) 24:724–30. doi: 10.1038/s41591-018-0040-8

72. Cafri G, Yossef R, Pasetto A, Deniger DC, Lu YC, Parkhurst M, et al. Memory T cells targeting oncogenic mutations detected in peripheral blood of epithelial cancer patients. *Nat Commun* (2019) 10:449. doi: 10.1038/s41467-019-08304-z

73. Bobisse S, Genolet R, Roberti A, Tanyi JL, Racle J, Stevenson BJ, et al. Sensitive and frequent identification of high avidity neo-epitope specific CD8 + T cells in immunotherapy-naive ovarian cancer. *Nat Commun* (2018) 9:1092. doi: 10.1038/s41467-018-03301-0

74. Garboczi DN, Hung DT, Wiley DC. HLA-A2-peptide complexes: refolding and crystallization of molecules expressed in Escherichia coli and complexed with single antigenic peptides. *Proc Natl Acad Sci U.S.A.* (1992) 89:3429–33. doi: 10.1073/pnas.89.8.3429

75. Rodenko B, Toebes M, Hadrup SR, van Esch WJE, Molenaar AM, Schumacher TNM, et al. Generation of peptide-MHC class I complexes through UV-mediated ligand exchange. *Nat Protoc* (2006) 1:1120–32. doi: 10.1038/nprot.2006.121

76. Bakker AH, Hoppes R, Linnemann C, Toebes M, Rodenko B, Berkers CR, et al. Conditional MHC class I ligands and peptide exchange technology for the human MHC gene products HLA-A1, -A3, -A11, and -B7. *Proc Natl Acad Sci* (2008) 105:3825–30. doi: 10.1073/pnas.0709717105

77. Saini SK, Hersby DS, Tamhane T, Povlsen HR, Amaya Hernandez SP, Nielsen M, et al. SARS-CoV-2 genome-wide T cell epitope mapping reveals immunodominance and substantial CD8+ T cell activation in COVID-19 patients. *Sci Immunol* (2021) 6:eabf7550. doi: 10.1126/sciimmunol.abf7550

78. Chang CXL, Tan AT, Or MY, Toh KY, Lim PY, Chia ASE, et al. Conditional ligands for Asian HLA variants facilitate the definition of CD8+ T-cell responses in acute and chronic viral diseases. *Eur J Immunol* (2013) 43:1109–20. doi: 10.1002/eji.201243088

79. Frøsig TM, Yap J, Seremet T, Lyngaa R, Svane IM, Thor Straten P, et al. Design and validation of conditional ligands for HLA-B*08:01, HLA-B*15:01, HLA-B*35:01, and HLA-B*44:05. *Cytometry Part A* (2015) 87:967–75. doi: 10.1002/cyto.a.22689

80. Luimstra JJ, Franken KLMC, Garstka MA, Drijfhout JW, Neefjes J, Ovaa H. Production and thermal exchange of conditional peptide-MHC I multimers. *Curr Protoc Immunol* (2019) 126:e85. doi: 10.1002/cpim.85

81. Overall SA, Toor JS, Hao S, Yarmarkovich M, Sara M, O'Rourke, et al. High throughput pMHC-I tetramer library production using chaperone-mediated peptide exchange. *Nat Commun* (2020) 11:1909. doi: 10.1038/s41467-020-15710-1

82. Murata K, Nakatsugawa M, Rahman MA, Nguyen LT, Millar DG, Mulder DT, et al. Landscape mapping of shared antigenic epitopes and their cognate TCRs of tumor-infiltrating T lymphocytes in melanoma. *Elife* (2020) 9:e53244. doi: 10.7554/eLife.53244

83. Pedersen LO, Nissen MH, Hansen NJV, Nielsen LL, Lauenmøller SL, Blicher T, et al. Efficient assembly of recombinant major histocompatibility cmplex class I molecules with performed disulfide bonds. *Eur J Immunol* (2001) 31:2986–96. doi: 10.1002/1521-4141(2001010)31:10<2986::AID-IMMU2986>3.0.CO;2-R

84. Ferré H, Ruffet E, Blicher T, Sylvester-Hvid C, Nielsen L, Hobley T, et al. Purification of correctly oxidized MHC class I heavy-chain molecules under denaturing conditions: A novel strategy exploiting disulfide assisted protein folding. *Protein Sci* (2003) 12:551–9. doi: 10.1110/ps.0233003

85. Lyu F, Ozawa T, Hamana H, Kobayashi E, Muraguchi A, Kishi H. A novel and simple method to produce large amounts of recombinant soluble peptide/major histocompatibility complex monomers for analysis of antigen-specific human T cell receptors. *N Biotechnol* (2019) 49:169–77. doi: 10.1016/j.nbt.2018.11.005

86. Wooster AL, Anderson TS, Lowe DB. Expression and characterization of soluble epitope-defined major histocompatibility complex (MHC) from stable eukaryotic cell lines. *J Immunol Methods* (2019) 464:22–30. doi: 10.1016/j.jim.2018.10.006

87. Mottez E, Jaulin C, Godeau F, Choppin J, Levy JP, Kourilsky P. A single-chain murine class I major transplantation antigen. *Eur J Immunol* (1991) 21:467–71. doi: 10.1002/eji.1830210232

88. Toshitani K, Braud V, Browning MJ, Murray N, McMichael AJ, Bodmer WF. Expression of a single-chain HLA class I molecule in a human cell line: presentation of exogenous peptide and processed antigen to cytotoxic T lymphocytes. *Proc Natl Acad Sci* (1996) 93:236–40. doi: 10.1073/pnas.93.1.236

89. Finton KAK, Brusniak M-Y, Jones LA, Lin C, Fioré-Gartland AJ, Brock C, et al. ARTEMIS: A novel mass-spec platform for HLA-restricted self and disease-associated peptide discovery. *Front Immunol* (2021) 12:658372. doi: 10.3389/fimmu.2021.658372

90. Lan H, Abualrous ET, Sticht J, Fernandez LMA, Werk T, Weise C, et al. Exchange catalysis by tapasin exploits conserved and allele-specific features of MHC-I molecules. *Nat Commun* (2021) 12:4236. doi: 10.1038/s41467-021-24401-4

91. Schumacher T, Heemels M, Neefjes J, Kast W, Melief C, Ploegh H. Direct binding of peptide to empty MHC class I molecules on intact cells and. *vitro. Cell* (1990) 62:563–7. doi: 10.1016/0092-8674(90)90020-f

92. Ljunggren H-G, Stam NJ, Öhlén C, Neefjes JJ, Höglund P, Heemels M-T, et al. Empty MHC class I molecules come out in the cold. *Nature* (1990) 346:476–80. doi: 10.1038/346476a0

93. Shimizu Y, Ogawa K, Nakayama M. Characterization of kinetic binding properties of unlabeled ligands via a preincubation endpoint binding approach. *J Biomol Screen* (2016) 21:729–37. doi: 10.1177/1087057116652065

Frontiers in Immunology

Explores novel approaches and diagnoses to treat immune disorders.

The official journal of the International Union of Immunological Societies (IUIS) and the most cited in its field, leading the way for research across basic, translational and clinical immunology.

Discover the latest Research Topics

See more →

Frontiers

Avenue du Tribunal-Fédéral 34
1005 Lausanne, Switzerland
frontiersin.org

Contact us

+41 (0)21 510 17 00
frontiersin.org/about/contact